IORT PAPERS IN—

nalytical methods
onomic geology
tuarine hydrology
eochemistry
eochronology
eomorphology
eophysics
laciology
round water
ydrologic techniques
leontology
trology
emote sensing
ratigraphy
ructural geology
rface water
ban hydrology

GEOLOGICAL SURVEY RESEARCH 1971

Chapter B

GEOLOGICAL SURVEY PROFESSIONAL PAPER 750–B

GEOLOGICAL SURVEY RESEARCH 1971

Chapter B

GEOLOGICAL SURVEY PROFESSIONAL PAPER 750–B

Scientific notes and summaries of investigations in geology, hydrology, and related fields

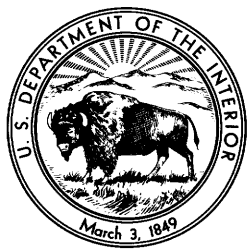

UNITED STATES GOVERNMENT PRINTING OFFICE, WASHINGTON: 1971

UNITED STATES DEPARTMENT OF THE INTERIOR

ROGERS C. B. MORTON, Secretary

GEOLOGICAL SURVEY

William T. Pecora, Director

For sale by the Superintendent of Documents, U.S. Government Printing Office
Washington, D.C. 20402 – Price $3.50

CONTENTS

GEOLOGIC STUDIES

Analytical methods

Remote sensing

Laboratory facilities

HYDROLOGIC STUDIES

Estuarine hydrology

Urban hydrology

Ground water

Surface water

Hydrologic techniques

INDEXES

GEOLOGICAL SURVEY RESEARCH 1971

This collection of 46 short papers is the first published chapter of "Geological Survey Research 1971." The papers report on scientific and economic results of current work by members of the Geologic and Water Resources Divisions of the U.S. Geological Survey.

Chapter A, to be published later in the year, will present a summary of significant results of work done in fiscal year 1971, together with lists of investigations in progress, reports published, cooperating agencies, and Geological Survey offices.

"Geological Survey Research 1971" is the twelfth volume of the annual series Geological Survey Research. The eleven volumes already published are listed below, with their series designations.

Geological Survey Research	*Prof. Paper*
1960	400
1961	424
1962	450
1963	475
1964	501
1965	525
1966	550
1967	575
1968	600
1969	650
1970	700

STRUCTURES RELATED TO THRUST FAULTS IN THE STANSBURY MOUNTAINS, UTAH

By E. W. TOOKER and R. J. ROBERTS, Menlo Park, Calif.

Abstract.—Structural studies of folded Paleozoic rocks in the Stansbury Mountains and regional geologic patterns suggest that this range consists of four imbricate thrust slices. Major unexposed thrust faults bound the east and west sides of the range. Similar thrust faults, fold structures, and comparable stratigraphic sequences are reported in the Sheeprock, West Tintic, and Gilson Mountains. Four conclusions can be drawn from these structures: (1) Paleozoic rocks now present in the Stansbury Mountains were deposited an unknown distance west of their present site. (2) The marked uplift and erosion during the Late Devonian (Stansbury uplift) recorded by the Stansbury Formation of Stokes and Arnold (1958) also took place farther west. (3) The Cambrian Tintic Quartzite now exposed high in the core of the range owes its presence to folding and upthrusting along the ramp of the Timpie thrust fault during the Sevier orogeny, not during the Stansbury uplift or to later epeirogenic movements. (4) The spatial distribution of igneous rocks and the metallization in thrust-fault zones here suggest potential target zones for prospecting in similar structures in the Great Basin.

The Stansbury Mountains are a north-trending range of the eastern Great Basin in north-central Utah, approximately 40 miles west of Salt Lake City (fig. 1) in the Deseret Peak and Timpie 15-minute quadrangles. The mountains are bounded on the north by Stansbury Island and the Great Salt Lake; on the east by the Tooele and Rush Valleys, which lie north and south, respectively, of a small transverse ridge, South Mountain; and on the west by Skull Valley. An extension of the range south of Johnson Pass is called the Onaqui Mountains. The Stansbury Mountains are approximately 30 miles long and 10 miles wide and attain a maximum elevation of 11,031 feet at Deseret Peak. The average valley elevation is about 4,500 feet. The rugged west slope of the range is dissected by steep-walled canyons; the eastern side is less rugged, except for the glacial cirques flanking Deseret Peak.

The geology of the Stansbury Mountains was known only in a general way from the reconnaissance of the Fortieth Parallel Survey of King (1878, p. 199) and the State geologic map of Butler (Butler and others, 1920, pl. 4) before publication of the summary edited by Rigby (1958), which included the Timpie and Deseret Peak 15-minute quadrangles (1:62,500 scale). The stratigraphy and structure of rocks of nearly comparable ages in the Stansbury Mountains is distinctly different from that reported for flanking ranges—the

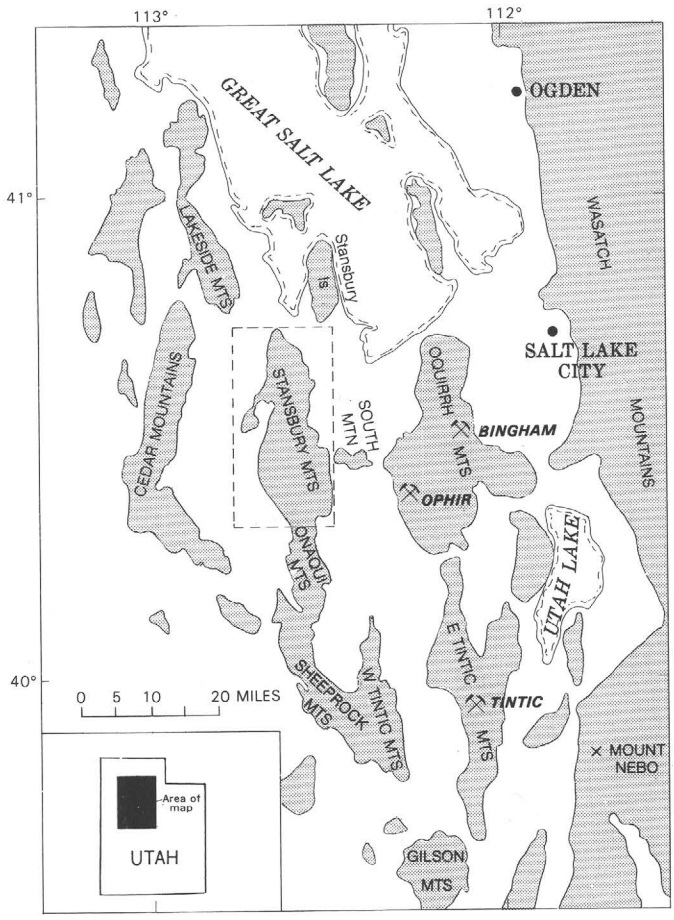

FIGURE 1.—Index map of north-central Utah, showing the Stansbury Mountains (area of figs. 2 and 4 outlined) and adjacent mountain ranges and valleys.

U.S. GEOL. SURVEY PROF. PAPER 750-B, PAGES B1-B12

Oquirrh Mountains to the east (Roberts and Tooker, 1961) and the Cedar Mountains to the west (Robert Maurer, oral commun., 1958). However, the southern end of Stansbury Island appears to be a northern continuation of the Stansbury Mountains (Palmer, 1969), and the Onaqui Mountains are a southern continuation (Rigby, 1958). We have made many reconnaissance studies of the stratigraphy and structure of the Stansbury Mountains since 1958 in an effort to resolve the marked geologic discontinuities between the Stansbury and Oquirrh Mountains. The data are now believed sufficient to substantiate our thesis that the main structural fabric of this region results from thrust faults.

Our detailed studies (1:24,000 scale) indicate that the Oquirrh Mountains are composed of rock units of different sedimentary facies brought into juxtaposition by, and folded along with, thrust faults. This interpretation also explains the seemingly incompatible structural relations of the Stansbury Mountains, which consist of an asymmetric north-trending block, and South Mountain, which consists of an asymmetric west-plunging fold. The South Mountain fold is closely related to the Oquirrh Mountain fold system. Similarly, marked facies differences between Devonian strata within the Stansbury Mountains and comparable strata in the Oquirrh Mountains[1] are also best explained by thrust faulting.

Our summary of Rigby's interpretation of geologic data is followed by the section "Thrust Fault Interpretation of Tooker and Roberts." We consider our thesis to be a working hypothesis, which we hope will stimulate discussion and lead to the detailed mapping and stratigraphic and paleontologic studies needed to solve the perplexing geologic problems here.

GEOLOGIC INTERPRETATION OF RIGBY

The rocks in the Stansbury Mountains (fig. 2, after Rigby, 1958, pls. 1–3) make up a sedimentary sequence ranging in age from the Cambrian through the Pennsylvanian distributed along north-northeast-trending open folds and tight, locally overturned folds. Most faults are north-trending basin-and-range normal faults. For convenience in discussion, Rigby's stratigraphic section has been broadly divided into three parts: lower Paleozoic (Cambrian through Silurian), Devonian, and upper Paleozoic (Mississippian and Pennsylvanian) (fig. 3).

Lower Paleozoic rocks crop out mainly in the western half of the range where they are nearly 9,500 feet thick. These rocks consist of (1) a Cambrian unit comprising 11 formations, approximately 8,700 feet thick, composed of a basal quartzite (4,200 feet), a middle shale, quartzite, and limestone (1,200 feet), and an upper limestone and dolomite (3,300 feet); (2) an Ordovician unit about 1,800 feet thick, comprising three formations composed of limestone, shale, and dolomite; and (3) a Silurian unit consisting of one formation as much as 920 feet thick, composed mainly of dolomite.

Devonian rocks consist predominantly of conglomerate-sand (Stansbury Formation), sandstone and clastic limestone (Victoria Formation), and limestone (Pinyon Peak Limestone) rock facies of variable thickness that interfinger in varying amounts from place to place in the Stansbury Mountains. Rigby (1958) also used the formational names Sevy Dolomite and Simonson(?) Dolomite for some of these rocks. At the north end of the range the Stansbury facies (shown in stippled pattern in figures 2 and 4) predominates, is approximately 1,700 feet thick, and consists primarily of coarse conglomerate interbedded with quartzite, dolomite, limestone, and calcareous sandstone. Lenses of quartzite in the lower part and limestone in the upper part resemble the Pinyon Peak Limestone and Victoria Formation in their type localities in the Tintic mining district (Morris and Lovering, 1961, p. 70 and 74) nearly 50 miles south of the range (fig. 1). In the low pass between the Stansbury Mountains and South Mountain, the unit is composed of clean white quartzite, at least 200 feet thick (Rigby, 1958, p. 37), that resembles quartzite in the Victoria Formation. Devonian strata in the western and southern parts of the range (shown in solid pattern) are composed of a much thinner (approximately 300 feet) unit that in a general way resembles the limestone, quartzite, and dolomite facies of the Stansbury but contains a much thinned pebble conglomeratic facies. These rocks more closely resemble the Pinyon Peak Limestone and Victoria Formation lithologic types, which also crop out in the uppermost part of the Stansbury Formation at its type locality. Rigby (1958) includes in addition as much as 370 feet of underlying dolomite in these Devonian rocks, which he included in the Sevy Dolomite and Simonson(?) Dolomite.

The upper Paleozoic section, consisting of as much as 20,200 feet of Mississippian and Pennsylvanian rocks, crops out mainly in the easterly half of the Stansbury Mountains. The formations consist of dolomite-rich beds as much as 650 feet thick at the base succeeded by limestone, sandstone, shale, and quartzite units.

The faults in the Stansbury Mountains shown by Rigby (1958) on figure 2 are interpreted by him as mostly north-trending range-front and related normal faults. A reverse fault, the Broad Canyon, separates upper Paleozoic rocks from older rocks in the north-

[1] Gilluly (1932, p. 22) described the discontinuous 3- to 4-foot-thick sandy carbonate unit underlying Mississippian formational units and resting on an irregular small-scale karst-surfaced Cambrian dolomite near the mouth of Ophir Canyon in the Oquirrh Mountains. Rigby (1959, p. 30) considered it to be an equivalent of the Pinyon Peak Limestone.

east part of the range. Rigby believes that this fault passes under Tertiary volcanic rocks and Quaternary sedimentary deposits and connects with a concealed fault immediately west of South Mountain.

Rigby (1958, p. 116–124) summarized the geologic history of the Stansbury Mountains in terms of two main periods of uplift and folding, each followed by substantial erosion, which occurred on or near the present site of the range. In his view, early Paleozoic deposition continued with minor breaks through the Early Devonian and was followed by the first, or Devonian, uplift, which resulted in some folding of the strata. Substantial erosion followed, during which the clastic Devonian formations were deposited. Sedimentation resumed with the deposition of Mississippian and Pennsylvanian formations. The second major tectonic event was the Laramide orogeny that broadly arched the range along the trend of the Devonian uplift. Reverse faults formed at this time during overfolding in the range. A major period of erosion resulted in the formation of pediment conglomerates. Contemporary igneous intrusion and volcanic flow activity followed a major period of normal faulting of the region. Subsequent rapid erosion cut broad pediments and formed great aprons of alluvium at the base of the range, completing the geomorphic form of today's Stansbury Mountains.

THRUST FAULT INTERPRETATION OF TOOKER AND ROBERTS

A regional pattern of thrust faults most logically explains both the regional geologic relations and the internal geologic features of distinctive stratigraphy and fold structures observed in four structural blocks in the Stansbury Mountains. The north-trending asymmetric fold system of the Stansbury Mountains lies nearly normal to the west-plunging asymmetric fold in South Mountain, a fold that appears to be closely related to the Oquirrh Mountain fold system. The concept of a thrust fault partly follows from Billingsley and Locke (1939, p. 43), who originally suggested one between the Stansbury Mountains and South Mountain. Roberts and others (1965) proposed the name Tintic Valley thrust for this fault because of its structural comparability with the one long inferred under the Tintic Valley. This fault has since been found by H. T. Morris (oral commun., 1967) to crop out farther south in the Gilson Mountains; it thus has regional significance. The lithologic sequences in the Oquirrh and East Tintic Mountains on the east show consistent difference from those in the Stansbury and West Tintic Mountains to the west (Tooker and Roberts, unpub. data; and Morris and Kopf, 1969). As a logical consequence of the thrust hypothesis, our field studies, and our interpretation of the data of Rigby (1958) (shown in fig. 2), we have subdivided the Stansbury Mountains into four structural units that are separated by thrust faults, namely, the Dolomite, Timpie Valley, Deseret Peak, and Salt Mountain structural blocks (shown in fig. 4).

Dolomite block

The Dolomite fault block is bounded on the east by the Tintic Valley thrust fault and on the west by the Broad Canyon thrust fault. We believe that the latter fault, the Broad Canyon reverse fault of Rigby (1958, p. 69), continues southward under the Tertiary volcanic rocks in the central part of the range, along the contact shown by Rigby as an angular unconformity between Mississippian and Pennsylvanian Manning Canyon Shale on the west side, and successively older parts of the Pennsylvanian Oquirrh Formation southward on the east side. Rigby supposed that the successive appearance of Atokan- and Morrowan-age parts of the Oquirrh Formation represented sedimentary overlap. On examining the Oquirrh Formation in Big Hollow, we found exposures at best exceedingly poor, but we found no evidence for shoreward facies changes such as a coarsening of sediments or other ecological features that should accompany overlap.

Our interpretation of these contact relations is based substantially on the geometry and sedimentary character of the beds in the adjoining Timpie Valley and Dolomite blocks. The Manning Canyon Shale in the Timpie Valley (hanging-wall) block roughly parallels the fault contact. At the contact the shale beds are the east limb of a tight north-trending fold, locally overturned to the east. The tightly folded character of the western part of the block is exposed by erosion in lower parts of the range in Timpie Valley at the north end and in Big Hollow at the south end. In contrast, strata in the footwall (Dolomite) block consist of Cambrian through Pennsylvanian formations, successively truncated southward from the north end to the middle of the range, the highest topographic point on the contact. We have already noted the same truncation in reverse order southward from this point. Because the contact is nearly everywhere poorly exposed, the precise angle of the dip is not discernible; however, the straight contact suggests that it is nearly vertical. The folds in the Dolomite block imply to us that the Broad Canyon fault has more regional significance than a simple high-angle reverse fault would have. Furthermore, the folded strata in the Dolomite block form a broad, arcuate, asymmetric syncline. At the north end of the range, the syncline plunges northeast, and the

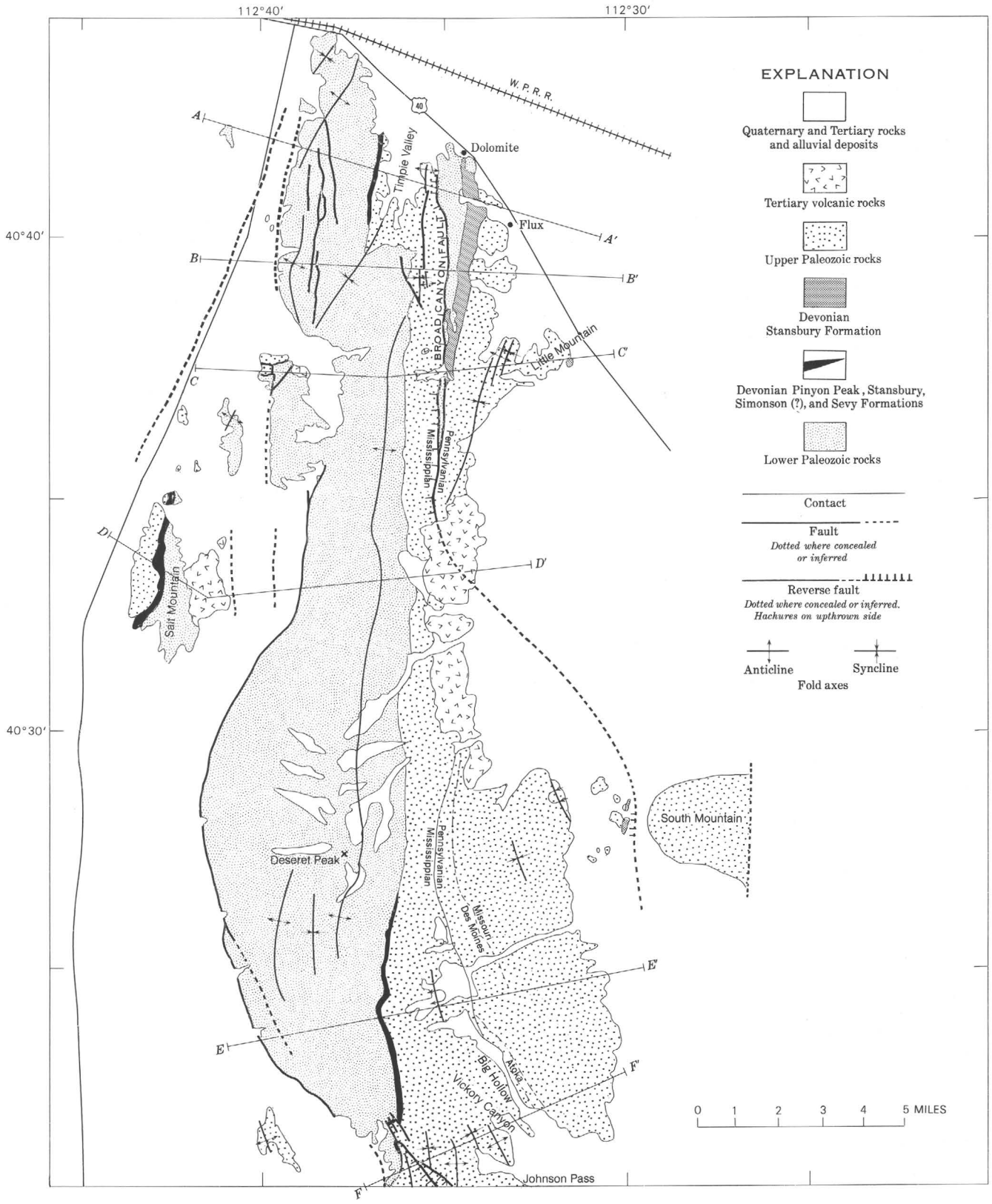
112°40′
112°30′
40°40′
40°30′
W. P. R. R.
40
Dolomite
Flux
Timple Valley
BROADCANYON FAULT
Little Mountain
Salt Mountain
Deseret Peak
South Mountain
Johnson Pass
Pennsylvanian
Mississippian
Missouri
Des Moines
Big Hollow
Vickory Canyon
Alpha
A
A′
B
B′
C
C′
D
D′
E
E′
F
F′
EXPLANATION
Quaternary and Tertiary rocks and alluvial deposits
Tertiary volcanic rocks
Upper Paleozoic rocks
Devonian Stansbury Formation
Devonian Pinyon Peak, Stansbury, Simonson (?), and Sevy Formations
Lower Paleozoic rocks
Contact
Fault
Dotted where concealed or inferred
Reverse fault
Dotted where concealed or inferred. Hachures on upthrown side
Anticline
Syncline
Fold axes
0 1 2 3 4 5 MILES

FIGURE 2.

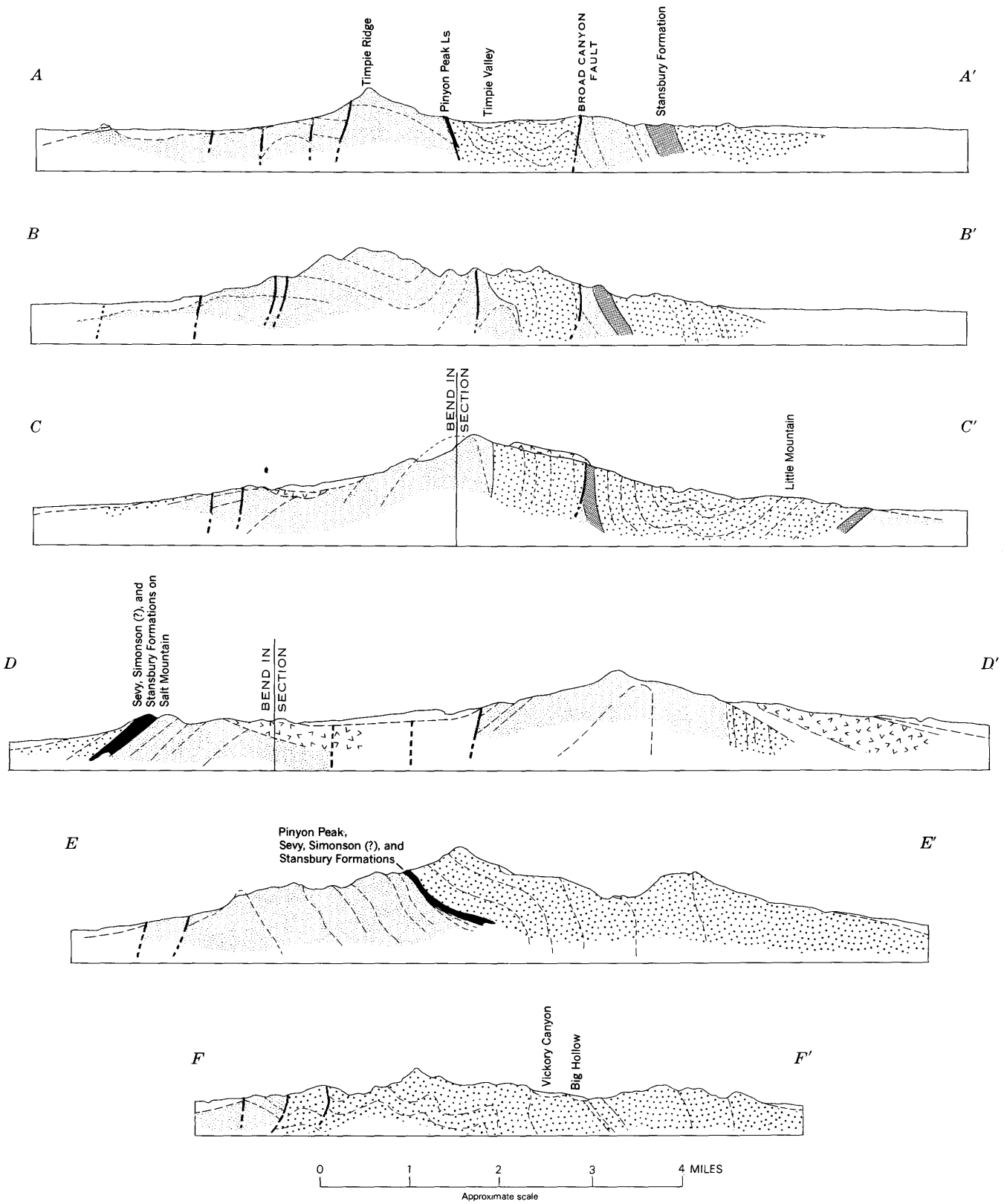

FIGURE 2.—Generalized geologic sketch map and diagrammatic sections of the Stansbury Mountains, after Rigby (1958, pls. 1, 2).

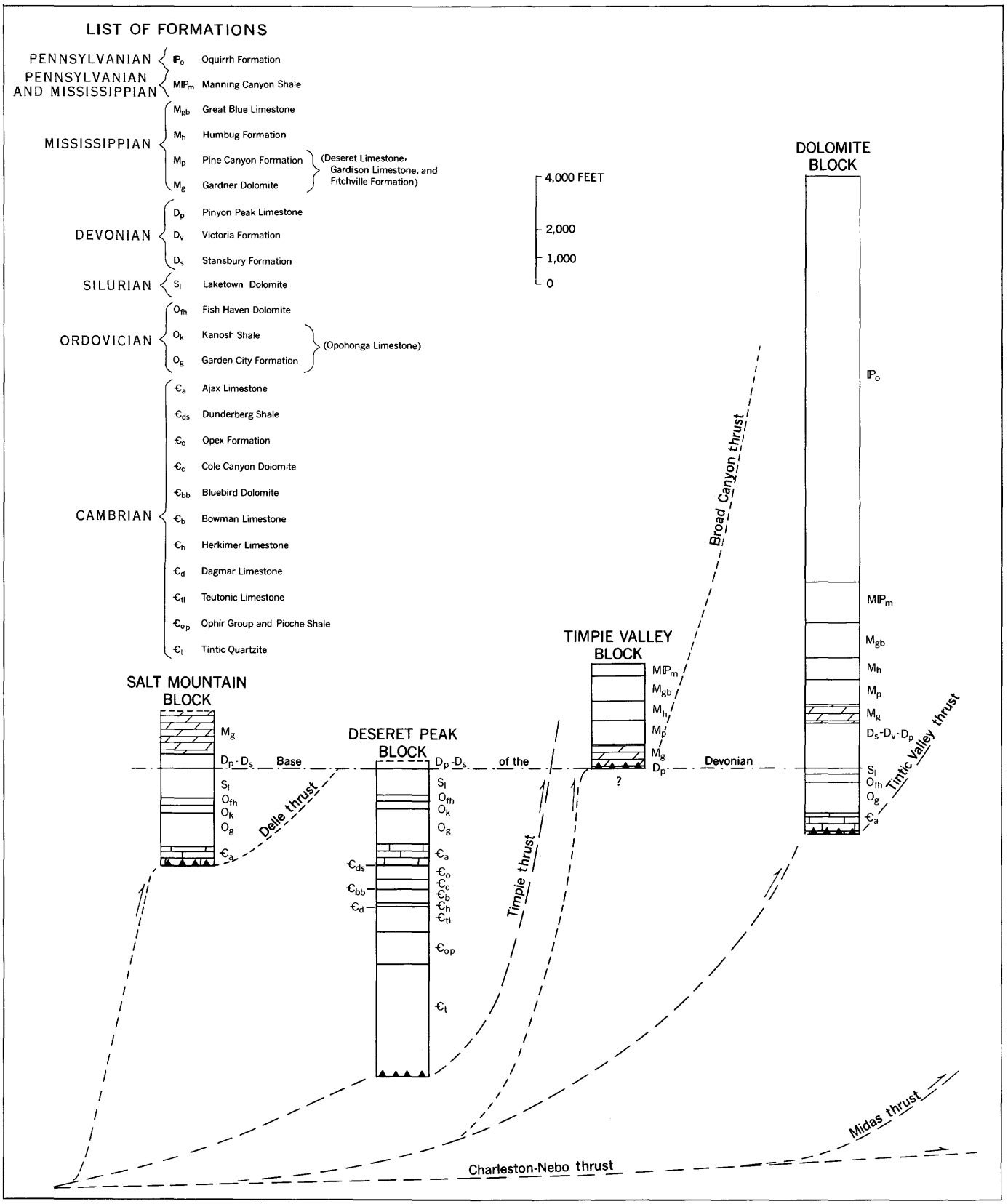

FIGURE 3.—Generalized columnar sections, largely after Rigby (1958), of the formational units in the Dolomite, Timpie Valley, Deseret Peak, and Salt Mountain structural blocks, showing their relations to the principal thrust faults. Formational names of correlative units in the Oquirrh and East Tintic Mountains are in parentheses. Long dashes represent extensive faults of large displacement, and short dashes represent faults of small displacement.

axial plane dips steeply to the west. At the south end, it broadens and bends to the southeast, and overfolds occur close to the trace of the Tintic Valley thrust near South Mountain. The bowing of folds in the Dolomite block resulting in a change in fold direction under the area of volcanic rocks in the central part of the range suggests to us that there may have been increased drag on the Tintic Valley thrust along the east-west Cortez-Uinta axis.

The Stansbury Formation, which includes the thickest section of Devonian conglomerate, crops out only in the Dolomote structural block; the type section is in sec. 6, T. 2 S., R. 6 W., and sec. 1, T. 2 S., R. 7 W. (Stokes and Arnold, 1958, p. 137) at the north end of the range on the ridge west of Dolomite and Flux, on the west limb of a syncline. We infer (*A–A* fig. 4) that this westward extension of the conglomerate in the Timpie Valley block is concealed by the overthrust Deseret Peak block. The east limb of the syncline is exposed on Little Mountain and in the pass between South Mountain and the Stansbury Mountains. The uppermost 60 feet of the type section above the conglomerate facies contains interbedded dolomite, limestone, and minor upper quartzite that Rigby assigns to the Pinyon Peak Limestone.

Timpie Valley block

The narrow, north-trending Timpie Valley block lies immediately east of, and parallel to, the crest of the Stansbury Mountains and extends southward from Timpie Valley to Vickory Canyon. Rocks in the block are carbonate rocks of Devonian and Mississippian age. The beds are tightly folded and locally overturned. A thin wedge of the Devonian Pinyon Peak Limestone occurs along the northernmost 2 miles of the fault contact on the west side of Timpie Valley in contact with the basal Mississippian dolomite. Whether the unit is truncated by stratigraphic pinchout or by the thrust fault cannot be determined. The block is bounded on the east and west sides by the Broad Canyon and Timpie thrust faults, respectively. Structural and stratigraphic evidence similar to that cited for the Broad Canyon thrust also defines the Timpie thrust. North-trending tight, asymmetric, and locally overturned, folds in the Timpie Valley block contrast with the broader, arcuate asymmetric folds in the Deseret Peak block to the west. Folding of the fault plane of the Timpie thrust fault and later erosion are inferred to have caused the apparent offset of the fault trace at the south end of Timpie Valley (fig. 4). Successively older parts of the Cambrian section in the adjacent Deseret Peak (hanging-wall) block are truncated at the fault contact southward into the central part of the range. This stratigraphic truncation is reversed farther south, where the fault successively exposes rocks of Cambrian through Devonian age.

Deseret Peak block

The Deseret Peak block underlies the topographically highest and westernmost part of the main ridge of the Stansbury Mountains. It is bordered on the east by the Timpie thrust fault and on the west by the Delle and Skull Valley thrusts. Although comparable lithologic units are found in the Deseret Peak and Salt Mountain blocks, the concealed Delle thrust is inferred because the folds exposed at the northwest end of the Stansbury Mountains are truncated by east-trending faults north of Salt Mountain. Not only are these intervening folds missing, but the covered area between the two blocks is insufficient to accommodate them. Thus, we infer telescoping of the syncline west of Salt Mountain against the Deseret Peak anticline. The Skull Valley thrust was postulated by Roberts and others (1965) on the basis of discordance of structure and stratigraphy between the Cedar and Stansbury Mountains.

The arcuate trend of the main asymmetrical, locally overturned Deseret anticline in the Deseret Peak block varies from northeasterly at the north end of the range, and generally northerly in the central part, to southeasterly at the south end. Adjacent folds, where present, parallel the Deseret anticline. This trend, concave to the east, contrasts with the general north trend of folds in the Timpie Valley block.

Several folds of the Timpie Valley block are exposed at the north and south ends of the range because of deep erosion in Timpie Valley and Vickory Canyon; in contrast, only the steep east limb of the easternmost fold is exposed in the higher, narrow central part of the block. The stratigraphic (fig. 3) and lithologic character of these rocks appears to be comparable with that of rocks in the Dolomite block, suggesting that closely related sedimentational units have been juxtaposed by the fault.

The Devonian strata exposed near Rock Springs in the southwest part of the Stansbury Mountains were tentatively divided by Rigby (1958) into the Sevy, Simonson(?), Stansbury, and lower part of the Pinyon Peak Formations. H. T. Morris (oral commun., 1968) believes that the strata identified as Sevy and Simonson actually correlate with beds in the middle part of the Bluebell Formation in the Tintic district to the south and should be reassigned to either the Bluebell Formation of Ordovician, Silurian, and Devonian age or to the Laketown Dolomite of Silurian age. The remaining upper beds resemble the clastic and fine-grained units in the Pinyon Peak Limestone. The coarser, lower beds

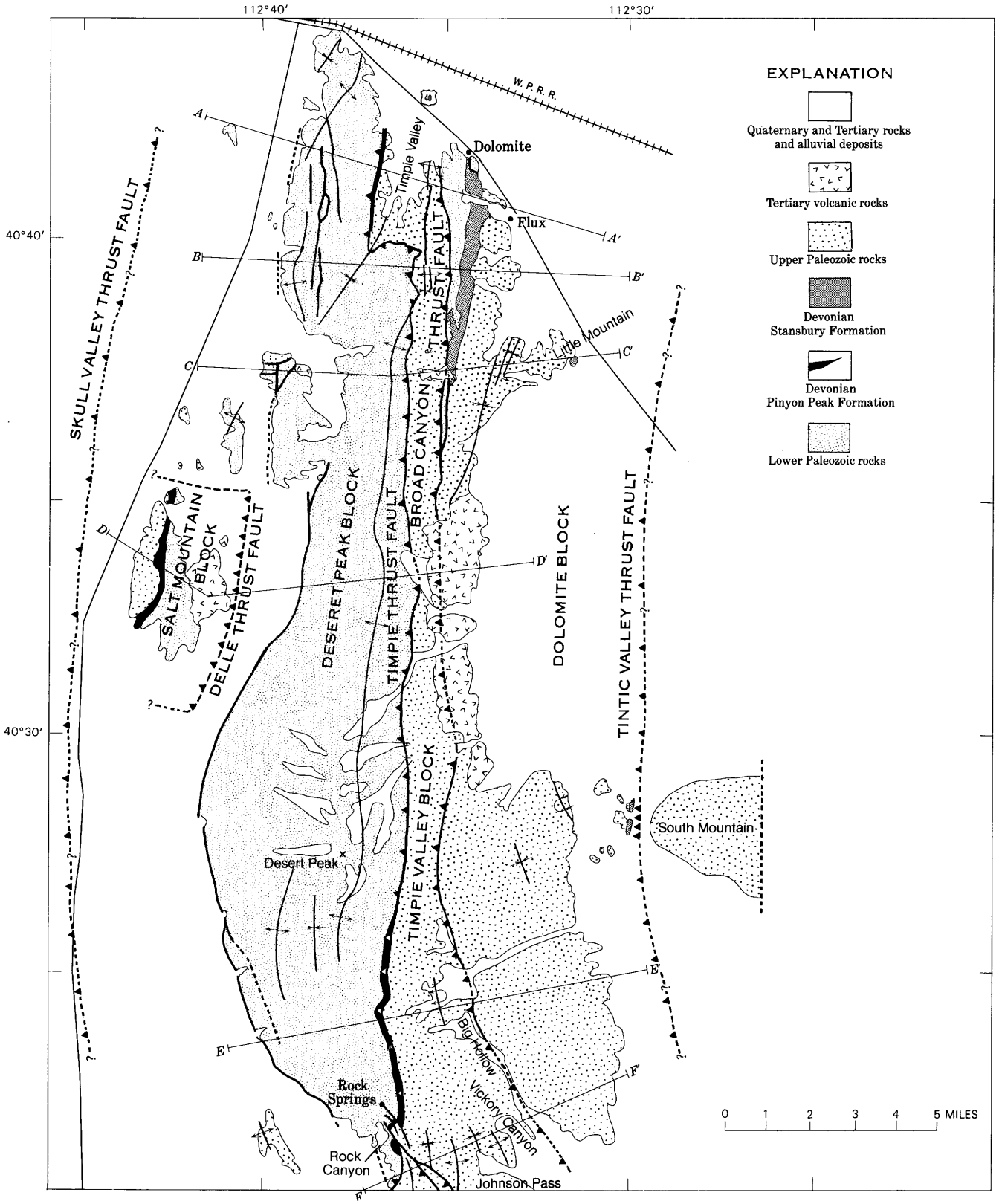
112°40′
112°30′
40°40′
40°30′
W. P. R. R.
40
Dolomite
Flux
Timpie Valley
Little Mountain
A
A′
B
B′
C
C′
D
D′
E
E′
F
F′
SKULL VALLEY THRUST FAULT
THRUST FAULT
BROAD CANYON
TIMPIE THRUST FAULT
DESERET PEAK BLOCK
DOLOMITE BLOCK
TINTIC VALLEY THRUST FAULT
SALT MOUNTAIN BLOCK
DELLE THRUST FAULT
TIMPIE VALLEY BLOCK
Desert Peak
South Mountain
Big Hollow
Vickory Canyon
Rock Springs
Rock Canyon
Johnson Pass
EXPLANATION
Quaternary and Tertiary rocks and alluvial deposits
Tertiary volcanic rocks
Upper Paleozoic rocks
Devonian Stansbury Formation
Devonian Pinyon Peak Formation
Lower Paleozoic rocks
0 1 2 3 4 5 MILES

FIGURE 4.

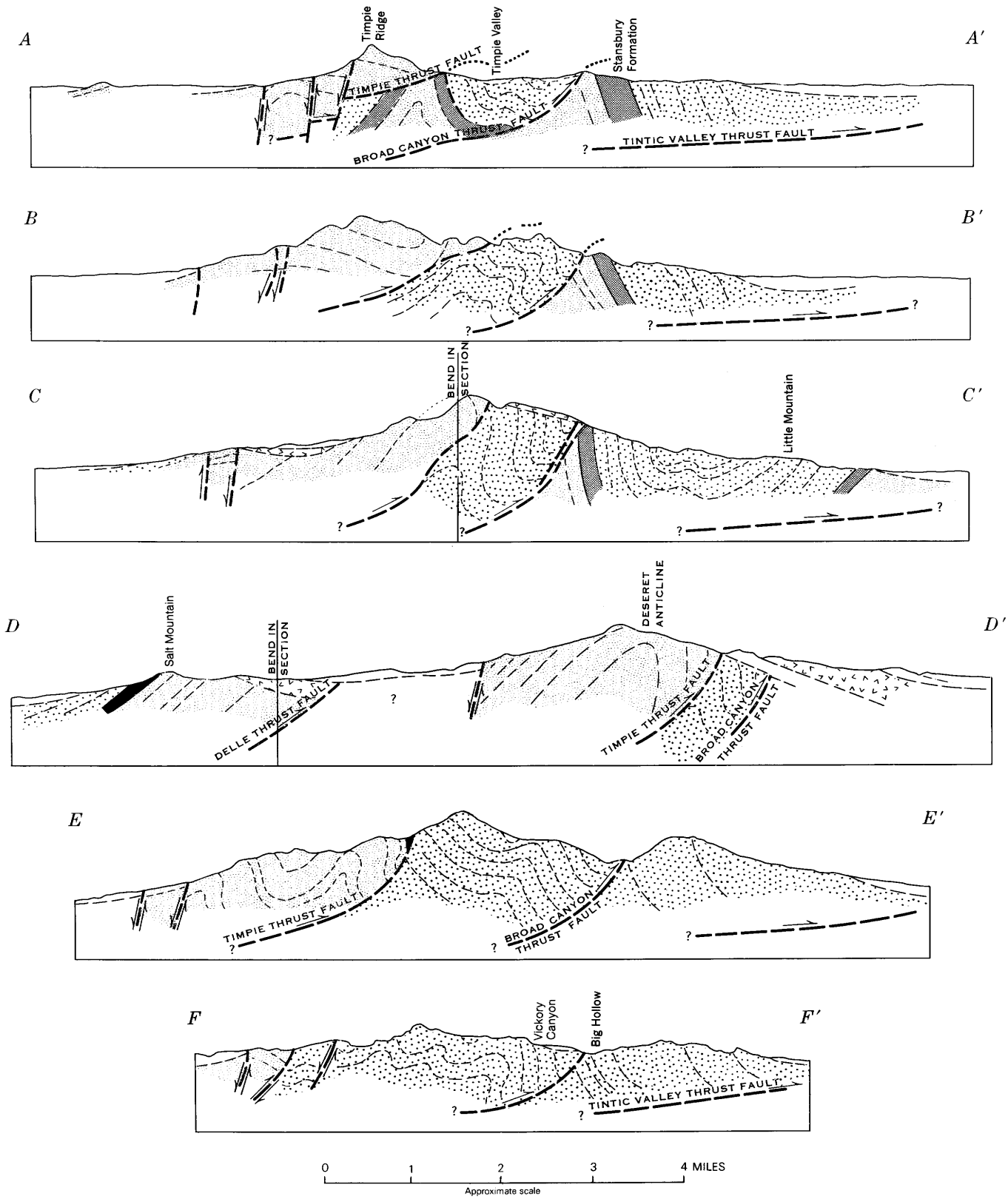

FIGURE 4.—Geologic sketch map and diagrammatic sections showing the thrust fault interpretation of the geology of the Stansbury Mountains, based on surface data of Rigby (1958). Listing of geologic units is given on figure 3.

may be considered Stansbury equivalents. The underlying Laketown Dolomite is much thicker in the Rock Springs area than in the Dolomite block (fig. 3), suggesting either that the Laketown was eroded more deeply in the Dolomite block or that original sedimentation was greater in the Deseret Peak block. Morris and Kopf (1969) have indicated in the West Tintic and Sheeprock Mountains south of this area that the Laketown thickens across the Sheeprock thrust. And Teichert (1959, p. 73) has recognized the Sheeprock thrust in the Onaqui Range as far north as Johnson Pass. If, as we believe, the Timpie thrust proves to be correlative with the Sheeprock thrust, a westward thickening of the normally deposited units also is expectable in the Stansbury Mountains. Another similarity between the Sheeprock and Stansbury Mountains is the presence of Cambrian strata on the upper plate, which have been thrust over middle and upper Paleozoic rocks.

Salt Mountain block

The Salt Mountain block is the upper plate of the Delle thrust, which separates Salt Mountain from the Deseret Peak block of the Stansbury Mountains. The block constitutes the east limb of a broad syncline that adjoins the overturned anticlinal structure of the Deseret Peak block. The Salt Mountain block is exposed only on Salt Mountain and thus areally is a much smaller unit than the Deseret Peak block, and may represent one of several broken discontinuous blocks that are poorly exposed along the west side of the Stansbury Mountains. The Timpie Valley syncline and Timpie Ridge anticline of Rigby (1958, p. 63, 64) that physically adjoin the Deseret anticline at the northwest end of the range do not seem to continue southward to the Salt Mountain block. These structures are believed to be overridden by the Delle thrust.

The beds in the Salt Mountain block assigned by Rigby to the Sevy and Simonson(?) Formations are considered here to be the upper part of the Laketown Dolomite. Thus the stratigraphic section here is comparable to that in the Deseret Peak block, although somewhat thicker (fig. 3). Thin Devonian sedimentary rocks, resembling both the Pinyon Peak and Stansbury Formations, are present in both the Deseret Peak and Salt Mountain blocks, again suggesting to us that the Delle thrust is of much lesser magnitude than the Timpie thrust. On Salt Mountain, Devonian rocks rest in erosional karstlike contact on Silurian Laketown Dolomite, suggesting that the Sevy and Simonson(?) Dolomites, if ever present in this block, were eroded along with some of the underlying Laketown Dolomite.

Geologic history

The structural evolution of the Stansbury Mountains can be explained only in terms of (1) accumulation of sediments in a basin an unknown distance west of the present site of the range and (2) folding and faulting during deformation that brought the rocks formed from these sediments to the present site. According to our concept, marine sediments gradually filled a broad shelf zone in western Utah and eastern Nevada beginning in the late Precambrian. During early Paleozoic time, deposition of carbonate, shale, and quartzose sediments apparently continued with only intermittent local interruption until the Late Devonian, when uplift commenced along the east-west Cortez-Uinta axis. On the basis of the thickness of the stratigraphic section, the magnitude of uplift along the Cortez-Uinta axis associated with the Stansbury uplift was at least 1,000 feet and probably more. Erosion of the Cambrian Tintic Quartzite locally formed the quartzite cobble and sand deposits of the Stansbury Formation. On other grounds, Rigby (1958, p. 87) has postulated as much as 7,000 feet of structural relief, a value considerably higher than would be required by the thrust-fault hypothesis. An asymmetry (highest on the north side) of this east-west uplift is suggested in the general distribution of the thicker deposits of coarser clastic debris on the northern side of the axis across Utah and Nevada (Roberts and Tooker, 1969). The clastic facies south of the arch appear to be largely sandy and dolomitic (Victoria quartzite facies) beds; beds containing small pebble-size clasts are local and thin. Normally, as in the Sheeprock Mountains, the clastic facies overlies the Laketown, Sevy, and Simonson succession, but in the Stansbury Mountains the clastic facies overlies a karst erosional surface on the Laketown Dolomite. The Pinyon Peak Limestone is present nearly everywhere, conformably overlying the clastic phase where present. We see no compelling evidence of folding associated with this deformation and therefore believe that the Pinyon Peak Limestone represents the end phase of the erosion cycle. We believe that in most of the Stansbury Mountains, the Silurian Laketown and Devonian Sevy and Simonson(?) deposits either may have been eroded during this uplift or were not deposited there. Following the Late Devonian, a thick sequence of Mississippian and Pennsylvanian strata was deposited over the entire basin.

During uplift accompanying the Sevier orogeny in Late Cretaceous time (Armstrong, 1968), large plates containing thick rock sequences became detached and moved eastward by gravity in the manner suggested by Rubey and Hubbert (1959). The eastward move-

ment stopped when these plates rode up against the craton, buckled, and became folded as they were stacked against each other. The Stansbury plates apparently represent basin deposits that lay west of rocks now seen on Mount Timpanogos in the Wasatch Mountains and in the Oquirrh Mountains. The plates were separated and subjected to differing forces. As they contained assemblages of rock having somewhat differing competency, the character of folding varied from block to block. In a general sense, the broad arching of folds, concave to the east, suggests that the thrusts were piled up athwart the Cortez-Uinta axis as it rose near the Wasatch Mountains, much as leaves floating in a stream are plastered against a rounded boulder. (In contrast, the broad arching of folds, convex to the east, on the upper plate of the Charleston-Nebo thrust in the Wasatch Mountains, results from their being thrust into the basin on the south flank of the Cortez-Uinta axis.) Well-defined differences in lithology and directions of apparent movement suggested by the folds in adjoining blocks suggest that the rocks exposed at the north end of the range in the Dolomite and Timpie Valley blocks may represent Devonian deposits more characteristic of those north of the axis, whereas rocks in the Deseret Peak and Salt Mountain blocks probably represent sedimentary features more characteristic of those south of this axis. We believe that the present location of the Salt Mountain section on line with the westward projection of the Cortez-Uinta axis presumably at the highest part of the axis, is inconsistent with the sedimentational character to be expected at such a site. The facies nearest the uplift ought to be either a thick clastic unit such as that we observed near Dolomite or an erosional hiatus as in the Oquirrh Mountains. However, the section at Salt Mountain differs little from that observed at Rock Springs at the south end of the Stansbury Mountains. All these observations support our hypothesis that the diverse assemblages of rocks seen in the Stansbury Mountains today can only have been deposited elsewhere and subsequently moved together.

Basin-and-range faulting and erosion have carved the present geomorphic form of the range. Tertiary intrusion and volcanic flows appear near the intersection of the Cortez-Uinta axis and the inferred traces of the thrust faults; we believe faults locally may have been feeder channels.

NATURE OF THE STANSBURY UPLIFT

Rigby (1958, p. 83–88) originally described the Stansbury uplift as primarily a Late Devonian feature that produced the conglomerate in the Stansbury Formation. He believed that the rock structures and the overlying Paleozoic sediments were subsequently deformed during the Laramide orogeny. As a result, the Cambrian rocks in the backbone of the range were folded, refolded, and uplifted twice along the structural pattern established in the Devonian. The Stansbury uplift in Rigby's terms is a composite of two events. Because we believe that the two episodes of deformation occurred in widely separated places, we are faced with the problem of deciding which of these events to name the Stansbury uplift.

We prefer to apply the name "Stansbury uplift" to Rigby's Late Devonian event and propose that Armstrong's name, "Sevier orogeny," be used for the Late Cretaceous thrusting and folding event. As a consequence of this episode of thrusting and folding, the lower Paleozoic rocks were brought to their present location at the crest of the range.

ECONOMIC POTENTIAL

Virtually all the metallic mineralization in the Stansbury Mountains is in the Timpie Valley block, generally close to the basal Broad Canyon thrust. Leakages of mineralized solutions along the Tintic Valley fault may be the source for the variscite deposits in the pass west of South Mountain. Volcanic rocks, intrusive dikes and plugs, and the hot springs at the north end of Timpie Valley also have close spatial relation to this Timpie Valley block and the thrust fault (Davis, 1959, p. 44). If the geologic structure of the Stansbury Mountains is primarily related to thrust faults, as proposed here, the metallic mineral potential of the range will be greatly enhanced. If the Broad Canyon fault is merely a high-angle reverse fault and is not related to underlying thrust surfaces, any exploration targets would be more or less confined to the vicinity of the fault below its outcrop. On the other hand, if the fault at depth is a thrust, a wider target area for hidden deposits would be offered in the hanging wall to the west, where favorable carbonate rocks might be expected. Any exploration for such deposits should of course be guided by well-planned geochemical and geophysical studies.

The Bingham and Tintic ore deposits (fig. 1) occur in a comparable structural and host-rock environment in the underlying Midas thrust plate. As very similar structural, stratigraphic, and hydrothermal features occur elsewhere in the Great Basin, these features may be useful as geologic tools in prospecting for ore deposits.

413-504 O - 71 - 2

REFERENCES

Armstrong, R. L., 1968, Sevier orogenic belt in Nevada and Utah: Geol. Soc. America Bull., v. 79, no. 4, p. 429–458.

Billingsley, P. R., and Locke, Augustus, 1939, Structure of ore districts in the continental framework: New York, Am. Inst. Mining Metall. Engineers, 51 p.

Butler, B. S., Loughlin, G. F., Heikes, V. C., and others, 1920, The ore deposits of Utah: U.S. Geol. Survey Prof. Paper 111, 672 p.

Davis, B. L., 1959, Petrology and petrography of the igneous rocks of the Stansbury Mountains, Tooele County, Utah: Brigham Young Univ. Research Studies Geology Ser., v. 6, no. 2, 56 p.

Gilluly, James, 1932, Geology and ore deposits of the Stockton and Fairfield quadrangles, Utah: U.S. Geol. Survey Prof. Paper 173, 171 p.

King, Clarence, 1878, Systematic geology: U.S. Geol. Explor. 40th Parallel (King), v. 1, 803 p.

Morris, H. T., and Kopf, R. W., 1969, Tintic Valley thrust and associated low-angle faults, central Utah [abs.]: Geol. Soc. America Programs for 1969, pt. 5, Rocky Mountain Sec., 22d Ann. Mtg., Salt Lake City, Utah, 1969, p. 55.

Morris, H. T., and Lovering, T. S., 1961, Stratigraphy of the East Tintic Mountains, Utah: U.S. Geol. Survey Prof. Paper 361, 145 p.

Palmer, D. E., 1969, Structure and stratigraphy of Stansbury Island, Tooele County, Utah [abs.]: Geol. Soc. America Programs for 1969, pt. 5, Rocky Mountain Sec., 22d Ann. Mtg., Salt Lake City, Utah, 1969, p. 62.

Rigby J. K., 1958, Geology of the Stansbury Mountains, eastern Tooele County, Utah, *in* Rigby, J. E., ed., Geology of the Stansbury Mountains, Tooele County, Utah: Utah Geol. Soc. Guidebook 13, p. 1–133.

——— 1959, Stratigraphy of the Southern Oquirrh Mountains, *in* Bissell, H. J., ed., Geology of the Southern Oquirrh Mountains and Fivemile Pass–Northern Boulter Mountain area, Tooele and Utah Counties, Utah: Utah Geol. Soc. Guidebook 14, p. 9–36.

Roberts, R. J., Crittenden, M. D., Jr., Tooker, E. W., Morris, H. T., Hose, R. K., and Cheney, T. M., 1965, Pennsylvanian and Permian basins in northwestern Utah, northeastern Nevada, and southcentral Idaho: Am. Assoc. Petroleum Geologists Bull., v. 49, no. 11, p. 1926–1956.

Roberts, R. J., and Tooker, E. W., 1961, Structural geology of the north end of the Oquirrh Mountains, Utah, *in* Cook, D. R., ed., Geology of the Bingham mining district and northern Oquirrh Mountains: Utah Geol. Soc. Guidebook 16, p. 36–48.

——— 1969, Age and regional significance of conglomerate in the Newfoundland and Silver Island Mountains, Utah [abs.]: Geol. Soc. America Programs for 1969, pt. 5, Rocky Mountain Sec., 22d Ann. Mtg., Salt Lake City, Utah, 1969, p. 69.

Rubey, W. W., and Hubbert, M. K., 1959, Role of fluid pressure in mechanics of overthrust faulting—II, Overthrust belt in geosynclinal area of western Wyoming in light of fluid-pressure hypothesis: Geol. Soc. America Bull., v. 70, no. 2, p. 167–206.

Stokes, W. L., and Arnold, D. E., 1958, Northern Stansbury Range and the Stansbury Formation, *in* Rigby, J. E., ed., Geology of the Stansbury Mountains, Tooele County, Utah: Utah Geol. Soc. Guidebook 13, p. 134–149.

Teichert, J. A., 1959, Geology of the southern Stansbury Range, Tooele County, Utah: Utah Geol. and Mineralog. Survey Bull. 65, 75 p.

DISPLACEMENT OF THE POCAHONTAS FORMATION BY THE RUSSELL FORK FAULT, SOUTHWEST VIRGINIA

By KENNETH J. ENGLUND, Washington, D.C.

Abstract.—Thickness and lithic variations in Upper Mississippian and Lower Pennsylvanian formations indicate approximately 4 miles of strike-slip movement along the Russell Fork fault. Economically important coal beds of the Pocahontas Formation, currently the objective of deep exploratory drilling, are displaced laterally by this movement.

Exploration for coal in the Pocahontas Formation in the subsurface of southwest Virginia has accelerated in recent years because of the increased demand for low-volatile and low-sulfur coal. The formation crops out principally in adjoining areas of southern West Virginia where the character and distribution of the Pocahontas coal beds have been disclosed by extensive exploration and mining. Previous geologic studies have generally overlooked the extension of the formation in the subsurface of southwest Virginia where equivalent strata have been included, undifferentiated, in the thicker and more widespread Lee Formation. However, recent deep drilling in the area has confirmed the presence of the Pocahontas coal beds and has resulted in the opening of several shaft mines. The areal distribution of the formation is controlled by various stratigraphic and structural features, including the Russell Fork fault at the northeast edge of the Cumberland overthrust sheet (fig. 1). The effect of this fault on the displacement of the Pocahontas Formation was determined by a stratigraphic study, which included the description of sections of core and drill-hole cuttings. Because much of the core data was obtained in confidence, only the locations of oil and gas tests are shown in figure 2. Several drill-hole descriptions were kindly furnished by the Virginia Division of Mineral Resources.

STRATIGRAPHIC UNITS

Strata displaced along the Russell Fork fault range from Devonian to Pennsylvanian in age. This study is primarily concerned with the Pocahontas Formation of Early Pennsylvanian age but also includes the Upper Mississippian and Lower Pennsylvanian units shown in figure 3.

The Pocahontas Formation underlies an area of approximately 3,500 square miles in parts of West Virginia, Virginia, and Kentucky. It is exposed only at the east edge of the Appalachian coal field, principally in a broad dissected area of relatively flat-lying beds in southern West Virginia. Southwestward in Virginia, the Pocahontas Formation and equivalent strata extend in a narrow belt of upturned beds to the southwest corner of the State. From a maximum thickness of about 700 feet in the central part of the outcrop area, the formation thins northwestward and wedges out in the subsurface. It consists of a typical coal-bearing sequence of sandstone, siltstone, shale, and underclay. Of these, light-gray, thin- to thick-bedded sandstone is most abundant. It commonly consists of 50–65 percent quartz, 4–11 percent feldspar, mica flakes, rock fragments, and a few heavy-mineral grains; in places it contains a few well-rounded white quartz pebbles. Well-sorted fine-grained quartzose sandstone occurs locally at the base of the formation. Shale and siltstone are medium to dark gray and are commonly carbonaceous. Coal, underlain by as much as a few feet of clayey or silty underclay, occurs in as many as 14 beds, of which 2 or 3 may be commercially important at a specific locality.

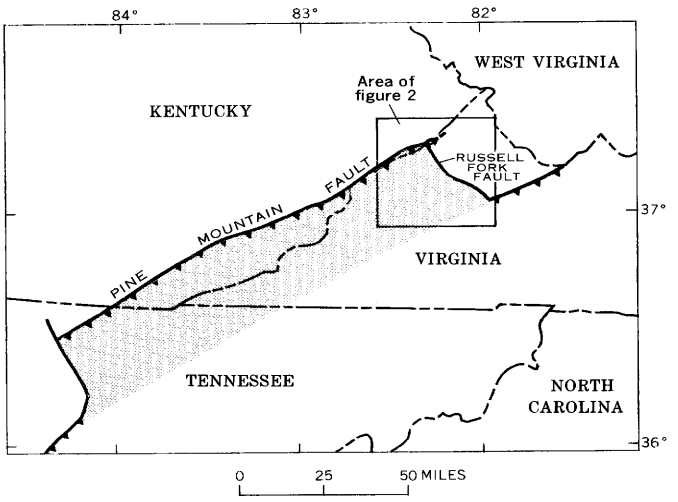

FIGURE 1.—Index map relating the area of figure 2 to the Cumberland overthrust sheet (stippled).

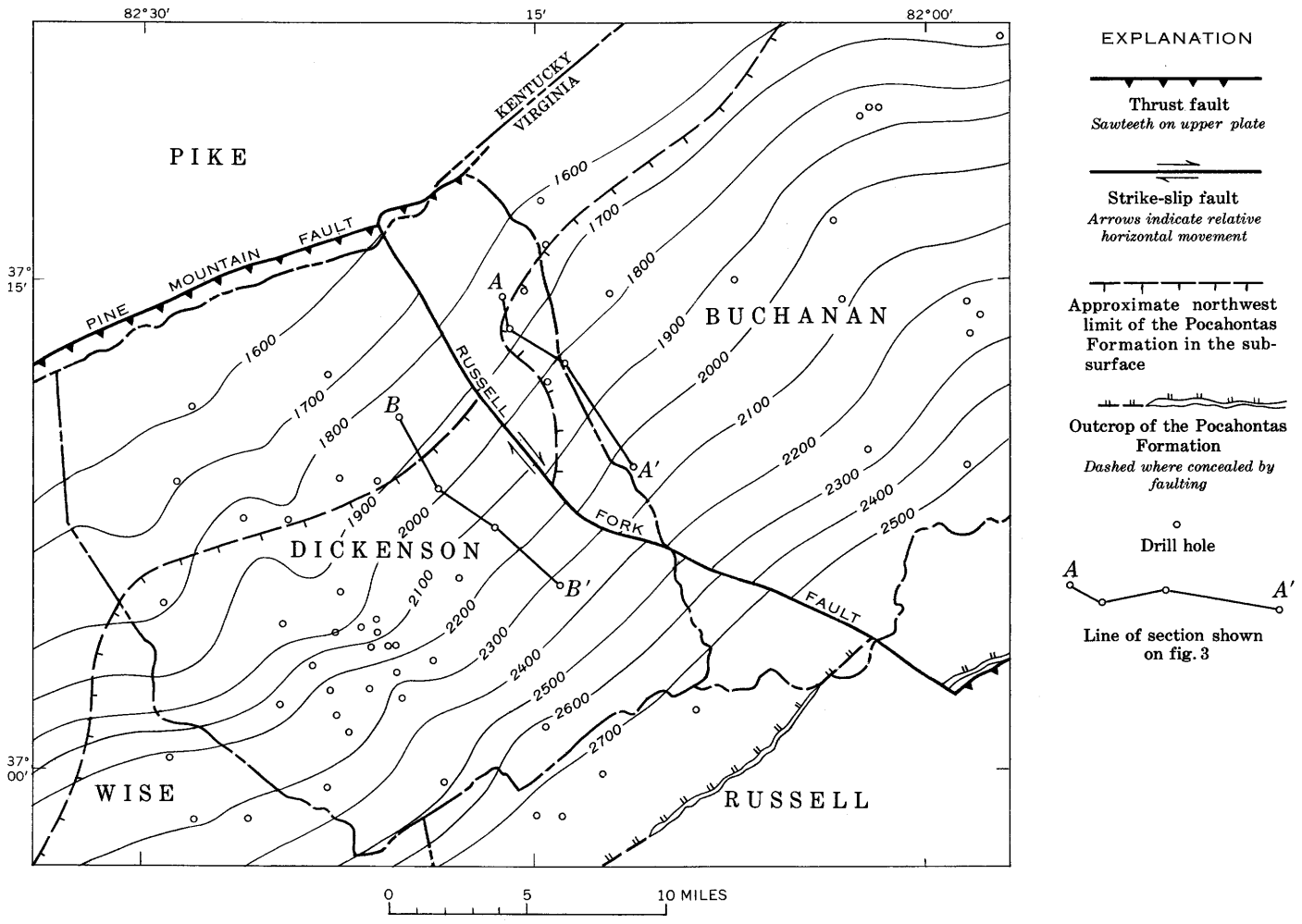

FIGURE 2.—Thickness map of rocks between the base of the Little Stone Gap Member of the Hinton Formation and the Jawbone coal bed, showing 4 miles of strike-slip movement along the Russell Fork fault.

The Pocahontas Formation was deposited in a transitional deltaic environment (Englund, 1969). Initial deposits consist of distributary sands that aggrade to the northwest and intertongue with prodeltaic varicolored shale of the underlying Bluestone Formation. Locally, the fringe of the delta is marked by well-sorted quartzose beach sand that forms lentils alined in a northeasterly direction at the base of the formation. Fluvial and swamp sediments were deposited in beds behind the delta front as the front advanced to the northwest.

Strata underlying the Pocahontas Formation are assigned to the Bluestone Formation of Late Mississippian to Early Pennsylvanian age. The upper part of the Bluestone Formation is characterized by greenish-gray, grayish-red, and gray slightly calcareous shale and siltstone. A few beds of very fine grained to fine-grained light-gray to light-greenish-gray sandstone are also present. The lower part of the formation is a persistent dark-gray shale which is correlated wth the Pride Shale Member of southern West Virginia. Also included in figure 3 are the uppermost beds of the Hinton Formation—the Tallery Sandstone Member, a locally quartzose and conglomeratic sandstone; and the Little Stone Gap Member, an argillaceous fossiliferous limestone.

The Pocahontas Formation is unconformably overlain by the Lee Formation, a widespread coal-bearing sequence of sandstone, siltstone, shale, and underclay. Regionally, the Lee is characterized by quartzose conglomeratic sandstone which occurs mostly in the basal and uppermost beds in the area of study. The unconformity at the base of the Lee truncates the Pocahontas Formation northwestward and marks a hiatus between the Mississippian and Pennsylvanian Systems where the Pocahontas and upper beds of the Bluestone are absent. Beds of sandstone, siltstone, shale, and coal in the lower part of the Norton Formation are also shown in figure 3.

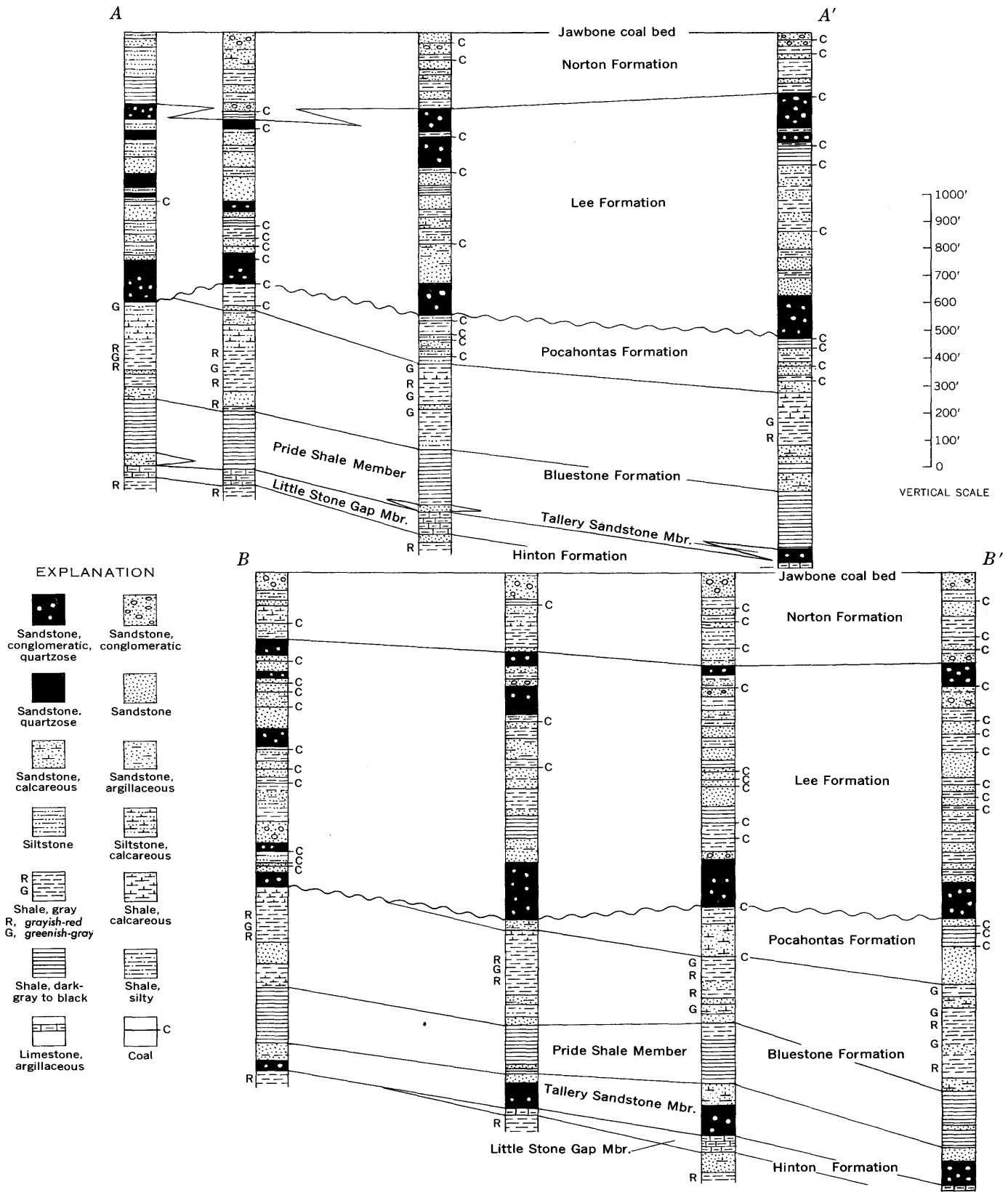

FIGURE 3.—Sections of Mississippian and Pennsylvanian units northeast (*A–A'*) and southwest (*B–B'*) of the Russell Fork fault, showing a similar but thicker sequence in the Cumberland overthrust sheet (*B–B'*). Location of sections shown in figure 2.

DISPLACEMENT OF THE RUSSELL FORK FAULT

The Russell Fork fault extends southeastward from the trace of the Pine Mountain fault for about 28 miles (fig. 2). Giles (1921, Wentworth (*in* Giles, 1921, p. 53–67; 1922), and Bates (1936) indicate that the movement of the Russell Fork fault is largely strike slip and occurs along a high-angle fault plane. They also noted a minor amount of thrusting and vertical displacement. The only determination of the amount of strike-slip movement is an unspecified estimate of about 2 miles by Wentworth (*in* Giles, 1921, p. 65). Movement of this magnitude is of particular importance in correlating beds and prospecting for coal, especially in the Pocahontas Formation where the beds wedge out to the northwest parallel to the direction of movement. To verify the amount of strike-slip movement involved, lateral changes in the physical characteristics of the rock were examined, particularly those that trend normal to the direction of movement. In contrast to the early estimate, the lateral changes observed indicate substantially greater movement than was previously estimated. For example, the amount of strike-slip movement can be demonstrated by the offset in thickness contours of strata between two readily identified beds, namely, the base of the Little Stone Gap Member of the Hinton Formation and the base of the Jawbone coal bed (fig. 3). As shown by the thickness map (fig. 2), these strata increase in thickness approximately 60 feet per mile to the southeast. Therefore, strike-slip movement to the northwest has placed a section of rocks in the overthrust sheet opposite a thinner counterpart across the Russell Fork fault. This difference in thickness indicates about 4 miles of movement.

Also indicative of the amount of strike-slip movement is the displacement of the Pocahontas Formation. Available thickness data show that it has been offset approximately 4 miles at the Russell Fork fault. This relation is not readily evident in a comparison of sections alined parallel to and within a few miles of the fault (fig. 3). Along the line of section A–A', the Pocahontas Formation actually extends farther to the north in the autochthonous plate because of a local change in the direction of the wedgeout from northwest to west near the fault. A similar change in direction, uninterrupted by faulting, is present along the edge of the formation near the Wise-Dickenson County line.

On the basis of available stratigraphic data, strike-slip movement measured along the Russell Fork fault is somewhat greater than previously estimated and is most likely on the order of 4 miles.

REFERENCES

Bates, R. L., 1936, The Big A Mountain area, Virginia: Virginia Geol. Survey Bull. 46–M, p. 167–204.

Englund, K. J., 1969, Relation of the Pocahontas Formation to the Mississippian-Pennsylvanian systemic boundary in southwestern Virginia and southern West Virginia [abs.]: Geol. Soc. America Abs. with Programs 1969, [v. 1] pt. 4, p. 21.

Giles, A. W., 1921, The geology and coal resources of Dickenson County, Virginia: Virginia Geol. Survey Bull. 21, 224 p.

———1922, The geology and coal resources of Russell County, Virginia: Virginia Geol. Survey Bull. 22, 179 p.

THE TWOWELLS SANDSTONE TONGUE OF THE DAKOTA SANDSTONE AND THE TRES HERMANOS SANDSTONE AS USED BY HERRICK (1900), WESTERN NEW MEXICO

By C. H. DANE,[1] E. R. LANDIS, and W. A. COBBAN,
Washington, D.C.; Denver, Colo.

Abstract.—The Twowells Sandstone Tongue of the Dakota Sandstone is an extensive unit that joins the undivided beds of the Dakota along a line trending northeast approximately through Window Rock, Ariz. It was deposited in a shallow-water marine shelf environment and over much of its extent contains a molluscan fauna having the same age as the Hartland Shale Member of the Greenhorn Limestone in southeastern Colorado and southwestern Kansas. The underlying Whitewater Arroyo Shale Tongue of the Mancos Shale is the same age as the Lincoln Limestone Member of the Greenhorn. Previous correlations of the Twowells with the Tres Hermanos Sandstone as named by Herrick (1900) have been in error; the Tres Hermanos at its type locality is a stratigraphically higher and younger sandstone of early Carlile age.

Since July 1966, we have been conducting a reconnaissance investigation of the Dakota Sandstone and the lower part of the Mancos Shale in west-central New Mexico and in adjacent areas (fig. 1). Stratigraphic sections were measured and molluscan faunas were collected at several levels. The work has in part been guided by and incorporates data from earlier reconnaissance studies dating back to 1954, some of the results of which have been previously reported (Dane and Bachman, 1957; Dane, 1959, 1960a, 1960b). A short paper by Marvin (1967) noted that these earlier reports and a paper by Owen (1966; see also Owen, 1963) disagree on several points. Marvin also pointed out, on the basis of subsurface correlation across the southern part of the San Juan Basin, that the three sandstones—numbers 1, 2, and 3 of Hunt (1936)—in the lower part of the Mancos Shale of the Mount Taylor region merge into the undivided Dakota Sandstone westward, the uppermost (number 3) becoming practically inseparable from the Dakota Sandstone at the Defiance monocline a short distance east of Window Rock, Ariz. We agree with these conclusions except for some details. The same general conclusions were also reached in a subsurface study by Tyrrell in 1959. Marvin's paper proposes in

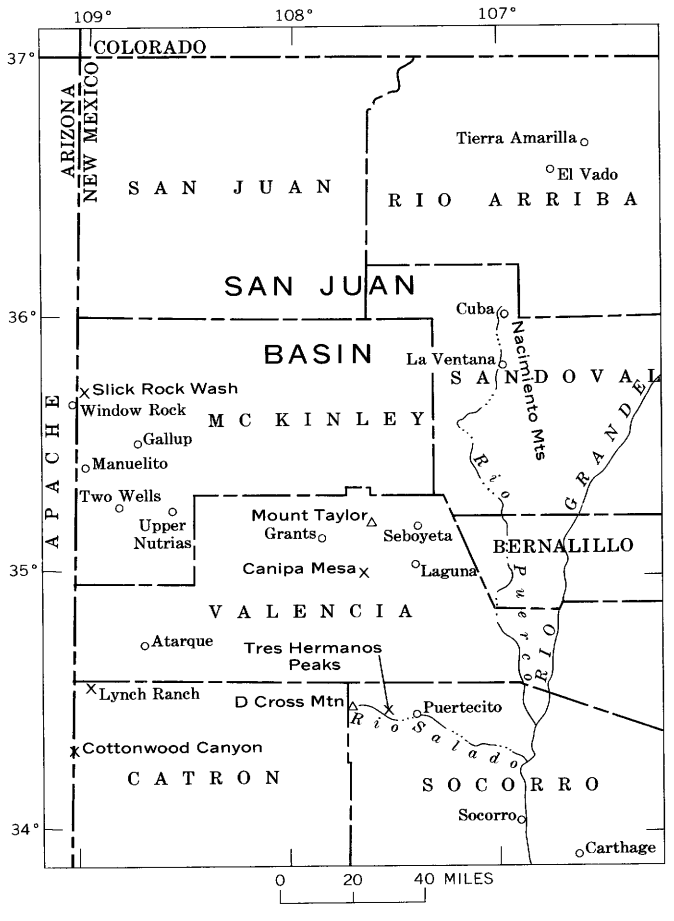

FIGURE 1.—Index map of west-central New Mexico and adjacent area, showing localities mentioned in text.

[1] Deceased June 24, 1968.

conclusion that "the member of the Dakota Sandstone overlying the Whitewater Arroyo Shale Member (Owen, 1966) be named the Twowells Member of the Dakota Sandstone." In the present paper we classify (1) the Twowells as a tongue of the Dakota rather than a member, and (2) the Whitewater Arroyo as a tongue of the Mancos Shale rather than a member of the Dakota. Data are now available to clear up some of the discrepancies in the previous literature, and it seems desirable to do so here.

TWOWELLS SANDSTONE AND WHITEWATER ARROYO SHALE TONGUES

The Twowells Sandstone Tongue, originally called a "sandstone lentil of the Mancos" by Pike (1947, p. 36), was named from "typical exposures near Two Wells in T. 12 N., R. 19 W." (Pike, 1947, p. 36). At the same locality, Owen (1966) measured the type section of his Whitewater Arroyo Shale Member of the Dakota Sandstone, which separated the Twowells from the thicker main ledges of the underlying Dakota Sandstone. We change his designation to Whitewater Arroyo Shale Tongue of the Mancos Shale, which more correctly describes its regional stratigraphic relationships. We measured the following section at that locality, mainly in the NE¼ sec. 17, T. 12 N., R. 19 W.:

	Thickness Feet	Thickness Inches
Mancos Shale (top of exposure):		
Shale, medium- to dark-gray, slightly calcareous, soft, flaky; contains yellow-weathering, rounded, discoidal, light-gray limestone concretions as much as 4 in. thick and 2 ft in diameter, about 5 ft above base. Both shale and limestone concretions contain *Exogyra levis* Stephenson and a broad thick-shelled form of the pelecypod described by Stanton (1893) as *Gryphaea newberryi* (USGS D7352)	7+	------
Twowells Sandstone Tongue of the Dakota Sandstone:		
Sandstone, very silty in part, very light gray, weathering to yellowish gray, mostly very fine grained, massive, soft; forms dip slope on back of cuesta ridge; uppermost few feet intensively burrowed; contains brown-weathering calcareous, concretionary, resistant parts 2 to 3 ft thick and 3 to 8 ft long. A clam (*Pholadomya* sp.; USGS D7350) was collected near base and an ammonite ("*Mantelliceras*" sp.) and an inoceramid (*Inoceramus* sp.; USGS D7351) from 15 ft above base. Thickness approximate because uppermost part is poorly exposed nearly everywhere	20±	------
Sandstone, light-gray, weathering to yellowish gray, fine-grained to very fine grained, massive, burrowed; resistant ledge-former	15	0
Twowells Sandstone Tongue of the Dakota Sandstone—Continued		
Sandstone, white, soft, massive, very fine grained; crossbedded in basal part	4	6
Siltstone, clayey and very sandy, and sandstone, very silty, weathers mostly dark yellowish brown, very fine grained, massive, soft; grades to overlying and underlying units	16	0
Sandstone, silty, light-gray, weathering to yellowish gray, very fine grained; mostly quartz but about 10 percent dark grains of other minerals and rocks; calcareous cement makes unit a weak ledge-former; massive to platy; thickness varies along outcrop	0	6
Total Twowells Sandstone Tongue	56	0
Whitewater Arroyo Shale Tongue of the Mancos Shale:		
Shale, silty in upper part, medium-dark-gray to olive-gray, slightly calcareous in part; USGS Mesozoic loc. D6155, *Exogyra* n. sp. from sparse, small limestone concretions at base	12	6
Bentonite	0	1
Shale, medium-dark-gray; brownish rounded limestone concretions scattered throughout; USGS Mesozoic loc. D7348 from 2 ft above base, "*Mantelliceras*" sp	8	6
Bentonite	0	1
Shale, medium-gray	10	0
Bentonite	0	2+
Shale, medium-gray	10	6
Bentonite		Streak
Shale, medium-gray	0	9
Bentonite	0	1
Shale, medium-gray	3	8
Total Whitewater Arroyo Shale Tongue	46	4
Dakota Sandstone (main body):		
Sandstone, pale-brown, calcareous, hard; USGS Mesozoic loc. D6154, *Acanthocardia tritis* (White) and *Exogyra levis* Stephenson	0	3
Sandstone, fine-grained, even-bedded; forms small ledge	1	8
Shale, carbonaceous, and interlaminated siltstone	7	0
Remainder of Dakota Sandstone not described here; slight channeled irregularity at base	114	6
Total Dakota Sandstone (main body)	123	5
Zuni Sandstone.		

The Twowells and Whitewater Arroyo thin northward; north of Manuelito the Twowells is only 20 feet thick, and the underlying Whitewater Arroyo seems to be represented by a concealed interval only 15 feet thick. We believe that the Twowells, which was measured as 28 feet thick by us, is the top ledge of the undivided Dakota at Window Rock. This ledge is overlain by a bed of gray shale and coaly shale 4 feet thick that is

succeeded by 14 feet of sandstone crowded with a broad thick-shelled form of the pelecypod described by Stanton (1893, p. 60, pl. 5, figs. 1–5) as *Gryphaea newberryi*. This sandstone bed, which we informally call the *Gryphaea* sandstone bed, was also recognized at Window Rock by Pike and by Owen. A similar section is exposed on the north side of Slick Rock Wash about 3 miles north of Window Rock, where 12 feet of the *Gryphaea* sandstone bed overlies 20 feet of interbedded shale, carbonaceous shale, coal, and bentonite above the main ledges of the Dakota. The *Gryphaea* bed seems not to be present at Manuelito, but the same fauna is present in the lower part of the shale overlying the Twowells Sandstone Tongue, as at the Twowells type locality. The *Gryphaea* sandstone bed was observed northeast of Gallup by Sears (1934) and a few miles north of there by Dane and Bachman (1957). As Pike (1947, p. 32) reported in his measured section 32 (near Window Rock),

> large numbers of *Gryphaea newberryi* were found in a thin sandstone 20 feet above the base of the Mancos. In the section near Gallup, Sears found the same faunal horizon in a 10-foot sandstone separated by 6 feet of shale from an underlying massive buff sandstone 25 feet thick. This sandstone in turn is separated from the highest sandstone of the Dakota(?) by 109 feet of marine shale. This 25-foot sandstone may be a tongue of Dakota(?) (Tres Hermanos, or possibly younger), and the 109 feet of marine shale may pinch out westward before reaching Section no. 32 where the overlying 25-foot sandstone or its equivalent would be considered the highest unit of the Dakota(?).

This is, except for the parenthetical clause, precisely our interpretation, but with the further conclusion that the 25-foot sandstone is also the Twowells, and the 109 feet of marine shale below it is the Whitewater Arroyo Shale Tongue. Although Dane (1960b) and Owen (1966, fig. 3) previously extended the Twowells north of Slick Rock Wash, it should probably not be extended north of Window Rock.

The *Gryphaea* sandstone bed also crops out, intermittently because of poor exposures, at least as far south as Upper Nutrias. Although the underlying Twowells seems to be unusually soft, silty, and thin bedded in this area, it presumably continues far to the south, because it is present northeast of Atarque in T. 7 N., R. 17 W. Farther south, exposures are few and widely separated, but the Twowells is present in the Lynch Ranch area, T. 4 N., R. 20 W. (see also Owen, 1963, pl. 1), and in the Cottonwood Canyon (Cienega Amarilla) area, T. 10 N., R. 31 E., Apache County, Ariz., and T. 1 N., R. 21 W., Catron County, N. Mex., where it was regarded by Young (1957) as the basal unit of the Mesaverde Formation.

The Twowells and the underlying Whitewater Arroyo crop out almost continuously eastward from Gallup to the Rio Puerco, but eastward from a point about 15 to 20 miles northwest of Grants the Whitewater Arroyo overlies the next lower sandstone tongue of the Dakota instead of overlying the main body of the Dakota. The tongues of the Dakota have been extensively mapped as parts of units in the lower part of the Mancos Shale by Thaden and his associates (Thaden and others, 1967; and other geologic quadrangle maps) in the Grants area and by Moench and Schlee (1967, p. 3, 23) and others in the Laguna area to the east. In both of these areas the uppermost mapped sandstone is the Twowells Sandstone Tongue.

TRES HERMANOS SANDSTONE AS USED BY HERRICK (1900)

Our studies show that the Twowells Sandstone Tongue is the "Tres Hermanos sandstone" as distinguished by Pike (1947, p. 65) at D Cross Mountain and as mapped by Givens (1957) east of D Cross Mountain and by Tonking (1957) in the Puertecito quadrangle; they also show that it is the only one of the three sandstones called Tres Hermanos of the Mount Taylor area present above the main part of the Dakota along Rio Salado northwest of Socorro. Dane (1959) was in error in correlating this sandstone (20 to 60 feet thick and lying about 250 feet above the thin basal Dakota Sandstone from D Cross Mountain east as far as the easternmost exposures of the Dakota and Mancos along Rio Salado) with the No. 2 sandstone of Hunt (1936) of the Rio Puerco valley east of Mount Taylor. The No. 2 sandstone of the Puerco Valley wedges out spectacularly on the west side of Canipa Mesa (see fig. 8, road logs, in report by Dane, 1959, where it is called No. 3 sandstone); however, the No. 3 sandstone of Hunt (1936) (Twowells of this report) caps Canipa Mesa and continues on to the south to be the unit that has been generally regarded as the Tres Hermanos Sandstone Member of the La Cruz Peak Formation and has been so mapped along Rio Salado (Tonking, 1957; Givens, 1957). We believe that the sandstone to which Herrick (1900, p. 341) originally applied the name Tres Hermanos is a sandstone that is 150 to 200 feet stratigraphically above the sandstone identified as "Tres Hermanos" (correctly Twowells) of the Rio Salado valley. This higher sandstone crops out about 1 mile east of Tres Hermanos Buttes (Peaks), where it was mapped by Givens (1957) as the basal member of the La Cruz Peak Formation of Tonking (1957), and where it is a "band of sandstone with enormous concretions" as required by Herrick's (1900) description. Some of the concretions are as much as 6 feet thick and 12 feet across,

whereas the Twowells Sandstone Tongue in this area has no concretions that large.

Pike (1947, footnote p. 32) correctly identified the type locality of the Tres Hermanos as "probably a mile east of Tres Hermanos Buttes, three volcanic necks in Alamosa Creek [now Rio Salado] valley, in sec. 26, T. 3 N., R. 7 W.," but later workers and Pike himself seem to have failed to correctly interpret the significance of this footnote as a guide to identifying the Tres Hermanos. The name Tres Hermanos should now be restricted to this higher sandstone, which contains a molluscan fauna of early Carlile age (*Collignoniceras woollgari* zone) as collected by us in the NE¼ sec. 25, T. 3 N., R. 7 W.

EXPOSURES ON EAST SIDE OF SAN JUAN BASIN

North and east of Rio Puerco (fig. 1), west of the Nacimiento Mountains, there is a drastic change in the thickness and stratigraphic position of the Twowells Sandstone Tongue and, to some degree, in its lithologic character. Although exposures are in part poor and in places widely separated, they do permit recognition of a continuous sandstone unit that extends throughout this area. Both the Twowells and the underlying Whitewater Arroyo thin markedly northeast from Rio Puerco. The Twowells, however, does not merge with the underlying Dakota as shown by Owen (1966, fig. 2), but continues northeastward and northward above the northeastern ends of the underlying sandstone tongues. The top of the Twowells on the eastern edge of the basin lies about 60 to 100 feet below the base of the Greenhorn Limestone Member of the Mancos Shale as it has generally been recognized in this area, and 95 to 150 feet above the top of the main body of the Dakota Sandstone. The Twowells is 10 to 20 feet thick, glauconitic and coarsely granular in some beds, and carries a characteristic ammonite fauna to be mentioned later. Although the northernmost section of the Twowells observed and measured by us is about 5 miles northeast of La Ventana, the unit may be present farther north along the steeply dipping foothills belt west of the Nacimiento Mountains. Speculatively, it may be represented in the well-exposed section along the west abutment of El Vado Dam in the northeastern part of the San Juan Basin by a zone (about 2 feet thick and about 55 to 60 feet below the base of the Greenhorn) in which there are several very thin siltstone beds. This zone lies about 75 feet above the top of the Dakota as mapped in the Tierra Amarilla quadrangle (Landis and Dane, 1967).

PALEONTOLOGY

The Twowells Sandstone Tongue in the area east from the type section to Rio Puerco contains a sparse fauna in both numbers of species and individuals, except for the uppermost part in which there locally are exceedingly numerous specimens of a broad thick-shelled form of Stanton's *Gryphaea newberryi* and smaller numbers of exogyras. These species range through a considerable interval downward from the top of the Twowells, as pointed out by Young (1960, p. 186). Otherwise, the fauna of the Twowells consists of the following:

"Mantelliceras" sp.
Metoicoceras defordi Young
Acanthocardia tritis (White)
Inoceramus sp.
Lopha sp. (large)
Pholadomya sp.
Pinna sp.
Cerithiopsis sp.

This fauna is the same age as the higher part of the Hartland Shale Member of the Greenhorn Limestone in southwestern Kansas and southeastern Colorado (middle Greenhorn). The assemblage is that of a shallow-water marine shelf environment (Kauffman, 1967, p. 119), which accords with the physical character and regional stratigraphic relations of the Twowells Sandstone Tongue.

The age of the top of the Twowells over much of its extent is more sharply defined by its relationship to a higher faunal zone in which a small baculitid, *Sciponoceras gracile* (Shumard), is present, though sparsely, nearly everywhere. Our collecting thus far indicates that this species is restricted to a zone no more than a few feet thick. At or very near the base of this zone is the lowest occurrence of Stanton's *Gryphaea newberryi* sensu strictu, a narrower and more convex form than the form present in the Twowells and underlying beds. The zone characterized by *Sciponoceras gracile* (Shumard) is of early Bridge Creek age. It lies as much as 50 feet above the top of the Twowells south of Gallup along the Nutria monocline, about 25 to 30 feet above the top of the *Gryphaea* sandstone bed (broad form) in the Four Corners area, from 50 to 60 feet above the top of the Twowells east of Rio Puerco, and from 15 to 20 feet above the top of the Twowells in the Rio Salado area.

The Whitewater Arroyo Shale Tongue is commonly characterized by much the same fauna as is present in the Twowells, but in some areas it also contains in its lower part distinctive but as yet undescribed exogyras

and a distinctive form of the pelecypod *Gryphaea newberryi* described by Stanton (1893). A large ammonite described by Haas (1949, p. 9, pls. 1–3; pl. 4; figs. 1, 2, 4) as *Mantelliceras canitaurinum* seems to characterize the Whitewater Arroyo in most areas, and a fragment of an ammonite found in the Twowells at its type section could be this species.

Southward from Atarque, the Twowells rises slightly stratigraphically; in the SW¼ sec. 15, T. 4 N., R. 20 W., Catron County, N. Mex., the top of it is only 3 feet below the level of a collection including *Kanabiceras* sp., a species indicating the *Sciponoceras gracile* zone. Fifteen miles farther south, in sec. 3, T. 10 N., R. 31 E., Apache County, Ariz., ammonites are present in some abundance in the upper 25 feet of the Twowells Sandstone Tongue, which is here about 90 feet thick. Collections from these beds were previously described by Keith Young (1957).

CONCLUSIONS

The Twowells Sandstone Tongue of the Dakota Sandstone is a very extensive offshore marine shelf sandstone that joins the main body of the Dakota near the Arizona–New Mexico State line in the vicinity of Window Rock, Ariz. From this point it extends southeastward for about 140 miles and has a maximum width at right angles to this axis of about 200 miles.

We concur with Owen's (1966, p. 1025) and Marvin's (1967, p. 172) proposal that the top of the Dakota be placed at the top of the Twowells, but we believe that the Twowells must be classified as a tongue of the Dakota rather than as a member of it. Marvin (1967, p. 172) notes that including the Twowells as part of the Dakota would permit "the contact to be consistently drawn across the southern San Juan Basin." This is true but does not hold farther afield geographically where the Twowells is absent or so thin as to be unrecognizable, and where the top of the Dakota must be placed at lower levels. Our definition of Twowells does not include the unit informally called by us the *Gryphaea* sandstone bed where this unit is separated from the Twowells by a marine or marginal marine shale unit on the western and northwestern side of the San Juan Basin. However, in other areas, sandy and silty beds containing the broad form of *Gryphaea* are indivisible from the underlying Twowells or from the underlying main part of the Dakota Sandstone where the Twowells is no longer recognizable.

Although its areal distribution suggests a source to the northwest like that of the lower tongues of the Dakota, the Twowells appears to rise stratigraphically toward the southwest from a level of Hartland age to a level probably just below that of the age of the Bridge Creek Limestone Member of Kansas. This stratigraphic rise and the thickening of the sandstone toward the southwest probably indicate a developing source to the southwest like that of the younger Cretaceous sandstones of the San Juan Basin. A southerly source for the Twowells has also been suggested by Owen (1963, p. 221) on the basis of metamorphic-type heavy minerals found in it.

The Tres Hermanos Sandstone as originally named by Herrick (1900, p. 341) is a stratigraphically higher sandstone than the Twowells and is of early Carlile age. It crops out extensively in the Rio Salado Valley, is present in the Carthage coal field, and probably also is present northeast of Socorro. It is represented in northwestern New Mexico and southwestern Colorado by a unit consisting of alternating silty shale and hard platy greenish-gray siltstone beds near the base of the beds of Carlile age. These beds characteristically contain impressions of *Collignoniceras woollgari* (Mantell), almost invariably small juvenile forms.

REFERENCES

Dane, C. H., 1959, Historical background of the type locality of the Tres Hermanos sandstone member of the Mancos shale *in* New Mexico Geol. Soc. Guidebook of west-central New Mexico, 10th Field Conf., 1959: p. 85–91.

——— 1960a, The boundary between rocks of Carlile and Niobrara age in San Juan Basin, New Mexico and Colorado: Am. Jour. Sci., v. 258A (Bradley volume), p. 46–56.

——— 1960b, The Dakota sandstone and Mancos shale of the eastern side of San Juan Basin, New Mexico *in* New Mexico Geol. Soc. Guidebook 11th Field Conf., Rio Chama Country, 1960: p. 63–74.

Dane, C. H., and Bachman, G. O., 1957, The Dakota sandstone and Mancos shale in the Gallup area [N. Mex.] *in* Four Corners Geol. Soc. Guidebook 2d Field Conf., Geology of southwestern San Juan Basin, 1957: p. 95–98.

Givens, D. B., 1957, Geology of Dog Springs quadrangle, New Mexico: New Mexico Bur. Mines and Mineral Resources Bull. 58, 40 p., geol. map.

Haas, Otto, 1949, Acanthoceratid Ammonoidea from near Greybull, Wyoming: Am. Mus. Nat. History Bull., v. 93, art. 1, 39 p., 15 pls.

Herrick, C. L., 1900, Report of a geological reconnaissance in western Socorro and Valencia Counties, New Mexico: Am. Geologist, v. 25, no. 6, p. 331–346.

Hunt, C. B., 1936, The Mount Taylor coal field, pt. 2 *of* Geology and fuel resources of the southern part of the San Juan Basin, New Mexico: U.S. Geol. Survey Bull. 860–B, p. 31–80.

Kauffman, E. G., 1967, Coloradoan macroinvertebrate assemblages, central Western Interior, United States, p. 67–143 *in* Paleoenvironments of the Cretaceous Seaway in the Western Interior—A symposium: Colorado School Mines Dept. Pubs., 266 p.

Landis, E. R., and Dane, C. H., 1967, Geologic map of the Tierra Amarilla quadrangle, Rio Arriba County, New Mexico (with description): New Mexico Bur. Mines and Mineral Resources Geol. Map 19.

Marvin, R. G., 1967, Dakota Sandstone—Tres Hermanos relationship, southern San Juan Basin area *in* Guidebook of Defiance-Zuni-Mt. Taylor region, Arizona and New Mexico—New Mexico Geol. Soc. 18th Field Conf., 1967: New Mexico Bur. Mines and Mineral Resources, p. 170–172.

Moench, R. H., and Schlee, J. S., 1967, Geology and uranium deposits of the Laguna district, New Mexico: U.S. Geol. Survey Prof. Paper 519, 117 p.

Owen, D. E., 1963, The (Cretaceous) Dakota Formation of the San Juan Basin, New Mexico and Colorado: Kansas Univ. Ph. D. dissert., 388 p., illus., incl. geol. map; [abs.], Dissert. Abs., v. 24, no. 12, pt. 1, p. 5336–5337, 1964.

———1966, Nomenclature of Dakota Sandstone (Cretaceous) in San Juan basin, New Mexico and Colorado: Am. Assoc. Petroleum Geologists Bull., v. 50, no. 5, p. 1023–1028.

Pike, W. S., Jr., 1947, Intertonguing marine and nonmarine Upper Cretaceous deposits of New Mexico, Arizona, and southwestern Colorado: Geol. Soc. America Mem. 24, 103 p.

Sears, J. D., 1934, The coal field from Gallup eastward toward Mount Taylor, with a measured section of pre-Dakota(?) rocks near Navajo Church, by J. D. Sears, pt. 1 *of* Geology and fuel resources of the southern part of the San Juan Basin, New Mexico: U.S. Geol. Survey Bull. 860–A, p. 1–29 [1935].

Stanton, T. W., 1893, The Colorado formation and its invertebrate fauna: U.S. Geol. Survey Bull. 106, 288 p., 45 pls.

Thaden, R. E., Santos, E. S., and Ostling, E. J., 1967, Geologic map of the Dos Lomas quadrangle, Valencia and McKinley Counties, New Mexico: U.S. Geol. Survey Geol. Quad. Map GQ–680.

Tonking, W. H., 1957, Geology of Puertecito quadrangle, Socorro County, New Mexico: New Mexico Bur. Mines and Mineral Resources Bull. 41, 67 p., illus., incl. geol. map.

Tyrrell, W. W., Jr., 1959, Dakota stratigraphy in the San Juan Basin area [Colo.–N. Mex.] *in* Am. Assoc. Petroleum Geologists Rocky Mtn. Sec. Geological record, 1959: Denver, Petroleum Inf., p. 43–54.

Young, Keith, 1957, Cretaceous ammonites from eastern Apache County, Arizona: Jour. Paleontology, v. 31, no. 6, p. 1167–1174.

Young, R. G., 1960, Dakota group of Colorado Plateau: Am. Assoc. Petroleum Geologists Bull., v. 44, no. 2, p. 156–194; discussions by several authors, v. 45, no. 9, p. 1582–1590, 1961.

LISBURNE GROUP, CAPE LEWIS–NIAK CREEK, NORTHWESTERN ALASKA

By A. K. ARMSTRONG, B. L. MAMET,[1] and J. THOMAS DUTRO, Jr.,
Menlo Park, Calif., Montreal, Canada, Washington, D.C.

Abstract.—Sections of Lisburne Group, Carboniferous (Mississipian), were measured in structurally complex terrane on rootless allochthonous thrust sheets. Exposures at Cape Lewis exceed 3,100 stratigraphic feet and consist of 1,284 feet of Viséan (lower Chester) shales and carbonates of the Nasorak Formation and 1,864 feet of "Namurian" (middle and upper Chester) carbonates of the Kogruk Formation. An incomplete 215-foot-thick section of the Nasorak Formation at Niak Creek is uppermost Meramec, lowermost Chester equivalent. On an underlying thrust sheet at Niak Creek, an incomplete section of the Kogruk Formation is 715 feet thick and is a Meramec age equivalent. Within these sections six foraminiferal assemblage zones are recognized and tied to the Cordilleran and Eurasian standards. A fauna of 14 taxa of lithostrotionoid carols is also present in the beds of Meramec and earliest Chester age. Corals are rare in beds younger than earliest Chester.

In 1968 Dutro and Armstrong measured and collected samples from five sections of the Lisburne Group on sea cliffs adjacent to the Arctic Ocean in northwestern Alaska (figs. 1 and 2). Carbonate classification used is Dunham's (1962). All the exposures studied are on rootless thrust sheets. The sea cliffs afford excellent exposures of these rocks, whereas inland, on the rubble-covered slopes of the Lisburne Hills, the Lisburne Group is very poorly exposed.

The 3,100-foot-thick composite section at Cape Lewis is formed by three measured sections, 68A–9, 68A–10, and 68A–11. These sections are believed to be one thrust sheet and make up a nearly complete representation of the Lisburne Group. The Cape Lewis section is truncated at its base by structurally complex terrane and tundra cover; the top of the section is tundra cover and a possible thrust fault surface (figs. 3, 4).

The two sections near Niak Creek are incomplete partial sections of the Lisburne Group. Section 68A–12, north of Niak Creek, is 715 feet thick. The base of the section is above a thick tectonic breccia zone and the top is a thrust fault surface (fig. 5*A*). Section 68A–13, south of Niak Creek, is 215 feet thick and is bounded by faults (fig. 5).

A foraminiferal zonation for the Lisburne Group in the central and eastern Brooks Range was established by Armstrong, Mamet, and Dutro (1970). The geographic and biostratigraphic relations of the measured sections on the sea cliffs of northwestern Alaska to the

[1] Université de Montréal.

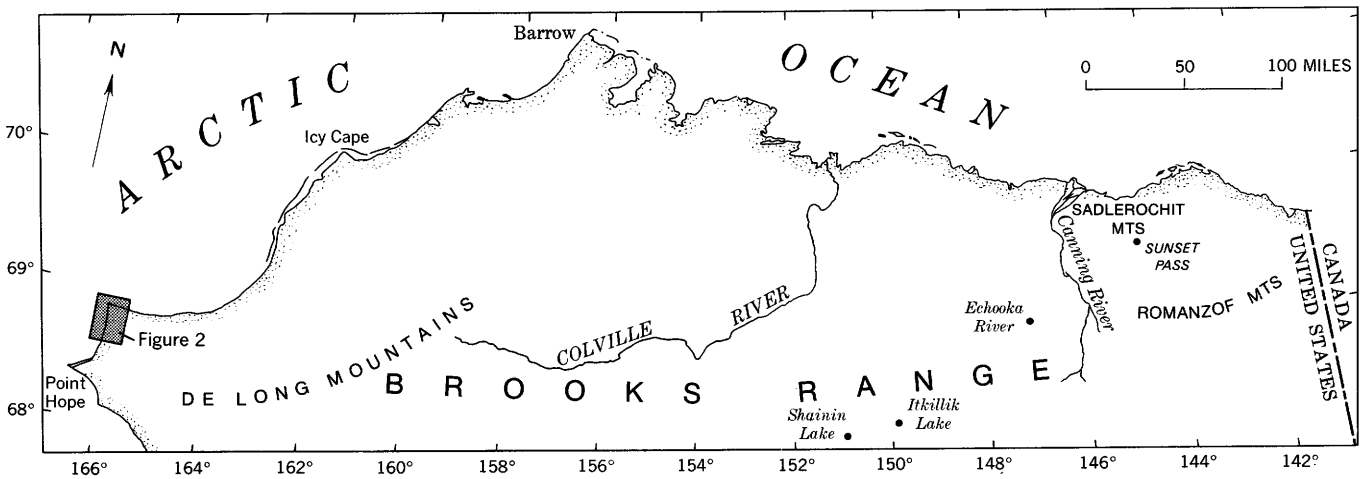

FIGURE 1.—Index map of arctic Alaska, showing location of sections referred to in figures 2 and 6.

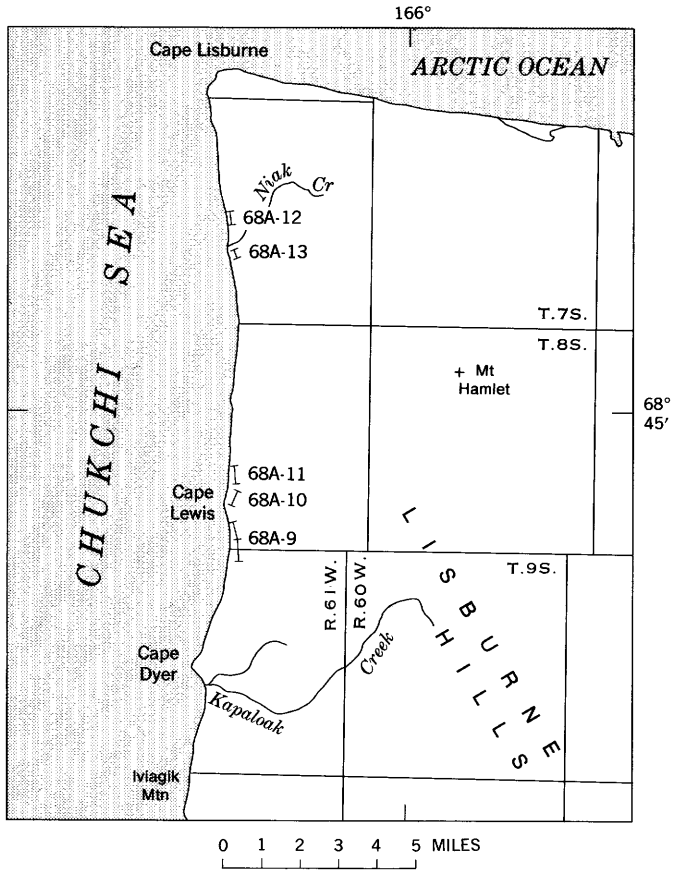

FIGURE 2.—Index map showing location of measured sections described.

Lisburne Group of the central and eastern Brooks Range is shown in figures 1 and 6.

The oldest carbonate rock found in the sea cliff sections is at the base of section 68A–12, north of Niak Creek. These rocks now rest on a thick zone of tectonic breccias. Undoubtedly, there were older carbonates in this section before the tectonic activity that produced the thick breccia zone (fig. 5*A*). The higher beds of section 68A–12 are extensively dolomitized; the Foraminifera present indicate an undetermined Viséan age for this interval.

Section 68A–13, on the south side of Niak Creek, is on a higher thrust sheet which overrides the thrust sheet bearing section 68A–12. Below the base of section 68A–13 is a sequence of paralic sediments: dark-gray shales, coals, siltstones, and sandstones. These sediments appear to be in gradational contact with the marine limestones of section 68A–13. Detailed study of these paralic clastic sediments is difficult because exposures are poor, and there are numerous small folds and faults. The Foraminifera of section 68A–13 are of late zone 15 and represent an age near or equivalent of the Meramec-Chester boundary.

The thick composite section at Cape Lewis comprising sections 68A–9, 68A–10, and 68A–11 is about 3,100 feet thick; microfossils indicate a late Viséan age (early Chester), zone 16_1 at the base and a "Namurian" zone 18 (late Chester) in the youngest exposed beds. As the top of section 68A–11 is covered by soil and tundra, beds younger than zone 18 may be present in the Kogruk Formation.

NASORAK FORMATION

The Nasorak Formation was named by Campbell (1967, p. 7), who designated as its type section a section in a sea cliff adjacent to the mouth of Nasorak Creek near Cape Thompson.

South of Cape Lewis, the Nasorak Formation is exposed in the sea cliffs (fig. 3*A*), where 1,282 feet of the lower part of section 68A–9 was assigned to this formation (figs. 4*A*, *B*). At this locality the Nasorak Formation can be divided into four lithic units.

The base of the measured section begins at or on the beach. Neither the composition nor the age of the underlying rocks is known, but they probably are Mississippian clastic rocks deposited in paralic or continental environments. The lowest unit consists of 355 feet of shales, siltstones, argillaceous limestones, limestones, and minor amounts of sandstones. The limestones and shale beds are generally 1 to 5 feet thick.

Unit 2, which is 295 feet thick, is composed primarily of dark-gray shales with lesser amounts of siltstone and sandstone. A massive limestone, about 15 feet thick, occurs near the middle of the unit. This limestone is overlain by gray to medium-brown calcareous shales that have a gradational contact with the massive cherty limestones of unit 3 (fig. 4*A*).

This dark-gray carbonaceous shale zone could possibly, under proper conditions, be a source bed for petroleum.

Unit 3 consists of 250 feet of massive-bedded light-gray to gray echinoderm-bryozoan packstone. Two covered intervals, 15 and 35 feet thick, are present (fig. 4*A*). The top of unit 3 is marked by a creek bed. The highest 20 feet of the unit contains a large number of lithostrotionoid corals. The gravel and soil associated with the creek bed covers some 150 stratigraphic feet of section.

Unit 4 is 232 feet thick. The base, exposed on the north side of the creek, is a 15-foot-thick sequence of thin-bedded gray limy mudstones and gray calcareous shales. The next 51 feet is covered. This is followed by 164 feet of shales, calcareous gray shales, and thin-bedded argillaceous lime mudstones.

The top of the Nasorak Formation at Cape Lewis was picked at the occurrence of the first massive gray

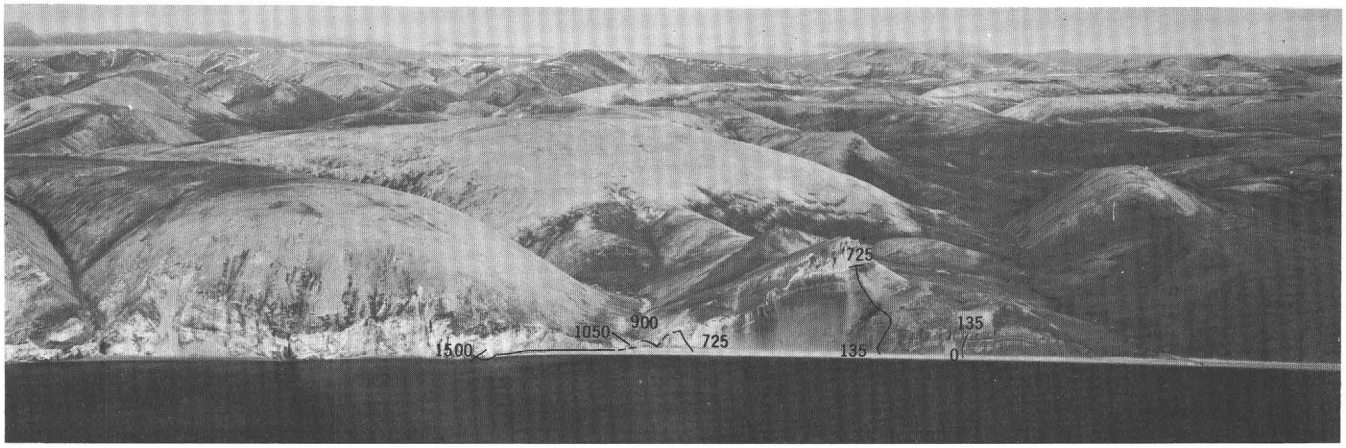

A

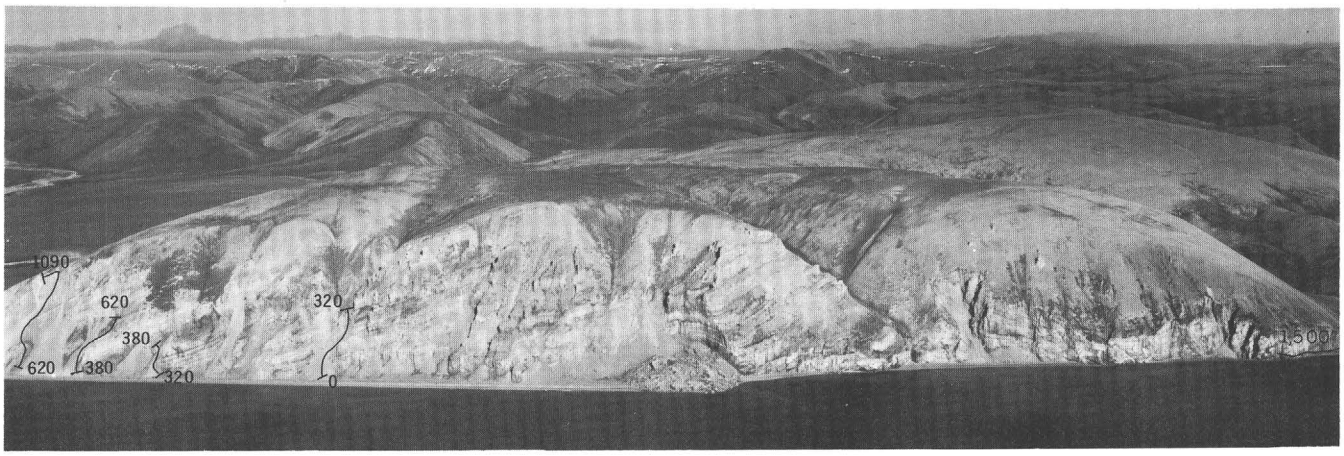

B

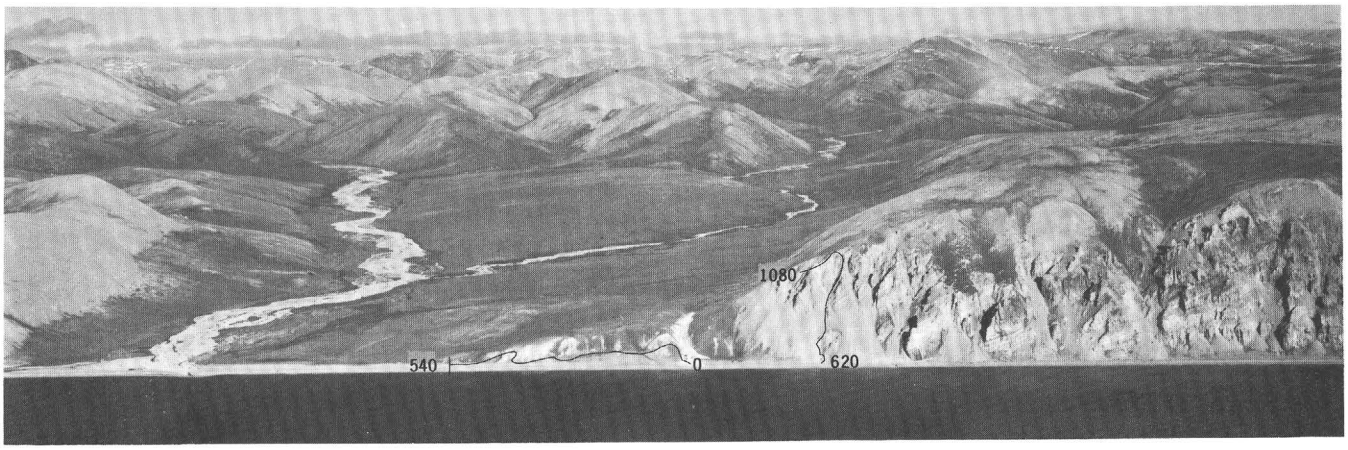

C

FIGURE 3.—Cape Lewis, oblique view to the east.

A, South end of sea cliff, showing location of section 68A–9.
B, Middle part of sea cliff, showing location of section 68A–10.
C, North end of sea cliff, 0–540, showing location of section 68A–11. The section marked "620–1090" is the upper part of section 68A–10 (See *B*).

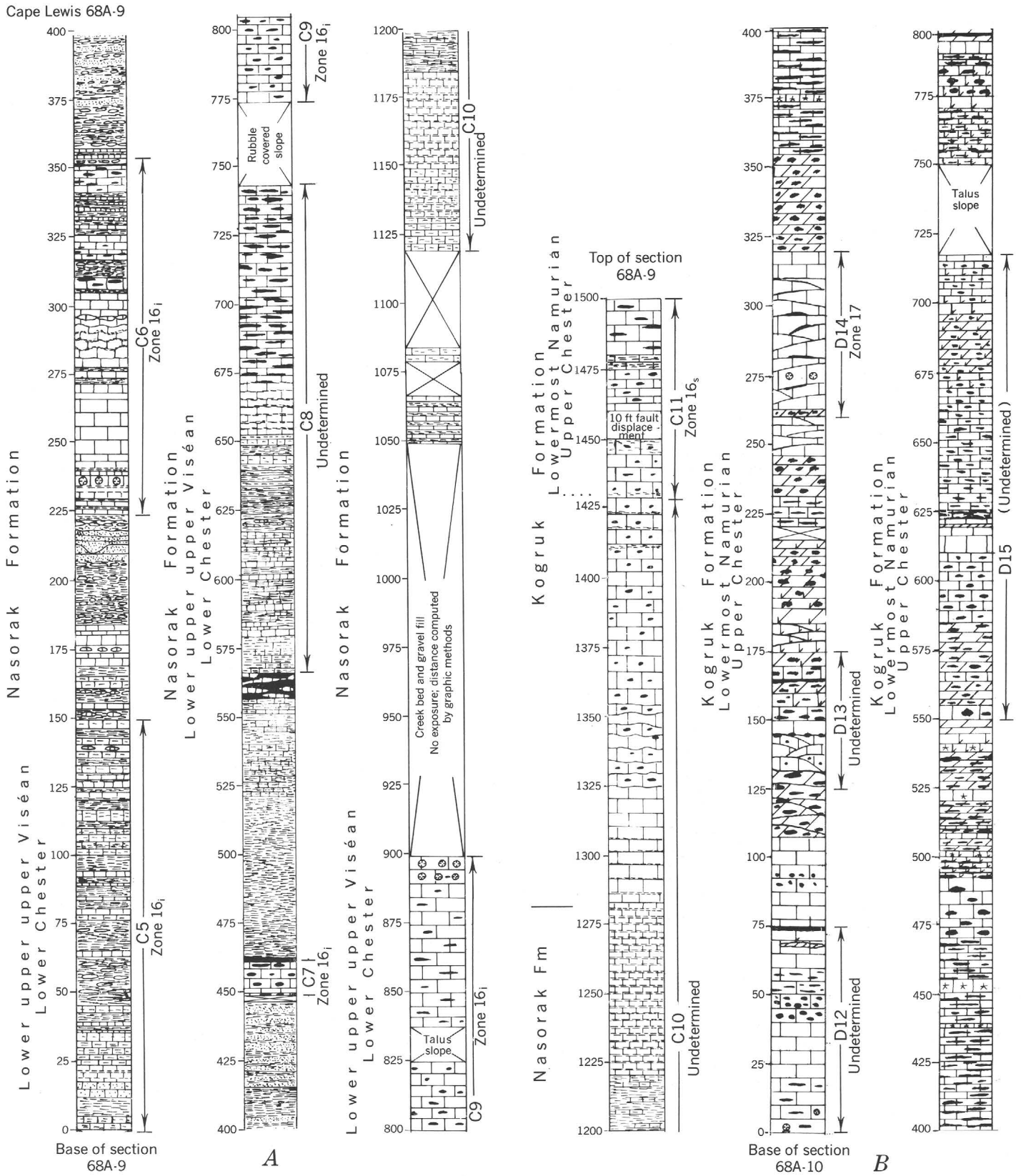

FIGURE 4.—Stratigraphic sections at Cape Lewis. Microfossil collections C5 to E17 shown in the section "Microfossil Lists."
A, Stratigraphic section 68A–9, Nasorak Formation.
B, Stratigraphic section 68A–9, continued; section 68A–10, Nasorak and Kogruk Formations.
C, Stratigraphic section 68A–10, continued; section 68A–11, Kogruk Formation.

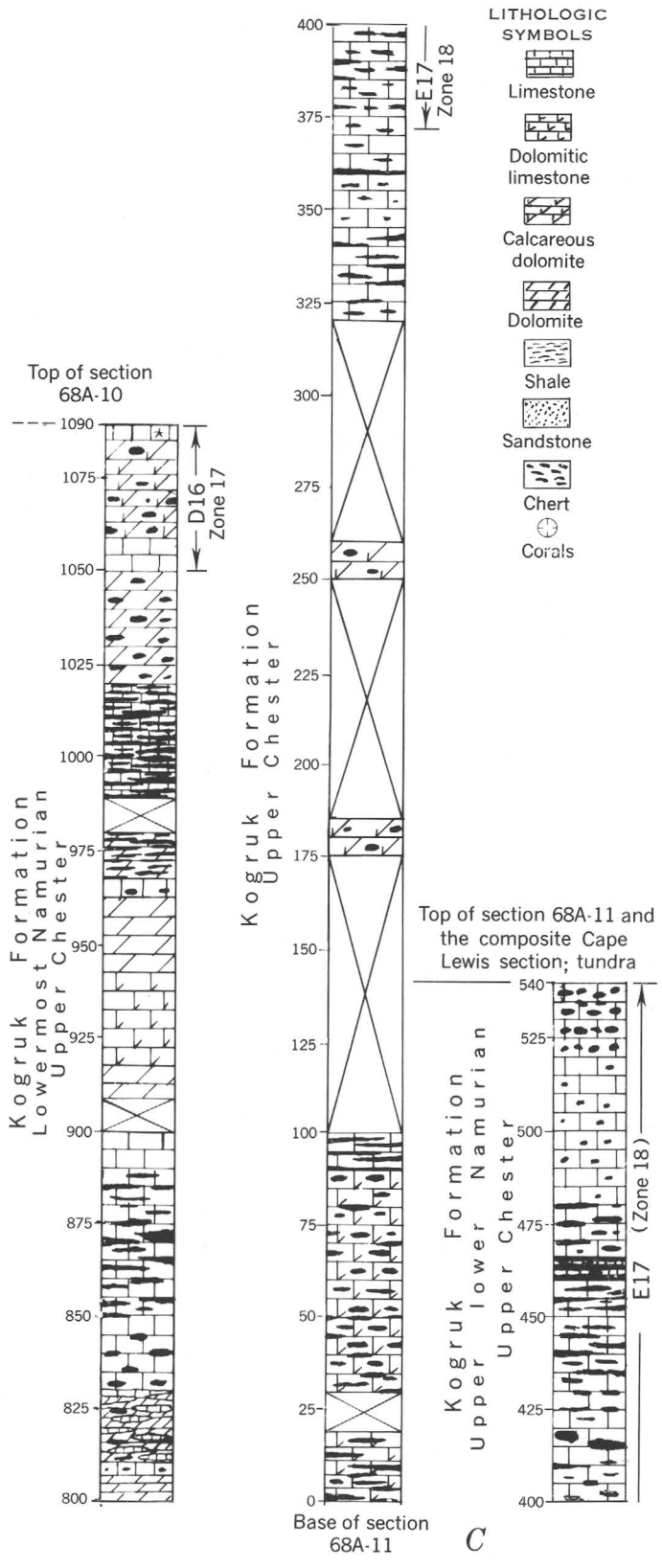

FIGURE 4.

echinoderm-bryozoan wackestones and packstones (figs. 3*A* and 4*B*) not followed by another cycle or sequence of shale or argillaceous limestone.

The section 68A–13, south of Niak Creek, is only 215 feet thick and is a partial representation of the lower part of Nasorak Formation. The section (fig. 5*A*, *B*) is a rhythmic sequence of dark-gray calcareous shales, argillaceous limestones, and 1- to 5-foot beds of medium- to dark-gray bryozoan-echinoderm wackestones and packstones. Dark-gray nodular chert is common, and commonly the limestones are slightly dolomitized. Dolomite is common as scattered rhombs within the micrite matrix.

KOGRUK FORMATION

Sable and Dutro (1961, p. 592) named the Kogruk Formation for the thick sequence of Carboniferous (Mississippian) limestone in the western DeLong Mountains. The Kogruk Formation in the Cape Lewis sections is more than 1,864 feet thick. The lower 232 feet of the Kogruk Formation is in the upper part of section 68A–9. These beds are massive, light-gray to gray, crossbedded echinoderm-bryozoan packstones and wackestones. An inaccessible interval, possibly 100 to 200 feet thick, that forms a cliff separates the top of section 68A–9 from the base of section 68A–10 (fig. 4*B*). Section 68A–10, which is 1,090 feet thick, is composed of massive carbonates. The lower 247 feet is a series of shallow-water cyclic carbonates. The cycles, each of which may be 20 feet thick or may exceed 120 feet, are formed by a series of 1- to 50-foot-thick beds which range in composition from grainstone formed by rounded bioclasts of bryozoans and echinoderms upward into packstones and wackestones that are capped by fine-grained siliceous and cherty dolomites. A 63-foot-thick light-gray, crossbedded echinoderm-bryozoan packstone-grainstone (fig. 4*B*) is present from 247 to 320 feet above the base of 68A–10. From 360 to 470 feet is a massive sequence of medium- to thin-bedded brownish-gray to brownish-black lime mudstone to well-sorted fine-grained bryozoan-echinoderm packstone. The unit contains 1- to 3-inch-long bodies of irregular-shaped grayish-black to black chert (fig. 7). From 570 to 1,090 feet is a sequence consisting of thin- to medium-bedded, gray to medium-gray cherty echinoderm grainstones that grade upward into lime mudstones and dolomites.

The base of section 68A–11 (fig. 4*C*) is believed to be within a few tens of feet stratigraphically from the top of 68A–10. Section 68A–11 is approximately 542 feet, thick, and the top is marked by tundra and soil cover. The nature of the beds that overlie this section is

413-504 O - 71 - 3

unknown. Section 68A–11 is composed of light-gray to gray limestone and dolomites containing light-gray to gray nodular chert. The limestones are primarily echinoderm-bryozoan wackestones and packstones. The beds tend to be massive.

Section 68A–12, north of Niak Creek (fig. 5*A*, *B*), is 715 feet thick and is an incomplete section of the Kogruk Formation bounded at its top and bottom by fault surfaces.

The bottom 45 feet of the section (fig. 8) is dark-gray argillaceous wackestones containing abundant colonial corals. The remaining 670 feet is composed of light- to medium-gray limestones and dolomites with nodular chert in varying amounts. The rock types are wackestones to echinoderm-bryozoan grainstones. Dolomitization is common. The beds from 35 to 225 feet above the base are light-brown-gray dolomites. The remainder of the section is a series of beds composed of lime mudstones, echinoderm-bryozoan packstones, and grainstones showing varying degrees of dolomitization.

BIOSTRATIGRAPHY

Microfaunal assemblage zones

Microfaunal assemblage zones are used in this study. These zones have been used by Mamet and Gabrielse (1969), Mamet and Mason (1968), and Mamet (1968) to correlate the Carboniferous of western Canada with the Carboniferous of the northern Cordilleran of the United States (Sando and others, 1969). Armstrong, Mamet, and Dutro (1970) used these microfaunal assemblage zones to correlate the Lisburne Group of the eastern and central Brooks Range.

The microfacies of Alaska, as in most of the Taimyr-Alaska foraminiferal realm (Mamet, 1962; Mamet and Belford, 1968), are generally poor in foraminifers and algae. Within the sections of the Lisburne Group studied in the sea cliffs of northwestern Alaska, six foraminiferal assemblages can be recognized and tied to the Cordilleran and Eurasiatic Carboniferous zonations (Sando and others, 1969).

The middle Viséan zone 13 is identified on the presence of archaediscids (*Archaediscus* of the Group *A. krestovnikovi* Rauzer-Chernoussova), endothyrids (*Eoendothyranopsis* of the group *E. pressa* Grozdilova *in* Lebedeva), *Globoendothyra* sp., eoforschiids (*Eoforschia*), and primitive bradyinids (*Endothyranopsis*).

No characteristic assemblage zone 14 has been found.

The top of zone 15 is recognized on the basis of endothyrids, and the $15/16_1$ boundary is placed at the extinction of *Eoendothyranopsis-Eoforschia; Endothyra* sensu stricto and *Zellerina* become an important element of the microfauna.

Zone 16_1 is poorly represented throughout the entire Cape Lewis 68A–9 section; the microfauna is reduced to scarce small endothyrids, archaediscids, and tetrataxids.

A

FIGURE 5.—Stratigraphic sections on Niak Creek. Microfossil collections A1 to B4 shown in the section "Microfossil Lists."

A, North Niak Creek section, 68A–12, and south Niak Creek section, 68A–13. Oblique view to the east.
B, Stratigraphic section 68A–12, north Niak Creek, and section 68A–13, south Niak Creek.

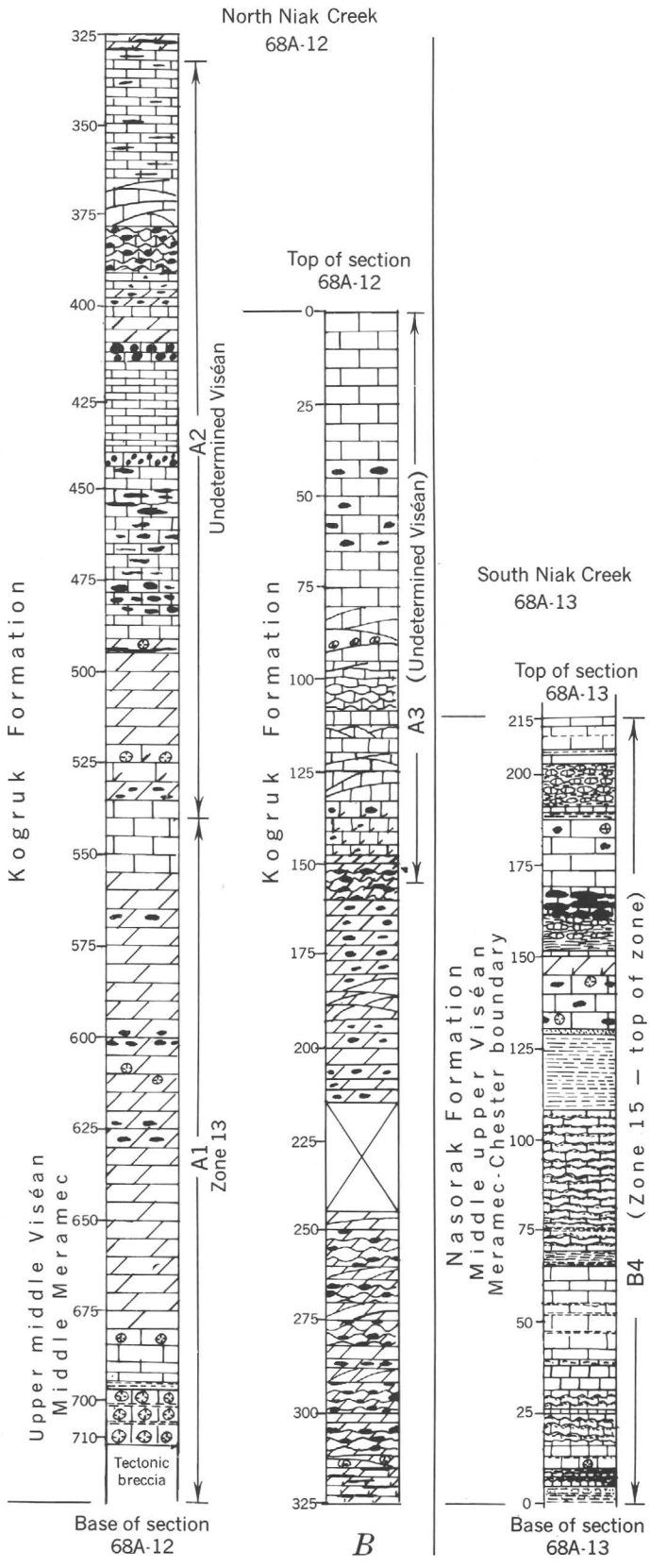

FIGURE 5.

Zone 16_s is characterized by the outburst of *Neoarchaediscus Planospirodiscus*, and zone 17 by the appearance of *Asteroarchaediscus*.

The youngest Carboniferous zone identified in this report is in the late early "Namurian" (*Eumorphoceras* equivalent) zone 18, identified on the presence of *Globivalvulina*? of the group *G. parva* Chernysheva mixed with very abundant *Asteroarchaediscus* and *Planospirodiscus*.

Microfossil lists (stratigraphic location shown on figs. 4 and 5)

A1 (0–220 feet)
Microfacies
Archaediscus sp.
Archaediscus of the group *A. krestovnikovi* Rauzer-Chernoussova.
Brunsia sp.
Calcisphaera sp.
Calcisphaera laevis Williamson.
Calcisphaera pachysphaerica (Pronina).
Earlandia, sp.
Earlandia clavatula (Howchin).
Earlandia vulgaris (Rauzer-Chernoussova and Reitlinger).
Endothyra sp.
Endothyra? of the group *E.*? *prisca* Rauzer-Chernoussova and Reitlinger.
Endothyranopsis sp.
Endothyranopsis compressa (Rauzer-Chernoussova and Reitlinger).
Eoendothyranopsis sp.
Eoendothyranopsis of the group *E. pressa* (Grozdilova *in* Lebedeva).
Eoendothyranopsis? *redwalli* (Skipp).
Eoforschia sp.
Globoendothyra sp.
Globoendothyra of the group *G. tomiliensis* (Grozdilova).
Palaeotextularia sp.
Parathurammina sp.
Age: zone 13, late middle Viséan, St. Louis equivalent.

A2 (220–400 feet)
Microfacies
Archaediscus sp.
Archaediscus of the group *A. krestovnikovi* Rauzer-Chernoussova.
Brunsia sp.
Calcisphaera sp.
Calcisphaera laevis Williamson.
Calcisphaera pachysphaerica (Pronina).
Endothyra sp.
Endothyra of the group *E. bowmani* Phillips *in* Brown.
Globoendothyra sp.
Age: undetermined Viséan zone.

A3 (600–710 feet)
Microfacies
Archaediscus of the group *A. krestovnikovi* Rauzer-Chernoussova.
Endothyra of the group *E. bowmani* Phillips *in* Brown.
Age: undetermined Viséan zone.

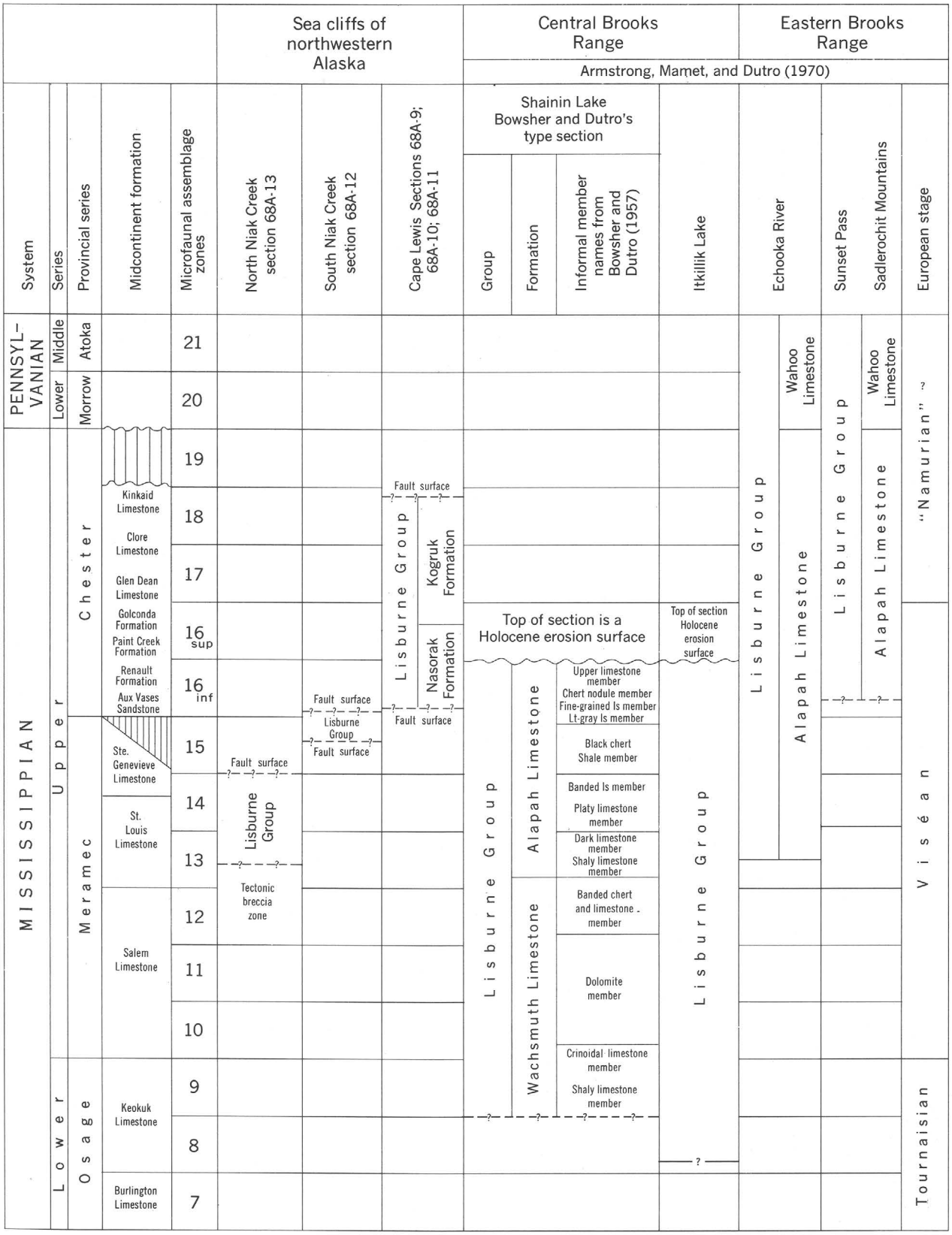

FIGURE 6.—Regional stratigraphic correlation chart for the Lisburne Group of northwestern Alaska with the Lisburne Group of the central and eastern Brooks Range.

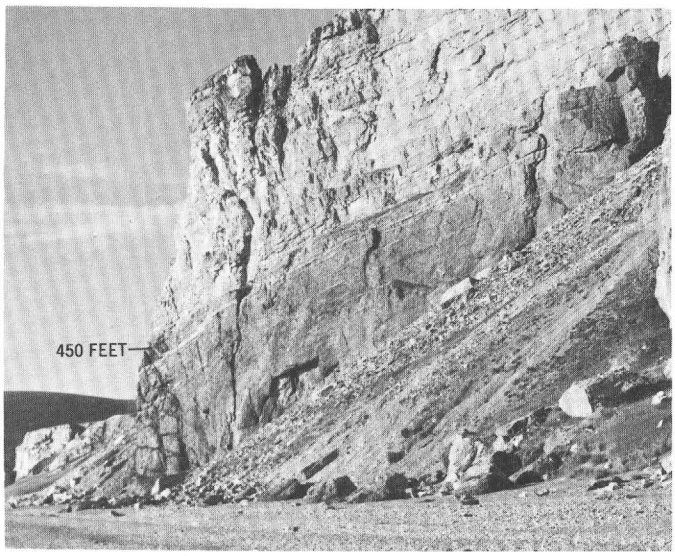

FIGURE 7.—Sea cliff showing the massive, thin-bedded dark-brownish-gray limestone present in section 68A–10, from 375 to 450 feet above the base. These beds are overlain by light-gray bryozoan-echinoderm wackestones and packstones.

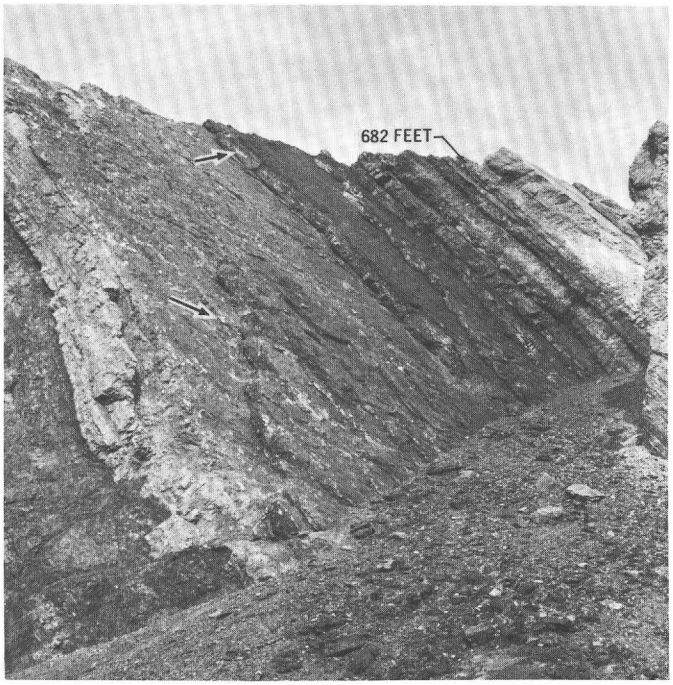

FIGURE 8.—View of the sea cliff at the base of section 68A–12, north of Niak Creek. Below the 715-foot level is a thick zone of tectonic breccia. The arrows point to two lithostrotionoid coral colonies. The bedding surface and the sides of the bed contain numerous coralla. Although coralla are very abundant, only 5 taxa are present.

B4 (0–215 feet)
Microfacies
Calcisphaera sp.
Calcisphaera laevis Williamson.
Calcisphaera sp.
Earlandia of the group *E. clavatula* (Howchin).
Earlandia of the group *E. vulgaris* (Rauzer-Chernoussova and Reitlinger).
Endothyra sp.
Endothyra of the group *E. bowmani* Phillips *in* Brown.
Endothyranopsis sp.
Endothyranopsis cf. *E. crassa* (Brady).
Eoendothyranopsis sp.
Eoendothyranopsis of the group *E. pressa* (Grozdilova *in* Lebedeva).
Globoendothyra sp.
Tetrataxis sp.
Age: zone 15 (top of the zone), middle late Viséan, Meramec-Chester boundary equivalent.

C5 (0–150 feet)
Microfacies
Archaediscus sp.
Calcisphaera laevis Williamson.
Cornuspira sp.
Endothyra sp.
Endothyra of the group *E. bowmani* Phillips *in* Brown.
Globoendothyra sp.
Tetrataxis sp.
Tetrataxis of the group *T. angusta* Vissarionova.
Tetrataxis of the group *T. conica* Ehrenberg *emend* von Möller.
Zellerina sp.
Age: zone 16_1, early late late Viséan, early Chester.

C6 (225–355 feet)
Microfacies
Calcisphaera sp.
Cornuspira sp.
Earlandia sp.
Endothyra sp.
Endothyra of the group *E. bowmani* Phillips *in* Brown.
Endothyra? of the group *E.? prisca* Rauzer-Chernoussova and Reitlinger.
Globoendothyra sp.
Tetrataxis sp.
Tetrataxis of the group *T. angusta* Vissarionova.
Tetrataxis of the group *T. conica* Ehrenberg *emend* von Möller.
Age: zone 16_1, early late late Viséan, early Chester equivalent.

C7 (450–460 feet)
Microfacies
Calcisphaera sp.
Earlandia sp.
Earlandia vulgaris (Rauzer-Chernoussova and Reitlinger).
Endothyra sp.
Endothyra of the group *E. bowmani* Phillips *in* Brown.
cf. *Neoarchaediscus* sp.
Tetrataxis sp.
Age: zone 16_1, early late late Viséan, early Chester equivalent.

C8 (575–740 feet)
Microfacies
Age: undetermined.
Earlandia sp.
Earlandia sp.
Endothyra sp.

C9 (770–900 feet)
Microfacies
Calcisphaera sp.
Earlandia sp.
Earlandia vulgaris (Rauzer-Chernoussova and Reitlinger).
Endothyra sp.
Endothyra of the group *E. bowmani* Phillips *in* Brown.
Endothyra? of the group *E.*? *prisca* Rauzer-Chernoussova and Reitlinger.
Globoendothyra sp.
Tetrataxis sp.
Tetrataxis of the group *T. angusta* Vissarionova.
Tetrataxis of the group *T. conica* Ehrenberg *emend von Möller.*
Age: zone 16_1, early late Viséan, early Chester equivalent.

C10 (1,120–1,415 feet)
Microfacies
Calcisphaera sp.
Earlandia sp.
Endothyra sp.
Age: undetermined

C11 (1,415–1,500 feet)
Microfacies
Archaediscus sp.
Archaediscus krestovnikovi Rauzer-Chernoussova.
Brunsia sp.
Diplosphaerina sp.
Earlandia sp.
Endothyra sp.
Neoarchaediscus sp.
Planospirodiscus sp.
Pseudoglomospira? sp.
Age: zone 16_2, latest Viséan, early Chester equivalent.

D12 (0–75 feet)
Microfacies
Archaediscus sp.
Archaediscus krestovnikovi Rauzer-Chernoussova.
Brunsia sp.
Calcisphaera sp.
Cornuspira sp.
Endothyra sp.
Kamaena sp.
Pseudoglomospira sp.
Stacheoides sp.
Age: undetermined.

D13 (125–175 feet)
Microfacies
Archaediscus sp.
Archaediscus krestovnikovi Rauzer-Chernoussova.
Brunsia sp.
Calcisphaera sp.
Cornuspira sp.
Endothyra sp.
Stacheoides sp.
Age: undetermined.

D14 (260–320 feet)
Microfacies
Archaediscus sp.
Archaediscus of the group *A. chernoussovensis* Mamet.
Archaediscus of the group *A. moelleri* Rauzer-Chernoussova.
Archaediscus krestovnikovi Rauzer-Chernoussova.
Asteroarchaediscus sp.
Brunsia sp.
Endothyra sp.
Age: zone 17, earliest "Namurian," Glen Dean equivalent of the Chester Series.

D15 (550–715 feet)
Microfacies
Calcisphaera sp.
Earlandia sp.
Eostaffella sp.
Age: undetermined.

D16 (1,050–1,090 feet)
Microfacies
Archaediscus sp.
Archaediscus of the group *A. chernoussovensis* Mamet.
Archaediscus krestovnikovi Rauzer-Chernoussova.
Archaediscus of the group *A. moelleri* Rauzer-Chernoussova.
Asteroarchaediscus sp.
Endothyra sp.
Endothyra of the group *E. bowmani* Phillips *in* Brown.
Eostaffella sp.
Palaeotextularia sp.
Planospirodiscus sp.
Age: zone 17, earliest "Namurian," Glen Dean equivalent of the Chester Series.

E17 (375–525 feet)
Microfacies
Archaediscus sp.
Archaediscus krestovnikovi Rauzer-Chernoussova.
Asteroarchaediscus sp.
Calcisphaera sp.
Cornuspira sp.
Endothyra sp.
Globivalvulian? of the group *G.*? *parva* Chernysheva.
Planospirodiscus sp.
Pseudoendothyra sp.
Stacheoides sp.
Age: zone 18, late early 'Namurian," late Chester equivalent.

Lithostrotionoid coral zones

The known stratigraphic distribution of lithostrotionoid coral species within the Lisburne Group (Mississippian) of the Lisburne Hills and sea cliff exposures and species from DeLong Mountains (Armstrong, 1970b) are shown in figure 9.

The base of the North Niak Creek **section 68A–12** contains the oldest coral fauna known in the region. Although a large number of lithostrotionoid corals were collected, thin-section studies reveal only four species: *Lithostrotion* (*Siphonodendron*) *warreni* Nelson, *Lithostrotionella banffensis* (Warren), and two new and undescribed species of *Lithostrotionella.* This coral fauna is found in association with a middle Viséan (middle Meramec), late zone 13 microfauna.

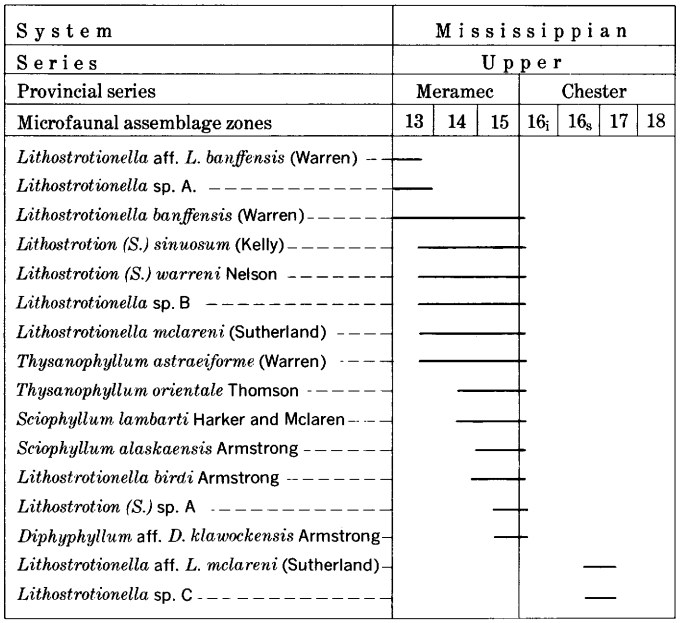

FIGURE 9.—Stratigraphic range of lithostrotionoid corals in the Lisburne Group of northwestern Alaska.

The South Niak Creek section 68A–13, which is at the zone 15–16 boundary, contains a prolific fauna of lithostrotionoid corals, *Lithostrotion* (*Siphonodendron*) *sinuosum* (Kelly), *L.* (*S.*) *warreni* Nelson, a new and undescribed species of *Lithostrotion* (*Siphonodendron*), *Diphyphyllum* aff. *D. klawockensis* Armstrong, *Lithostrotionella banffensis* (Warren), *L. birdi* Armstrong, *L. mclareni* (Sutherland), *Thysanophyllum astraeiforme* (Warren), *Sciophyllum lambarti* Harker and McLaren, and *S. alaskaensis* Armstrong.

The lower 900 feet of the Cape Lewis section 68A–9 is equivalent to the basal Chester, zone 16_i as indicated by the Foraminifera, and has a lithostrotionoid coral fauna of *Lithostrotion* (*Siphonodendron*) *sinuosum* (Kelly), *L.* (*S.*) *warreni* Nelson, a new species of *Lithostrotion* (*Siphonodendron*), *Diphyphyllum* aff. *D. klawockensis* Armstrong, *Lithostrotionella banffensis* (Warren), *L. birdi* Armstrong, *L. mclareni* (Sutherland), *Thysanophyllum astraeiforme* (Warren), and *Sciophyllum lambarti* Harker and McLaren.

Many of the species collected from the Lisburne Hills sea cliffs are known to occur in the Kogruk Formation of the DeLong Mountains. Armstrong (1970b) reports the following species of coral from the Meramec zones 14 and 15 of the Kogruk Formation of the DeLong Mountains: *Lithostrotion* (*Siphonodendron*) *sinuosum* (Kelly), *L.* (*S.*) *warreni* Nelson, *Lithostrotionella banffensis* (Warren), *L. birdi* Armstrong, *L. mclareni* (Sutherland), *Thysanophyllum astraeiforme* (Warren), *Sciophyllum lambarti* Harker and McLaren, and *S. alaskaensis* Armstrong.

A middle to late Meramec coral fauna that is associated with a Foraminifera fauna is reported by Armstrong (1970a) from the northwestern coastal regions of the Prince of Wales Island, southeastern Alaska. This coral fauna has in common with the fauna of this report the following species: *L.* (*S.*) *warreni* Nelson, *Diphyphyllum klawockensis* Armstrong, *L. banffensis* (Warren), *L. birdi* Armstrong, *T. astraeiforme* (Warren), and *S. alaskaensis* Armstrong.

Comparison of the coral faunas of the Lisburne Group with the four coral assemblages of Macqueen and Bamber (1968) from the Mount Head Formation of southwestern Alberta suggests that the extinction of *L.* (*S.*) *warreni* Nelson, *Thysanophyllum astraeiforme* (Warren), and *Lithostrotionella mclareni* (Sutherland) could be slightly later in Alaska than in Alberta, Canada.

Foraminifera suggest that the Lisburne Group coral fauna at the north of the Niak Creek section (68A–12) is a time equivalent of Macqueen and Bamber's faunal assemblage 2 from the Mount Head Formation and of Sando, Mamet, and Dutro's coral zone E from the northern Cordillera of the United States. The coral fauna from South Niak Creek section 68A–13 and the lower 900 feet of the Cape Lewis section 68A–9 is an equivalent of Macqueen and Bamber's fossil assemblage 4 and of the upper part of Sando, Mamet, and Dutro's (1969) coral zone F.

The limitations encountered in attempting to compare the coral fauna of northwestern Alaska with those of Alberta are greatly magnified when comparisons are made with coral faunas of the northern Cordillera of the United States. Sando, Mamet, and Dutro's list of fossil corals (1969, p. E7) from the Cordilleran region of the United States shows no species in common with the Lisburne Group faunas.

The microfossil assemblage (fig. 9) indicates that the prolific Kogruk Formation coral fauna straddles the Meramec-Chester boundary and extends into the lower Chester. Field studies in the Cape Lewis–Niak Creek region, and also across the Brooks Range, indicate that this coral assemblage became extinct during the early part of zone 16_i.

Above zone 16_i, colonial corals are relatively rare. Specimens of two new species of lithostrotionid corals were collected in the carbonates of zone 16_s at Cape Lewis. A few solitary corals were the only corals found at Cape Lewis in the upper Chester limestones of zones 17 and 18.

REFERENCES

Armstrong, A. K., 1970a, Mississippian rugose corals, Peratrovich Formation, west coast, Prince of Wales Island, southeastern Alaska. U.S. Geol. Survey Prof. Paper 534, 44 p.

——— 1970b, Carbonate facies and lithostrotionid corals of the Mississippian Kogruk Formation, DeLong Mountains, northwestern Alaska: U.S. Geol. Survey Prof. Paper 664, 38 p.

Armstrong, A. K., Mamet, B. L., and Dutro, J. T., Jr., 1970, Foraminiferal zonation and carbonate facies of the Mississippian and Pennsylvanian Lisburne Group, central and eastern Brooks Range, Alaska: Am. Assoc. Petroleum Geologists Bull., v. 54, no. 5, p. 687–698, 4 figs.

Bowsher, A. L., and Dutro, J. T., Jr., 1957, The Paleozoic section in the Shainin Lake area, central Brooks Range, Alaska: U.S. Geol. Survey Prof. Paper 303–A, 39 p., 6 pls., 4 figs.

Campbell, R. H., 1967, Areal geology in the vicinity of the Chariot site, Lisburne Peninsula, northwestern Alaska: U.S. Geol. Survey Prof. Paper 395, 71 p., 1 pl., 28 figs.

Dunham, R. J., 1962, Classification of carbonate rocks according to depositional texture, *in* Classification of carbonate rocks—A symposium: Am. Assoc. Petroleum Geologists Mem. 1, p. 108–121, 8 pls.

Macqueen, R. W., and Bamber, E. W., 1968, Stratigraphy and facies relationship of the upper Mississippian Mount Head Formation, Rocky Mountains and foothills, southwestern Alberta: Canadian Assoc. Petroleum Geologists Bull., v. 16, no. 3, p. 225–287.

Mamet, B. L., 1962, Remarques sur la microfaune de Foraminiferes du Dinantien: Soc. Geol. Belgique Bull., v. 70, no. 2, p. 166–173.

——— 1968, Foraminifera, Etherington Formation (Carboniferous), Alberta, Canada: Canadian Assoc. Petroleum Geologists Bull., v. 16, no. 2, p. 167–179.

Mamet, B. L., and Belford, D. J., 1968, Carboniferous Foraminifera, Bonaparte Gulf Basin, northwestern Australia: Micropaleontology, v. 14, no. 3, p. 339–347.

Mamet, B. L., and Gabrielse, H., 1969, Foraminiferal zonation and stratigraphy of the type section of the Nizi Formation (Carboniferous systems, Chesteran Stage), British Columbia: Canada Geol. Survey Paper 69–16, p. 1–21, 6 figs.

Mamet, B. L., and Mason, D., 1968, Foraminferal zonation of the lower Carboniferous Connor Lake section, British Columbia: Canadian Assoc. Petroleum Geologists Bull., v. 16, no. 2, p. 147–166.

Sable, E. G., and Dutro, J. T., Jr., 1961, New Devonian and Mississippian Formations in DeLong Mountains, northern Alaska: Am. Assoc. Petroleum Geologists Bull., v. 45, no. 5, p. 585–593, 4 figs.

Sando, W. J., Mamet, B. L., and Dutro, J. T., Jr., 1969, Carboniferous megafaunal and microfaunal zonation in the northern Cordillera of the United States: U.S. Geol. Survey Prof. Paper 613–E, 29 p.

STRATIGRAPHIC INTERPRETATIONS OF SOME CRETACEOUS MICROFOSSIL FLORAS OF THE MIDDLE ATLANTIC STATES

By JACK A. WOLFE and HELEN M. PAKISER,
Menlo Park, Calif.

Abstract.—Palynologic analysis of surface samples from the Patuxent, Patapsco, Raritan, and Magothy Formations indicates that these rock units can be divided into two major sequences separated by a major hiatus. The lower sequence includes the Potomac Group (Patuxent, Arundel, and Patapsco Formations) of Maryland and Virginia and the Raritan Formation of northern New Jersey. The Potomac Group is thought to range in age from probable late Aptian or early Albian (Early Cretaceous) through earliest Cenomanian (Late Cretaceous), and the Raritan Formation is thought to be entirely of Cenomanian Age. The upper sequence—the Magothy Formation—is thought to be of Santonian and earliest Campanian (Late Cretaceous) Age. The Amboy stoneware clay, which was formerly included in the Raritan Formation, has a rich flora closely allied to that of the Morgan and Cliffwood beds of the Magothy and was recently reassigned as the basal unit of the Magothy Formation. The Old Bridge Sand Member of the Raritan Formation also contains a flora closely allied to that of the Magothy and is herein removed from the Raritan Formation and made the basal member of the Magothy Formation.

Lithostratigraphic relationships in the lowermost outcropping beds of the northern Atlantic Coastal Plain have received little attention since the early part of this century. At that time, these beds were subdivided, oldest to youngest, into the Potomac Group (Patuxent, Arundel, and Patapsco Formations) and the Raritan and Magothy Formations. Environmental interpretations of these units indicate that most were deposited in a nonmarine environment. Some thin marine beds are, however, present in the upper part of this sequence.

Up to the mid-1950's, the stratigraphic section most commonly cited from Maryland to New Jersey was as shown in table 1.

The various lithologies within the Potomac Group and the Raritan Formation were deposited irregularly over a long time interval. As a result, some investigators have doubted the existence, particularly in the Potomac Group, of valid mappable formations (Jordan, 1962; Owens, 1969).

Several papers have appeared in recent years concerning the palynology of the Cretaceous formations of the Atlantic Coastal Plain. The work of Brenner (1963) on the oldest units—the Patuxent, Arundel, and Patapsco Formations of the Potomac Group—is the most extensive treatment yet to appear on eastern North American Cretaceous microfossil floras. Our knowledge of the Late Cretaceous palynology of eastern North America stems largely from the papers of Groot, Penny, and Groot (1961), Leopold and Pakiser (1964), Kim-

TABLE 1.—*Part of the Cretaceous stratigraphic section in Maryland and New Jersey as described up to the mid-1950's*

Series	Stage	Maryland	Northern New Jersey
Upper Cretaceous	Turonian	Magothy	Magothy
		UNCONFORMITY	
	Cenomanian	Raritan	Raritan: Amboy stoneware clay[1]; Old Bridge Sand Member[2]; South Amboy fire clay[1]; Sayreville Sand Member[2]; Woodbridge clay[1]; Farrington Sand Member[2]; Raritan fire clay[1]
		UNCONFORMITY	
Lower Cretaceous		Potomac Group: Patapsco, Arundel, Patuxent	

[1] Economic subdivisions defined by Kümmel and Knapp (1904).
[2] Names added by Barksdale and others (1943).

yai (1966), Gray and Groot (1966), and Doyle (1969) and from the unpublished dissertation of Steeves (1959).

The name "Raritan" was first applied in Maryland by Berry (1910) to exposures at Elk Neck in the northeastern part of the State. Correlation with the Raritan of New Jersey was made on floral rather than lithic similarities.

In 1966, the Elk Neck locality of Berry was examined by Owens (1969) and samples were collected from the various formations reported by Bascom and Miller (1920). Although Miller thought an unconformity separated the Raritan and Patapsco Formations, the contact was found to be gradational. There is, however, a well-defined unconformity between the Raritan and overlying Magothy as evidenced by a sharp contact and a 2-foot bed of reworked gravel in the base of the Magothy.

The conformable relationship between the Raritan and Patapsco is borne out by palynological data which indicate that the change in pollen from the Patapsco of Early Cretaceous age to the Raritan of Late Cretaceous age is gradual rather than abrupt, as postulated by Brenner (1963). In addition, the Raritan of Maryland is older than the Raritan of New Jersey. Doyle (1969) has also noted similar relationships.

The realization that an age difference existed between the Raritan of Maryland and the Raritan of New Jersey precipitated the detailed study of the palynology of the Raritan Formation at its type locality.

We have examined only 28 samples, but we think that the present work, combined with the published work cited previously, is adequate to support the conclusions presented here. The sample localities are plotted in figure 1. The precise locality data and field stratigraphic assignments for localities in northern Maryland and in New Jersey are given at the end of this article. Numbers without a letter prefix are registered in the U.S. Geological Survey Paleobotany Locality Catalog in Washington, D.C.; numbers prefixed by "D" are registered in the U.S. Geological Survey Locality Catalog in Denver, Colo.

We have not attempted to determine the systematic position or stratigraphic ranges of all the pollen and spore types represented in the samples. Many of the gymnospermous pollen and filicaceous spore types appeared to have such long ranges that for the purposes of this study, which were largely stratigraphic, these types have little value. Particular attention was directed to the ranges of the striate spores of the ferns belonging to Schizaeaceae (generally placed in the form genera *Appendicisporites* and *Cicatricosisporites*). Although we

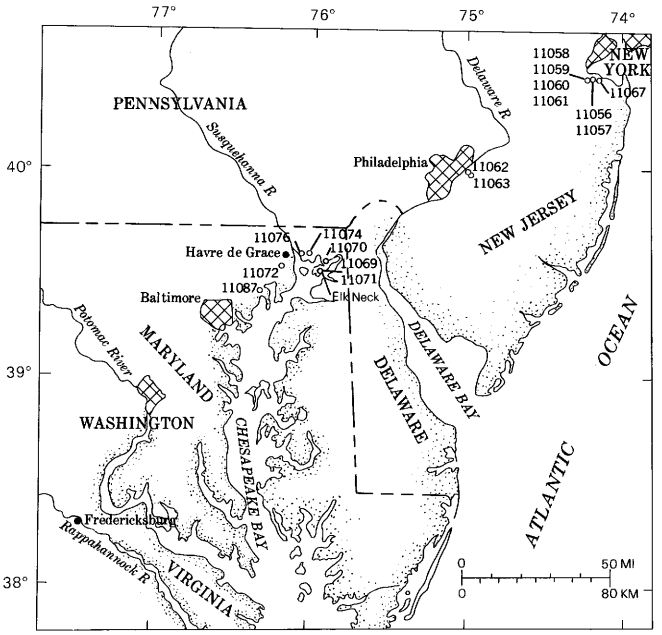

FIGURE 1.—Map of part of the Middle Atlantic States, showing sample localities discussed in this report.

may have recognized an excess of form species of these two genera, many of the 75 species appear to have stratigraphic utility. The diversity of schizaeaceous foliage especially in the megafossil flora of the Potomac Group, however, indicates that the family should be well represented in the microfossil flora.

Pollen of Dicotyledonae, specifically triaperturate types, was also examined in detail. Some of the pollen can be assigned to the various from genera instituted by Pflug (1953), Krutzsch (1957, 1959), and Góczán and others (1967) for European Cretaceous dicotyledonous pollen of the Normapolles group. Some of the species can be assigned to those erected by other workers who have dealt with the North American Cretaceous, but most of the species appear to be undescribed.

We have ignored the data based on megafossil floras as they pertain to correlations. None of the Cretaceous megafossil floras of the Atlantic Coastal Plain or Gulf Coast have been studied with modern techniques, and, until such time as these floras are properly studied, no stratigraphic interpretations based on them should be considered to have validity.

Acknowledgments.—We wish to acknowledge the assistance of J. P. Owens in collecting most of the samples and in consultation regarding physical stratigraphy, as well as for his indefatigable interest in this study. R. H. Tschudy and E. B. Leopold assisted in suggesting the taxonomic relationships of some of the palynomorphs and their stratigraphic significance.

POTOMAC GROUP

Patuxent and Arundel Formations

Brenner (1963) noted that the pollen and spore floras of the Patuxent and Arundel Formations are indistinguishable, and he therefore included both formations in his Zone I. This indicates that probably no hiatus exists between the Patuxent and Arundel—a conclusion in contrast to that of Dorf (1952). The Arundel may in fact be a local facies of the Patuxent, and in this report we imply both Patuxent and Arundel when the term Patuxent is used.

In addition to the northern Maryland samples, we have also examined several samples from the Patuxent Formation in the Washington, D.C., area. Two samples from the Fredericksburg, Va., Patuxent were obtained from specimens in the U.S. National Museum. Both assemblages compare well with the Patuxent microfossil flora as described by Brenner (1963).

Few palynomorphs appear to be restricted to the Patuxent Formation; almost all extend upward into the Patapsco. Brenner (1963, p. 22) lists only four species that appear to be restricted to the Patuxent microfossil flora. Of these four, we have found one—*Ephedripites virginiaensis* Brenn.—in one Patapsco sample (11071-A). The remaining three index species are so rare that, as Brenner concluded, they have little stratigraphic utility; we have not found any of these three species in any of our Patuxent samples. Several species of *Appendicisporites* and *Cicatricosisporites* have been found only in the Patuxent Formation, but the individual species occur in only one or two samples and are thus of little value. Brenner relied in part on the greater abundance or frequency of occurrence of certain species in the Patuxent than in the Patapsco in order to distinguish the microfossil floras of the two units; this approach may have some validity in attempting to correlate extensively sampled sections, but it cannot be relied on to place stratigraphically one or a few samples from isolated sections.

The primary distinction between the Patuxent and Patapsco microfossil floras is the lack in the Patuxent of certain palynomorphs that are found, typically in abundance, in the Patapsco. The most notable group lacking in the Patuxent assemblages is the triaperturate pollen of the dicotyledons.

Sample 11076 from near Havre de Grace, Md., was collected from clays that grade upward into gravels that have previously been considered to be of late Tertiary age. Such a young age is clearly contradicted by the microfossil flora; triaperturate dicotyledonous pollen is absent, and the sample contains an abundant and diverse flora indicative of an Early Cretaceous age. Among the dozens of taxa present are: *Appendicisporites* (seven species), *Cicatricosisporites* (19 species), *Trilobosporites marylandensis* Brenn., *Minerisporites venustus* Singh, *Maexisporites*, *Erlansonisporites*, *Kuylisporites*, and *Taurocusporites*. This assemblage indicates that the beds from which the sample came are equivalent in age to the Patuxent Formation. Sample 11074, which was collected from beds also gradational with so-called upper Tertiary gravels contained few taxa, but the dominance of *Trilobosporites marylandensis* and absence of triaperturate pollen probably indicate a Patuxent age.

The Patuxent Formation is not of early Neocomian Age as thought by Dorf (1952). The occurrence in the Patuxent microfossil flora of taxa such as *Clavatipollenites hughesi* Coup. and *Ephedripites* indicate a maximal age at about the Hauterivian-Barremian boundary (Couper, 1964), that is, late Neocomian. Other species, for example *Appendicisporites crickmayi* Poc. and *Minerisporites venustus* Singh, have been previously found only in beds of Albian Age (Singh, 1964). Part of the evidence on the age of the Patuxent must be the age of the lower part of the Patapsco Formation, because of the conformable contact between the two units and the gradational nature of the pollen and spore floras. The lower part of the Patapsco contains triaperturate dicotyledonous pollen; no documentation has been presented of the occurrence of this pollen type in beds unquestionably of pre-Albian Age (Hughes, 1961). Even many early Albian floras apparently lack triaperturate dicotyledonous pollen; the Lower Greensand of England, which is of early Albian Age in its upper part, lacks this pollen type (Hughes, 1961), and Singh (1964) reports that this pollen type is lacking in Alberta even in beds of middle Albian Age. On the basis of present evidence, the lower part of the Patapsco is considered to be somewhere in the later half of the Albian Stage. The Patuxent (including the Arundel) Formation, therefore, is at least in part of earlier Albian Age, although we cannot exclude the possibility that the lower part of the Patuxent is of Aptian Age. This age assignment is in accord with the somewhat debatable evidence from the Arundel dinosaurs (Dorf, 1952, p. 2176–2177).

Patapsco Formation

The primary characteristic of the pollen and spore assemblages described by Brenner (1963) from the Patapsco Formation is the occurrence of a few species of tricolpate pollen and the lack of more advanced dicotyledonous types. All surface samples from the Patapsco examined by Brenner, as well as those that we have ex-

amined, contain at least two species of tricolpate pollen, although in two subsurface samples Brenner did not find this pollen type. The other pollen and spore types listed by Brenner (1963, p. 23) as restricted to the Patapsco (Brenner's Zone II) are of limited use; one of these types—*Apiculatisporis babsae* Brenn.—has been found in one Patuxent sample. Most of the other spore and pollen types thought to be restricted to the Patapsco by Brenner have not been noted in the current study in any of our Patapsco samples.

Brenner (1963) recognized two subzones of his Zone II. The lowest subzone, which has rare tricolpate pollen, is transitional between the upper part of Zone II and the Patuxent Formation. If any hiatus is present between the Patuxent and Patapsco Formations, it is not indicated by the pollen and spore assemblages. The work of Brenner is in fact indicative of continuous deposition from the Patuxent into the Patapsco. Some new forms were introduced during Patapsco time, but, in relation to the total known flora, these are few.

The beds exposed on Elk Neck show a lithologic gradation between the Patapsco Formation and what some workers have referred to as the Raritan Formation. The microfossil floras of these beds also display a gradation (see also the treatment of these floras by Doyle, 1969). The lowest sample (11071–A), which was obtained from definite Patapsco, can be referred to Brenner's (1963) subzone II–B. Included in the lowest Elk Neck assemblage are: *Taurocusporites segmentatus* Stov., *Granabivesiculites*, and *Rugubivesiculites*, as well as three species of tricolpate dicotyledonous pollen. The striate schizaeaceous spores are also diverse and contain numerous species that have not been found in the Raritan Formation.

Sample 11071–B, which is also from the Patapsco, has a fern-gymnospermous flora that is also allied to that of Patapsco assemblages elsewhere in Maryland. The dicotyledonous flora, however, is notably richer than that of Brenner's subzone II–B. Sample 11071–B has five tricolpate species, including *Psilatricolpites* sp. of Brenner (1967) and one tricolporate species; no tricolporates are known from subzone II–B. Sample 11071–C contains four tricolpate and two tricolporate species, including "*Tricolporopollenites*" *triangulus*.

Our highest Elk Neck sample (11069) was obtained from beds that are in the transitional interval between definite Patapsco and the so-called Raritan (J. P. Owens, oral commun., Jan. 1968); older geologic maps place this sample in the Raritan. The dicotyledonous flora from this sample is richer than that of the lower Elk Neck samples; seven tricolpates and two tricolporates, including "*Tricolporopollenites*" *triangulus* (fig. 2, *r*) are present. One of the tricolpates represents "*Striatopollis sarstedtensis*" of Groot and Groot (1962) (fig 2, *s*; our material compares well with that from the Portuguese Cenomanian but not with typical *S. sarstedtensis* Krutzsch, which has all striae emanating from the poles). The fern and gymnospermous flora, however, are of the Patapsco type. Ten species of striate schizaeaceous spores are known, including some (for example, fig. 2, *w*) that are typical of the Potomac Group and have not been found in the Raritan.

The Elk Neck pollen and spore assemblages indicate that the so-called Raritan of Maryland probably represents the uppermost part of the Patapsco Formation. Because of the numerous triaperturate dicotyledonous species (particularly the presence of tricolporates) this uppermost Patapsco is considered to represent earliest Cenomanian. The Patapsco Formation, therefore, is of both Albian (Early Cretaceous) and Cenomanian (Late Cretaceous) Age.

Sample 11063 is from beds from which Berry (1911a) obtained a small megafossil flora (11 species) near Camden, N.J. Berry considered this assemblage to be from the upper part of the Raritan, but neither the field relations (J. P. Owens, oral commun., Jan. 1968) nor the megafossil flora indicate such a stratigraphic assignment. The 11 triaperturate pollen species include eight tricolpates and three tricolporates; one of the tricolporates is "*Tricolporopollenites*" *triangulus*. All the dicotyledons are thus of simple construction as in the uppermost Patapsco at Elk Neck, and at least six of the Camden dicotyledonous species are also represented in the uppermost Elk Neck sample. Notable as well is the presence of a diverse schizaeaceous flora; some of the species (for example, figs. 2, *v*, *x*) have been found in definite Patapsco but not in the type Raritan of northern New Jersey. The palynologic data indicate that the beds from which sample 11063 was obtained are correlative with the uppermost Patapsco at Elk Neck (the Raritan of some authors).

FIGURE 2.—Pollen and spores from the Potomac Group and Raritan Formation. × 1,000.

a, b. Atlantopollis sp. Loc. 11060, South Amboy fire clay, Raritan Formation.

c–g, o. Complexiopollis spp. *c–f*, loc. 11060, South Amboy fire clay; *g, o*, Woodbridge clay; Raritan Formation.

h, j–n. Tricolporites spp. *h, j, l–n*, loc. 11060, South Amboy fire clay; *k*, Woodbridge clay; Raritan Formation.

i, Tricolpites sp. Loc. 11060, South Amboy fire clay.

p, u. Dicotetradites sp. Loc. 11069, Patapsco Formation.

q. Tricolporites sp. Loc. 11069, Patapsco Formation.

r. "*Tricolporopollenites*" *triangulus* Groot, Penny, and Groot. Loc. 11069, Patapsco Formation.

s. "*Striatopollis sarstedtensis*" of Groot and Groot, 1962. Loc. 11069, Patapsco Formation.

t. Rugubivesiculites sp. Loc. 11069, Patapsco Formation.

v–x. Cicatricosisporites spp. *v*, loc. 11087–A; *w*, loc. 11071–C; *x*, loc. 11070; Patapsco Formation.

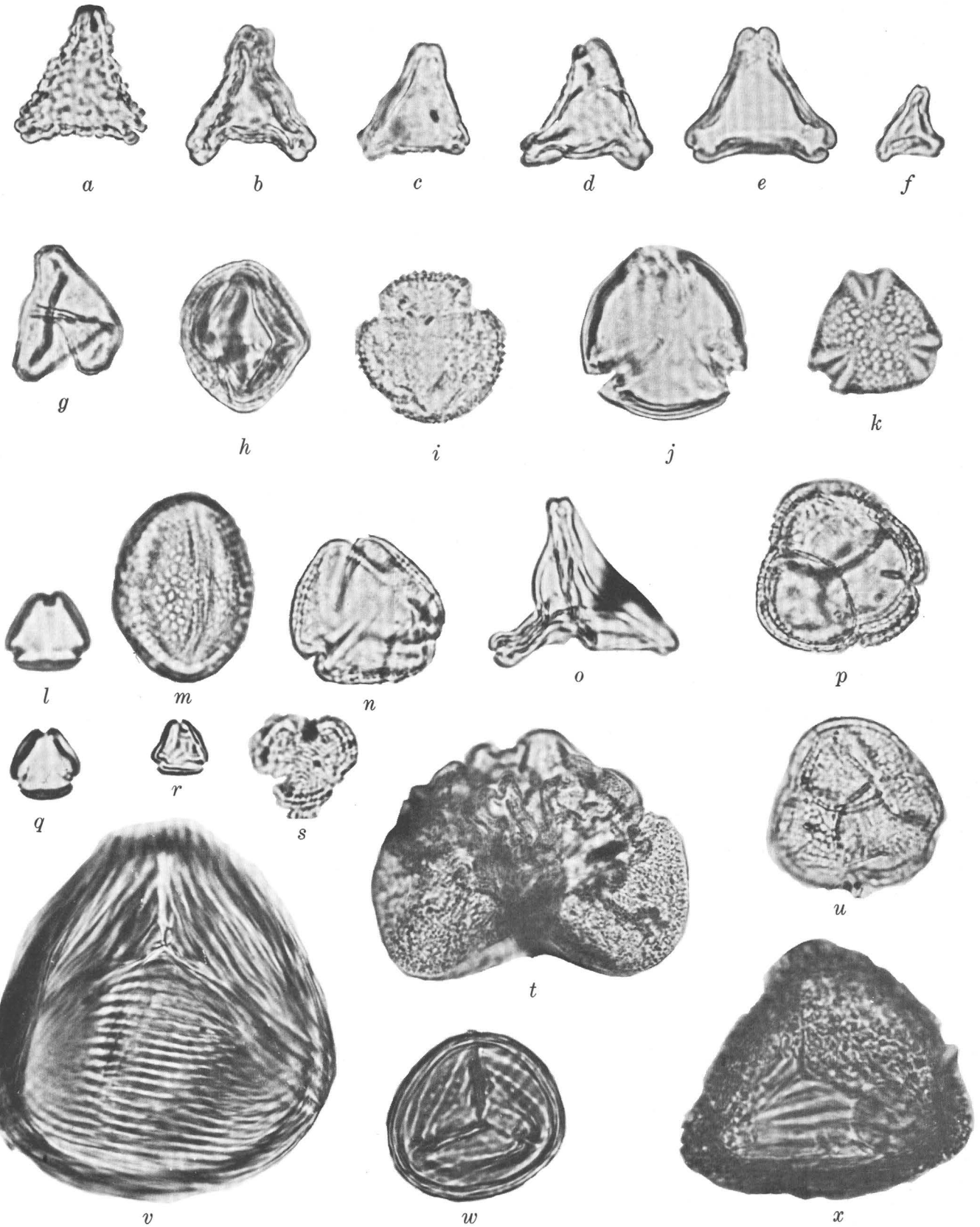

FIGURE 2.

The Camden area is, significantly, included by Owens, Minard, and Sohl (1968) in the Salisbury embayment, which was—during the Cretaceous—distinct from the Raritan embayment of northern New Jersey. We have not seen any samples of the so-called Raritan in the Salisbury embayment that are as young as the samples of the type Raritan Formation from the Raritan embayment. We suggest, therefore, that the "Raritan" of the Salisbury embayment represents the uppermost Patapsco and that the Raritan Formation is lacking in the Salisbury embayment.

Raritan Formation

Assemblages of plant microfossils have been described from the Raritan Formation (Raritan fire clay, Woodbridge clay, and South Amboy fire clay) by Groot, Penny, and Groot (1961) and Kimyai (1966). Our analysis of samples from the Woodbridge clay and definite South Amboy fire clay indicates that these samples differ strikingly in composition from the sample from the Amboy stoneware clay (the uppermost part of the Raritan) and a sample that is, on field evidence, either from the Amboy stoneware clay or South Amboy fire clay.

The microfossil flora of the basal part of the Raritan Formation of northern New Jersey—the Raritan fire clay—is known only from the work of Groot, Penny, and Groot (1961). Their one Raritan fire clay sample contains only six triaperturate species, but included are both tricolpates and tricolporates. A diverse assemblage of striate schizaeaceous spores was not reported, however, indicating that the Raritan fire clay probably is slightly younger than the uppermost Patapsco.

The samples from the Woodbridge clay and South Amboy fire clay are similar to one another in having fewer (an average of five) species of striate schizaeaceous spores in contrast to the considerable diversity of this spore type (an average of 12 species in the Patapsco, for example) lower in the section. These samples also contain about the same diversity of triaperturate pollen as the samples reported on by Groot, Penny, and Groot (1961) and Kimyai (1966) for the Woodbridge and South Amboy. Our two Woodbridge samples have 14 and 12 species (a total of 18 for the two samples and a total of 21 including previous workers' samples from the Woodbridge) of triaperturate pollen; of these 21, five are triporate and are members of the Normapolles group. The South Amboy sample is richer (21 species) in triaperturate forms than any individual Woodbridge clay sample. Including the species illustrated by Groot, Penny, and Groot (1961), at least 30 triaperturate species are known from the South Amboy fire clay. Most of the triporate species, however, represent *Atlantopollis* or *Complexiopollis*, which are two of the characteristic Normapolles genera in the European Cenomanian; these two genera are, however, not restricted to the Cenomanian. *Atlantopollis* is known in Europe in beds of late Cenomanian or younger age, as is the "*Latipollis*" type of *Complexiopollis* (fig. 2, *g*).

Groot, Penny, and Groot (1961) concluded that the South Amboy fire clay was probably of Turonian Age. Although the known age ranges of the South Amboy fire clay Normapolles genera are permissive for such an age assignment, they are not indicative. Both *Atlantopollis* and *Complexiopollis* are known in the Woodbridge clay, which, on the basis of marine mollusks, is of mid-Cenomanian Age (N. F. Sohl, oral commun., Jan. 1968). The South Amboy flora, although somewhat richer in triaperturate species, is similar to the Woodbridge flora, and we think that there is little age difference between the two floras. The pollen flora of the Coker Formation, the lower of two formations in the Tuscaloosa Group of Alabama, contains one additional Normapolles genus, *Tenerina*, as well as *Atlantopollis* and *Complexiopollis*. In numbers of species of the Normapolles group, the Coker assemblage is more like the South Amboy than the Woodbridge assemblage. Groot, Penny, and Groot (1961) and Leopold and Pakiser (1964) considered the Coker in Alabama to be of Turonian Age, but the foraminiferal and molluscan evidence indicates that the Coker in Alabama is of late Cenomanian Age (Applin, 1964; Sohl, 1964). All Coker Normapolles genera are indeed also known in the later Cenomanian of Europe, and there is thus no valid reason for considering the lower part of the Tuscaloosa to be of other than later Cenomanian Age and approximately correlative with the South Amboy fire clay.

The age assignment by Doyle (1969) of the Woodbridge clay to the latest Cenomanian is probably not justified by either the mollusks or pollen. Sohl, as stated previously, considers the mollusks from the Woodbridge to be of probable middle Cenomanian, and not of latest Cenomanian, Age. The fact that Normapolles types are not known from the middle Cenomanian microfossil floras, such as the Woodbine of Oklahoma or the so-called Dakota of Minnesota, indicated to Doyle (1969, p. 16) that the Woodbridge "* * * is probably younger than most of the Middle Cenomanian * * *". Areas such as Oklahoma and Minnesota would probably have received most of their pollen rain and sediments (including pollen) from the region west of the epicontinental sea and thus do not represent the Normapolles province. The appearance (or lack) of Normapolles in such areas is irrelevant to the Atlantic Coastal Plain sequence.

MAGOTHY FORMATION

Old Bridge Sand Member

Our knowledge of the palynology of the Old Bridge Sand Member, which heretofore has been considered to be part of the Raritan, is largely based on the work of Doyle (1969). Although Doyle's sample came from beds stratigraphically intermediate between the South Amboy fire clay and Amboy stoneware clay, it is uncertain whether the samples represent the now largely buried Old Bridge Sand Member (J. P. Owens, oral commun., April 1969). Doyle (1969) illustrates only two grains from the presumed Old Bridge. One species represents, as Doyle notes, the genus *Pseudoplicapollis*, which first appears in Europe in the middle Turonian. As shown later, the oldest occurrence of this genus elsewhere in North America is in the upper McShan assemblage, which, largely on meager stratigraphic evidence, has been considered to be of Coniacian Age (Murray, 1961). The second illustrated Old Bridge species is the one that we refer to *Heidelbergipollis* (fig. 4, *q*), which first appears in Europe in the early half of the Santonian. Although Doyle (1969) questions whether this type of grain represents a Normapolles type, the complicated and thickened pore structure indicates that Góczán and others (1967) were probably correct in considering *Heidelbergipollis* to be a member of the Normapolles group. A sample obtained from the same pit as Doyle's contains grains of the Santonian or younger *Praebasopollis*. The significant point, however, is that both illustrated Old Bridge genera occur in the Amboy stoneware clay and are unknown in the South Amboy and older Raritan assemblages. We suggest that the unit that Doyle sampled represents the basal sand of the Magothy Formation.

Amboy stoneware clay

Sample 11056, from the Amboy stoneware clay, and sample 11061, from either the Amboy stoneware clay or the South Amboy fire clay, have markedly similar dicotyledonous pollen floras; about 75 percent of the 68 triaperturate pollen species are found in both samples. Previously described Normapolles genera, with their known lowest occurrences in Europe, that are present in the two samples are listed in figure 3, and are illustrated in figure 4. At least 10 additional Normapolles genera are thought to be represented, but these are apparently new. All are morphologically similar to *Plicapollis* or *Pecakipollis* or closely related genera. Except for *Semioculopollis*, the more morphologically bizarre Normapolles genera—for example *Endopollis*, *Extratriporopollenites*, and *Oculopollis*—are lacking, but these genera are typically unknown or rare in any North American Cretaceous pollen flora. The known stratigraphic ranges in Europe of the previously described Normapolles genera that occur in the Amboy stoneware clay indicate that this unit is no older than Senonian and that the lower age limit is probably Santonian. The palynologic and molluscan evidence on the age of the overlying Morgan and Cliffwood beds indicates that the Amboy stoneware clay is probably older than Campanian; the available evidence, therefore, indicates that the Amboy stoneware clay is probably of Santonian Age.

Morgan and Cliffwood beds

The six samples from the Morgan and Cliffwood beds are very similar to one another in dicotyledonous pollen content. These represent a sampling of the beds overlying the Amboy stoneware clay. The number of triaperturate species in individual samples varies from 42 to 57, which is about the same as in the Amboy stoneware clay samples. The total of 71 and 81 triaperturate pollen species in the Morgan beds and Cliffwood beds, respectively, represents a moderate increase over the Amboy stoneware flora. This increase is due primarily to an increase in species that have tricolpate and tricolporate grains; the number of triporate species in fact decreases.

The flora from the Morgan beds (fig. 5) has an especially strong similarity in the composition of the Normapolles flora to the Amboy stoneware flora. Except for *Semioculopollis*, all the Amboy stoneware genera of the Normapolles group also occur in the Morgan flora. The Cliffwood flora, however, lacks some Normapolles

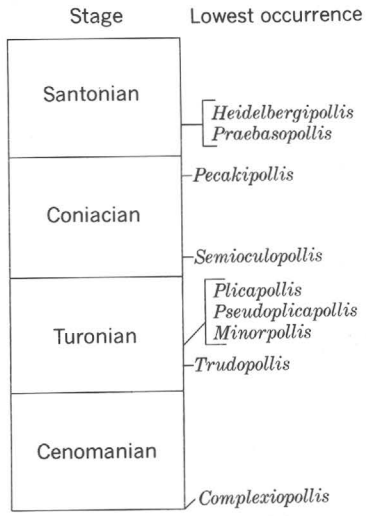

FIGURE 3.—Lowest occurrences in Europe of previously described Normapolles genera represented in the Amhoy stoneware clay.

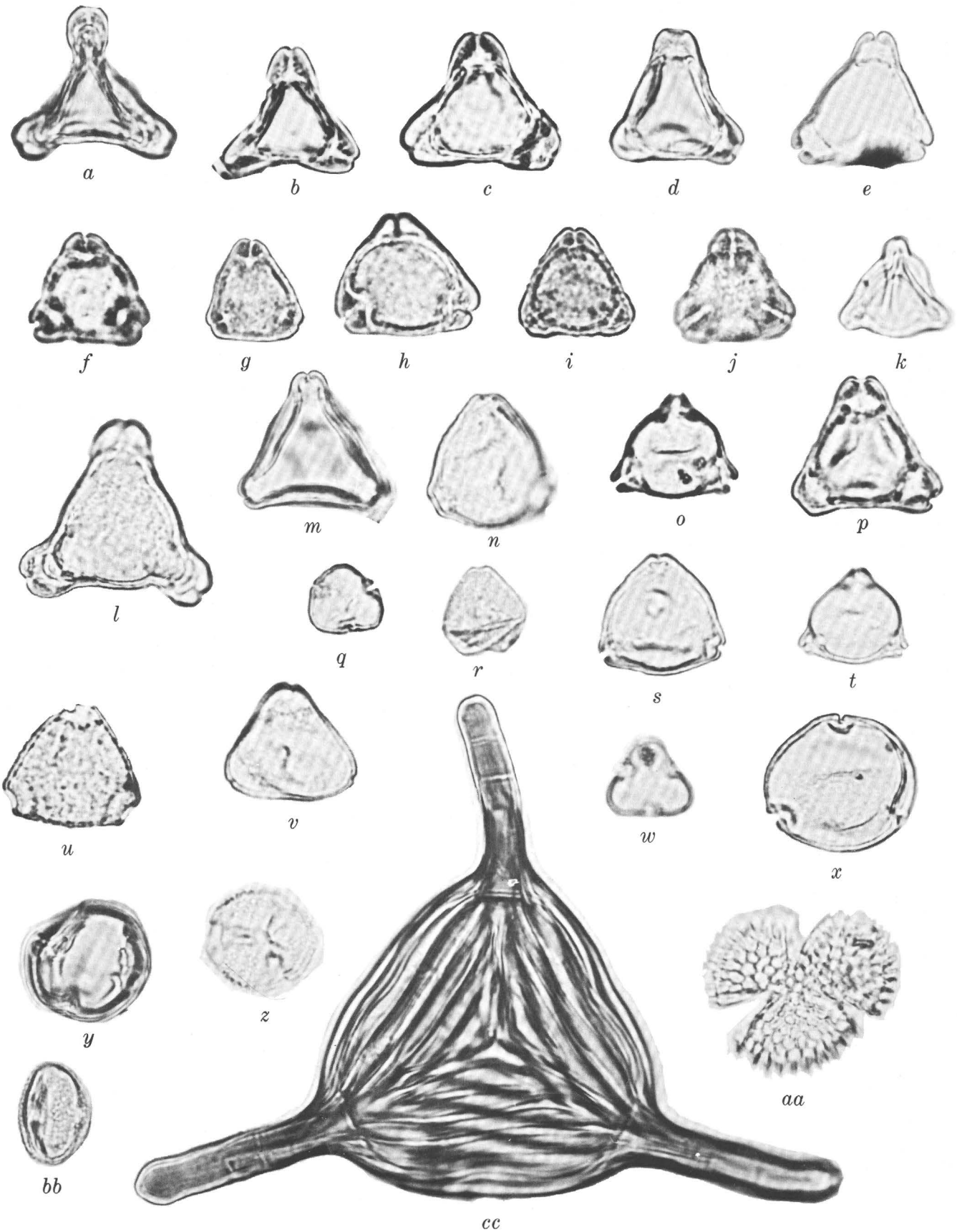

FIGURE 4.

genera that are found lower in the section, for example, *Heidelbergipollis*, *Pecakipollis*, and several of the new Normapolles genera have not been found in the Cliffwood samples. In addition, the number of species within genera such as *Plicapollis* and *Pseudoplicapollis* is less in the Cliffwood than in the Morgan flora, whereas the number of tricolpate and tricolporate species that have complicated sculpture is greater in the Cliffwood. One of these tricolpate species (fig. 5, *aa*) belongs to a genus that has previously been found in Campanian and younger beds in the Gulf Coastal Plain (Tschudy, 1970). Conifer grains, which typically form less than 25 percent of the pollen counted in the Amboy stoneware clay and Morgan beds, account for over half the specimens in the Cliffwood beds. The Morgan flora, in its strong similarity to the Amboy stoneware, is probably of Santonian Age. The Cliffwood flora, however, contains some forms that have previously been found only in Campanian or younger rocks. The molluscan fauna from the base of the Cliffwood beds is of late Santonian or early Campanian Age (N. F. Sohl, oral commun., Jan. 1968), and thus is permissible evidence for considering the Cliffwood flora to be of Campanian Age. The fauna of the overlying Merchantville is also of early but not earliest Campanian Age (N. F. Sohl, oral commun., Jan. 1968); all the triaperturate pollen species recorded from the Merchantville by Gray and Groot (1966) also occur in the upper Magothy flora.

FIGURE 4.—Pollen and spores from the Amboy stoneware clay of the Magothy Formation. × 1,000.

a. *Praebasopollis* sp. Loc. 11056.
b, c. New genus A (aff. *Praebasopollis*). Loc. 11061.
d. New genus *B* (aff. *Praebasopollis*). Loc. 11061.
e. *Pecakipollis* sp. Loc. 11061.
f–h. *Trudopollis* spp. Loc. 11061.
i, j. *Semioculopollis* sp. Same grain, loc. 11061.
k. *Pseudoplicapollis* sp. Loc. 11061.
l. New genus C (aff. *Praebasopollis*). Loc. 11061.
m. New genus D (aff. *Megatriopollis*). Loc. 11061.
n. New genus E (aff. *Neotriangulipollis*). Loc. 11061.
o. New genus F (aff. *Minorpollis*). Loc. 11061.
p. New genus G (aff. *Plicapollis*). Loc. 11056.
q. *Heidelbergipollis* sp. Loc. 11061.
r. *Complexiopollis* sp. Loc. 11061.
s. New genus H (aff. *Primipollis*). Loc. 11061.
t. *Minorpollis* sp. Loc. 11061.
u. New genus I (aff. *Neotriangulipollis*). Loc. 11061.
v. New genus J (aff. *Vacuopollis*). Loc. 11056.
w. *Intratriporopollenites* sp. Loc. 11061.
x–z, bb. *Tricolporites* spp. Loc. 11061.
aa. *Tricolpites* sp. Loc. 11061.
cc. *Appendicisporites tricuspidatus* Weyl. and Greif. Loc. 11056.

The pollen floras of the Amboy stoneware clay, Morgan and Cliffwood beds of the Magothy Formation, and the Merchantville Formation represent a continuum that appears to show only a gradual change in floristic composition. This continuum probably began in the Santonian (Amboy stoneware and Morgan floras) and continued into the Campanian (Cliffwood and Merchantville floras). The fact that the Old Bridge Sand Member has floras that are allied to that of the Magothy Formation indicates that the Old Bridge Sand Member should no longer be considered a member of the Raritan Formation. It is hereby reassigned as the basal member of the Magothy Formation.

The age relationship of the Magothy Formation of northern New Jersey, which has supplied the samples discussed in this report, to the Magothy at its type section in Maryland is not certain. Stover (1964), however, illustrates a specimen of *Trisectoris stoveri* (our fig. 5, *aa*) from the type Magothy; this genus we have only found in the Cliffwood beds and younger formations. The type Magothy thus probably includes age equivalents of the Cliffwood beds.

Correlations with the pre-Selma rocks of Alabama

As noted previously, the Tuscaloosa Group of Alabama contains some pollen assemblages that indicate an approximate correlation with the South Amboy fire clay. The pollen assemblage that particularly indicates such a correlation is from locality D1109–7 (see Leopold and Pakiser, 1964, for locality data), which is from the middle of the lower (Eoline) member of the Coker Formation of the Tuscaloosa. Mollusks of late Cenomanian Age occur stratigraphically above this pollen assemblage (Sohl, 1964). The upper formation—the Gordo—of the Tuscaloosa Group contains a Normapolles assemblage that is generically similar to that of the Eoline as well as to the assemblage from the South Amboy. Some of the Normapolles species of the Gordo, however, are unknown from either the Eoline or the South Amboy; the Gordo assemblage, moreover, is the only Tuscaloosa assemblage dominated by *Rugubivesiculites*. The meager data indicate that the Gordo is palynologically distinct from the South Amboy and the Eoline assemblages. Whether the Gordo is latest Cenomanian or Turonian cannot be determined at present.

413-504 O - 71 - 4

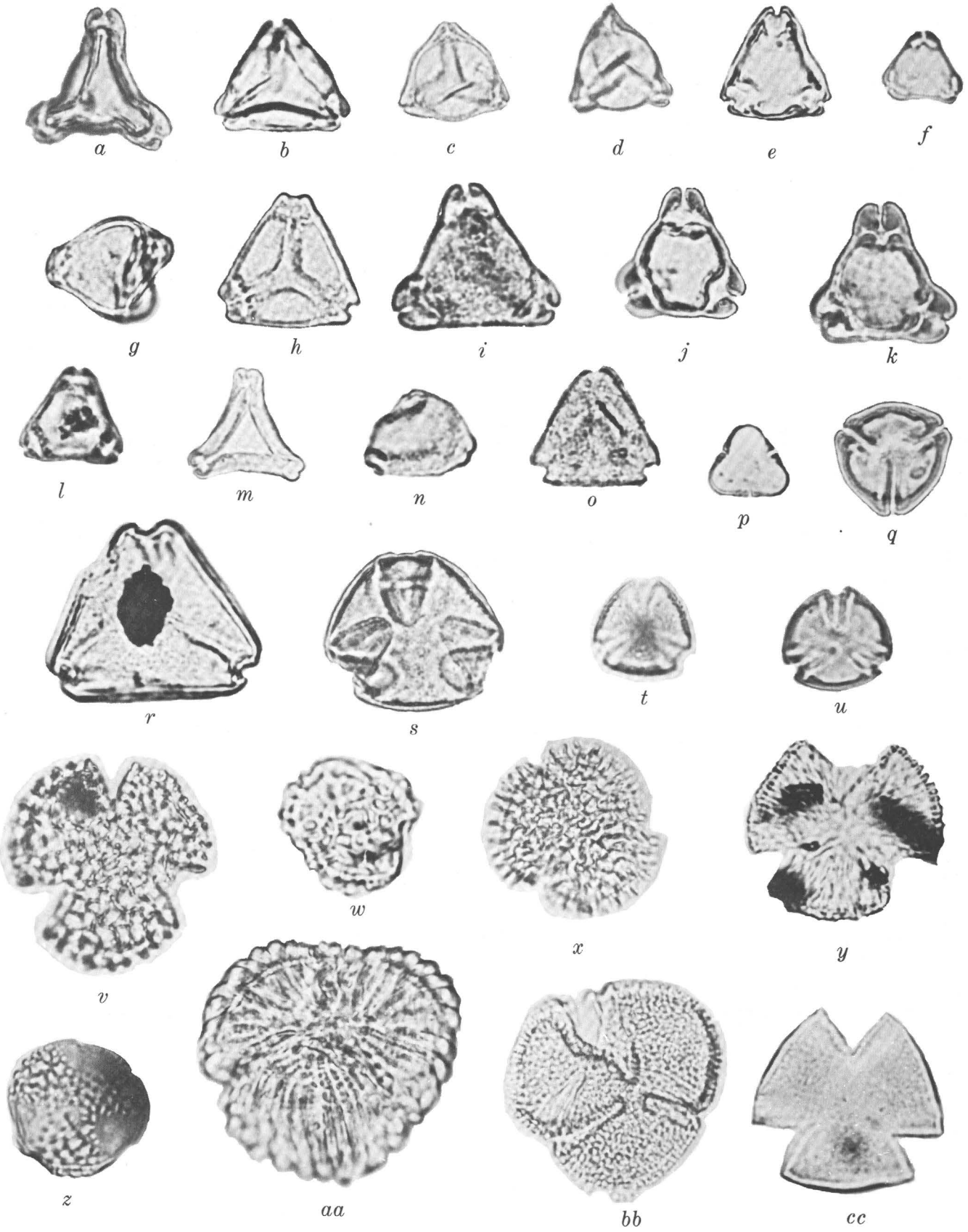

FIGURE 5.

Pollen assemblages were also reported by Leopold and Pakiser (1964) from parts of the McShan Formation, which unconformably overlies the Tuscaloosa, and the Eutaw Formation, which is probably conformable on the McShan. All the McShan and Eutaw assemblages were, for purposes of correlation, treated as a single assemblage by Leopold and Pakiser (1964) and were considered to be of Turonian and pre-Magothy age. The McShan assemblages came from two widely separated stratigraphic levels: (1) D1456–5 and 6, which are in the basal half of the McShan, and (2) D1456–4, which is near the top of the formation. Both lower assemblages contain fewer (7 and 8) triaperturate species than the upper assemblage, which has 18. The Normapolles flora of the lower McShan contains only pollen of the *Vacuopollis* type, whereas the upper McShan assemblage contains *Complexiopollis*, *Pseudoplicapollis*, *Vacuopollis*, and our new genera E (fig. 4, *n*) and H (fig. 4, *s*). Although *Complexiopollis*, might be expected in the lower McShan (the genus is represented in both older and younger beds in this area), we think that the greater diversity of the Normapolles group in the upper than in the lower McShan is significant. In the paucity of Normapolles and other triaperturate types and in the abundance of *Rugubivesiculites* the lower McShan assemblage is similar to Gordo assemblage, although the occurrence of the *Vacuopollis* type in the lower McShan indicates a younger age for this assemblage. We suggest that the lower McShan assemblage may be of later Turonian Age.

The age of the upper McShan assemblage we tentatively consider to be Coniacian. Lacking in the upper McShan assemblage are such characteristic Amboy stoneware genera as *Praebasopollis* and *Trudopollis*. This lack also characterizes the known Eutaw assemblages, which came from the middle of the formation. The Eutaw assemblages, however, contain additional Normapolles types such as *Pecakipollis* and our new genus M (fig. 5, *m*). Both the upper McShan and middle Eutaw assemblages are, therefore, recognizably older than the Amboy stoneware and hence pre-middle Santonian. The middle Eutaw assemblage is similar to that of the Old Bridge Sand Member (basal Magothy) and probably of early Santonian Age, and by inference the upper McShan is of probable Coniacian Age (fig. 6).

PHYTOGEOGRAPHIC CONSIDERATIONS

Góczán and others (1967) concluded that eastern North America was, during the Late Cretaceous, part of the Normapolles province. This conclusion would in turn indicate that there was not a major barrier to plant migration between Europe and eastern North America during the Late Cretaceous. Three of the four Normapolles genera present in the European Cenomanian have also been recorded from the Cenomanian of eastern North America, which indicates that during all or some part of the Cenomanian these two areas were not separated by any significant migrational barrier. After the

FIGURE 5.—Pollen from the Morgan beds and Cliffwood beds of the Magothy Formation. × 1,000.

a. *Praebasopollis* sp. Loc. 11068, Morgan beds.
b–d. *Pseudoplicapollis* spp. *b*, loc. 11067–A; *d*, loc. 11067–B; Cliffwood beds. *c*, loc. 11057, Morgan beds.
e. *Primipollis* sp. Loc. 11068, Morgan beds.
f. New genus K. Loc. 11057, Morgan beds.
g. *Complexiopollis* sp. Loc. 11067–B, Cliffwood beds.
h. *Plicapollis* sp. Loc. 11068, Morgan beds.
i. New genus L (aff. *Oculopollis*). Loc. 11068, Morgan beds.
j, k. *Trudopollis* spp. Loc. 11057, Morgan beds.
l. *Neotriangulipollis* sp. Loc. 11067–B, Cliffwood beds.
m. New genus M (aff. *Interpollis*). Loc. 11062–A, Cliffwood beds.
n. New genus N (aff. *Quedliniburgipollis*). Loc. 11062–B, Cliffwood beds.
o. *Proteacidites*? sp. Loc. 11068, Morgan beds.
p. *Intratriporopollenites* sp. Loc. 11067–B, Cliffwood beds.
q, r, t, u. *Tricolporites* spp. *q*, loc. 11062–A; *r*, loc. 11067–A; *u*, loc. 11067–B; Cliffwood beds. *t*, loc. 11057, Morgan beds.
s, v–cc. *Tricolpites* spp. *s, w, aa*, loc. 11062–B; *cc*, loc. 11067–B; Cliffwood beds. *v, y, bb*, loc. 11057; *x, z*, loc. 11068; Morgan beds.

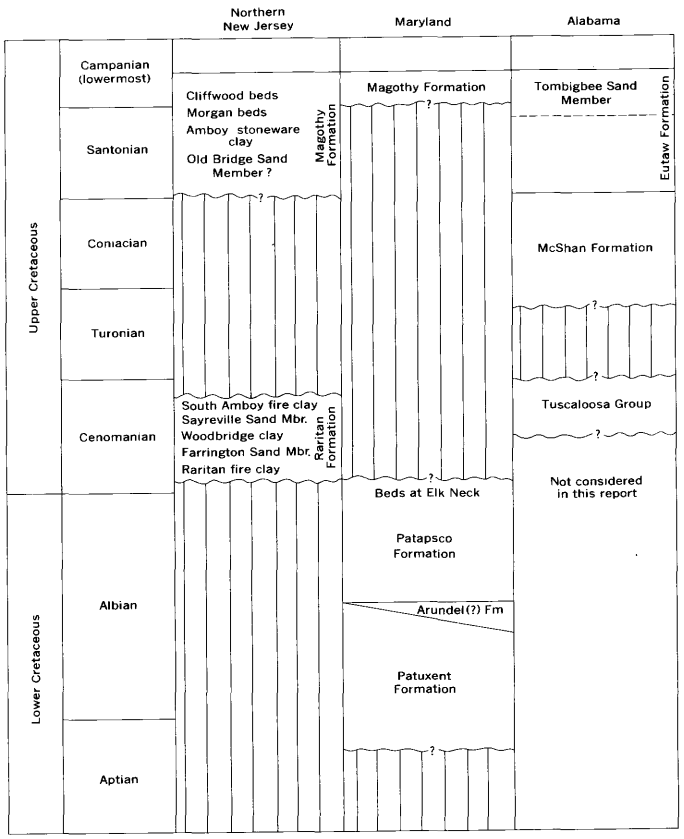

FIGURE 6.—Correlation of some Cretaceous formations of the Eastern United States.

Cenomanian, however, the similarity is actually very weak, despite the presence and diversity of the Normapolles group in both areas. The North American Turonian floras lack some of the fundamental Normapolles types, such as *Trudopollis* and *Plicapollis*, which are present in Europe in the middle Turonian. Apparently, the *Trudopollis* stock did not arrive in North America until the Coniacian or Santonian, and the *Plicapollis* stock arrived in the Coniacian. The American Turonian appears to contain only two Normapolles stocks: the presumably primitive *Complexiopollis* stock and the *Vacuopollis* stock. This is in striking contrast to the European Turonian, when the *Trudopollis*, *Plicapollis*, and *Oculopollis* stocks first appear; even more significant is the lack in North America of the bizarre *Emscheripollis*, *Lusatipollis*, and *Pflugipollis*.

The difference between Europe and North America in pollen floras is even more striking during the Santonian. The North American floras, although having a diversity of Normapolles genera, have almost none of the morphologically bizarre genera found in Europe. The North American Normapolles genera are mostly members of the *Plicapollis*, *Vacuopollis*, and *Trudopollis* stocks, and the majority of these American genera are unknown in Europe. Even so, the bizarre members of these stocks (*Piolencipollis*, *Santonipollis*, and *Pompeckjoidaepollenites*) have not been found in North America. Indeed, the only morphologically bizarre genera yet known from eastern North America are *Semioculopollis and Oculopollis*. Groot, Penny, and Groot (1961) recorded *Quedliniburgipollis* from the Magothy Formation, and we have found grains that match the description and illustration of their species; these grains, however, lack the ektexinal extension that covers the pore, which is a diagnostic feature of the genus. In the European Santonian, in contrast, the *Extratriporopollenites*, *Basopollis*, *Papillopollis*, and *Endopollis* stocks are well represented. Of the 44 Normapolles genera described from the pre-Campanian of Europe, only 12 are known in the North American pre-Campanian, and 3 of these are present in the Cenomanian of both areas.

In addition to the Normapolles group, the North American Cretaceous has distinctive groups not found in the European Cretaceous. For example, "*Intratriporopollenites*", which does not appear in Europe until the Tertiary, is present in the Amboy stoneware, Morgan, and upper Magothy floras. The tricolpate and tricolporate floras in the North American Upper Cretaceous are consistently more diverse than in the European Upper Cretaceous.

The evidence appears, therefore, to indicate that there was little floristic interchange between Europe and eastern North America after the Cenomanian and until the Tertiary. The appearance of genera such as *Semioculopollis* in North America can be thought of as the result of long-distance dispersal. The other Normapolles genera that were shared by Europe and eastern North America could well be the result of parallel evolution from the three basic stocks that, also through long-distance dispersal, arrived in North America from Europe. These concepts have an important bearing on the use of palynology to correlate between Europe and North America. If, as Góczán and others (1967) suggested, Europe is the center of evolution for the Normapolles group, then the first appearance of a genus such as *Semioculopollis* in North America must be at least slightly younger than the first appearance of the genus in Europe.

LOCALITY DATA

Locality numbers are registered in the U.S. Geological Survey Paleobotany Catalog, Washington, D.C. Letters denote progressively higher samples at the same locality.

11046. Lat 40°27.0′ N., long 74°17.5′ W., South Amboy quadrangle, New Jersey. Collector J. P. Owens. Amboy stoneware clay.

11057. Lat 40°26.0′ N., long 74°17.7′ W., South Amboy quadrangle, New Jersey. Collector J. P. Owens. Morgan beds.

11058. Lat 40°27.1′ N., long 74°21.6′ W., South Amboy quadrangle, New Jersey. Collector J. P. Owens. South Amboy fire clay or Woodbridge clay.

11059. Lat 40°28.2′ N., long 74°21.2′ W., South Amboy quadrangle, New Jersey. Collector J. P. Owens. Woodbridge clay.

11060. Lat 40°28.0′ N., long 74°19.0′ W., South Amboy quadrangle, New Jersey. Collector J. P. Owens. South Amboy fire clay.

11061. Lat 40°25.4′ N., long 74°21.7′ W., South Amboy quadrangle, New Jersey. Collector J. P. Owens. South Amboy fire clay or Amboy stoneware clay.

11062–A, –B. Lat 40°59.2′ N., long 75°1.5′ W., Camden quadrangle, New Jersey. Collector J. P. Owens. Cliffwood beds.

11063. Lat 40°59.3′ N., long 75°2.3′ W., Camden quadrangle, New Jersey. Collector J. P. Owens. Raritan Formation.

11067–A, –B. Lat 40°26.8′ N., long 74°12.6′ W., Keyport quadrangle, New Jersey. Collector J. P. Owens. Cliffwood beds.

11068. Lat 40°27.7′ N., long 74°16.7′ W., South Amboy quadrangle, New Jersey. Collector J. P. Owens. Morgan beds.

11069. Lat 39°29.2′ N., long 75°59.8′ W., Earleville quadrangle, Maryland. Collector J. P. Owens, Uppermost Patapsco.

11070. Lat 39°35.4′ N., long 76°56.9′ W., North East quadrangle, Maryland. Collector J. P. Owens. Patapsco Formation.

11071–A, –B, –C. Lat 39°27.5′ N., long 76°0.7′ W., Spesutie quadrangle, Maryland. Collector J. P. Owens and J. A. Wolfe. Patapsco Formation.

11072. Lat 39°31.4′ N., long 76°11.2′ W., Aberdeen quadrangle, Maryland. Collector J. P. Owens. Patapsco Formation.

11074. Lat 39°35.2′ N., long 76°5.3′ W., Havre de Grace quadrangle, Maryland. Collector J. P. Owens. Potomac Group.

11076. Lat 39°35.4′ N., long 76°3.9′ W., Havre de Grace quadrangle, Maryland. Collector J. P. Owens. Potomac Group.

11077. Lat 39°29.0′ N., long 76°15.3′ W., Edgewood quadrangle, Maryland. Collector J. P. Owens. Patapsco Formation.

11087–A, –B, –C. Lat 39°28.8′ N., long 76°15.5′ W., Edgewood quadrangle, Maryland. Collector J. P. Owens. Patapsco Formation.

REFERENCES

Applin, E. R., 1964, A microfauna from the Coker Formation, Alabama: U.S. Geol. Survey Bull. 1160–D, p. 65–70.

Barksdale, H. C., Johnson, M. E., Schaefer, E. J., Baker, R. C., and DeBuchananne, G. D., 1943, The ground-water supplies of Middlesex County, N.J.: New Jersey Water Policy Comm. Spec. Rept. 8, 160 p.

Bascom, Florence, and Miller, B. L., 1920, Description of the Elkton and Wilmington quadrangles: U.S. Geol. Survey Geol. Atlas Folio 211.

Berry, E. W., 1910, The evidence of the flora regarding the age of the Raritan Formation: Jour. Geology, v. 18, p. 252–258.

——— 1911a, The flora of the Raritan formation: New Jersey Geol. Survey Bull. 3, 233 p.

——— 1911b, The Lower Cretaceous floras of the world *in* Lower Cretaceous: Maryland Geol. Survey, p. 99–151.

Brenner, G. J., 1963, The spores and pollens of the Potomac Group of Maryland: Maryland Dept. Geology, Mines, and Water Resources Bull. 27, 215 p.

——— 1967, Early Angiosperm pollen differentiation in the Albian to Cenomanian deposits of Delaware (U.S.A.), *in* Palaeophytic and Mesophytic palynology—International Conference Palynology, 2d, Utrecht, 1966: Rev. Paleobotany and Palynology, v. 1, nos. 1–4 (spec. vol.), p. 219–227.

Couper, R. A., 1964, Spore-pollen correlation of the Cretaceous rocks of the northern and southern hemispheres: Soc. Econ. Paleontologists and Mineralogists Spec. Pub. 11, p. 131–142.

Dorf, Erling, 1952, Critical analysis of Cretaceous stratigraphy and paleobotany of the Atlantic Coastal Plain: Am. Assoc. Petroleum Geologists Bull., v. 36, p. 2161–2184.

Doyle, J. A., 1969, Cretaceous angiosperm pollen of the Atlantic Coastal Plain and its evolutionary significance: Arnold Arboretum Jour., v. 50, p. 1–35.

Góczán, Ferenc, Groot, J. J., Krutzsch, Wilfried, and others, 1967, Die Gattungen des "Stemma Normapolles Pflug 1953b" (Angiospermae); Neubeschreibungen und Revision europäischer Formen (Oberkreide bis Eozän): Paläontologische Abh., ser. B, v. 2, no. 3, p. 429–525.

Gray, T. C., and Groot, J. J., 1966, Pollen and spores from the marine Upper Cretaceous Formations of Delaware and New Jersey: Palaeontographica, ser. B, v. 117, p. 114–134.

Groot, J. J., and Groot, C. R., 1962, Plant microfossils from Aptian, Albian, and Cenomanian deposits of Portugal: Portugal, Serv. Geol., Comm., v. 46, p. 133–171.

Groot, J. J., Penny, J. S., and Groot, C. R., 1961, Plant microfossils and age of the Raritan, Tuscaloosa and Magothy formations of the eastern United States: Palaeontographica, v. 108, ser. B, p. 121–140.

Hughes, N. F., 1961, Geology, *in* Recent advances in science: Science Progress, v. 49, no. 193, p. 84–102.

Jordan, R. R., 1962, Stratigraphy of the sedimentary rocks of Delaware: Delaware Geol. Survey Bull. 9, 51 p.

Kimyai, Abbas, 1966, New plant microfossils from the Raritan Formation (Cretaceous) in New Jersey: Micropaleontology, v. 12, no. 4, p. 461–476.

Krutzsch, Wilfried, 1957, Sporen- und Pollengruppen aus der Oberkreide und dem Tertiär Mitteleuropas und ihre stratigraphische Verteilung: Zeitschr. angew. Geologie, v. 3, no. 11–12, p. 509–548.

——— 1959, Einige neu Formgattungen und -arten von Sporen und Pollen aus der mitteleuropäischen Oberkreide und dem Tertiär: Palaeontographica, v. 105, ser. B, no. 5–6, p. 125–155.

Kümmel, H. B., and Knapp, G. N., 1904, Part II, The stratigraphy of the New Jersey Clays, *in* Clay industry of New Jersey: New Jersey Geol. Survey Final Rept., Ser. State Geol., v. 6, p. 117–203.

Leopold, E. B., and Pakiser, H. M., 1964, A preliminary report on the pollen and spores of the pre-Selma Upper Cretaceous strata of western Alabama: U.S. Geol. Survey Bull. 1106–E, p. 71–95.

Murray, G. E., 1961, Geology of the Atlantic and gulf coastal province of North America: New York, Harper and Row Publishers, 692 p.

Owens, J. P., 1969, Coastal Plain rocks, *in* Maryland Geological Survey, The Geology of Harford County, Maryland: Baltimore, Md., Maryland Geol. Survey, p. 77–103.

Owens, J. P., Minard, J. P., and Sohl, N. F., 1968, Cretaceous deltas in the northern New Jersey Coastal Plain, Trip B, *in* Guidebook to field excursions—New York State Geological Association, 40th Annual Meeting, Flushing, N.Y., 1968: Brockport, N.Y., State Univ. Coll. Dept. Geology, p. 33–48.

Pflug, H. D., 1953, Zur Entstehung und Entwicklung des angiospermiden Pollens in der Erdgeschichte: Palaeontographica, v. 95, ser. B, no. 4–6, p. 60–171.

Singh, Chaitanya, 1964, Microflora of the Lower Cretaceous Manville Group, east-central Alberta: Research Council Alberta Bull. 15, 238 p.

Sohl, N. F., 1964, Pre-Selma larger invertebrate fossils from well core samples in western Alabama: U.S. Geol. Survey Bull. 1160–C, p. 55–64.

Steeves, M. W., 1959, The pollen and spores of the Raritan and Magothy formations (Cretaceous) of Long Island: Radcliffe Coll., Cambridge, Mass., Ph. D. thesis.

Stover, L. E., 1964, Comparison of three Cretaceous spore-pollen assemblages from Maryland and England, *in* Cross, A. T., ed., Palynology in oil exploration: Soc. Econ. Paleontologists and Mineralogists Spec. Pub. 11, p. 143–152.

Tschudy, R. H., 1970, Two new pollen genera (Late Cretaceous and Paleocene) with possible affinity to the Illiciaceae: U.S. Geol. Survey Prof. Paper 643–F, p. F1–F13.

PALEOCENE MOLLUSKS FROM THE GULF OF ALASKA TERTIARY PROVINCE—A SIGNIFICANT NEW OCCURRENCE ON THE NORTH PACIFIC RIM

By WARREN O. ADDICOTT and GEORGE PLAFKER,
Menlo Park, Calif.

Abstract.—Marine mollusks of Paleocene age occur near the base of a sequence of continental and marine strata mapped as the Kulthieth Formation in the foothills of the St. Elias Mountains, southern Alaska. The gastropod *Turritella merriami brevitabulata* Merriam and Turner indicates correlation with the upper Paleocene "Meganos Stage" of the Pacific coast of the conterminous United States. The fossils from the Malaspina district (lat 60° N.) provide evidence of the oldest marine strata thus far recorded from the Gulf of Alaska Tertiary province, the oldest previously known strata being of middle or late Eocene age. They also record the first occurrence of marine Paleocene from north of California (lat 40° N.). Accordingly, Paleocene seas were not of restricted distribution but in fact extended over broad areas along the North Pacific rim.

One of the more puzzling aspects of the paleogeographic history of the North Pacific basin has been the apparent constriction of marine deposition during the Paleocene in contrast to the widespread occurrence of marine strata of Late Cretaceous and Eocene age. Marine Eocene strata, for example, occur along the west coast of the conterminous United States, Canada, and southern Alaska, but rocks of Paleocene age have previously been reported only from low latitudes—no farther north than northern California near lat 40° N. (fig. 1).

In this paper we report the first documentation of marine strata of Paleocene age from the north Pacific margin near lat 60° N. The new record is based upon the gastropod *Turritella merriami brevitabulata* Merriam and Turner (1937). The collection was made in 1968 by George Plafker in a remote part of the rugged southern foothills of the St. Elias Mountains within the Gulf of Alaska Tertiary province (fig. 2).

STRATIGRAPHIC OCCURRENCE

The *Turritella* and indeterminate fragments of mollusks, including a nuculanid, were collected from a hard, massive sandstone near the base of a sequence of

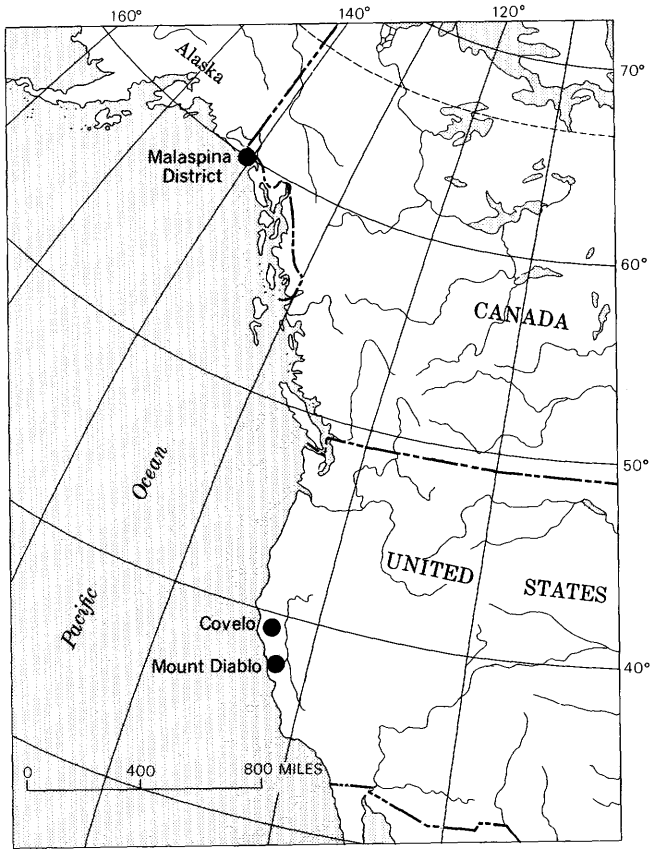

FIGURE 1.—Index map of the northeastern part of the Pacific Basin, showing Paleocene occurrences of *Turritella Merriami brevitabulata* Merriam and Turner.

U.S. GEOL. SURVEY PROF. PAPER 750-B, PAGES B48-B52

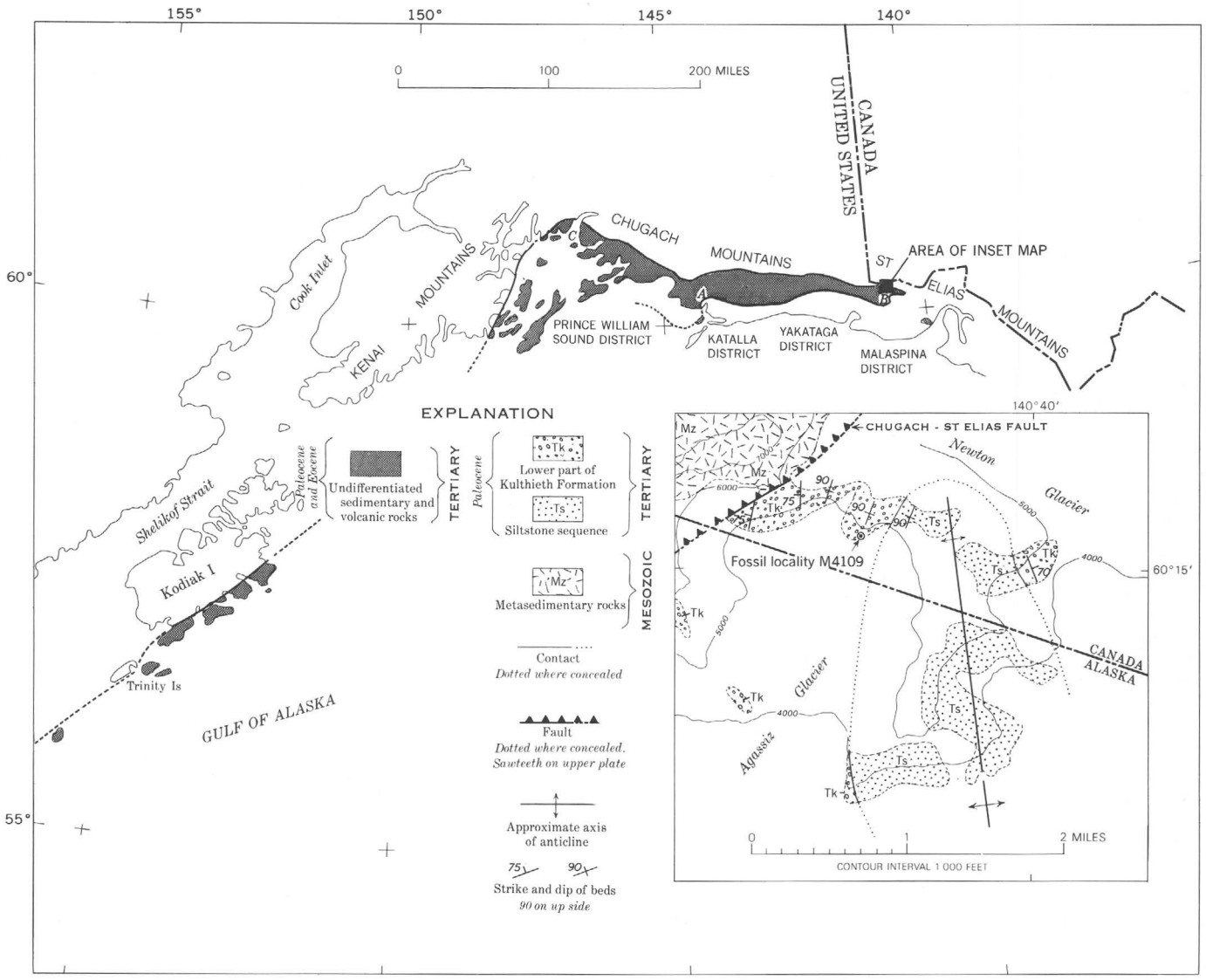

FIGURE 2.—Index map of the northern Gulf of Alaska region, showing the approximate outcrop areas of lower Tertiary rocks and localities referred to in the text.

terrestrial and marine strata mapped by Plafker and Miller (1957) as the Kulthieth Formation. The Kulthieth Formation is part of a belt of Paleogene sedimentary and volcanic rocks that fringes the margin of the Gulf of Alaska from the vicinity of Yakutat Bay westward to the Trinity Islands (fig. 2). At the fossil locality (USGS M4109), at least 3,900 feet of the Kulthieth Formation is exposed in a homoclinal section that strikes roughly north and dips between 90° and 75°, with tops to the west (fig. 2). The sequence consists predominantly of uniformly bedded, light-gray to greenish-gray, hard, arkosic sandstone, pebbly sandstone, and sandy pebble conglomerate. Interbedded with the coarse clastic rocks are subordinate amounts of reddish-brown- to orange-weathering, leaf-bearing calcareous sandstone, dark-gray siltstone, and thin beds of sheared bituminous coal.

The Kulthieth Formation is in contact to the east with a highly contorted and sheared sequence of greenish-gray-weathering, gray to dark-gray siltstone containing minor amounts of fine-grained laminated sandstone in thin beds or lenses. These rocks were mapped as an unnamed siltstone sequence by Plafker and Miller (1957). The contact between the two units is crudely conformable but is marked by crumpling and slickensiding indicative of differential fault movement between the Kulthieth Formation and the relatively incompetent siltstone sequence. The general map rela-

tionships shown in figure 2 suggest that rocks of the Kulthieth Formation are exposed on the flanks of a complex, north-south-trending anticlinorium which is cored by the siltstone sequence. Elsewhere in its outcrop area the upper part of the siltstone sequence appears to intertongue with coal-bearing rocks of the Kulthieth Formation. The bulk of the siltstone unit, which totals several thousand feet in thickness, lies stratigraphically below the Kulthieth in the Malaspina district.

The Kulthieth Formation was assigned a Paleocene(?) and Eocene age by Plafker and Miller (1957). Mainly on the basis of one specifically identifiable fossil, *Turritella uvasana sargeanti* Anderson and Hanna, they postulated that the unit was mostly of Eocene age, probably largely, if not entirely, of late Eocene age. As will be discussed subsequently, restudy of this *Turritella* indicates that it was misidentified and is in fact a species known only from rocks of middle Eocene age.

The siltstone sequence was considered by Plafker and Miller to be older than the Kulthieth Formation and younger than the Late(?) Cretaceous Yakutat Group on the basis of structural, stratigraphic, and lithologic evidence. A few poorly preserved marine mollusks subsequently collected from this unit in the Malaspina and Yakataga districts have proven to be nondiagnostic as to age, but detrital limestone from a probable outcrop of the siltstone sequence in the Yakataga district has yielded middle Eocene orbitoid Foraminifera (Stoneley, 1967). On the basis of the limited available evidence, it appears that the siltstone sequence includes strata ranging in age from Paleocene through middle Eocene.

PALEONTOLOGY

Turritella merriami brevitabulata Merriam and Turner (1937, p. 105, pl. 6, figs. 1, 2) is represented by an external mold preserved in very fine grained sandstone. A latex rubber cast has been compared with specimens from California including the holotype and paratype figured by Merriam (1941, pl. 14, figs. 1–7). Although the earliest whorls on the specimen from the Malaspina district are not preserved, crisp spiral sculpture and faint growth lines are discernible on later whorls (fig. 3). This specimen has the channeled sutures, sculpture, and straight-sided, nontabulate whorl profile characteristic of *T. merriami brevitabulata*. Details of the growth lines on the Alaskan specimen also indicate affinity with the California species. Segments of the delicate growth lines preserved on one of the whorls indicate a moderately deep antispiral sinus with the apex near, or just below, the middle of the whorl. The growth line angle on this specimen is narrow, about 10° to 12°.

AGE AND CORRELATION

This subspecies is the earliest representative of the late Paleocene to early Eocene *Turritella merriami* stock of Merriam (1941, p. 41). It differs from other species assigned to this stock principally in lacking a subsutural flange. *Turritella merriami brevitabulata* is reported from several localities near Mount Diablo, Contra Costa County, Calif., and from a locality near Covelo, Mendocino County, Calif. (Merriam and Turner, 1937; Clark, 1940). These occurrences are in strata assigned to the "Meganos Stage" of Clark and

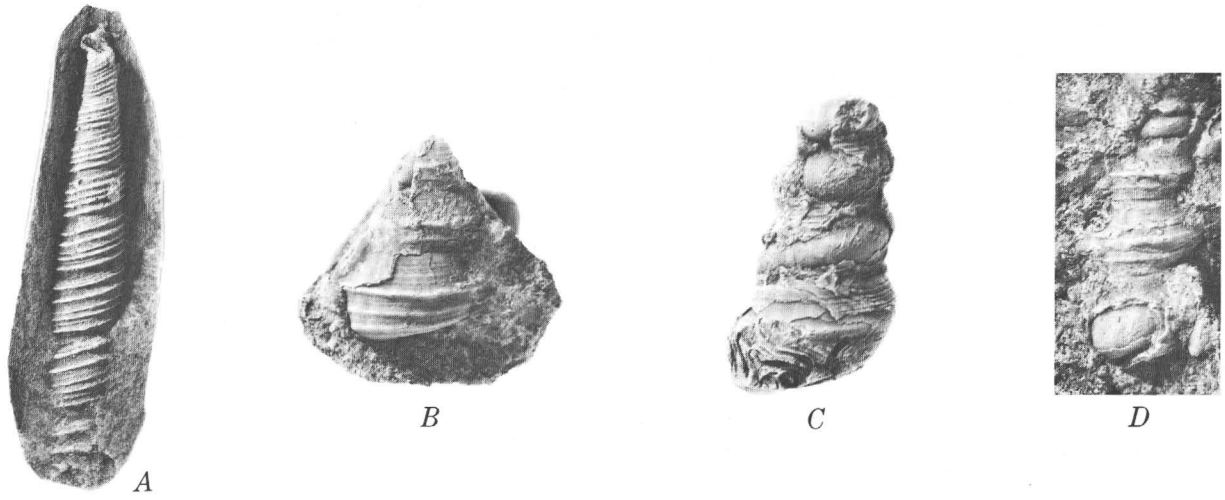

FIGURE 3.—Turritellas from the Kulthieth Formation, Malaspina district, Alaska.
A. Turritella merriami brevitabulata Merriam and Turner. × 1. USNM 646,470, a rubber cast. USGS Cenozoic loc. M4109.
B. Cristispira pugetensis Allison. × 2. USNM 646, 471. USGS loc. D333(T).
C. Cristispira pugetensis Allison. × 2. USNM 646, 472. USGS loc. D333(T).
D. Cristispira pugetensis Allison. × 1½. USNM 646, 473. USGS loc. D333(T).

Vokes (1936), a unit considered to be of late Paleocene age in the standard Pacific coast chronology (Weaver and others, 1944; Durham, 1954).

DISCUSSION

Although marine strata of Paleocene age have long been suspected to occur in the higher latitudes of the marginal eastern North Pacific, the present record provides the first evidence of marine strata of this age from north of Mendocino County, Calif. (near lat 40° N.). Weaver and others (1944, chart 11) postulated that the Metchosin Volcanics of southwestern Canada and northwestern Washington would prove to be of Paleocene age, but so far fossils of Paleocene age have not been recovered from marine sedimentary rocks interbedded with this volcanic sequence.

The oldest strata previously recognized from the Gulf of Alaska Tertiary province include the Stillwater Formation in the Katalla district, the Kulthieth Formation in the Malaspina district, and the Orca Group in the Prince William Sound district (localities *A*, *B*, *C*, fig. 2). The Stillwater Formation of the Katalla district was considered to be of middle Eocene age on the basis of sparse, poorly preserved specimens of crabs, bivalves, gastropods, and echinoids (MacNeil and others, 1961; Miller, 1961). Turritellas collected as float on Wingham Island in the Katalla district were believed by C. W. Merriam to represent a middle Eocene species, but he further noted that the specimens also resembled a Late Cretaceous species (Miller, 1961).

Mollusks from two localities in the Samovar Hills, Malaspina district, were previously regarded as of late Eocene age (Plafker and Miller, 1957), but restudy of the *Turritella* upon which this determination was based (fig. 3) indicates that it is *Cristispira pugetensis* Allison, rather than the late Eocene *T. uvasana sargeanti* Anderson and Hanna. These specimens are differentiated from *T. uvasana sargeanti* by the development of two rather than five strong primary spiral ribs, a prominent medial keel, and a concave subsutural whorl profile. The occurrence of *C. pugetensis* suggests that the Kulthieth is in part of middle Eocene age, the species having been described from the middle Eocene Raging River Formation of northwestern Washington (Allison, 1965). It should be noted that the Kulthieth also contains marine invertebrate assemblages of undoubted late Eocene age (Miller, 1957; Plafker, 1967), as well as plants of early Oligocene age (Wolfe, 1969). The further possibility that part of the Kulthieth Formation may be of early Eocene age is suggested by the occurrence of very poorly preserved Turritellas that resemble *T. buwaldana crooki* Merriam and Turner in collections by Plafker from this general area (USGS loc. M4112 and M4119). This subspecies is of widespread occurrence in rocks assigned to the lower Eocene "Capay Stage" of Clark and Vokes (1936) in California. Thus, available data indicate that the Kulthieth Formation includes marine strata ranging in age from late Paleocene through late Eocene, and nonmarine strata of early Oligocene age. The associated unnamed siltstone unit is probably largely of Paleocene age, although it may include strata as young as middle Eocene in the Yakataga district (Stoneley, 1967).

On the basis of a single collection of fossil crabs and mollusks, the lower part of the Orca Group in the Prince William Sound district was assigned a probable middle to late Eocene age by Plafker and MacNeil (1966). The known stratigraphic ranges of the crabs from the Orca Group suggest a late Eocene age. It should be emphasized, however, that the lower limits of the ranges of these crustaceans are poorly known owing to the paucity of pre-upper Eocene stratigraphic records (Rathbun, 1926). The much better documented biozone of *Acila decisa*, the only specifically determined mollusk in the collection from the Orca Group, is from the lower Paleocene "Martinez Stage" to the upper Eocene "Tejon Stage" in the conterminous United States. Accordingly, the possibility that the Orca Group may be, in part, of Paleocene age should not be ruled out.

In summary, the newly reported occurrence of marine Paleocene mollusks in southern Alaska indicates that Paleocene seas covered a much broader area along the North Pacific rim than was previously known. It further seems probable that marine strata of this age may be more widely distributed in the Paleogene sequence of the Gulf of Alaska margin than has hitherto been suspected. Dating of these rocks is hampered, however, by the scarcity of diagnostic fossils, a scarcity resulting from the prevailing structural complexity and thorough induration of the rocks, and from local mild metamorphism.

REFERENCES

Allison, R. C., 1965, Apical development in turritellid classification with a description of *Cristispira pugetensis* gen. et sp. nov.: Palaeontology, v. 8, pt. 4, p. 666–680, pl. 92.

Clark, B. L., and Vokes, H. E., 1936, Summary of marine Eocene sequence of western North America: Geol. Soc. America Bull., v. 47, no. 6, p. 851–878.

Clark, S. G., 1940, Geology of the Covelo district, Mendocino County, California: California Univ., Dept. Geol. Sci. Bull., v. 25, no. 2, p. 119–142, 7 figs.

Durham, J. W., 1954, The marine Cenozoic of southern California, [pt.] 4 *in* chap 3 *of* Jahns, R. H., ed., Geology of southern California: California Dept. Nat. Res., Div. Mines Bull. 170, p. 23–31.

MacNeil, F. S., Wolfe, J. A., Miller, D. J., and Hopkins, D. M., 1961, Correlation of Tertiary formations of Alaska: Am. Assoc. Petroleum Geologists Bull., v. 45, no. 11, p. 1801–1809.

Merriam, C. W., 1941, Fossil Turritellas from the Pacific Coast region of North America: California Univ., Dept. Geol. Sci. Bull., v. 26, no. 1, p. 1–214, pls. 1–41.

Merriam, C. W., and Turner, F. E., 1937, The Capay middle Eocene of northern California: California Univ., Dept. Geol. Sci. Bull., v. 24, no. 6, p. 91–114, pls. 5, 6.

Miller, D. J., 1957, Geology of the southeastern part of the Robinson Mountains, Yakataga district, Alaska: U.S. Geol. Survey Oil and Gas Inv. Map OM–187, scale 1: 63,360.

——— 1961, Geology of the Katalla district, Gulf of Alaska Tertiary Province, Alaska: U.S. Geol. Survey open-file map.

Plafker, George, 1967, Geologic map of the Gulf of Alaska Tertiary Province, Alaska: U.S. Geol. Survey Misc. Geol. Inv. Map I–484.

Plafker, George, and MacNeil, F. S., 1966, Stratigraphic significance of Tertiary fossils from the Orca Group in the Prince William Sound region, Alaska, *in* Geological Survey Research 1966: U.S. Geol. Survey Prof. Paper 550–B, p. B62–B68.

Plafker, George, and Miller, D. J., 1957, Reconnaissance geology of the Malaspina district, Alaska: U.S. Geol. Survey Oil and Gas Inv. Map OM–189, scale 1: 125,000.

Rathbun, M. J., 1926, The fossil stalk-eyed Crustacea of the Pacific slope of North America: U.S. Natl. Mus. Bull. 138, 155 p., 39 pls.

Stoneley, Robert, 1967, The structural development of the Gulf of Alaska sedimentary province in southern Alaska: Geol. Soc. London Quart. Jour., v. 123, p. 25–27.

Weaver, C. E., chm., and others, 1944, Correlation of the marine Cenozoic formations of western North America [Chart 11]: Geol. Soc. America Bull., v. 55, no. 5, p. 569–598.

Wolfe, J. A., 1969, Paleogene floras from the Gulf of Alaska region: U.S. Geol. Survey open-file rept., 110 p.

TWO NEW FOSSIL POLLEN GENERA FROM UPPER CAMPANIAN (CRETACEOUS) ROCKS OF MONTANA

By BERNADINE D. TSCHUDY, Denver, Colo.

Abstract.—Two new fossil pollen species typifying two new genera were well represented in rock samples from the upper Campanian of Montana. These are similar to, and are probably relatives of, several pollen species previously described from Upper Cretaceous sediments from the Western-Siberian lowland of the U.S.S.R. The new genera and species from Montana are described and illustrated, and five species from the U.S.S.R. are transferred from the genus *Proteacidites* to one of the new genera.

In this report, two new genera and their type species are described; and their similarities to, and differences from, several formerly described genera and species are discussed.

The taxons which are dealt with here were considered to merit detailed study because of: (1) their resemblance to several medium to large pollen species previously described from Upper Cretaceous rocks of the Western-Siberian lowland of the U.S.S.R., (2) their suspected stratigraphic importance, and (3) the abundance of specimens available for study. The two species, though resembling six species from the Western-Siberian lowland of the U.S.S.R., as shown in photographs and drawings, were found to be morphologically different from the Russian species. *Siberiapollis montanensis* n. sp. was abundantly represented in sample D3726–E from the Parkman Sandstone Member of the Judith River Formation; however, it occurred as only 1 percent of a total pollen and spore count in that sample. A few specimens of the same species were also found in samples from five other localities (see table 1). *Montanapollis endannulatus* was found only in sample D4067 (basal part of the Bearpaw Shale or uppermost part of the Judith River Formation) and in that sample only in very low concentration—the 25 specimens studied were recovered from a total of 12 slides. In the Rocky Mountain area, as far as is known, the two taxons investigated are limited to upper Campanian rocks.

Acknowledgments.—I am grateful to Ivan J. Mittin for translations from essential parts of Russian publications and to W. A. Cobban and J. R. Gill for their correlation of several of the samples with stratigraphic units and ammonite zones.

PHOTOGRAPHY AND TYPE SLIDES

The photographs that illustrate the new species in this report were taken on Zeiss photoscopes. Figure 3, *b* was taken under Nomarski phase contrast on Polaroid type 55 P/N film. Neofluar 54× and Apochromatic 40× oil-immersion objectives and 35-mm KB–14 film were used for the remainder of the photographs.

All specimens illustrated in this report are deposited in the type-slide files of the U.S. Geological Survey laboratory at Denver, Colo. The type specimens are within the ink-circled areas on the slides; they may also be located by the mechanical stage coordinates which are given in the plate explanations and with the individual holotype and paratype assignments. My coordinate readings for the center point of a 1- by 3-inch standard microscope slide are 108.2 ×12.4 mm (horizontal × vertical axes); with the slide label placed to the left on the microscope stage, the vertical coordinates decrease toward the bottom edge of the slide, and the horizontal coordinates decrease toward the right edge. Conversion of coordinates to those of another mechanical stage can be made by the methods of Traverse (1958) and Tschudy (1966).

SYSTEMATIC DESCRIPTIONS

Group NORMAPOLLES Pflug, 1953

Normapolles Pflug, 1953, p. 95.
Normapolles Pflug, 1953. In Góczán and others, 1967, p. 434–445.

Remarks.—Genera of the Normapolles Group are characterized by highly differentiated, widely variable,

U.S. GEOL. SURVEY PROF. PAPER 750–B, PAGES B53–B61

TABLE 1.—*Stratigraphic distribution of* Siberiapollis montanensis *and* Montanapollis endannulatus *in upper Campanian rocks from Montana*

USGS Paleobot. loc. No.	Stratigraphic unit	Western Interior ammonite zone	Estimated age of zone (millions of years) [1]	*Siberiapollis montanensis*	*Montanapollis endannulatus*	Locality				Collector of sample
						County	Section	T.	R.	
D1613	Minor Creek Formation.			X		Park	NW¼ 20	2 S.	9 E.	A. E. Roberts.
D1612	do			X		do	SE¼ 19	2 S.	9 E.	Do.
D4067	Bearpaw Shale (basal part) or Judith River Formation (uppermost part).	*Baculites scotti.*[2]	75–76	X	X	Phillips	NW¼NE¼ 31	22 N.	24 E.	J. R. Gill.
D3725–D	Judith River Formation (upper part).	do	75–76	X		Blaine	NW¼ 26	24 N.	17 E.	J. R. Gill and L. G. Schultz.
D3726–A	Judith River Formation (Parkman Sandstone Member).[3]	*Baculites asperiformis.*[2]	78–79	X		Fergus	C. NE¼ 31	23 N.	17 E.	Do.
D3726–E	do	do	78–79	X		do	C. NE¼ 31	23 N.	17 E.	Do.

[1] Gill and Cobban (1966, p. A35).
[2] W. A. Cobban (oral commun., Aug. 6, 1970).
[3] J. R. Gill (oral commun., Sept. 29, 1970).

and bizarre apertures. Affinities of most genera of this group with modern families of plants are uncertain, and genetic relationships within the group are not implied.

Form-genus *Siberiapollis* n. gen.

Type species.—*Siberiapollis montanensis* n. sp., USGS Paleobot. loc. D3726–E, slide (6) at 80.5×4.9; figure 2, *a* (holotype); center NE¼ sec. 31, T. 23 N., R. 17 E., Fergus County, Mont.; Judith River Formation (Parkman Sandstone Member), upper Campanian.

Description.—Tricolporate, angulaperturate, isopolar to subisopolar pollen grains. Shape in polar view triangular; sides of triangle plane, concave, convex, or irregular; corners rounded or bifurcating (owing to gaping colpi). Shape in equatorial view rhomboidal to oval. Colpi slitlike to V shaped, extending less than half the distance to poles. Endopores with simple collarlike endannuli, which are located near base of colpi. Exine variable in thickness; endexine and ektexine extending to colpal exits. Surface sculpture varied (verrucate, gemmate, clavate, reticulate, or areolate; not psilate, echinate, or striate). Grains without arci or plicae.

New combinations.—The following species, on the basis of the authors' descriptions and figures, appear to conform to *Siberiapollis* and are here transferred from *Proteacidites.*

Siberiapollis deruptus (Chlonova, 1961, p. 71, pl. 14, figs. 103, 103a) n. comb.

Siberiapollis occulatus (Samoilovitch, *in* Samoilovitch and others, 1961, p. 176–178, pl. 55, figs. 1a–d) n. comb.

Siberiapollis crassiporus (Samoilovitch, *in* Samoilovitch and others, 1961, p. 183–184, pl. 58, figs. 1a–d, 2) n. comb.

Siberiapollis angulatus (Samoilovitch, *in* Samoilovitch and others, 1961, p. 187–188, pl. 60, figs. 1a–c, 2a–d) n. comb.

Siberiapollis trilobatus (Samoilovitch, *in* Samoilovitch and others, 1961, p. 190–191, pl. 61, figs. 4a–d) n. comb.

Note.—Srivastava's (1969, p. 1573) transfers of *Proteacidites occulatus* Samoilovitch, *Proteacidites angulatus* Samoilovitch, and *Proteacidites trilobatus* Samoilovitch to *Beaupreaidites* Cookson emend. Srivastava, 1969, are not recognized here because I do not believe that *Beaupreaidites* as emended by Srivastava is a legitimate genus. Srivastava's designation of vestibulate apertures for *Beaupreaidites* would exclude its type species, *B. elegansiformis* Cookson (lectotype: *in* Cookson, 1950, pl. 1, fig. 4 designated by Potonié, 1960, p. 121), which does not have vestibulate apertures.

Remarks.—*Siberiapollis* n. gen. was erected as a form-genus to accommodate a group of pollen species having morphological similarity to each other but doubtful affinity with any particular modern plant family. In addition to the type species, I have included in this new genus several species from the Upper Cretaceous of the Western-Siberian lowland, descriptions and illustrations of which were published by Chlonova and by Samoilovitch (see new combinations above) under the genus *Proteacidites.* It was in recognition of the Siberian species that the name *Siberiapollis* was chosen.

Affinity.—Uncertain. Neither in the modern-pollen files of the U.S. Geological Survey laboratory at Denver, Colo., nor in illustrations of the literature (Cookson

and Erdtman, *in* Erdtman, 1952, p. 339–369; Wodehouse, 1932, p. 335–336, pl. 21, figs. 21, 26; Cranwell, 1942, pl. 55, fig. 19) have I found any modern proteaceous pollen species to which species of *Siberiapollis* have close similarity. Slight resemblance of *Siberiapollis* species to pollen of some members of the families Rubiaceae, Oenotheraceae, and Proteaceae is seen, but I do not believe the likeness is sufficient to justify assignment to any one of these modern families.

Comparison with other fossil pollen genera.—Within the Normapolles Group, *Siberiapollis* probably most closely resembles *Bakonyipollis* Góczán, *in* Góczán and others, 1967 (p. 447–448). *Siberiapollis*, in common with *Bakonyipollis*, has endopores with endannuli, but it differs from *Bakonyipollis* in that it does not have plicae and has distinctly different exinal structure in the apertural areas. (See Góczán *in* Góczán and others, 1967, text fig. 15, p. 447.)

Siberiapollis, because of its complex colporate apertures, is distinct from *Proteacidites* Cookson ex Couper, 1953 (p. 42), which has porate apertures, and from *Beaupreaidites* Cookson ex Couper, 1953 (p. 43), which has colpate apertures.

Siberiapollis is distinguishable from *Montanapollis* n. gen. by its longer colpi, by its simple rather than banded pore rings, and by its lack of the multiple lateral branches from the endexine in the apertural zone.

Siberiapollis montanensis n. sp.

Figures 1, 2

Holotype.—USGS Paleobot. loc. D3726–E, slide (6) at 80.5×4.9; figure 2, *a*; center NE¼ sec. 31, T. 23 N., R. 17 E., Fergus County, Mont.; Judith River Formation (Parkman Sandstone Member), upper Campanian.

Paratype.—USGS Paleobot. loc. D3726–E, slide (9) at 82.1×7.5; figure 2, *b*; same locality data as for holotype.

Paratype.—USGS Paleobot. loc. D3726–E, slide (5) at 109.8×2.1; figure 2, *c*; same locality data as for holotype.

Distribution.—See table 1.

Description (based on 70 specimens in polar view and 10 in equatorial view).—Tricolporate, angulaperturate, isopolar pollen grains. Shape in polar view triangular; sides of triangle plane, slightly concave, slightly convex, or irregular; in some specimens the equatorial outline of grain is slightly modified owing to indentations at the base of the apertural areas. Shape in equatorial view rounded-rhomboidal to oval. Diameter 42μ–84μ (commonly 48μ–70μ), polar axis 34μ–59μ. *Apertures:* Colpi (as seen in polar view of grains) slitlike to V shaped, extending approximately one-third the distance from corners of grain to poles; colpal lips approximately 3μ wide, tapering to become narrow at base of colpus; lips prominent in some specimens, in others indistinct or apparently lacking; colpal margins smooth to rough or unevenly serrate. Endopores located near base of colpi, 12μ–17μ in diameter, each bordered by a smooth pore ring (endannulus) 2.5μ–5.0μ wide; endannulus, at least in some specimens, not a complete ring (figs. 1; 2, *d*); in pale or eroded specimens pore rings indistinct to fragmentary. *Pollen wall:* Exine consisting of endexine and ektexine. Endexine 0.5μ–2.0μ thick on body of grain, thickening in apertural areas to as much as 3μ in most specimens (to as much as 5μ in a few specimens). Ektexine composed of a basal columnar layer and a surface sculptural layer; ektexine 0.5μ–1.5μ thick, thinning near apertural areas, becoming very thin in apertural zone. Ektexinal columnar layer very thin, in some specimens not clearly discernible; individual columnar elements very short and slender—these visible in some specimens at × 1,000 oil-immersion magnification. Surface sculptural layer consisting of closely spaced, more or less isodiametric elements having rounded tops, these elements becoming very short in apertural areas and merging—forming a thin, almost smooth surface layer. Surface sculpture areolate (negative reticulum); areolae (in surface view of grains) round, rounded triangular, or irregular in outline, 1.0μ–5.0μ in diameter; negative net irregular and in part discontinuous (where areolae fuse and break the net); individual areolae supported on one or more delicate columellae; areolae in some specimens appear to hover over endexine with only a very thin space between them and the endexine; in other specimens, or parts of individual grains, the areolae appear to lie directly on the endexinal layer; size of areolae varies from grain to grain, as well as on individual grains; areolae arranged almost like parts of a jigsaw puzzle, or less closely

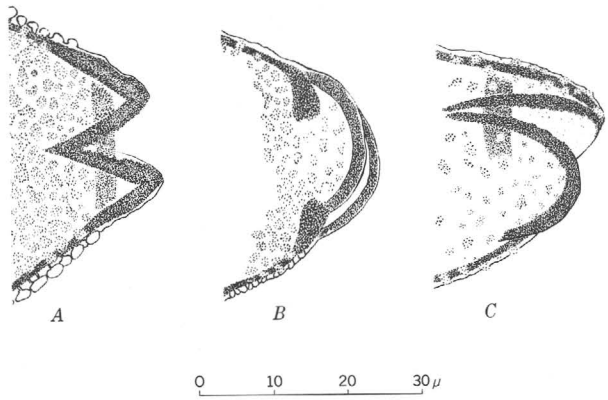

FIGURE 1.—Diagrammatic drawings of apertural area of *Siberiapollis montanensis* n. sp. *A*, grain in polar view; *B*, grain in equatorial view; *C*, grain in oblique view.

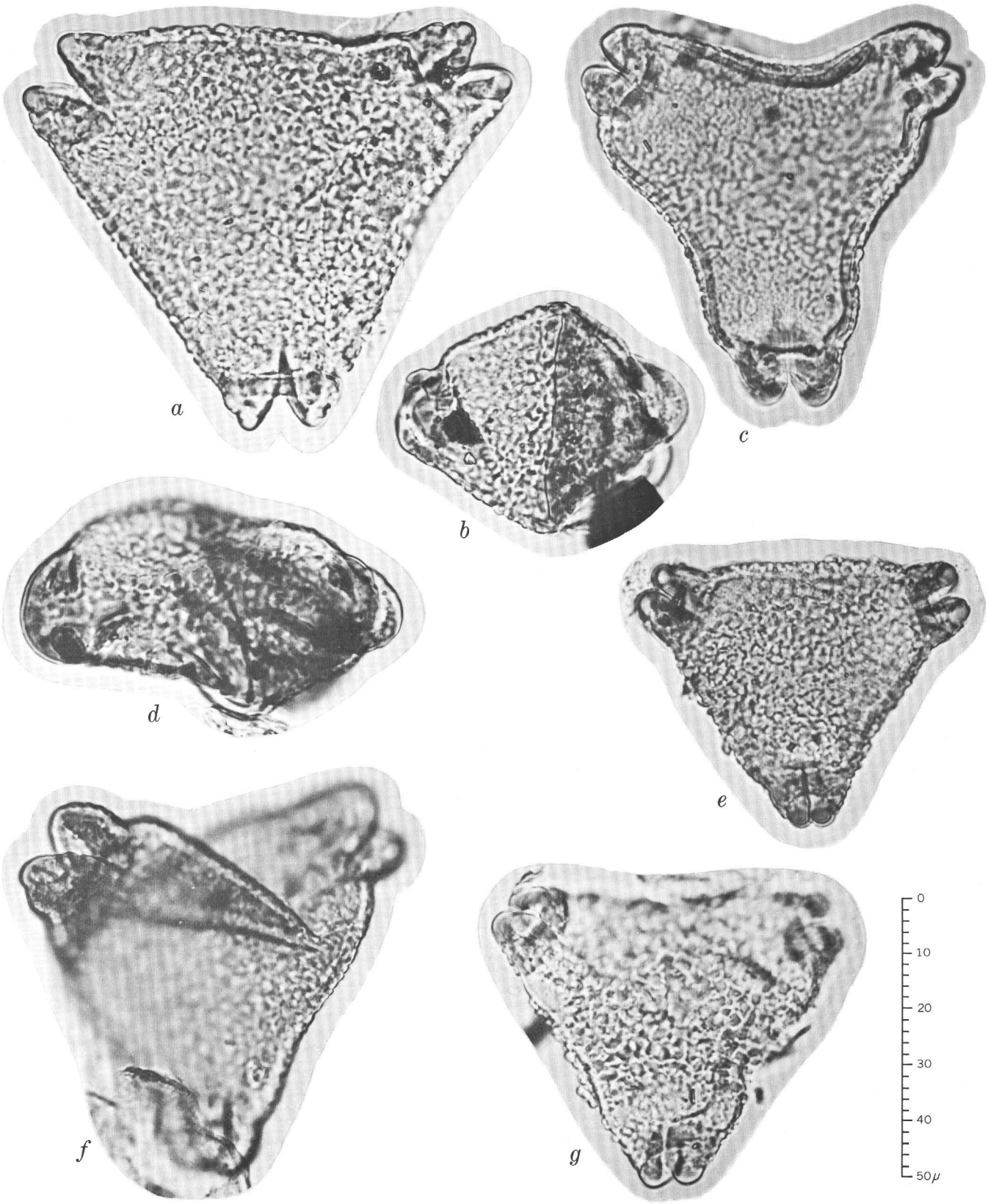

FIGURE 2.

spaced, but diameters of areolae usually greater than width of spaces between them. On surface view of well-preserved grains (at × 1,000 oil-immersion magnification) the highest focal level shows the round, angular, and irregular areolae; at slightly lower focal level the tops of the individual columns appear, with resultant display of a much finer subsurface texture. Surface ornamentation the same on distal and proximal hemispheres of grain; in some specimens ornamentation slightly coarser on polar areas than in vicinity of apertures. Grains without arci or plicae.

Remarks.—The specimen called *Beaupreaidites angulatus* (Samoilovitch) Srivastava, 1969 (pl. 1, figs. 3–5) from the Edmonton Formation of Alberta, Canada, as illustrated in photographs, appears to be very similar to some of the specimens of *S. montanensis;* however, the aperture structure of *Beaupreaidites* Cookson emend. Srivastava 1969 (p. 1573, text fig. 2), to which the species was assigned, does not correspond to that of *S. montanensis.*

Similar species.—In respect to size of grain, pore-collar appearance, and surface ornamentation, *S. montanensis* resembles *Siberiapollis* (*Proteacidites*) *deruptus* (Chlonova, 1961, p. 71, pl. 14, figs. 103, 103*a*) n. comb.; however, the colpi of *S. montanensis* are shorter and less gaping than those of *S. deruptus;* and the endexine in the apertural area of *S. montanensis* thickens appreciably, whereas it appears to become thinner in that area in *S. deruptus.*

S. montanensis n. sp. also resembles but is distinct from several large pollen species classified under the genus *Proteacidites* by Samoilovitch (*in* Samoilovitch and others, 1961, p. 175–191). Some similarities to and difference from these species are as follows:

1. *S. montanensis* differs from *Proteacidites magnus* Samoilovitch by its very prominent colpi and also by shorter and more delicate columellae in its columnar layer.
2. In shape and size, many of my specimens of *S. montanensis* strikingly resemble Samoilovitch's (pl. 55, fig. 1*a*) photograph of *Proteacidites occulatus* (= *Siberiapollis occulatus* n. comb.); however, on the basis of a careful examination of her photographs and of her (pl. 55, fig. 1*b*) detailed drawing, as well as of her description, the two species are judged to be distinctly different. Samoilovitch stated that her *P. occulatus* is subisopolar; as seen from equatorial views, *S. montanensis* is isopolar. The pores and colpi of *S. montanensis* are apparently very similar to those of *S. occulatus;* however, the structure of the exine in the apertural areas in the two species is distinctly different—the endexine of *S. occulatus* apparently thickens at the base of the aperture area, then thins abruptly and becomes very thin at the colpal rim, whereas the endexinal layer of *S. montanensis* thickens in the apertural area, and in most specimens it attains its maximum thickness at the colpal exit.
3. *S. montanensis*, in common with *Siberiapollis* (*Proteacidites*) *crassiporus* (Samoilovitch) n. comb., has a thickened endexinal layer near the colpal exit ("pore aperture" of Samoilovitch) and has internal pores with thickenings; however, *S. montanensis* differs in that it has much less thickening of the exine on the mesoporiums, and its exine sculpture is coarser than that of *S. crassiporus.* The pore apertures of *S. crassiporus* were described as short, slit shaped, and very narrow or locked together, whereas the colpi of most specimens of *S. montanensis* are gaping.
4. *S. montanensis* has apertures which are apparently very similar to those of *Siberiapollis* (*Proteacidites*) *angulatus* (Samoilovitch) n. comb., and the surface sculpture of these two species appears to be very similar. *S. montanensis* differs from *S. angulatus* in that its columnar layer is discontinuous in the apertural area, whereas in *S. angulatus* this layer remains about the same thickness in the apertural areas (as stated by Samoilovitch). The endexine of *S. montanensis* is about equal in thickness to the ektexine, whereas Samoilovitch stated that the sexine is twice as thick as the nexine in *S. angulatus.* As shown in photographs of *S. angulatus*, the columnar layer is thicker and much more distinct than in *S. montanensis.* In *S. montanensis* the endexine thickens in the apertural area; this thickening is not a characteristic of *S. angulatus*, either as described or as illustrated.

FIGURE 2.—*Siberiapollis montanensis* n. sp.

a. Polar view of holotype. USGS Paleobot. loc. D3726–E, slide (6) at 80.5×4.9.
b. Equatorial view of a paratype. USGS Paleobot. loc. D3726–E, slide (9) at 82.1×7.5.
c. Polar view of a paratype. USGS Paleobot. loc. D3726–E, slide (5) at 109.8×2.1.
d. Equatorial view, showing ends of incomplete pore ring. USGS Paleobot. loc. D3726–E, slide (1) at 114.8×14.0.
e. Polar view. USGS Paleobot. loc. D3726–E, slide (5) at 91.5 ×19.6.
f. Oblique polar view. USGS Paleobot. loc. D3726–E, slide (5) at 114.8×9.8.
g. Polar view of a grain with sculptural layer partially detached. USGS Paleobot. loc. D3726–E, slide (1) at 81.0 ×10.2.

Among the large number of variable but merging grains described under the species *S. montanensis* are three grains (for example, fig. 2, *c*) whose shape resembles that of *Siberiapollis* (*Proteacidites*) *trilobatus* (Samoilovitch) n. comb.; however, they are distinctly different from *S. trilobatus* in that their surface sculpture is much coarser.

Form-genus *Montanapollis* n. gen.

Type species.—*Montanapollis endannulatus* n. sp., USGS Paleobot. loc. D4067, slide (4) at 92.9×21.1; figure 3, *d* (holotype); NW¼NE¼ sec. 31, T. 22 N., R. 24 E., Phillips County, Mont.; Bearpaw Shale (basal part) or Judith River Formation (uppermost part), upper Campanian.

Description.—Tricolporate, brevissimicolpate, angulaperturate pollen grains. Shape in polar view triangular; sides of triangle plane, slightly convex, slightly concave, or irregular; angles rounded, each angle notched by a shallow aperture. Colpi very short, slitlike, U or V shaped, closed or gaping. Endopores (ora) encircled by banded pore ring consisting of several endannuli which originate from lateral branching of endexine in apertural area. Ektexine thinner in apertural area than on body of grain. Endexine and ektexine extending to colpal exits. Vestibulum not present between endexinal and ektexinal wall layers in apertural area. Surface sculpture varied. Grains medium to large in size (>40μ in diameter). Grains without arci or plicae.

The distinguishing features of this genus are the banded pore rings encircling the endopores and the very short colpi.

Affinity.—Uncertain.

Comparison with other fossil pollen genera.—*Montanapollis* n. gen. is distinct from *Siberiapollis* n. gen. by reason of its shorter colpi, its banded pore rings, and by the lateral branching of the endexine in its apertural zones.

The multiple endannuli of the ora of *Montanapollis* resemble those of *Atlantopollis* Krutzsch, *in* Góczán and others, 1967 (p. 445–446, text fig. 13) and *Neotriangulipollis* Góczán, Groot, and Krutzsch, *in* Góczán and others, 1967 (p. 479–480, text fig. 42) as shown in the authors' text figures; however, *Montanapollis* is easily distinguishable from those genera as indicated below. The sculptural and columnar wall layers of *Montanapollis* become thinner in the apertural area, whereas those of *Atlantopollis* are approximately the same thickness in the apertural area as on the body of the grain. *Montanapollis* also differs from *Atlantopollis* in that it does not have an enlarged endannulus adjacent to its apertural exits. The outermost wall layer of *Montanapollis* thins in the apertural area, whereas in *Neotriangulipollis* it thickens. The outer wall layers of *Montanapollis* do not separate in the area adjacent to the apertural exit to form a vestibulum as they do in *Neotriangulipollis*.

The colporate apertures and banded pore rings of *Montanapollis* distinguish it from both *Proteacidites* Cookson ex Couper, 1953 (p. 42) and *Beaupreaidites* Cookson ex Couper, 1953 (p. 43).

Montanapollis endannulatus n. sp.

Figures 3, 4

Holotype.—USGS Paleobot. loc. D4067, slide (4) at 92.9×21.1; figure 3, *d*; NW¼NE¼ sec. 31, T. 22 N., R. 24 E., Phillips County, Mont.; Bearpaw Shale (basal part) or Judith River Formation (uppermost part), upper Campanian.

Paratype.—USGS Paleobot. loc. D4067, slide (3) at 75.0×10.7; figures 3, *a*, *b*; same locality data as for holotype.

Paratype.—USGS Paleobot. loc. D4067, slide (10) at 76.0×8.8; figure 3, *g*; same locality data as for holotype.

Distribution.—To date found only in USGS Paleobot. loc. D4067 (Bearpaw Shale, basal part; or Judith River Formation, uppermost part).

Description (based on 25 specimens in polar view; species has not been observed in equatorial view).—Tricolporate, brevissimicolpate, angulaperturate pollen grains. Shape in polar view triangular; sides of triangle plane, slightly concave, or irregular; angles rounded, each notched by a shallow aperture; in some specimens equatorial outline slightly modified by in-

FIGURE 3.—*Montanapollis endannulatus* n. sp.

a. Polar view of a paratype, USGS Paleobot. loc. D4067, slide (3) at 75.0×10.7.
b. Same grain as *a*, Nomarski phase-contrast photograph showing surface detail.
c. Polar view, USGS Paleobot. loc. D4067, slide (11) at 105.2 ×13.8.
d. Polar view of holotype, USGS Paleobot. loc. D4067, slide (4) at 92.9×21.1.
e. Polar view, USGS Paleobot. loc. D4067, slide (11) at 98.2×2.9.
f. Oblique polar view, USGS Paleobot. loc. D4067, slide (12) at 76.7×9.3.
g. Polar view of a paratype, USGS Paleobot. loc. D4067, slide (10) at 76.0×8.8.

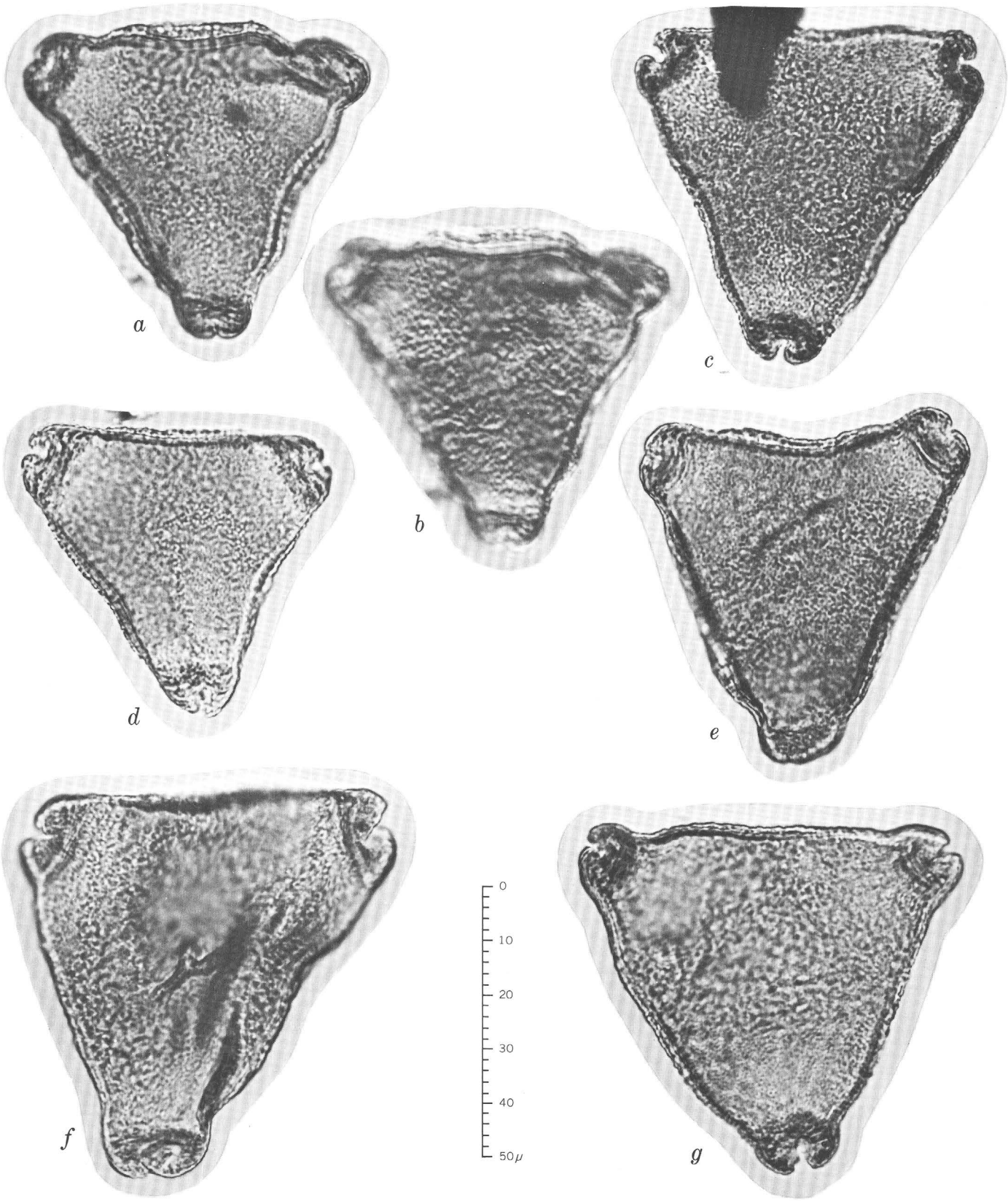

FIGURE 3.

413-504 O - 71 - 5

dentations at the base of the apertural areas. Diameter 45μ–70μ. *Apertures:* Colpi slitlike, U or V shaped, very short, terminating at approximate top of endopore ring; colpal margins smooth, not thickened. Endopores (ora) encircled by banded pore rings 3μ–7μ wide; pore ring consisting of a series of narrow, interfingering, incomplete endannuli, the endannuli originating from lateral branches of endexine. *Pollen wall:* Exine on body of grain 2μ–4μ thick. Endexine on body 1μ–2μ thick, in some specimens slightly thinner near base of apertural areas than on the remainder of body. In lower and midparts of apertural areas the endexine repeatedly branches laterally and forms several narrow, interfingering, discontinuous endannuli, which make up the banded pore ring; in some specimens endexinal branching and banded pore ring very distinct, in others these not clearly visible. Ektexine made up of a basal columnar layer and a surface sculptural layer. Columnar layer thin, with maximum thickness of approximately 0.5μ on body of grain; columnar elements delicate, distinct at × 1,000 oil-immersion magnification in some specimens, not clearly visible in others where the columnar layer appears as an interloculum (or space) between the sculptural layer and the endexine; columnar layer very thin to nondiscernible in apertural areas. Ektexinal sculptural layer 0.5μ–1.5μ thick on body, in some specimens appearing to be partially detached (figs. 3, *a*, *e*)—apparently owing to structural weakness of the underlying columnar layer; sculptural layer becoming very thin near base of, and in, apertural areas. Surface of grains appearing rugulate to irregularly reticulate at high focal level at × 1,000 magnification. Surface ornamentation the same on distal and proximal hemispheres of grain.

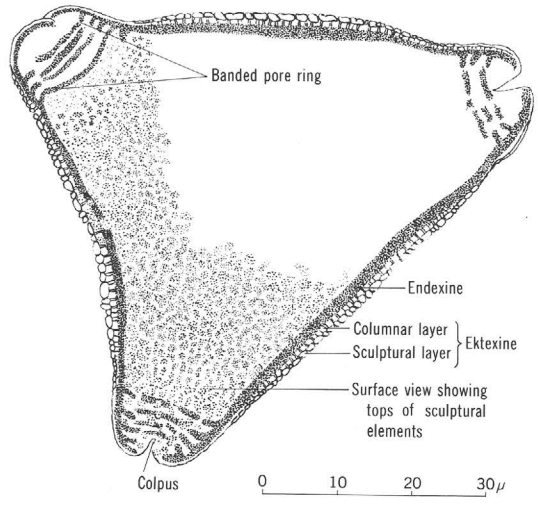

FIGURE 4.—Diagrammatic drawing of *Montanapollis endannulatus* n. sp., showing aperture and wall detail.

This species is assumed to have a shorter polar axis than equatorial diameter, because of the fact that specimens have been found only in polar view.

Similar species.—Montanapollis endannulatus may be related to a pollen taxon from the "Maestrichtian-Danian" of the Western-Siberian lowland called *Proteacidites crassiporus* subspecies *pachysexinius* Samoilovitch, *in* Samoilovitch and others, 1961 (p. 184–185, pl. 58, figs. 3a–d). The photograph of *P. crassiporus* subsp. *pachysexinius* shows only a suggestion of a banded pore ring and an indication of branching of the endexine in only one of the apertures. *M. endannulatus* differs from *P. crassiporus* subsp. *pachysexinius* in that it has thinner ektexine on the body of the grain, has less differentiation between the ektexinal thickness on the body and in the apertural areas, and does not have the thickened endexinal layer (endannulus) adjacent to the colpal exits.

REFERENCES

Chlonova, A. F., 1961, Spory i pyl'tsa verkhnei poloviny verkhnego mela vostochnoi chasti Zapadno-Sibirskoi nizmennosti [Spores and pollen of upper part of the Upper Cretaceous of the eastern part of the Western Siberian Lowland]: Akad. Nauk SSSR Sibirsk. Otdeleniye Inst. Geologii i Geofiziki Trudy, v. 7, 138 p., 17 pls.

Cookson, I. C., 1950, Fossil pollen grains of proteaceous type from Tertiary deposits in Australia: Australian Jour. Sci. Research, Ser. B—Biol. Sci., v. 3, no. 2, p. 166–177, 3 pls.

Couper, R. A., 1953, Upper Mesozoic and Cainozoic spores and pollen grains from New Zealand: New Zealand Geol. Survey Paleontology Bull. 22, 77 p., 9 pls.

Cranwell, L. M., 1942, New Zealand pollen studies, 1. Key to the pollen grains of families and genera in the native flora: Auckland Inst. and Mus. Recs., v. 2, pt. 6, p. 280–308, 3 pls.

Erdtman, Gunnar, 1952, Pollen morphology and plant taxonomy—angiosperms (An introduction to palynology, 1): Waltham, Mass., Chronica Botanica Co., 539 p.

Gill, J. R., and Cobban, W. A., 1966, The Red Bird section of the Upper Cretaceous Pierre Shale in Wyoming, *with a section on* A new echinoid from the Cretaceous Pierre Shale of eastern Wyoming, by P. M. Kier: U.S. Geol. Survey Prof. Paper 393–A, 73 p.

Góczán, Ferenc, Groot, J. J., Krutzsch, Wilfried, and Pacltová, Blanka, 1967, Die Gattungen des "Stemma Normapolles Pflug 1953b" (Angiospermae); Neubeschreibungen und Revision Europäischer Formen (Oberkreide bis Eozän): Paläont. Abh., Sec. B, v. 2, no. 3, p. 429–525, 19 pls.

Pflug, H. D., 1953, Zur Entstehung und Entwicklung des angiospermiden Pollens in der Erdgeschichte: Palaeontographica, v. 95, Sec. B, nos. 4–6, p. 60–171, 11 pls.

Potonié, Robert, 1960, Nachträge Sporites, fortsetzung Pollenites, pt. 3 *of* Synopsis der Gattungen der Sporae Dispersae: Geol. Jahrb. Beihefte, v. 39, 189 p., 9 pls.

Samoilovitch, S. R., and others, eds., 1961 Pyl'tsa i spory zapadnoĭ Sibiri, Iura-Paleotsen [Pollen and spores of western Siberia, Jurassic to Paleocene]: Leningrad, Vses. Neft. Nauchno-Issled. Geol.-Razved. Inst. Trudy, new ser., no. 177, 657 p., 149 pls.

Srivastava, S. K., 1969, Upper Cretaceous proteaceous pollen from the Edmonton Formation, Alberta (Canada) and their paleoecologic significance: Canadian Jour. Botany, v. 47, no. 10, p. 1571–1578, 1 pl.

Traverse, Alfred, 1958, Locating plant microfossils on mixed slides: Micropaleontology, v. 4, no. 2, p. 207–208.

Tschudy, R. H., 1966, Associated megaspores and microspores of the Cretaceous genus *Ariadnaesporites* Potonié, 1956, emend., *in* Geological Survey Research 1966: U.S. Geol. Survey Prof. Paper 550–D, p. D76–D82.

Wodehouse, R. P., 1932, Tertiary pollen. I, Pollen of the living representatives of the Green River flora: Torrey Bot. Club Bull., v. 59, no. 6, p. 313–340, 3 pls.

THE LANDFALL PEAK ADAMELLITE AND REGIONAL COMPARISON OF PETROCHEMICAL AND AGE DATA FROM THE THURSTON ISLAND–EIGHTS COAST AREA, WEST ANTARCTICA

By AVERY ALA DRAKE, JR.,[1] R. F. MARVIN,[2]
T. W. STERN,[1] and HAROLD A. HUBBARD,[1]
[1] Washington, D.C., [2] Denver, Colo.

Work supported by the National Science Foundation

Abstract.—Plutonic rocks of two different types crop out on Thurston Island. A group of rocks petrographically and petrochemically identical with the Eights Coast batholith is probably Late Pennsylvanian in age. The Landfall Peak Adamellite is distinct from other west Antarctic intrusive rocks but is petrochemically similar to older volcanic rocks of the Jones Mountains. Mineral concentrates from the Landfall Peak Adamellite gave K–Ar ages of 150 and 145 m.y. and a lead-alpha age of 250 m.y. The Landfall Peak Adamellite may date from the Paleozoic and contain reset isotopic clocks, or it may be of Jurassic age.

Thurston Island, between the Amundsen and Bellingshausen Seas, in West Antarctica (figs. 1 and 2) was first visited by the 1959–60 U.S. National Science Foundation–U.S. Navy expedition to the Bellingshausen Sea. Seven localities were examined by Campbell Craddock and H. A. Hubbard (Craddock and Hubbard, 1961; Craddock and others, 1964b).

During the 1960–61 austral summer, two adjacent areas were reconnoitered: the Eights Coast (figs. 1, 2) by A. A. Drake, Jr., on the U.S. National Science Foundation–U.S. Navy expedition (Drake, 1962; Drake and others, 1964), and the Jones Mountains (figs. 1, 2) by geologists from the University of Minnesota (Craddock and others, 1964a).

More recently, geologists from the University of Wisconsin have made more detailed studies of areas of outcrop along the Eights Coast, Jones Mountains, and Thurston Island (Craddock and others, 1969).

The purpose of this paper is to describe rocks collected on Thurston Island, to present isotopic mineral ages of adamellite from the western end of the island,

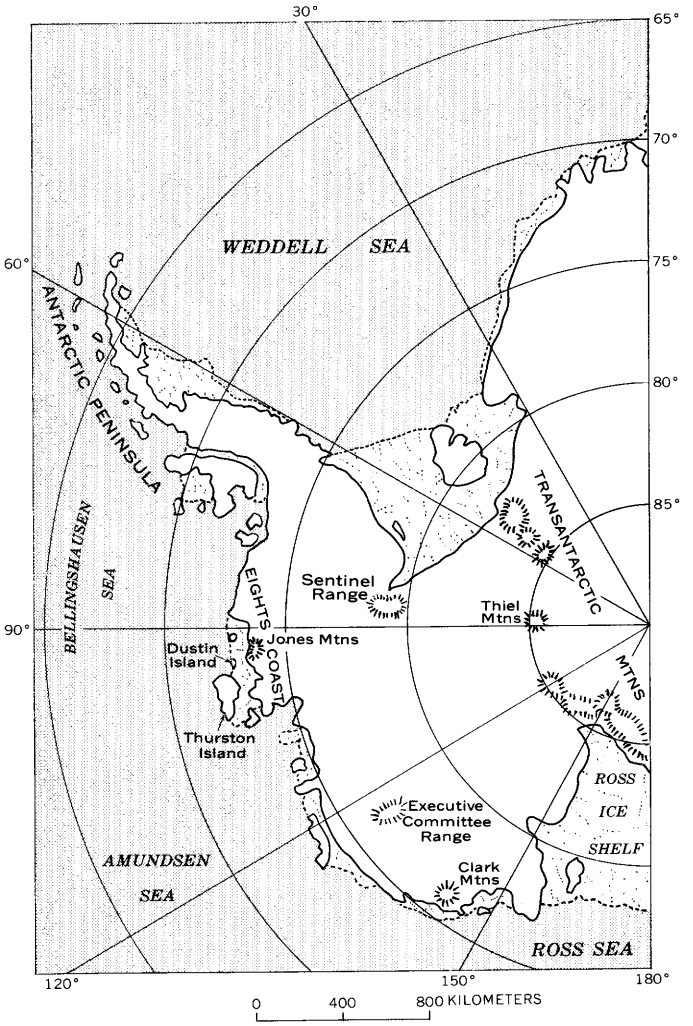

FIGURE 1.—Index map of West Antarctica, showing location of Thurston Island, Eights Coast, and Jones Mountains.

U.S. GEOL. SURVEY PROF. PAPER 750-B, PAGES B62-B73

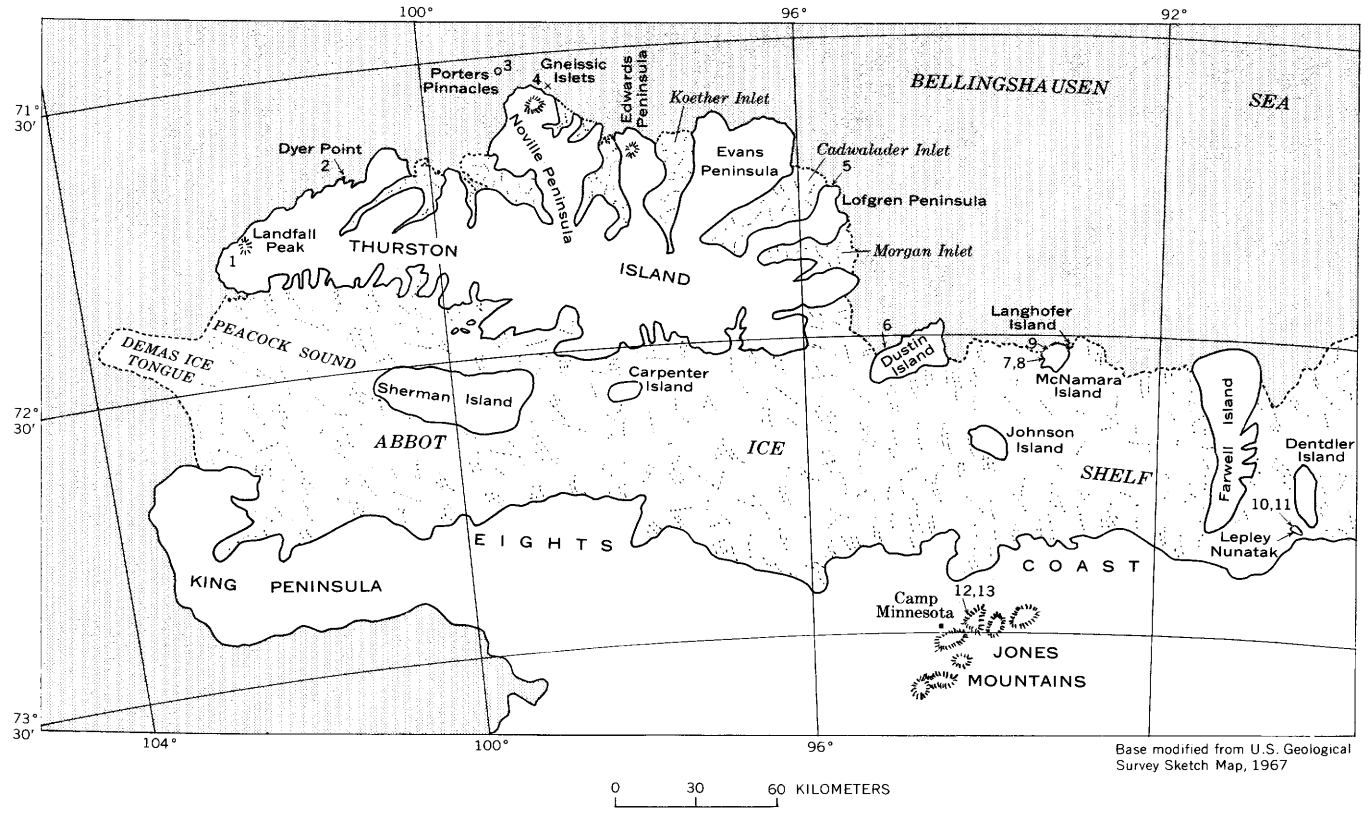

FIGURE 2.—Map of Thurston Island and Eights Coast, showing sample locations.

and to suggest some possible relations between the rocks of Thurston Island, the Eights Coast, and the Jones Mountains.

We wish to acknowledge the work of Campbell Craddock, Hubbard's geologic partner on the 1959–60 expedition, who examined outcrops on the eastern part of Thurston Island, whilst Hubbard examined those west of long 98° W. In addition, Craddock supplied us with samples of gneissic quartz diorite from eastern Thurston Island as well as samples of granite and intrusive felsite from the Jones Mountains.

GEOLOGIC SETTING

Rocks described from the Eights Coast–Thurston Island area consist mostly of quartz diorite or quartz diorite gneiss (Craddock and Hubbard, 1961; Drake, 1962; and Craddock and others, 1964b; Drake and others, 1964). These rocks are intrusive into metasedimentary rocks on Thurston Island and at places along the Eights Coast (Craddock and Hubbard, 1961; Drake, 1962) and cut gabbroic rocks on Dustin Island (fig. 2) (Drake and others, 1964). The quartz diorite from the Eights Coast area also has adamellite, granodiorite, and gabbro phases. These rocks have been assigned to the Eights Coast batholith (Drake, 1962; Drake and others, 1964). The rocks are very light gray, medium to coarse grained and have a poorly to well-developed foliation resulting from a parallel arrangement of biotite, hornblende, and plagioclase crystals. Typical modes (6, 7, 9, 10) of quartz diorite and leucogabbro are given in table 1. Amphibolite inclusions are common in the outcrops visited, as are mafic dikes.

Quartz diorite of the Eights Coast batholith is intruded by pink granitic rock on McNamara Island and Lepley Nunatak. These pink rocks are fine grained and are characterized by myrmekitic textures. They range from granodiorite to granite in composition and are probably small hypabyssal intrusive bodies. Typical modes (8 and 11) are given in table 1.

Quartz diorite gneiss similar to that of the Eights Coast batholith has been described from the eastern part of Thurston Island (Craddock and Hubbard, 1961; Craddock and others, 1964b). This Thurston Island rock has been interpreted as having a metamorphic origin (Craddock and others, 1964b); however, a sample (sample 5, table 1) furnished us by Craddock, although foliated, has the interlocking texture and delicately oscillatorily zoned plagioclase typical of intrusive rocks. More recently, Craddock and others (1969) have also reported intrusive rocks from

TABLE 1.—*Chemical analyses, CIPW norms, and modes of plutonic rocks from Thurston Island, Eights Coast, and Jones Mountains, Antarctica*

	1	2	3	4	5	6	7	8	9	10	11	12	13
Chemical analyses (weight percent)													
SiO_2	67.8	68.2	73.3	------	62.0	48.2	62.9	75.7	60.9	70.1	73.1	74.4	72.9
Al_2O_3	15.5	15.6	13.1	------	17.7	24.6	17.2	13.1	18.3	15.7	13.9	13.3	13.7
Fe_2O_3	1.3	1.1	.93	------	3.4	1.5	1.9	.80	3.7	1.1	1.5	.80	.95
FeO	2.6	2.2	2.3	------	2.6	2.8	2.4	.44	2.8	1.0	.65	.18	.50
MgO	.8	.7	.7	------	2.3	5.1	1.8	.1	1.9	1.0	.51	.42	.68
CaO	2.4	2.1	2.1	------	6.3	14.8	6.2	.20	6.4	3.2	1.1	.64	1.0
Na_2O	4.1	4.2	4.2	------	3.5	1.5	4.5	4.2	4.4	4.0	4.0	3.7	3.3
K_2O	4.4	4.3	1.5	------	.23	.34	1.2	4.5	.16	2.0	4.1	4.8	5.1
H_2O+	.57	.1	.14	------	.67	.16	.60	.12	.60	.21	.31	.48	.35
H_2O-	.05	.58	1.2	------	.31	.81	.05	.45	.06	1.2	.65	.52	.75
TiO_2	.51	.50	.34	------	.71	.31	.97	.21	.80	.32	.34	.11	.20
P_2O_5	.17	.12	.05	------	.40	.08	.44	.03	.30	.21	.12	.16	.17
MnO	.12	.12	.09	------	.13	.05	.08	.05	.12	.02	.06	.04	.05
CO_2	.05	.11	.11	------	.05	.08	.05	.09	.05	.07	.08	.05	.05
Total	100.4	99.9	100.1	------	100.3	100.33	100.2	100.0	100.5	100.1	100.4	99.6	99.7
CIPW norms													
Quartz	19.9	21.2	37.1	------	25.4	1.5	17.8	33.5	18.7	32.2	31.6	33.0	32.3
Orthoclase	26.1	25.6	8.9	------	1.1	1.7	7.2	27.1	1.1	11.7	24.5	28.9	30.6
Albite	34.6	35.6	36.1	------	29.3	12.6	38.2	36.1	37.2	34.1	34.1	32.0	27.8
Anorthite	11.1	10.3	9.7	------	28.6	59.2	23.4	1.1	29.5	15.0	4.7	2.5	4.2
Corundum		.3	1.0	------	1.4			.8		1.6	1.0	1.0	1.
$CaSiO_3$						5.6	2.1		.1				
$MgSiO_3$	2.0	1.8	1.8	------	5.7	12.8	3.4	.2	4.8	2.5	1.3	1.1	1.37
$FeSiO_3$	3.0	2.5	3.0	------	1.1	3.6	2.3		.9	.4			
Magnetite	1.9	1.6	1.4	------	4.9	2.1	2.8	.6	5.3	1.6	1.2	------	1.2
Ilmenite	.9	.9	.6	------	1.4	.6	1.8	.5	1.5	.6	.6	.2	.5
Apatite	.3	.3	.3	------	1.0	.3	1.0		.7	.3	.3	.3	.3
Hematite								.3			.6	.8	.2
Total	99.8	100.1	99.9	------	99.9	100.0	100.0	100.2	99.8	100.0	99.9	99.8	100.1
Modes (volume percent)													
Plagioclase	31.4	34.7	41.4	66.9	64.1	76.6	60.6	12.4	70.2	63.4	31.1		
Quartz	16.4	15.3	43.2	21.0	20.7	Tr.	22.5	36.9	18.6	23.3	34.3		
K-feldspar	44.2	42.0	6.0	2.8				48.4		2.3	31.4		
Biotite	4.7	5.1		3.7	3.8	5.7	7.1		3.9	1.1	17.0		
Hornblende	1.9	1.6	.8	.3	5.6	9.9	6.1		3.3	.2			
Chlorite	Tr.	Tr.	5.1	3.0	2.2	1.0		.8	1.1	6.5			
Opaque minerals	.8	.7	.3	1.6	2.5	Tr.	.8	.2	2.2	2.3	.9		
Sphene	Tr.	Tr.	Tr.	Tr.	.6	Tr.	1.6		.6	.5	.2		
Apatite	Tr.	Tr.	Tr.	------	.3	Tr.	.8	Tr.	Tr.	Tr.			
Myrmekite							Tr.			Tr.			
Epidote	Tr.	Tr.	3.1	.5	Tr.	1.0	Tr.	.6		.3			
Zircon	Tr.	Tr.	Tr.	------	Tr.		Tr.	Tr.	Tr.	Tr.	Tr.		
Carbonate minerals			Tr.					Tr.					
Clinopyroxene						4.9							

1. Medium-grained adamellite from Landfall Peak, Thurston Island. Plagioclase is calcic oligoclase as determined optically in oils. Collected by H. A. Hubbard.
2. Medium-grained adamellite from unnamed islet just off Dyer Point, Thurston Island. Plagioclase is calcic oligoclase as determined optically in oils. Collected by H. A. Hubbard.
3. Medium-grained granodiorite from dredge station 26, near Porter's Pinnacles, Bellingshausen Sea. Plagioclase is sodic andesine as determined optically in oils. Collected by H. A. Hubbard.
4. Fine- to fine-medium-grained hornblende-biotite quartz diorite from "Gneissic Islet," Thurston Island area. Plagioclase is andesine as determined optically in oils. Collected by H. A. Hubbard.
5. Medium-grained quartz diorite from east part of Lofgren Peninsula, Thurston Island. Plagioclase is sodic andesine as determined optically in oils. Collected by Campbell Craddock.
6. Gabbro from pavement outcrops near astro station on Dustin Island. Plagioclase is sodic bytownite as determined optically in oils. Collected by A. A. Drake, Jr.
7. Medium-grained quartz diorite from "Peelers Pinnacles," McNamara Island, Eights Coast (Drake and others, 1964). Plagioclase is sodic andesine as determined optically in oils.
8. Fine-grained granite from same location as 7. Plagioclase is sodic oligoclase as determined optically in oils. Rock has a granophyric texture and contains abundant myrmekite, the components of which were counted individually. Collected by A. A. Drake, Jr.
9. Medium-grained quartz diorite from northwest corner of McNamara Island. Plagioclase is sodic andesine as determined optically in oils. Collected by A. A. Drake, Jr.
10. Medium-grained quartz diorite from Lepley Nunatak, Eights Coast. Plagioclase is sodic andesine as determined optically in oils. Collected by A. A. Drake, Jr.
11. Fine-grained adamellite from same location as 10. Rock has a granophyric texture. Plagioclase is oligoclase. Collected by A. A. Drake, Jr.
12. Felsite dike from Avalanche Ridge, Jones Mountains. No thin section available for modal analysis. Collected by Campbell Craddock.
13. Pink granite from Avalanche Ridge, Jones Mountains. No thin section available for modal analysis. Collected by Campbell Craddock.

eastern Thurston Island. Intrusive and high-grade metamorphic rocks are very probably interlayered in this area.

South of the Eights Coast in the Jones Mountains (fig. 2), coarse-grained pink granite (sample 11, table 1) is in fault contact with felsic extrusive rocks (called herein Jones Mountains older volcanic rocks) (Craddock and others, 1964a). Both the granite and older volcanic rocks are cut by basalt and felsite (sample 10, table 1) dikes of Cretaceous(?) age and are unconformably overlain by flat-lying extrusive and hypabyssal bodies of olivine-basalt (Craddock and others, 1964a).

Four different rock types are known on the western part of Thurston Island: basement amphibolite, hornblende-biotite quartz diorite, hornblende-biotite adamellite, and hornblende granodiorite known only from a dredge sample.

The easternmost area visited by Hubbard, informally known as the gneissic islets, is at lat 71°50′30″ S., long 98°18′ W. (locality *4*, fig. 2). Here are two small islets, the larger of which is about 50–65 m long by 20–25 m wide. The exposed rock is gneissic, very light gray hornblende-biotite quartz diorite that contains conformable thin to thick layers of basement gneiss which here is "salt and pepper" amphibolite. Foliation dips steeply northeast and is marked in both diorite and amphibolite by oriented hornblende and plagioclase. A fault probably lies between the islets and the coast of Thurston Island, and apparently approximately parallels the coast. Rock similar to that of the islets crops out about halfway up the largely snow- and ice-covered cliff of the coast.

Amphibolite

The "salt and pepper" amphibolite is fine grained, the largest crystals being about 3 mm long. The amphibolite is composed principally of andesine and hornblende, but clinopyroxene and biotite are also present. Much of the andesine in the rock has been altered to sericite and epidote. Some plagioclase grains are normally zoned and appear similar to the feldspar in the biotite-hornblende diorite and are probably related to the emplacement of that unit. Much of the clinopyroxene has been altered to uralite. Biotite forms at the expense of hornblende and seems spatially related to zoned feldspars. Hornblende, including that in uralite, is commonly altered to mixtures of chlorite, epidote, and opaque minerals which have reaction rims of sphene.

Hornblende-biotite quartz diorite

The hornblende-biotite quartz diorite is fine to fine medium grained; most minerals range from 1 to 3 mm in maximum dimension, although some plagioclase phenocrysts are as much as 5 mm long. Paragenetically early well-twinned andesine, incipiently altered to sericite, forms large to medium-sized anhedral grains. Some of these grains are bent or broken. Other andesine forms medium-sized oscillatorily zoned crystals that have calcic oligoclase rims and occur spatially with late quartz. The quartz is strained and embays and penetrates hornblende and biotite. Much of the hornblende has been altered to pale-green chlorite, epidote, and opaque minerals which are spatially associated with sphene, which probably formed by reaction. The biotite is brown, and much of it has also been altered to chlorite. Apatite is abundant within the biotite. A mode (sample 4) is given in table 1.

Biotite-hornblende adamellite

Biotite-hornblende adamellite was studied at two places on Thurston Island. The first of these is at lat 71°56′ S., long 100°32′ W., just west of Dyer Point (loc. *2*, fig. 2). Here two of three small islets were examined. The rock exposed on the islets is massive, contains pinkish-gray potassium feldspar and light-gray plagioclase, and is characterized by clots of mafic minerals. The unit contains feldspathized inclusions of fine-grained amphibolite.

Adamellite also crops out on Landfall Peak at lat 72°00′30″ S., long 102°01′ W. on the northwesternmost end of Thurston Island (fig. 2). The peak rises from a gentle snow slope at an altitude of about 400 feet to about 1,300 feet. The east face is nearly vertical.

The rock exposed in this cliff is light- to medium-gray medium-grained biotite-hornblende adamellite. The rock has a faint flow structure which dips about 55° S. and is marked by parallelism of tabular minerals. Some phases of the adamellite are coarse grained and have sharp contacts with the medium-grained rock. Inclusions of partly digested feldspathized fine-grained amphibolite are present in the cliff. Numerous quartz veins range from ⅛ to 1 inch in width, average less than ½ inch, strike about east, and dip from vertical to about 55° S.

The biotite-hornblende adamellite is medium to coarse grained, the feldspars ranging from about 4 to 10 mm in size. The other minerals are less than 4 mm in maximum dimensions. The potassium feldspar is orthoclase microperthite, the exsolved well-twinned albite forming both patch and string intergrowths. Andesine forms both early subhedral zoned crystals and later well-twinned anhedral grains. The more calcic zones of the plagioclase are incipiently altered to sericite. Quartz is unstrained and encloses zircon, sphene, and apatite. Both biotite and hornblende are brown and are partly altered to chlorite and opaque minerals. The alteration

of the biotite and hornblende probably is the result of late-stage deuteric alteration, as evidence of post consolidation metamorphism is lacking. Modes (1 and 2) are given in table 1.

Hornblende granodiorite

Granitic rock was also collected in a dredge sample from near Porter's Pinnacles (loc. *3*, fig. 2). This rock, hornblende granodiorite, is pinkish gray to grayish orange pink and medium grained. Although plagioclase (andesine) and quartz grains average 3 to 4 mm, some plagioclase grains are as much as 9 mm in maximum dimension; mafic minerals occur in 1- to 2-mm clusters. Plagioclase is intergrown with large quartz grains. Some plagioclase is antiperthitic and has patches and rims of potassium feldspar. Late quartz forms small rounded grains and embays plagioclase. The rock is strongly altered, the andesine being saussuritized and the hornblende being largely altered to chlorite. A mode (13) is given in table 1.

PETROGRAPHIC COMPARISONS

The modal compositions of rocks collected from Thurston Island are compared with modes of other plutonic rocks from West Antarctica in table 1 and on figure 3. The hornblende-biotite quartz diorite from the gneissic islets (table 1, sample 4) clearly is petrographically similar to rocks of the Eights Coast batholith (table 1, samples 6, 7, 9, 10; Drake, 1962; Drake and others, 1964) as well as to gneissic quartz diorite collected by Craddock from the east end of Thurston Island (sample 5). The rock from the gneissic islets, as well as those from the east part of Thurston Island (Craddock and others, 1964b), contains abundant amphibolite layers and inclusions and may be a border phase of the Eights Coast batholith.

The Landfall Peak Adamellite (table 1, samples 1 and 2) does not plot with the Eights Coast rocks, nor does it resemble rocks of generally similar composition of the Andean granite-gabbro suite, the best known suite of west Antarctic rocks. The adamellite could conceivably be related to some of the poorly understood pre-Andean rocks of the Antarctic Peninsula. In any case, it is clear that the Landfall Peak rocks belong to a separate pluton.

The affinities of the dredged hornblende granodiorite (table 1, sample 3) are uncertain. It plots relatively near the Landfall Peak Adamellite and has clustered mafic minerals as does the adamellite. Its different appearance may be due to alteration, and it may well belong to the Landfall Peak Pluton.

AGE OF LANDFALL PEAK ADAMELLITE

Mineral concentrates separated from adamellite (1), collected at Landfall Peak, were dated radiometrically. The K-Ar ages of biotite and hornblende, together with

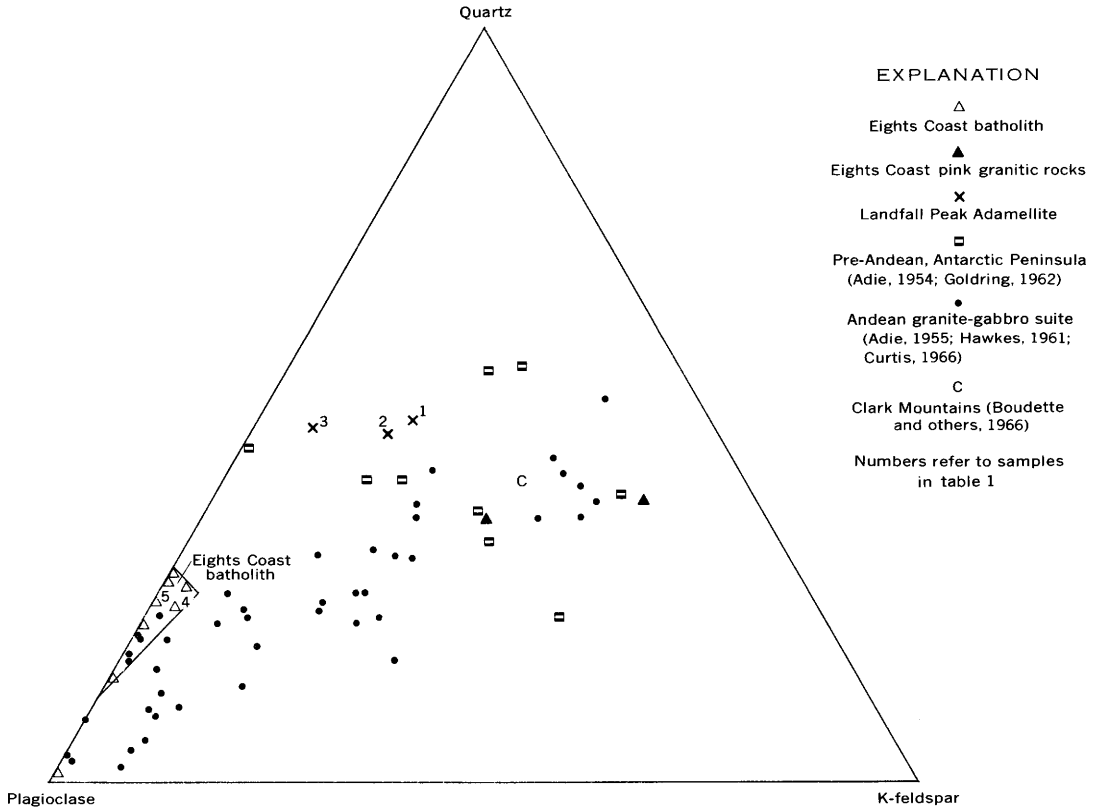

FIGURE 3.—Plot comparing modes of some intrusive rocks from West Antarctica.

TABLE 2.—*Analytical data and K-Ar ages of biotite and hornblende from adamellite 1, Landfall Peak, Thurston Island, Antarctica*

[Analysts: R. F. Marvin, H. H. Mehnert, H. H. Lipp, and Wayne Mountjoy. Approximate location of sample (field number 1): lat 72°00'30" S., long 102°01'15" W.]

Sample	K_2O (percent average)	K^{40} (ppm)	$*Ar^{40}$ (ppm)	$\frac{*Ar^{40}}{\text{Total } Ar^{40}}$ (percent)	$\frac{*Ar^{40}}{K^{40}}$	Age (m.y.)
Biotite	7. 29	7. 38	0. 0671	93	0. 00912	150±6
Hornblende [1]	. 871	. 882	. 00777	88	. 00883	145±5

Symbol: *, radiogenic isotope.
Decay constants: $K^{40}=0.585\times10^{-10}$/yr.
$=4.72\times10^{-10}$/yr.
Abundance: K $=1.22\times10^{-4}$ g/gK.
Potassium determinations, 7.23 percent and 7.38 percent K_2O for biotite. Ar determined by isotope-dilution techniques.

[1] Potassium determined by isotope dilution by W. T. Henderson and H. H. Mehnert: 0.876 percent and 0.866 percent K_2O.

the corresponding analytical data, are given in table 2. Although the K-Ar ages are slightly discordant, they indicate that the adamellite has a minimum age of about 150 m.y. (million years) (Jurassic).

The lead-alpha age of a zircon concentrate and corresponding analytical data are given in table 3. The lead-alpha age, 250 m.y., suggests a Permian age for the adamellite, but as lead-alpha ages can be anomalously old because of the presence of xenocrystic zircons or inherited lead, we will assume the K-Ar age to be approximately correct. We are aware, alternatively, that the K-Ar age may be a reduced age and that the system may have initially started during the Permian.

PETROCHEMICAL COMPARISON OF IGNEOUS ROCKS IN WEST ANTARCTICA

Petrochemical data from West Antarctica exclusive of the Transantarctic Mountains are few, but a comparison is important to better understand the few isotopic ages available. Granitic rocks of possible Tertiary age crop out in the southern part of the Antarctic Peninsula (Knowles, 1945). These rocks probably belong to the Andean granite-gabbro suite defined by Adie (1955). Late Cretaceous or early Tertiary isotopic ages were reported for similar rocks from the north part of the Antarctic Peninsula by Halpern (1962). Adie (1954) recognized older plutonic rocks in the Marguerite Bay of the Antarctic Peninsula and believed that these rocks were of early Paleozoic age. Drake and others (1964) showed that the rocks exposed along the Eights Coast differ petrochemically from the Andean suite, are distinctly older, and belong to a large composite batholith. Boudette and others (1966) found that adamellite in the Clark Mountains is of Late Jurassic age. Adie (1964) found that the Upper Jurassic volcanic group and Andean granite-gabbro suite of the Antarctic Peninsula are geochemically very much like each other as well as like the Jurassic volcanic and the Cretaceous intrusive suite of the West Patagonian Cordillera.

Halpern (1967) found that intrusive rocks in eastern Ellsworth Land are petrochemically similar to the Andean granite-gabbro suite and are of Cretaceous age. In a later paper, Halpern (1968) suggests that a late Paleozoic "Samfrau" orogenic-plutonic belt occupies most of West Antarctica and that the Cretaceous Andean orogenic-plutonic belt is marginal to or superposed on the "Samfrau belt" and follows the circum-Pacific margin of Antarctica toward New Zealand.

The chemistry of the Landfall Peak Adamellite and some other rocks from West Antarctica is compared in several variation diagrams. Rocks from the Andean granite-gabbro suite are included in all plots, as this is the only well-defined igneous suite in West Antarctica.

In the silica variation diagram (fig. 4), the Landfall Peak Adamellite contains more K_2O and total Fe and less CaO, MgO, and Al_2O_3 relative to SiO_2 than either Eights Coast of Andean rocks. MgO and Na_2O differ little in the three rock types. The Landfall Peak Adamellite differs most markedly from the Eights Coast rocks in K_2O and CaO content. Pink granitic rocks from the Eights Coast, Jones Mountains intrusive rocks, and the Clark Mountains Adamellite plot near the Andean variation curves. There is a suggestion that the Jones Mountains older volcanic rocks may be related to the Landfall Peak Adamellite.

TABLE 3.—*Lead-alpha age of zircon from adamellite 1 from Landfall Peak, Thurston Island, Antarctica*

[Alpha activity measurement by T. W. Stern; spectrographic analysis of lead by Harold Westley]

Alpha counts per milligram per hour	Lead [1] (ppm)	Calculated age [2] (m.y.)
188	19	250±30

[1] Average of duplicate determinations.
[2] Age calculated by the equation $t = C$ lead/alpha, where C, a constant based upon an assumed Th/U ratio of 1, equals 2,485, lead = lead content in parts per million, and alpha = alpha activity in alpha counts/mg-hr.

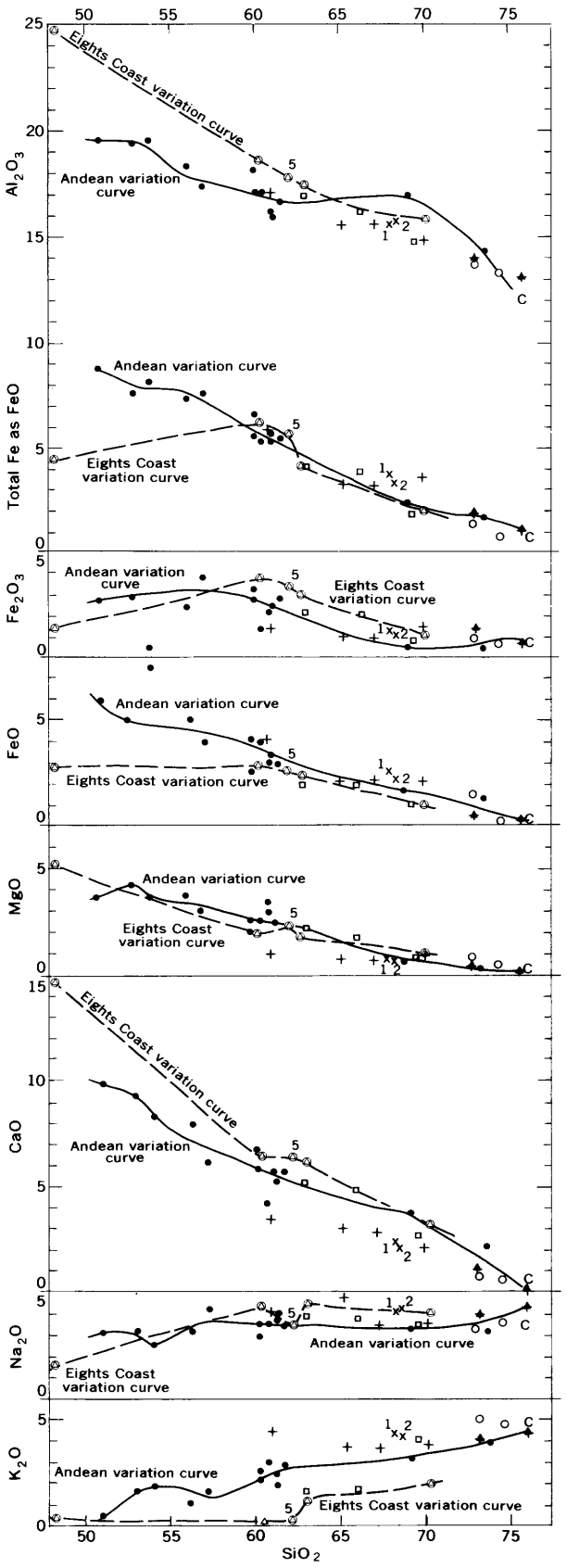

Rocks of the Marguerite Bay basement complex (Adie, 1964) are compared with the other west Antarctic rocks in figure 5. The Marguerite Bay, Andean, and Eights Coast rocks plot along distinctly different curves, and it is readily apparent that the Landfall Peak Adamellite is unrelated to any of these rocks. These plots also suggest that the Eights Coast pink granitic rocks may be related to the Andean suite, as are most of the rocks collected by the Expédition Antarctique Française.

Normative comparisons of the rocks discussed above are shown on figures 6 and 7. Analyses of the Marguerite Bay basement complex are not available for comparison, as only variation diagrams were published by Adie (1964). Rocks from the Eights Coast batholith and the Andean granite-gabbro suite plot in clearly defined fields as do the older volcanic rocks from the Jones Mountains. The Landfall Peak Adamellite plots within the Jones Mountains older volcanic field on both diagrams, supporting the suggested relation shown on the silica variation diagram (fig. 4). The dredge sample of hornblende granodiorite (table 1, sample 3) shows no systematic relation to any group of rocks. A genetic relation between the Andean suite and pink granitic rocks from the Eights Coast, Clark Mountain Adamellite, and intrusive rocks from the Jones Mountains is not well supported by these data.

West Antarctic rocks are also compared in Larsen diagrams (fig. 8). The tie lines of rocks from the Eights Coast batholith (fig. 8*A*) plot characteristically and differ markedly from those of the Andean suite (fig. 8*B*) and other west Antarctic igneous rocks. Plots of Landfall Peak Adamellite (fig. 8*C*) again differ markedly from the Andean and west Antarctic groups of rocks, but are similar to those of the Jones Mountains old volcanic rocks. The plots of the Eights Coast pink granitic rocks, Jones Mountains intrusive rocks, and Clark Mountain Adamellite resemble one another but are not like those of other rocks.

EXPLANATION

- △ Eights Coast batholith
- ▲ Eights Coast pink granitic rocks
- ▫ Antarctic Peninsula, Expedition Antarctique Française, 1903-05 (Hamilton, 1961)
- • Andean granite-gabbro suite (Adie, 1955)
- \+ Jones Mountains older volcanic rocks (Craddock and others, 1964a)
- o Jones Mountains intrusive rocks (Craddock and others, 1964a)
- x Landfall Peak Adamellite
- C Clark Mountains (Boudette and others, 1966)

FIGURE 4.—Silica variation diagram comparing the chemistry of some west Antarctic rocks.

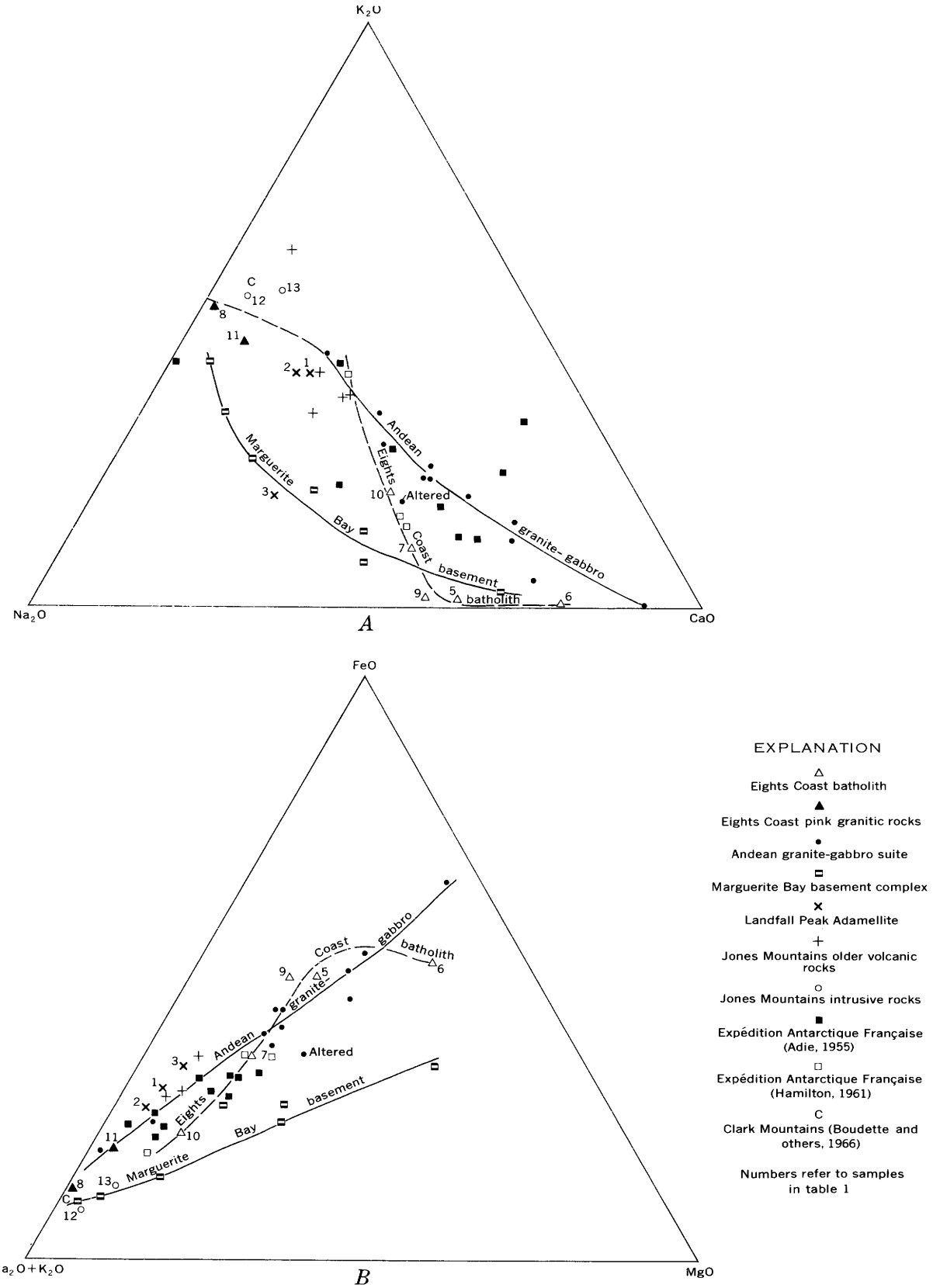

FIGURE 5.—Comparison of the compositions of some rocks from West Antarctica. *A*, K_2O–Na_2O–CaO; *B*, FeO–Na_2O+K_2O–MgO. Total iron as FeO (weight percent). Variation curves for Andean granite-gabbro suite and Marguerite Bay basement complex from Adie (1955, 1964). Numbers refer to sample numbers in table 1.

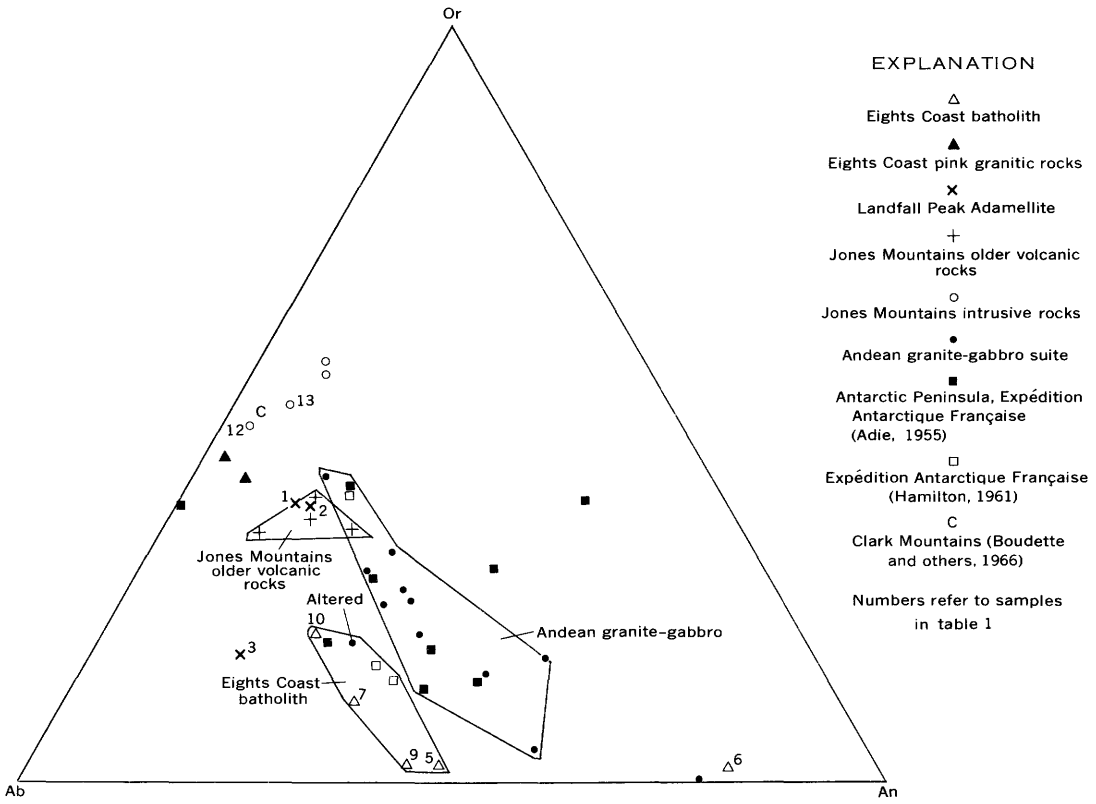

FIGURE 6.—Plot comparing norms of some igneous rocks from West Antarctica.

AGE CORRELATIONS

The Eights Coast batholith has been interpreted to be at least Jurassic (150 m.y.) in age (Drake and others, 1964) and to have undergone a thermal event about 97 m.y. ago. The foliated quartz diorite from the east end of Thurston Island is similar chemically and petrographically to the foliated rocks of the Eights Coast batholith and is probably of the same age. Craddock and others (1964b), however, report a Rb-Sr biotite age of 280 m.y. (Late Pennsylvanian-Early Permian) for the gneissic quartz diorite. It seems likely, therefore, that the Eights Coast batholith, including the quartz diorite from Thurston Island, is at least as old as Late Pennsylvanian. The lead-alpha age of zircon, 150 m.y. (Jurassic), from the Eights Coast sample is considered anomalously young.

The Landfall Peak Adamellite is not foliated, nor is there any petrographic evidence of recrystallization. A Permian age, however, is certainly not impossible, as suggested by the 250-m.y. lead-alpha age. Pink granite in the Jones Mountains has a minimum Late Triassic age, so Mesozoic plutonism is not impossible. If, on the other hand, the Landfall Peak Adamellite is related to the older volcanic rocks in the Jones Mountains, as suggested by the scanty available data, the 150-m.y. (Jurassic) age as given by the K-Ar method would be reasonable, as the volcanic rocks probably are between 104 and 199 m.y. old (Craddock and others, 1964a). It is also possible that the Eights Coast batholith, the Landfall Peak Adamellite, and the Jones Mountains pink granite all date from the Paleozoic, the contained isotopic clocks being variously reset by Andean plutonism. This solution would mesh nicely with Halpern's concept of an Andean plutonic-orogenic belt marginal to or superposed on a Paleozoic "Samfrau" plutonic-orogenic belt in this area.

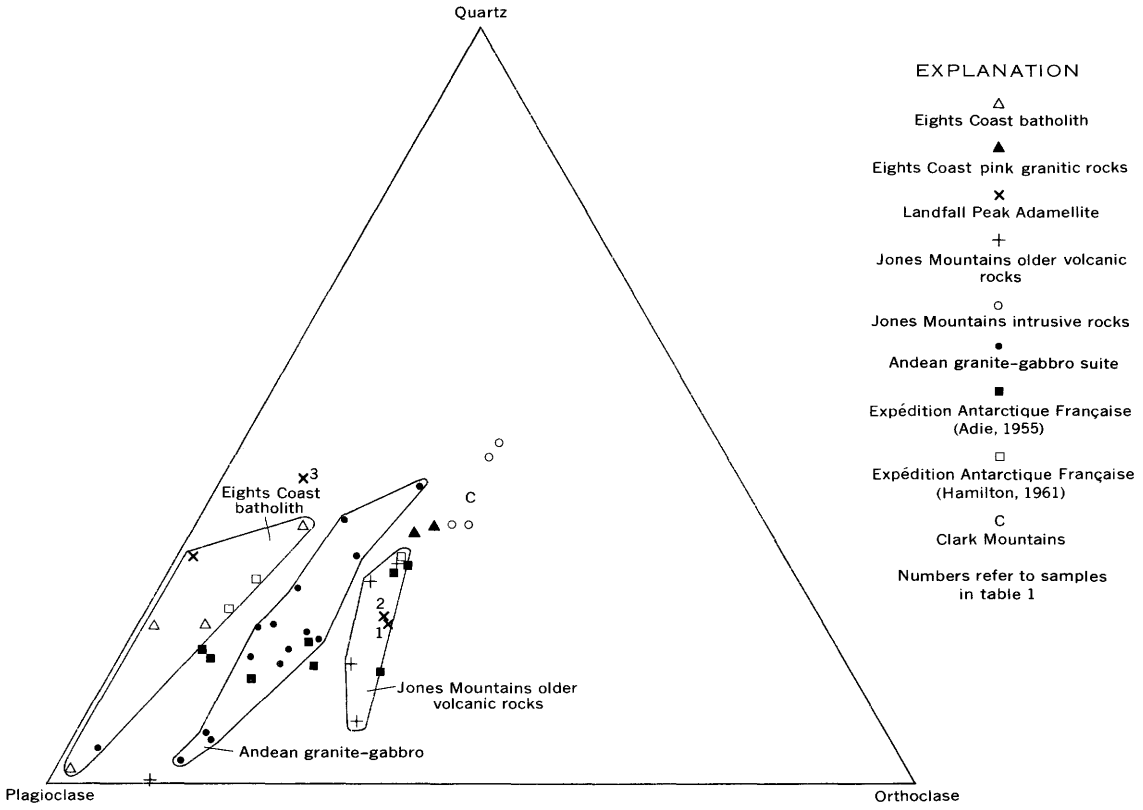

FIGURE 7.—Plot of norms of some igneous rocks from West Antarctica.

REFERENCES

Adie, R. J., 1954, The petrology of Graham Land; I, The basement complex; early Paleozoic plutonic and volcanic rocks: Falkland Islands Dependencies Survey, Sci. Rept. 11, 22 p.

——— 1955, The petrology of Graham Land; II, The Andean granite-gabbro intrusive suite: Falkland Islands Dependencies Survey, Sci. Rept. 12, 39 p.

——— 1964, The geochemistry of Graham Land, *in* Adie, R. J., ed., Antarctic geology: Amsterdam, North-Holland Pub. Co., p. 541–547.

Boudette, E. L., Marvin, R. F., and Hedge, C. E., 1966, Biotite, potassium-feldspar, and whole-rock ages of adamellite, Clark Mountains, West Antarctica: U.S. Geol. Survey Prof. Paper 550–D, p. D190–D194.

Craddock, Campbell, and Hubbard, H. A., 1961, Preliminary geologic report on the 1960 U.S. Expedition to Bellingshausen Sea, Antarctica: Science, v. 133, no. 3456, p. 886–887.

Craddock, Campbell, Bestien, T. W., and Rutford, R. H., 1964a, Geology of the Jones Mountains area, *in*, Adie, R. J., ed., Antarctic geology: Amsterdam, North-Holland Pub. Co., p. 171–187.

Craddock, Campbell, and others, 1964b, Rubidium-strontium ages from Antarctica: Geol. Soc. America Bull, v. 75, no. 3, p. 237–240.

Craddock, Campbell, White, C. M., and Rutford, R. H., 1969, The geology of the Eights Coast: Antarctic Jour., v. 4, no. 4, p. 93–94.

Curtis, R., 1966, The petrology of the Graham Coast, Graham Land: British Antarctic Survey Sci. Rept. 50, 51 p.

Drake, A. A., Jr., 1962, Preliminary geologic report on the 1961 U.S. Expedition to Bellingshausen Sea, Antarctica: Science, v. 135, no. 3504, p. 671–672.

Drake, A. A., Jr., Stern, T. W., and Thomas, H. H., 1964, Radiometric ages of zircon and biotite in quartz diorite, Eights Coast, Antarctica: U.S. Geol. Survey Prof. Paper 501–D, p. D50–D53.

Goldring, D. C., 1962, The geology of the Loubet Coast, Graham Land: British Antarctic Survey Sci. Rept. 36, 50 p.

Halpern, Martin, 1962, Potassium-argon dating of plutonic bodies in Palmer Peninsula and southern Chile: Science, v. 138, no. 3546, p. 1261–1262.

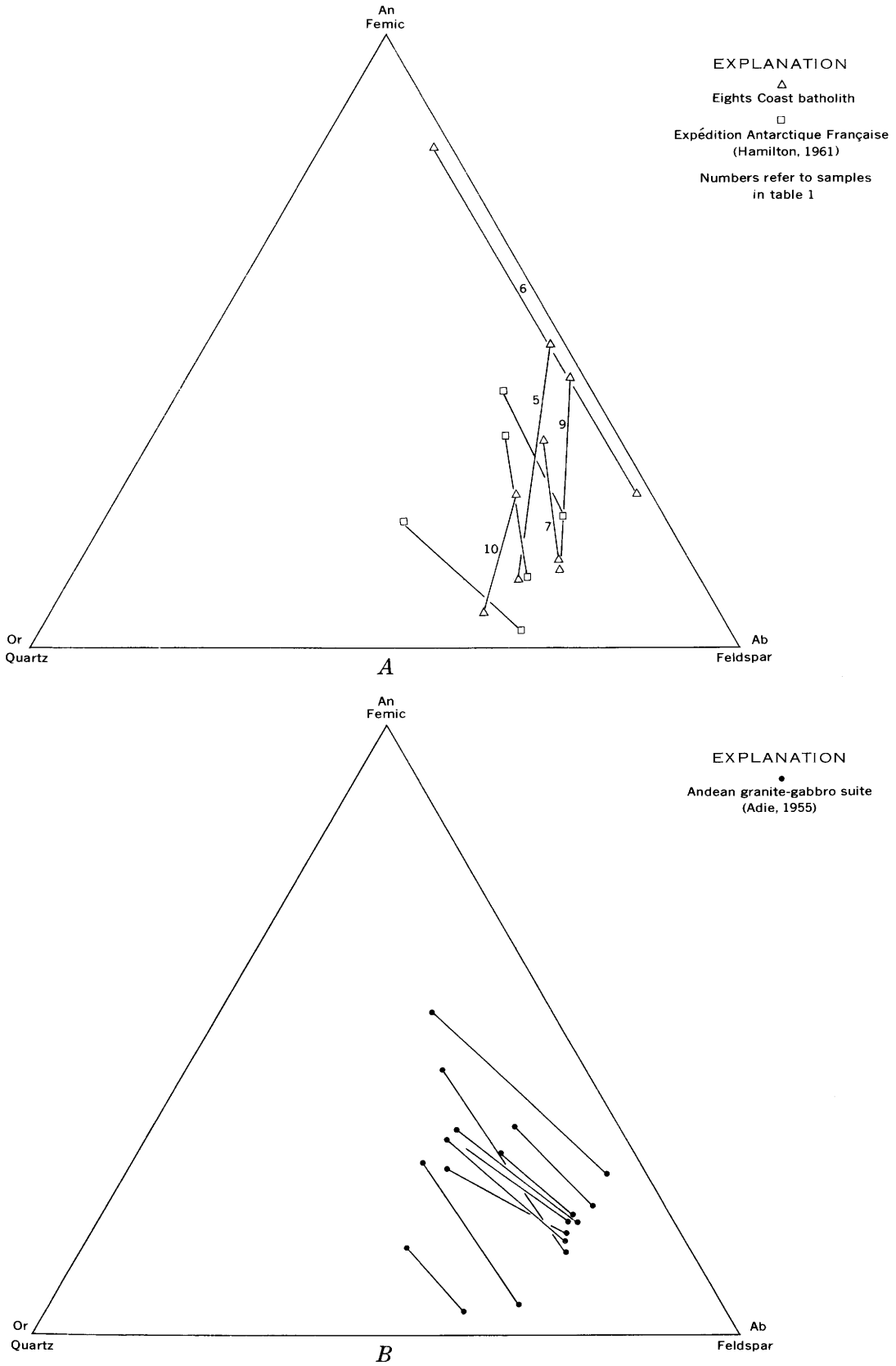
An
Femic
EXPLANATION
Eights Coast batholith
Expédition Antarctique Française
(Hamilton, 1961)
Numbers refer to samples
in table 1
6
5
9
7
10
Or
Quartz
Ab
Feldspar
A
An
Femic
EXPLANATION
Andean granite-gabbro suite
(Adie, 1955)
Or
Quartz
Ab
Feldspar
B

FIGURE 8.

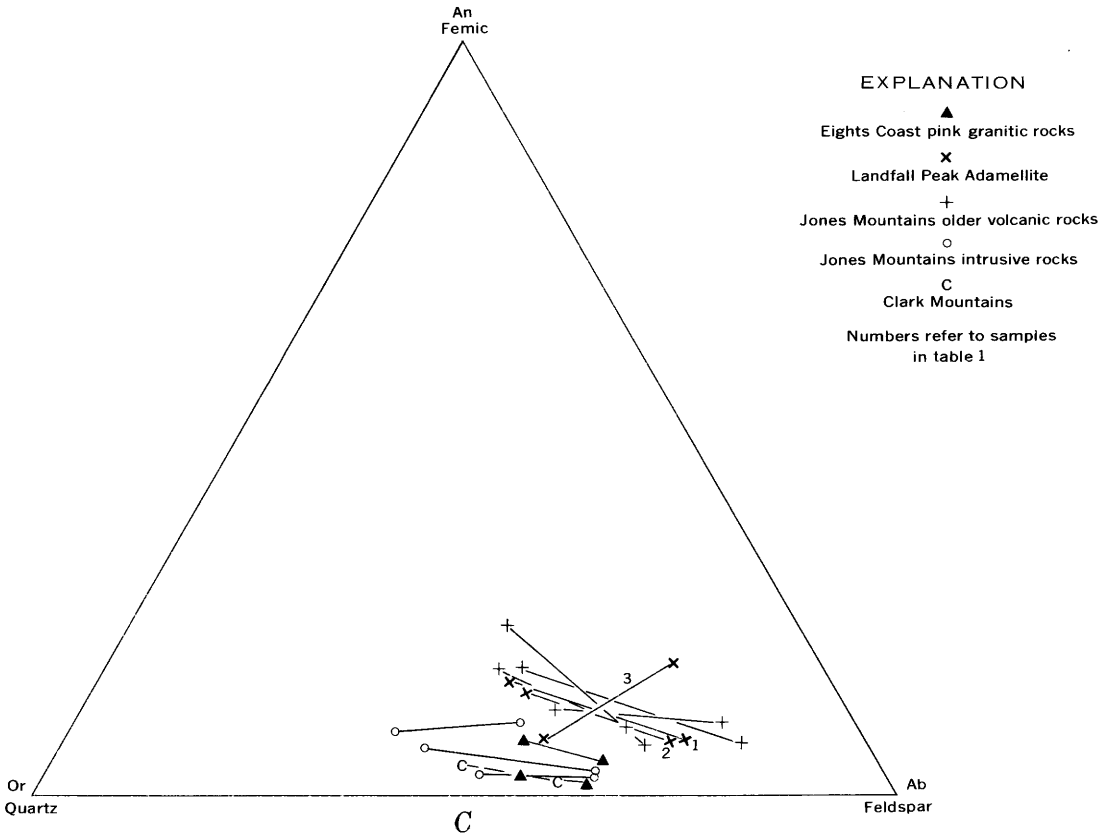

FIGURE 8.—Larsen plots showing normative comparison of some rocks from West Antarctica. *A*, Eights Coast batholith, Expédition Antarctique Française (Hamilton, 1961); *B*, Andean granite-gabbro suite (Adie, 1955); *C*, Landfall Peak Adamellite, Jones Mountains older volcanic rocks, Eights Coast pink granitic rocks, Jones Mountains intrusive rocks, and Clark Mountains rocks.

Halpern, Martin, 1967, Rubidium-strontium isotopic age measurements of plutonic igneous rocks in eastern Ellsworth Land and northern Antarctic Peninsula, Antarctica: Jour. Geophys. Research, v. 72, no. 20, p. 5133–5142.

——— 1968, Ages of Antarctic and Argentine rocks bearing on Continental drift: Earth and Planetary Sci. Letters, v. 5, no. 3, p. 159–167.

Hamilton, Warren, 1961, Petrochemistry of probable Paleozoic granitic rocks from the Ross Sea region, Antarctica: Art. 225 *in* U.S. Geol. Survey Prof. Paper 424–C, p. C209–C212.

Hawkes, D. D., 1961, The geology of the South Shetland Islands; I, The petrology of King George Island: Falkland Islands Dependencies Survey Sci. Rept. 26, 28 p.

Knowles, P. H., 1945, Geology of southern Palmer Peninsula, Antarctica: Am. Philos. Soc. Proc., v. 89, no. 1, p. 132–145.

AMPHIBOLITES NEAR SALIDA, COLORADO

By RALPH E. VAN ALSTINE, Washington, D.C.

Work done in cooperation with the Colorado Geological Survey

Abstract.—Field and chemical evidence is given for the origin of five Precambrian amphibolite samples from the Salida area, Colorado. It is concluded that concordant bodies of amphibolite were metagabbro sills at three of the localities and metabasalt flows at the other two. The chemistry and mineralogy of these two types of amphibolite are contrasted. The gabbroic rocks have lower differentiation indices and higher crystallization indices than the basaltic rocks. The amphibolites follow trends of basic- or middle-stage differentiates and not those of sedimentary rocks. The plotted relationships of Ni, Cr, and Niggli ti to Niggli mg for these amphibolites also are typical of basic igneous rocks.

In the Salida area, Chaffee County, Colo., many amphibolite masses are conformably interlayered in a Precambrian crystalline complex predominantly of sedimentary origin. Comparable bodies of hornblende gneiss and schist in areas immediately to the west (Dings and Robinson, 1957, p. 6) and north (Van Alstine, 1969, p. 6) were considered to have been produced by metamorphism of sedimentary rocks, although, in the western area, Stark (1934, p. 1005–1006) had recognized that the schist "grades into ellipsoidal greenstone not unlike the pillow lavas of the Lake Superior region." Rocks in the Salida area are less metamorphosed than those to the north and west, however, and it was thought that study of these amphibolites might reveal their origin. Five of the amphibolite masses, therefore, were examined in the field and studied petrographically in thin section, and chemical analyses were tested statistically to determine whether the rocks were of sedimentary or igneous origin. The investigation is part of a project conducted in cooperation with the Colorado Geological Survey.

On the basis of the field and laboratory studies, the five amphibolites are of igneous origin. Three are interpreted as metagabbro sills and two as metabasalt flows. This paper describes the evidence leading to these conclusions. Statistical testing of the chemical analyses followed techniques developed by Leake (1963, 1964), Shaw and Kudo (1965), and van de Kamp (1969).

FIELD AND PETROGRAPHIC RELATIONS

The amphibolites are interlayered with metasedimentary rocks consisting of black fine-grained amphibolitic and biotitic schists and phyllites, light-colored arkosic gneisses and quartzites, quartz-andalusite-sillimanite-garnet micaceous schist, quartz-plagioclase-cordierite schist, and skarn. The cordierite-bearing rock locally contains zoisite, phlogopite, talc, chlorite, gahnite, garnet, tourmaline, and accessory magnetite, sphene, apatite, and zircon.

Except for dikelike extensions from sills, the amphibolite bodies have concordant contacts with the adjacent rocks. In the area north of Salida (fig. 1) the amphibolites strike about N. 50° E. and dip 60° SE.; southwest of Salida those sampled strike north and dip 60° W. (fig. 2). In the area to the north the amphibolites range in thickness from about 2 to 350 feet, whereas those investigated to the southwest are 1–3 feet thick.

The original textures of the now strongly foliated amphibolites were largely obliterated during recrystallization to the almandite-amphibolite facies of regional metamorphism, but locally diabasic and amygdaloidal textures are present, and crystals of hornblende contain remnants of diopsidic pyroxene. Green hornblende forms 45–65 percent of the metagabbros and 73–74 percent of the metabasalts. The rest of the rocks consist largely of plagioclase; indices of refraction indicate that the composition is An_{53} to An_{85} in metagabbros and about An_{50} in metabasalts. One medium-grained metagabbro contains plagioclase crystals as long as 7 mm; all the other rocks are fine grained. A few flakes of biotite are found in one of the metagabbros, and quartz forms nearly 15 percent of another metagabbro. Quartz also is present in amygdules in the metabasalt, where

U.S. GEOL. SURVEY PROF. PAPER 750-B, PAGES B74-B81

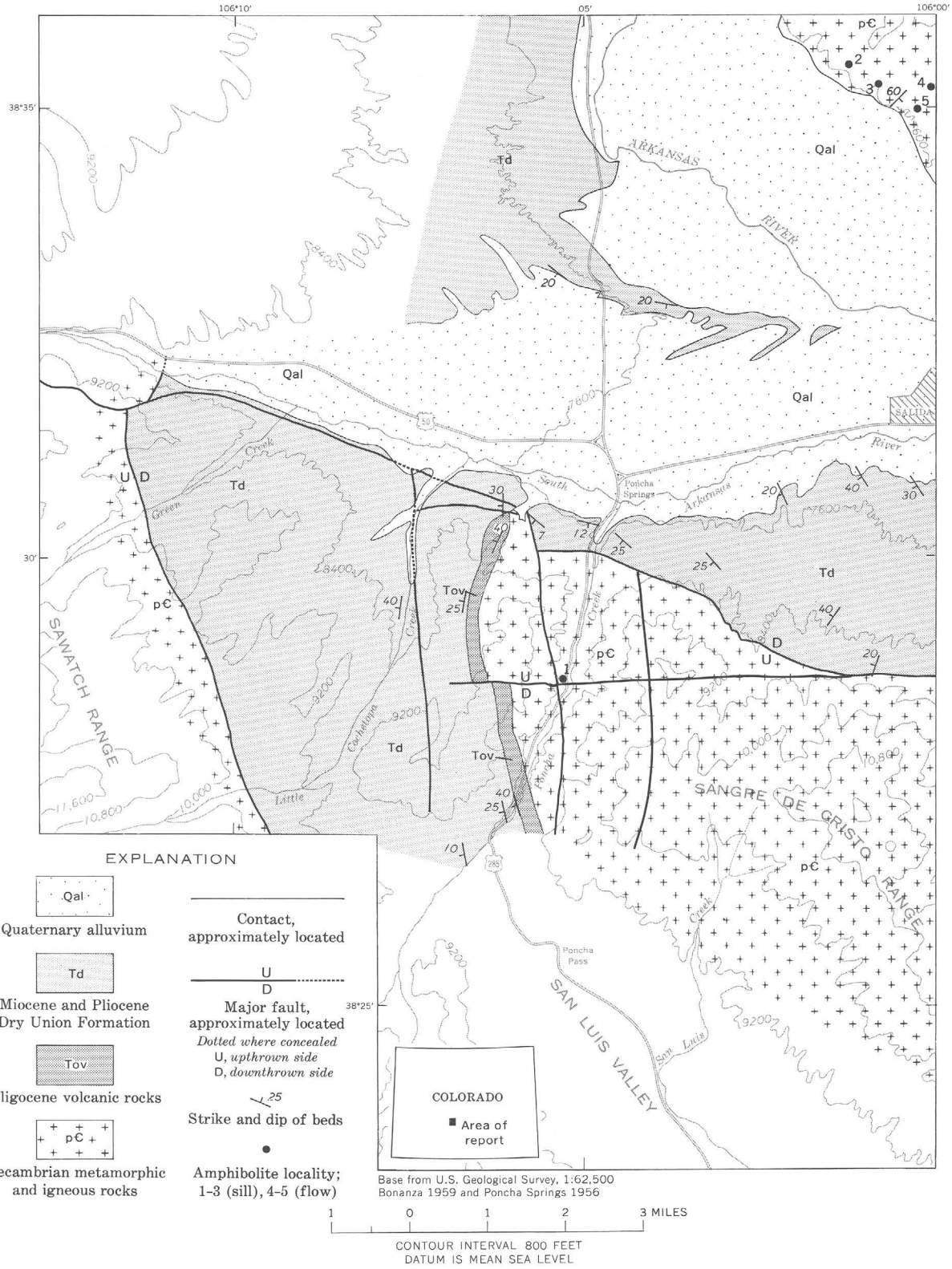

FIGURE 1.—Generalized geologic map of the Salida area, Chaffee County, Colo., showing five amphibolite localities.

413-504 O - 71 - 6

FIGURE 2.—Amphibolite along U.S. Highway 285 southwest of Salida, Colo. Black sills of metagabbro cut light-colored gneiss; pick (right center) shows scale.

it constitutes an estimated 2 percent of the rock. Hornblende appears to have formed later than plagioclase. In the quartz gabbro, quartz and magnetite embay the hornblende and other earlier formed minerals.

CHEMICAL RELATIONS

Comparison of analyses of the amphibolites in table 1 indicates some chemical differences between the metagabbros and metabasalts. The metagabbros are higher in magnesium oxide and calcium oxide contents than the metabasalts; total iron exceeds magnesia in all samples. The metabasalts have higher values of SiO_2, K_2O, Be, Nb, Pb, Sr, V, Y, Yb, and Zr than the metagabbros. These amphibolites have no normative corundum and almost no carbonate; thus they are not aluminous or calcareous metasediments. All these rocks have low Niggli k values, 0.15 or less, which is typical of orthoamphibolites. With respect to normative minerals and Niggli parameters (Niggli, 1954), the metabasalts have more orthoclase, ferrosilite, apatite, alk, and si than the metagabbros, but have no forsterite or fayalite and contain a less calcic normative plagioclase.

The two metagabbros have 4.5 and 10.5 normative olivine and are olivine tholeiites. In the Needle Mountains of southwestern Colorado, amphibolites considered by Barker (1969, p. A7–A9) to be metamorphosed olivine tholeiites have similar chemical analyses and mineralogy; pillow structures show that they are at least partly metavolcanic. Barker (1969, p. A19–A21) reported that other amphibolites in the area are interlayered with gneiss and have tholeiitic basalt compositions, normative quartz, hypersthene, and no olivine.

TABLE 1.—*Chemical compositions of amphibolites, Salida area, Chaffee County, Colo.*

	Metagabbro			Metabasalt	
Specimen no.	1	2	3	4	5
Chemical analyses [1] (weight percent)					
SiO_2	48.56	47.24	49.58	51.82	51.40
Al_2O_3	15.70	19.79	16.27	17.80	15.07
Fe_2O_3	2.96	3.17	6.88	2.62	3.98
FeO	7.25	6.44	5.49	6.60	8.91
MgO	8.46	5.57	6.57	5.00	3.99
CaO	10.65	12.82	11.18	9.33	9.64
Na_2O	2.94	2.12	.75	3.45	2.78
K_2O	.35	.57	.14	.83	.58
H_2O-	.14	.16	.08	.02	.02
H_2O+	1.19	1.00	1.00	1.08	1.36
TiO_2	.90	.80	1.30	.96	1.48
P_2O_5	.33	.34	.35	.41	.45
MnO	.29	.14	.38	.17	.23
F	.14	.10	.17	.12	.16
CO_2	.00	.02	.02	.04	.02
Subtotal	99.86	100.28	100.16	100.25	100.07
Less O	.06	.04	.15	.07	.10
Total	99.80	100.24	100.01	100.18	99.97
Semiquantitative 6-step spectrographic analyses [2]					
Ag	L	L	L	L	L
Ba	0.010	0.015	0.020	0.1	0.020
Be	L	N	L	.0001	.0001
Co	.005	.002	.005	.003	.005
Cr	.02	.003	.01	.01	L
Cu	.0007	.003	.003	.003	.003
Ga	.0015	.0015	.0015	.0015	.0015
Mo	.0003	N	.0003	.0007	N
Nb	N	N	.0003	.0005	.0005
Ni	.015	.003	.005	.007	L
Pb	N	N	N	.0015	.0010
Sc	.005	.0015	.005	.003	.005
Sr	.02	.03	.05	.07	.05
V	.015	.01	.02	.015	.03
Y	.002	.0015	.003	.003	.005
Yb	.0002	.00015	.0003	.0003	.0005
Zr	.005	.002	.005	.007	.007
Norms (weight percent)					
Quartz	0	0	13.6	1.3	6.8
Corundum	0	0	0	0	0
Orthoclase	2.1	3.4	0.8	4.9	3.5
Albite	25.3	18.1	6.4	29.5	23.8
Anorthite	29.0	43.2	41.0	30.9	27.3
Wollastonite	9.0	7.6	4.9	5.2	7.2
Enstatite	11.5	10.1	16.5	12.6	10.1
Ferrosilite	5.4	5.9	3.0	8.8	11.2
Forsterite	6.9	2.7	0	0	0
Fayalite	3.6	1.8	0	0	0
Magnetite	4.4	4.6	10.1	3.8	5.8
Ilmenite	1.7	1.5	2.5	1.8	2.8
Apatite	.8	.8	.8	1.0	1.1
Fluorite	.2	.1	.3	.2	.3
Total	99.9	99.8	99.9	100.0	99.9

See footnotes at end of table.

TABLE 1.—*Chemical compositions of amphibolites, Salida area, Chaffee County, Colo.*—Continued

	Metagabbro			Metabasalt	
Specimen no.	1	2	3	4	5
	Niggli values				
al	20. 61	26. 50	22. 68	26. 59	22. 85
fm	47. 11	36. 79	47. 04	38. 25	42. 68
c	25. 42	31. 21	28. 34	25. 34	26. 58
alk	6. 85	5. 50	1. 93	9. 82	7. 89
si	108. 20	107. 34	117. 31	131. 36	132. 26
ti	1. 51	1. 37	2. 31	1. 83	2. 86
p	. 31	. 33	. 35	. 44	. 49
h	8. 84	7. 58	7. 89	9. 13	11. 67
k	. 07	. 15	. 11	. 14	. 12
mg	. 60	. 51	. 49	. 49	. 36
si ′	127. 39	121. 98	107. 73	139. 28	131. 55
qz	−19. 20	−14. 64	9. 58	−7. 92	. 71
Salic	55. 71	64. 04	61. 26	65. 87	60. 57
Femic	43. 04	34. 92	37. 68	33. 00	38. 01
Differentiation index	27. 4	21. 5	20. 8	35. 7	34. 1
Crystallization index	52. 4	59. 6	58. 0	44. 0	39. 3

L, element detected, but below limit of determination; N, element looked for but not detected. Other elements looked for but not detected: As, Au, B, Bi, Cd, Ce, Eu, Ge, Hf, In, La, Li, Pd, Pt, Re, Sb, Sn, Ta, Te, Th, Tl, U, W, Zn.

[1] Standard rock analysis by Ann Vlisidis, Paul Elmore, and Sarah Berthold.
[2] Semiquantitative spectrographic analysis by Joseph Harris. Spectrographic results are reported in percent to the nearest number in the series 1.0, 0.7, 0.5, 0.3, 0.2, 0.15, 0.1, and so forth, which represents approximate points of group data on a geometric scale.

In figure 3, which is a ternary diagram for alk (K_2O+Na_2O), F ($FeO+2Fe_2O_3+MnO$), and M (MgO), the two olivine metagabbros plot near each other; the two metabasalts are close to them but are

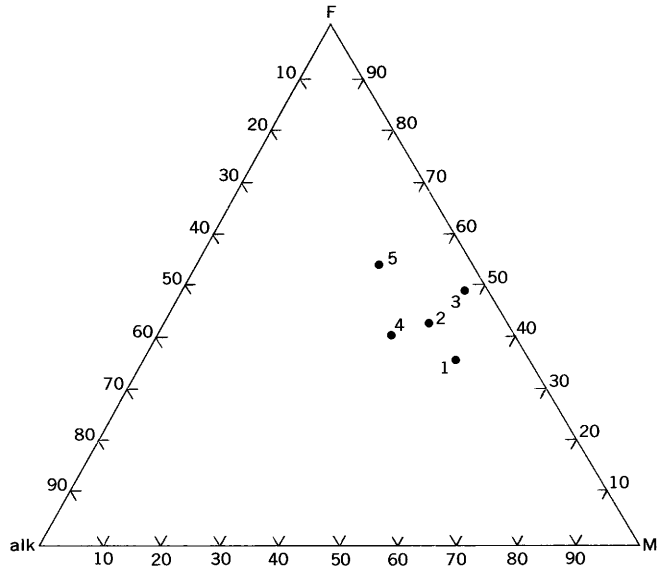

FIGURE 3.—Ternary variation diagram of alk (K_2O+Na_2O), F ($FeO+2Fe_2O_3+MnO$), and M (MgO) relations for five amphibolites, Salida area, Colorado. Specimens are same as in table 1.

richer in alkalies and poorer in magnesia. The third metagabbro, which actually is a quartz gabbro, is high in Al_2O_3, Fe_2O_3, and normative quartz, and low in FeO, Na_2O, and K_2O. It contains the most calcic normative plagioclase (An_{86}); its Fe_2O_3/FeO ratio is 1.3, whereas that ratio for the other four rocks ranges from 0.40 to 0.49.

Two methods [1] for distinguishing orthoamphibolites and para-amphibolites gave slightly different results when applied to the five analyses of amphibolites from the Salida area. The X_1 discriminant function, using Cr, V, Ni, Co, Sc, Sr, Ba, and Zr, gave positive (igneous) values for all five rocks analyzed (table 2); rocks

TABLE 2.—*Amphibolite discriminant functions for five rocks from the Salida area, Colorado*

[Methods of Shaw and Kudo (1965)]

Specimen number	1	2	3	4	5
Discriminant X_1	5. 8	2. 9	9. 3	4. 8	12. 0
Discriminant X_3	1. 4	−. 5	. 4	−. 4	1. 5

of sedimentary origin have negative values by this method. The X_3 discriminant function, using oxides of Ti, Al, Fe, Mn, Mg, Ca, P, and C, gave positive (igneous) values for two of the analyses. The calculations for the other three amphibolites were so close to zero that little confidence could be given to their discriminatory value; two amphibolite calculations gave slightly negative (sedimentary) values, and one result was slightly positive (igneous). An X_2 discriminant function of Shaw and Kudo (1965, p. 431) was not calculated for the amphibolites as it uses only values of cobalt and scandium and was regarded by the authors as less reliable than their two other discriminant functions.

Niggli mg-c plots (fig. 4) for the five amphibolites are closer to the differentiation trend of mafic igneous rocks than to trends of sedimentary rocks approximately at right angles to this trend (Leake, 1964, fig. 1). All five analyses plot with mafic igneous rocks and not with pelitic rocks or graywackes (Rivalenti and Sighinolfi, 1969, fig. 2). A triangular plot of Niggli mg, c, and al-alk (fig. 5) similarly shows that the five analyses closely follow the trend of Karroo dolerites rather than sedimentary compositional trends (Leake, 1964, fig. 2). All five analyses fall within the area of middle-stage differentiates.

[1] Discriminant functions after Shaw and Kudo (1965):
$X_1 = -2.69 \log Cr - 3.18 \log V - 1.25 \log Ni + 10.57 \log Co + 7.73 \log Sc + 7.54 \log Sr - 1.95 \log Ba - 1.99 \log Zr - 19.58$
$X_3 = 7.07 \log TiO_2 + 1.91 \log Al_2O_3 - 3.29 \log Fe_2O_3 + 8.48 \log FeO + 2.97 \log MnO + 4.81 \log MgO + 7.80 \log CaO + 3.92 \log P_2O_5 + 0.15 \log CO_2 - 15.08$
Major oxides in weight percent.
Trace elements in parts per million.

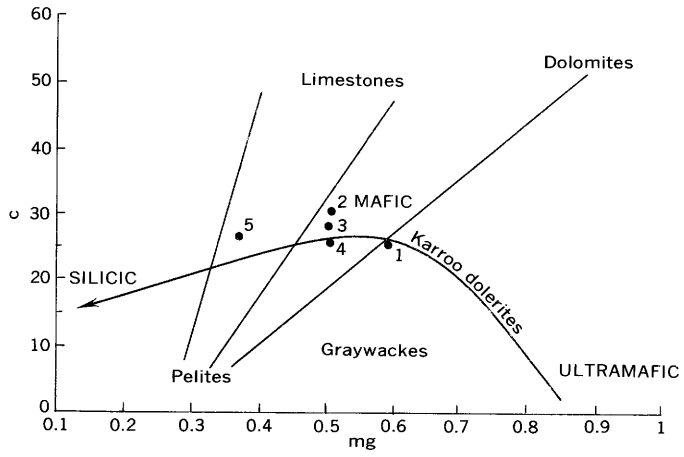

FIGURE 4.—Niggli c (CaO) and mg (MgO/FeO+MnO+2Fe_2O_3+MgO) variation diagram for five amphibolites, Salida area, Colorado. Trend lines for Karroo dolerites and for sedimentary mixtures from Leake (1964, fig. 1) and Rivalenti and Sighinolfi (1969, fig. 2).

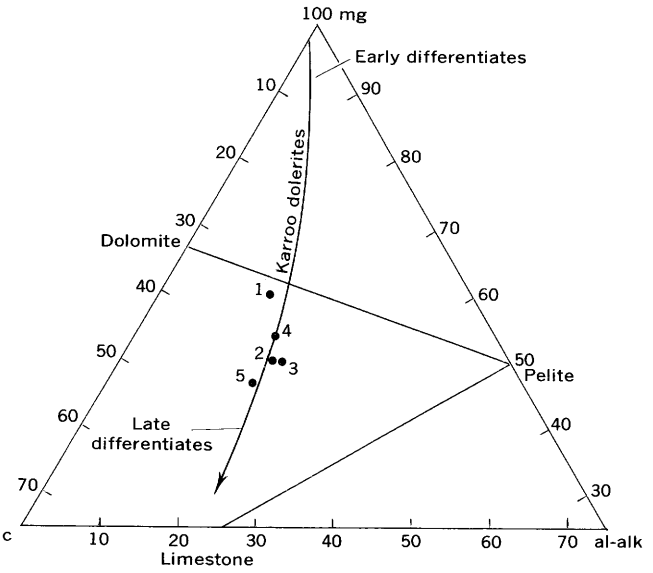

FIGURE 5.—Ternary variation diagram of Niggli mg×100, c, and al-alk (Al_2O_3—Na_2O+K_2O), recalculated to 100, for five amphibolites, Salida area, Colorado. Trend lines for Karroo dolerites and for sedimentary mixtures from Leake (1964, fig. 2).

Plots of Niggli mg and c against si (fig. 6) show that mg and c vary inversely with si for the five orthoamphibolites. For graywackes, Rivalenti and Sighinolfi (1969, p. 180–183) found no such correlation between these values. A plot of Niggli c against al-alk (fig. 7) shows that the five amphibolites are well within the boundary of the igneous field and not with graywackes on the boundary of the igneous and sedimentary fields (Rivalenti and Sighinolfi, 1969, p. 180).

As Orville (1969) suggested, all hornblende-plagioclase assemblages regardless of their igneous or sedimentary origin have compositions very much like those of

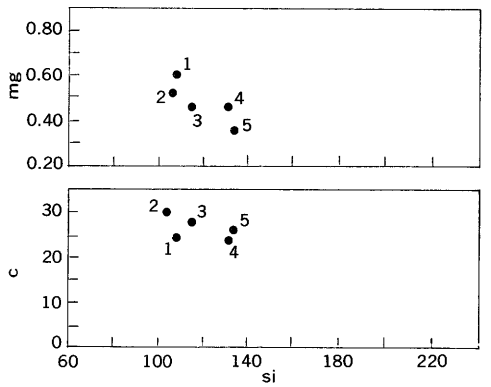

FIGURE 6.—Plot of Niggli mg, c, and si for five amphibolites, Salida area, Colorado.

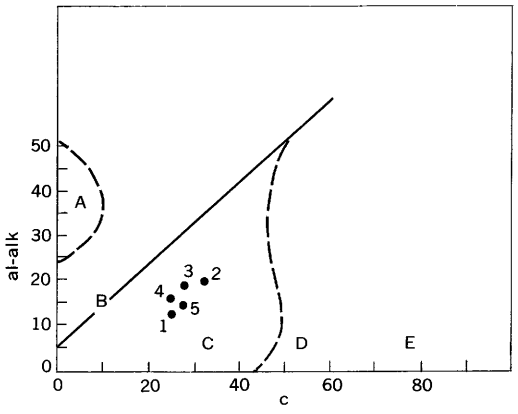

FIGURE 7.—Plot of Niggli c and al-alk for five amphibolites, Salida area, Colorado, A, B, C, D, and E approximate the fields of pelites, graywackes, igneous rocks, dolomites, and limestones, respectively. Partly from Rivalenti and Sighinolfi (1969, fig. 3) and from van de Kamp (1969, fig. 1).

mafic igneous rocks; therefore, bulk compositions are not necessarily diagnostic of origin, and certain minor elements, such as Ni, Cr, and Ti, may be more discriminatory than other constituents. In figure 8, which is a plot of Niggli ti and nickel and chromium contents against Niggli mg values for the five amphibolites, an increase of mg is accompanied by a marked increase in nickel and chromium and a decrease in ti. These abundance ranges and relationships are typical of mafic igneous rocks, whereas nickel and chromium in mixtures of pelitic sedimentary rocks with dolomite or limestone increase with decrease of mg (Leake, 1963, p. 1194; van de Kamp, 1969, fig. 3). A chemical analysis (Joseph Harris, U.S. Geological Survey, analyst, July 1, 1966) of a metasedimentary quartz-feldspar gneiss near the amphibolites north of Salida shows that all five amphibolites are consistently higher than the gneiss in Al, Cr, Fe, Mg, Ni, Sc, Sr, Ti, and V, and lower in Be, K, and Si.

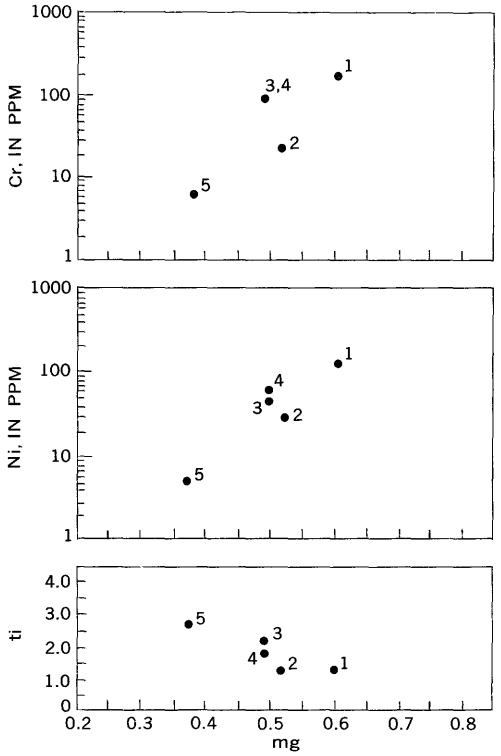

FIGURE 8.—Plot of Niggli mg, Niggli ti, and Ni and Cr contents for five amphibolites, Salida area, Colorado.

Plots of the differentiation indices of the amphibolites against the major oxides (fig. 9) show that these indices vary directly with SiO_2 and inversely with MgO and CaO. The differentiation indices (Thornton and Tuttle, 1960), which are the sums of the weight percentages of normative quartz, orthoclase, and albite, range from 20.9 to 27.3 in the metagabbros and from 34.1 to 35.7 in the metabasalts (table 1). The above relations between the indices and these major oxides are those shown by other igneous rocks whose composition becomes progressively more mafic, as suggested by Thornton and Tuttle (1960, p. 676).

Crystallization indices (Poldervaart and Parker, 1964, p. 285), measures of the progression of igneous rocks from the primitive system anorthite-diopside-forsterite, were calculated for the five amphibolites of the Salida area (table 1). As the indices for the three metagabbros range from 52.4 to 59.6 and those of the metabasalts are 39.3 and 44.0, the olivine metagabbros are less differentiated than the metabasalts. All but one of the rocks are within the gabbro (basalt) field when the crystallization indices are plotted against normative quartz (fig. 10).

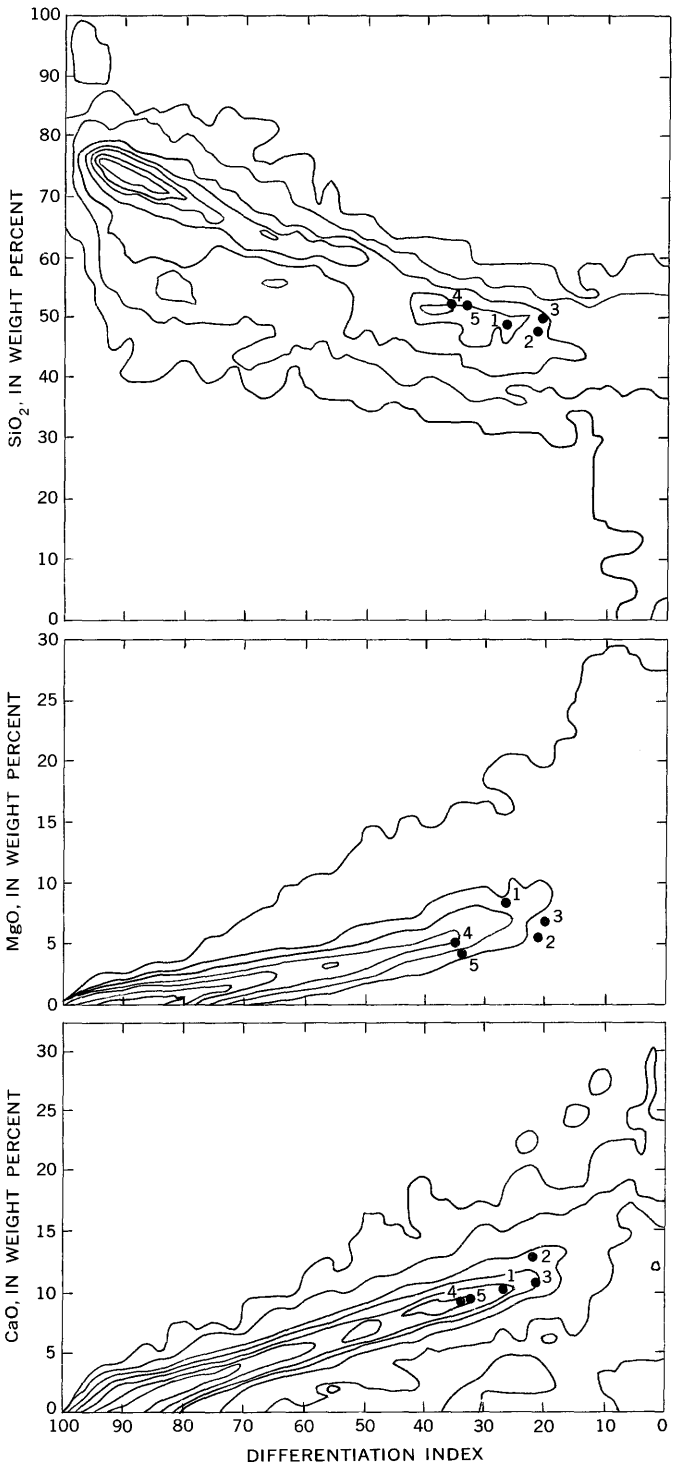

FIGURE 9.—Plot of the differentiation indices of five Salida area, Colorado, amphibolites against SiO_2, MgO, and CaO. Contoured diagrams represent 5,000 analyses of igneous rocks from Washington's tables (Thornton and Tuttle, 1960, p. 674–678).

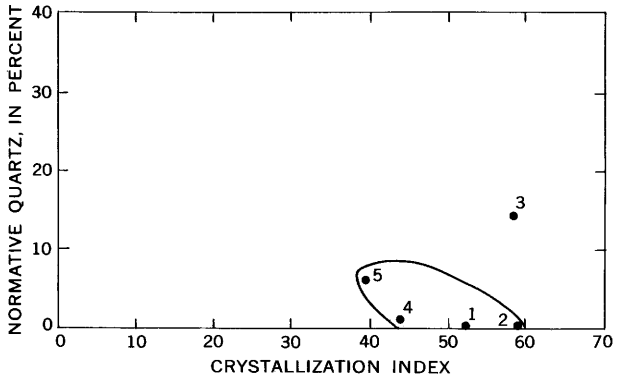

FIGURE 10.—Plot of the crystallization indices and normative quartz for five amphibolites, Salida area, Colorado. Four indices fall within the outlined gabbro (basalt) field (Poldervaart and Parker, 1964, fig. 2).

As an indication of the oxidation state, oxidation ratios expressed as mols $\frac{2Fe_2O_3 \times 100}{2Fe_2O_3 + FeO}$ were calculated for the five amphibolites from the Salida area (table 3). As this ratio gives the percentage of ferric atoms in total iron atoms, a rock containing only magnetite would have an oxidation ratio of 66.6 (Chinner, 1960, p. 186–187). If the quartz metagabbro that is richest in magnetite (specimen 3) is excluded, the average oxidation ratio of the amphibolites is 28, which agrees well with oxidation ratios for some other mafic igneous rocks. The average Connemara striped amphibolites of Ireland, which Evans and Leake (1960, p. 354, 361) showed to be metamorphosed rocks of basaltic composition, have an oxidation ratio of 28.9, and the average Watchung Basalt of New Jersey has an oxidation ratio of 26.1 (Preto, 1970, p. 780).

Barth (1948; 1955, p. 354) has reported that in the association of 100 cations with approximately 160 oxygens in ordinary rocks, the oxygen shows a strong tendency to accumulate in quartz and feldspars near the surface and to become scarcer with depth in olivines, pyroxenes, and related silicates. The numbers of oxygen ions needed to combine with cations in the five amphibolites of the Salida area are calculated at 153 and 155 for the two metagabbros and 157 and 158 for the two metabasalts. For the quartz metagabbro, the number of such oxygen ions is 160; this slightly greater number may be a reflection of the late-formed quartz and magnetite in this rock. Although the genetic relations of the metagabbros to the metabasalts are unknown and the rocks probably were emplaced at different levels of the crust, any slightly greater oxygen values originally in the extrusive rocks may have been preserved in spite of metamorphism of both rock types to the amphibolite stage.

TABLE 3.—*Oxidation ratios of amphibolites from the Salida area, Colorado*

[Fe_2O_3 and FeO values in weight percent]

Specimen number	1	2	3	4	5
Fe_2O_3	2. 96	3. 17	6. 88	2. 62	3. 98
FeO	7. 25	6. 44	5. 49	6. 60	8. 91
Oxidation ratio	26. 8	30. 7	53. 1	26. 2	28. 6

CONCLUSIONS

Chemical analyses of Precambrian amphibolites of the Salida area support field evidence that the concordant bodies were metagabbro sills and metabasalt flows. One method for discriminating between orthoamphibolites and para-amphibolites gave igneous values for all five amphibolites from the Salida area. A second method gave igneous values for two of the analyzed rocks, and calculations for the other three were so close to zero that they lack discriminatory value. These amphibolites follow trends of middle-stage differentiates and not those of sedimentary rocks.

REFERENCES

Barker, Fred, 1969, Precambrian geology of the Needle Mountains, southwestern Colorado: U.S. Geol. Survey Prof. Paper 644–A, 35 p.

Barth, T. F. W., 1948, The distribution of oxygen in the lithosphere: Jour. Geology, v. 56, no. 1, p. 41–49.

———1955, Presentation of rock analyses: Jour. Geology, v. 63, no. 4, p. 348–363.

Chinner, G. A., 1960, Pelitic gneisses with varying ferrous/ferric ratios from Glen Clova, Angus, Scotland: Jour. Petrology, v. 1, no. 2, p. 178–217.

Dings, M. G., and Robinson, C. S., 1957, Geology and ore deposits of the Garfield quadrangle, Colorado: U.S. Geol. Survey Prof. Paper 289, 110 p.

Evans, B. W., and Leake, B. E., 1960, The composition and origin of the striped amphibolites of Connemara, Ireland: Jour. Petrology, v. 1, no. 3, p. 337–363.

Leake, B. E., 1963, Origin of amphibolites from northwest Adirondacks, New York: Geol. Soc. America Bull., v. 74, no. 9, p. 1193–1202.

——— 1964, The chemical distinction between ortho- and para-amphibolites: Jour. Petrology, v. 5, no. 2, p. 238–254.

Niggli, Paul, 1954, Rocks and mineral deposits: San Francisco, W. H. Freeman and Co., 559 p.

Orville, P. M., 1969, A model for metamorphic differentiation origin of thin-layered amphibolites: Am. Jour. Sci., v. 267, no. 1, p. 64–86.

Poldervaart, Arie, and Parker, A. B., 1964, The crystallization index as a parameter of igneous differentiation in binary variation diagrams: Am. Jour. Sci., v. 262, no. 3, p. 281–289.

Preto, V. A. G., 1970, Amphibolites from the Grand Forks quadrangle of British Columbia, Canada: Geol. Soc. America Bull., v. 81, no. 3, p. 763–782.

Rivalenti, Giorgio, and Sighinolfi, G. P., 1969, Geochemical study of graywackes as a possible starting material of para-amphibolites: Contr. Mineralogy and Petrology, v. 23, p. 173–188.

Shaw, D. M., and Kudo, A. M., 1965, A test of the discriminant function in the amphibolite problem: Mineralog. Mag., v. 34, no. 268, p. 423–435.

Stark, J. T., 1934, Reverse faulting in the Sawatch Range: Geol. Soc. America Bull., v. 45, no. 6, p. 1001–1015.

Thornton, C. P., and Tuttle, O. F., 1960, Chemistry of igneous rocks—[Pt.] 1, Differentiation index: Am Jour. Sci., v. 258, no. 9, p. 664–684.

Van Alstine, R. E., 1969, Geology and mineral deposits of the Poncha Springs NE quadrangle, Chaffee County, Colorado: U.S. Geol. Survey Prof. Paper 626, 52 p.

van de Kamp, P. C., 1969, Origin of amphibolites in the Beartooth Mountains, Wyoming and Montana—New data and interpretation: Geol. Soc. America Bull., v. 80, no. 6, p. 1127–1135.

MINOR-ELEMENT CHANGES IN PELITIC BELT ROCKS CAUSED BY METAMORPHISM IN THE PEND OREILLE AREA, IDAHO–MONTANA

By J. E. HARRISON and J. C. HAMILTON, Denver, Colo.

Abstract.—Changes in trace-element content during regional and cantact metamorphism of certain Belt argillites and siltites have been examined by means of quantitative spectrographic and wet chemical analyses. Identification of changes during metamorphism is complicated by a considerable range in original content plus increased variability in both rock types during metamorphism. Trends suggest loss of B, Co, Cr, and Ni, and perhaps Ba, Pb, Sc, and V. Sr and perhaps Ga have increased in contact-metamorphosed rocks. Data on Cu do not indicate clearly whether the Cu content has increased or decreased during metamorphism. They do indicate that Cu has been redistributed to some degree, which suggests that metamorphic processes should not be discarded as potential contributors to stratabound copper deposits in Belt rocks.

Recent comparative studies of the geochemistry of Belt rocks from two widely separated areas in Idaho and Montana (Harrison and Grimes, 1970) suggested that further investigation of the Idaho area might pinpoint changes in minor-element content during regional and contact metamorphism of Belt rocks. The earlier studies used semiquantitative spectrographic methods of analysis, which revealed some trends of change and hinted that others might be present. We hoped that quantitative spectrographic analysis would document trends identified in the earlier studies as well as reveal further trends not identifiable by the less precise semiquantitative method.

We selected a total of 88 samples of 2 rock types from each of 2 formations for the current study. Previous studies indicated that the pelitic rocks—argillites and siltites—were more uniform from place to place than psammitic or carbonate rocks. The pelitic rocks, therefore, offered a better opportunity to examine small chemical changes due to a metamorphic process, because the original chemical variability was small and not as likely to mask small differences resulting from metamorphism. In addition, certain pelitic rock types could be identified with confidence in the higher grade metamorphic zones where schists and gneisses had been formed from the argillites and siltites.

Spectrographic analytical techniques used in this study have been described elsewhere (Bastron and others, 1960). The generally low content of lead and zinc required that we use a wet chemical method described by Holmes (1945) for determination of these elements. Precision of the spectrographic method for several elements in sedimentary rocks similar in minor-element content and general chemistry to Belt rocks is given by Barnett (1961) in terms of the coefficient of variation for a single spectrographic determination. The precision ranges from 6 to 20 percent, with most elements at about 10 percent. Using similar calculations, we determined the precision for a single determination by the wet chemical method used for low-level lead and zinc to be 17 percent for lead and 32 percent for zinc.

GEOLOGIC SETTING

The Pend Oreille area is almost entirely in the Idaho panhandle (fig. 1). Bedrock of the area is predominantly rocks of the Belt Supergroup that have been intruded by scattered plutons of granodiorite of Cretaceous age.

Belt rocks of the area are a monotonous sequence, at least 42,000 feet thick, of argillite and siltite, minor quartzite, and sparsely scattered limestone or dolomite. Metamorphism increases from top to bottom: the Missoula Group rocks, uppermost in the Belt, are in the chlorite–sericite zone of the greenschist facies; secondary biotite first appears in parts of the Wallace Formation; and the Ravalli Group and the Prichard Formation are in the biotite zone of the greenschist facies.

Metamorphism has also resulted from intrusion of Precambrian gabbroic sills, Tertiary porphyry dikes, and Cretaceous granodiorite plutons. Contact metamorphic effects from the sills and dikes are generally

U.S. GEOL. SURVEY PROF. PAPER 750-B, PAGES B82-B91

limited to a few feet of hornfels host rocks on each side of the intrusive sheet, but the Cretaceous plutons have metamorphic aureoles a few hundred to a few thousand feet wide approximately proportional to the size of the now-exposed pluton.

Structurally, the Pend Oreille area represents a highly faulted west limb of a large syncline trending approximately north. Large upright to overturned folds related to thrusting occur in the northwest part of the area, and smaller folds are scattered throughout the remainder of the area where faulting or forceful intrusion of the Cretaceous plutons has disturbed the rocks. A major fault, the Hope, transects the center of the area (fig. 1); apparent movement along this fault is about 16 miles right lateral.

Two formations are particularly suited to a study of metamorphic effects. The Wallace Formation contains pelitic rocks that are in the chlorite–sericite zone of regional metamorphism in some areas and, mostly in lower parts of the formation, are in the biotite zone of regional metamorphism. The Prichard Formation contains pelitic rocks that are everywhere in the biotite zone of regional metamorphism, and, at places, are in the biotite or garnet zone of contact metamorphism. In addition, increased metamorphism has changed the normally bedded but biotitic rocks into schistose or gneissic rocks that still retain some of the original bedding structures, such as thin black-and-white laminations or the salt-and-pepper aspects of poorly laminated, even-grained siltites. The number of samples of each metamorphic grade, rock type, and formation used in this study is given in table 1.

CHEMICAL DATA

Analytical results on selected minor elements of each sample are given in table 2. Sample localities are shown on figure 1.

Table 3 presents statistical summaries of the various groups of samples listed in table 2 on all elements except beryllium, the concentration of which was reported as at or below the sensitivity limit for most samples. For purposes of calculation, a small number about halfway between the sensitivity limit and zero was substituted for the L's in table 2 as follows: Co, 2; Cu, 1; Ga, 5; Nb, 10; Ni, 2; and Sc, 2. Where more than half the samples in a given group were reported as L, no statistical calculations were made; the mean ($\overline{X}$) is reported in table 3 as less than the sensitivity limit for the element (for example, L(50) for boron in one group of Prichard argillites). All statistical results are reported to two significant figures, in accordance with standard practice.

TABLE 1.—*Distribution of samples among formations, rock types, and metamorphic grades, Pend Oreille area, Idaho*

Formation	Rock type	Metamorphic grade ←Regional→ ←Contact→		
		Chlorite–sericite	Biotitic but bedded	Biotitic gneiss or schist
Wallace	Argillite	6	5	---
	Siltite	5	11	---
Prichard	Argillite		14	24
	Siltite		8	15

INTERPRETATION OF DATA

The standard deviations for most of the elements are fairly large (table 3). The ratio of the standard deviation to the mean, expressed in percent (coefficient of variation), ranges from 1 to 169 and averages about 40. Figure 2 expresses this ratio graphically and also gives some information about the rocks and the processes that have affected them.

Large standard deviations in these analyses could result from imprecision in analytical technique, errors in sampling or grouping the rock types, original sedimentary ranges in trace-element composition, and variations resulting from metamorphism. Precision of the analytical technique averages about 10 percent, which is considerably less than the average coefficient of variation for the sample groups. Much of the copper is in discrete sulfide minerals unevenly distributed in the sample; the exceptionally large coefficients of variation (fig. 2) are in part due to the particulate nature of the small amounts of copper in these Belt rocks (Harrison and Grimes, 1970). Element content near the sensitivity limit of the method results in significant loss of precision. In the graphs (fig. 2) for Co, Ga, Nb, and Ni, this is a factor that should cause larger than normal coefficients of variation. The rocks have been grouped on the basis of formation, grain size, mineralogy, and degree of recrystallization. Each of these factors is readily discernible, although most require petrographic examination and X-ray analysis. This extra care in grouping and splitting of pelitic rocks into argillites and siltites stems from the experience of Shaw (1954), who had difficulty in discovering trends of trace-element change during metamorphism, because of considerable range in parent-rock composition. For most elements, therefore, the graphs are believed to portray a measure of the original variation in element content and to give some indication of metamorphic trends.

A consistently large coefficient of variation (all bars in the graph for a given element are tall) indicates a large original variation not reduced significantly during metamorphism. This seems true in general for copper and lead.

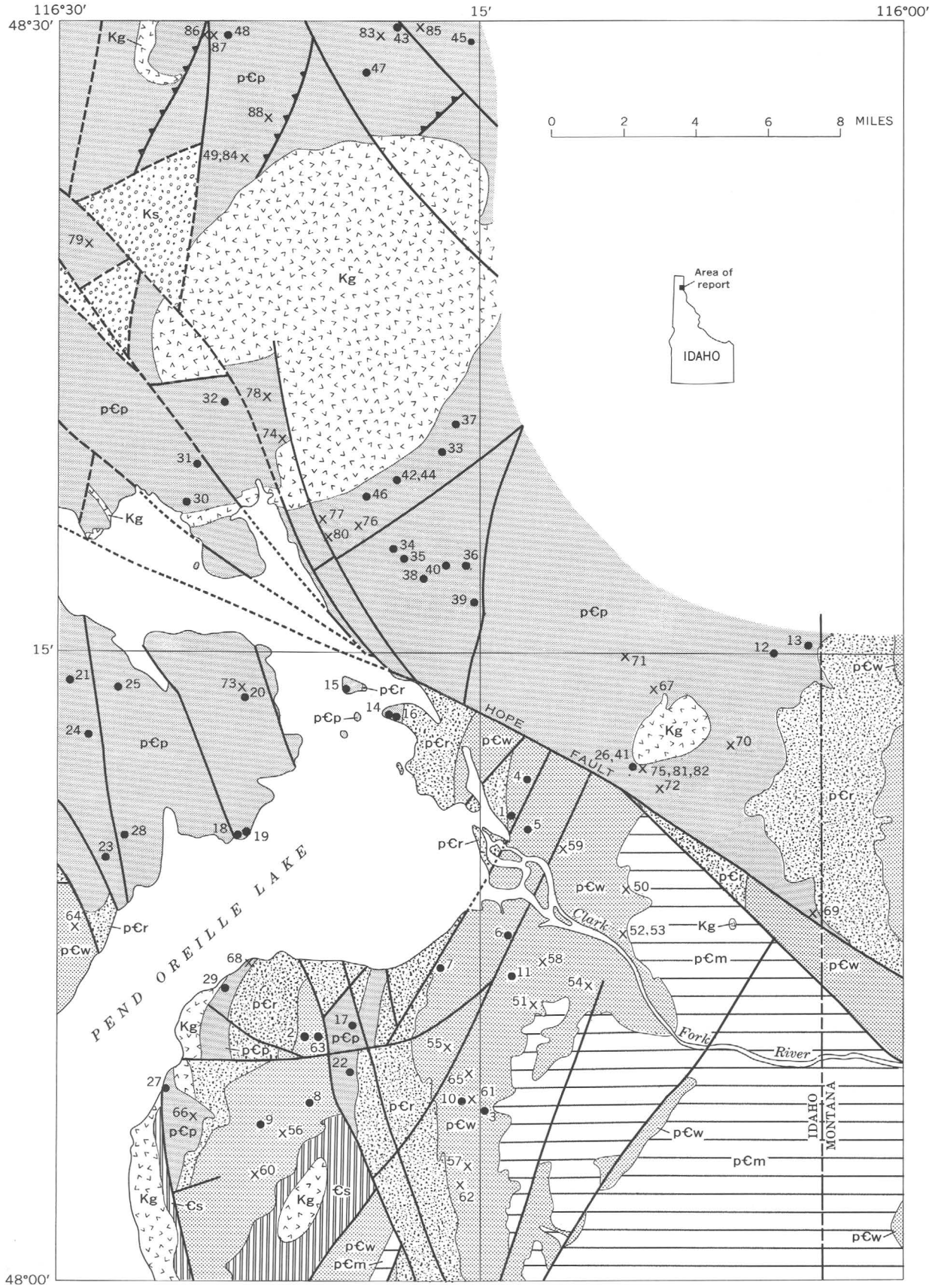
116°30′
15′
116°00′
48°30′
48°00′
0 2 4 6 8 MILES
Area of report
IDAHO
PEND OREILLE LAKE
HOPE FAULT
Clark Fork River
IDAHO
MONTANA
Kg
Ks
p€p
p€r
p€w
p€m
€s

FIGURE 1.

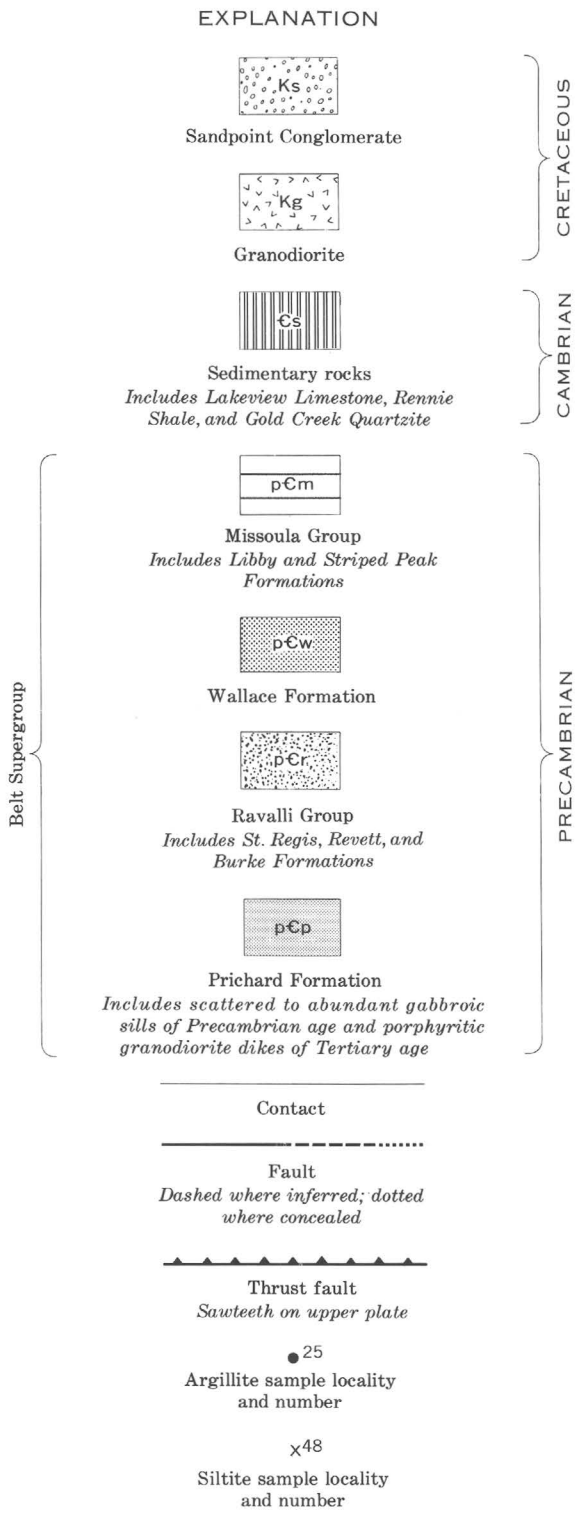

FIGURE 1.—Simplified bedrock geologic map of the Pend Oreille area, Idaho–Montana, showing localities sampled for argillites and siltites of the Wallace and Prichard Formations.

The graphs (fig. 2) also show some patterns that have geologic meaning. The Wallace Formation represents rocks that are in the incomplete process of being transformed from chlorite–sericite-zone to biotite-zone metamorphic grade by regional metamorphism. The Prichard Formation represents rocks that approach or are at equilibrium in the biotite zone of regional metamorphism, but that at places have been prograded by contact metamorphism and folding to biotitic schists and gneisses, some of which contain sparse, tiny garnets. The Prichard Formation is everywhere at least in the biotite zone of regional metamorphism, and the Wallace Formation shows no contact metamorphic effects. We cannot, therefore, study a direct continuum from chlorite–sericite metamorphic grade to biotitic but bedded grade to gneissic biotite grade, because we cannot assume that the original minor-element content of the Prichard Formation rocks was identical with that of the Wallace rocks. We can, however, examine trends of regional metamorphism in the Wallace rocks and trends of contact metamorphism in the Prichard rocks. If we consider the paired groups of samples on figure 2 (C–B, B–G, C–B, B–G), it seems evident that for most elements the metamorphic processes have resulted in greater variability (the left side of the pair is lower than the right), or at least the processes at the stage at which we are examining them have done little to homogenize the trace-element content for most elements. If this tendency to shift elements around so as to make the rocks more variable even at these low levels of metamorphism is combined with a tendency to concentrate or remove certain elements, then such processes operating over the vast areas of Belt rocks could lead to economic deposits of certain elements.

Possible changes in element content during metamorphism are shown on figure 3, where the data from table 3 have been plotted on a semilogarithmic scale for convenience. Here again, because of the variability of the parent rocks and the generally increased variability caused by metamorphism, we must look only for patterns and not for apparent differences of mean values. If, however, a pattern of gain or loss is consistent in two rock types of a formation, or in two rock types of two formations, then some evidence for an actual change exists.

TABLE 2.—*Minor-element content of argillites and siltites from the Wallace and Prichard Formations, Pend Oreille area, Idaho*

[L, sample reported as containing less than the sensitivity limit for the element; leaders (----), not determined. Quantitative spectrographic analyses by J. C. Hamilton (85 samples) and P. R. Barnett (3 samples); wet-chemical analyses by J. B. McHugh, H. G. Neiman, and E. P. Welsch]

	Quantitative spectrographic analyses (ppm)																Wet chemical analyses (ppm)	
Element	B	Ba	Be	Co	Cr	Cu	Ga	Mn	Nb	Ni	Sc	Sr	V	Y	Yb	Zr	Pb	Zn
Sensitivity limit of analytical method	(50)	(3)	(5)	(5)	(2)	(2)	(10)	(2)	(2)	(5)	(5)	(10)	(10)	(20)	(2)	(20)	(2)	(5)
ARGILLITES AND ARGILLITIC ROCKS																		
Wallace Formation																		
Chlorite–sericite rocks:																		
1	140	1,200	----	7	52	3	----	130	----	22	15	26	86	40	----	240	9	80
2	120	760	----	8	38	3	----	82	----	18	13	25	66	40	----	260	10	110
3	130	1,100	----	13	55	10	----	890	----	16	17	40	64	40	----	210	4	40
4	100	500	----	7	58	30	----	250	----	21	17	19	74	40	----	220	5	90
5	130	1,000	----	6	49	9	----	60	----	14	13	30	78	50	----	450	6	32
6	120	740	5	9	60	7	19	------	30	22	14	40	77	60	8	460	6	55
Biotitic but bedded rocks:																		
7	70	850	L	L	15	4	L	440	20	6	9	13	31	40	7	250	5	18
8	80	680	L	11	69	11	12	350	20	24	21	17	130	40	5	270	5	38
9	80	540	L	8	37	22	L	110	20	14	12	24	54	30	3	220	34	95
10	70	420	8	9	35	12	L	240	L	16	13	21	69	40	4	210	7	50
11	110	660	L	9	69	26	11	180	30	20	23	26	110	50	6	290	22	65
Prichard Formation																		
Biotitic but bedded rock:																		
12	80	960	6	L	66	9	20	430	30	6	17	89	85	70	6	290	24	80
13	60	880	----	L	66	13	----	320	----	L	18	40	68	30	----	180	46	38
14	50	1,100	L	11	74	40	19	640	20	25	16	90	79	50	6	280	22	110
15	70	1,000	6	11	62	23	15	500	20	19	22	63	110	50	6	280	36	110
16	50	830	L	7	50	32	10	380	20	18	15	33	74	50	5	260	8	50
17	70	1,100	----	9	51	19	----	500	----	18	16	70	72	40	----	300	19	80
18	200	1,200	L	14	62	43	19	430	20	24	18	44	90	40	7	230	14	65
19	120	1,300	L	11	65	52	21	570	20	25	18	42	130	60	7	300	14	80
20	120	1,200	L	L	82	8	19	310	20	L	21	74	100	50	7	320	13	42
21	90	1,000	L	L	28	26	12	310	20	L	12	72	44	30	5	200	8	30
22	50	990	9	14	69	38	15	340	20	20	22	55	110	50	6	220	14	75
23	70	1,000	L	11	52	9	17	590	30	21	15	66	96	50	7	250	16	80
24	110	1,400	L	8	49	31	24	500	30	10	21	42	120	30	5	240	11	85
25	60	1,400	L	8	44	6	16	560	20	14	15	65	66	50	6	260	22	85
Biotitic schist or gneiss:																		
26	L	2,000	L	6	90	4	40	900	30	9	25	140	130	80	9	330	22	70
27	L	510	L	6	34	5	L	240	L	12	10	22	44	30	4	260	90	48
28	100	980	L	10	47	18	13	540	20	20	14	59	79	50	5	250	34	75
29	L	1,100	6	L	81	23	21	370	20	L	27	97	130	40	5	240	19	38
30	160	1,200	L	6	47	33	19	740	20	11	14	45	86	50	6	240	16	48
31	80	1,300	L	13	59	80	23	780	20	22	17	92	87	50	6	280	28	95
32	L	1,200	L	L	54	34	24	560	30	6	19	110	110	80	6	320	14	60
33	L	1,500	L	L	66	11	25	370	30	L	19	90	70	40	4	230	14	40
34	L	1,100	L	L	70	9	21	110	30	5	14	120	60	50	5	260	9	38
35	L	1,000	L	L	61	20	24	320	30	L	16	110	60	50	4	240	14	40
36	L	1,300	L	L	62	28	23	70	30	L	18	55	70	60	4	240	14	30
37	L	900	L	L	60	12	19	690	30	L	15	190	70	60	6	300	15	70
38	L	890	L	L	39	42	20	460	20	5	16	77	60	40	4	240	28	60
39	L	1,400	L	L	68	32	23	460	30	8	19	31	100	60	5	240	14	50
40	110	1,200	L	8	64	32	24	420	30	16	17	37	100	60	5	210	7	90
41	L	1,300	8	8	10	4	10	690	30	12	23	76	110	70	7	310	25	95
42	L	1,200	L	L	62	19	24	270	20	L	18	56	100	40	3	180	20	42
43	L	1,600	L	L	41	8	18	240	20	L	10	140	66	40	4	230	15	29
44	L	1,000	L	L	30	L	17	150	20	L	10	68	49	40	4	240	5	10
45	L	920	L	L	51	6	19	430	20	L	14	210	86	40	4	260	20	38
46	L	780	L	L	30	8	12	180	20	L	14	140	46	40	3	260	5	10
47	L	940	L	L	65	14	29	570	30	L	19	96	120	60	6	290	15	45
48	L	950	L	L	49	16	23	350	20	L	13	98	72	80	7	290	5	37
49	L	1,200	L	8	67	24	26	450	30	14	22	84	120	80	6	270	30	44

TABLE 2.—*Minor-element content of argillites and siltites from the Wallace and Prichard Formations, Pend Oreille area, Idaho*—Continued

[L, sample reported as containing less than the sensitivity limit for the element; leaders (----), not determined. Quantitative spectrographic analyses by J. C. Hamilton (85 samples) and P. R. Barnett (3 samples); wet-chemical analyses by J. B. McHugh, H. G. Neiman, and E. P. Welsch]

	Quantitative spectrographic analyses (ppm)																Wet chemical analyses (ppm)	
Element	B	Ba	Be	Co	Cr	Cu	Ga	Mn	Nb	Ni	Sc	Sr	V	Y	Yb	Zr	Pb	Zn
Sensitivity limit of analytical method	(50)	(3)	(5)	(5)	(2)	(2)	(10)	(2)	(2)	(5)	(5)	(10)	(10)	(20)	(2)	(20)	(2)	(5)
SILTITES AND SILTY ROCKS Wallace Formation																		
Chlorite-sericite rocks:																		
50	190	1,000	----	13	69	16	----	62	----	21	18	23	76	40	----	280	25	42
51	150	820	----	6	42	8	----	670	----	22	11	26	59	30	----	260	9	38
52	320	820	----	14	51	10	----	200	----	15	14	28	76	30	----	240	34	75
53	90	730	----	19	29	20	----	93	----	20	6	24	40	30	----	190	24	38
54	110	780	----	L	48	12	----	130	----	21	10	29	52	30	----	310	8	80
Biotitic but bedded rocks:																		
55	70	630	L	9	35	20	L	180	20	17	12	21	52	40	4	220	19	60
56	60	410	L	7	41	28	L	200	L	14	10	24	62	30	4	350	18	48
57	110	860	7	6	54	9	L	530	20	20	13	17	74	30	4	230	18	85
58	60	360	L	10	48	7	13	------	30	21	12	50	58	40	5	370	9	65
59	140	880	----	13	44	13	----	160	----	27	14	28	68	50	----	270	15	65
60	50	200	L	13	33	64	L	460	L	26	8	13	42	30	4	300	12	140
61	70	440	8	13	40	92	L	340	20	29	13	24	67	50	5	280	7	50
62	50	760	L	L	25	18	L	46	20	11	9	14	40	30	4	220	19	70
63	90	1,700	L	L	23	360	L	100	L	15	9	82	32	40	5	340	6	32
64	90	710	L	6	25	22	L	200	20	12	8	33	52	30	4	180	26	110
65	50	250	L	L	30	16	L	180	20	11	11	23	37	50	6	570	60	90
Prichard Formation																		
Biotitic but bedded rocks:																		
66	L	670	L	7	20	4	L	28	L	9	9	35	29	40	5	300	8	8
67	L	970	L	8	52	19	13	440	30	10	18	65	78	40	5	340	12	30
68	50	890	L	9	55	26	16	440	20	17	20	55	86	60	7	290	19	85
69	L	680	----	8	41	17	----	340	----	13	13	62	54	40	----	200	16	85
70	L	800	L	8	52	11	12	410	30	15	16	93	81	60	5	430	10	36
71	50	610	L	15	55	56	10	700	30	31	16	150	81	50	5	350	26	120
72	L	460	L	7	31	30	L	340	30	12	10	45	42	40	3	330	13	38
73	L	460	L	12	22	34	L	390	L	16	8	57	40	30	3	180	36	42
Biotitic gneiss or schist:																		
74	L	690	L	L	23	3	12	400	20	10	8	110	40	40	4	330	14	50
75	L	740	7	7	110	10	20	670	30	11	19	230	120	70	7	370	28	85
76	L	540	L	L	26	4	16	440	20	9	8	180	40	40	4	260	11	42
77	L	520	L	L	26	26	13	320	30	5	10	120	40	70	6	390	13	32
78	L	530	L	7	22	3	16	540	30	9	10	88	40	50	4	260	13	75
79	L	110	L	L	11	4	L	210	20	5	8	130	40	40	3	210	14	36
80	L	960	L	L	19	8	L	460	20	L	5	110	40	40	4	420	75	46
81	L	890	7	7	68	14	10	480	20	L	17	98	82	60	5	360	20	40
82	L	610	L	L	22	5	L	350	20	L	8	74	34	40	3	320	15	12
83	L	880	L	L	45	4	12	270	20	8	9	260	54	40	3	240	5	10
84	L	360	L	L	23	4	L	300	20	L	L	96	22	40	3	590	5	10
85	L	470	L	L	18	3	L	220	L	L	L	37	20	40	3	360	20	10
86	L	380	L	14	81	19	23	1,000	30	44	24	290	110	90	9	550	15	67
87	L	670	L	13	30	34	14	200	20	26	8	76	47	50	4	330	5	27
88	L	780	L	L	52	8	24	340	30	L	16	140	92	70	7	290	5	43

TABLE 3.—*Average minor-element content, in parts per million, of argillites and siltites from the Wallace and Prichard Formations, Pend Oreille area, Idaho*

[Metamorphic grade: C, chlorite–sericite; B, biotitic but bedded; G, biotitic gneiss or schist. $\bar{x}$, mean; s, standard deviation. L followed by number in parentheses, indeterminate amount less than the number given; leaders (---), insufficient data]

	Argillites and argillitic rocks								Siltites and silty rocks							
	Wallace Formation				Prichard Formation				Wallace Formation				Prichard Formation			
	C		B		B		G		C		B		B		G	
	$\bar{x}$	s	$\bar{x}$	s	$\bar{x}$	s	$\bar{x}$	s	$\bar{x}$	s	$\bar{x}$	s	$\bar{x}$	s	$\bar{x}$	s
B	120	14	82	16	86	42	L(50)		170	91	76	29	L(50)		L(50)	
Ba	880	260	630	160	1,100	180	1,100	300	830	100	650	420	690	190	610	230
Co	8.3	2.5	7.8	3.4	8.0	4.4	L(5)		11	6.8	7.5	4.4	9.2	2.8	L(5)	
Cr	52	7.9	45	24	59	14	54	18	48	15	36	10	41	15	38	28
Cu	10	10	15	8.9	23	16	20	17	13	4.8	59	100	25	16	9.9	9.5
Ga			L(10)		15	7.2	21	6.8			L(10)		8.2	5.3	12	6.4
Mn	280	350	260	130	460	110	430	220	110	57	190	130	390	180	410	210
Nb			20	7.1	19	9.2	25	5.9			18	8.1	20	12	23	5.9
Ni	19	3.4	16	6.8	15	8.7	6.8	6.3	20	2.8	18	6.6	15	7.0	9.1	12
Pb	6.7	2.3	15	13	19	11	18	18	20	11	19	15	18	9.4	16	18
Sc	15	1.8	16	6.1	18	3.0	17	4.5	12	4.5	11	2.1	14	4.4	10	6.2
Sr	30	8.5	20	5.3	60	18	93	47	26	2.5	30	20	70	36	140	73
V	74	8.2	79	41	89	24	84	26	61	16	53	14	61	23	55	31
Y	45	8.4	40	7.1	46	11	54	15	32	4.5	38	8.7	45	11	52	16
Yb			5.0	1.6	6.1	.08	5.1	1.4			4.5	.71	4.7	1.4	4.6	1.8
Zn	68	30	53	29	72	25	50	23	55	21	74	31	55	37	39	24
Zr	310	120	250	33	260	41	260	35	260	45	300	110	300	81	350	110

Elements that appear to have decreased during both regional (as shown by the Wallace Formation) and contact (as shown by the Prichard Formation) metamorphism are B, Co, Cr, and Ni, and perhaps Ba, Pb, Sc, and V. No elements appear to have increased during both regional and contact metamorphism, but strontium and perhaps gallium show increases during contact metamorphism alone. The same patterns for B, Co, Ni, and Sr were suggested by previous semiquantitative spectrographic analyses of Prichard rocks (Harrison and Grimes, 1970). The high variability and particulate nature of original sedimentary copper, an element of especial current interest in Belt rocks, make measurements of its absolute change during metamorphism difficult. A large number of samples of rocks containing more abundant copper might yield more conclusive results. It does seem probable, from its increased variability with metamorphism (fig. 2), that copper has been redistributed somewhat by metamorphic processes. If so, the possible effects of metamorphic changes should not be overlooked as a potential concentrating mechanism of stratabound copper ores in Belt rocks.

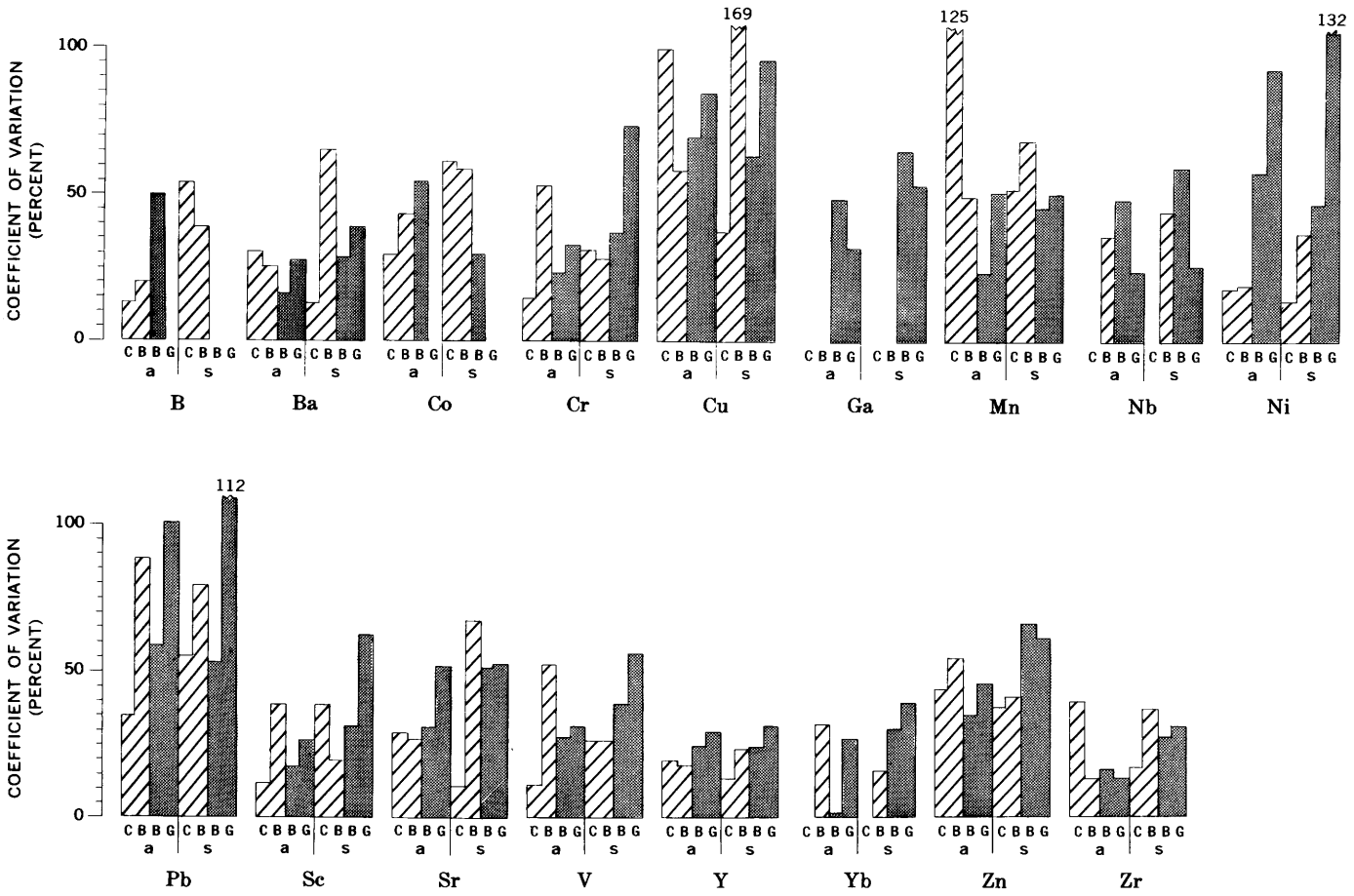

FIGURE 2.—Coefficient of variation of minor elements in different formations, rock types, and metamorphic grades. Formations: hachured, Wallace; solid, Prichard. Rock types: a, argillite; s, siltite. Metamorphic grade: C, chlorite–sericite; B, biotitic but bedded; G, biotitic gneiss or schist.

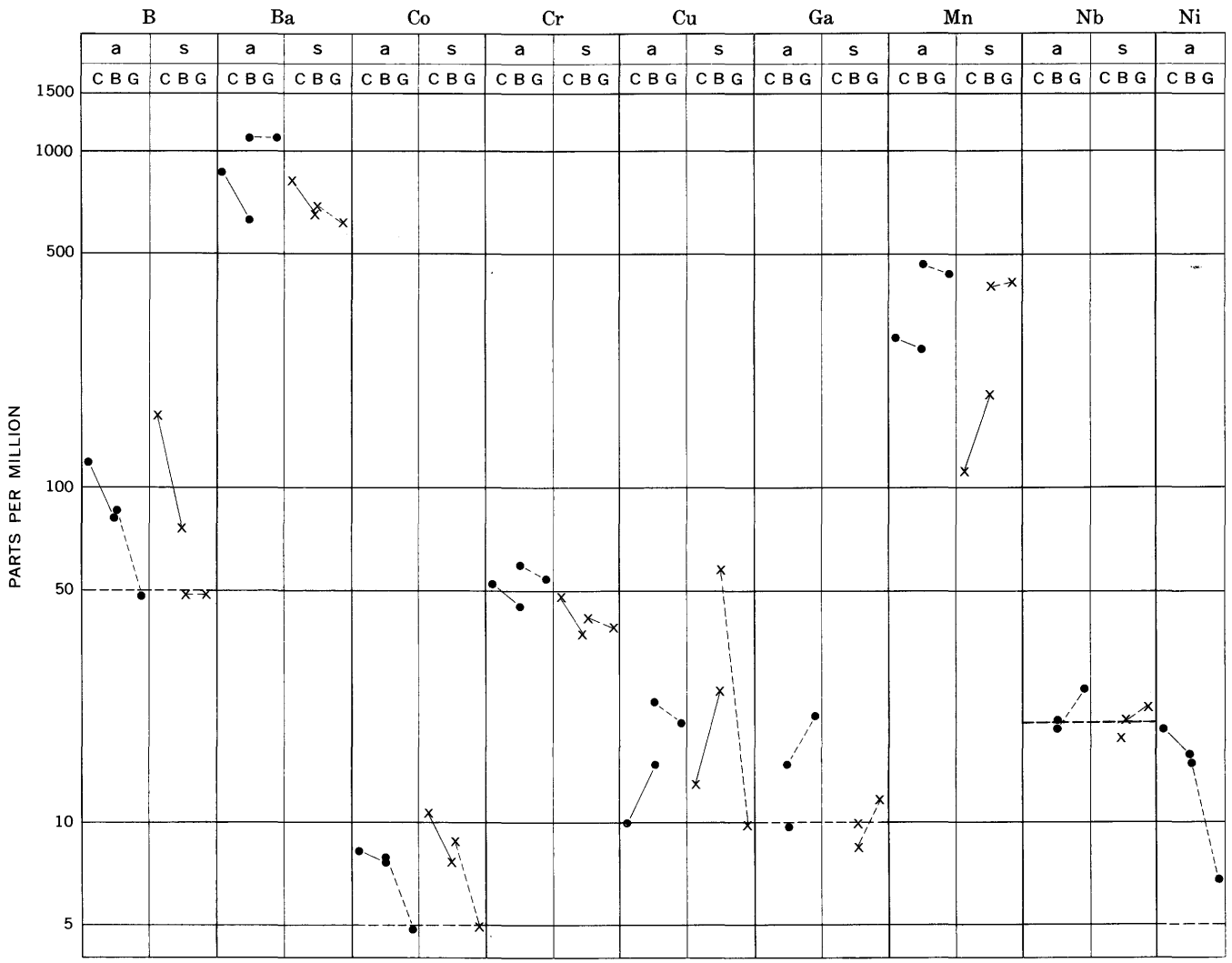
B
Ba
Co
Cr
Cu
Ga
Mn
Nb
Ni
a
s
C B G
1500
1000
500
100
50
10
5
PARTS PER MILLION

FIGURE 3.

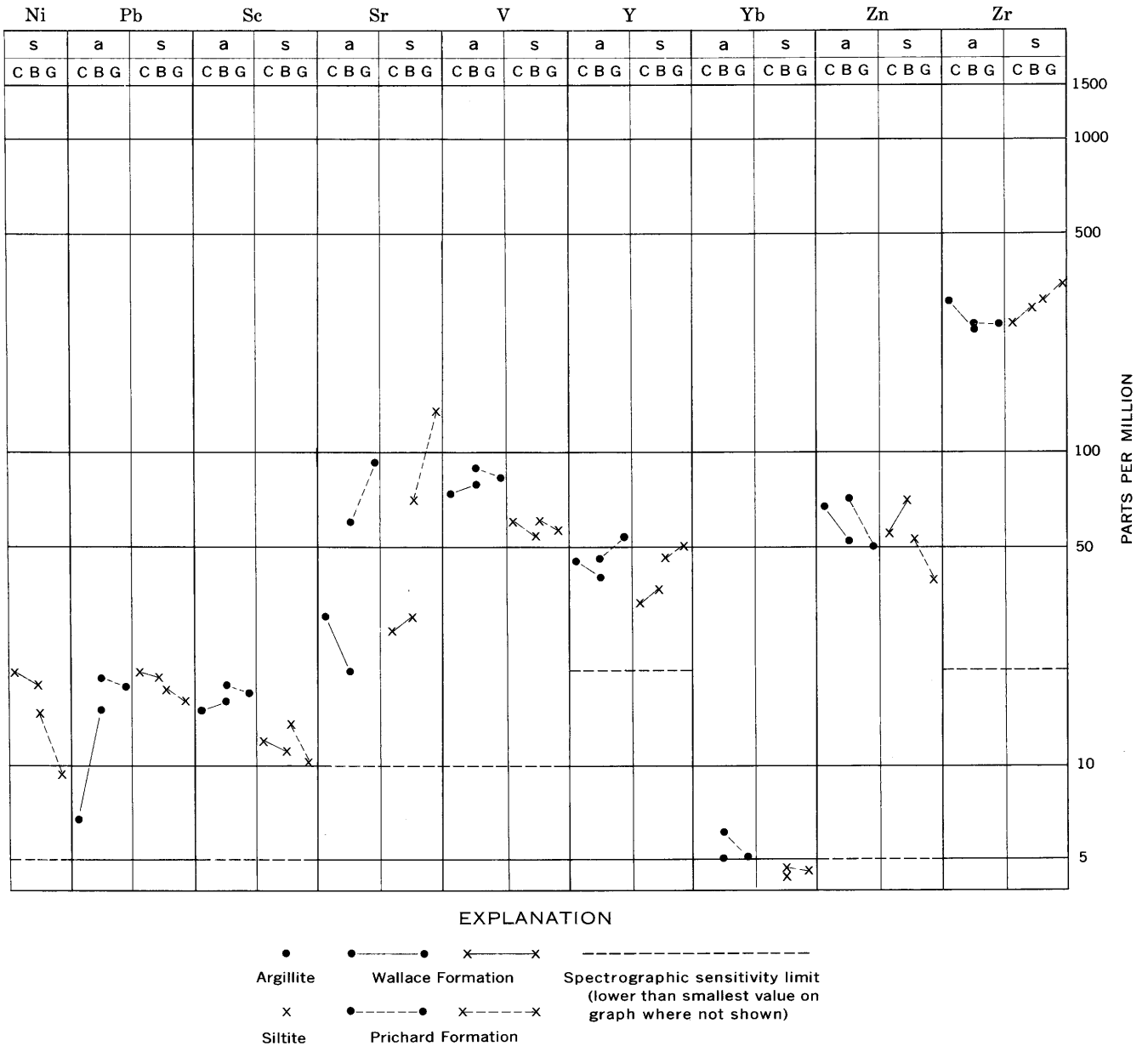

FIGURE 3.—Graphs showing changes in average minor-element content during metamorphism, Rock type: a, argillite; s, siltite. Metamorphic grade: C, chlorite-sericite; B, biotitic but bedded; G, biotitic gneiss or schist.

REFERENCES

Barnett, P. R., 1961, Spectrographic analysis for selected minor elements in Pierre shale: U.S. Geol. Survey Prof. Paper 391–B, 10 p.

Bastron, Harry, Barnett, P. R., and Murata, K. J., 1960, Method for the quantitative spectrochemical analysis of rocks, minerals, ores, and other materials by a powder d-c arc technique: U.S. Geol. Survey Bull. 1084–G, p. 165–182.

Harrison, J. E., and Grimes, D. J., 1970, Mineralogy and geochemistry of some Belt rocks, Montana and Idaho: U.S. Geol. Survey Bull. 1312–O, p. O1–O48.

Holmes, R. S., 1945, Determination of total copper, zinc, cobalt, and lead in soils and soil solutions: Soil Sci., v. 59, p. 77–84.

Shaw, D. M., 1954, Trace elements in pelitic rocks [N.H.]—pt. 1, Variation during metamorphism: Geol. Soc. America Bull., v. 65, no. 12, pt. 1, p. 1151–1166.

413-504 O - 71 - 7

STRONTIUM ISOTOPIC COMPOSITION OF TWO BASALTS REPRESENTATIVE OF THE SOUTHERN SNAKE RIVER VOLCANIC PROVINCE

By EDWIN H. McKEE and ROBERT K. MARK,[1]
Menlo Park, Calif., Stanford, Calif.

Abstract.—The isotopic ratios $^{87}Sr/^{86}Sr$ from two samples of Pliocene olivine basalt from north-central Nevada are 0.7056 and 0.7058. These values are similar to those from Snake River Plain basalts and other upper Cenozoic basalts in north-central Nevada and support field evidence that the Snake River volcanic province extends about 100 miles, in a southerly direction, from Idaho into Nevada. These basalts have very similar bulk chemistry to ocean-ridge tholeiites but have $^{87}Sr/^{86}Sr$ values that indicate a significant enrichment in Sr^{87} compared with ocean-ridge tholeiites.

Recently published data on the strontium isotopic composition of basalts from the Western United States have outlined the general framework on which further isotopic studies, more closely tied to geologic details, can be related. In particular, the papers of Hedge and Walthall (1963), Hedge (1966), Leeman (1970), and Leeman and Manton (1970) have delineated areas within the Great Basin and adjacent regions (Sierra Nevada, Snake River Plain, Colorado Plateaus, and the Arizona part of the Basin and Range province) in which basalts seem to have consistent and different $^{87}Sr/^{86}Sr$ values.

In general, basalts from the central part of the Great Basin have lower $^{87}Sr/^{86}Sr$ values (about 0.704) than those from surrounding regions (about 0.706). It should be noted, however, that the limited number of samples from this large region and the lack of geologic control, especially age, may prove such generalizations invalid.

GEOLOGIC SETTING

In this study the isotopic composition of strontium was measured in two samples of olivine basalt from north-central Nevada (fig. 1). The samples are from the top flow of a series of more than 20 upper Miocene to Pliocene flows that have been mapped and dated by K/Ar methods, and on which whole-rock analyses are available. Because the geologic control is good, and because this flow is representative of a much larger basalt field, it was felt that its strontium isotopic composition would have more than average geologic importance.

Primarily on the basis of geologic mapping, but supported by petrographic studies and age relationships, the basaltic field north of the town of Battle Mountain, Nev. (fig. 1), has been considered a southern extension of the Snake River volcanic province by McKee and Silberman (1970). The top flow in a series of flows in the Sheep Creek Range north of the town of Battle Mountain can be traced continuously for about 30 miles northward. Beneath this uppermost flow are more than 1,000 feet of basaltic flows, most of which are not olivine bearing. All the basalts are part of the same volcanic field, which thins southward and pinches out about 20 miles southeast of Battle Mountain. North of the Sheep Creek Range, basalts of this volcanic field are found in the area around Midas (fig. 1), and to the northeast and northwest of Midas similar basalts merge with units from the Snake River Plain.

Most of the volcanic rocks south of Battle Mountain are unrelated to Snake River volcanic rocks. These central Nevada rocks are older, between 20 and 35 m.y. (million years) old, and are mostly rhyolite ash-flow sheets or lava flows of intermediate composition (McKee and Silberman, 1970).

SELECTION AND ANALYSIS OF BASALTS

The two samples of Pliocene (10 m.y. old by K/Ar methods; McKee and Silberman, 1970) olivine basalt from the top flow north of the town of Battle Mountain are alkali-poor tholeiitic basalts chemically very simi-

[1] Stanford University.

U.S. GEOL. SURVEY PROF. PAPER 750-B, PAGES B92-B95

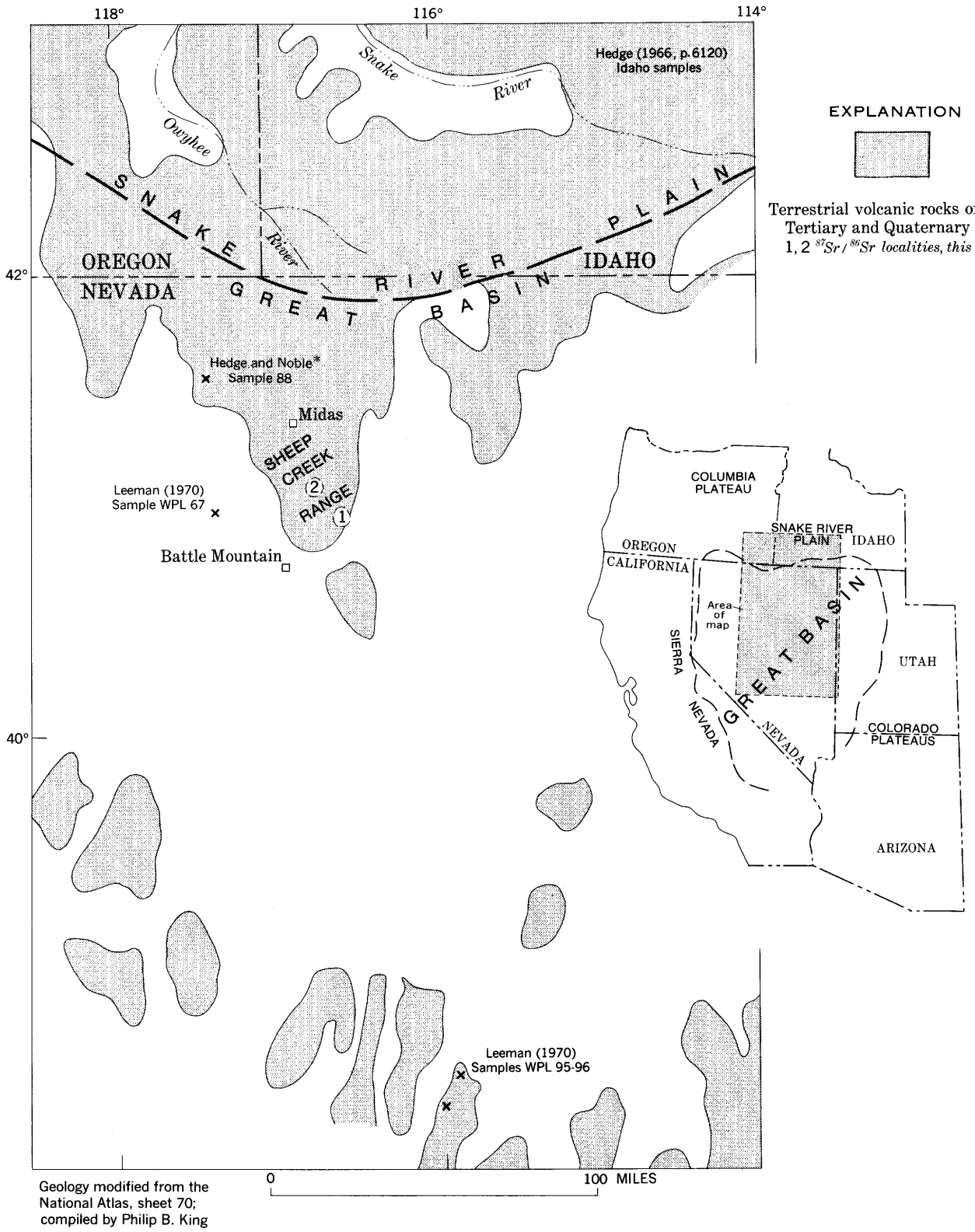

FIGURE 1.—Map of the central part of the Great Basin and southern part of the Snake River Plain. The shaded areas are mostly lava flows of basaltic and andesitic composition and rhyolite ash-flow sheets. Most of these rocks are of late Miocene age or younger. *C. E. Hedge and D. C. Noble (written commun., 1970).

lar to ocean-ridge tholeiites from both the Atlantic and Pacific oceans (Kay and others, 1970). Whole-rock analyses of them are given in table 1. The other olivine-free flows in the series tend to be andesitic basalts on the basis of chemical analyses (Gilluly and Gates, 1965, table 7). The upper alkali-poor tholeiitic flow was selected for strontium isotopic analysis because it seemed to most nearly represent a "primitive" oceanic basalt. Low amounts of K, P, Rb, Sr and Zr and relatively high amounts of Cr and Sc, comparable to values given by Engel, Engel, and Havens (1965) for oceanic tholeiites, characterize this flow. The barium content, however, is higher than the average for oceanic tholeiites (Engel and others, 1965).

TABLE 1.—*Chemical analyses of two samples of Pliocene olivine basalt from north of Battle Mountain (Sheep Creek Range), Nev.*

[Samples analyzed by methods described in U.S. Geol. Survey Bull. 1144-A (Shapiro and Brannock, 1962), supplemented by atomic absorption. Analyzed by Leonard Shapiro, project leader; SrO analyzed by Lois B. Schlocker using flame photometric methods]

	Location (fig. 1)	
	1	2
Weight percent		
SiO_2	48.2	47.4
Al_2O_3	16.6	16.7
Fe_2O_3	2.5	1.4
FeO	6.6	8.1
MgO	8.9	9.3
CaO	12.1	11.3
Na_2O	2.1	2.1
K_2O	.17	.34
H_2O-	.30	.44
H_2O+	.68	.21
TiO_2	.86	1.2
P_2O_5	.23	.26
MnO	.17	.19
CO_2	.14	.05
SrO	.033	.033
Total	100	99
Parts per million		
Ba	300	[1] 200
Co	50	[1] 70
Cr	300	[1] 500
Ni	200	[1] 30
Sc	70	[1] 70
V	300	[1] 300
Zr	30	[1] 70
Rb	7.8	[2] 6.7
Partial semiquantitative 6-step spectrographic analyses [3]		
$^{87}Sr/^{86}Sr$[2]	0.7058±0.0005	0.7056±0.0002

[1] Results are identified with geometric brackets whose boundaries are 1.2, 0.83, 0.56, 0.38, 0.26, 0.18, 0.12, and so forth, but are reported arbitrarily as midpoints of these brackets, 1, 0.7, 0.5, 0.3, 0.2, 0.15, 0.1, and so forth. The precision of a reported value is approximately plus or minus 1 bracket at 68 percent, or 2 brackets at 95-percent confidence.

[2] Rb analyzed by Carl E. Hedge by X-ray fluorescence with an uncertainty of ± 2 ppm.

[3] Corrected to Eimer and Amend $SrCO_3$ standard of 0.7080. ± indicates standard deviation of internal ratios.

Samples were dissolved in hydrofluoric and perchloric acids, and strontium was separated using a cation exchange resin. The strontium blank was less than 0.1 μg per analysis. Mass analyses were made on a 30-cm radius, 90°-sector, single-focusing mass spectrometer using a triple filament source configuration and Faraday cage collector. Outgassed rhenium filaments were used. Isotopic fraction was corrected for by normalizing $^{86}Sr/^{88}Sr$ to 0.1194. Rubidium correction to mass 87 is less than 0.02 percent. The $^{87}Sr/^{86}Sr$ measured on the Eimer and Amend $SrCO_3$ standard is 0.70824±0.00009 (standard deviation 7 analyses). All data are corrected to a value for the Eimer and Amend standard of 0.7080. Replicate analyses of other basalts yield a standard deviation of approximately 0.0002 for $^{87}Sr/^{86}Sr$.

DISCUSSION OF RATIOS OBTAINED

The $^{87}Sr/^{86}Sr$ values of the basalts from the Sheep Creek Range are shown in table 1. These ratios (0.7056 ±0.0002 and 0.7058±0.0005) show that this flow is enriched in radiogenic strontium compared with typical oceanic basalts (average about 0.704; Gast, 1967, Hamilton, 1968). The flow is comparable to the basalt analyzed by Leeman (1970; value of 0.7052,[1] sample WPL–67) from about 40 miles to the west and a sample (No. 88, fig. 1) analyzed by C. E. Hedge and D. C. Noble (written commun., 1970) with a value of 0.7057, collected about 60 miles to the northwest of the Sheep Creek Range. It is also about the same as one of the basalts from the Snake River Plain reported by Hedge (1966; 0.7060, sample locality Clover Creek, Idaho) and the average values for the Snake River Plain basalts given by Leeman and Manton (1970), but lower than three other Snake River Plain basalts reported by Hedge (1966; 0.7066, 0.7075, and 0.7077, sample localities Wendell, Dietrich, and Shoshone, Idaho).

CONCLUSIONS

The $^{87}Sr/^{86}Sr$ values of two samples of Pliocene (10 m.y. old by K-Ar methods) olivine basalt from the Sheep Creek Range, north of Battle Mountain, Nev., are slightly less than 0.706. This value is similar to those reported for basalts of the Snake River Plain (Hedge, 1966; Leeman and Manton, 1970) and for upper Ceno-

[1] Leeman's $^{87}Sr/^{86}Sr$ value of 0.7056 corrected to an Eimer and Amend $SrCO_3$ standard of 0.7080.

zoic basalts in northern Nevada (Leeman, 1970). Strontium ratios of upper Cenozoic basalts from central Nevada are less radiogenic (about 0.704; Leeman, 1970). The similarity in strontium isotopic composition between the basalts in the Sheep Creek Range of northern Nevada, other upper Cenozoic basalts in north-central Nevada, and the Snake River Plain basalts supports field evidence that the Snake River Plain volcanic province extends into north-central Nevada about as far south as the town of Battle Mountain.

On the basis of major-element chemistry, the basalts from the southern Snake River Plain described here are almost identical with ocean-ridge tholeiites described by Kay and others (1970). $^{87}Sr/^{86}Sr$ values for the southern Snake River Plain basalts, however, indicate a significant enrichment in radiogenic strontium when compared with the average of ocean-ridge tholeiites. This Sr^{87} enrichment indicates a fundamental difference in the evolution of these two otherwise similar tholeiitic basalts.

ACKNOWLEDGMENTS

We express our appreciation to Marvin A. Lanphere, U.S. Geological Survey, and Donald C. Noble, Harvard University, for discussion and review of this paper. Carl E. Hedge, of the U.S. Geological Survey, and Donald C. Noble made available unpublished strontium isotopic analyses of one sample (referred to in this paper as No. 88), and Hedge kindly analyzed the rubidium and strontium content of the two basalts described here.

REFERENCES

Engel, A. E. J., Engel, C. G., and Havens, R. G., 1965, Chemical characteristics of oceanic basalts and the upper mantle: Geol. Soc. America Bull., v. 75, no. 7, p. 719–734.

Gast, P. W., 1967, Isotope geochemistry of volcanic rocks *in* Hess, H. H., and Poldervaart, A., eds., Basalt, v. 1: New York, Wiley-Interscience, p. 325–358.

Gilluly, James, and Gates, Olcott, 1965, Tectonic and igneous geology of the northern Shoshone Range, Nevada: U.S. Geol. Survey Prof. Paper 465, 153 p.

Hamilton, E. I., 1968, The isotopic composition of strontium applied to problems of the origin of the alkaline rocks *in* Hamilton, E. I. and Farquhar, R. M., eds., Radiometric dating for geologists: New York, Wiley-Interscience, p. 437–463.

Hedge, C. E., 1966, Variations in radiogenic strontium found in volcanic rocks: Jour. Geophys. Research, v. 71, p. 6119–6126.

Hedge, C. E., and Walthall, F. G., 1963, Radiogenic strontium-87 as an index of geologic processes: Science, v. 140, p. 1214–1217.

Kay, R., Hubbard, N. J., and Gast, P. W., 1970, Chemical characteristics and origin of ocean ridge volcanic rocks: Jour. Geophys. Research, v. 75, p. 1585–1614.

Leeman, W. P., 1970, The isotopic composition of strontium in late Cenozoic basalts from the Basin-Range province, western United States: Geochim. et Cosmochim. Acta, v. 34, p. 857–872.

Leeman, W. P., and Manton, W. I., 1970, Sr^{87}/Sr^{86} ratios of Snake River Plain basalts [abs.]: Trans. Am. Geophys. Union, v. 51, p. 444.

McKee, E. H., and Silberman, M. L., 1970, Geochronology of Tertiary igneous rocks in central Nevada: Geol. Soc. America Bull., v. 81, p. 2317–2328.

Shapiro, Leonard, and Brannock, W. W., 1962, Rapid analysis of silicate, carbonate, and phosphate rocks: U.S. Geol. Survey Bull. 1144–A, p. A1–A56.

VOLCANIC-SEDIMENTARY BELTS AND SULFIDE OCCURRENCES IN WISCONSIN

By CARL E. DUTTON, Madison, Wis.

Work done in cooperation with the University Extension—
The University of Wisconsin Geological and Natural History Survey

Abstract.—Several areas in Wisconsin have exposures of Precambrian volcanic-sedimentary sequences similar to the Archean greenstone belts from which commercially important amounts of copper, lead, zinc, gold, and silver are obtained in Ontario and Quebec, Canada. The areas of principal interest in Wisconsin total about 1,600 square miles; sparse data from scattered outcrops and explorations for iron ore, and from magnetic surveys (both dip-needle and aeromagnetic), suggest that additional areas, which total about 1,000 square miles, are underlain by similar sequences. The amount of exposed bedrock in the areas ranges widely and is generally so sparse that geophysical surveys must supplement geologic mapping in order to plan explorations for potential mineral deposits.

The Archean greenstone belts of Canada (fig. 1) contain many massive sulfide ore deposits. These belts are volcanic-sedimentary sequences that consist of abundant greenstone with associated rhyolite-dacite and metasedimentary rocks (Goodwin, 1965); lithologically similar assemblages of the same or younger Precambrian age are present in central and northern Wisconsin (fig. 2) in Marathon and Lincoln Counties, Florence and Marinette Counties, Oneida County, and Iron and Ashland Counties, and possibly other localities. The similarity of the geology in these areas to that in Canadian ore-bearing volcanic belts makes them appear favorable for prospecting, and the results of an 18-month drilling campaign on a promising copper prospect near the center of Rusk County are now being evaluated.

According to Leith, Lund, and Leith (1935, pl. 1) northern Wisconsin is underlain by small areas of mafic volcanic rocks and large areas of "undifferentiated Huronian series [that] * * * probably includes some

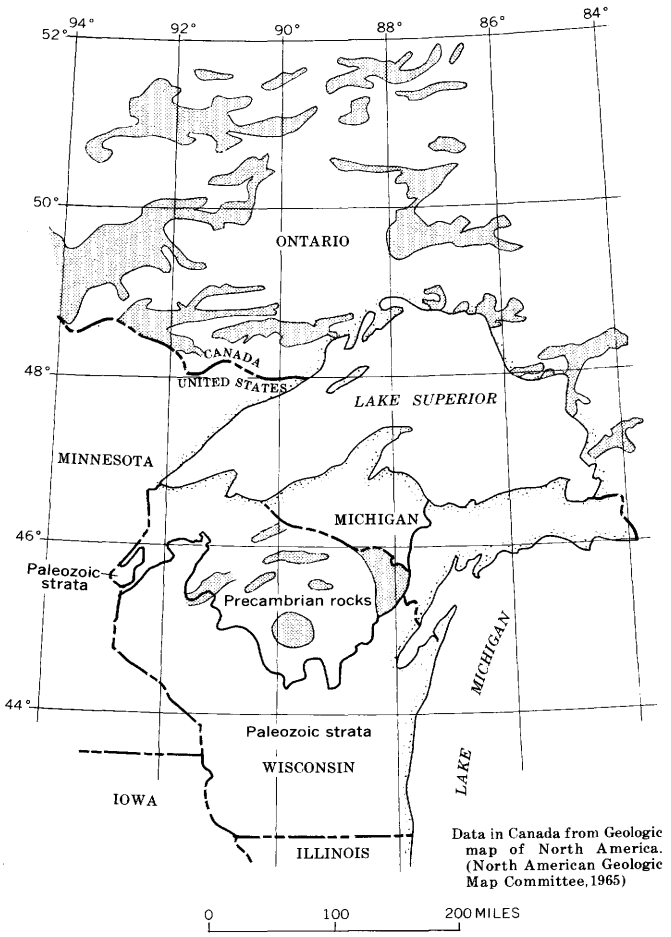

FIGURE 1.—Map showing areas (shaded) of Archean greenstone belts in Canada and volcanic-sedimentary sequences in Wisconsin.

U.S. GEOL. SURVEY PROF. PAPER 750-B, PAGES B96-B100

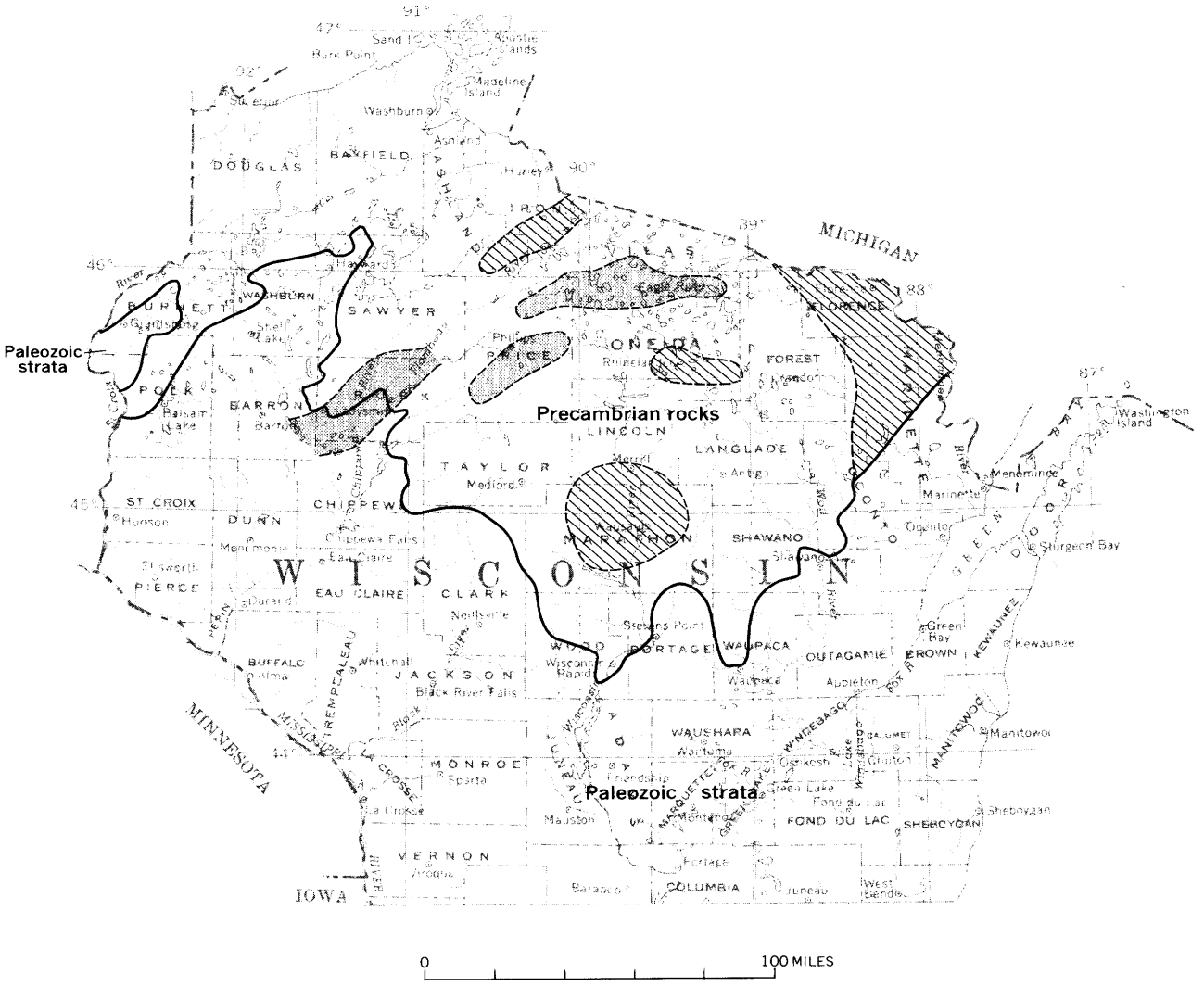

FIGURE 2.—Generalized geologic map showing approximate extent of Precambrian volcanic-sedimentary sequences and associated granite in northern Wisconsin. Diagonal lines indicate principal areas referred to in text, and stipple indicates the inferred areas. Geology is not known in adjacent unshaded areas, except that granite is abundant between the Wausau area of Marathon and Lincoln Counties and the edge of the Paleozoic strata.

magnetic igneous rocks." These areas and the one in central Wisconsin, as well as the geologic data on which they are based, are also shown by Dutton and Bradley (1970). The areas of "undifferentiated Huronian series" are locally to possibly extensively underlain by mafic and felsic rocks of flow and pyroclastic origin with associated metamorphosed argillaceous and some cherty ferruginous rocks. All these rocks are commonly in the biotite or garnet grade of metamorphism and locally in the staurolite grade.

A summary of information on the relationship of massive sulfide deposits and volcanism by Anderson (1969) provides a good basis for initially appraising the significance of these associated lithologies in Wisconsin relative to their mineral resource potential. The geologic age of about one-third of the 103 deposits considered in that summary is Precambrian. About two-thirds of the hosts for the 103 deposits are almost equally classed as silicic or mafic volcanic rocks, and hosts for most of the other deposits are tuffaceous beds with associated chert and iron-formation. The massive sulfide deposits contain pyrite or pyrrhotite and commonly also one or more associated sulfides of copper, lead, and zinc. The mineralized areas tend to be tabular or lenticular forms that parallel bedding or foliation. The discussion includes the suggestions of various geol-

ogists as to derivation of the ore-forming constituents from igneous rocks, transport by vapor or hydrous fluids, and deposition in eugeosynclines.

MARATHON AND LINCOLN COUNTIES

An area of about 900 square miles around Wausau in Marathon and Lincoln Counties (fig. 1) that includes townships 27 through 31 north and part of each range from 3 through 9 east is of special interest. Glacial drift of pre-Wisconsin age is discontinuous over the area, but the relative and total amounts of exposed Precambrian bedrock are probably the highest in the State (Dutton and Bradley, 1970). This area was examined by Weidman (1907) and was also studied during the mineral lands classification by the Wisconsin Geological and Natural History Survey from 1914 to 1921. A description of interesting exposures in the area and a related modification of the geologic map by Weidman (1907) were prepared by LaBerge and Weis (1969). Geologic and geophysical data on the Wausau area and all other areas of Precambrian rocks in Wisconsin have been compiled and interpreted by Dutton and Bradley (1970). The areal geology and the sequence of rock types, however, have not been adequately deciphered, nor have the possibilities for sulfide deposits been studied.

Felsic igneous rock is the principal lithologic group with four or possibly five general megascopic subdivisions: (1) granite is widely distributed and in several varieties; (2) syenite and nepheline syenite are west of Wausau—mainly in T. 29 N., Rs. 6 and 7 E.; (3) felsite and porphyritic rhyolite-dacite are also near Wausau—mainly T. 29 N., Rs. 7, 8, and 9 E.; (4) foliated to gneissic rocks of probable igneous affinities but unknown specific origin are in the southern part of the area; and (5) in some areas stratified material is in part or mainly of direct pyroclastic derivation or was deposited after transport by streams. Rubidium-strontium ratios in whole-rock analyses indicate that the geologic ages are 1.64 billion years for rhyolite and 1.60 billion years for the granite; these are probably the youngest igneous rocks in the area. Rhyolite contains locally a small amount of visible sulfide that is mainly or exclusively pyrite, but no samples have been chemically analyzed insofar as is known.

Mafic igneous rock is widely distributed but is only locally a dominant or major feature. Three general megascopic subdivisions are present: (1) Phaneritic rocks are gabbro and diorite which thus far have not been mapped separately, nor have relative amounts been determined. (2) Aphanitic rocks are greenstone, some of which is locally ellipsoidal; the exposed amounts of aphanitic and phaneritic mafic rock appear to be about equal. (3) Foliated rocks of undetermined origin are presumably derived from the other subdivisions but have not been distinguishable or mapped separately. The greenstone areas near Wausau locally contain very small amounts of visible chalcopyrite, malachite, and azurite.

Metasedimentary rock is exposed or has been penetrated only sparingly and locally. The subdivisions are (1) quartzite, which is topographically prominent at Rib Hill near Wausau and Powers Bluff northwest of Wisconsin Rapids, and (2) undifferentiated others (slate, phyllite, schist, and graywacke) northwest of Wausau.

The association in this area of greenstone, rhyolite, graywacke, and at least minor occurrences of copper-bearing minerals suggests the possibility that a volcanic-sedimentary sequence may be present and that its potential should be investigated.

FLORENCE AND MARINETTE COUNTIES

Florence and Marinette Counties are in northeastern Wisconsin. The area of outcrops is triangular, about 35 miles wide across the northern side, and extends about 60 miles southward (fig. 2). Glacial drift is widespread in the area.

The abundance of outcrops ranges from moderately abundant in the terminal parts to very sparse in the central part of the area. Associated volcanic and sedimentary rocks underlie about 200 square miles of Florence County, 150 square miles in the northern part of Marinette County, and 50 square miles in the southern part. Phaneritic igneous rocks are the most commonly exposed and in decreasing order of approximate areal extent are granites, granodiorite, quartz diorites, and metagabbro. Metabasalt that is locally ellipsoidal is the most common aphanitic rock and is second to granites in order of abundance of exposures and probable areal extent. Mafic rocks at the southern end of the area are metamorphosed tuff, agglomerate, and basalt; the visible pyrite and pyrrhotite in these rocks is estimated to be more than 10 percent locally. Rhyolite and porphyritic rhyolite are present at both extremities of the area and also at one small locality in the central part. Conglomerate is present in the southern part, quartzite occurs locally in the central part, and both are present in Florence County.

Most of the rocks in the area are probably of middle Precambrian age, but about half the metabasalt (Quinnesec Formation) may be older. The sequence of the units has not been definitely determined (Mancuso, 1957, 1960; Prinz, 1965; Cain, 1964, 1966; Bayley and others, 1966; and Banks and Cain, 1969), except for general but not unanimous agreement that the Quinnesec Formation is probably the oldest unit.

The Quinnesec Formation consists of older metabasalt with minor phyllite and gruneritic iron-formation and younger rhyolite and porphyritic rhyolite. This assemblage is lithologically similar to Archean greenstone belts that contain massive base metal sulfide deposits in Ontario and Quebec, but significant occurrences of sulfide deposits in Wisconsin have not been indicated by examinations thus far. Exploration in the NE¼SW¼ sec. 16, T. 36 N., R. 21 E., is reported to have yielded a sample that contained 12.39 oz (ounces) of silver and 0.61 oz of gold per ton. Five other samples had from 0.01 to 0.1 oz of silver per ton. Short fiber chrysotile asbestos occurs locally along fractures in small knobs of serpentinized basalt in SE¼ sec. 24, T. 36 N., R. 21 E. Small occurrences of quartz-talc-magnesite with minor magnetite and chromite are in sec. 21, T. 37 N., R. 21 E.

The Hoskin Lake Granite of middle Precambrian age has pyrrhotite with associated fluorite in sec. 7, T. 38 N., R. 20 E. Molybdenite-bearing quartz veins are in this granite in sec. 33, T. 38 N., R. 19 E., and in the Belongia Granite in sec. 18, T. 33 N., R. 20 E.

Pieces of core from a drill hole in the Michigamme Slate of middle Precambrian age in sec. 27, T. 39 N., R. 18 E., contain veinlets and disseminated grains of pyrrhotite.

ONEIDA COUNTY

The area of interest in Oneida County includes much of T. 36 N., Rs. 10, 11, and possibly 8 and 9 E., and part of T. 35 N., R. 10 E.; its extent is about 100 square miles (fig. 2). Glacial drift is widespread, swamps are numerous, and outcrops are generally small and scattered.

Greenstone, which is locally ellipsoidal, is the most common rock exposed. Felsite and porphyritic rhyolite are least exposed and crop out only in the central part of the area. The abundances of phaneritic mafic and felsic rocks are about equal.

The rhyolite contains minor occurrences of sulfide, probably pyrite, but the resource potential of the area has not been investigated.

IRON AND ASHLAND COUNTIES

Minor ellipsoidal basalt, associated garnet-biotite-quartz schist, and several occurrences of metamorphosed iron-formation underlie an area of about 200 square miles mainly in Iron and Ashland Counties near the middle of the north boundary of Wisconsin. The few outcrops are in the western half of the area where metabasalt and schist are equally abundant but are in separate parts of the area. Iron-formation and associated rocks in several loctaions have been penetrated by exploratory drilling to appraise suitability of the iron-formation for beneficiation, but no sulfide other than pyrite has been reported in any of the rocks. Kalliokoski (1968) interpreted geologic relations in an area of Ontario east of Lake Superior and extending into western Quebec as suggesting that the environment favorable for deposition of massive base-metal sulfides was presumably less favorable for accumulation of major iron-formation deposits. Hutchinson (1970) reported that similar contrasts in metal distribution formerly suggested for other parts of Ontario and Quebec were no longer so distinctive.

INFERRED AREAS

The results of magnetic surveys in the areas considered thus far suggest that the underlying rock is more magnetic than the mapped exposures; in any case, the association of magnetic anomalies with the volcanic-sedimentary belts suggests that magnetic surveys might help in the search for new belts. Metabasalt is commonly somewhat magnetic, and some local anomalies determined by ground surveys with a magnetometer have been reported to be caused by felsic rocks. Linear magnetic anomalies and rather sparse outcrop information suggest that the Price-Oneida-Vilas area and the Rusk County area are also volcanic belts.

Data from geologic and dip-needle surveys (Hotchkiss and others, 1915 and 1929) and an aeromagnetic survey (Patenaude, 1966) may possibly indicate that geologic conditions of interest underlie a poorly defined area that extends northeasterly from southwestern Price County through parts of Oneida and Vilas Counties. The area is about 85 miles long and as much as 25 miles wide. Granite crops out locally along a central longitudinal strip, and associated low magnetic values separate high magnetic values in Vilas and Price Counties to the north from those in Price County to the south. Mafic rocks crop out sparsely in the northern part. Local drilling in the southern part has been reported to have penetrated mainly magnetic hornblende schist, but one hole was reported to have been in graywacke, sericite schist, and slate.

Another magnetically anomalous area trends northeastward from western Rusk County; it is about 50 miles long and has a maximum width of about 15 miles. Geologic data are rather scarce, but the area is of special interest because of locally mineralized rock. There are a few granite outcrops, fewer of diorite-gabbro, and very locally some metabasalt, graywacke, and quartzose sericitic rock that may be altered metasedimentary or volcanic rock. Quartzite that unconformably overlies the older rocks is at, south of, and northwest of the location of the anomaly. Strata of late Cambrian age

between and beyond the quartzite areas cover most of the other Precambrian rocks, which, according to reported information from local drilling in southwestern Rusk County, include rhyolite, granite, and syenite. Specimens of quartzose sericitic rock collected by a Wisconsin Geological Survey party on August 14, 1914, from the bottom of a 50-foot dug well that was 10 feet into bedrock in the SE¼SE¼ sec. 16, T. 33 N., R. 6 W., contain small amounts of scattered malachite. Two samples from the well were reported (Hotchkiss and others, 1915, p. 169) to contain 1 oz of silver per ton, and one sample contained 0.75 percent copper but the other had none. An occurrence of similar rock with less evidence of copper was reported to be in a pit 15 feet deep in the northeast corner of the SE¼ sec. 16. A third occurrence is mentioned in the field notes of May 15, 1910, as "schistose granite mineralized with copper sulphides and carbonate" from a pit 12 feet deep in the SW¼NW¼ sec. 15, T. 33 N., R. 6 W. Also of interest and possible significance is a fine-grained siliceous and sericitic rock that contains much disseminated pyrite as exposed along the highway in the SW¼ sec. 10, T. 34 N., R. 8 W. Large quantities of pyrite in "highly mashed acid porphyries" were reported in sec. 19, T. 36 N., R. 7 W. (Hotchkiss and others, 1915, p. 211), but no pyrite was seen when the locality was visited about 1965.

A different occurrence of copper in this area is that of considerable malachite associated with quartz veins in sheared greenstone exposed in the SE¼ sec. 35, T. 36 N., R. 8 W. Limonitic stain and sulfides, which are probably pyrite, are in diorite associated with graywacke in the NW¼ sec. 17, T. 35 N., R. 6 W.

The possibility of volcanic-sedimentary sequences in and near Rusk County and the recent drilling of a promising copper prospect near Ladysmith, Wis., suggest that the resource potential of the indicated areas and others that may be found merit further investigation.

REFERENCES

Anderson, C. A., 1969, Massive sulfide deposits and volcanism: Econ. Geology, v. 64, no. 2, p. 129–146.

Banks, P. O., and Cain, J. A., 1969, Zircon ages of Precambrian granitic rocks, northeastern Wisconsin: Jour. Geology, v. 77, no. 2, p. 208–220.

Bayley, R. W., Dutton, C. E., and Lamey, C. A., 1966, Geology of the Menominee iron-bearing district, Dickinson County, Michigan, and Florence and Marinette Counties, Wisconsin: U.S. Geol. Survey Prof. Paper 513, 96 p.

Cain, J. A., 1964, Precambrian geology of the Pembine area, northeastern Wisconsin: Michigan Acad. Sci., Arts and Letters Papers, v. 49, p. 81–103.

——— 1966, Investigations in part of the Wisconsin batholith, northeastern Wisconsin [abs.]: Geol. Soc. America Spec. Paper 87, p. 24–25.

Dutton, C. E., and Bradley, R. E., 1970, Lithologic, geophysical, and mineral commodity maps of the Precambrian of Wisconsin: U.S. Geol. Survey Misc. Geol. Inv. Map I–631, 6 sheets.

Goodwin, A. M., 1965, Mineralized volcanic complexes in the Porcupine-Kirkland Lake-Noranda region, Canada: Econ. Geology, v. 60, no. 5, p. 955–971.

Hotchkiss, W. O., and others, 1915, Mineral land classification showing indications of iron formation . . .: Wisconsin Geol. and Nat. History Survey Bull. 44, 378 p.

——— 1929, Mineral lands of part of northern Wisconsin: Wisconsin Geol. and Nat. History Survey Bull 46, 212 p.

Hutchinson, R. W., 1970, Mineral potential in greenstone belts of northwestern Ontario [abs.]: Institute on Lake Superior Geology, 16th ann. meeting, Lakehead Univ., Thunder Bay, Ontario, Proc., p. 22–23.

Kalliokoski, J. O., 1968, Structural features and some metallogenic patterns in the southern part of the Superior Province, Canada: Canadian Jour. Earth Sci., v. 5, no. 5, p. 1199–1208.

LaBerge, G. L., and Weis., L. W., 1969, Central Wisconsin volcanic belt—Field trip guidebook for 15th Annual Institute on Lake Superior Geology, May 1969: [Oshkosh, Wis., Wisconsin State Univ.—Oshkosh], 31 p.

Leith, C. K., Lund, R. J., and Leith, Andrew, 1935, Pre-Cambrian rocks of Lake Superior region, a review of newly discovered geologic features with a revised geologic map: U.S. Geol. Survey Prof. Paper 184, 34 p.

Mancuso, J. J., 1957, Geology and mineralization of the Mountain area, Wisconsin: Madison, Univ. Wisconsin, M. Sc. thesis, 32 p.

——— 1960, The stratigraphy and structure of the McCaslin district, Wisconsin: East Lansing, Michigan State Univ., Ph. D. thesis, 135 p.

North American Geologic Map Committee, 1965, Geologic map of North America: U.S. Geol. Survey, 2 sheets, scale 1:5,000,000.

Patenaude, R. W., 1966, A regional aeromagnetic survey of Wisconsin *in* Steinhart, J. S., and Smith, T. J., eds., The earth beneath the continents—A volume of geophysical studies in honor of Merle A. Tuve: Am. Geophys. Union Geophys. Mon. 40 (Natl. Acad. Sci.—Natl. Research Council Pub. 1467), p. 111–126.

Prinz, W. C., 1965, Marinette Quartz Diorite and Hoskin Lake Granite of northeastern Wisconsin, *in* Cohee, G. V., and West, W. S., Changes in stratigraphic nomenclature by the U.S. Geological Survey 1964: U.S. Geol. Survey Bull. 1224–A, p. A53–A55.

Weidman, Samuel, 1907, The geology of north central Wisconsin: Wisconsin Geol. and Nat. History Survey Bull. 16, 697 p.

CHANGES IN COASTAL MORPHOLOGY OF MONOMOY ISLAND, CAPE COD, MASSACHUSETTS [1]

By R. N. OLDALE, J. D. FRIEDMAN, and R. S. WILLIAMS, JR.,
Woods Hole, Mass.; Washington, D.C.

Work done in cooperation with the Terrestrial Sciences Laboratory, U.S. Air Force Cambridge Research Laboratories, Bedford, Mass., and the Woods Hole Oceanographic Institution, Woods Hole, Mass.

Abstract.—Monomoy Island, an active spit undergoing short- and long-term changes in its coastline, projects southward from the elbow of Cape Cod. The 1969 shoreline was determined from cartographic aerial photography using Ektachrome Aero, Ektachrome infrared Aero, and Plus-X Aerographic films. Comparison of this shoreline with older shorelines, of as long ago as 1887, showed numerous changes in the configuration of the spit. The north end of the island has been receding since 1948. If retreat of the northern half of the Atlantic Ocean shore continues at the current rate of about 40 feet per year, the island may separate into two parts in 70 or 80 years. Eastward progradation of the southern half of the island has continued at a rate of about 40 feet per year since at least 1853. The present encroachment of the south end of Monomoy Island into two deep basins to the southeast and southwest may result in a major reduction in the rate of southward progradation of the spit and may lead to increased erosion of the western shore.

The Terrestrial Sciences Laboratory, of the U.S. Air Force Cambridge Research Laboratories, along with the U.S. Geological Survey in 1969 initiated a cooperative project to study selected segments of the coastline of New England with airborne cartographic cameras and an airborne infrared line-scan system, supported by ground and sea-surface observations. Two objectives of the project are to monitor temporal changes in shoreline and tidal-zone movement of sediment on the coast of Massachusetts.

Monomoy Island was chosen as the subject of this paper because it is an active spit undergoing rapid short-term changes as a result of storms and also slower long-term changes resulting from erosion and deposition by nonstorm waves and currents. Recent geologic quadrangle maps (Koteff and others, 1968; Oldale and Koteff, 1970) show some of the changes in the Monomoy Island shoreline as far back as 1887. With this previous information and the aerial photography acquired in 1969 the long-term trends can be recognized and reasonable predictions can be made as to the future configuration of Monomoy Island.

METHODS

In May 1969, complete 1:24,000-scale film coverage of Monomoy Island was obtained as part of a larger aerial survey project, utilizing Ektachrome Aero, Ektachrome infrared Aero, and Plus-X Aerographic films in 9-inch ×9-inch format, using gyrostabilized K–17 and KC–1B cameras in a U.S. Air Force JC–130A aircraft. The scale was deliberately chosen for rapid comparison with existing U.S. Geological Survey topographic and geologic maps. Overlay plots of frame-by-frame coverage were made to determine the amount of stereoscopy available and to determine whether orthorectification of these frames is necessary for geologic mapping purposes. Little or no rectification was found to be necessary for the present study of Monomoy Island.

The Ektachrome infrared Aero film recorded the greatest amount of detail in the shallow waters of the tidal and subtidal zones and gave the best shoreline detail of the three film types. In exposure of the Ektachrome infrared Aero film, a Wratten No. 12 filter was used to eliminate virtually all light reflectance at wave-

[1] Contribution No. 2438 of the Woods Hole Oceanographic Institution.

U.S. GEOL. SURVEY PROF. PAPER 750-B, PAGES B101-B107

lengths shorter than 510 nanometers (fig. 1). The yellow-dye layer of the film, sensitive to the green spectral region, was relied upon most heavily to yield variations in tonal density depending on intensity of apparent light reflectance from the ocean bottom below the water of the tidal zones. This dye layer recorded the greatest detail in bottom morphology. The cyan-dye layer of the film, sensitive to infrared radiation (fig. 1), which is readily absorbed by a water column as a function of its depth, gave sharp discrimination of shorelines in shallow water of tidal flats and shoal areas.

Stereoscopic pairs were used to plot the planimetric shoreline of Monomoy Island as recorded on Ektachrome infrared Aero film on May 7, 1969, at midday, between low tide and mean tide. The mean tide in this area is about 3.7 feet, although the range is 6.5 feet on the Atlantic Ocean shore of Monomoy Island and 4.1 feet on the Nantucket Sound shore of Monomoy.

GEOGRAPHY AND GEOLOGY

Monomoy Island is a sand spit that projects southward from the elbow of Cape Cod (fig. 2). It is one of the many spits and shoals that characterize the shore and nearshore areas in this region and that form a barrier between Nantucket Sound and the open Atlantic. On the ocean side of the spit, waves and currents generated by easterly winds erode and redeposit the sand and gravel. Waves and currents generated by westerly winds similarly affect the western shore of the spit but have less energy. North of the island the outer shore of Cape Cod is made up of Nauset Beach, a spit that protects the glacial sand and gravel northward to Coast Guard Beach (fig. 2). From this point northward to Pilgrim Heights (fig. 2) the Atlantic shore is made up of a narrow beach at the base of sea cliffs as much as 150 feet high, cut in the sandy glacial deposits. These deposits are the source of the sand and gravel that make up the spits of Nauset Beach and Monomoy Island (Zeigler and others, 1965, p. R310). The sand is transported southward by waves and currents. Much of the sand is deposited to form the seaward part of the shoal upon which Monomoy Island rests. Some sand is carried around Monomoy Point and deposited to form the western part of the Monomoy Island shoal. Aerial photographs (for example, fig. 3) show submarine sand waves formed during the northward transportation of the sand on the west side of Monomoy.

Adjacent to Monomoy Island the bathymetry is characterized by shoals with minimum depths of a few feet and by channels tens of feet deep (fig. 4). South of the shoals and channels, Great Point, a large spit attached to Nantucket Island (fig. 2), projects northward toward Monomoy Island. Monomoy Island rests atop a broad platform defined by the 12- and 18-foot bathymetric contours (fig. 4). This shoal is separated from Handkerchief Shoal by a channel with maximum depths of 44 feet and from Stone Horse Shoal by Butler Hole with maximum depths of more than 100 feet (fig. 4).

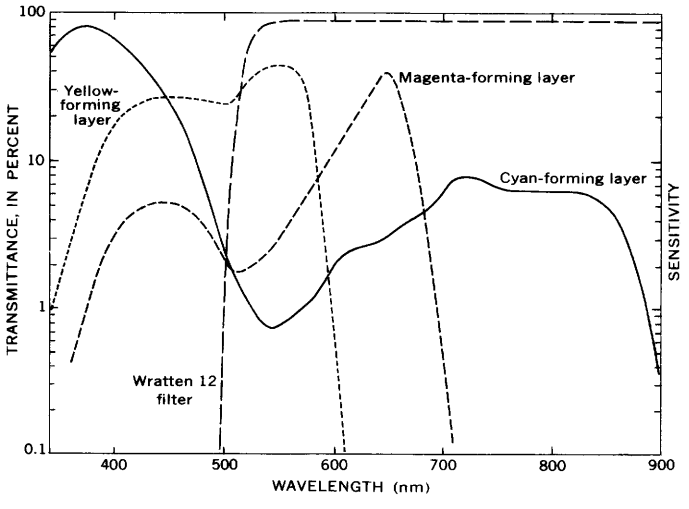

FIGURE 1.—Spectral sensitivities of the three film layers of Ektachrome infrared Aero film (type 8443), utilized to plot the 1969 shoreline features of Monomoy Island. During exposure of the film the Wratten No. 12 filter, the spectral transmittance of which is also shown, was used to eliminate short-wavelength reflectance and dispersion of light from water surfaces. After Fritz (1967).

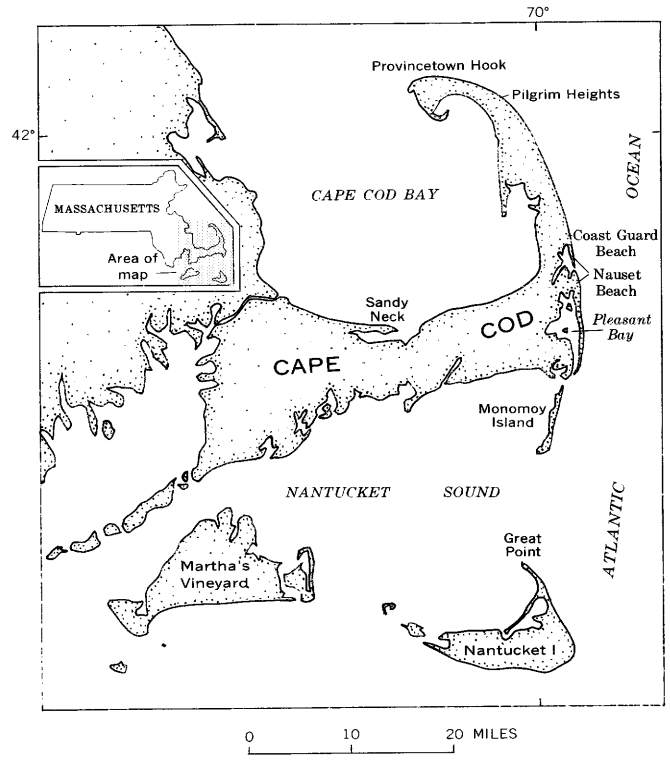

FIGURE 2.—Index map of Cape Cod, Mass., showing the location of Monomoy Island.

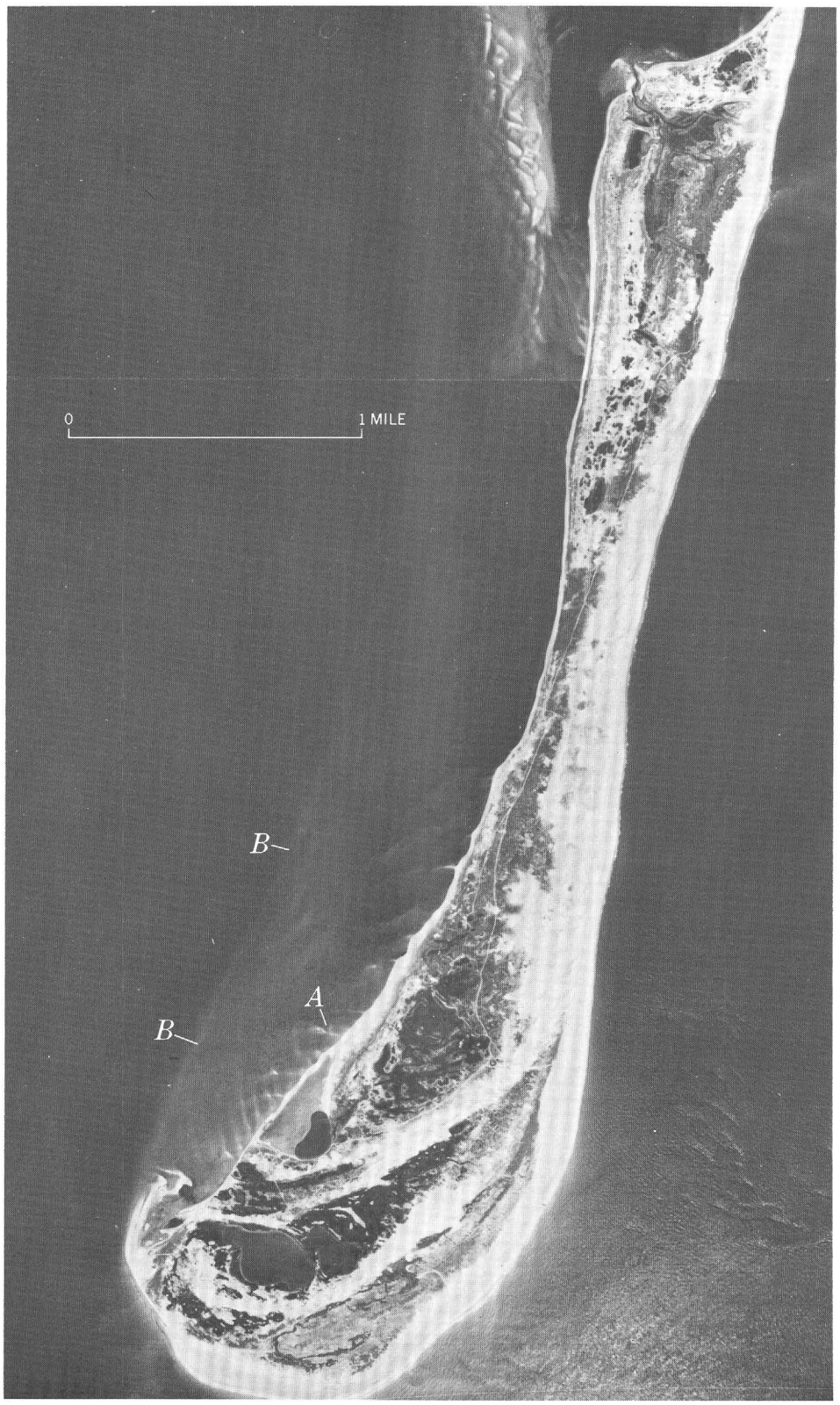

FIGURE 3.—Southern part of Monomoy Island at 11:49 a.m., e.d.t., May 7, 1969, about 59 minutes after low tide at Monomoy Point. Mosaic of black and white prints from frames 65 and 66, roll 43, Ektachrome infrared Aero film, type 8443. Taken with a K–17 aerial cartographic camera from an altitude of 24,000 feet on a north-south flight line. Camera focal length 12 inches; angular field of view 41°06′; original image scale 1:24,000, 9-inch × 9-inch format. Submarine sand waves (*A*) developed on the shoal west of Monomoy Island are visible through approximately 2 feet of water. Submerged bar (*B*) is at a depth of 3 feet.

70°00′
69°57′30″
69°55′00″
41°40′
Chatham
Harding Beach
MORRIS ISLAND
NAUSET BEACH
48
38
2
CHATHAM QUADRANGLE
70°2′30″
41°37′30″
MONOMOY POINT QUADRANGLE
Shooters Island
Hammonds Bend
1
21
SOUND
ISLAND
6
12
18
30

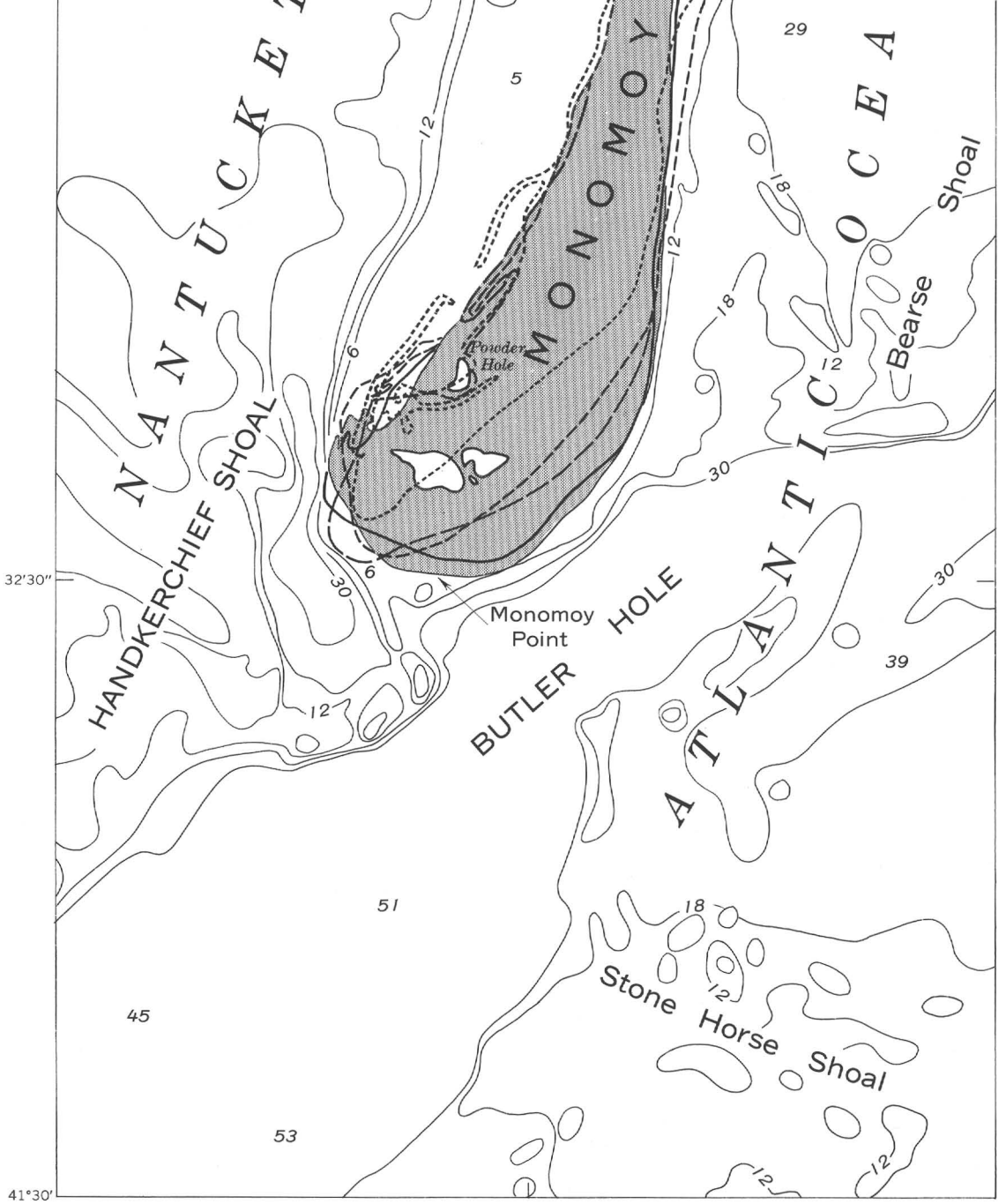

EXPLANATION

1887 shoreline from U.S. Geological Survey 15-minute topographic maps of Chatham and Yarmouth quadrangles

1940

1947–53

1961–64

Shorelines from U.S. Geological Survey 7½-minute topographic maps of Chatham and Monomoy Point quadrangles

1969 landform determined from stereoscopic pairs as recorded on Ektachrome infrared aerographic film on May 7, 1969, between low and mean tide

Where later shoreline conflicts with earlier shoreline, generally the earlier one is shown

Bathymetry, in feet, from Chatham quadrangle (1961) and Monomoy Point quadrangle (1964)

0 1 MILE

FIGURE 4.—Map of Monomoy Island, showing the shorelines of 1887, 1940, 1947–53, and 1961–64 from U.S. Geological Survey topographic maps, and the recent shoreline, determined by aerial photographs taken in May 1969.

Monomoy Island is composed mainly of beach deposits, mostly sand and some gravel and boulders as much as 10 inches in diameter. The beach deposits have maximum altitudes of a foot or two above sea level. Dune sand overlies the beach deposits in most places and locally may be as much as 40 feet thick.

The early history of Monomoy spit may be inferred from data obtained elsewhere on Cape Cod. As a result of the postglacial rise in sea level, the sea reached the vicinity of Cape Cod about 6,000 years ago to begin marine erosion of the glacial deposits (Zeigler and others, 1965, p. R305). Development of the spit began sometime after this and may have been similar to the development of Sandy Neck spit in Barnstable (fig. 2). The initiation of Sandy Neck occurred as much as 4,000 years ago, and the spit has grown eastward at a rate of as much as 13 feet per year for the past 3,000 years (Redfield, 1965). Changes in Monomoy spit, from 1887 to 1964, are summarized by Koteff, Oldale, and Hartshorn (1968) and Oldale and Koteff (1970). These changes in the Monomoy Island shoreline can be seen by comparing the data given in the above references with the shoreline visible on the May 1969 photographs (fig. 3).

The north end of the island continues to retreat southward. Erosion of this part was probably initiated by the major breakthrough that occurred during 1957–58 winter storms, possibly as a result of closing the channel between Morris Island and Chatham. The hurricane of September 21, 1938, originally created the channel between Morris Island and Chatham.[1] Erosion and deposition in this area may also be presently influenced in part by the sand dike constructed from Harding Beach to Morris Island in 1965. Progradation appears to be taking place along the Nantucket Sound shore of Monomoy Island at the site of the breakthroughs shown by the 1947 shoreline. Southward from there to Hammonds Bend the progradation shown by the 1969 shoreline (fig. 3) may be in part apparent because the photographs were taken near low tide and may show the sand flat west of the island as dry land. However, the photographs appear to show vegetation in the area between the offshore dunes and the shoreline of 1961, suggesting that progradation is actually taking place. The shore at Hammonds Bend and the west shore southward for about 2½ miles appear to be very stable, showing little change from the 1887 shoreline and virtually no change since 1940. On the ocean side of Monomoy Island, the shore north of a point 2½ miles north of Monomoy Point shows only minor configurational changes between 1964 and 1969. However, the shore as a whole in this area appears to be retreating westward, probably at a rate of about 40 feet per year as determined from the position of earlier shorelines. Progradation of the ocean shore has continued at a similar rate in the southern part of the island. This rapid progradation has continued since at least 1853, when the shore was in a position marked by the dune ridge just southeast of Powder Hole (Zeigler and others, 1965, p. R307). The eastern part of the tip of Monomoy Point has continued to prograde southward while the western part has retreated northward, trends first shown by the 1964 shoreline. Recurving of the spit at Monomoy Point (as best seen in the 1887 shoreline) was shown much reduced by the 1940, 1953, and 1964 shorelines, but as shown by the 1969 shoreline, the curve appears to be redeveloping. A point of stability on the eastern coast 1.7 miles north of Monomoy Point has continued to exist since at least 1940. North of this point, the shoreline retreats, and south of this point the shoreline progrades; hence the longitudinal axis of Monomoy Island is shifting to approximately a north-south position. A similar straightening of the outer arm of Cape Cod by longshore drift was recognized and described by Davis (1896, p. 713–715, fig. 112) during the last century.

[1] U.S. Army Corps of Engineers, 1968, Survey report, Pleasant Bay—Chatham, Orleans, Harwich, Massachusetts: Waltham, Mass., 61 p., appendices A–F, variously paged.

CONCLUSIONS

The shoreline of Monomoy Island will continue to change as a result of erosion and deposition by (1) major storm waves of yearly winter gales and sporadic late summer hurricanes along the New England coast, and (2) waves and currents generated under fair-weather conditions. Some idea of the future of the island may be gained from the recent changes in the shoreline and from trends previously described. The southward retreat of the north end of the island will probably continue for some time, although possibly at a reduced rate as a result of the progradation of the west shore in this area. The stability of the shore at Hammonds Bend and the rapid retreat of the ocean shore on the east side of the island may result in the separation of Monomoy Island and Shooters Island in 70 or 80 years, not unlike the configuration shown by the shoreline in 1887. Separation could occur much sooner because this narrow neck of the island is low, and hence vulnerable to storm erosion.

The encroachment of Monomoy Point on Butler Hole and the smaller depression southwest of the point may result in major changes of the growth and development of the spit. The source of sand for Monomoy Island is the exposed glacial deposits to the north, and entrapment of this sand in these depressions should retard greatly the southward progradation of the spit. A present result of the entrapment of sand in the depressions

may be the retreat of the southwestern part of Monomoy Point, so that the 1969 and 1887 shorelines are in about the same position. Possibly a more important effect is that the supply of sand nourishing the west side of Monomoy Island will be cut off. The result may be retrogradation or lack of progradation, a condition now existing along much of the Nantucket Sound shore. Either of these conditions coupled with continued retreat of the northern part of the ocean shore will result in a narrowing of the spit.

It seems probable that growth of the spit has been impeded by similar depressions in the past. The persistent embayment at Hammonds Bend may represent the location of one of these depressions. The narrow waist of the island may be the location of another depression as suggested by deep water east and west of the island. Conversely, the increase in width of the island at the south end may be caused by deposition on a shoal, the eastern and western ends of which are now represented by Bearse and Handkerchief shoals.

REFERENCES

Davis, W. M., 1896, The outline of Cape Cod: Am. Acad. Arts and Sci. Proc., v. 31, p. 303–332; also pub. in Geographical essays, New York, Dover Pub., p. 690–724, 1954.

Fritz, N. L., 1967, Optimum methods for using infrared-sensitive color films: Photogramm. Eng., v. 33, no. 10, p. 1128–1138.

Koteff, Carl, Oldale, R. N., and Hartshorn, J. H., 1968, Geologic map of the Monomoy Point quadrangle, Barnstable County, Cape Cod, Massachusetts: U.S. Geol. Survey Geol. Quad. Map GQ–787.

Oldale, R. N., and Koteff, Carl, 1970, Geologic map of the Chatham quadrangle, Barnstable County, Cape Cod, Massachusetts: U.S. Geol. Survey Geol. Quad. Map GQ–911.

Redfield, A. C., 1965, Ontogeny of a salt marsh estuary: Science, v. 147, no. 3653, p. 50–55.

Zeigler, J. M., Tuttle, S. D., Tasha, H. J., and Giese, G. S., 1965, The age and development of the Provincelands Hook, Outer Cape Cod, Massachusetts: Limnology and Oceanography, v. 10, supp., p. R298–R311.

MOVEMENT MEASUREMENTS ON TWO ROCK GLACIERS IN THE EASTERN ELK MOUNTAINS, COLORADO

By BRUCE BRYANT, Denver, Colo.

Abstract.—On two cirque rock glaciers at 11,500–12,000 feet in altitude at lat 39°00′ N. in the eastern Elk Mountains of Colorado, maximum surface movement amounted to about 2 feet (60 cm) per year over a 4-year period. Practically no disruption of their surface cover took place during that period, and little change along surface profiles was detected. In both rock glaciers there appeared to be a lateral component of movement away from the highest valley wall.

Rock glaciers are abundant in the eastern Elk Mountains of western Colorado at about 39° N. (fig. 1). In the Maroon Bells 7½-minute quadrangle more than 50 rock glaciers are mapped (Bryant, 1969). Both cirque and valley-wall types (Outcalt and Benedict, 1965) occur, but cirque types predominate. Cirque types are commonly surrounded by an apron of talus along their sides and upper ends. Most of them head at about 12,000 feet and terminate on the average at 11,200 feet, but some end as low as 10,800 feet and others as high as 11,600 feet. They are commonly half a mile long and 500–1,000 feet wide, but some reach a length of a mile and a width of 1,500 feet.

For purposes of mapping, the rock glaciers are divided into two groups: one which lacks soil and vegetation and which is believed to be active and one on which soil and vegetation have developed and which is believed to be inactive. Some intermediate types are found; these may be older rock glaciers on which slow movement has continued to the present or they may be older rock glaciers that were only partly reactivated when the newer rock glaciers formed. The younger cirque rock glaciers have irregular surfaces formed by ridges, furrows, and lobes, and are composed of coarse angular blocks that lack lichens (figs. 2–4). The rock glaciers have the convex cross sections of active ice glaciers, with steep fronts shedding talus and revealing sand and silt. They override older rock glaciers and

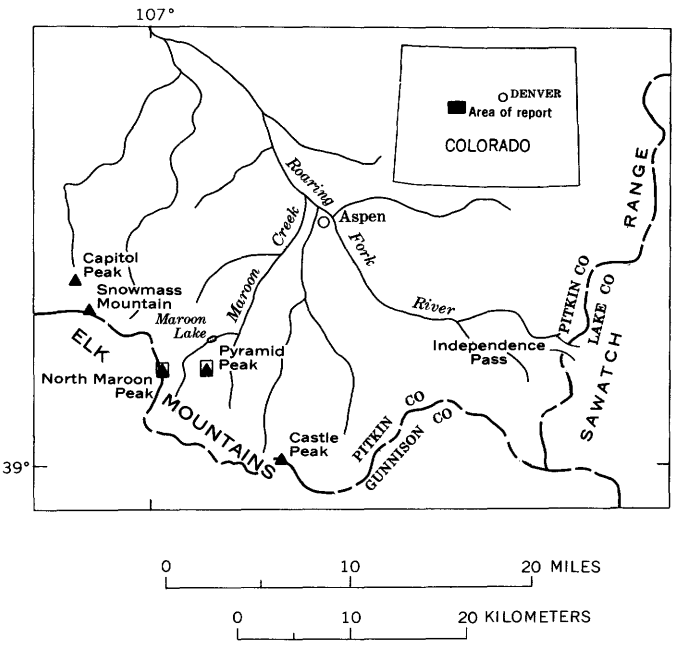

FIGURE 1.—Location of area of rock glaciers on which movement measurements were made, in the eastern Elk Mountains. Solid triangles indicate 14,000-foot peaks; squares outline area of figures 6*A*, *B*.

neoglacial moraines of the Temple Lake Stade (fig. 5). They are the sources of streams during the summer season.

LOCATION AND SETTING OF ROCK GLACIERS MEASURED

Movement measurements were made on two rock glaciers in the drainage of West Maroon Creek, near Aspen, Colo. The measured glaciers are the one north of North Maroon Peak (figs. 2, 6*A*) and the one north of Pyramid Peak (figs. 3, 6*B*). These two glaciers were selected because they appeared to be as active as any in the area, and they could be readily reached from the roadhead at Maroon Lake.

U.S. GEOL. SURVEY PROF. PAPER 750-B, PAGES B108-B116

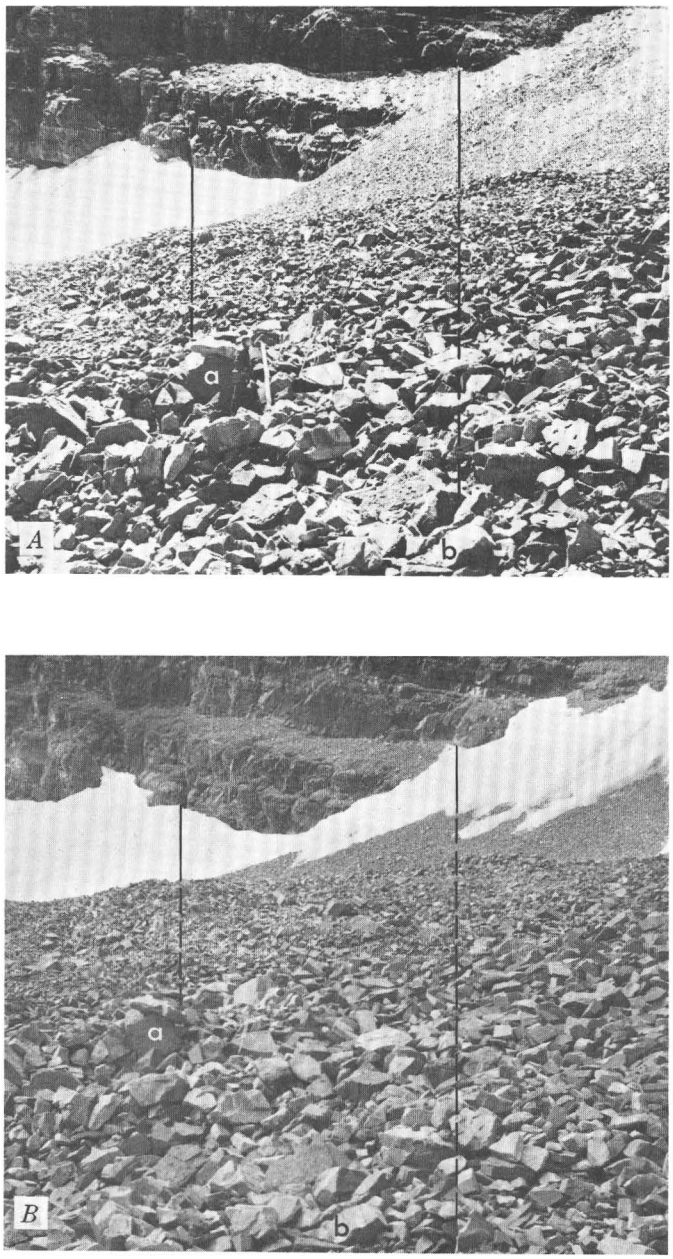

FIGURE 2.—Views across Maroon rock glacier at about 11,830 feet altitude from station 1 toward station 5 (fig. 6*A*), showing downvalley movement of glacier without any rearrangement of surface rocks. Perpendicular lines are drawn from features on valley walls to aid detection of movement; a and b identify the same rocks in the two pictures. *A*, Aug. 28, 1964; *B*, Aug. 21, 1968.

The Maroon rock glacier is 2.5 airline miles S. 63° W. from the outlet of Maroon Lake where the Maroon Creek road now ends. It flows east from a cirque on the north side of North Maroon Peak (fig. 6*A*). The head of the rock glacier grades into talus at an altitude of 12,200 feet, and the south side grades into talus derived from the north face of the peak down to an altitude of about 11,600 feet. The north side of the rock glacier is marked by a well-defined marginal trench above the 11,800-foot contour and by a steep front below that altitude. The north margin of the glacier truncates a neoglacial moraine at about 11,550 feet. Rocks of the Maroon Formation, which consists of grayish-red sandstone, conglomerate, and siltstone, form the cirque walls and furnish the material of the rock glacier. The numerous sandstone and conglomerate beds tend to weather into large angular blocks that are unstable on the steep cirque walls. Bedding in the Maroon Formation on the high south side of the cirque dips 15°–20° toward the rock glacier. The dip toward the rock glacier increases the supply of blocks from that direction through rockslides down bedding planes, as well as through rockfall. Thin dikes of Tertiary igneous rocks make scant contribution to the rock glacier.

The Pyramid rock glacier is about 1.4 miles S. 25° W. from the outlet of Maroon Lake in a north-facing cirque below Pyramid Peak (figs. 3, 4, 6*A*, 9*B*). Bedrock on Pyramid Peak, which is the main source area for the rock glacier, is similar to that on North Maroon Peak. Strata dip 5°–10° toward the rock glacier. The rock glacier grades into talus at its head just below 12,000 feet and terminates in a steep front at 11,400 feet in altitude. Both sides of the rock glacier are marked by well-defined troughs. One interesting feature on the Pyramid rock glacier is a pond that was judged in 1963 to be about 40 feet long and 12 feet wide. Its surface then was about 12 feet below the lip of a closed basin. Comparison of photographs of the pond taken from the same spot at the same time of year in 1964 and 1968 shows that the water level was several feet higher in 1968. Ives (1940) reported ponds on an active rock glacier in the Front Range of Colorado.

MEASUREMENTS

In late August 1964, two straight lines were surveyed across each glacier with a Wild T–12 theodolite. Distances were measured by stadia. The position of the lines was dictated by location of easily accessible bedrock outcrops to furnish stationary tie points at each end. Instrument stations were marked and numbered with orange paint, and intermediate rod points were marked with a spot of paint. Vertical profiles were constructed (fig. 7). In late August 1968, the lines were resurveyed. Although the survey points were difficult to find because the bright orange paint of 1964 had weathered to light gray, all the instrument stations were located, except one on the lower line on the Pyramid glacier. That line proved less useful in this study than the others because of its small angle with the direction of movement of the rock glacier.

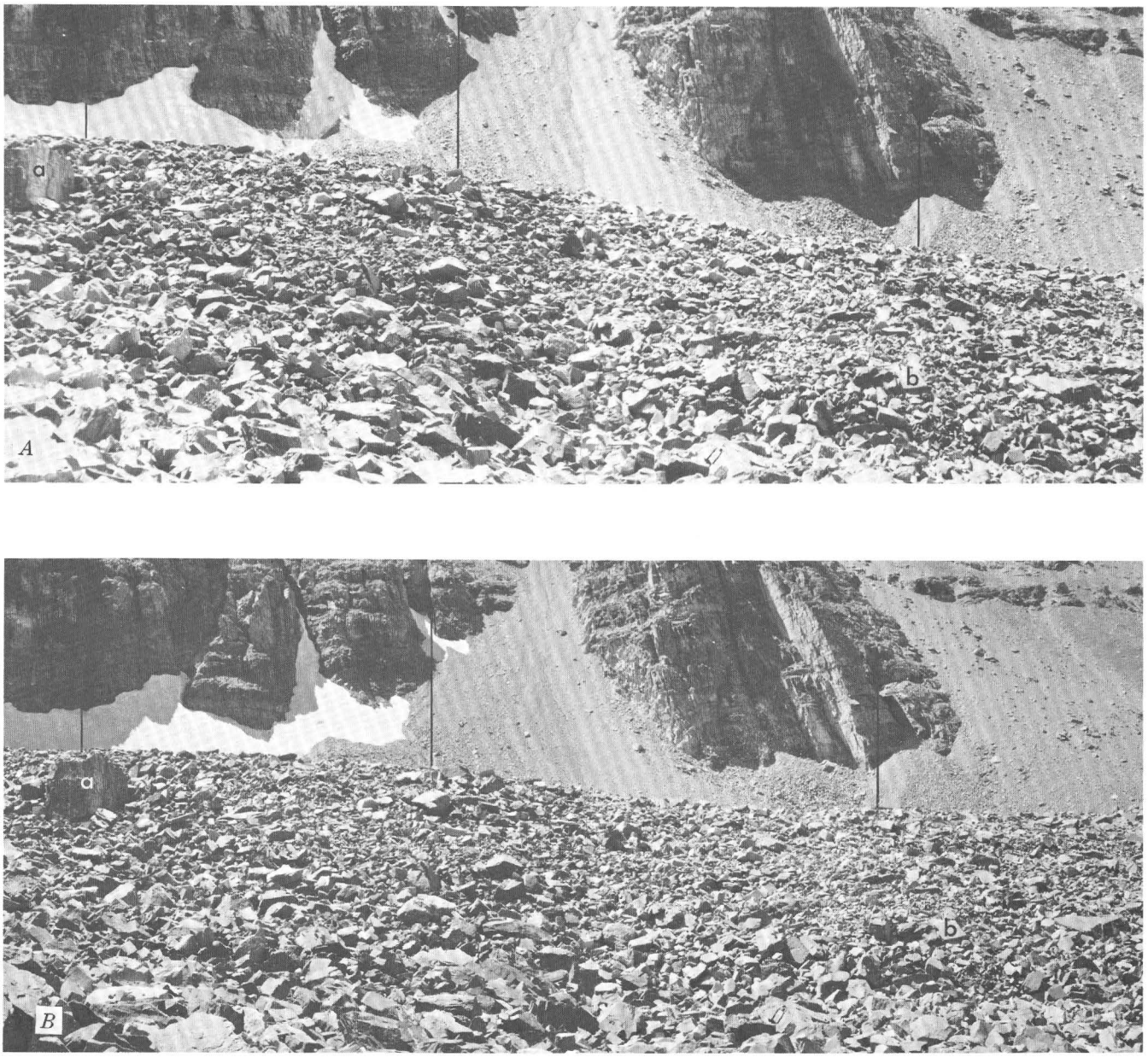

FIGURE 3.—Views across Pyramid rock glacier at about 11,900 feet altitude from station 6 toward station 1 (fig. 6*B*), showing downvalley movement of glacier. Note that most of the distinctive larger rocks on the talus slopes behind the glacier have not moved. Perpendicular lines are drawn from distinctive features on valley walls to aid detection of rock-glacier movement; a and b identify the same rocks in the two pictures. *A*, Aug. 31, 1964; *B*, Aug. 22, 1968.

Displacements of the survey points are measured from calculations of their positions in 1964 and 1968 on a grid by use of a system of latitudes and departures. The x coordinate is parallel to the initial shot in the resurvey of 1968, from the first instrument station on the glacier to the end of the line on outcrop adjacent to the glacier (fig. 8). Thus, the x coordinate is almost parallel with the original survey line of 1964, and the y coordinate is almost perpendicular to it. The positions of points in the y coordinate depend mainly on the small angles measured with the instrument, which can be read to the nearest minute. The positions of points in the x coordinate depend mainly on stadia readings, which are much less accurate. Consequently, the displacement of points in the y coordinate (table 1) may be considered a minimum displacement, and the total displacement, made by calculating the vector sum of the x and y displacements, is a maximum (table 1, fig. 9). This system of measurement is superior to range lines and taping, because it permits detection of lateral displacement (in the x coordinate) that is not parallel to the trend of the rock-glacier axis.

FIGURE 4.—Panoramas across lower part of Pyramid rock glacier at about 11,700 feet from station 8 (fig. 6*B*) showing that lobe has moved downvalley. Perpendicular lines are drawn from distinctive features on valley walls to aid detection of movement; a and b identify the same rocks in the two pictures. *A*, Aug. 31, 1964; *B*, Aug. 22, 1968.

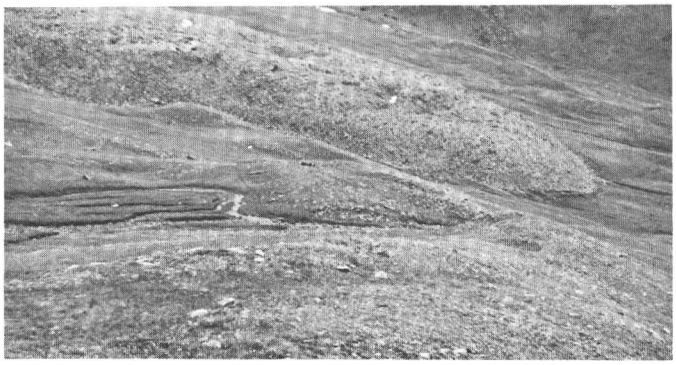

FIGURE 5.—Rock glacier at the head of West Maroon Creek cutting inner of two neoglacial morainal loops of the Temple Lake Stade.

Maximum movement measured for any point was 8.9 feet (272 cm), an average of 2.2 feet (68 cm) a year. Maximum movement in the y (approximately down-glacier and almost perpendicular to the line of the 1964 survey) direction of any point is 8.5 feet (255 cm), an average of 2.1 feet or 63 cm a year (table 1; fig. 9). Movements of that amount occurred along both the lower line on the Maroon rock glacier and the upper line on the Pyramid rock glacier. The upper line of Maroon rock glacier showed only half as much movement. The upper Pyramid line gave evidence of less movement at the margin of the rock glacier than in the center (table 1; figs. 7, 9). Movement in the x direction apparently occurred at points on all three lines, and that movement was away from the highest wall of the cirque. On both rock glaciers the component of movement in x was opposite to the direction of resurvey. Is this a significant relation, considering the lower accuracy of stadia determination of the x coordinate? It appears to be at least qualitatively significant, because amount of movement in the x direction for the most part has a systematic relation with movement in the y direction. A large amount of random error in measurement of the x direction should produce more variation in vectors of movement. Movement becomes systematically greater on the upper Maroon line independently of amount of movement in the y direction, probably because of large amounts of rock supplied to that area from the north face of North Maroon Peak. Point 6a of the lower line of Maroon rock glacier shows movement dominantly in the x direction, because that point is on the gradational line between rock glacier and talus feeding it by downslope movement.

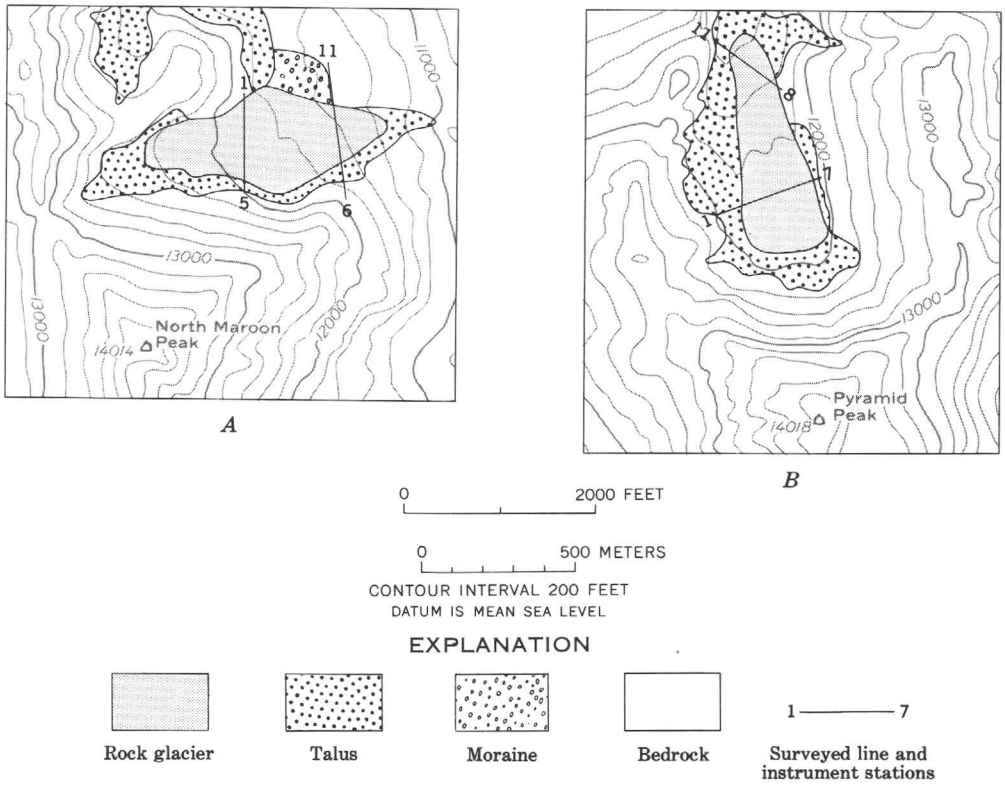

FIGURE 6.—Setting of rock glaciers and position of surveyed lines. Base from U.S. Geological Survey Maroon Bells quadrangle, 1:24,000, 1960; geology from Bryant (1969). *A*, Maroon rock glacier. *B*, Pyramid rock glacier.

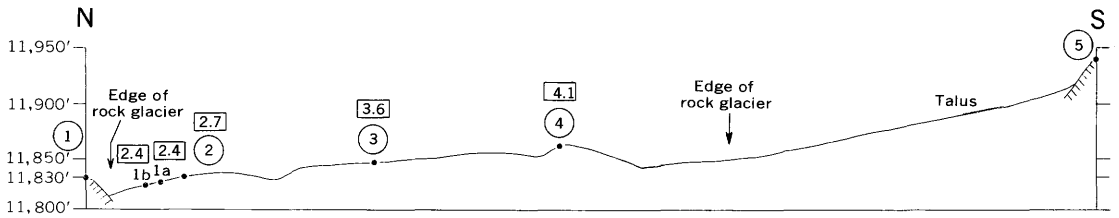

A. Maroon rock glacier–upper line

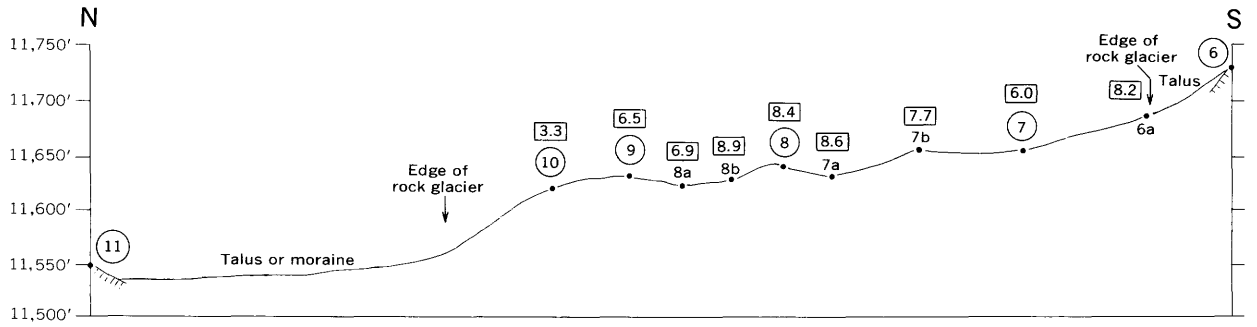

B. Maroon rock glacier–lower line

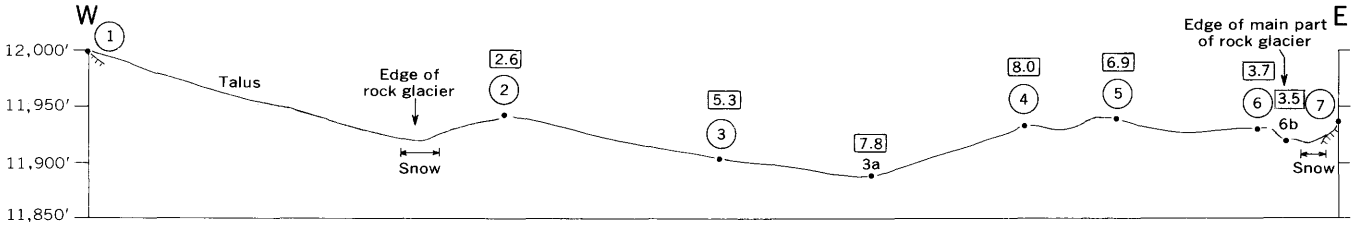

C. Pyramid rock glacier–upper line

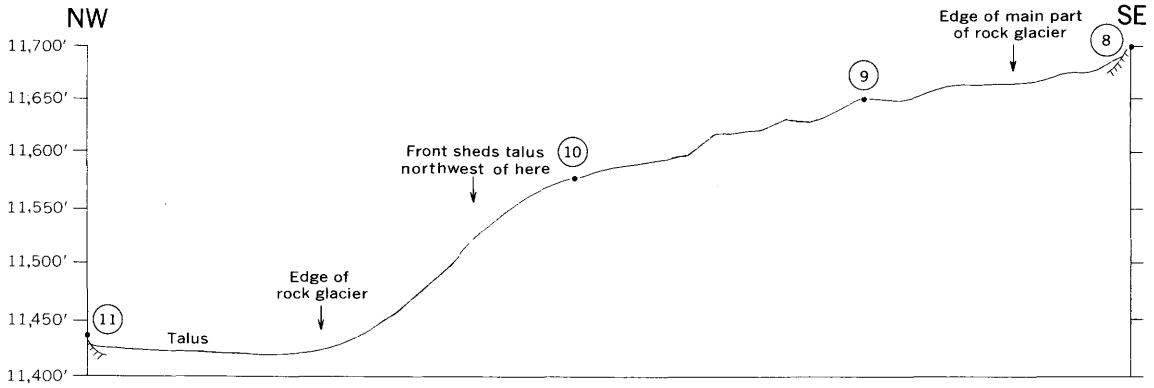

D. Pyramid rock glacier–lower line

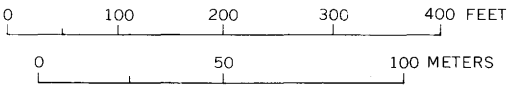

FIGURE 7.—Profiles along lines of original survey made in 1964. Instrument stations are circled numbers. Other numbers are rod stations recovered in 1968 resurvey. Numbers in boxes are calculated total movement, in feet, of each point between 1964 and 1968. Station 10 on lower line of Pyramid rock glacier was not recovered. No movement calculations were made for that line because of this and the small angle the line made with direction of movement. Vertical scale equals horizontal scale.

TABLE 1.—*Calculated amounts of movement of survey points, in feet*

[All *y* components are in downglacier direction. All *x* components are toward the point of origin of the 1968 resurvey]

Survey point	Component		Total (vector sum)	Direction of movement
	x	*y*		
Maroon rock glacier—lower line Direction of line S. 11° E.				
10	1.2	3.1	3.3	N. 58° E.
9	3.2	5.6	6.5	N. 49° E.
8b	6.8	5.8	8.9	N. 30° E.
8a	4.1	5.5	6.9	N. 42° E.
8	5.1	6.7	8.4	N. 42° E.
7b	4.2	6.4	7.7	N. 46° E.
7a	1.7	8.5	8.6	N. 68° E.
7	2.9	5.2	6.0	N. 50° E.
6a	8.0	2.0	8.2	N. 3° E.
Maroon rock glacier—upper line Direction of line South				
1b	0	2.4	2.4	East
1a	0	2.4	2.4	East
2	1.1	2.5	2.7	N. 66° E.
3	2.4	2.7	3.6	N. 48° E.
4	3.8	1.5	4.1	N. 22° E.
Pyramid rock glacier—upper line Direction of line N. 70° E.				
2	2.4	1.1	2.6	N. 85° W.
3	2.7	4.6	5.3	N. 50° W.
3a	4.6	6.3	7.8	N. 56° W.
4	4.9	6.3	8.0	N. 58° W.
5	3.9	5.7	6.9	N. 54° W.
6	2.5	2.4	3.5	N. 68° W.
6b	2.0	1.5	2.5	N. 73° W.

Vertical surface profiles calculated from the 1968 survey generally did not reveal significant differences as compared with the 1964 profiles. Surveying error, which was indicated by discrepancy in elevation difference between the bedrock tie points on the ends of the lines, was less than 2 feet for all the lines except the lower one on the Pyramid rock glacier. There the discrepancy was 5.5 feet. It is unfortunate that the latter line did seem to have some significant profile changes as indicated by local parts of the profile where control was good.

Photographs taken in 1964 and 1968 from survey points on bedrock beside the rock glaciers clearly show that the glaciers have moved downvalley (figs. 2–4). Spatial relations between individual boulders identifiable in the photographs remained the same for the most part, but movement of the whole rock glacier can be detected by carefully comparing positions of individual boulders or groups of boulders with distinctive features in outcrops. Note also that most of the distinctive large boulders on the talus slopes or the valley walls have not moved during the 4-year period, and they may also be used as reference points for detecting movement of the rock glaciers (fig. 3).

DISCUSSION

Movement in the *x* direction, oblique to the rock-glacier axes, indicates that direction of rock-glacier movement may be influenced by the amount of rock supplied by rockfall and avalanche, which was much greater on the south side than on the north side of the Maroon rock glacier. On that rock glacier the steepness of the north margin and front as compared with that of the south margin grading to talus (fig. 7*A*, *B*) suggests that the component of lateral movement away from North Maroon Peak is real and is not due to a surveying error. On the Pyramid rock glacier the upper profile shows trenches at both margins of the glacier, although the valley side east of the glacier is higher than that to the west (figs. 6*B*, 7*C*, *D*). However, the lower part of the Pyramid rock glacier is asymmetrical in relation to the valley. The main mass of the glacier is concentrated on the east side of the valley so that at 11,600 feet in altitude only a small marginal trench separates the glacier from the east valley wall, whereas the west side of the glacier at the same altitude resembles a glacier front in height and steepness.

Pattern of movement downvalley on Pyramid and Maroon rock glaciers is similar to that reported by Outcalt and Benedict (1965) and Waldrop and White (1965) for Arapaho rock glacier in the Front Range west of Boulder, Colo. Points near the rock-glacier margins moved less than those in the center on two of three lines on Pyramid and Maroon rock glaciers. Slumping exposed glacial ice less than 1 meter below

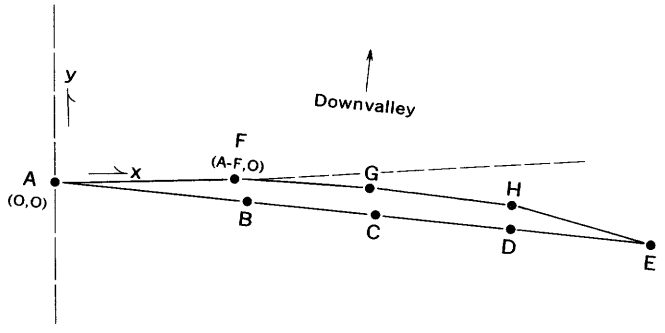

FIGURE 8.—Orientation of grid system for calculating position of survey points. ABCDE is line of original (1964) survey. AFGHE is line of resurvey (1968). x direction is determined by shot from F to A; y direction is perpendicular to it. Point A is arbitrary point of origin of grid system and is assigned the coordinates 0,0. Point F has the coordinates A–F,0.

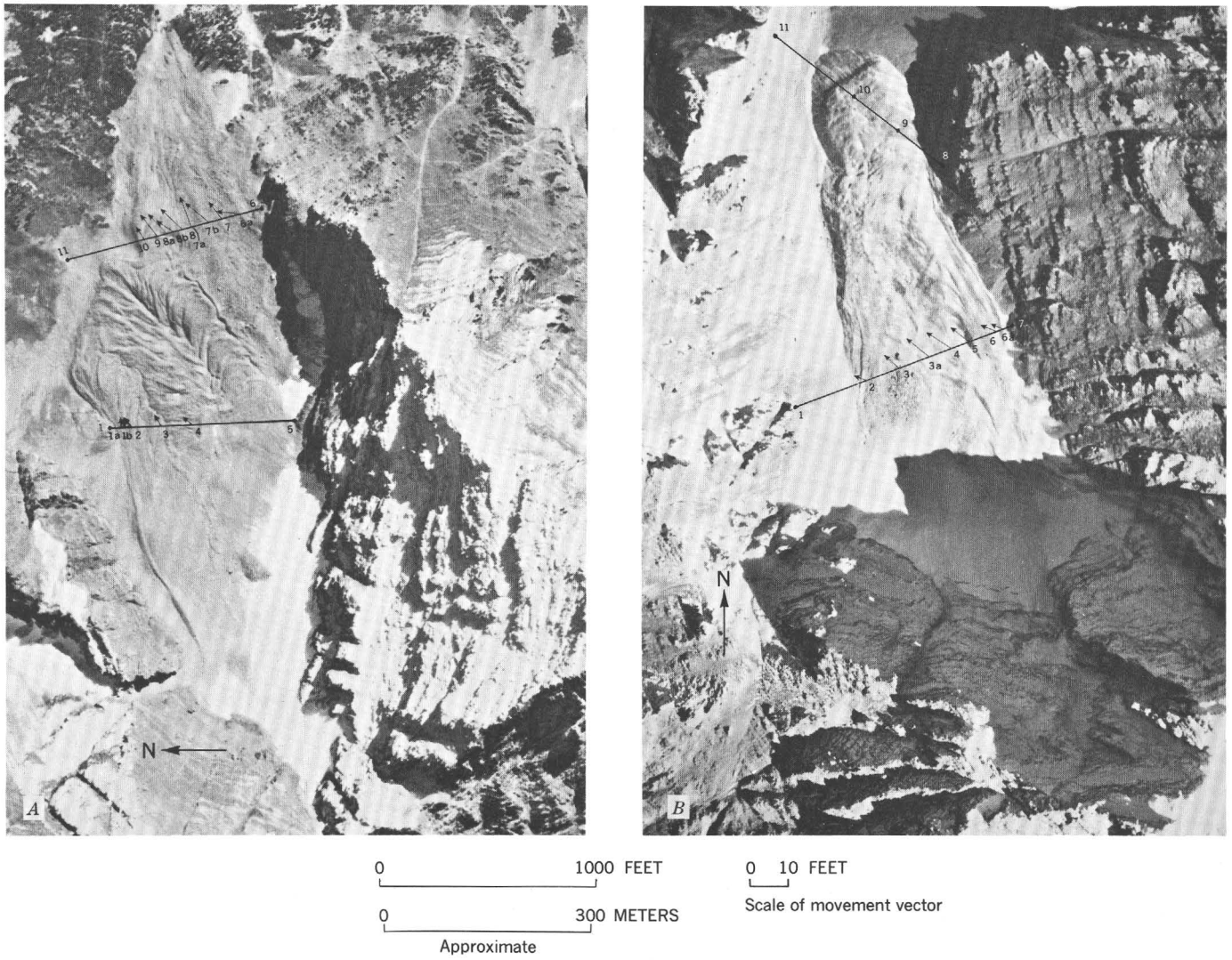

FIGURE 9.—Movement vectors on surveyed lines across rock glaciers. Downvalley is at top. *A*, Maroon rock glacier. From enlargement of U.S. Forest Service photograph ESK–1–279 taken Sept. 14, 1967. *B*, Pyramid rock glacier. From enlargement of U.S. Forest Service photograph ESK–3–9 taken Sept. 21, 1967.

the surface of Arapaho rock glacier 1,300 feet (400 m) downvalley from the base of the cirque headwall; however, movement rates there were only 20 cm/yr at the most (Outcalt and Benedict, 1965).

Maximum rate of movement measured on Pyramid and Maroon rock glaciers is comparable with the value of 80 cm/yr measured by Potter (1968) on the upper part of Galena Creek rock glacier in the northern Absaroka Range of Wyoming at lat 44°38′ N. and 8,800–10,400 feet in altitude. The upper part of this rock glacier has only 1–1.5 m of debris over glacial ice. Similar movement rates have been reported for rock glaciers in Alaska (Wahrhaftig and Cox, 1959; Foster and Holmes, 1965).

No direct observations in the eastern Elk Mountains show whether the rock glaciers consist of glacial ice mantled with debris as described by Potter (1968), or have a smaller core of glacial ice as revealed by a mine tunnel in one rock glacier in the San Juan Mountains of southwestern Colorado (Brown, 1925), or have only interstitial ice, as indicated by Wahrhaftig and Cox (1959) for rock glaciers of the Alaska Range and as revealed by excavation in a rock stream at lower altitude in southern Colorado (Johnson, 1967). Because of a difference in morphology, altitude, and physiographic setting, I think all three types occur in the eastern Elk Mountains and that there are intergradations among them. The truth will not be known until

some method, possibly geophysical, is found to determine how much and what kind of ice is beneath or inside rock glaciers.

ACKNOWLEDGMENTS

Kirby W. Bay assisted in surveying lines across the rock glaciers in 1964; Stephen G. Pollack assisted in the resurvey of 1968. John C. Reed, Jr., gave valuable advice on calculations of amount of movement of the points based on the survey data.

REFERENCES

Brown, W. H., 1925, A probable fossil glacier: Jour. Geology, v. 33, no. 4, p. 464–466.

Bryant, Bruce, 1969, Geologic map of the Maroon Bells quadrangle, Pitkin and Gunnison Counties, Colorado: U.S. Geol. Survey Geol. Quad. Map GQ–788.

Foster, H. L., and Holmes, G. W., 1965, A large transitional rock glacier in the Johnson River area, Alaska Range, *in* Geological Survey Research 1965: U.S. Geol. Survey Prof. Paper 525–B, p. B112–B116.

Ives, R. L., 1940, Rock glaciers in the Colorado Front Range: Geol. Soc. America Bull., v. 51, no. 9, p. 1271–1294.

Johnson, R. B., 1967, Rock streams on Mount Mestas, Sangre de Cristo Mountains, southern Colorado, *in* Geological Survey Research 1967: U.S. Geol. Survey Prof. Paper 575–D, p. D217–D220.

Outcalt, S. I., and Benedict, J. B., 1965, Photo-interpretation of two types of rock glacier in the Colorado Front Range: Jour. Glaciology, v. 5, no. 42, p. 849–856.

Potter, Noel, Jr., 1968, Galena Creek rock glacier, northern Absaroka Mountains, Wyoming, *in* Abstracts for 1967: Geol. Soc. America Spec. Paper 115, p. 438.

Wahrhaftig, Clyde, and Cox, Allan, 1959, Rock glaciers in the Alaska Range: Geol. Soc. America Bull., v. 70, no. 4, p. 383–436.

Waldrop, H. A., and White, S. E., 1965, Arapaho Glacier and Arapaho Rock Glacier, Trip 1 *in* Guidebook for one-day field conferences, Boulder area, Colorado—Internat. Assoc. Quaternary Research 7th Con., U.S.A., 1965: Lincoln, Nebr., Nebraska Acad. Sci., p. 5–10.

MAGNETIC INTENSITIES IN A DIFFERENTIATED GABBROIC BODY, THE DUFEK INTRUSION, PENSACOLA MOUNTAINS, ANTARCTICA

By MYRL E. BECK, JR.,[1] and NANCY LINDSLEY GRIFFIN,[2]
Bellingham, Wash., Riverside, Calif.

Abstract.—The following relationships are found to hold for the Dufek intrusion, a large stratiform mafic body exposed in the Pensacola Mountains, Antarctica:

$$k_a = 1.56V^{1.88} \times 10^{-3} \text{ emu/oe},$$

and

$$J_r = 1.54V^{1.80} \times 10^{-3} \text{ emu},$$

where k_a is apparent magnetic susceptibility, J_r is intensity of natural remanent magnetization, and V is volume percentage of opaque minerals, nearly all iron-titanium oxides in the Dufek intrusion. For a rock body whose magnetic intensity is described by these expressions, concentration of opaque minerals can be estimated from magnetic anomaly patterns, if geometry and depth of burial of the anomaly-producing mass and the direction of J_r are known. The average value of Q, the ratio of remanent intensity to induced intensity, for such a body will be approximately equal to the reciprocal of T, the magnetic field intensity. For the Dufek intrusion, as for many other floored mafic intrusions that have differentiated in place, total magnetic intensity is found to vary markedly with height above base. Magmatic differentiation in such bodies evidently can produce strong gradational contrasts in magnetization. The nonlinear relationship between k_a and V in Dufek intrusion rocks tentatively may be attributed to the effect of self-demagnetization and to an increase in intrinsic magnetic susceptibility with grain size. The similarity in k_a–V and J_r–V relationships suggests that thermoremanent magnetization in Dufek intrusion rocks may be carried by single-domain regions magnetically isolated within multidomain grains by the presence of exsolution-oxidation lamellae of ilmenite.

The Dufek intrusion is a stratiform complex similar to the Stillwater and Duluth Gabbro Complexes of North America and the Bushveld Complex of Africa. It is exposed in the Dufek Massif and in the Forrestal Range (located near lat 83° S., long 52° W.), part of the Pensacola Mountains in West Antarctica.

[1] U.S. Geological Survey.
[2] Department of Geological Sciences, University of California.

The Dufek intrusion is estimated by Ford and Boyd (1968) to be at least 7 km thick and to have an areal extent sufficient to make it one of the world's largest stratiform complexes. Although approximately 40 percent of the intrusion is unavailable for sampling because of erosion or ice cover, a wide variety of rock types is exposed. Represented lithologies range from anorthosite in the lowest exposures through pyroxene gabbro, pyroxenite, leucogabbro, and fairly iron-rich gabbro, to granophyre in the highest exposures. These different varieties of mafic rocks apparently have developed by ordinary magmatic processes from a silica-saturated basaltic magma that is similar to the tholeiitic magma type found distributed over much of the earth's surface and throughout the entire geological column. Relationships worked out in Dufek rocks thus may be expected to have wide application to the study of other mafic rocks.

The Dufek intrusion is currently under investigation by the U.S. Geological Survey (see Ford and Boyd, 1968, and Ford, 1970, for a discussion of geology and petrology). Data reported here were collected during paleomagnetic studies that are still in progress (Beck and others, 1968; Griffin, 1969). Seismic, gravity, and aeromagnetic studies in the Pensacola Mountains have been described by Behrendt, Meister, and Henderson (1966).

METHODS AND GENERAL OBSERVATIONS

Magnetic properties of 172 oriented samples have been studied to date. These samples are representative of the complete exposed stratigraphic thickness and much of the exposed areal extent of the Dufek intrusion. Thin sections have been prepared from 27 of these samples, and the volume percentage (V) of opaque

U.S. GEOL. SURVEY PROF. PAPER 750-B, PAGES B117-B121

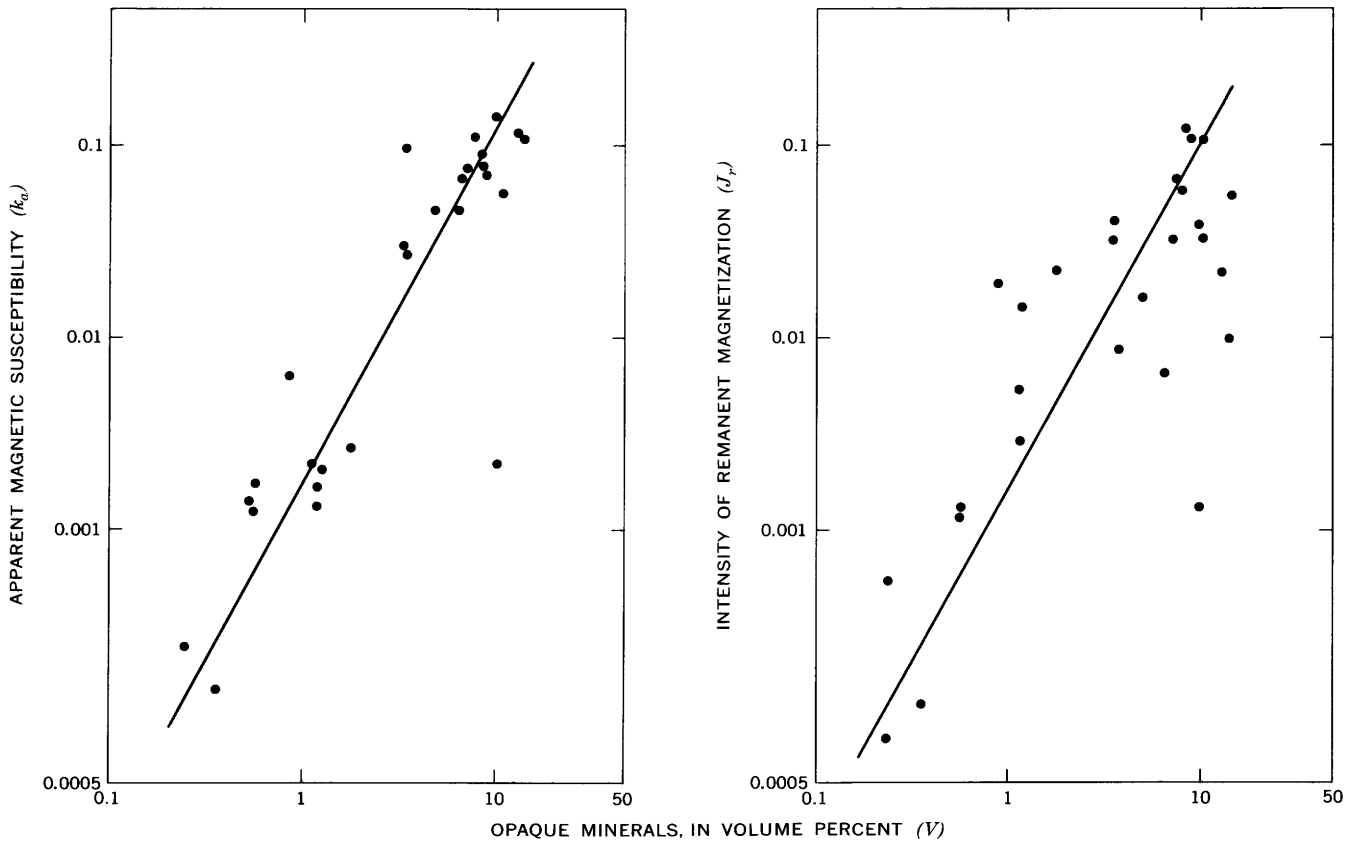

FIGURE 1.—Plot of volume percentage of opaque minerals (V) versus apparent magnetic susceptibility (k_a, in emu/oe) and intensity of remanent magnetization (J_r, in emu) for samples from the Dufek intrusion. Lines are least-squares best fit.

minerals has been determined at moderate magnification by standard petrographic point-counting techniques. At least 1,000 points were counted for each thin section. Visible opaque grains in these samples consist almost entirely of iron-titanium oxide minerals, mainly intergrowths of magnetite and ilmenite, although a few sulfide grains are present in some samples (Griffin, 1969; Aughenbaugh, 1961). For the purposes of this report, V can be regarded as a very good estimate of abundance of magnetic oxide minerals. Volume percentage of opaque minerals is shown plotted against (1) apparent magnetic susceptibility (k_a) and (2) intensity of natural remanent magnetization (J_r) in figure 1.

As expected, both k_a and J_r increase with increasing content of opaque minerals. The regularity of the relationship is interesting, however, and allows several useful functional relationships to be established empirically. For example, the equations of the least-squares lines shown in figure 1,

$$k_a = 1.56V^{1.88} \times 10^{-3} \text{ emu/oe}, \quad (1)$$

and

$$J_r = 1.54V^{1.80} \times 10^{-3} \text{ emu}, \quad (2)$$

in which emu/oe is electromagnetic units per oersted, together with the expression for total magnetization (J),

$$\vec{J} = \vec{J}_r + k\vec{T}, \quad (3)$$

where $\vec{T}$ is the total intensity of the geomagnetic field, allow prediction of the magnetic anomaly to be expected from any given concentration of opaque minerals. The direction of $\vec{J}_r$ must of course be determined from measurements on oriented samples. If the opaque fraction is assumed to consist mainly of iron-titanium oxide minerals, the anomaly amplitude range likely to indicate ore may be predicted. Conversely, if the approximate shape, size, and depth of the anomalous mass are known, opaque concentrations may be estimated from magnetic maps by means of equations 1–3.

Expressions similar to equation 1 have been used by several authors to describe the relationship between magnetic susceptibility and fraction of magnetic mineral in various rock types. Bath (1962) and Jahren (1963) reported $1.16V^{1.39} \times 10^{-3}$ emu/oe for a Mesabi iron formation. Mooney and Bleifuss (1953) gave

$2.89V^{1.01}\times10^{-3}$ emu/oe for a suite of seven rock types from Minnesota and $1.23V^{0.36}\times10^{-3}$ emu/oe for gabbro samples alone. Balsley and Buddington (1958) reported $2.6V^{1.33}\times10^{-3}$ emu/oe for igneous and metamorphic rocks from the Adirondack Mountains, N.Y. Similar investigations also have been made by others; for example, Slichter (1929) and Werner (1945). The most conspicuous result of these investigations is to show that no simple relationship exists between magnetic susceptibility and content of magnetic mineral. Evidently, rock type and geological history exert considerable control over the magnetic properties of rocks. This appears to be a promising field for further useful research.

SELF-DEMAGNETIZATION

The important role played by self-demagnetization in determining rock magnetic properties has been discussed by several authors. It can be shown (for example, Nagata, 1961, p. 130) that, for $p \ll 1$,

$$k_a=\frac{pk}{1+Nk}, \tag{4}$$

where k_a, k, and N are apparent magnetic susceptibility, intrinsic magnetic susceptibility, and demagnetizing factor, respectively, and p is the volume fraction of magnetic mineral ($p=V\times10^{-2}$). For large values of k this gives approximately $k_a=p/N$. Since $N\approx3.9$ for a typical assemblage of magnetic grains (Stacey, 1963), the relationship $k_a=0.26p$ should hold approximately for large k. This is equivalent to $k_a=2.6V\times10^{-3}$, not unlike Mooney and Bleifuss' (1953) expression for Minnesota rocks. For small and variable k, however, equation 4 predicts a more complicated relationship between magnetic susceptibility and content of magnetic oxide minerals. In particular, if k increases with p, a relationship similar to the Jahren (1963) and Bath (1962) expression for Adirondack rocks, or to equation 1 of this paper, might result. For instance, if it is assumed that k increases linearly with p ($k=ap$), then

$$k_a=\frac{ap^2}{1+Nap}=ap^2-Na^2p^3. \tag{5}$$

Equation 5 gives results very close to those of equation 1 for suitably small values of p. Intrinsic susceptibility (k) might be expected to increase with p if part of the variation in p was due to variation in grain size. This follows because k is to some extent an increasing function of grain size (Stacey, 1963, p. 71; Nagata, 1961, p. 99). In rocks from the Dufek intrusion a notable increase in grain size accompanies increase in the total volume percentage of opaque minerals.

It follows from equations 1 and 2 that for the Dufek intrusion a good estimate of the average value of Q, a quantity defined (Koenigsberger, 1938) as

$$Q=\frac{J_r}{kT}, \tag{6}$$

is given by T^{-1} for all values of V. Thus, for all likely values of geomagnetic field intensity,

$$1.3<Q_{avg}<5, \tag{7}$$

indicating that accurate interpretation of total intensity magnetic data requires that both remanent and induced magnetization be taken into consideration. Actual values of Q for the 27 samples shown in figure 1, calculated for $T=0.5$ oe, range from 0.3 to 30 and average 2.02.

VARIATION OF k_a AND J_r WITHIN THE DUFEK INTRUSION

Variations in magnetic susceptibility and intensity of natural remanent magnetization do not occur randomly throughout the thickness of the Dufek intrusion; rather, k_a and J_r have a strong tendency to increase with height above base until the granophyre zone near the roof is reached, whereupon they drop abruptly. The tendency for magnetic intensity to increase upward is not confined to the Dufek intrusion; it is found in many other mafic bodies that have differentiated in situ (examples include those of Jaeger and Joplin, 1955; Beck, 1966; Beck and Lindsley, 1969). Increase of magnetization with decreasing depth may result from differentiation trends characterized by increase in the ferric–ferrous ratio, accompanied by increasing or nearly constant iron content; this differentiation is produced under conditions which permit the crystalline material to sink to the floor of the magma chamber. Thus, early-formed material that rests near the floor of the intrusion tends to be relatively free of iron-titanium oxide minerals, whereas late oxide-rich material is located near the roof. The uppermost parts of some differentiated mafic bodies also have relatively low magnetization. This low magnetization probably results from a tendency for a small amount of early-crystallized material to adhere to the roof of the magma chamber, but for some mafic bodies (such as the Dufek intrusion) it is caused by the presence near the roof of a granophyric residuum nearly devoid of iron-bearing minerals. Strong magnetization contrasts may be produced within a differentiated mafic intrusion by this mechanism. Figure 2 shows variation in remanent and induced magnetization within the Dufek intrusion, based on

413-504 O - 71 - 9

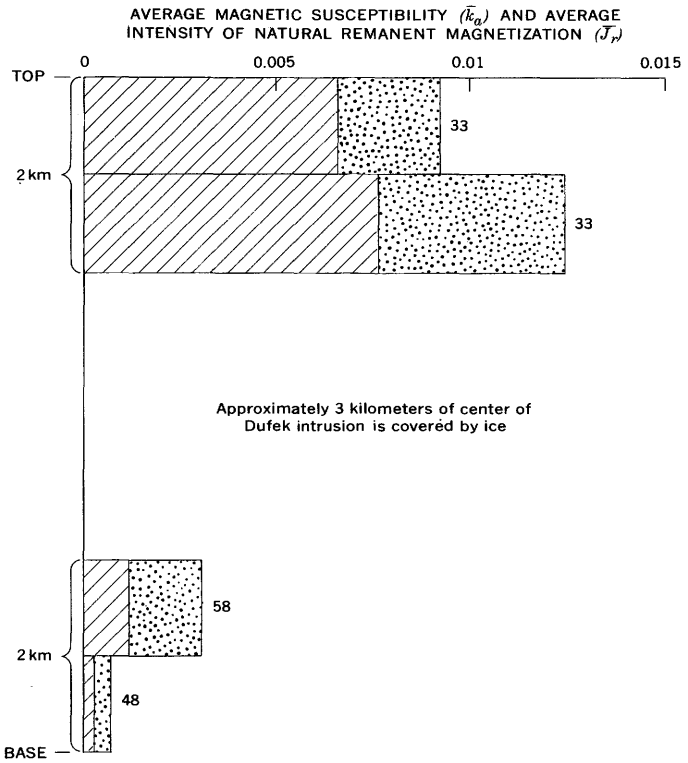

FIGURE 2.—Average magnetic susceptibility (k_a, indicated by diagonal pattern) and average intensity of natural remanent magnetization (J_r, indicated by dotted pattern) for arbitrary thick zones within the Dufek intrusion. Numerals opposite each bar indicate number of samples averaged per group.

measurements of 172 samples. From this diagram it is evident that if the Dufek intrusion were strongly deformed it would present a complex pattern of magnetic anomalies. Many of these anomalies would be caused by gradational magnetization contrasts, reflected by low anomaly gradients relative to gradients resulting from abrupt magnetic contrasts of equal magnitude between juxtaposed, contrasting lithological units at the same depth. The possible existence of such gradational magnetization contrasts should be considered when computing depth to basement by gradient techniques.

SOURCE OF k_a AND J_r

The fact that virtually identical empirical relationships exist between concentration of opaque minerals and magnetic susceptibility and between opaque minerals concentration and intensity of remanent magnetization is of some interest. The greater scatter shown by the V–J_r diagram (fig. 1) undoubtedly reflects the complex origin of remanent magnetization, a process not yet wholly understood. However, difference in scatter does not alter the close similarity between the V–k_a and V–J_r diagrams. Apparently magnetic susceptibility and remanent magnetization are somehow similarly related to the large opaque grains that dominate the point counts. Magnetic susceptibility is clearly a multidomain process (Stacey, 1963), but remanent magnetization (specifically thermoremanent magnetization) is more probably single-domain or pseudosingle-domain in character (Evans and others, 1968; Evans and McElhinny, 1969; Stacey, 1967). For instance, Evans, McElhinny, and Gifford (1968) have shown that nearly half the intensity of thermoremanent magnetization of the Modipe gabbro is contributed by magnetite particles (diameter 17μ or less) found as exsolution products within pyroxene grains. For the Dufek intrusion, Q values are too high (all but two are in excess of 0.5) to satisfy Stacey's (1967) criterion for true multidomain behavior; yet it appears that intensity of remanent magnetization bears a consistent relationship to the volume of visible opaque minerals in the rock. Moreover, the relationship between V and J_r is virtually identical to that between induced magnetization, a known multidomain process, and volume of large opaque grains. Dufek intrusion samples show a high to moderate magnetic stability, so it is unlikely that the greater part of the remanent magnetization is viscous or isothermal in origin (M. E. Beck, Jr., unpub. data). Apparently the number of single-domain regions contributing to the remanent magnetization of Dufek intrusion rocks is proportional to the volume of opaque minerals visible in thin section. The simplest explanation for this observation, following Strangway, Larson, and Goldstein (1968), is that the single-domain behavior originates in small regions within the large opaque grains that have been isolated by ilmenite lamellae, which are formed by relatively low-temperature exsolution and subsolidus oxidation. More laboratory work is necessary to test this idea.

ACKNOWLEDGMENTS

The measurements upon which this paper is based were made on oriented hand specimens collected by A. B. Ford, W. W. Boyd, Jr., D. L. Schmidt, and W. H. Nelson. Ford and W. T. Hanna acted as reviewers. This assistance is gratefully acknowledged.

REFERENCES

Aughenbaugh, N. B., 1961, Preliminary report on the geology of the Dufek Massif, chap. 8 *in* Reports of Antarctic geological observations, 1956–60: Internat. Geophys. Year Glaciological Rept. 4, p. 155–193.

Balsley, J. R., and Buddington, A. F., 1958, Iron-titanium oxide minerals, rocks, and aeromagnetic anomalies of the Adirondack area, New York: Econ. Geology, v. 53, no. 7, p. 777–805.

Bath, G. D., 1962, Magnetic anomalies and magnetizations of the Biwabik iron-formation, Mesabi area, Minnesota: Geophysics, v. 27, no. 5, p. 627–650.

Beck, M. E., Jr., 1966, The effect of magmatic differentiation on the magnetic properties of diabase sheets of southeastern Pennsylvania *in* Geological Survey Research 1966: U.S. Geol. Survey Prof. Paper 550–D, p. D109–D116.

Beck, M. E., Jr., Ford, A. B., and Boyd, W. W., Jr., 1968, Paleomagnetism of a stratiform intrusion in the Pensacola Mountains, Antarctica: Nature, v. 217, no. 5128, p. 534–535.

Beck, M. E., Jr., and Lindsley, N. C., 1969, Paleomagnetism of the Beaver Bay Complex, Minnesota: Jour. Geophys. Research, v. 74, no. 10, p. 2002–2013.

Behrendt, J. C., Meister, Laurent, and Henderson, J. R., 1966, Airborne geophysical study in the Pensacola Mountains of Antarctica: Science, v. 153, no. 3742, p. 1373–1376.

Evans, M. E., and McElhinny, M. W., 1969, An investigation of the origin of stable remanence in magnetite-bearing igneous rocks: Jour. Geomagnetism and Geoelectricity, v. 21, p. 757–774.

Evans, M. E., McElhinny, M. W., and Gifford, A. C., 1968, Single domain magnetite and high coercivities in a gabbroic intrusion: Earth and Planetary Sci. Letters, v. 4, no. 2, p. 142–146.

Ford, A. B., 1970, Development of the layered series and capping granophyre of the Dufek intrusion of Antarctica *in* Symposium on the Bushveld igneous complex and other layered intrusions: Geol. Soc. South Africa Spec. Pub. 1, p. 492–510.

Ford, A. B., and Boyd, W. W., Jr., 1968, The Dufek Intrusion, a major stratiform gabbroic body in the Pensacola Mountains, Antarctica: Internat. Geol. Cong., 23d, Prague 1968, Rept., v. 2, p. 213–228.

Griffin, N. L., 1969, Paleomagnetic properties of the Dufek intrusion, Pensacola Mountains, Antarctica: Riverside, California Univ. M.S. thesis, 93 p. (unpub.).

Jaeger, J. C., and Joplin, Germaine, 1955, Rock magnetism and the differentiation of dolerite sill: Geol. Soc. Australia Jour., v. 2, p. 1–19.

Jahren, C. E., 1963, Magnetic susceptibility of bedded iron-formation: Geophysics, v. 28, no. 5, pt. 1, p. 756–766.

Koenigsberger, J. G., 1938, Natural residual magnetism of eruptive rocks: Terrestrial Magnetism Atmospheric Electricity, v. 43, no. 2, p. 119–130.

Mooney, H. M., and Bleifuss, Rodney, 1953, Analysis of field results, pt. 2 *of* Magnetic susceptibility measurements in Minnesota: Geophysics, v. 18, no. 2, p. 383–393.

Nagata, Takesi, 1961, Rock magnetism [revised ed.]: Tokyo, Maruzen Co., Ltd., 350 p.

Slichter, L. B., 1929, Certain aspects of magnetic surveying, *in* Geophysical prospecting: Am. Inst. Mining and Metall. Engineers Trans., v. 81, p. 238–260.

Stacey, F. D., 1963, The physical theory of rock magnetism: Advances in Physics, v. 12, no. 45, p. 45–133.

——— 1967, The Koenigsberger ratio and the nature of thermoremanence in igneous rocks: Earth and Planetary Sci. Letters, v. 2, no. 1, p. 67–68.

Strangway, D. W., Larson, E. E., and Goldstein, M., 1968, A possible cause of high magnetic stability in volcanic rocks: Jour. Geophys. Research, v. 73, no. 12, p. 3787–3795.

Werner, Sture, 1945, Determinations of the magnetic susceptibility of ores and rocks from Swedish iron ore deposits: Sveriges Geol. Undersökning Årsb., Ser. C, v. 39, no. 5, 79 p.

GEOPHYSICAL DATA RELATING TO A POSSIBLE PLEISTOCENE OVERFLOW OF LAKE BONNEVILLE AT GEM VALLEY, SOUTHEASTERN IDAHO

By DON R. MABEY, Denver, Colo.

Abstract.—Electrical resistivity soundings and aeromagnetic surveys in Gem Valley, Idaho, an area covered by Pleistocene basalt flows, are interpreted as indicating that (1) prior to the flooding of the valley by basalt flows the south end of the valley was a topographic low and (2) a broad channel along the west side of the valley reached north to the Portneuf River canyon. The base of this channel is now about 5,100 feet above sea level, which is slightly lower than the level of Lake Bonneville at the time of the initial overflow at Red Rock Pass. The concealed topography beneath the basalt suggests that drainage of the south end of the valley was, as it is now, south through the Oneida Narrows into the Lake Bonneville basin. If the Oneida Narrows were open before Gem Valley was flooded by basalt flows, the low point in the rim of the Lake Bonneville basin may have been at the head of the Portneuf River canyon, and overflow may have occurred through the Portneuf River. Blocking of this drainage by basalt flows could have produced a rise in the lake level and overflow at Red Rock Pass.

A segment of the surface-water divide between the Great Salt Lake and the Snake River drainages is an almost imperceptible feature on the surface of Pleistocene basalt flows in Gem Valley, a large intermontane basin in southeastern Idaho (fig. 1). Gem Valley as used in this report includes all the valley area between the Portneuf and Fish Creek Ranges on the west and the Chesterfield Range, Soda Springs Hills, and Bear River Range on the east. The Portneuf River, which drains the north end of the valley through a canyon (here called the Portneuf River canyon) into the Snake River, could be diverted southward into the Great Basin by a dam 250 feet high. The Bear River, which flows through the southern part of the valley into Great Salt Lake, could be diverted northwestward into the Portneuf River by a slightly lower dam.

The Bear River is the largest river flowing into Great Salt Lake; diversion of it by the basalt flows in Gem Valley could have had an important effect on Lake Bonneville, a Pleistocene lake in the Great Salt Lake basin. An excellent summary of previous ideas concerning the Pleistocene drainage in Gem Valley was presented by Bright (1963). The tangible record of Pleistocene drainage in Gem Valley, however, is concealed by basalt flows, which occupy the valley and gaps in the adjoining ranges. Recent geophysical studies which provide some new perspective on the Pleistocene drainage in key areas are the subject of this report.

The major items of visible evidence relating to the Pleistocene events in Gem Valley (fig. 2) are:

1. Extensive basalt flows cover the valley and extend down the Portneuf River canyon almost 50 miles.
2. A surface divide between the Bear and Portneuf Rivers on the basalt flows has a minimum elevation of about 5,525 feet above sea level.
3. Shorelines and sediments in the south end of Gem Valley indicate a Pleistocene lake at a maximum elevation of 5,445 feet above sea level (Bright, 1963).
4. Lake Bonneville catastrophically overflowed at Red Rock Pass at an elevation above 5,100 feet and possibly as high as 5,200 feet above sea level (Malde, 1968).[1] Prior to this overflow, Lake Bonneville rose in the Alpine maxima to a level a few feet below the elevation at which overflow occurred at Red Rock Pass (Crittenden, 1963).
5. Lake Bonneville extended into the south end of Gem Valley through the Oneida Narrows (Bright, 1963).

[1] A problem in comparing elevations of shorelines and related features in the Bonneville basin is caused by the differential isostatic subsidence and rebound that resulted from variations in time of the water load in the basin. The elevation of the Bonneville shoreline, for example, ranges from 5,085 feet at Red Rock Pass to 5,300 feet above sea level in the area of deepest water (Crittenden, 1963).

U.S. GEOL. SURVEY PROF. PAPER 750-B, PAGES B122-B127

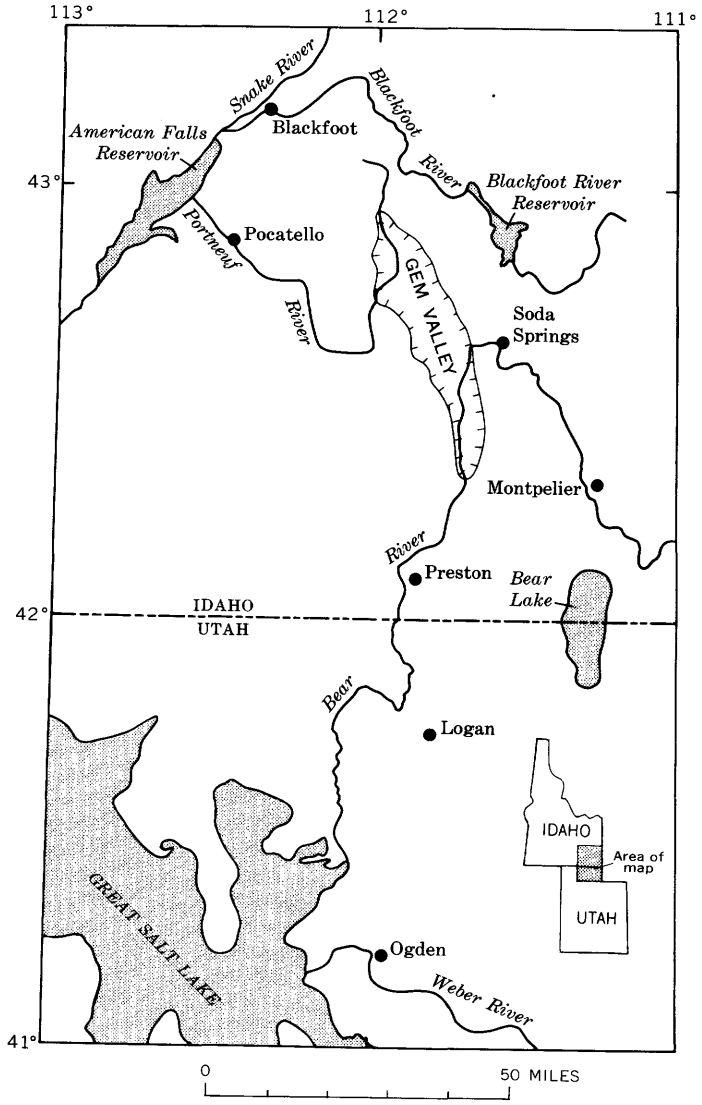

FIGURE 1.—Index map of northern Utah and southeastern Idaho, showing location of Gem Valley.

GEOPHYSICAL DATA

Gravity and magnetic surveys in Gem Valley have been interpreted by Mabey and Armstrong (1962) and Mabey and Oriel (1970). The gravity data indicate a prism of low-density material several thousand feet thick under most of the valley. On the basis of geologic evidence, this low-density material is thought to be largely Tertiary sedimentary rocks that fill a graben. Aeromagnetic anomalies over the valley are produced by basalt flows and by eruptive centers. A magnetic high along the west side of the valley has been interpreted as indicating that a basalt-filled channel extends southward from the head of the Portneuf River canyon.

Portneuf River canyon

The elevation of the concealed bedrock divide between Gem Valley and the Portneuf River canyon is crucial to reconstruction of the Pleistocene drainage. The aeromagnetic anomaly measured at this divide suggests that 200–300 feet of basalt is present, and a detailed gravity profile suggests that the base of the basalt is at or near bedrock, without a substantial thickness of intervening low-density sediments (Mabey and Oriel, 1970). Two Schlumberger resistivity soundings were made in this area under the direction of A. A. R. Zohdy (fig. 3). The

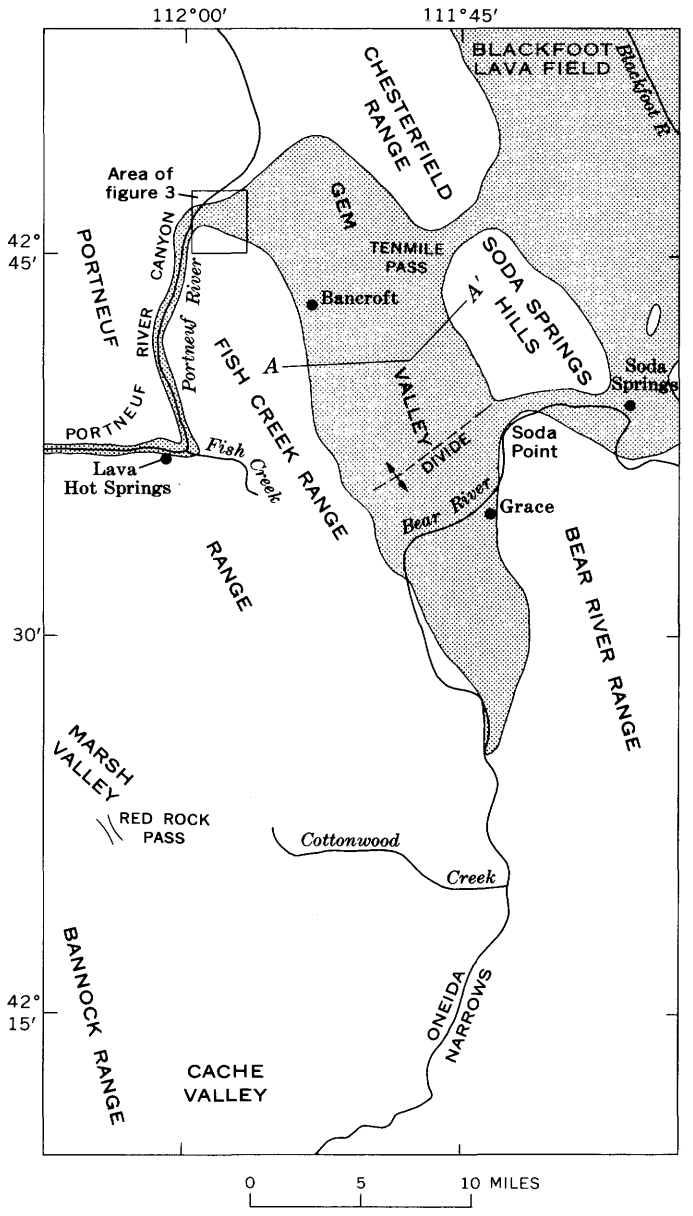

FIGURE 2.—Map of Gem Valley, showing extent of exposed basalt flows (stippled), area of figure 3, and location of profile *A–A′*.

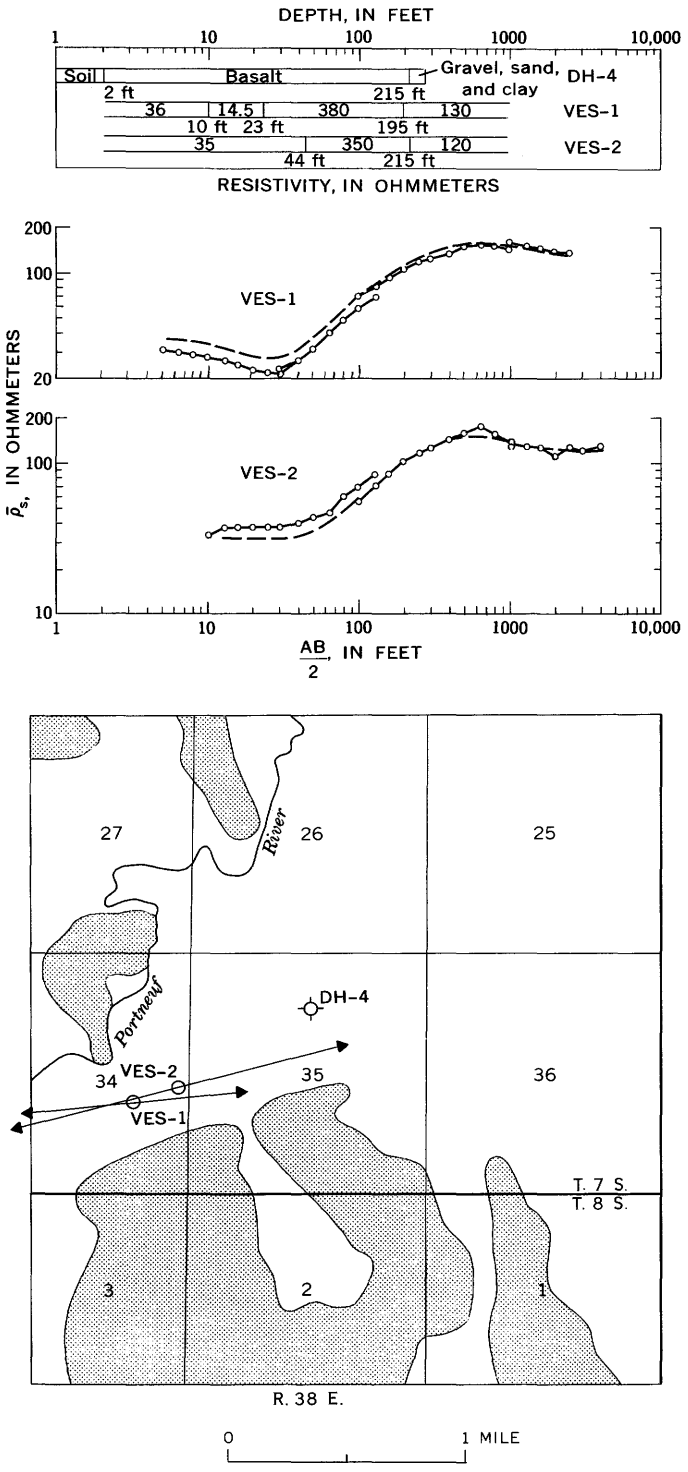

FIGURE 3.—Resistivity soundings (VES–1 and VES–2) at the head of the Portneuf River Canyon. DH–4, well. Stippled area is pre-Tertiary rock. Resistivity survey and interpretation by A. A. R. Zohdy.

interpretation of these soundings indicates that about 200 feet of basalt having a resistivity of 350–380 ohmmeters underlies a thin layer of lower resistivity material. The basalt, in turn, is underlain by material with a resistivity of about 125 ohmmeters, which is approximately the resistivity measured on nearby outcrops of Paleozoic rocks. A much lower resistivity (10–25 ohmmeters) was measured for fine-grained sediments under basalt in the central part of Gem Valley. The material with 125-ohmmeter resistivity under the basalt at the concealed divide could be either Paleozoic rock or sand and gravel—probably it is both—but it is not likely to be fine-grained lake sediments. Therefore, interpretation of the resistivity sounding strongly suggests that the base of the basalt at the concealed divide at the head of the Portneuf River canyon is a little more than 200 feet below the surface (or about 5,100 feet above sea level) and that it is not underlain by lake sediments. A well (DH–4) northeast of the soundings, where the surface elevation is about 5,335 feet, went through basalt to a depth of 215 feet (elevation about 5,120 feet), then through 57 feet of clay, sand, and gravel, and was bottomed in clay, thus confirming the basalt thickness inferred from the geophysical data. Possibly the divide is a few tens of feet below 5,100 feet above sea level, because neither the resistivity soundings nor the drill holes are likely to indicate the maximum thickness of basalt.

Magnetic data over the Portneuf River canyon downstream to the junction with Fish Creek (Mitchell and others, 1965) reflect the presence of the basalt in the canyon, but do not indicate any local source for it. Rather, the magnetic data strongly suggest that all the basalt above Fish Creek flowed down the canyon from Gem Valley.

Gem Valley

A profile of Schlumberger resistivity soundings by A. A. R. Zohdy across the central part of Gem Valley provides additional information on the topography below the basalt (fig. 4). On the west edge of the valley the resistivity soundings confirm the existence of a basalt-filled channel indicated by the magnetic data. The channel is about 2 miles wide and about 300 feet deep, and may have a central trough possibly 100 feet deeper. The elevation of the base of the broad inferred channel is about 5,150 feet, and the central trough is about 5,050 feet above sea level. Three wells (DH–1, DH–2, and DH–3) within 2 miles of the resistivity soundings provide support for the interpretation of geophysical data. DH–1 did not penetrate basalt and is assumed to be west of the inferred channel. DH–2 was drilled through interbedded basalt and sediments to a depth of 283 feet (elevation about 5,170 feet) and then through sediments to 355 feet. DH–3 found interbedded basalt and sediments to a depth of 271 feet (elevation about 5,170 feet), but was bottomed at 275 feet after drilling 4 feet of sediment; more basalt may exist below 275 feet. The resis-

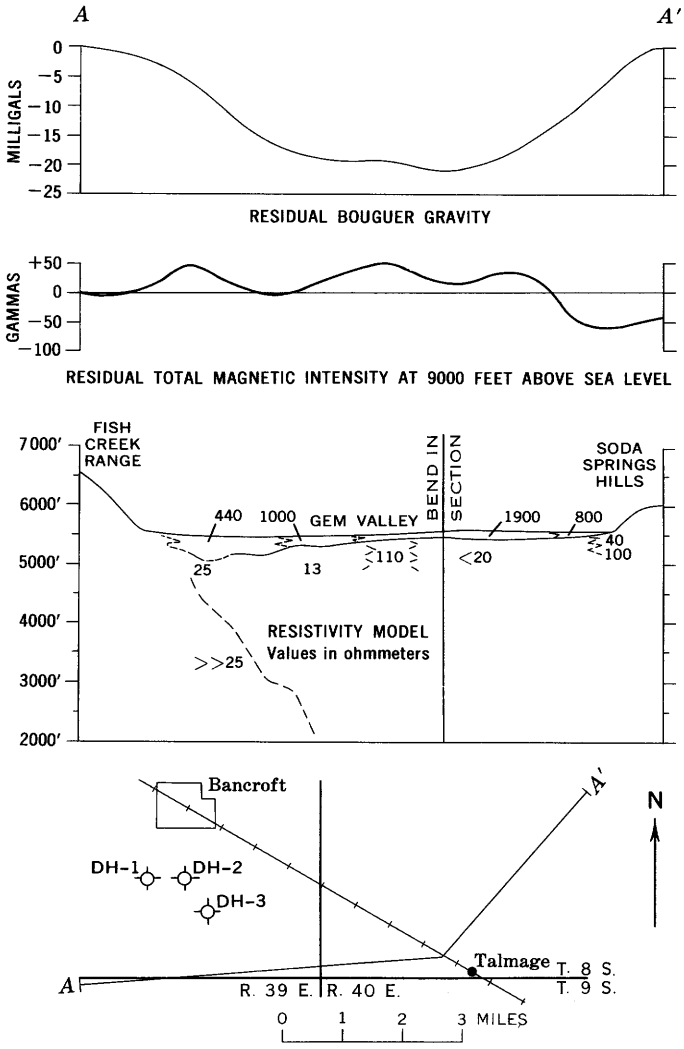

FIGURE 4.—Gravity and aeromagnetic profiles and resistivity model across Gem Valley. DH–1, DH–2, and DH–3, wells. Resistivity survey and interpretation by A. A. R. Zohdy.

tivity soundings did not reveal any evidence of a major basalt-filled channel in the central or eastern part of the profile.

Aeromagnetic data, which are available over only the northern three-quarters of Gem Valley, have been interpreted as indicating a subbasalt surface of moderate relief (Mabey and Oriel, 1970). North of the resistivity profile the basalt is locally thin or absent, and in the northern part of the valley neither the geophysical data nor drill holes suggest that basalt is present at elevations much below 5,100 feet above sea level. Apparently the basalt was emplaced on a valley floor that had been dissected by erosion and that probably included several alluvial fans along the east side of the valley. The floor of the valley may have resembled the present floor of southern Marsh Valley, which is the next major valley west of Gem Valley.

The lowest known elevation of basalt in the valley is about 4,950 feet in the south end (Bright, 1963). Except in a possible area of subsidence associated with the volcanic craters near Grace (fig. 2), neither the geophysical nor the drill-hole data indicate basalt at any lower elevation. Thus, seemingly the south end of the valley was a topographic low before the overlying basalt was emplaced.

Areas east of Gem Valley

Basalt flows occur in gaps in the ranges at Soda Point and Tenmile Pass on the east side of the valley, in the divide between the Bear and Blackfoot Rivers north of Soda Springs, and along much of the course of the Blackfoot River (fig. 2). Knowledge of the thickness of the basalt in these areas is a key to inferring the course of the Blackfoot and Bear Rivers before the time of the basalt flows. The only geophysical data available on the thickness of the basalt in these areas are the data used in preparing the magnetic contour map of Mabey and Oriel (1970) and an unpublished aeromagnetic profile across the gaps at Soda Point and Tenmile Pass. Quantitative interpretation of the magnetic data without some subsurface control is subject to large uncertainties, and thickness estimates based on the magnetic data alone should be used with great caution.

The basalt thickness inferred from the magnetic data suggests some possible courses of the Blackfoot and Bear Rivers before the low areas east of Gem Valley were flooded with basalt. At Soda Point the magnetic profile suggests a broad prism of basalt about 500–600 feet thick occupying most of the area between the Soda Springs Hills and the Bear River Range. Thus, an elevation of about 5,100–5,200 feet for the base of the basalt at Soda Point is probable. At Tenmile Pass the basalt appears to be thin on the north side but rather thick in a narrow wedge just north of the Soda Springs Hills. The magnetic anomaly does not provide a good indication of the maximum thickness of this wedge, but a thickness of between 500 and 1,000 feet seems most likely. The subbasalt elevation of Tenmile Pass remains a major uncertainty; it might be as low as 5,100 feet but could be several hundred feet higher. East of Tenmile Pass the geophysical data suggest considerable relief on the buried pre-Tertiary rock, but there is no evidence of a bedrock barrier higher than at Tenmile Pass. North of Soda Springs the magnetic data indicate basalt to be continuous, with a minimum thickness of several hundred feet. In the canyon of the Blackfoot River, northeast of the Blackfoot River Reservoir, the magnetic data suggest that about 400 feet of basalt underlies the river, placing the subbasalt surface at about

5,600 feet above sea level (Mabey and Oriel, 1970). Before the basalt was emplaced, the Blackfoot River may have been tributary to the Bear River through the gaps north of Soda Springs or may have entered Gem Valley through Tenmile Pass, but the Bear River probably did not flow north through the present course of the Blackfoot River.

PLEISTOCENE DRAINAGE SUGGESTED BY GEOPHYSICAL DATA

The geophysical data and the elevation of basalt penetrated in drill holes suggest that before emplacement of the basalt the topographic low in Gem Valley was in the southern part of the valley about 4,900 feet above sea level, with drainage of at least the southern part of the valley southward through the Oneida Narrows. If the Oneida Narrows existed in virtually the present form before the basalt was emplaced and the elevation of Red Rock Pass was above 5,100 feet above sea level before the overflow, the low point in the rim of the basin before Lake Bonneville time could have been in Gem Valley or at the head of the Portneuf River canyon at an elevation of about 5,100 feet above sea level. During high stands in the Bonneville basin, the lake would have extended into the south end of Gem Valley and overflowed through the channel indicated by the geophysical data along the west side of the valley into the Portneuf River canyon (fig. 5). During low stands of the lake the Bear River would have flowed southward through the Oneida Narrows, removing sediment from the south end of the valley and producing a topographic low similar to what exists today (fig. 6). The divide in Gem Valley could have been the control for the elevation of Lake Bonneville during the Alpine maxima when the lake apparently reached a maximum level a few feet below the subsequent Bonneville maximum controlled by Red Rock Pass (Crittenden, 1963).

Northward overflow through Gem Valley would have been prevented by basalt flows entering the valley at Tenmile Pass and Soda Point and by basalt from vents within Gem Valley itself, events which raised this segment rim of the Bonneville basin to more than 5,200 feet above sea level. The Portneuf River would have been ponded to form a lake in the north end of the valley, and the Bear River would have continued to flow south from Soda Point. The next overflow of the lake in the Bonneville basin would have been over a divide not higher than 5,200 feet above sea level at Red Rock Pass and would have produced the catastrophic flooding in the Snake River Plain.

The series of events proposed on the basis of the thickness of the basalt inferred from the geophysical data is

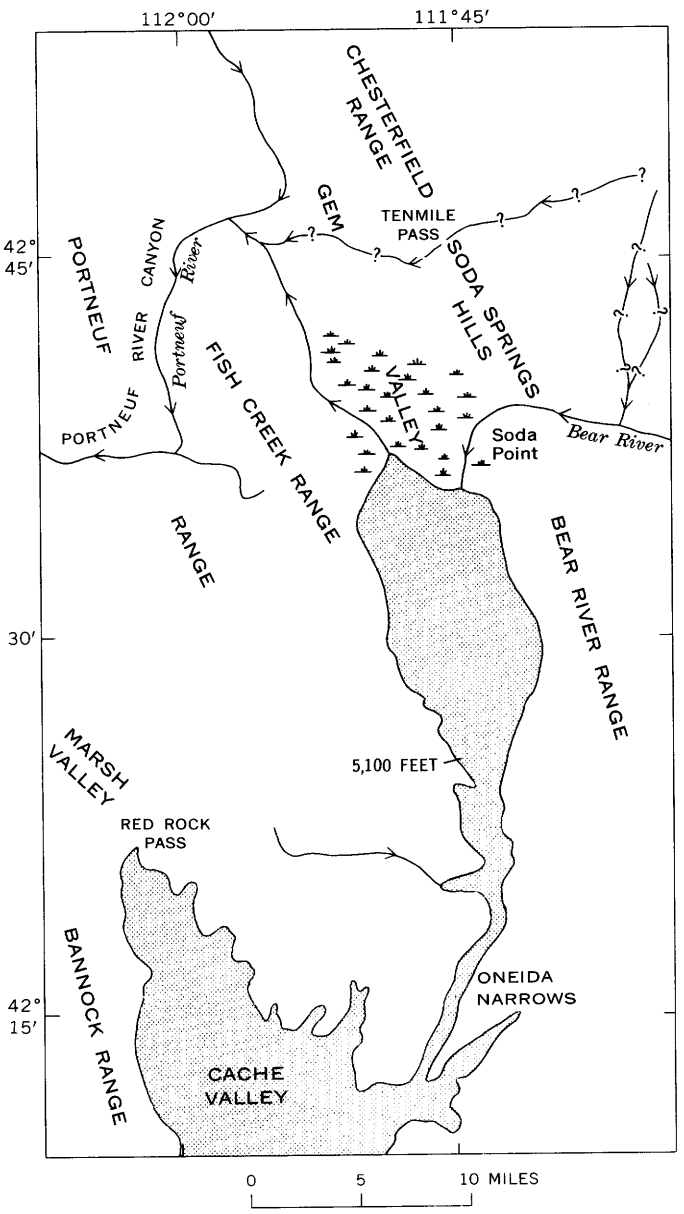

FIGURE 5.—Proposed drainage in Gem Valley before emplacement of basalt and during overflow of lake in Bonneville basin.

quite different from the Pleistocene history deduced by Bright (1963). A major weakness in this hypothesis is the lack of an explanation for the presence of lake deposits in the south end of Gem Valley at a maximum elevation of 5,445 feet above sea level. Indeed, the existence of these lake deposits, which are, at least in part, younger than the basalt, and the absence of equally high deposits in Cache Valley indicate that the Oneida Narrows was not open when the higher deposits were formed. Development of a dam in the narrows after the emplacement of basalt in Gem Valley seems unlikely but not impossible. However, the alternate Pleistocene his-

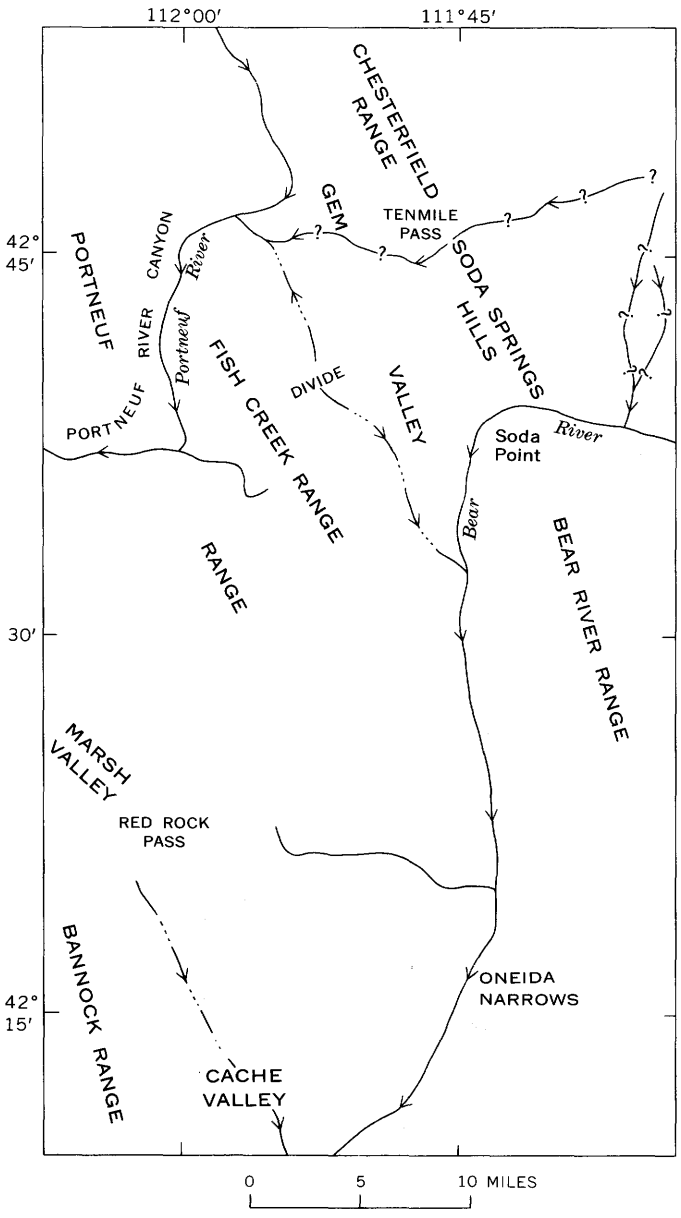

FIGURE 6.—Proposed drainage in Gem Valley before emplacement of basalt and during low stands of lake in Bonneville basin.

tory proposed by Bright to account for the features he has observed requires the development of a dam at least 340 feet high in the Portneuf River canyon prior to the emplacement of the basalt in Gem Valley. (Bright concluded that (1) the elevation at the head of the Portneuf River canyon must have been less than 4,783 feet to account for the elevation, before emplacement of the basalt, in the south end of Gem Valley by northward drainage through the Portneuf River canyon and (2) the canyon was dammed to produce a lake with a surface elevation of 5,125 feet.)

Although the interpretation of geophysical data should not be considered rigid, these data do suggest several features of the topography before the basalt was emplaced that must be integrated into any reconstruction of the Pleistocene drainage. The principal uncertainty to be resolved is the direction of drainage of the south end of the valley before the emplacement of the basalt flows. Until more surface and subsurface information becomes available on this problem, two quite different Pleistocene histories should be considered.

REFERENCES

Bright, R. C., 1963, Pleistocene lakes Thatcher and Bonneville, southeastern Idaho: Minneapolis, Minnesota Univ. Ph. D. thesis, 292 p.

———1967, Late Pleistocene stratigraphy in Thatcher Basin, southeastern Idaho: Tebiwa, v. 10, no. 1, p. 1–7.

Crittenden, M. D., Jr., 1963, New data on the isostatic deformation of Lake Bonneville: U.S. Geol. Survey Prof. Paper 454–E, 31 p.

Mabey, D. R., and Armstrong, F. C., 1962, Gravity and magnetic anomalies in Gem Valley, Caribou County, Idaho: Art. 140 *in* U.S. Geol. Survey Prof. Paper 450–D, p. D73–D75.

Mabey, D. R., and Oriel, S. S., 1970, Gravity and magnetic anomalies in the Soda Springs region, southeastern Idaho: U.S. Geol. Survey Prof. Paper 646–E, 15 p.

Malde, H. E., 1968, The catastrophic late Pleistocene Bonneville Flood in the Snake River Plain, Idaho: U.S. Geol. Survey Prof. Paper 596, 52 p.

Mitchell, C. M., Knowles, F. F., and Petrafeso, F. A., 1965, Aeromagnetic map of the Pocatello-Soda Springs area, Bannock and Caribou Counties, Idaho: U.S. Geol. Survey Geophys. Inv. Map GP–521.

GRAVITY AND MAGNETIC DATA IN THE VICINITY OF THE CALAVERAS, HAYWARD, AND SILVER CREEK FAULTS NEAR SAN JOSE, CALIFORNIA

By STEPHEN L. ROBBINS, Menlo Park, Calif.

Abstract.—A gravity survey along the east side of San Jose, Calif., with stations spaced about 1–1½ miles (2–3 km) apart, shows a long, narrow 30-mgal gravity low, which may be caused in part by a graben extending into the lower crust and possibly into the upper mantle. The gravity gradients along the sides of this feature coincide with the Calaveras and Silver Creek faults, with what appears to be the northwestward extension of the Silver Creek fault, and with what may be an old inactive fault in line with the still active Hayward fault. On the west side of San Jose a 25-mgal negative gravity anomaly is believed to indicate that the surface there is underlain by Tertiary and Quaternary rocks more than 4 km thick. Aeromagnetic data also show that the Silver Creek fault extends northwestward beyond the area in which it is exposed.

Little is known about the subsurface geology in the vicinity of San Jose, Calif., especially about the subsurface configurations of the Calaveras, Hayward, and Silver Creek faults. The gravity and aeromagnetic data presented here have been obtained within the area outlined in figure 1, and were used, along with the known geology of the area, in making the following subsurface structure interpretations.

Acknowledgments.—I am indebted to Leon Page and the Santa Clara Valley Water Conservation District for making it possible for me to obtain many of the gravity stations and to the California Department of Water Resources for allowing me to use their geologic base map (California Dept. of Water Resources, 1967, plate 3). I also wish to thank Dr. John Brooke and Dr. Norman Dolloff, of San Jose State College, and several members of the U.S. Geological Survey, for guidance and for helpful criticism of this report.

GEOLOGY

The oldest rocks known to underlie the area described in this report—what are commonly termed "basement rocks"—are those of the Franciscan Formation, which in this area are of Jurassic or Early Cretaceous age east of the Calaveras fault and of mid-Cretaceous age in the Santa Cruz Mountains (Bailey and others, 1964, p. 150). This formation consists mainly of sandstone and shale but contains lesser amounts of chert, serpentinite, and greenstone. Relatively unaltered mafic and ultramafic rocks such as diorite, gabbro, and pyroxenite are exposed in the Oak Hills (fig. 2) (Crittenden, 1951, p. 21). There are also many small bodies of diorite, diabase, and gabbro in the areas mapped by Crittenden (1951, pl. 1) as serpentinite. Crittenden mapped a number of small bodies of a rock that he referred to as silica-carbonate rock and believed to have formed by alteration of serpentinite.

The area here described includes a miogeosynclinal sequence of Mesozoic sedimentary rocks, the oldest and most abundant of which belong to the Knoxville Formation, of Jurassic age, and consist mainly of shale and siltstone, but it also contains Cretaceous rocks, mainly shale, conglomerate, and sandstone.

The thickest known section of Tertiary rocks in the area, possibly as much as 2.3 km thick, is exposed in the hills east of San Jose (Crittenden, 1951, p. 22). These rocks are mostly shallow-water marine sediments.

Still higher in the stratigraphic sequence is the Santa Clara Formation, mainly of Quaternary age but partly of Pliocene age. This formation is at least 0.7 km thick on the west side of San Jose (Dibblee, 1966), where the beds in its lower part are but little consolidated and those at the top so wholly unconsolidated that it is sometimes impossible to locate the boundary between them and the overlying alluvial deposits.

On the east side of San Jose, according to Crittenden (1951, p. 22, 45), about 0.5 km of what he regards as Holocene alluvium has been deposited, but a part of this material may be the upper part of the Santa Clara Formation (California Dept. of Water Resources, 1967, p. 21).

U.S. GEOL. SURVEY PROF. PAPER 750-B, PAGES B128-B139

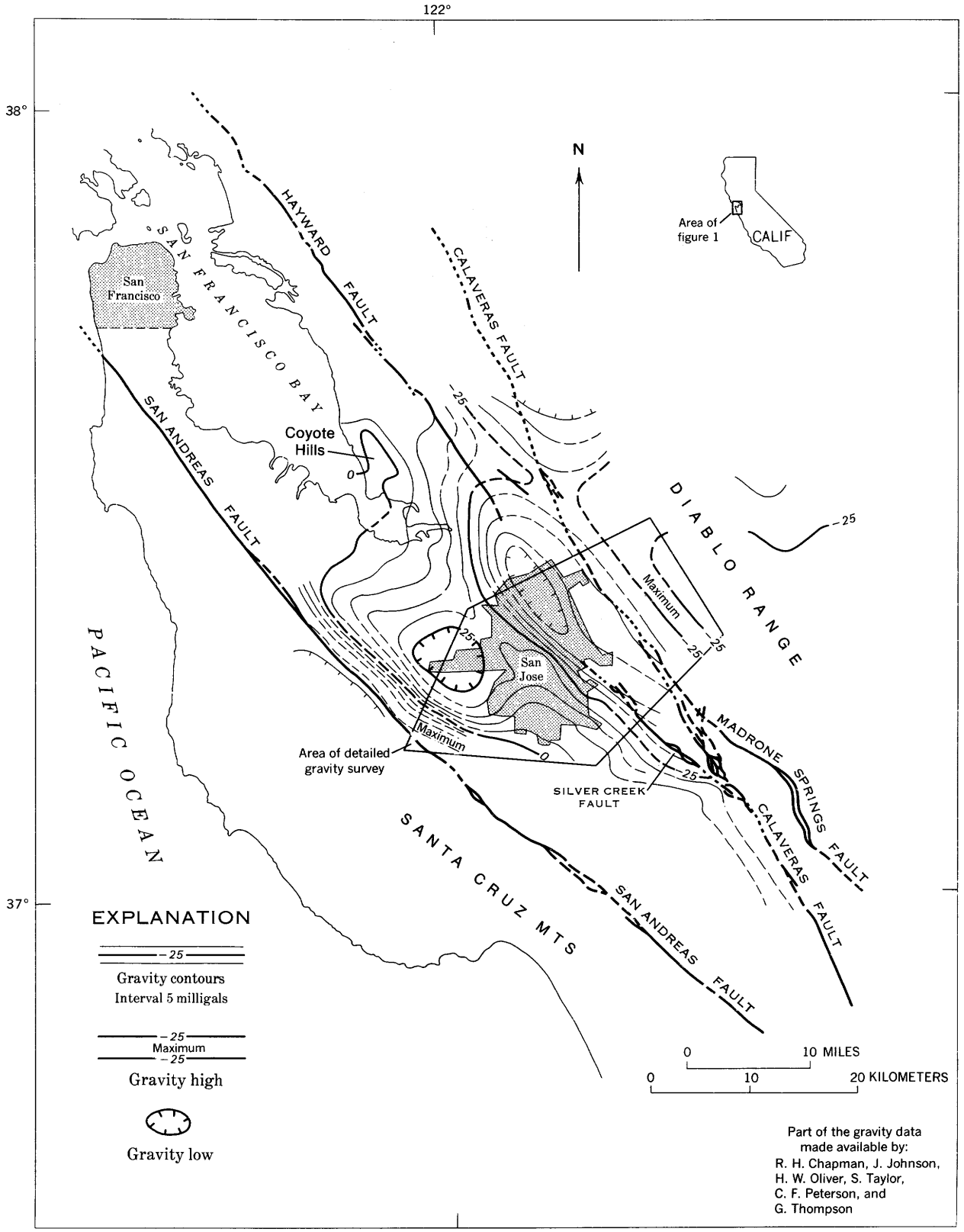

FIGURE 1.—Regional Bouguer gravity map of the area near San Jose, Calif., described in this report.

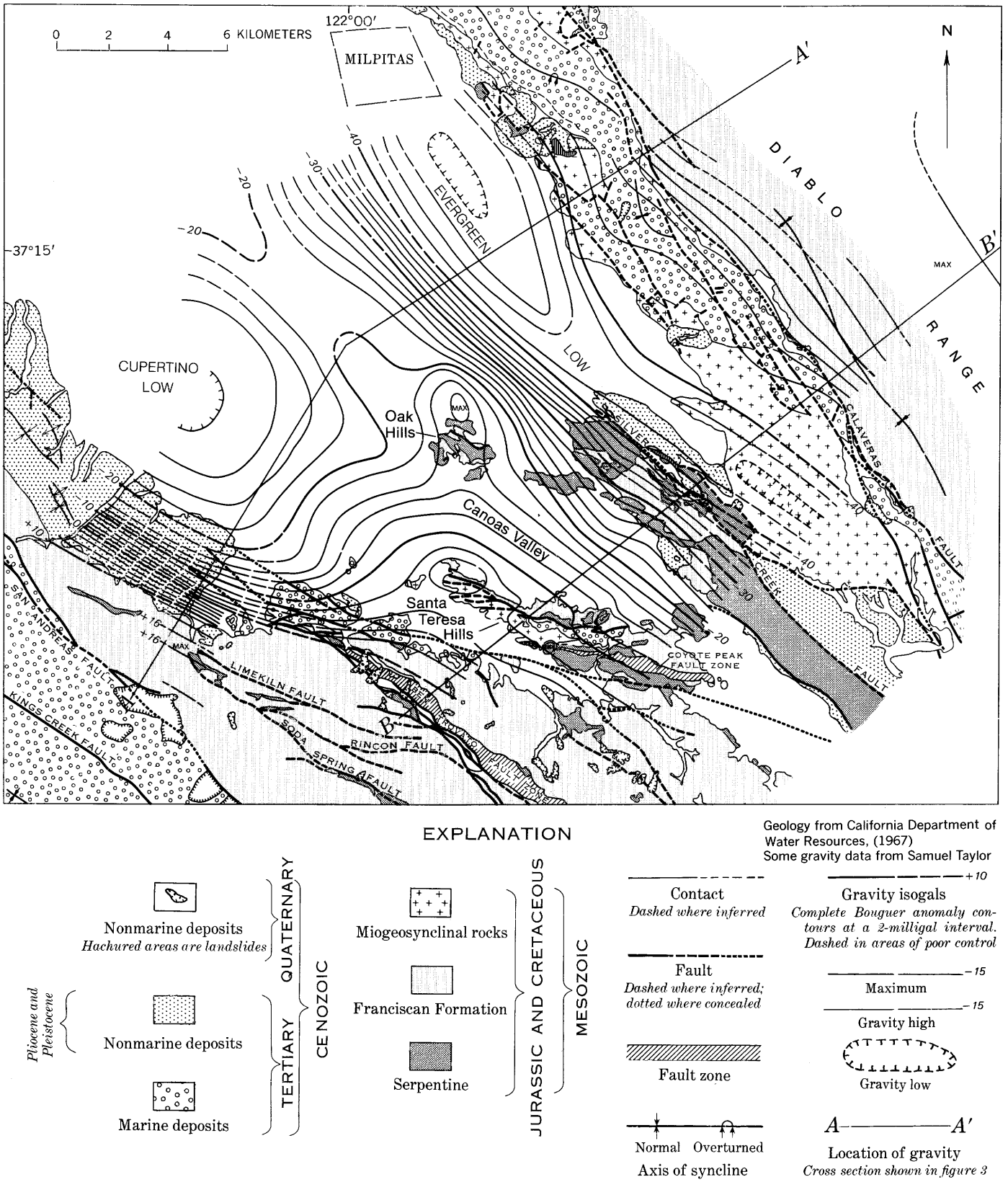

FIGURE 2.—Complete Bouguer gravity and geologic map of the San Jose, Calif., area.

GEOPHYSICAL DATA

The complete Bouguer gravity map (fig. 2) is based on observations made at about 200 gravity stations, spaced at intervals of 2–3 km (1–1½ miles). At 102 of these stations, a Worden Educator gravity meter with a 0.4909 mgal/scale-division scale constant was used, and at 49 stations a LaCoste-Romberg gravity meter was used. The latter was also used in reoccupying most of the gravity stations on Taylor's Evergreen profile (Taylor, 1956, pl. 1) and about half the stations on his San Jose profile, and also for tying all base stations to the California gravity network (Chapman, 1966, p. 10). Taylor's Santa Clara profile also has been used in figure 2, but with gravity values modified in accordance with differences observed between Taylor's and the reoccupied values on the San Jose and Evergreen profiles.

The data were reduced on the assumption that the rocks had an average density of 2.67 g/cc. The terrain effect was removed by using the U.S. Coast and Geodetic Survey system (Swick, 1942, p. 67) through zone O, and the resultant values were contoured at an interval of 2 mgal.

Figure 1 is a regional Bouguer gravity map covering the area of special interest and some of the surrounding area. It is based on part of the data compiled by Howard W. Oliver and me for the "Transcontinental Geophysical Survey (35°–39° N.) Bouguer Gravity Map" (U.S. Air Force Aeronautical Chart and Information Center, 1968). Few of the gravity stations outside the area outlined in figure 1 have been terrain corrected.

Table 1 shows the ranges of density and average density in most stratigraphic units exposed in this general region. The samples on which they are based were all taken at the surface, and most of them in places outside of the area surveyed, but they are all representative of stratigraphic units exposed within the survey area.

TABLE 1.—*Rock densities in the San Francisco Bay area, as determined by Taylor (1956, p. 31), Greve (1962, p. 15), Clement (1965, p. 2), and Robbins (6 samples)*

[Based on over 200 samples]

Rock group	Density (g/cc)	
	Range (max)	Average
Quaternary nonmarine deposits	1. 57–2. 05	1. 9
Pliocene and Pleistocene nonmarine deposits.	1. 90–2. 30	2. 2
Tertiary marine deposits	2. 03–2. 53	2. 3
Mesozoic rocks:		
Miogeosynclinal rocks	2. 41–2. 68	2. 5
Franciscan Formation:		
Sedimentary rocks	2. 30–3. 10	[1]2. 7
Serpentinite	1. 96–2. 89	[1]2. 5
Greenstone	1. 81–2. 99	[1]2. 8

[1]2.7 or commonly 2.67.

Bailey, Irwin, and Jones (1964, p. 141) have collected many samples of graywacke from the Franciscan Formation, and some from the Mesozoic miogeosynclinal formations. Their density figures for Franciscan graywackes (181 samples in the Bay area) agree closely in the range and in average value with those listed in table 1, but those for individual samples of miogeosynclinal graywackes all exceed the average density for miogeosynclinal rocks given in table 1. One reason for this is that the miogeosynclinal rocks exposed at the surface in the surveyed area are mostly shales, siltstones, and conglomerates of greater average density than the graywackes. Another reason may be that most of the samples of graywacke that Bailey, Irwin, and Jones took from the miogeosyncline were collected outside the Bay area.

Seven northeast-trending aeromagnetic profiles flown by the U.S. Geological Survey in 1959 in the northern part of the Santa Clara Valley, at 1-mile (1.6 km) spacing and 500 feet (150 m) above the ground surface, are reproduced in figure 4, in which a regional gradient of 10 gammas per mile has been removed (U.S. Coast and Geodetic Survey, 1965). These magnetic data are variations in the total intensity relative to an arbitrary datum.

To judge from surface exposures, the only rocks within the area that could produce magnetic anomalies as large as those shown in figure 4 are the serpentinites, greenstones, and mafic and ultramafic rocks in the Franciscan Formation, and it is unlikely that any rocks as magnetic as these lie buried within the miogeosynclinal and Tertiary formations.

GRAVITY INTERPRETATION

In order to interpret the gravity anomalies, two profiles were selected and linear regional gradients removed (see fig. 2). These gradients were picked by assuming that the gravity values over the Franciscan Formation at both ends of the profiles were near zero. The gradients were 1.8 mgal/mile (2.9 mgal/km) for profile *A–A′* and 1.2 mgal/mile (1.9 mgal/km) for profile *B–B′*.

When first studying the gravity and geologic map (fig. 2) it seemed reasonable to assume that the gravity anomalies are caused by rocks at shallow depth, and the upper models in figure 3 are based on this assumption. In these models, the Evergreen low is assumed to be caused by Mesozoic rocks that are 0.2 g/cc less dense than the Franciscan rocks, and the Cupertino low caused by Tertiary rocks that are 0.4 g/cc less dense than the Franciscan rocks (table 1). From this, a first approximation to the basement configuration was obtained by means of the Bott (1960) two-dimensional

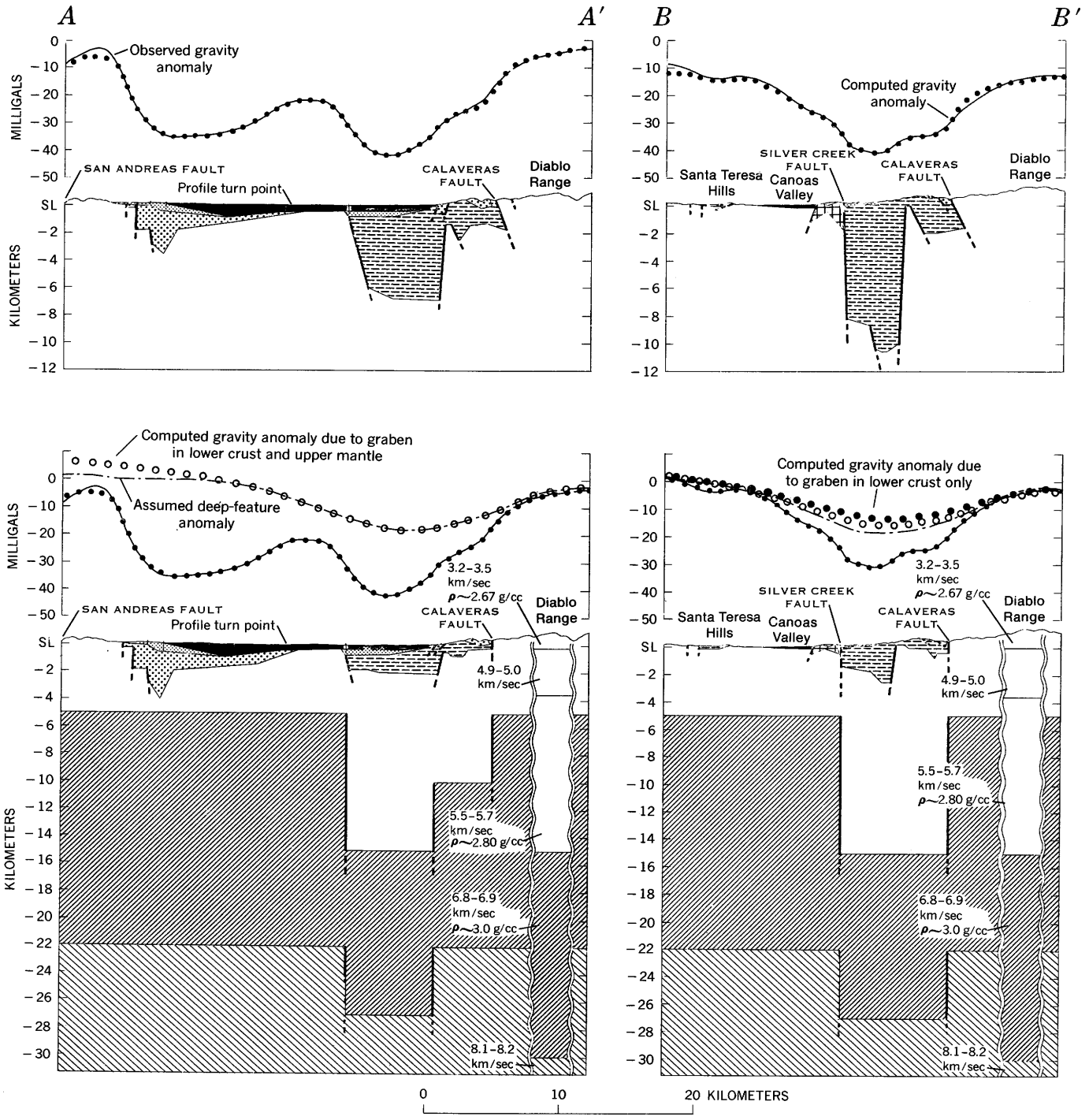
A
A′
B
B′
MILLIGALS
KILOMETERS
Observed gravity anomaly
Computed gravity anomaly
SAN ANDREAS FAULT
Profile turn point
CALAVERAS FAULT
Diablo Range
SILVER CREEK FAULT
Santa Teresa Hills
Canoas Valley
SL
Computed gravity anomaly due to graben in lower crust and upper mantle
Assumed deep-feature anomaly
Computed gravity anomaly due to graben in lower crust only
3.2–3.5 km/sec ρ~2.67 g/cc
4.9–5.0 km/sec
5.5–5.7 km/sec ρ~2.80 g/cc
6.8–6.9 km/sec ρ~3.0 g/cc
8.1–8.2 km/sec
0
10
20 KILOMETERS

FIGURE 3.

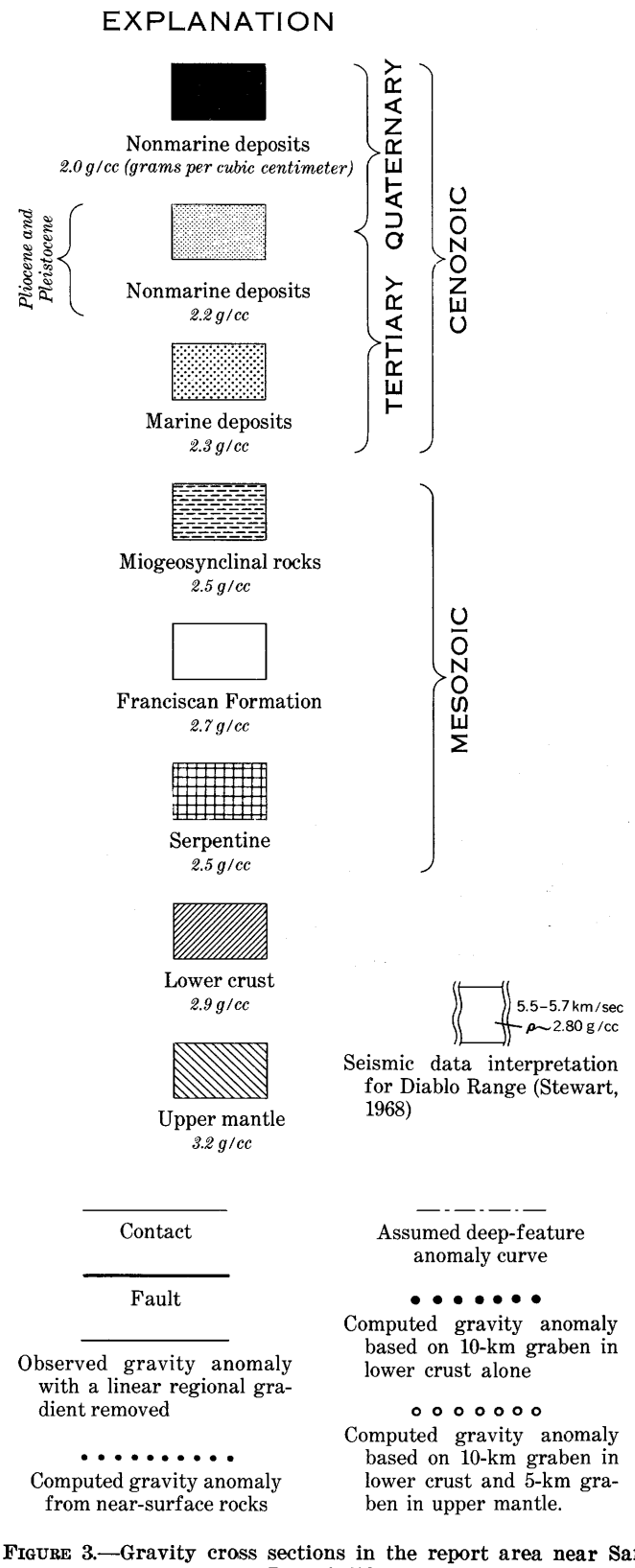

FIGURE 3.—Gravity cross sections in the report area near San Jose, Calif.

gravity-mass-computation computer program which produced, as output, a one-density-contrast model after eight successive iterations were performed on an input of observed gravity values with the regional gradient removed. From this first approximation, modified by data obtained from geologic features observed at the surface (California Dept. of Water Resources, 1967; Crittenden, 1951; and Dibblee, 1966), by data from the logs of three drill holes on profile A–A', and from density differences taken from table 1 as constraints, multidensity models were assumed. The average density of the Quaternary deposits was assumed to be 2.0 g/cc rather than 1.9 g/cc, because the latter value was based on material that included samples of mud taken from San Francisco Bay north of the survey area. The surface gravity attraction of these multidensity models was next computed by means of the Talwani (Talwani and others, 1959) two-dimensional gravity-interpretation computer program. The models were then so adjusted as to obtain close fits between the computed and the observed gravity values (upper models, fig. 3).

The upper models show two features that seem unreasonable: (1) the depth to which the Mesozoic miogeosynclinal rocks extend seems too great relative to the width, and (2) there is a large unexplained residual between the computed and observed gravity values east of the Calaveras fault on profile B–B' (upper model, fig. 3). These discrepancies suggest that part of the measured gravity anomaly is produced by a deep-seated anomalous mass. By assuming that some such mass does exist, despite lack of indication as to its thickness and extent, one can superimpose anomaly curves representing the largest possible anomalous mass, for which the observed gravity could reasonably account, upon the observed gravity curves (lower models, fig. 3). The residuals between these curves were used to compute new multidensity models of the rocks within a short distance of the surface by the procedure using the Talwani computer program (Talwani and others, 1959). These new multidensity models represent minimum thicknesses for the various known rock formations, whereas the upper models in figure 3 represent maximum thicknesses.

Bodies of rock in the lower crust and upper mantle are also shown in the lower models of figure 3, along with their values of attraction as computed by means of Talwani's program (Talwani and others, 1959) in an attempt to determine the approximate form and structure of some deep feature that could account for the observed anomalies. The upper boundaries of these bodies are based on a profile from Thompson and Tal-

wani (1964, p. 4820), and on the assumption that large grabens exist between the Silver Creek and Calaveras faults. In both profiles of the lower models on figure 3, one curve represents anomalies caused by grabens extending into both the lower crust and the upper mantle, and in profile *B–B′* there is also a curve that represents the attraction caused by a graben that extends only into the lower crust.

AEROMAGNETIC INTERPRETATION

In the interpretation of the magnetic profiles shown in figure 4, I have assumed that the magnetization vector in the magnetic bodies is parallel to the earth's field, and have disregarded the small, sharp anomalies caused by manmade surface features such as railroad tracks and radio towers.

The location and shape of the magnetic curves indicate the approximate shape and boundaries of the magnetic bodies (Heirtzler and others, 1962, p. 3–11). Depths and susceptibilities were calculated for the large anomaly on profiles 1–4 (fig. 4) by a graphical method based on the half width of the anomaly (Heirtzler and others, 1962, p. 4–10).

GEOLOGIC SIGNIFICANCE OF DATA

The Evergreen gravity low east of San Jose (fig. 2) extends northwestward to a point north of Milpitas and, according to Jeff Johnson (oral commun., 1967), southeastward to a point southeast of Anderson Lake. The Knoxville Formation is exposed in the middle of this gravity low southeast of profile *B–B′* (fig. 3), and it is assumed that the northwestward continuation of this low is also mainly caused by these rocks or other Mesozoic miogeosynclinal rocks. Just northwest of profile *B–B′* (fig. 3), Pliocene and Pleistocene rocks within the Evergreen gravity low are in direct contact with the miogeosyncline rocks, which indicates that little or no Tertiary rock is associated with this low. An interpretation of this low on profile *A–A′* (upper model, fig. 3) based on the gravity data and a 0.5-km-deep drill hole, shows 0.4 km of Quaternary alluvium, 0.4 km of Pliocene and Pleistocene rocks, and about 7 km of Mesozoic miogeosynclinal rocks. The Mesozoic rocks in profile *B–B′* (upper model, fig. 3) are shown to be about 11 km thick.

In both the upper and lower models (fig. 3), the gravity gradients on both the southwest and northeast sides of the Evergreen gravity low indicate steep slopes on the buried surface of the basement rocks. The slope in profile *B–B′*, on the southwest side of that low, is directly under the surface trace of the Silver Creek fault, and the slope in profile *A–A′*, is probably on the extension of this fault. The magnetic profiles in figure 4 also indicate that the northeast boundary of the Oak Hills magnetic body nearly coincides with this fault extension at depth. The location and shape of the magnetic anomalies indicate that the northeastern boundary of the top of the magnetic body lies southwest of the fault, and that the northeast side of this body dips northeastward until it is cut off by the fault. The Silver Creek fault may reach San Francisco Bay and may connect with a fault that is believed by Chapman (California Dept. of Water Resources, 1967, plate 3) to extend along the east side of the Coyote Hills (fig. 1).

On the northeast side of the Evergreen gravity low, the complex gravity gradient shown in the upper models of figure 3 indicates a major vertical fault, which displaces the basement rocks and may be an extension of the still active Hayward fault. This fault is flanked on the east by a buried ridge of basement rocks, and there is a small graben between the ridge and the Calaveras fault (fig. 3). No surface expression of it has been recognized in the vicinity of profile *B–B′*. The existence of the buried ridge is further supported by Crittenden's mapping of several small bodies of serpentinite, of a very small body of what he regards as Franciscan sedimentary rock, of several small bodies of silica-carbonate rock, and of a body of rhyolite, all exposed at the surface in the area believed to be underlain by the ridge (Crittenden, 1951). The magnetic field increases northeastward toward this ridge, along whose crest there is a possible magnetic high, as indicated by profile 5 (fig. 4). All these facts appear to indicate that the basement ridge is similar in lithology and origin to the Oak Hills. As shown in profile *B–B′* (upper model, fig. 3), the top of this ridge is 0.5 km below the surface, and the graben east of it extends to a depth of 2.7 km below the surface.

According to my interpretation of the lower models in figure 3, the gravity gradients on the southwest and northeast sides of the Evergreen low represent the same structure as that interpreted for the upper models, with the Mesozoic miogeosynclinal rocks associated with the Evergreen gravity low being only 3.1 km thick along profile *B–B′* as compared to 11 km for the interpretation of the upper models, and with profile *A–A′* being underlain by 2.1 km of miogeosynclinal rocks, 0.3 km of Quaternary alluvial deposits, and 0.4 km of Pliocene and Pleistocene rocks. The top of the buried basement ridge is again about 0.5 km from the surface, but the computed thickness of the rocks in the graben east of the ridge is 1.2 km, in contrast to the 2.7-km thickness interpreted from the upper models.

In an attempt to determine what crustal and subcrustal structure could contribute to the Evergreen gravity low, a crustal model was assumed (Thompson and Talwani, 1964, p. 4820) in which a surface

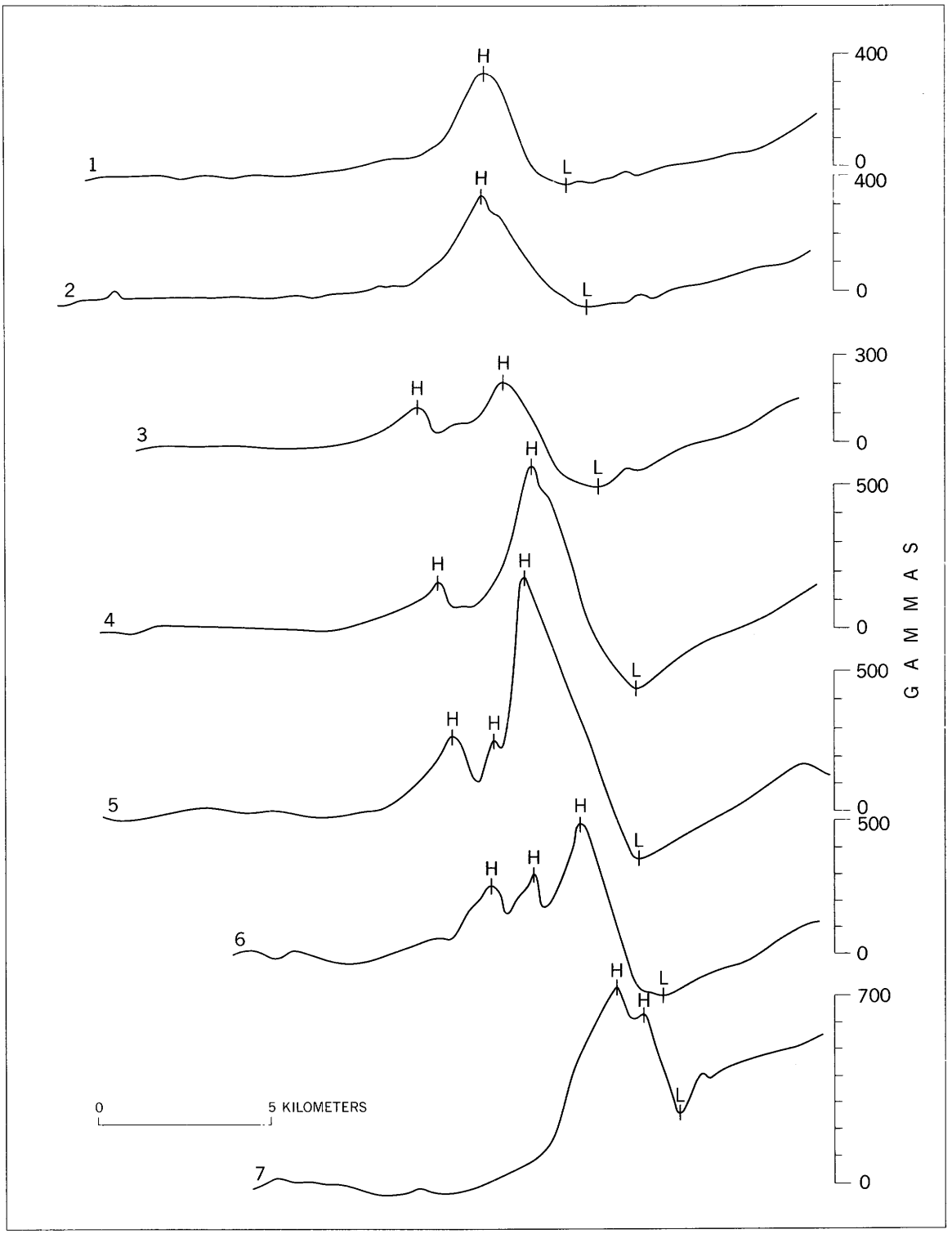

FIGURE 4.—Aeromagnetic profiles (locations and respective highs, H, and lows, L, are shown in fig. 5) flown at an altitude of 500 feet (150 m) above ground surface, near San Jose, Calif.

413-504 O - 71 - 10

density of 2.7 g/cc increases to 2.9 g/cc at a depth of 5 km and to 3.2 g/cc at the Mohorovičić discontinuity, which is assumed to lie 22 km below the surface (lower models, fig. 3). These are the largest increases of density and minimum depths that are consistent with the views expressed in Thompson and Talwani's paper. To obtain the anomaly curve shown in the lower models of figure 3, a graben 10 km deep had to be introduced into the lower crustal layer (the 2.9-g/cc density layer), and a graben 5 km deep into the upper mantle; the sides of both grabens were assumed to be vertical extensions of the Silver Creek and Calaveras faults. Profile *A–A′* suggests that an extension of the Hayward fault may extend into the mantle. According to profile *B–B′*, however, the anomaly caused by both grabens differs more from the assumed anomaly curve than the anomaly caused by the lower crustal graben alone. Both grabens produced anomalies with the inflection points of the gradients farther displaced from those of the assumed gradients with only a small increase in the amplitude of the anomaly. It is possible that the anomalies caused by the two graben models would not differ so greatly if the eastern sides of the grabens in profile *B–B′* were farther west as they are in profile *A–A′*. This suggests the extension of the Hayward fault even farther southward. The main difference between the anomalies computed from the grabens and those ascribed to the assumed anomaly is that the latter have steeper gradients, indicating that the density contrasts must be nearer to the surface than those shown in the lower models (fig. 3). Seismic delay times measured at about a dozen seismograph stations scattered throughout the area indicate that local departures from the regional crustal structure occur in the vicinity of the Evergreen gravity low (John Roller, oral commun., 1968). This may be caused by a greater depth to the Mohorovičić discontinuity, as was just suggested; however, it may be due to lithologic variations within the crust.

Recent seismic refraction data (Stewart, 1968, data shown in fig. 3) indicate that the crust under the Diablo Range is about 30 km thick, and if this is so it becomes more difficult to interpret the structure at the Mohorovičić discontinuity. Stewart calculates the Franciscan Formation to be as much as 16 km thick, and believes it to be subdivided into three layers whose seismic velocities range from 3.2 to 5.7 km/sec. The velocities in the first kilometer range from 3.2 to 3.5 km/sec, and those in the second and third layers appear to be about 5.0 and 5.7 km/sec, respectively. These velocities probably represent a density range of only 2.67 to 2.8 g/cc. Stewart also calculates that under the Diablo Range the velocity in the lower crust is higher (6.8–6.9 km/sec) than in Thompson and Talwani's model (6.2 km/sec). This indicates that the density of the lower crust is probably at least 3.0 g/cc. The attraction of a body that could account for the anomaly ascribed to an assumed deep feature as calculated from Stewart's crustal model will produce a smaller anomaly than is indicated by Thompson and Talwani's model, used in figure 3. Since Stewart's model for the Diablo Range produces a smaller anomaly, and since no graben seems likely to be as much as 10 km deep (few are likely to be more than 5 km deep), part of the anomaly supposedly caused by a deep-seated feature must in fact be due to variations of density in the upper crust, or to thicker formations near the surface. Variations of density are perhaps most likely to occur in the Franciscan Formation and in the Mesozoic rocks. It still appears probable that the crust on the west side of the Silver Creek fault is as little as 22 km thick, and such a thickness would better accord with Thompson and Talwani's model. The seismic-delay times in the Evergreen gravity low indeed indicate variation in the thickness of the crust, but they could be due to some other cause, such as variation in lithologic character (John Roller, oral commun., 1968).

Since the upper models in figure 3 are herein considered unreasonable (see section, "Gravity Interpretation"), and since the anomaly ascribed to an assumed deep feature (lower models, fig. 3) is probably due in part to density variation near the surface and to the presence of unusually thick Mesozoic miogeosynclinal and Tertiary deposits near the surface, the formation thicknesses shown in both upper and lower models (fig. 3) probably represent maximums and minimums, respectively, with the actual thicknesses possibly being between one-third and two-thirds of the extremes. It appears reasonable to assume that at the center of the Evergreen gravity low where it is crossed by profile *A–A′* the Quaternary alluvial deposits are about 0.4 km thick, that the Pliocene and Pleistocene rocks are of about the same thickness, and that the thickness of Mesozoic miogeosynclinal rocks is between 3.0 and 5.0 km. The Mesozoic rocks in profile *B–B′* are probably from 5.0 to 6.0 km thick. Most of the top of the buried basement ridge is probably about 0.5 km below the surface, and the graben east of it is as much as 2.0 km in depth. Exposures on the surface (Crittenden, 1951, p. 22) indicate that the Tertiary rocks in this graben may

be thicker than are indicated in figure 3, and if so, the graben is shallower.

The gravity high over the Oak Hills (fig. 2) indicates that the Franciscan rocks, of which the exposed hills are mostly composed, extend northwestward as a buried ridge. The gravity data along profile *A–A′* (fig. 3) indicate that the distance from the land surface to the top of this ridge ranges from 0.3 to 0.4 km. Calculations of depths and susceptibilities from magnetic profiles over the buried ridge are variable. The results yield depths of 0.2 to 1.3 km and susceptibilities of 1×10^{-3} to 5×10^{-3} cgs units. These values are only approximate and could be as much as 50 percent in error. However, the variation of the results is not caused by any calculation error and is probably due, at least in part, to the unevenness of the top of the buried ridge caused by differential erosion. The variation may also be partly due to differences in the size, shape, and lithology of magnetic bodies in the ridge, and their irregular distribution. In a report on an area several miles to the north (California Dept. of Water Resources, 1967, p. 44), it is suggested that the Coyote Hills may be a northwestward extension of this buried ridge. This view is supported by the fact that the Coyote Hills and the Oak Hills are in line with the buried ridge; they resemble it, moreover, in the character of their rocks and in the magnitude of their gravity highs (California Dept. of Water Resources, 1967, plate 8).

The Cupertino gravity low, west of San Jose (fig. 2), is interpreted from profile *A–A′* (fig. 3) as being caused by the presence of nearly 4.0 km of Tertiary rocks, 0.6 km of Pliocene and Pleistocene rocks (Santa Clara Formation), and up to 0.9 km of alluvial material in its northeastern half. The center of this low is northwest of profile *A–A′*, at a place where the Santa Clara Formation may be more than 1.0 km thick. To the southwest of the anomaly, the interpretation shows the Tertiary rocks to be separated from the Franciscan Formation by at least three high-angle faults (probably reverse faults), which are probably members of the Shannon fault system (Taylor, 1956, p. 44). The small amplitude of the magnetic highs in the Cupertino low (fig. 4) indicates that the basement under it consists of Franciscan sedimentary rocks.

The hills between the Silver Creek fault and Canoas Valley (fig. 2), where traversed by profile *B–B′* (fig. 3), have been mapped as consisting of Franciscan rocks, with a large percentage of serpentinite. The gravity data indicate that the rocks in these hills are of lower density than basement rocks in surrounding areas. There are two possible reasons for this: (1) the hills are composed predominantly of low-density serpentinite that extends to a depth of 1.0 or 2.0 km and encloses only small bodies of Franciscan sedimentary rocks, or (2) the surrounding area may be underlain by basement rocks with a higher density than 2.67 g/cc.

In Canoas Valley there is only a very small negative gravity anomaly (profile *B–B′*, fig. 3), probably because the basement is here immediately overlain by about 0.2 km of alluvium that has a density of 2.0 g/cc. In the Santa Teresa Hills, southwest of Canoas Valley (profile *B–B′*, fig. 3), the Cretaceous rocks appear to be about 0.3 km thick.

CONCLUSIONS

The Evergreen gravity low cannot be regarded as being wholly due either to the structure of the rocks exposed at the surface or to some hypothetical deep-seated features. It is here ascribed to a combination of shallow and deep structures with as much as 6 km of Mesozoic miogeosynclinal rocks in the upper crust, and a graben that is mainly in the lower crust but may extend into the upper mantle, both of which may have been vertically displaced some 5 to 10 km along the Silver Creek, Hayward, and Calaveras faults.

The buried basement ridge (fig. 5) east of the Evergreen low is probably separated from the thick body of Mesozoic rocks southwest of it by an inactive extension of the still active Hayward fault. There is no evidence, however, that this fault extends into the lower crust south of profile *B–B′*.

The Silver Creek fault probably extends northwestward beneath the alluvium (fig. 5) and may connect with a fault passing along the east side of the Coyote Hills. A buried ridge of Franciscan rocks, west of the fault, is believed to extend from the Oak Hills to the Coyote Hills, in both of which these rocks are exposed.

On the southwest side of the Cupertino low, at least 4.0 km of Quaternary and Tertiary rocks are in fault contact against the Franciscan Formation (Dibblee, 1966).

The basement rocks associated with the Cupertino gravity low and those under Canoas Valley are Franciscan sedimentary rocks of rather low magnetic susceptibility and may be faulted against the more strongly magnetic rocks exposed in the Oak Hills (figs. 4 and 5).

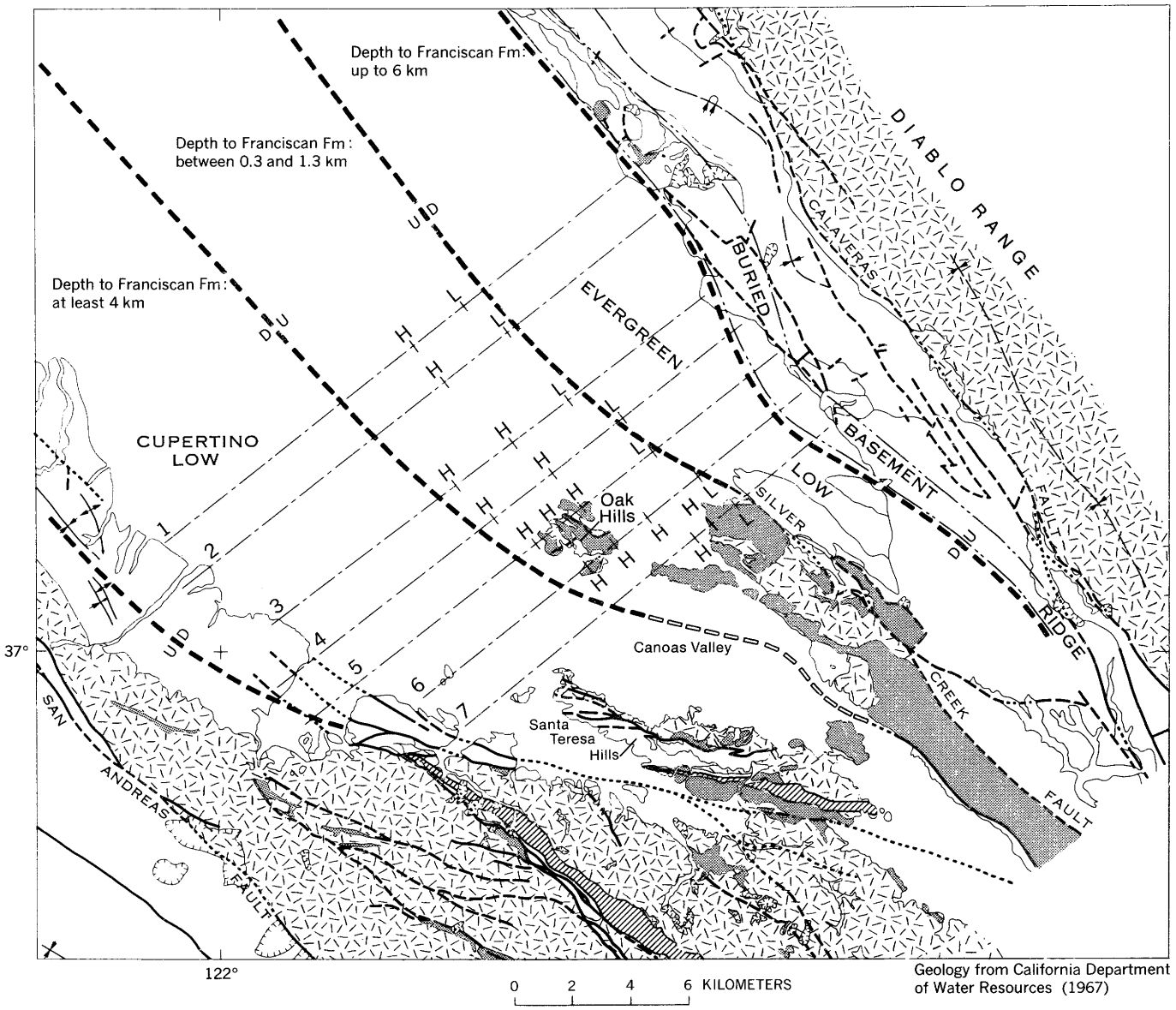

EXPLANATION

Nonbasement rocks

Basement rocks

Serpentine

Subsurface fault or faults
Interpreted from geophysical data

Inferred subsurface fault or faults

BURIED BASEMENT RIDGE

Interpreted buried ridge

1 H L

Location of magnetic profiles and location of high and low points along profiles shown in figure 4

Note: Other symbols are explained on figure 2

FIGURE 5.—Structural interpretation map of the report area near San Jose, Calif.

REFERENCES

Bailey, E. H., Irwin, W. P., and Jones, D. L., 1964, Franciscan and related rocks, and their significance in the geology of western California: California Div. Mines and Geology Bull. 183, 177 p.

Bott, M. H. P., 1960, The use of rapid digital computing methods for direct gravity interpretation of sedimentary basins: Royal Astron. Soc. Geophys. Jour., v. 3, no. 1, p. 63–67.

California Department of Water Resources, 1967, Evaluation of ground water resources—South Bay, Appendix A; Geology: California Dept. of Water Resources Bull. 118–1A, 153 p.

Chapman, Rodger, 1966, Gravity base station network: California Div. Mines and Geology, Spec. Rept. 90, 49 p.

Clement, W. G., 1965, Complete Bouguer gravity map of the northern part of the San Francisco Bay area and its geologic interpretation: U.S. Geol. Survey Geophys. Inv. Map GP–468.

Crittenden, M. D., Jr., 1951, Geology of the San Jose–Mount Hamilton area, California: California Div. Mines and Geology Bull. 157, 74 p.

Dibblee, T. W., Jr., 1966, Geology of the Palo Alto quadrangle, Santa Clara and San Mateo Counties, California: California Div. Mines and Geology Map Sheet 8.

Greve, Gordon, 1962, An investigation of the earth's gravitational and magnetic fields on the San Francisco peninsula, California: Stanford Univ., unpub. Ph. D. thesis, 108 p.

Heirtzler, J. R., Peter, G., Talwani, Manik, and Zurflueh, E. G., 1962, Magnetic anomalies caused by two-dimensional structure; their computation by digital computers and their interpretation: Palisades, N.Y., Lamont Geol. Observatory Tech. Rept. 6, 124 p.

Peterson, C. F., 1960, A gravity investigation of the Red Mountain area, California: Unpub. Student Research Project, Stanford Univ., Palo Alto, Calif., 16 p.

———1962, A gravity investigation of Livermore Valley, California: Unpub. Student Research Project, Stanford Univ., Palo Alto, Calif., 7 p.

Stewart, S. W., 1968, Preliminary comparison of seismic traveltimes and inferred crustal structure adjacent to the San Andreas fault in the Diablo and Gabilan Ranges of central California: Stanford Univ. Pubs. Geol. Sci., v. 11, p. 218–230.

Swick, C. H., 1942, Pendulum gravity measurements and isostatic reductions: U.S. Coast and Geod. Survey Spec. Pub. 232, 82 p.

Talwani, Manik, Worzel, J. L., and Landisman, Mark, 1959, Rapid gravity computations for two-dimensional bodies with application to the Mendocino submarine fracture zone: Jour. Geophys. Research, v. 64, no. 1, p. 49–59.

Taylor, S. G., Jr., 1956, Gravity investigation of the Southern San Francisco Bay area, California: Stanford Univ., Unpub. Ph. D. thesis, 105 p.

Thompson, G. A., and Talwani, Manik, 1964, Crustal structure from Pacific Basin to central Nevada: Jour. Geophys. Research, v. 69, no. 22, p. 4813–4837.

U.S. Air Force Aeronautical Chart and Information Center, compilers, 1968, Transcontinental geophysical survey (35°–39° N) Bouguer gravity map from 112° W. longitude to the coast of California: U.S. Geol. Survey Misc. Geol. Inv. Map I–532–B.

U.S. Coast and Geodetic Survey, 1965, Total intensity chart of the United States, 1965: U.S. Coast and Geod. Survey chart 3077 f.

THE EFFECT OF A STRONG OXIDIZING ENVIRONMENT ON THE STABILITY OF THE GOLD IODIDE COMPLEX

By CHARLES W. GALE 3d, Denver, Colo.

Abstract.—Although manganese dioxide is an effective oxidant for the formation of gold chloride and gold bromide complexes, it decreases the solubility of the gold iodide complex, because iodide, the complexing agent, is removed from the system by oxidation to iodine. In a laboratory study of possible mechanisms for the movement of gold in natural systems, gold leaf was dissolved by the addition of sodium iodide to a solution prepared to approximate copper porphyry input leach solutions used in recovering metals from porphyry copper dumps. The gold was then precipitated from the solution by exposing the pregnant leach solution to an environment made strongly oxidizing by the addition of manganese dioxide.

In a study of possible mechanisms for the movement of gold in natural systems, the behavior of the gold iodide complex in an acidic solution of ferric sulfate, cupric sulfate, and aluminum sulfate was found to be quite different from the behavior of either the bromide or chloride complexes of gold in similar solutions (tables 1 and 2). Although it is necessary for the solution of gold in the chloride and bromide solutions, manganese dioxide reduces the solubility of gold in the iodide solution. The author performed the following experiments to further investigate the behavior of the gold iodide complex in the presence of manganese dioxide.

TABLE 1.—*Gold dissolved in 0.001 molar sodium iodide–acidic sulfate solutions*

[From H. W. Lakin, unpub. data, 1970]

MnO_2 added (mg/liter)	Gold content (ppm) of solutions after contact with gold leaf for—		
	1 week	2 weeks	3 weeks
100	0. 06	<0. 04	<0. 04
20	1. 2	. 6	. 3
0	4. 8	5. 0	4. 4

TABLE 2.—*Gold dissolved in 0.005 molar sodium halide–acidic sulfate solutions*

[From H. W. Lakin, unpub. data, 1970]

MnO_2 added (mg/liter)	Gold content (ppm) of solutions after contact with gold leaf for 1 week		
	NaCl	NaBr	NaI
100	2. 0	2. 0	14.
20	. 6	. 7	30.
0	<. 04	<. 04	27.

EXPERIMENTAL PROCEDURES AND RESULTS

An experiment was designed to determine if gold is soluble as a complex iodide ion in the presence of ferric iron and if a stronger oxidant will remove dissolved gold from solution. Sodium iodide was added to a solution (table 3) prepared to approximate input leach solutions now being used to leach porphyry copper dumps in the southwestern United States. Solutions of this composition can also occur in natural systems by rainwater leaching of pyritic deposits (Beall, 1965).

TABLE 3.—*Composition of test solution*

[pH: 2.0, adjusted with H_2SO_4]

Constituent	*Molarity*
$Al_2(SO_4)_3 \cdot 18H_2O$	0. 002
$CuSO_4 \cdot 5H_2O$	. 002
$Fe_2(SO_4)_3$	. 002
NaI	. 001

Two hundred and fifty milliliters of the test solution (table 3) was placed with 3.6536 g of cleaned gold turnings in one chamber of the system illustrated in figure 1. The other chamber contained 0.1 g of powdered MnO_2. After 1 week the solution was forced by air pressure

U.S. GEOL. SURVEY PROF. PAPER 750–B, PAGES B140–B142

from the chamber containing gold to the chamber containing manganese dioxide. Thereafter, the solution was moved from chamber to chamber daily. A 0.45μ filter was placed between the two chambers to prohibit transfer of any gold which was not in solution.

After 1 month, components of the system were analyzed (table 4). Nearly 90 percent of the gold dissolved in the test solution was precipitated by the oxidizing action of manganese dioxide. The manganese dioxide grains and associated precipitates were used for analysis by X-ray diffraction in an unsuccessful attempt to identify the form of the precipitated gold, but they were not quantitatively analyzed for gold. However, several grains of manganese dioxide which had been caught on a filter during separation contained 145 μg of gold.

A second experiment was designed to monitor the stability of the gold iodide complex in both the presence and absence of manganese dioxide. Two beakers were filled with the test solution (table 1), which was modified to be 0.005 molar in sodium iodide. The iodide concentration was increased in order to dissolve gold more rapidly. Leaf gold was placed on the surface of each solution. After 1 day the 2 solutions were passed through a 0.45μ filter to exclude free gold from the solution, and 0.1 g of MnO_2 powder was then placed in one of the solutions. Both solutions were analyzed for gold periodically for 10 days. Figure 2 illustrates that the gold iodide complex is less stable in the presence of manganese dioxide.

The iodide–sulfate solutions containing dissolved gold were initially amber colored in all experiments. As the solutions were placed in contact with manganese dioxide, they developed a deep reddish-brown color owing to the increased rate of formation of iodine; but they became clear and nearly colorless as iodine escaped, indicated by a discoloration of clear plastic tubing above the solution to reddish brown. No gold was found in the colorless solutions, but gold was detected in association with a green precipitate which had formed around the manganese dioxide grains.

TABLE 4.—*Analyses of system components for gold*

Source of gold	Amount (μg)
Dissolved by test solution (determined by loss in weight of gold turnings)	4, 000
Removed from system for analysis during experiment	28
Remaining in solution at end of experiment (0.1 μg/ml in 236 ml)	24
Cleaned from vessel walls, tubing, and filters by washing with 0.5-percent Br in concentrated hydrobromic acid	438
Subtotal	490
Gold precipitated (obtained by difference)	3, 510

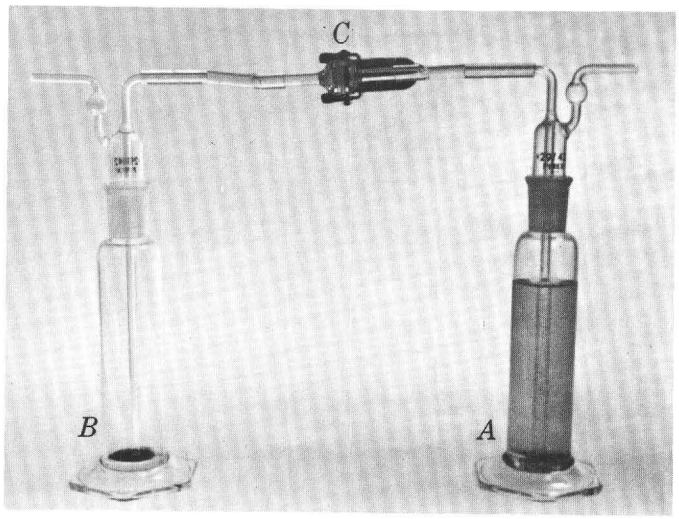

FIGURE 1.—Experimental apparatus. *A*, chamber containing 3.6536 g of gold turnings and 250 ml of the test solution; *B*, chamber containing 0.1 g of MnO_2; *C*, 0.45-micron filter.

ANALYTICAL METHODS

Gold analyses were made by an atomic absorption method (Thompson and others, 1968). In preparation of solutions for analysis, a 10-ml aliquot was passed through a 0.45μ filter to insure that any gold detected was in solution and not particulate. Precipitates and

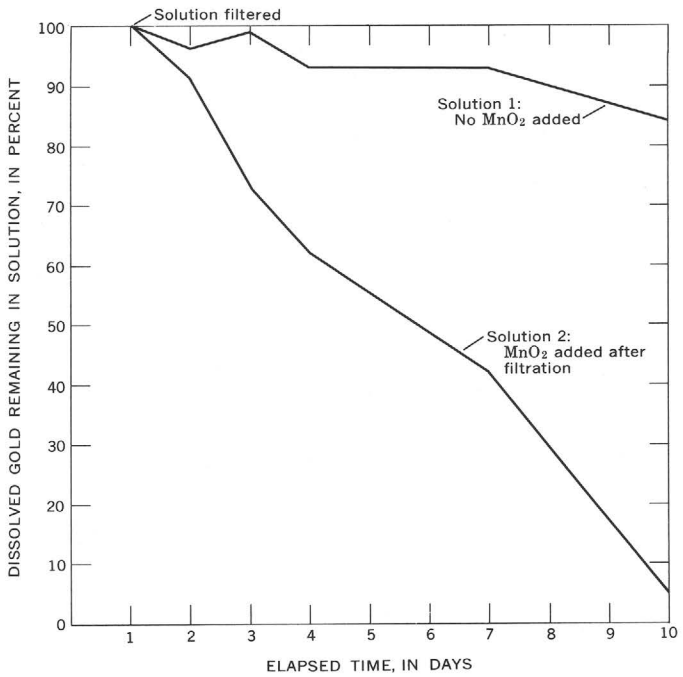

FIGURE 2.—Stability of gold iodide complex with time in an approximated copper porphyry input leach solution.

manganese dioxide grains were separated from the solutions by filtration and required no additional preparation.

DISCUSSION

Gold does not exist as a simple ion in aqueous solution. The gold iodide complex is probably the AuI_2^- species, because the aurous ion is particularly suited to complexing with the very large iodide ion. This conclusion is supported by (1) the observation that gold is very soluble in an iodide solution and (2) the metal-ligand characteristics reported by Jorgensen (1962). The instability of the complex arises from the elimination of iodide ions from the system by oxidation to molecular iodine.

If one considers the equilibrium

$$Au(s)+Fe^{3+}+2I^- \overset{H^+}{\rightleftarrows} AuI_2^-+Fe^{2+}, \quad (1)$$

an approximate equilibrium constant can be represented as follows:

$$K \doteq \frac{[AuI_2^-][Fe^{2+}]}{[I^-]^2[Fe^{3+}][Au(s)]}. \quad (2)$$

(Note: Any oxidizing agent of sufficient strength could replace ferric iron in reaction 1.)

The concentration of a solid is considered equal to 1. When there is a large excess of Fe^{3+} or if some stronger oxidizing agent oxidizes any Fe^{2+} to Fe^{3+}, the ratio $[Fe^{2+}]/[Fe^{3+}]$ remains practically constant. It has been demonstrated that manganese dioxide does oxidize Fe^{2+} to Fe^{3+} in an acidic sulfate solution; thus equilibrium expression 2 reduces to:

$$K' \doteq \frac{[AuI_2^-]}{[I^-]^2}. \quad (3)$$

Therefore the solubility of gold as an iodide complex in this system depends upon the concentration of iodide present. Reaction 1 is in competition for iodide ions with the oxidation of iodide to iodine.

According to Krauskopf (1951), gold may be mobilized as a gold (III) chloride complex in an acid solution in the presence of a strong oxidizing agent such as manganese dioxide:

$$2Au+12H^++3MnO_2+8Cl^-=3Mn^{2+}+2AuCl_4^-+6H_2O \quad (4)$$

According to the standard oxidation potentials in table 5, iodide ions are more easily oxidized than either chloride or bromide ions. The chloride–chlorine couple could oxidize gold to $AuCl_4^-$, and the bromide-bromine couple could oxidize gold to $AuBr_4^-$. The iodide–iodine couple will not oxidize gold to an iodide complex. The strong oxidizing conditions necessary for solution of gold as a chloride complex cause the oxidation of iodide, and, further, the elimination of a complexing agent, iodide, prohibits gold from existing in solution.

The stability of gold iodide in the systems considered is influenced by oxidizing agents other than manganese dioxide. Dissolved oxygen and ferric iron are also able to oxidize iodide to iodine; however, the action of manganese dioxide is much more rapid.

TABLE 5.—*Oxidation potentials*

[From Latimer (1952)]

Half-reaction	*E° (volts)*
$Au=Au^++e^-$	−1. 68
$Au=Au^{3+}+3e^-$	−1. 42
$Au+4Cl^-=AuCl_4^-+3e^-$	−1. 00
$Au+4Br^-=AuBr_4^-+3e^-$	−. 87
$Au+I^-=AuI+e^-$	−. 50
$2Cl^-=Cl_2+2e^-$	−1. 3595
$2Br^-=Br_2+2e^-$	−1. 0652
$2I^-=I_2+2e^-$	−. 5355
$Mn^{2+}+2H_2O=MnO_2+4H^++2e^-$	−1. 28
$2H_2O=O_2+4H^++4e^-$	−1. 229
$Fe^{2+}=Fe^{+3}+e^-$	−. 771
$Cu^+=Cu^{2+}+e^-$	−. 153
$H_2=2H^++2e^-$	. 00

CONCLUSIONS

Gold is soluble in acid solution as an iodide complex if iodide is readily available and if an oxidant of strength comparable to ferric iron is available. However, an oxidant of the strength of manganese dioxide reduces the solubility of gold by eventually removing most of the iodide from solution by oxidation to molecular iodine. This oxidation and subsequent escape of iodine is much slower than the solution of gold as an iodide complex, but, because the iodine can escape, that reaction is driven practically to completion. Experimental results suggest that gold may be leached by adding sodium iodide to acid sulfate leach solutions now being used to recover metals from porphyry copper dumps, and that gold may be precipitated by exposing the pregnant leach solution to a strong oxidizing environment.

REFERENCES

Beall, J. V., 1965 Southwest copper—A position survey: Mining Eng., v. 17, no. 10, p. 77–92.

Jorgensen, C. K., 1962, Absorption spectra and chemical bonding in complexes: New York, Pergamon Press, 352 p.

Krauskopf, K. B., 1951, The solubility of gold: Econ. Geology, v. 46, no. 8, p. 858–870.

Latimer, W. M., 1952, Oxidation states of the elements and their potentials in aqueous solutions [2d ed.]: Englewood Cliffs, N.J., Prentice-Hall, Inc., 392 p.

Thompson, C. E., Nakagawa, H. M., and VanSickle, G. H., 1968, Rapid analysis for gold in geologic materials, *in* Geological Survey Research 1968: U.S. Geol. Survey Prof. Paper 600–B, p. B130–B132.

GEOCHEMICAL RECONNAISSANCE OF THE CURAÇÁ RIVER BASIN AREA, BAHIA, BRAZIL

By RICHARD W. LEWIS, JR.; SYLVIO de QUEIROS MATTOSO,[1] and RAYMUNDO JOSÉ PORTELLA BRIM,[1]
Rio de Janeiro, Brazil; Salvador, Bahia, Brazil

Work done in cooperation with the Departamento Nacional da Produção Mineral and the Universidade Federal da Bahia (Salvador, Bahia, Brazil), under the auspices of the Government of Brazil and the Agency for International Development, U.S. Department of State

Abstract.—Geological and geochemical reconnaissance of 8,000 sq km of Precambrian rocks in northeast Brazil revealed a belt containing mafic and ultramafic rocks with which copper mineralization is associated. These mafic-ultramafic bodies are covered by a chestnut-brown heavy clay soil that supports a distinctive leguminous-spurge vegetation. Detailed geochemical exploration disclosed that several copper anomalies, at least one of which may have economic potential, are associated with these mafic and ultramafic bodies.

The Curaçá River basin is in north-central Bahia state, about 380 km northwest of the state capital, Salvador, and approximately 80 km south of the São Francisco River (fig. 1). The area reconnoitered, which covers about 8,000 sq km between the towns of Juàzeiro, Patamuté, Uauá, and Jaguarari (30–35 km south of Barrinha), was chosen for study because of the numerous showings of copper minerals.

The climate of this area is hot and semiarid; most of the annual precipitation is concentrated in one period, from late spring to summer (November to April).

The soils are largely residual, varying in composition, texture, and color in accordance with the underlying parent rock. Dusky-red and chestnut-brown clay soils were of special interest and assistance in geochemical exploration, as these soils overlie mafic-ultramafic bodies that were the specific targets for geochemical prospecting.

[1] Universidade Federal da Bahia.

Vegetation is typical of the arid and semiarid areas in northeast Brazil (von Luetzelburg, 1923) and is dominated by members of the Leguminoseae (pulse), Euphorbiaceae (spurge), Cactaceae (cactus), Bromeliaceae (bromelid), and Anacardiaceae (cashew) families. Six distinct vegetation assemblages were recognized, the most important of which for mineral prospecting is the caatingueira (*Caesalpina pyramidales*)-pinhão (*Jatropha pohliana*)-matapasto (*Cassia bicapsularis*) assemblage characteristic of the heavy clay soils formed above mafic-ultramafic rocks. This assemblage is strikingly less dense than the thorny thickets found over the more siliceous rock types; it is generally characterized by a low creeping blue flower, nana or erva de Santa Luzia (*Evolvus krameroides*).

GEOLOGY

Most of the study region is underlain by highly deformed metamorphic rocks of middle Precambrian age (fig. 1). The oldest of these is an assemblage of highly deformed migmatite, granitic gneiss, amphibolite, leptite, and mafic-ultramafic rocks. Next is a sequence of leptite, gneiss, amphibolite, and schist, followed by a unit of schist, amphibolite, and quartzite. The youngest middle Precambrian rocks are the syenitic augen gneiss and foliated granite. Overlying these middle Precambrian rocks are upper Precambrian calcareous rocks and quartzite, phyllite and quartzite, and Cenozoic limestone and conglomerate.

U.S. GEOL. SURVEY PROF. PAPER 750-B, PAGES B143-B150

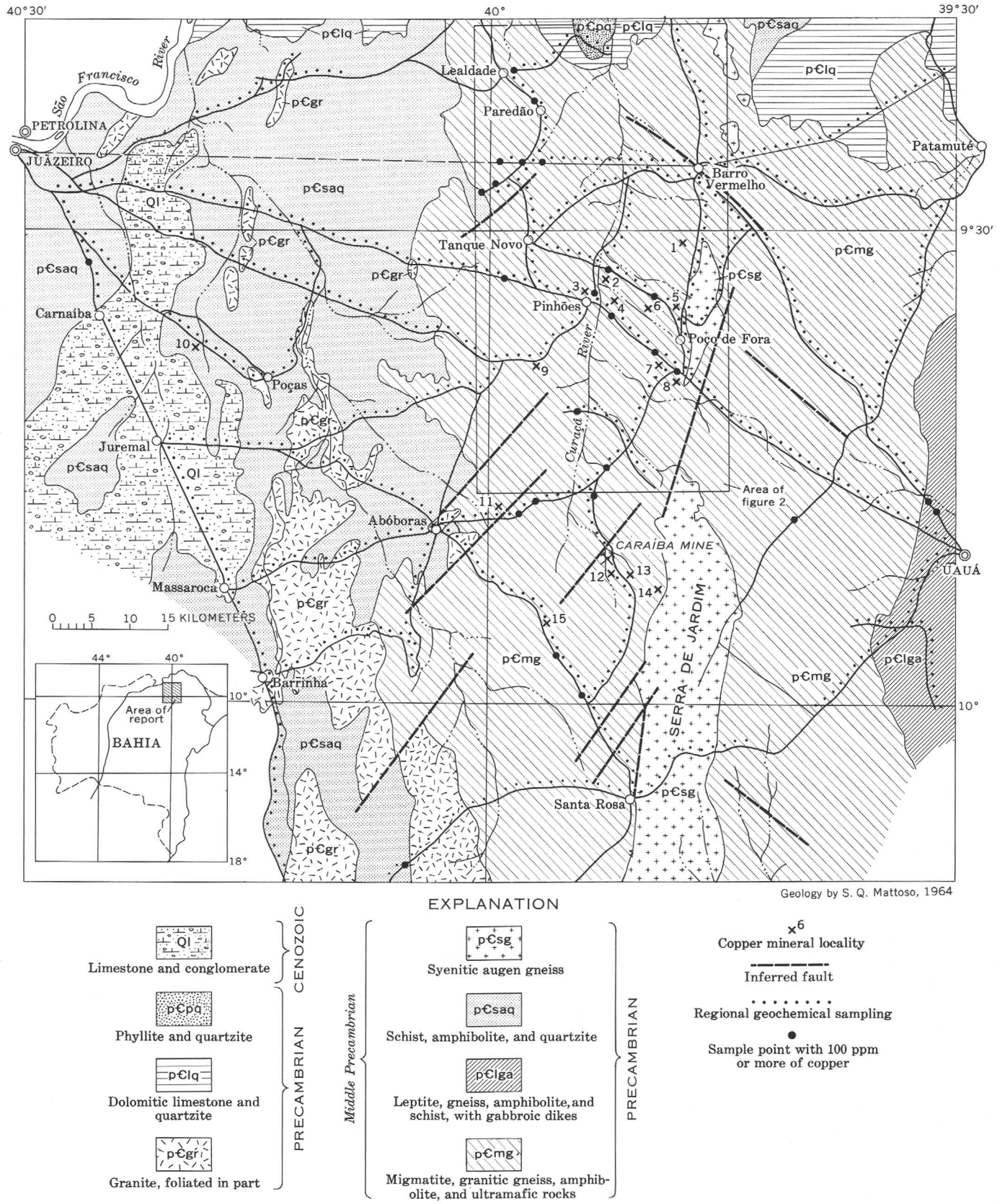

FIGURE 1.—Generalized geologic map of the Curaçá region, Bahia state, Brazil, showing regional geochemical sampling net and localities of copper mineralization. Names of localities and types of mineralization are given in table 1.

The oldest Precambrian rocks include numerous semiconcordant bodies of gabbro, norite, and pyroxenite, most of which lie in a 20-km-wide belt just east of the Curaçá River (fig. 2). These ultramafic rocks are of particular interest because they are the host rock to most of the primary copper mineralization of the region.

MINERAL OCCURRENCES

Copper minerals were seen at 15 localities in the Curaçá River basin area (table 1); these localities have been plotted on figure 1. The deposits may be classified under four types according to their lithologic and structural associations: (1) disseminations in ultramafic complexes, (2) disseminations in amphibolite, (3) mineralized fracture zones, and (4) quartz veinlets with chalcopyrite.

The most important of these types is the first—disseminations and veinlets of chalcopyrite and bornite in pyroxenite and, to a lesser extent, in norite, as found at Caraíba. The tenor of copper in these mineralized bodies is low, about 1.0 percent, but tonnages may be on the order of tens of millions of metric tons (Mello Jr. and others, 1962).

The second type of copper mineralization is present as disseminated primary sulfides, mostly chalcopyrite, in hornblende-rich amphibolites, such as seen at Fazenda Angico. This mineralization is erratic in distribution, seldom occupying a width of more than 10 m or extending for more than 50 m along the strike. Nevertheless, these mineralized amphibolites may represent intermediate rocks that commonly surround ultramafic complexes, and they should be studied in detail.

The third and most obvious type is secondary copper mineralization associated with large fractures and shear zones. Mineralized zones generally range in width from 20 cm to 5 m and contain chrysocolla, some malachite, brochantite, small amounts of azurite, and concentrations of chalcocite and cuprite. Spotty mineralization and low tonnages have discouraged extensive exploration, although mineralized fractures are possible leads to mineralized ultramafic bodies.

Narrow veins of milky quartz containing disseminated chalcopyrite, the fourth type of copper mineralization, also have been found cutting schists and amphibolites in the western part of the area around Poças and in Precambrian limestones north of the area studied. No veins of this type were observed in the middle Precambrian gneisses and migmatites containing the other three types of mineralization.

TABLE 1.—*Locality and type of surficial showings of copper mineralization in the Curaçá River basin area, Bahia, Brazil*

Locality (fig. 1)	*Type of mineralization*
1. Fazenda Angico (Lagoa da Mina).	Disseminations in amphibolite.
2. Lagoa de Pedras	Mineralized fracture zone in gneiss.
3. Pinhões	Do.
4. Fazenda Lisbôa	Disseminations in ultramafic complex.
5. Buiões	Mineralized fracture zone in gneiss.
6. Fazenda Surubim	Disseminations in mafic complex.
7. Southwest of Poço de Fora.	Mineralized fracture zone in mafic complex.
8. South of Poço de Fora	Do.
9. Fazenda Lages	Mineralized fracture zone in amphibolite.
10. Poças [1]	Quartz veinlets.
11. East of Abóboras	Mineralized fracture zone in gneiss.
12. Caraíba	Disseminations in ultramafic complex.
13. Southeast of Caraíba	Mineralized fracture zone in gneiss.
14. Fazenda Riachuelo	Disseminations in amphibolite.
15. Southwest of Caraíba (Riacho da Mina).	Mineralized fracture zone in gneiss.

[1] In another river basin just west of the Curaçá River basin.

GEOCHEMICAL INVESTIGATIONS

Geochemical sampling of soils was made on regional, semiregional, and detailed bases. All samples were collected in the B soil horizon and analyzed for copper by standard procedures as described by Ward and others (1963).

Regional geochemical sampling

Soil samples were collected along more than 1,000 km of major and secondary roads in the region, at intervals of approximately 1 km (fig. 1). Regional background values of copper in the soils over the various heterogeneous rock units are tabulated in table 2. The background of copper in soils overlying the migmatites and banded gneisses that contain the mafic and ultramafic bodies is slightly higher than copper values for soils over other lithologic units. This belt of rocks contains most of the surficial copper showings and 17 of the 23 regional sample points from which samples were taken containing 100 ppm or more of copper.

Background values of copper in soils over individual rock types are similar to those found at the Caraíba copper deposit (Lewis, 1966) and are tabulated in table 3.

The difference in background values between soil types representing rock types or units of potential interest and those with no potential is too small to permit the use of regional geochemical sampling as a guide to areas of mineralization.

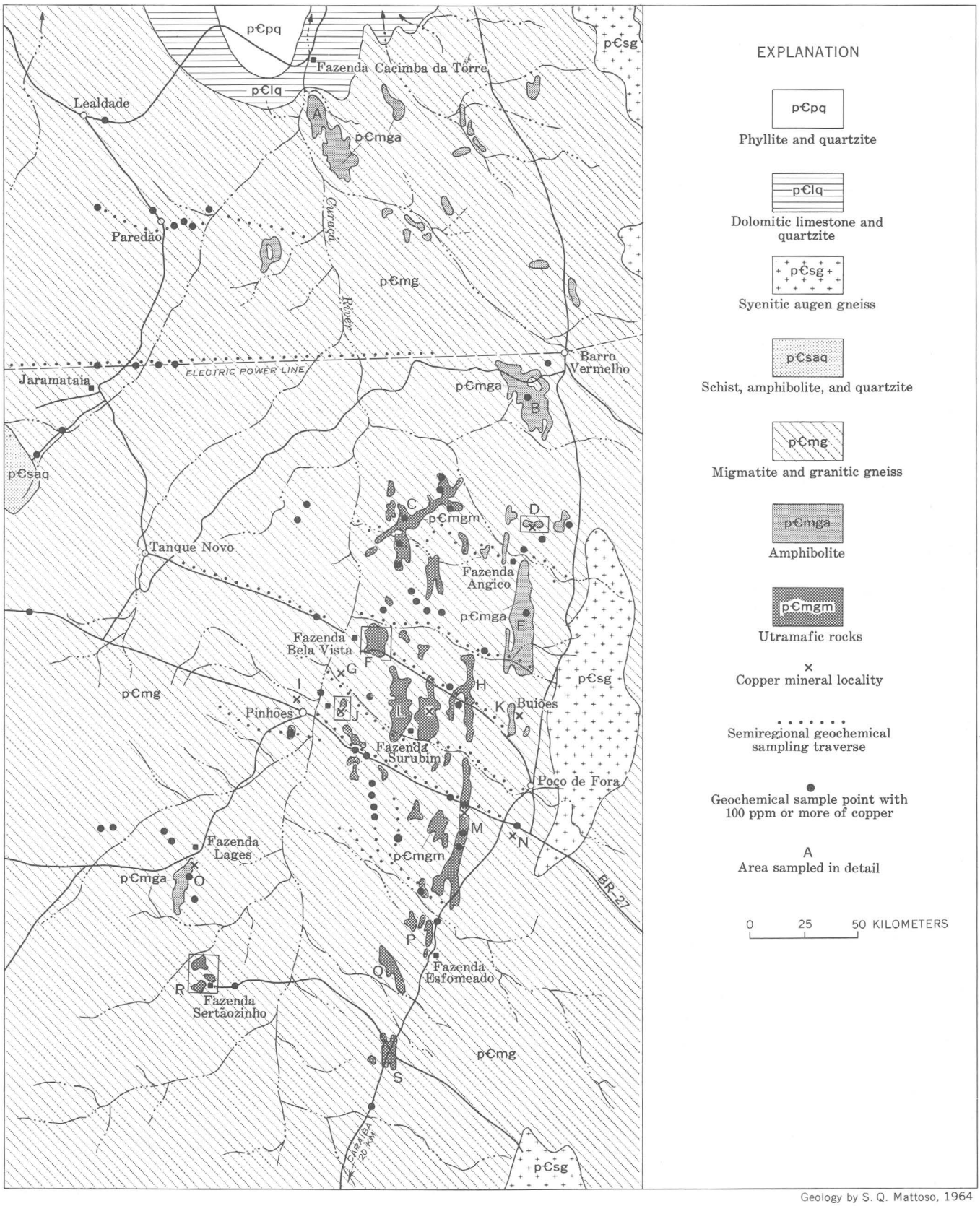

FIGURE 2.—Sketch map of mineralized belt in the Curaçá River basin, Bahia, Brazil, showing sample traverses and localities. Lithology and copper content of principal patterned mafic-ultramafic bodies indicated by letter on map are shown in table 4.

TABLE 2.—*Regional background copper content, in parts per million, in soils over principal rock units of the Curaçá River basin area, Bahia, Brazil*

[Tr., trace]

Rock unit (letters in parentheses refer to unit on fig. 1)	Number of samples	Range	Arithmetic mean	Geometric mean	Median	Mod_e
Limestone and conglomerate (Ql)	21	10–30	18. 9	17. 8	20	20
Foliated granite (p€gr)	21	Tr.–50	13. 9	10. 9	10	10
Syenitic augen gneiss (p€sg)	19	Tr.–25	10. 2	7. 9	5	12. 5
Schist, amphibolite, and quartzite (p€saq)	21	Tr.–50	15. 9	12. 5	10	10
Leptite, gneiss, amphibolite, and schist (p€lga)	21	Tr.–100	21. 0	11. 8	10	10
Migmatite, gneiss, amphibolite, and mafic-ultramafic rocks (p€mg)	21	5–50	26. 9	23. 2	25	25

TABLE 3.—*Estimated background values of copper, in parts per million, in soils above different rock types in the Curaçá River basin area Bahia, Brazil*

[Tr., trace]

Rock type	Number of samples	Range	Arithmetic mean	Geometric mean	Median	Mode
Amphibolite	13	10–150	45. 6	33. 7	35	50
Diabase	11	10–100	37. 9	26. 7	25	25
Gabbro	12	10–150	43. 8	38. 0	50	50
Gneiss, banded	13	5–50	20. 6	15. 4	10	10
Gneiss, nebulitic, granitic	9	Tr.–50	20. 3	13. 4	12. 2	10, 25
Gneiss, syenitic augen	9	Tr.–20	13. 4	10. 3	12. 5	12. 5, 17. 5
Granite	9	10–50	24. 2	20. 3	17. 5	----------
Leptite	9	Tr.–50	24. 1	12. 4	17. 5	50
Limestone	11	Tr.–25	18. 3	14. 6	20	10
Mica schists	7	Tr.–50	16. 6	10. 3	10	10
Migmatite	9	Tr.–75	30. 4	12. 1	17. 5	12. 5
Milonite	5	5–17. 5	12. 0	11. 1	12. 5	12. 5
Pegmatite	5	Tr.–50	22. 2	12. 6	25	25
Quartzite	5	Tr.–25	13. 2	8. 9	12. 5	----------
Ultramafic rocks (unmineralized)	11	17. 5–100	40. 2	35. 4	25	25

Semiregional geochemical sampling

The semiregional sampling program was undertaken to investigate the effectiveness of sampling at intervals of 200 to 500 m in locating belts or areas of potential mineralization. About 300 soil samples were taken at intervals along 7 traverses across the belt of rocks containing most of the mafic and ultramafic bodies between the Curaçá River and the Caraíba-Poço de Fora-Barro Vermelho road, and along 5 traverses west of the Curaçá River (fig. 3). These traverses were 6 to 12 km long and followed either roads or stream courses, most of which were oriented approximately N. 60° W.

The results of this semiregional sampling are inconclusive, as belts of known ultramafic rocks having mineral potential are not consistently marked by notable increases of copper over background values in the overlying soil.

Detailed geochemical sampling

Soils at more than 30 localities of known mineralization or mafic-ultramafic rocks were sampled in detail to determine the presence and extent of mineralization. Sampling was started on a random basis and expanded to systematic traverses and grids where geochemical analyses showed values of 100 ppm or more of copper, or where float, soil type, and vegetation assemblage indicated the presence of an ultramafic body.

Criteria developed during the study of the Caraíba copper deposit (Lewis, 1966) were used for evaluating geochemical data as follows: Sample localities showing 100 ppm or more of copper were considered as areas of potential interest; sites having 250 ppm or more of copper were considered as possible indicators of nearby mineralization; and soils with a copper content of 1,000 ppm or more were assumed to mark the possible presence of cupriferous ultramafic bodies near the surface.

Areas sampled in detail are marked on figure 2, and the results are tabulated in table 4. Some of the best individual geochemical anomalies are shown on figure 4.

The copper anomaly found at Fazenda Bela Vista is above an ultramafic body and shows vegetation, soil types, and copper values similar to those found at the Caraíba deposit; it thus may represent a mineralized

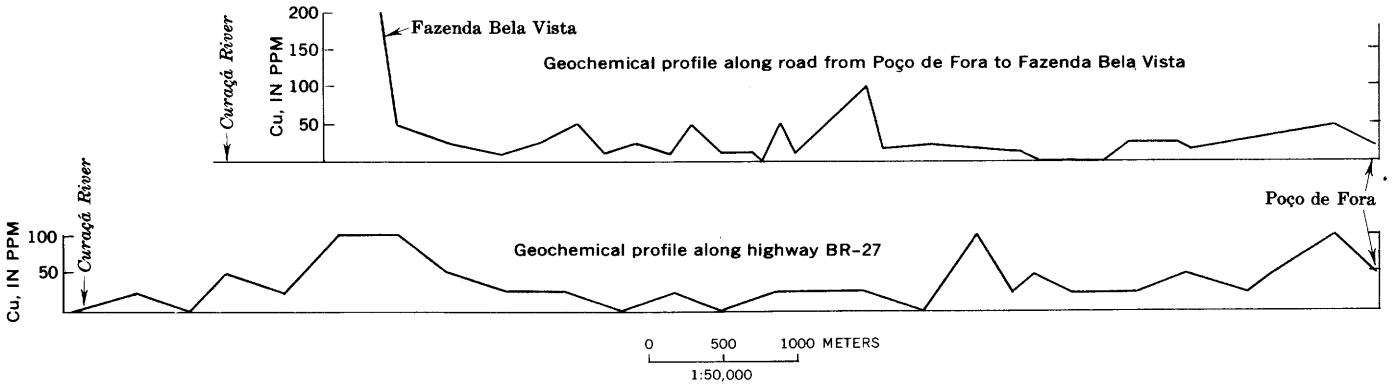

FIGURE 3.—Semiregional geochemical profiles, projected on an east-west line, Curaçá River basin area (fig. 2), Bahia, Brazil.

ultramafic body of economic potential. The anomaly at Fazenda Lisbôa (*J*, fig. 2), although smaller than that at Bela Vista, is also believed to represent a mineralized mafic or ultramafic body that might possibly be worked economically in conjunction with other nearby ore bodies.

The copper anomaly found above amphibolite at Fazenda Angico is in a large area of ground containing 100 ppm or more of copper. Although the rock type at this locality is not the most favorable for deposits of economic grade and dimensions, the possibility that the mineralized amphibolite represents an intermediate facies surrounding mineralized ultramafic rock merits further investigation.

Other areas of promise are the low but obvious copper anomalies found in the mafic complexes west of Fazenda Angico, at Fazenda Surubim, southwest and south of Poço de Fora, and at Fazendas Esfomeado and Sertãozinho.

The remaining areas listed in table 4, and other localities that have copper mineralization at the surface, do not seem promising; they might best be investigated only after more is known about the region as a whole.

TABLE 4.—*Results of detailed geochemical exploration of the principal mafic-ultramafic bodies in the Curaçá River basin area, Bahia, Brazil*

Number on figure 1	Letter on figure 2	Locality	Number of samples	Highest copper concentration (ppm)	Copper minerals observed	Lithology
-------	A	Fazenda Cacimba da Tôrre	57	100	No	Amphibolite.
-------	B	Barro Vermelho	15	150	No	Do.
-------	C	West of Fazenda Angico	40	200	No	Mafic complex.
1	D	Fazenda Angico	70	3,000	Yes	Amphibolite.
-------	E	South of Fazenda Angico	107	100	No	Do.
-------	F	Fazenda Bela Vista	170	8,000	No	Ultramafic complex.
2	G	Lagoa de Pedras	10	350	Yes	Gneiss.
-------	H	Northwest of Poço de Fora	42	100	No	Mafic complex.
3	I	Pinhões	6	500	Yes	Gneiss and amphibolite.
4	J	Fazenda Lisbôa	24	1,200	Yes	Ultramafic complex.
5	K	Buiões	14	150	Yes	Gneiss and amphibolite.
6	L	Fazenda Surubim	69	200	Yes	Mafic complex.
7	M	Southwest of Poço de Fora	56	100	Yes	Mafic-ultramafic complex.
8	N	South of Poço de Fora	8	750	Yes	Do.
9	O	Fazenda Lages	47	500	Yes	Amphibolite.
-------	P	Fazenda Esfomeado	27	100	No	Mafic complex.
-------	Q	Southwest of Fazenda Esfomeado	17	70	No	Mafic-ultramafic complex.
-------	R	Fazenda Sertãozinho	19	200	No	Ultramafic complex.
-------	S	Crossroads south of Fazenda Esfomeado	34	50	No	Mafic complex.

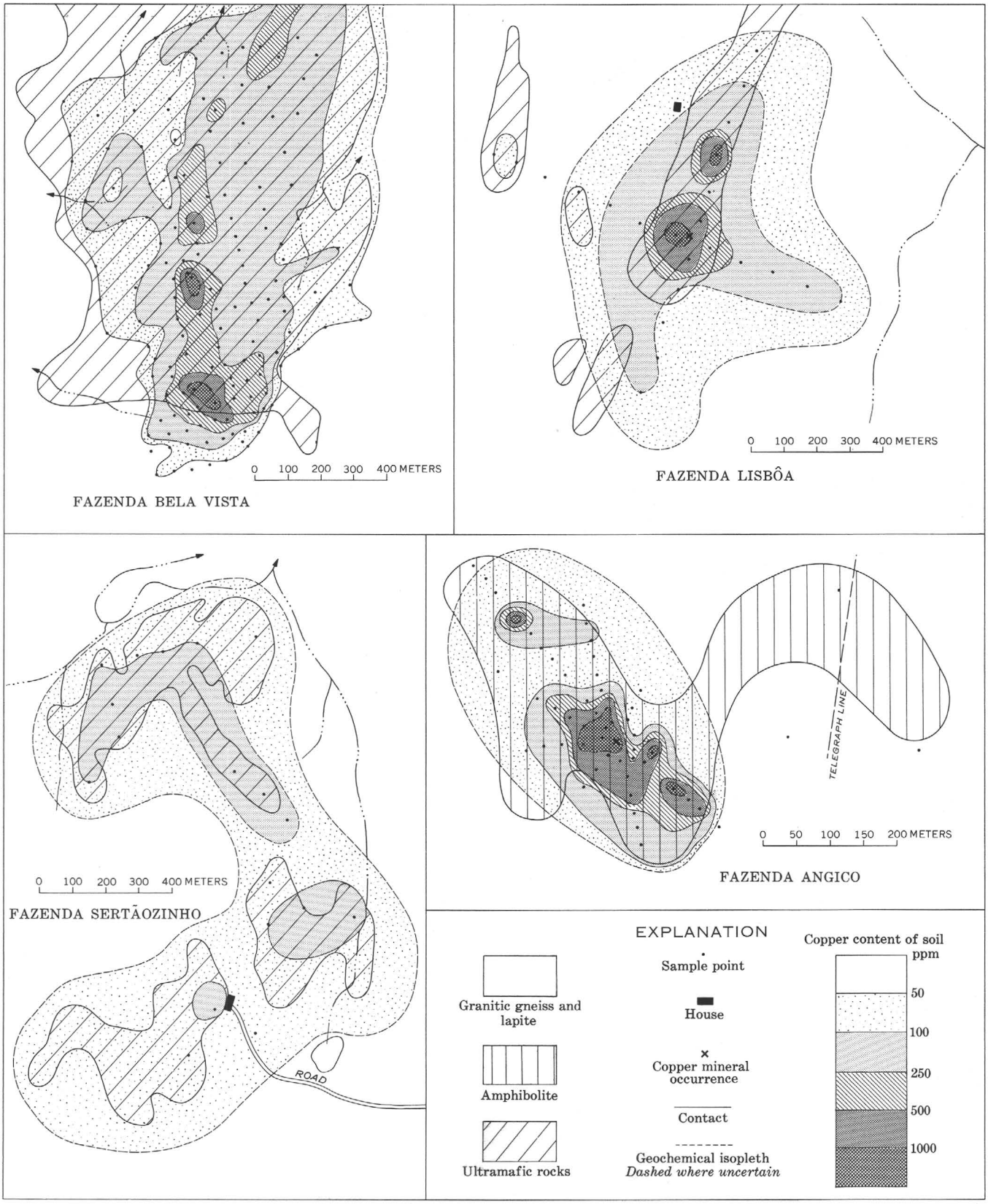

FIGURE 4.—Sketch maps of selected copper anomalies in soils in the Curaçá River basin area, Bahia, Brazil.

REFERENCES

Lewis, R. W., Jr., 1966, A geochemical investigation of the Caraíba copper deposit, Bahia, Brazil, *in* Geological Survey Research 1966: U.S. Geol. Survey Prof. Paper 550–C, p. C190–C196.

Luetzelburg, Phillip von, 1923, Estudo botânico do Nordeste: Brazil, Min. Viação e Obras Públicas, Insp. Fed. Obras Contra Sêcas Pub. 57, ser. 1, pt. A, v. 3, 283 p.

Mello, Jr., J. L. de, Pouchain, E. B., and Castiel, Nassim, 1962, Relatório sôbre a jazida de Caraíba, Bahia: Brazil, Dept. Nac. Produção Mineral, Div. Fomento Produção Mineral Bol. 117, 137 p.

Ward, F. N., Lakin, H. W., Canney, F. C., and others, 1963, Analytical methods used in geochemical exploration by the U.S. Geological Survey: U.S. Geol. Survey Bull. 1152, 100 p.

EXTRAORDINARY TRACE-ELEMENT ACCUMULATIONS IN ROADSIDE CEDARS NEAR CENTERVILLE, MISSOURI

By J. J. CONNOR, H. T. SHACKLETTE, and J. A. ERDMAN,
Denver, Colo.

Abstract.—Unusually high concentrations of lead, copper, zinc, and cadmium were found in samples of cedar (*Juniperus virginiana* L.) collected on the roadside of State Highway 21–72 about 4 miles northeast of Centerville, Mo. For 15 samples, geometric mean concentrations for these elements in cedar ash were, in parts per million: Pb, 5,800; Cu, 190; Zn, 940; and Cd, 12. The high concentrations are thought to reflect vehicular transport of lead-bearing ores from mine to smelter, rather than mineralized rock at depth.

Connor, Erdman, Sims, and Ebens (1971), in a study of the roadside effect on the trace-element content of natural materials in Missouri, noted that the principal effect is a twofold to threefold increase of lead concentrations in vegetation growing within 50 feet of the pavement compared to similar vegetation growing more than 300 feet from the pavement. They concluded that most of this increased amount of lead originates from automotive exhaust. The objective of that study, which was made in the summer of 1969, was to determine the roadside effect as it bears on sampling rocks, soils, and vegetation in geochemical programs.

During the course of the study an extraordinarily high concentration of lead was found in a roadside cedar tree (*Juniperus virginiana* L.) at a sampling locality near Centerville in southeastern Missouri (fig. 1). This cedar contains more than 70 times the expected amount of lead in cedars growing on roadsides and is remarkable not only in its lead content, but also in its content of other metals (table 1). Its cadmium content is five times, its copper content more than four times, and its zinc content nearly three times the respective amounts expected to occur in cedars along roads. Further evidence of the unusual geochemical environment at this locality is provided by the lead content of a cedar 320 feet from the road that is six times the content expected in such cedars. Moreover, a sample of subsurface soil collected at a depth of 2–4 inches from under the canopy of the roadside cedars contains nearly 36 times the amount of lead and 3 times the amount of zinc that are expected in roadside subsurface soils.

The unusual geochemical environment reflected in these materials strongly suggests that a source of these elements other than automotive exhaust must be looked for. The most obvious alternative explanation is the fact that the sample locality lies within an area of extensive lead mineralization (fig. 1), as described by Weigel (1965, p. 78); some of the lead deposits have been mined for many years, and the high lead concentrations found here may reflect widespread lead-rich

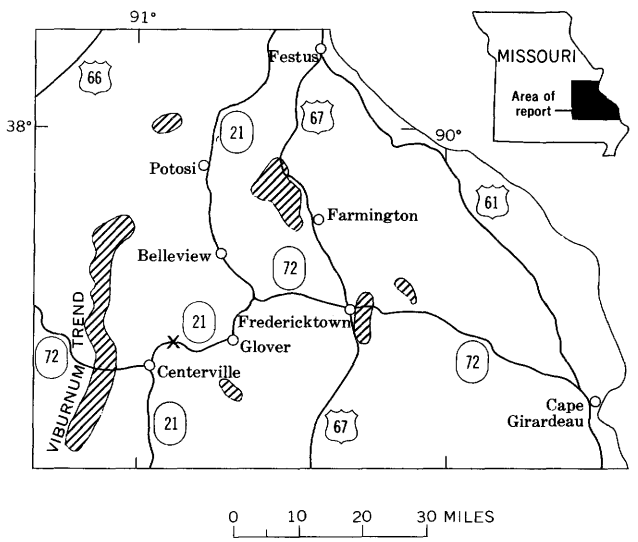

FIGURE 1.—Index map of part of southeastern Missouri, showing highway routes, sample locality X, and major areas of lead mineralization (patterned) (adapted from Weigel, 1965).

U.S. GEOL. SURVEY PROF. PAPER 750-B, PAGES B151-B156

413-504 O - 71 - 11

TABLE 1.—*Concentrations of certain elements in 2 samples of cedar trees and 2 associated soils collected in the summer of 1969 at the Centerville, Mo., locality, and average concentrations of these elements in 32 similar samples from 16 localities in southern Missouri*

[Adapted in part from Connor, Erdman, Sims, and Ebens (1971, pl. 3). Fe, Mg, Ca, and Ti in percent; other elements in parts per million, in cedar ash and dry soil. Averages are geometric means. Analysts: T. F. Harms, J. M. Nishi, and C. S. E. Papp]

Element	Cedar ash [1]				Subsurface soil			
	Centerville		Average, all cedars		Centerville		Average, all soils	
	On road	Off road	On road	Off road	On road	Off road	On road	Off road
Fe	0.5	0.2	0.39	0.31	1.5	2.0	2.2	2.3
Mg	7	7	7.4	7.7	.3	.2	.29	.20
Ca	28	27	26	28	.2	.07	.28	.18
Ti	.03	.02	.08	.04	.3	.3	.47	.40
B	500	300	230	260	10	10	<10	<10
Ba	<20	1,000	400	680	200	50	130	70
Cd	9.3	2.8	1.7	1.8	<1	<1	<1	<1
Co	15	15	8.4	7.9	7	10	12	12
Cr	70	30	75	50	50	70	71	71
Cu	300	100	68	51	7	15	15	11
Mn	2,000	5,000	2,400	4,000	700	700	1,100	930
Ni	50	70	46	47	15	20	16	17
Pb	20,000	700	280	114	500	<10	14	15
Sc	<10	<10	<10	<10	5	7	5.4	5.8
Sr	200	500	840	920	100	<100	<100	<100
V	<20	<20	<20	<20	30	50	62	56
Y	<20	<20	<20	<20	15	10	18	17
Zn	1,080	390	380	300	195	52	57	47
Zr	30	20	40	30	300	200	260	260

[1] Ash content of the Centerville cedar, and average ash content of all cedar samples, was 6 percent of dry weight.

substrata. The strongest argument against this explanation, however, is the fact that the off-road cedars and subsurface soils at this locality contain much less lead than those along roads.

The high metal concentrations found in the soil and cedar ash at this locality prompted a subsequent geochemical reconnaissance and sampling program at the locality in the fall of 1969. This study area lies along State Highway 21–72 about 4 miles northeast of Centerville, Mo. (fig. 1). A diagrammatic sketch of the locality is shown in figure 2 and a photograph in figure 3. The road here is cut into the base of a wooded hillside on the northwestern side of a narrow northeast-descending stream valley. An almost continuous outcrop of dolomite is exposed along the uphill side of the road. The dolomite is gray, well bedded, and generally fine grained, and contains a few included shale beds. It is thought to be part of the Potosi Dolomite of Cambrian age. A bench has been cleared above the dolomite outcrop where a powerline has been installed. Cedars ranging in height from a few inches to about 15 feet grow abundantly on this bench, some of them visibly rooted in crevices of the bedrock. The hillside is mantled with an extensive deposit of iron-rich chert-bearing clay commonly referred to as residuum. This clay is generally thought to be the product of intense and long-continued weathering of the underlying dolomite.

A pile of sulfide-bearing aggregate was observed near the roadside cedar that was sampled in the original study (fig. 2). This aggregate is composed of crushed dolomite and rhyolite, both of which contain visible sulfide minerals. However, the pile of aggregate is small (probably less than an ordinary dump-truck load), and it rests on the lip of the dolomite bench more than 20 feet downslope from the originally sampled cedar.

SAMPLE DESIGN AND ANALYTICAL METHODS

The two cedars and subsurface soil sites sampled in the original study were located and resampled in October 1970. Additional cedars, estimated to range in age from 5 to 25 years, and subsurface soils were sampled both along the road and at sites more distant from the road. Cedars are abundant on the roadside, but only a few grow in the oak-hickory-pine forest that borders the right-of-way. As in the original study, each cedar tree was sampled by collecting a set of terminal parts of branches over the crown of the tree, and the subsurface soil beneath the tree canopy was sampled at a depth of 2–4 inches. Exposures of dolomite bedrock along the edge of the road also were sampled.

Twenty cedars were sampled at the Centerville locality; 15 were growing on the roadside and 5 were at various distances from the road. The locations and lead

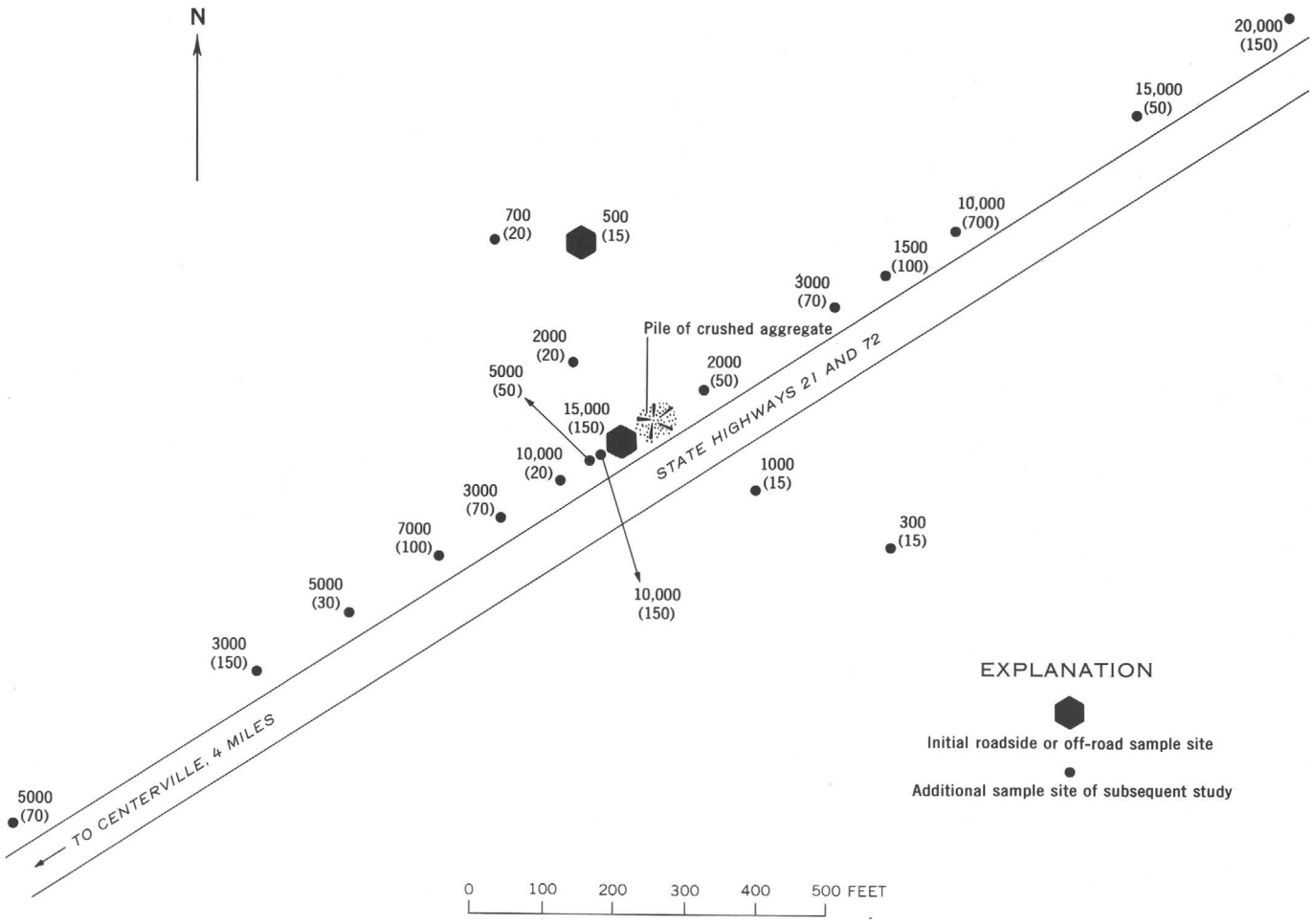

FIGURE 2.—Sketch of the Centerville, Mo., locality, showing the locations of sample sites and the lead concentrations in cedar ash (upper value) and soil (in parentheses). All values are in parts per million. All analyses are those made in the subsequent study. Analyses of samples collected during the initial study of the roadside and off-road sites are given in table 1.

contents of the individual cedar trees, and the lead contents of the soils in which the trees are growing, are given in figure 2. Five samples of residuum, 13 samples of bedrock dolomite, and 2 samples of the aggregate were also collected. The concentrations of elements in these materials are given in table 2. These concentrations are compared with the expected average amounts in compositionally similar materials (as reported in the literature) in the same table; in addition, the element contents of the Centerville cedars may be compared to the average element contents of all Missouri cedar samples given in table 1.

All samples were analyzed in laboratories of the U.S. Geological Survey in Denver, Colo., by both semiquantitative spectrographic and atomic absorption techniques. The spectrographic methods were described by Myers, Havens, and Dunton (1961). Before analysis, all surfaces of the rock samples were trimmed, the dried soils and residuum samples were pulverized in a ceramic mill to approximately 100-mesh particle size, and the cedar samples were burned to ash in an electric muffle. Samples of each material were analyzed in a random sequence for approximately 40 elements; the results of lead, copper, zinc, and cadmium analyses only are presented in table 2.

Averages for all elements included in this study are given as geometric means. A geometric mean concentration of a particular element may be considered to be the typical or expected concentration for the element in the material that was analyzed. Because trace-element studies commonly include at least a few samples in which some elements are present in quantities too small to be evaluated, computation of geometric means for these elements must rely on special statistical methods. These and other methods of evaluating trace-element data were described by Shacklette, Sauer, and Miesch (1970).

FIGURE 3.—View, looking northwest, of the Centerville, Mo., sampling locality, showing the highway pavement, the dolomite outcrop, and some of the cedar trees that were sampled. The man is standing to the left of the roadside cedar first discovered to have a highly anomalous lead concentration in samples of its branches; a posthole digger stands in a pile of sulfide-bearing aggregate dumped along the roadside. An oak-hickory-pine forest lies behind the utility line right-of-way. Photographed September 12, 1970.

RESULTS

The analyses of the single roadside tree originally sampled (table 1) and the trees sampled in the subsequent study (fig. 2) indicate that all roadside cedars at this locality contain extraordinarily large amounts of lead; the off-road cedars contain much less lead, but still more than was found in samples of off-road cedars elsewhere in Missouri. The ash produced by burning the roadside cedar samples ranged from 4 to 5 percent of the dry weight of the sample; that from the off-road cedar samples ranged from 4 to 7 percent. These ash percentages are within the range expected in tree samples (see Shacklette and others, 1970, p. C16–C17) and indicate that the samples did not contain large amounts of surficial particulate matter as would result from deposits of roadside dust. The two trees of the original study were dry when sampled, and the samples were not washed. These and the other trees used in the subsequent study were sampled during a period of heavy rainfall which thoroughly washed the branches. Analyses of the original samples collected when dry (table 1), and analyses of the same trees resampled when wet (fig. 2), show that somewhat more lead was present in the dry samples; the differences in these analyses, however, are within one standard error of the analytical techniques and may not be significant. These facts suggest that the lead found in the tree samples is largely incorporated in the tissues of the trees and is not just a component of particulate surficial deposits on the tree branches.

The amounts of lead in roadside subsurface soil at this locality also are generally anomalous, whereas the lead concentrations in off-road soil samples are well within the expected range (table 1, fig. 2). Thus the analyses of both cedars and soils indicate that amounts of lead in these materials are closely related to distance of the sample sites from the road.

TABLE 2.—*Geometric mean concentrations, in parts per million, of lead, copper, zinc, and cadmium in natural materials on the roadside at the Centerville, Mo., locality, and published averages for comparable materials*

[From analyses of Centerville samples by J. P. Cahill, H. G. Neiman, V. E. Shaw, and J. A. Thomas. Leaders (---), no data available]

Material	Number of samples	Pb	Cu	Zn	Cd
Centerville locality					
1. Dolomite bedrock	13	<10	0.88	9.1	---
Dolomite, in aggregate	1	15	200	10	---
2. Rhyolite, in aggregate	1	30	3	105	<1
3. Residuum	5	20	47	140	.66
4. Subsurface soil	15	85	29	110	.81
5. Cedar ash	15	5,800	190	940	12
Averages reported in comparable materials					
1. Carbonate rock [1]		9	4	20	0.035
2. Low-Ca granitic rock [1]		19	10	39	.13
3. Shale [1]		20	45	95	.3
4. Soils, United States [2]	863	16	18	44	---
5. Ash of various plants [3]	1,501 for Pb and Zn, 1,498 for Cu	111	112	1,010	---

[1] Turekian and Wedepohl (1961, table 2).
[2] Shacklette, Hamilton, Boerngen, and Bowles (1971).
[3] Shacklette (1965, p. D14).

Lead concentrations in the underlying residuum and dolomite bedrock along the road seem to be of an ordinary magnitude (table 2), in contrast to the high lead concentrations in cedars and subsurface soil. The highest concentration of lead measured in residuum was 30 ppm and the highest concentration in bedrock was 20 ppm.

Lead in the aggregate appears to be of an ordinary magnitude; 15 ppm lead was found in the dolomite component and 30 ppm in the rhyolite component. The aggregate is unusual, however, in that the dolomite contains 200 ppm copper and the rhyolite contains 105 ppm zinc. Although the aggregate might possibly serve as a source of copper and zinc for the originally sampled cedar, it can hardly serve as a source of lead.

DISCUSSION

An intensive study of the roadside environment near Centerville confirms an earlier observation that roadside cedars here have accumulated unusually large amounts of lead. The amount of accumulation is largest in trees growing nearest the road. We conclude from this fact that the anomalous accumulation of lead in these trees is actually a roadside effect, although this effect is much more pronounced here than in other parts of Missouri. Therefore, a source of lead other than, or in addition to, vehicle emissions must be sought to account for the extremely high lead values found in the Centerville roadside cedars and associated soils.

The fact that this locality lies in a major lead-mining district and the discovery that the suite of accumulated elements includes lead, zinc, copper, and cadmium suggest that a mineralized (lead-zinc) source of some kind is responsible for these concentrations. Specific possible sources of these metals include mineralized bedrock or ground water, or perhaps some factor associated with lead mining, such as mill tailings that may have been used in road materials or ore haulage and spillage along the highway.

The anomalous concentrations of lead in the cedars and soils probably do not reflect an unusual occurrence of lead minerals in bedrock. No such occurrence was observed in the bedrock exposures, and the highest lead content measured in outcrop was only 20 ppm.

Similarly, lead accumulations in these trees and soils are difficult to attribute to a ground-water source. Most of the roadside cedars appear to be growing in contact with dolomite bedrock. The generally near-surface distribution of the tree roots (at least in areas of shallow soil over bedrock) indicates that the cedars most likely are using near-surface (runoff) water rather than true ground water. The dolomite at the Centerville locality is generally dense and of low porosity; these qualities preclude much movement of ground water in the bedrock itself. Moreover, three off-road trees are located uphill from the roadside and presumably are using the same or a similar water source as are the roadside cedars, yet they have low lead concentrations compared to those of the roadside cedars (fig. 2). It seems improbable, therefore, that the excessive metal accumulations in the roadside cedars can be attributed to mineralized or otherwise unusual water.

Residuum at the Centerville locality was shown by analysis not to be unusually enriched in lead or other metals (table 2). Moreover, residuum is widespread throughout southern Missouri, including areas where no excessive accumulations of lead in cedars have been found.

The pile of sulfide-bearing aggregate (and perhaps similar piles along highways in this part of the State) might serve as a source of metals in the local roadside environment. Clearly, however, the pile of aggregate observed at the Centerville locality could not have served as a source of metals to more than a few trees. Moreover, because of its very low lead content the aggregate pile could not have been a significant source of lead in any of the trees that were sampled.

Because it is difficult to account for the large lead accumulations in cedars and soils as results of the processes discussed, other sources of the metals must be considered. The most obvious possible source is lead ore or other lead-bearing materials that are transported by trucks on the highway. A reasonable mechanism for lead accumulation in roadside soils may be the continual escape of fine-grained particulate lead-bearing cargo from ore trucks passing by the locality. Some of the particulate matter may also be deposited directly on the surfaces of the cedar trees, but most of the lead in the trees may have been absorbed from the soil through the root systems. Attributing the roadside contamination to this source may be all the more reasonable in view of the fact that the Centerville locality lies on the shortest highway route between one of the largest (and also one of the newest) lead mining areas in the district (the Viburnum trend of Weigel, 1965, p. 77) and a lead smelter at Glover, Mo.

In conclusion, the anomalous concentrations of lead and other metals in cedar trees and soils along Highway 21–72 near Centerville are thought not to reflect the presence of mineralized ground. Rather, it seems apparent that they are part of a roadside effect. This effect on metal concentrations in natural roadside materials in Missouri is thought to consist of at least two distinct components: (1) lead accumulations attributed to automotive exhaust, and (2) lead and other metal accumula-

tions probably resulting from highway transport of lead-bearing materials. Both components greatly affect the trace-metal content of roadside vegetation, but only the second appears to have a detectable effect on roadside subsurface soils.

REFERENCES

Connor, J. J., Erdman, J. A., Sims, J. D., and Ebens, R. J., 1971, Roadside effects on trace element content of some rocks, soils, and plants in Missouri, *in* Hemphill, D. D. ed., Trace substances in environmental health, Missouri Univ. 4th Ann. Conf., Proc. [In press]

Myers, A. T., Havens, R. G., and Dunton, P. J., 1961, A spectrochemical method for the semiquantitative analysis of rocks, minerals, and ores: U.S. Geol. Survey Bull. 1084–I, p. 207–229.

Shacklette, H. T., 1965, Element content of bryophytes: U.S. Geol. Survey Bull. 1198–D, 21 p.

Shacklette, H. T., Sauer. H. I., and Miesch, A. T., 1970, Geochemical environments and cardiovascular mortality rates in Georgia: U.S. Geol. Survey Prof. Paper 574–C, 39 p.

Shacklette, H. T., Hamilton, J. C., Boerngen, J. G., and Bowles, J. M., 1971, Elemental composition of surficial materials in the conterminous United States: U.S. Geol. Survey Prof. Paper 574–D. [In press]

Turekian, K. K., and Wedepohl, K. H., 1961, Distribution of the elements in some major units of the Earth's crust: Geol. Soc. America Bull., v. 72, no. 2, p. 175–191.

Weigel, W. W., 1965, The inside story of Missouri's exploration boom, Pt. 1: Eng. and Mining Jour., v. 166, no. 11, p. 77–86, 170–172.

AGES OF SOME TERTIARY ANDESITIC AND LATITIC VOLCANIC ROCKS IN THE PRESCOTT–JEROME AREA, NORTH-CENTRAL ARIZONA

By MEDORA H. KRIEGER, S. C. CREASEY, and RICHARD F. MARVIN, Menlo Park, Calif.; Denver, Colo.

Abstract.—Three isotopic ages obtained by the potassium-argon method have shown that some volcanic rocks in the Prescott-Jerome area, north-central Arizona, are of Oligocene and Miocene age. The two older dates (23.4 and 26.7 m.y.) are from latitic flows to which the name Sullivan Buttes Latite is given. The youngest date (14.6 m.y.) is from flows at the base of the Hickey Formation and suggests that these flows are Miocene in age.

GEOLOGIC RELATIONS

Cenozoic rocks in the Prescott-Jerome area of central Arizona (fig. 1) have been considered Pliocene and Pleistocene(?) on the basis of (1) lithologic similarity to other Pliocene and Pleistocene rocks in Arizona, (2) the tentative age of vertebrate fossils found near Prescott, Ariz., and (3) the relations of the Cenozoic rocks to Basin and Range deformation and to erosion cycles (Anderson and Creasey, 1958; Lehner, 1958; Krieger, 1965, 1967). Three isotopic ages obtained by the potassium-argon method, however, have revealed volcanic rocks of Oligocene and Miocene age. The isotopic ages were determined on (1) biotite from a trachyandesite in the Hickey Formation collected from the north-central part of the Mingus Mountain quadrangle (*A–43*, fig. 1), (2) hornblende from a hornblende latite in the Sullivan Buttes Latite collected from the central part of the Paulden quadrangle (*A–44*, fig. 1), and (3) biotite from a biotite latite, also in the Sullivan Buttes Latite, collected from the southeast corner of the Paulden quadrangle (*A–45*, fig. 1). All these units are fresh flows; the minerals used for dating are unaltered. We have no reason to doubt that the isotopic ages are the cooling ages of the flows.

In the Jerome area, Anderson and Creasey (1958) separated the Hickey Formation, composed of volcanic rocks (largely basaltic) and gravels, from the Verde Formation, a sedimentary basin deposit containing minor intercalations of basalt. The Hickey Formation is older than the Basin and Range deformation, whereas the Verde Formation is younger, having accumulated in a basin formed by that deformation. In the Clarkdale quadrangle, Lehner (1958) recognized these two formations plus the Perkinsville Formation, composed of basaltic and sedimentary rocks. This formation he correlated with the Verde Formation to the extent that both are younger than the Basin and Range deformation and younger than the initiation of the present drainage system. At the time of the descriptions and correlations no diagnostic fossils had been found in these formations. The Hickey Formation, however, was assigned a Pliocene(?) age and the Verde and Perkinsville a Pliocene(?) and Pleistocene(?) age.

In her early work in the Paulden quadrangle, Krieger (1965) recognized a local stratigraphy in the Cenozoic rocks: older gravel and local patches of older basaltic rocks are separated from younger basaltic and sedimentary rocks by volcanic rocks then called andesite, but now called latites on the basis of chemical analyses (table 1, A–44 and A–45). Krieger (1967) showed that these latitic rocks extend westward into the east-central part of the Simmons quadrangle (fig. 1). It seems desirable that this important sequence of volcanic rocks be recognized by formational status; therefore this unit is here named the Sullivan Buttes Latite for the exposures in Sullivan Buttes, the type locality (fig. 1). The Sullivan Buttes Latite consists of plugs, domes, flows, breccias, agglomerate, and mudflows, and of latitic gravels related to the latitic period of eruption.

U.S. GEOL. SURVEY PROF. PAPER 750-B, PAGES B157–B160

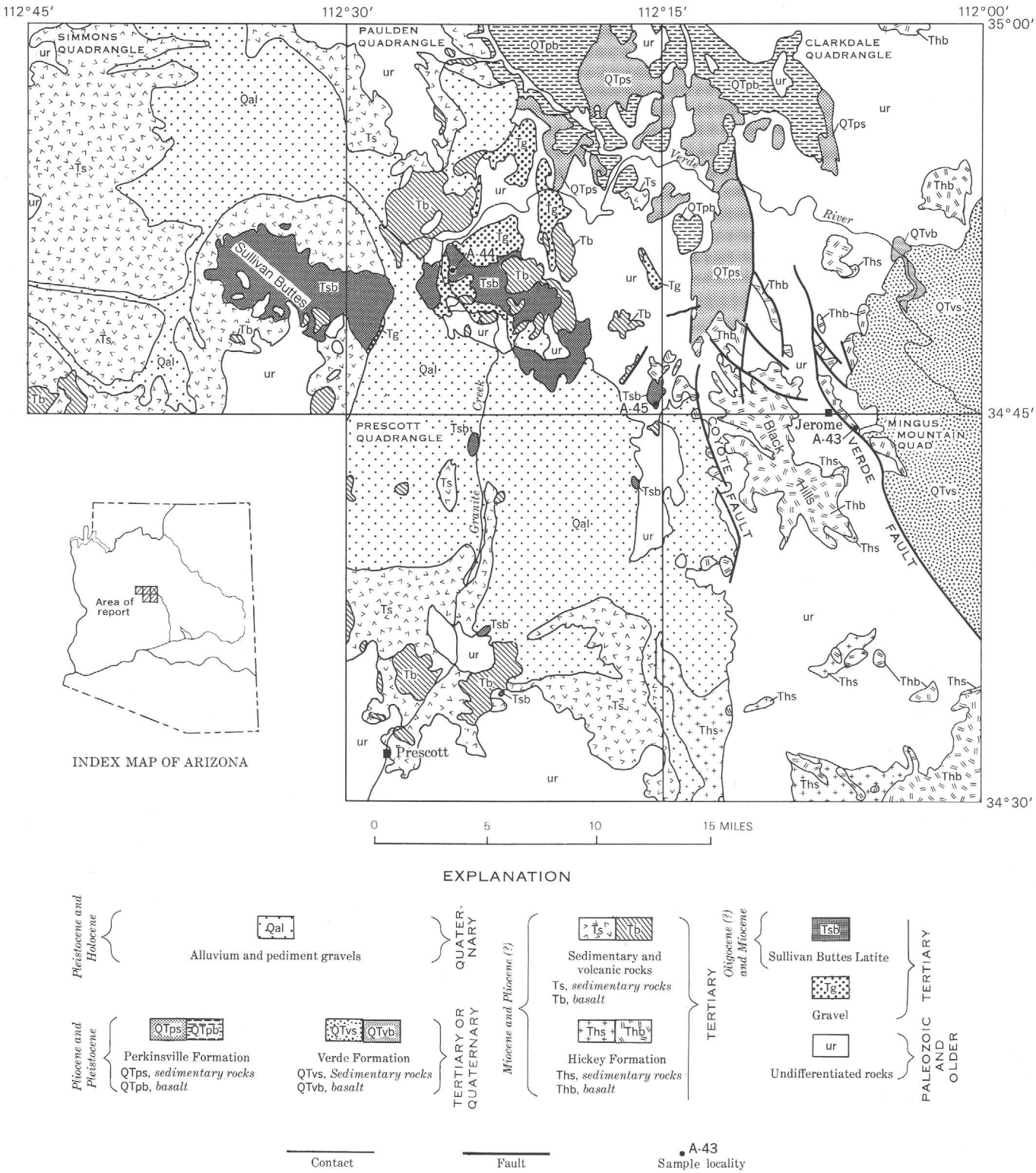

FIGURE 1.—Generalized geologic map of the Cenozoic rocks in the Prescott-Jerome area, north-central Arizona.

TABLE 1.—*Chemical analyses, in weight percent, of the three Tertiary volcanic rocks in the Prescott-Jerome area, north-central Arizona*

[Analysts: P. L. Elmore, John Glenn, Lowell Artis, James Kelsey, and H. Smith]

	A–43	A–44	A–45
SiO_2	50.1	62.0	61.3
Al_2O_3	12.6	15.6	14.0
Fe_2O_3	7.6	3.7	2.6
FeO	1.4	1.7	3.0
MgO	6.1	2.4	3.9
CaO	7.4	4.9	5.4
Na_2O	2.4	3.6	2.6
K_2O	4.3	3.5	4.2
H_2O^-	2.0	.17	.18
H_2O^+	2.1	1.0	1.4
TiO_2	1.6	.89	.89
P_2O_5	1.6	.38	.36
MnO	.17	.14	.15
CO_2	<.05	<.05	<.05

A–43, trachyandesite, Hickey Formation, Mingus Mountain quadrangle.
A–44, hornblende latite, Sullivan Buttes Latite, Paulden quadrangle.
A–45, biotite latite, Sullivan Buttes Latite, Paulden quadrangle.

In the Prescott and Paulden quadrangles, structures produced by the Basin and Range deformation are not obvious, and consequently the relations of the Cenozoic rocks to the Basin and Range structures in most places are obscure. Therefore, separation of the Cenozoic rocks into pre- and post-Basin and Range deformation was not possible at that time, and correlation with similar-appearing rocks in the Clarkdale and Jerome areas to the east was ambiguous. Geologic field relations, which are shown on figure 1, strongly suggest that some of the basalts and interbedded gravels in the Paulden quadrangle are westward continuations of rocks mapped to the east as the Hickey and Perkinsville Formations.

POTASSIUM-ARGON AGES

Three potassium-argon ages (table 2) were determined on latitic and andesitic rocks: two from the latites that separate older basalt and gravel from younger basalt and gravel in the Paulden quadrangle, and one from andesite at the base of the Hickey Formation near Jerome (fig. 1). It was originally thought that these volcanic rocks might be of the same age and therefore could be used as a marker unit in unraveling the Cenozoic stratigraphy. However, the determined ages of 14.6, 23.4, and 26.7 million years (table 2) show that the rocks are not the same age. The potassium-argon ages, however, are a start toward ordering the Cenozoic stratigraphy of north-central Arizona, although many more dates will be necessary before the stratigraphic relations of all the Cenozoic units are known.

The base of the Hickey Formation on the east side of the Black Hills is a trachyandesite flow (sample A–43, fig. 1, tables 1 and 2) of limited distribution. The rock has conspicuous biotite flakes as much as 1.5 mm in diameter and greenish prismatic pyroxene crystals as much as 0.3 mm in length that have the extinction angles of normal augite. The groundmass consists of oligoclase laths separated by granular pyroxene and black opaque minerals. Patches of weakly birefringent to isotropic colorless material may be potassium feldspar and (or) glass. Corundum crystals 0.1 mm long are accessory. We call the rock trachyandesite because Williams (Williams and others, 1954, p. 97) extended that term to include all andesites that contain more than 10 percent normative potassium feldspar, and this rock contains 26 percent normative potassium fedspar. The trachyandesite rests unconformably on Precam-

TABLE 2.—*Potassium-argon ages and analytical data for three Tertiary volcanic rocks in the Prescott-Jerome area, north-central Arizona*

[Analysts: R. F. Marvin, H. H. Mehnert, and Violet Merritt]

Formation, field number, and location (lat. N., long. W.)	Rock type, analyzed mineral	[1] K_2O (percent)	$*Ar^{40}$ (10^{-10} moles/g)	$\frac{*Ar^{40}}{\text{Total } Ar^{40}}$	$\frac{*Ar^{40}}{K^{40}}$	Age (m.y.) $\pm 2\sigma$
Hickey Formation A–43 34°44′29″, 112°06′25″.	Trachyandesite Biotite	7.20	1.556	0.61	0.000855	14.6±1.1
Sullivan Buttes Latite A–44 34°51′08″, 112°25′19″.	Latite Hornblende	1.86	.7366	.76	.00157	26.7±1.1
Sullivan Buttes Latite A–45 34°45′23″, 112°15′28″.	Latite Biotite	8.76	3.051	.84	.00138	23.4±1.0

Decay constants, K^{40}: $\lambda_\epsilon = 0.584 \times 10^{-10}$ yr^{-1}; $\lambda_\beta = 4.72 \times 10^{-10}$ yr^{-1}.
Atomic abundance: $K^{40}/K = 1.19 \times 10^{-4}$.
$*Ar^{40}$, radiogenic argon.

[1] Average of duplicate determinations.

brian rocks and marks the beginning of the accumulation of the Hickey Formation at that locality. Thus, near Jerome, the age of the base of the Hickey Formation is 14.6 m.y. (late Miocene). Potassium-argon ages of younger volcanic rocks in the formation will have to be obtained in order to determine whether any of the Hickey Formation is Pliocene.

The ages of two flows (samples A–44 and A–45, fig. 1, tables 1 and 2) in the Sullivan Buttes Latite in the southern half of the Paulden quadrangle are 26.7 m.y. (very late Oligocene or very early Miocene) and 23.4 m.y. (early Miocene), respectively. Thus the Sullivan Buttes Latite is considered very late Oligocene(?) and early Miocene. The dates are the oldest obtained from Cenozoic volcanic rocks in north-central Arizona. As these rocks locally unconformably overlie basalt and gravel, and are unconformably overlain by other basalt and gravel, they are neither the oldest nor the youngest Cenozoic rocks in the area. Whether the younger basalt is the same age as the Hickey or Perkinsville Formations, or whether its age is different from the age of both, is not known. Certainly there are no volcanic rocks in the Jerome area that are as old as the dated latites or older basalt in the Paulden quadrangle.

REFERENCES

Anderson, C. A., and Creasey, S. C., 1958, Geology and ore deposits of the Jerome area, Yavapai County, Arizona: U.S. Geol. Survey Prof. Paper 308, 185 p.

Krieger, M. H., 1965, Geology of the Prescott and Paulden quadrangles, Arizona: U.S. Geol. Survey Prof. Paper 467, 127 p.

——— 1967, Reconnaissance geologic map of the Simmons quadrangle, Yavapai County, Arizona: U.S. Geol. Survey Misc. Geol. Inv. Map I–503.

Lehner, R. E., 1958, Geology of the Clarkdale quadrangle, Arizona: U.S. Geol. Survey Bull. 1021–N, p. 511–592.

Williams, Howel, Turner, F. J., and Gilbert, C. M., 1954, Petrography—An introduction to the study of rocks in thin sections: San Francisco, Calif., W. H. Freeman and Company, 406 p.

RAPID SCANNING TECHNIQUE FOR LOW LEVELS OF CO_2 IN SILICATE ROCKS

By LEONARD SHAPIRO, Washington, D.C.

Abstract.—Carbon dioxide evolved from a 25-mg sample of pulverized rock is caught in a small bulge of a modified test tube, and its volume estimated by comparison against similarly processed standards. The method is restricted to CO_2 concentrations ranging from 0.0 to 0.1 percent and is especially applicable to most igneous rocks and silicate minerals. The standard deviation is 0.02 percent CO_2. Samples can be analyzed rapidly at the rate of 2 minutes each. The procedure is useful for screening samples containing more than 0.1 percent CO_2, where greater accuracy in analysis is warranted.

A reliable method for the determination of carbon dioxide in silicate rocks has been reported previously (Shapiro and Brannock, 1955). It is based on collecting carbon dioxide evolved with acid in a test tube with a side arm. This procedure requires 1 g of sample to obtain sufficient accuracy for the range 0–2 percent CO_2; the determination takes about 7 minutes.

Data accumulated on many thousands of samples indicate that approximately 80 percent of the silicate samples that we have analyzed contain 0.1 percent CO_2 or less. A simplified version of this method, described in this paper, was developed specifically for such samples. This simplified method will at the same time identify those samples containing more than 0.1 percent CO_2, for which more accurate methods of determination could be used.

APPARATUS AND REAGENTS

Small borosilicate test tube, 10×75 mm: Modified by addition of a bulge, made by heating the test tube over a bunsen burner flame and pressing from within with an opened paper clip with a small hook at one end, about ¾ inch (18 mm) from the bottom (fig. 1).

Small dipper: For measuring approximately 25 mg of powdered sample. Prepared by drilling a hole ⅛ inch in diameter and ⅛ inch deep into the end of a ¼-inch round brass bar.

Test tube clamp.

Desk lamp.

Hotplate.

Squeeze-type pipet: Suitable for transferring 0.1–0.2 ml of liquid.

Bunsen burner.

Wash bottle with water.

Saturated mercuric chloride solution: For use, transfer 20 ml of the saturated solution to a small beaker and add 20 ml of concentrated HCl.

Standard rock powder containing approximately 0.1 percent CO_2: Convenient standard is the granite G–1 taken as containing 0.08 percent CO_2.

PROCEDURE

At the beginning of a run, place the small beaker containing the $HgCl_2 + HCl$ on the hotplate, set to bring the solution nearly to boiling.

Transfer approximately 25 mg of the standard powder (80 mesh or finer) by dipper to the modified test tube. Add water to about ¼ inch above the bulge. Bring the contents of the test tube rapidly to a boil by passing the tube in and out of the bunsen burner flame. Holding it vertically in front of a table lamp, tap the tube gently to displace any bubbles from the bulge, then tilt the tube about 45° (bulge upward) and squirt 0.1–0.2 ml of the hot acid solution into the tube. It is important for best reproducibility that both the water solution and the acid be hot. Within a few seconds carbon dioxide bubbles will rise from the sample and accumulate in the bulge. In about 15–20 seconds nearly all of the producible carbon

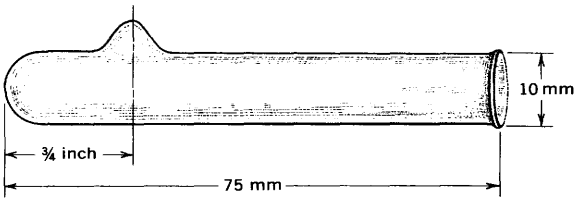

FIGURE 1.—Modified test tube used in scanning technique for low levels of carbon dioxide in silicate rocks.

U.S. GEOL. SURVEY PROF. PAPER 750-B, PAGES B161-B162

dioxide will have come off. With G–1 as the standard (0.08 percent CO_2) and 25 mg of sample the bubble of carbon dioxide should occupy about one-half the available volume. Observe the amount which then serves as the standard at 0.08 percent.

Rinse out the contents of the tube, then repeat the procedure with an unknown sample. Drying the tube is unnecessary. If a sample yields approximately the same volume of carbon dioxide as the standard, it is reported as having the same carbon dioxide content. If it yields roughly half the volume, a sample would contain 0.04 percent CO_2 (relative to the G–1). Approximations made by this rough comparison are rarely in error by more than a few hundredths of a percent.

If the volume exceeds that produced by G–1 by more than a small amount, the carbon dioxide content is too high to be accurately determined by this method; such samples should be run by the other procedures available. Rougher estimates can be made using a dipper one-tenth the size of the one described, but the results can be in error by an order of magnitude.

DISCUSSION OF RESULTS

Standard samples suitable for testing the procedure are practically unavailable. Conventional procedures on available standards have given values which vary too much for the samples to serve as good reference materials. This can be seen from a recent study (Flanagan, 1969) on six U.S. Geological Survey standards. In table 1 are presented the average carbon dioxide content and the range of values reported for each of six rock types. The table also shows values obtained by the described method on three separate occasions. It can be seen that the agreement among five of the six samples is within 0.04 percent for the average of both methods. In sample GSP–1 the discrepancy is 0.08 percent, but there is high variability in the literature value.

The discrepancy in values for sample GSP–1 was investigated by analyzing two 10-g samples using a gas-evolution method (Goldich and others, 1959). The results obtained were 0.095 and 0.097 percent, which agree better with those of the proposed method and indicate that the reported average by conventional methods is poor.

To gain a better idea of the precision of the proposed method, 10 determinations were made on GSP–1. The results ranged from 0.04 to 0.08 percent. Such a spread can be at least partly explained by variations of temperature and of manner of injection of the acid. The absolute difference is small, however, and less than that obtained by conventional procedures.

To test the usefulness of the procedure as a scanning technique, 75 samples which had been analyzed by the routine procedure described by Shapiro and Brannock (1962) were also run by the described method. All results were within 0.03 percent of the values given by the routine procedure. In the routine procedure, the determination limit is 0.05 percent CO_2; values below this are reported as <0.05 because variability in blank prevents the reporting of a more definitive value. Because with the new technique the blank is zero, values down to 0.01 become meaningful. The time required for the run of the 75 samples with the routine technique averaged 7 minutes per sample, or nearly 9 hours for the set. The new technique required an average of 2 minutes per sample, or 2.5 hours total. In this example 5 hours were saved in the analysis of 75 samples. This laboratory analyzes between two and three thousand samples each year.

It is quite clear that the objective of a rapid scan method for carbon dioxide levels of 0.1 percent and less can be achieved by the procedure described. An auxiliary advantage arises from the small sample size required. At times small specimens of minerals are available for which it is important to establish the level of carbon dioxide as a function of the freshness of the sample. With a sample size of 25 mg it becomes feasible as well as convenient to make this determination.

TABLE 1.—*Comparison of results, in percent, from conventional and proposed methods for the determination of carbon dioxide in rock samples*

Sample type	Reported values by conventional methods (Flanagan, 1969)		Values by proposed method		
	Average	Range	Run 1	Run 2	Run 3
G–2 granite	0. 08	0. 04–. 15	0. 04	0. 03	0. 04
GSP–1 granodiorite	. 15	. 06–. 33	. 07	. 06	. 08
AGV–1 andesite	. 05	. 01–. 11	. 03	. 02	. 02
PCC–1 peridotite	. 12	. 02–. 18	. 09	. 10	. 09
DTS–1 dunite	. 08	. 03–. 17	. 03	. 04	. 04
BCR–1 basalt	. 03	. 01–. 06	. 03	. 02	. 02

REFERENCES

Flanagan, F. J., 1969, U.S. Geological Survey standards—II. First compilation of data for the new USGS rocks: Geochim. et Cosmochim. Acta, v. 33, p. 81–120.

Goldich, S. S., Ingamells, C. O., and Thaemlitz, Doris, 1959, The Chemical composition of Minnesota lake marl—comparison of rapid and conventional chemical methods: Econ. Geology, v. 54, p. 285–300.

Shapiro, Leonard, and Brannock, W. W., 1955, Rapid determination of CO_2 in silicate rocks: Anal. Chemistry, v. 27, p. 1796–1797.

———1962, Rapid analysis of silicate, carbonate, and phosphate rocks: U.S. Geol. Survey Bull. 1144–A, 56 p.

DETERMINATION OF SULFUR IN PYRITIC ROCKS BY A SINGLE PRECIPITATION OF BARIUM SULFATE AFTER NITRATE FUSION

By LAURA E. REICHEN, Washington, D.C.

Abstract.—Sulfur in pyritic rocks is determined gravimetrically by a single precipitation of barium sulfate. After sodium carbonate–potassium nitrate fusion, the addition of hydroxylamine hydrochloride to the acidified filtrate destroys nitrate and prevents its occlusion. The precipitate thus obtained is sufficiently pure to require no reprecipitation.

Total sulfur in pyritic rocks is commonly determined by fusing the sample with a sodium carbonate–potassium nitrate flux, leaching the cake with water, and precipitating barium sulfate from the acidified filtrate. The precipitate thus obtained is impure and strongly contaminated with nitrate, requiring that a second precipitation of barium sulfate be made following a second fusion with sodium carbonate alone. This paper presents a procedure which avoids the occlusion of the nitrate and gives satisfactory results with only one precipitation of barium sulfate.

The fact that nitrate causes difficulties in the determination of barium sulfate is well known (Kolthoff and Elving, 1961, p. 61; Hillebrand and others, 1953, p. 717; Kolthoff and Sandell, 1952, p. 322–331). Maxwell in his new book on rock and mineral analysis (1968, p. 441) avoids the problem of nitrate by using a sodium carbonate–sodium peroxide flux for silicates. In the procedure to be described, nitrate is destroyed with hydroxylamine hydrochloride prior to the precipitation of barium sulfate.

REAGENTS

Flux: Na_2CO_3–KNO_3, 9 to 1.

Hydroxylamine hydrochloride: 5 g dissolved in 25 ml of water.

Barium chloride solution: 10 percent w/v.

PROCEDURE

Add 5 g of flux to an accurately weighed sample containing not more than 0.100 g sulfur in a platinum crucible. Fuse as usual (Hillebrand and others, 1953, p. 848), but continue the fusion until most of the nitrate has been decomposed, indicated by a thickening of the liquid to the same consistency as if only sodium carbonate had been used.

Leach the melt overnight on the steam bath and filter into a 400-ml beaker. Neutralize the solution with hydrochloric acid and add a few drops in excess.

Heat the solution on a hotplate and continue heating gently until most of the carbon dioxide has been expelled. Add more hydrochloric acid, if necessary, to maintain acidity. Add the solution of hydroxylamine hydrochloride and boil for one minute.

Precipitate the barium sulfate as usual with 10 ml of $BaCl_2$ (Hillebrand and others, 1953, p. 720); then fill the beaker to capacity with hot water so that the hydroxylamine is as dilute as possible. Let stand overnight.

Filter off the barium sulfate, burn off the filter paper, and treat the precipitate with hydrofluoric acid; ignite the precipitate, and weigh as barium sulfate.

RESULTS AND DISCUSSION

The seriousness of the nitrate contamination is demonstrated by the first four samples in table 1. These rocks contained a major percentage of pyrite and were analyzed for total sulfur. In the double precipitation of barium sulfate, the first precipitate was weighed (column 2) before making the second precipitation (column 4). The least contaminated had an error of 0.0009 g of sulfur, and the most 0.0013 g of sulfur.

U.S. GEOL. SURVEY PROF. PAPER 750–B, PAGES B163–B164

The possibility of destroying nitrate with hydroxylamine hydrochloride was explored. It was found that 5 g added in solution to the acidified filtrate, followed by boiling, destroyed the nitrate. In table 1, the values for sulfur in column 3 were obtained from a single precipitation according to the new procedure outlined; results obtained on reprecipitation are shown in column 4. In all samples the appearance of the white precipitate from the hydroxylamine solution was satisfactory in that there were no stains present which are characteristic of nitrate contamination.

Next, it was necessary to know if hydroxylamine hydrochloride would have any adverse affect on the precipitation of barium sulfate. Again the pyritic rocks were used as well as standardized sodium sulfate (table 2). The "taken" sulfur values for the rock samples were obtained by a sodium carbonate–potassium nitrate fusion and double precipitation of the barium sulfate. The close agreement of the sulfur found with the sulfur taken shows that quantitative determination of barium sulfate was made in the presence of 5 g of hydroxylamine hydrochloride in 400 ml of solution. However, using more than 5 g of hydroxylamine is not recommended, since a greater amount tends to retard the precipitation of barium sulfate.

In conclusion, sulfur is determined satisfactorily by a single precipitation of barium sulfate after the nitrate from the fusion has been destroyed by hydroxylamine hydrochloride. This single precipitation greatly shortens the time required to determine sulfur over that required when the purification of barium sulfate is done by fusion and reprecipitation.

TABLE 1.—*Sulfur, in grams, obtained under various conditions of precipitation*

Rock sample (0.2000 g)	First precipitation, no hydroxylamine	First precipitation, 5 g of hydroxylamine	Second precipitation, no hydroxylamine	Difference
1	0. 0521		0. 0512	+0. 0009
2	. 0942		. 0932	+. 0010
3	. 0958		. 0947	+. 0011
4a	. 0797		. 0784	+. 0013
4b		0. 0788	. 0788	. 0000
5		. 0321	. 0323	−. 0002
6		. 0558	. 0555	+. 0003
7		. 0595	. 0593	+. 0002
8		. 0856	. 0860	−. 0004
9		. 0932	. 0931	+. 0001
10		. 0992	. 0994	−. 0002

TABLE 2.—*Precipitation of barium sulfate in a 400-ml solution containing 5 g of hydroxylamine hydrochloride*

Source of sulfur	Sulfur (grams)	
	Taken	Found
Sodium sulfate	0. 0321	0. 0322
Do	. 0640	. 0640
Rock	[1] . 0784	. 0788
Do	[1] . 0897	. 0899

[1] Determined by sodium carbonate-potassium nitrate fusion of sample and double precipitation of barium sulfate.

REFERENCES

Hillebrand, W. F., Lundell, G. E. F., Bright, H. A., and Hoffman, J. I., 1953, Applied inorganic analysis, 2d ed: New York, John Wiley & Sons, Inc., 1034 p.

Kolthoff, I. M., and Elving, P. J., 1961. Treatise on analytical chemistry, pt. II, v. 7: New York, Interscience Publishers, 567 p.

Kolthoff, I. M., and Sandell, E. B., 1952, Textbook of quantitative inorganic analysis, 3d ed.: New York, The Macmillan Company, 759 p.

Maxwell, J. A., 1968, Rock and mineral analysis: New York, Interscience Publishers, 584 p.

CHEMICAL ANALYSIS OF SPHENE—SPECTROPHOTOMETRIC DETERMINATION OF SILICON, ALUMINUM, TITANIUM, TOTAL IRON, AND PHOSPHORUS

By ROBERT MEYROWITZ, Washington, D.C.

Abstract.—Silicon, titanium, total iron, and phosphorus are directly determined spectrophotometrically in sphene, using molybdenum blue, hydrogen peroxide, 1,10-phenanthroline, and heteropoly blue procedures, respectively. Aluminum is determined spectrophotometrically with pyrocatechol violet after separating titanium and iron by precipitation using cupferron.

Relatively few complete chemical analyses of sphenes (titanites) and other titaniferous silicate minerals have been published. Papers concerned with the chemistry of sphenes and other titaniferous minerals either contain no description of analytical methods or have very vague outlines (Bellanca, 1942, p. 213; Sahama, 1946, p. 92; Kauffman and Jaffe, 1946, p. 586; Konta, 1949, p. 3–4; Takubo and Nishimura, 1953, p. 325; Omori and Hasegawa, 1956, p. 141).

Sphene is for the most part a calcium titanium silicate and may also contain hydrogen as hydroxyl, fluorine, chlorine, sodium, potassium, rare earth elements, yttrium, scandium, manganese, thorium, uranium, strontium, barium, aluminum, iron, magnesium, niobium, tantalum, vanadium, chromium, zirconium, and phosphorus. This paper describing microprocedures and semimicroprocedures is the first in a series which, on completion, will provide the schematics for the complete chemical analysis of small samples of sphene. The procedures described herein are based on methods in use at the U.S. Geological Survey for the analysis of small samples of minerals.

PREPARATION OF SAMPLE SOLUTION, 1.2*N* PERCHLORIC ACID, FOR THE DETERMINATION OF TiO_2, TOTAL IRON, AND P_2O_5.

Reagents and apparatus

Perchloric acid, $HClO_4$, 6*N*.
Hydrofluoric acid, HF, concentrated.
Nitric acid, HNO_3, 8*N*.
Dish, evaporating, platinum, 35-ml.
Stirring rod, Teflon; ⅛ in.×68–70 mm.
Dish, petri; 55×14 mm.
Funnel, filter, plastic; 40 mm wide, 80 mm long, with 7-mm tip.
Tongs, platinum-tipped, Blair-form.
Cylinders, glass; 48-mm outside diameter and 20–22-mm height. These are used to support the 35-ml platinum dish in the hot-air bath.
Hotplate, thermostatically controlled.
Surface temperature thermometer, 0°–540°C.

Procedure

1. Weigh duplicate 40- to 50-mg ($\pm$0.1 mg) < 200-mesh samples in a 35-ml platinum evaporating dish. Two other dishes serve for the preparation of procedural blanks.
2. Moisten the sample with a few drops of water. Add 4.0 ml of 6*N* $HClO_4$. Add dropwise (using a plastic pipet) 4.0 ml of concentrated HF. If organic matter is present, add 1.0 ml of 8*N* HNO_3. Mix, using a small Teflon stirring rod. The Teflon rod remains in the dish. Digest in a hot-air bath. Evaporate to the first appearance of perchloric acid fumes. Cool. Add 4.0 ml of 6*N* $HClO_4$.
3. Cool. Rinse down the inside surface of the dish. Evaporate the solution in the hot-air bath until the first appearance of perchloric acid fumes. Place the evaporating dish in one-half of a petri dish and place on a hotplate whose surface temperature is approximately 250°C. Fume strongly.
4. Repeat step 3.
5. Cool. Add 1 ml of water dropwise to the dish and mix. Rinse down the inside surface of the dish, adding sufficient water to dissolve all salts on warming and subsequent cooling. Stir and transfer, using a plastic filter funnel, to a 100-ml volumetric flask.
6. Add 12.0 ml of 6*N* $HClO_4$ to the flask. Cool to room temperature, dilute to volume, mix, and transfer the solution to a dry plastic bottle.

U.S. GEOL. SURVEY PROF. PAPER 750–B, PAGES B165–B170

Discussion

The author prefers to use a hot-air bath, formed by supporting the platinum dishes on glass cylinders resting on the hotplate, instead of using a steam bath. The air temperature is varied by changing the temperature of the hotplate and (or) the height of the glass cylinders. Blair-form rather than straight platinum-tipped tongs are used to handle the platinum dishes to prevent contamination and possible loss of the sample if the tips become wet with the solution in the dish.

Duplicate samples should differ in weight by 10–20 percent. This variation provides a built-in quality control for the reliability of the analysis. If the slope of the standard curve of a spectrophotometric procedure is not correct, the two results for a given constituent will not agree when the amounts of the constituent differ by 10–20 percent.

The 1.2*N* $HClO_4$ solution of the sphene can be used for the determination of calcium, magnesium, sodium, potassium, and manganese.

SPECTROPHOTOMETRIC DETERMINATION OF TiO_2, USING HYDROGEN PEROXIDE

Reagents and apparatus

Sulfuric acid, H_2SO_4, 10*N*.

Hydrogen peroxide, H_2O_2, 3-percent (v/v). Prepare fresh daily from 30-percent H_2O_2.

Titanium solution, 1,000-ppm TiO_2, approximately 1.8*N* H_2SO_4. Prepare using U.S. National Bureau of Standards standard titanium dioxide No. 154a. Follow directions in "Procedure for Use as a Standard in Colorimetry" as given in the certificate of analysis provided with the standard.

Titanium solution, 100-ppm TiO_2, approximately 0.18N H_2SO_4.

Spectrophotometer.

Cells, absorption, 2-cm light path.

Procedure

1. Transfer duplicate 5.00-ml aliquots from each of the 1.2*N* $HClO_4$ solutions of the procedural blanks and the samples to 50-ml volumetric flasks. Rinse down the necks of the flasks. Add 9.4 ml of 10*N* H_2SO_4.
2. Transfer aliquots of 0.00, 5.00, 7.00, 8.00, 9.00, 10.00 and 15.00 ml of 1-ppm TiO_2 solution to 50-ml volumetric flasks. Add 10.0 ml of 10*N* H_2SO_4 to the first two flasks, 9.8 ml to the next four flasks, and 9.7 ml to the last flask.
3. Rinse down the necks of all flasks. Dilute to approximately 40 ml and mix. Add 3.0 ml of 3-percent H_2O_2. Mix and dilute to volume.
4. Determine the absorbances at 410 mμ in 2-cm cells, using water as the reference solution.
5. Subtract the absorbance of the appropriate procedural blanks from the absorbance of the standard and the unknown solutions to obtain the net absorbance.
6. Plot a standard TiO_2 curve from the data of the standard solutions.
7. Calculate the TiO_2 content of the unknowns from the standard curve.

Discussion

In a 2*N* H_2SO_4 and 0.18-percent H_2O_2 (v/v) solution, 5.0 ppm Fe_2O_3 (Fe^{3+}), 2.0 ppm V_2O_5, 2.0 ppm UO_3, 2.0 ppm Ce_2O_3, 2.0 ppm Cr_2O_3 (Cr^{3+}), 2.0 ppm Nb_2O_5, and 2.0 ppm Nb_2O_5 plus 2.0 ppm Fe_2O_3 (Fe^{3+}) do not interfere in the hydrogen peroxide procedure for the determination of titanium dioxide as described above. These observations can be expressed in another way. If the aliquot of solution analyzed for titanium dioxide is equivalent to 2.5 mg of sample, then 10 percent of Fe_2O_3 (total iron) and 4 percent each of the other oxides mentioned do not interfere. The concentrations of these elements usually found in sphene are less than those tested. All the flasks contain approximately 100 meq (milliequivalents) of H^+ before the addition of the hydrogen peroxide.

SPECTROPHOTOMETRIC DETERMINATION OF TOTAL IRON, USING 1,10-PHENANTHROLINE

Reagents and apparatus

Perchloric acid, $HClO_4$, 1.2*N*.

Iron solution, 1,000-ppm Fe_2O_3, 0.12*N* $HClO_4$. Dissolve 4.9112 g of ferrous ammonium sulfate hexahydrate, $Fe(NH_4)_2(SO_4)_2 \cdot 6H_2O$ in distilled water, add 20.0 ml of 6*N* $HClO_4$, and dilute to 1 liter.

Iron solutions containing 80.0, 8.00, and 2.00 ppm Fe_2O_3 in 1.2*N* $HClO_4$, prepared by appropriate dilutions.

Hydroxylamine hydrochloride, $NH_2OH \cdot HCl$, 10-percent (w/v). Prepare 250 ml. Filter through a fast paper.

1,10-phenanthroline, 0.25-percent (w/v). Prepare 250 ml of solution in the cold, using a magnetic stirrer to dissolve the reagent. Filter through a fast paper.

Sodium citrate, $Na_3C_6H_5O_7 \cdot 2H_2O$, 20-percent (w/v). Prepare 250 ml of solution. Filter through a fast paper.

Sodium acetate, $NaC_2H_3O_2 \cdot 3H_2O$, 25-percent (w/v). Prepare 500 ml of solution. Filter through a fast paper.

Cells, absorption, 2-cm and 5-cm light path.

Procedure

1. Transfer duplicate 5.00-ml aliquots of the 1.2*N* $HClO_4$ solutions of the procedural blanks and samples to 25-ml volumetric flasks. Rinse down the necks of the flasks with a small portion of water. Add 2.0 ml of 1.2*N* $HClO_4$.
2. Transfer aliquots of 0.00, 3.00, 4.00, 5.00, 6.00, and 7.00 ml of 8.00-ppm Fe_2O_3 solution to 25-ml volumetric flasks. For the range 0.1–0.8 percent Fe_2O_3 use the 2.00-ppm Fe_2O_3 solution. Rinse down the necks of the flasks with a small portion of water. Add in turn 7.0, 4.0, 3.0, 2.0, 1.0, and 0.0 ml of 1.2*N* $HClO_4$.

3. Add 2.0 ml of hydroxylamine hydrochloride, 2.0 ml of 1,10-phenanthroline, 1.5 ml of sodium citrate, and 6.0 ml of sodium acetate solution. Rinse down the necks of the flasks, dilute to mark, mix and let stand for 60 minutes.
4. Determine the absorbances at 510 mμ in 2-cm cells for the range 0.8–2.4 percent Fe_2O_3 and in 5-cm cells for the range 0.1–0.8 percent Fe_2O_3, using water as the reference solution.
5. Measure the pH of all final solutions.
6. Subtract the absorbance of the appropriate procedural blanks from the absorbance of the standard and unknown solutions to obtain the net absorbance.
7. Plot a standard Fe_2O_3 curve from the data of the standard solutions.
8. Calculate the Fe_2O_3 content of the unknown from the standard curve.

Discussion

Titanium interferes by precipitation in the spectrophotometric determination of iron when 1,10-phenanthroline is used in acetate medium. Norwitz and Codell (1954, p. 350) prevented its precipitation by the addition of ammonium tartrate. Hibbits, Davis, and Menke (1961, p. 163) prevented the precipitation of titanium by the addition of citric acid before the adjustment of pH to 4.0±0.1 by the addition of a solution of sodium hydroxide. The procedure described in this paper does not require the adjustment of pH by the addition of a base. The amount of acid present in the solution must contain the equivalent of 7.0 ml of 1.2*N* H^+ before the addition of the hydroxylamine hydrochloride reagent. The pH of the final solutions will range from 4.0 to 4.3. If this pH is not obtained, check the solutions used and repeat the determination. At this pH in the presence of citric acid, 100 ppm of TiO_2 and 4 ppm of Cr_2O_3, UO_3, V_2O_5, ThO_2, ZrO_2, and Nb_2O_5 do not interfere. The concentrations of these elements usually found in sphene are less than those tested. This procedure should be useful in the determination of trace amounts of iron in rutile and anatase.

SPECTROPHOTOMETRIC DETERMINATION OF P_2O_5, USING THE HETEROPOLY BLUE METHOD

Reagents and apparatus

Sulfuric acid, H_2SO_4, 1.2*N*.

Sulfuric acid, 10*N*.

Ammonium paramolybdate, $(NH_4)_6Mo_7O_{24}\cdot 4H_2O$, 2.25-percent (w/v) in 10*N* H_2SO_4.

Dissolve 5.63 g of $(NH_4)_6Mo_7O_{24}\cdot 4H_2O$ in 10*N* H_2SO_4 and dilute to 250 ml with 10*N* H_2SO_4. Filter through a slow paper and store in glass.

Hydrazine sulfate, $N_2H_4\cdot H_2SO_4$, 0.15-percent (w/v).

Prepare 250 ml. Filter through a medium paper.

Phosphorus solution, 1,000-ppm P_2O_5. One liter of solution contains 1.917 g of U.S. National Bureau of Standards standard potassium dihydrogen phosphate, KH_2PO_4, or equivalent, dried at 120°C for 2 hours.

Phosphorus solution, 100-ppm P_2O_5.

Phosphorus solution, 1.00-ppm P_2O_5.

Hot-water bath. This is made of a borosilicate crystallizing dish, 190×100 mm, and 6 small water-bath thermometer clamps (overall length, 3½ inches). The rim of the dish is covered with a small piece of slit rubber tubing before the clamp is attached. The dish is supported on an iron tripod and heated by a Meker-type gas burner.

Procedure

1. Transfer duplicate 5.00-ml aliquots from each of the 1.2*N* $HClO_4$ solutions of the procedural blanks and the unknown sample to 50-ml flasks. Rinse down the necks of the flasks. Add 5.0 ml of 1.2*N* H_2SO_4.
2. Transfer 0.00, 2.00, 4.00, 6.00, 8.00, and 10.00 ml of 1.00-ppm P_2O_5 to 50-ml volumetric flasks. Add 10.0 ml of 1.2*N* H_2SO_4 to each of these flasks.
3. Rinse down the necks of all flasks and mix. Add 4.0 ml of ammonium paramolybdate solution, rinse down the necks of the flasks, and mix.
4. Add 2.0 ml of hydrazine sulfate solution, rinse down the necks of the flasks, mix, and dilute with water to approximately 45 ml (there should be a small vacant space below the neck of the flask). Mix.
5. Place the flasks in a boiling hot-water bath for 10 minutes.
6. Cool rapidly in a cold-water bath containing ice until the flask is at room temperature. Dilute to volume and mix well.
7. Determine the absorbances at 830 mμ in 5-cm cells using water as the reference solution.
8. Subtract the absorbance of the appropriate procedural blanks from the absorbance of the standard and the unknown solutions to obtain the net absorbance.
9. Plot a standard P_2O_5 curve from the data of the standard solutions.
10. Calculate the P_2O_5 content of the unknowns from the standard curve.

Discussion

This method is virtually the heteropoly blue procedure described by Boltz (1958, p. 32–35). The amount of acid present in the solutions must be 12 meq of H^+ before the addition of the ammonium paramolybdate reagent. The final acidity is 1*N* with respect to perchloric and (or) sulfuric acid. The 4.0 ml of ammonium paramolybdate solution used here is equivalent (molybdenum content) to 5.0 ml of the Boltz 2.5-percent sodium molybdate solution.

Two ppm each of UO_3, V_2O_5, ZrO_2, Nb_2O_5, CrO_3, ThO_2, Ce_2O_3, La_2O_3, Y_2O_3, and Nd_2O_3 do not interfere.

Neither Boltz and Mellon (1947, p. 875) nor Boltz (1958, p. 32–33) mention the effect of titanium. Codell

and Mikula (1953, p. 1445) added phosphorus-free titanium to the standard phosphorus solutions used to prepare the calibration curve for their procedure for the determination of phosphorus in titanium alloys. However, their reductant is stannous chloride. Guyon and Mellon (1962, p. 873–875) used reduced molybdotitanic acid for the spectrophotometric determination of titanium with stannous chloride as reducing reagent. Similarly, Reznik and Vorotyagina (1968) used the reduced titanium-molybdenum complex to determine titanium with ascorbic acid as the reducing agent.

Titanium does not interfere in the Boltz heteropoly blue procedure. Because U.S. National Bureau of Standards titanium dioxide (No. 154 and No. 154a) contains determinable amounts of phosphorus, it could not be used in the experiments described below. L. Paul Greenland, U.S. Geological Survey, determined the phosphorus content of two different lots of pure titanium dioxide by neutron activation analysis and found one of them to contain less than 0.01 percent P_2O_5. This was confirmed by determining the phosphorus pentoxide content by the above procedure. The titanium dioxide was dissolved by boiling with sulfuric acid and ammonium sulfate. The absorbances of a reagent blank, a procedural blank for the preparation of the titanium dioxide solution, and the titanium dioxide solution containing 10,000 μg of TiO_2 were 0.008, 0.010, and 0.010 absorbance units, respectively, with water as the reference solution. Therefore, it is possible to determine directly the phosphorus content not only of sphene but also of rutile, using the Boltz heterpoly blue procedure.

SPECTROPHOTOMETRIC DETERMINATION OF SiO_2, USING THE MOLYBDENUM BLUE PROCEDURE

The silicon dioxide content of a 3- to 5-mg sample is determined by a molybdenum blue procedure using 1-amino-2-naphthol-4-sulfonic acid as the reducing agent (Meyrowitz, 1969). The sample is decomposed by sodium hydroxide fusion in a gold crucible, and a hydrochloric acid solution of the melt is used for the determination.

PREPARATION OF SAMPLE SOLUTION FOR THE DETERMINATION OF ALUMINUM

Reagents and apparatus

Sulfuric acid, H_2SO_4 (1+1).
Nitric acid, HNO_3, concentrated.
Hydrochloric acid, HCl, 1.2*N*.
Filter-paper pulp.
Cupferron solution, 6-percent (w/v). Prepare 100 ml. Store in the cold. One ml of solution is equivalent to approximately 10 mg of Fe_2O_3 or approximately 8 mg of TiO_2.
Cupferron-H_2SO_4 wash solution. Prepare when needed and store in the cold. Two hundred and fifty ml contains 7.5 ml of 6-percent cupferron (cold) plus 50.0 ml of (1+3) H_2SO_4 (cold).
Beakers, Vycor or quartz, 250-ml.

Procedure

1. Weigh duplicate 40- to 50-mg ($\pm$0.1 mg) <200-mesh samples in a 35-ml platinum evaporating dish. Two other dishes serve for the preparation of procedural blanks.
2. Moisten the sample with a few drops of water. Add 4.0 ml of (1+1) H_2SO_4. Add dropwise (using a plastic pipet) 4.0 ml of concentrated HF. Digest on a steam bath or in a hot-air bath. Evaporate to fumes of sulfuric acid.
3. Cool. Rinse down the inside surface of the dish, evaporate to fumes of sulfuric acid. Place the evaporating dish in one-half of a petri dish on a hotplate whose surface temperature is approximately 270° C. Fume strongly.
4. Repeat Step 3.
5. Cool. Add 1 ml of water dropwise to the dish and mix. Rinse down inside surface of the dish, adding sufficient water to dissolve all salts on warming and subsequent cooling.
6. Transfer the sulfuric acid solution to a 100-ml borosilicate beaker. Add 60 ml of (1+1) H_2SO_4, dilute to 50 ml, and mix well.
7. Cool in an ice bath the (a) sample solution, (b) blank, (c) 6-percent cupferron solution, and (d) cupferron-H_2SO_4 wash solution.
8. Place the sample solution beaker in an ice bath. Add 2.5 ml of cold 6-percent cupferron solution dropwise with constant stirring. Let the precipitate settle. Add a drop of cupferron solution to the supernatant liquid. The appearance of a fine white precipitate which dissolves on stirring indicates the presence of excess cupferron.
9. Add 1 ml excess of 6-percent cupferron, stir, and let stand in an ice bath for 3 to 5 minutes. Add a small amount of filter-paper pulp and stir.
10. Filter through an 11-cm medium filter paper into a 250-ml Vycor or quartz beaker. Test the filtrate for complete precipitation, using a few drops of 6-percent cupferron solution.
11. Wash the precipitate with cold cupferron-H_2SO_4 wash solution. Discard precipitate.
12. Evaporate the filtrates to approximately 50 ml. Add 25 ml of concentrated HNO_3 and cover with a watch glass. Place in a hot-air bath or on a low-temperature hotplate. As the decomposition of the cupferron proceeds, effervescence will take place. Watch carefully. If effervescence is rapid, remove

the beaker from the hot-air bath or from the hotplate; when it ceases, resume heating.

13. Evaporate to approximately 50 ml, and raise the temperature of the hotplate to 200° C. Place the beaker on the hotplate and evaporate to a small volume. Cool. Rinse the watch glass into the beaker, using water. Rinse down the inside surface of the beaker.
14. With the beaker uncovered, heat until most of the nitric acid has been evaporated. Cover the beaker with a watch glass and evaporate to fumes of sulfuric acid. Raise the temperature of the hotplate to 250° C. Remove the beaker from the hotplate and cool.
15. Add dropwise a small amount of water through the lip of the beaker while swirling it. Rinse the watch glass into the beaker and rinse down the inside surface of the beaker. Cover with the watch glass, evaporate the water, and fume for 5 minutes. The procedural blanks will require additional concentrated nitric acid to completely decompose the cupferron.
16. Cool. Add dropwise a small amount of water through the lip of the beaker, swirling the beaker. Add 5 ml of concentrated HNO_3.
17. Evaporate to fumes of sulfuric acid twice as directed in steps 13, 14, and 15, except omit the addition of nitric acid.
18. Filter through a fast filter paper into a 100-ml volumetric flask. Wash the silica precipitate with water. Dilute to approximately 80 ml. Cool to room temperature, dilute to volume, and mix. Discard precipitate.

Discussion

There are no gravimetric, titrimetric, or spectrophotometric procedures for the determination of aluminum in the presence of large amounts of titanium. The determination of aluminum by classical "wet" chemical procedures is usually by difference, an intrinsically unreliable approach which, in the case of sphene (titanite) and other high-titanium silicate minerals, is even more unreliable because of the usual low concentrations of aluminum. Frequently titanium is removed before the determination of aluminum. The method for separation of titanium from aluminum adopted by the author is the time-tested precipitation of titanium as the cupferrate.

Titanium, iron, niobium, tantalum, vanadium, and zirconium are completely precipitated by cupferron from (1+9) H_2SO_4 solution; rare earths and thorium are partially precipitated (Cheng, 1961, p. 128). The amounts of rare earths, thorium, yttrium, scandium, manganese, uranium, and chromium left in solution (considering the size of sample and usual concentrations in the sample) do not interfere with the spectrophotometric determination of aluminum, using pyrocatechol violet (Meyrowitz, 1970).

SPECTROPHOTOMETRIC DETERMINATION OF ALUMINUM, USING PYROCATECHOL VIOLET

Reagents and apparatus

Perchloric acid, $HClO_4$, 0.12*N*

Perchloric acid, $HClO_4$, 0.06*N*

Mercaptoacetic acid, 4-percent (v/v). Prepare fresh daily.

Pyrocatechol violet, 0.03-percent (w/v). Prepare 500 ml, filter through a slow paper, and store in glass. Discard after 5 days.

Ammonium acetate, 50-percent (w/v). Prepare 1,000 ml, filter through a fast paper, and store in glass.

Aluminum solution, 1,000-ppm Al_2O_3; 0.6*N* HCl. One liter of solution contains 4.730 g of $AlCl_3 \cdot 6\ H_2O$ plus 100 ml of 6*N* HCl. Standardize gravimetrically using 8-quinolinol.

Aluminum solution, 100-ppm Al_2O_3, 0.06*N* HCl.

Aluminum solution, 5.00-ppm Al_2O_3, 0.06*N* H^+. Two hundred ml of solution contains 10.00 ml of 100-ppm Al_2O_3, 0.06*N* HCl plus 1.9 ml of 6*N* $HClO_4$.

Cells, absorption, 1-cm light path.

Dish, evaporating, platinum, 25-ml.

Procedure

1. Transfer duplicate 10.00-ml aliquots of the 100-ml cupferron filtrate solutions and blanks to 25-ml platinum evaporating dishes.
2. Evaporate to almost dryness using a hotplate, the surface temperature of which is approximately 110°C.
3. Raise the temperature of the hotplate to approximately 220°C. When fumes of sulfuric acid appear, raise the temperature to 270°C and heat until all of the sulfuric acid has been removed.
4. Cool. Add 7.0 ml of 0.12*N* $HClO_4$. Warm in a hot-air bath to dissolve salts. Wash the inside surface of the dish with the solution by inclining the dish while rotating it.
5. Add 5.0 ml of water. Warm in an air bath. Mix and transfer the solution to a 100-ml volumetric flask, using water. Cool.
6. Transfer aliquots of 0.00, 5.00, 6.00, 7.00, 8.00, 9.00, and 10.00 ml of 5.00-ppm Al_2O_3, 0.06*N* H^+ to 100-ml volumetric flasks. Rinse down the necks of the flasks and add respectively 14.0, 9.0, 8.0, 7.0, 6.0, 5.0, and 4.0 ml of 0.06*N* $HClO_4$ to each of the flasks. All the flasks contain 0.84 meq of H^+.
7. Add 5.0 ml of mercaptoacetic acid solution to all flasks, rinse down the necks of the flasks, and mix. Allow to stand for 10 minutes.
8. Add 10.00 ml of pyrocatechol violet solution with a transfer pipet. Allow to stand for 10 minutes.

9. Dilute with water to approximately 80 ml and add 10.0 ml of ammonium acetate solution while swirling the flask.
10. Dilute to mark, mix, and allow to stand for 60 minutes.
11. Determine the absorbances at 580 mμ, using a 1-cm cell path. Use water as the reference solution.
12. Subtract the absorbance of the appropriate procedural blanks from the absorbance of the standard and the unknown solutions to obtain the net absorbance.
13. Plot a standard Al_2O_3 curve from the data of the standard solutions.
14. Calculate the Al_2O_3 content of the unknowns from the standard curve.

Discussion

The aluminum content of sphene ranges from less than 0.1 percent Al_2O_3 to as much as 10 percent. The semiquantitative spectrographic analysis of the mineral provides a guide for determining the volume of the aliquot of sample solution to be taken for the aluminum determination. Beer's law is obeyed from 0.2 to 0.8 ppm of Al_2O_3. For a 50 mg sample, 40.00 ml of the sample solution is used when the Al_2O_3 content is 0.1 to 0.4 percent, 10.00 ml when it is 0.4 to 1.5 percent, and 5.00 ml when it is 0.8 to 3.2 percent. If the aluminum oxide content is higher than 3.2 percent, a proper dilution is made so that at least a 5.00-ml aliquot of solution is taken for analysis.

The absorbances of the solutions in the same set (procedural blanks, reagent blank, standards, and unknown) are measured in the same order in which the solutions were prepared to insure that the standing time for all is approximately the same. The amount of acid present in the solutions must be 0.84 meq of H^+ before the addition of the mercaptoacetic acid reagent. The pH of the final solution should be 6.0, but may be within the range of 5.9 to 6.2. However, samples and standards within a set should not differ by more than 0.1 pH unit. If this pH range is not obtained, check the solutions used and repeat the determination.

REFERENCES

Bellanca, Angelo, 1942, Sulla titanite di Isernia (Campobaso) e sulla costituzione chimica delle titaniti in genere: Period. Mineralogia, v. 13, p. 209–217.

Boltz, D. F., 1958, Colorimetric determination of nonmetals: New York, Interscience Publishers, Inc., 372 p.

Boltz, D. F., and Mellon, M. G., 1947, Determination of phosphorus, germanium, silicon, and arsenic by the heteropoly blue method: Anal. Chemistry, v. 19, p. 873–877.

Cheng, K. L., 1961, Cupferron precipitation of the elements: Chemist-Analyst, v. 50, p. 126, 128.

Codell, Maurice, and Mikula, J. J., 1953, Determination of phosphorus in titanium alloys: Anal. Chemistry, v. 25, p. 1444–1446.

Guyon, J. C., and Mellon, M. G., 1962, Spectrophotometric determination of titanium as reduced molybdotitanic acid: Anal. Chemistry, v. 34, p. 856–859.

Hibbits, J. O., Davis, W. F., and Menke, M. R., 1961, The determination of iron with 1,10-phenanthroline: Talanta, v. 8, p. 163–164.

Kauffman, A. J., Jr., and Jaffe, H. W., 1946, Chevkinite (tscheffkinite) from Arizona: Am. Mineralogist, v. 31, p. 582–588.

Konta, Jiri, 1949, Příčiny různého zbarvení titanitu: Třídy Českе Akad., Rozpravy II, v. 59, p. 1–16.

Meyrowitz, Robert, 1969, The direct microdetermination of silicon and aluminum in silicate minerals, *in* Geological Survey Research 1969: U.S. Geol. Survey Prof. Paper 650–B, p. B136–B139.

———1970, A pyrocatechol violet spectrophotometric procedure for the direct microdetermination of aluminum in silicate minerals, *in* Geological Survey Research 1970: U.S. Geol. Survey Prof. Paper 700–D, p. D225–D229.

Norwitz, George, and Codell, Maurice, 1954, Colorimetric determination of iron in titanium alloys: Anal. Chim. Acta, v. 11, p. 350–358.

Omori, Keiichi, and Hasegawa, Shuzo, 1956, Titanite from a pegmatite at Ishikawa town, Fukushima Prefecture: Tohoku Univ. Sci. Repts., ser. 3, v. 5, p. 139–142.

Reznik, B. E., and Vorotyagina, V. D., 1968, Photometric determination of titanium as its titanomolybdenum complex: Zhur. Anal. Khimii, v. 23 p. 1230–1231.

Sahama, Th. G., 1946, On the chemistry of the mineral titanite: Finlande Comm. Géol. Bull., No. 138, p. 88–120.

Takubo, Jitsutaro, and Nishimura, Shinichi, 1953, On tscheffkinite from Kobe-mura, Kyoto Prefecture, Japan: Kyoto Univ. Coll. Sci., Mem. Ser. B, v. 20, p. 323–328.

DETERMINATION OF MERCURY IN CRUDE OILS

By M. E. HINKLE, Denver, Colo.

Abstract.—The frequent association of mercury with solid and liquid hydrocarbons in mercury deposits and with petroleum in oil wells makes determination of the mercury content of hydrocarbon materials imperative to the fuller understanding of the geochemistry of mercury. In the proposed procedure the oil sample is quickly and completely oxidized in an oxygen flask, the combustion products are absorbed in dilute chlorine water, and the dissolved mercury is collected on a silver screen that is immersed in the chlorine-water solution. The screen is heated, and the evolved mercury is measured by a mercury-vapor absorption detector. From 10 to 400 nanograms of mercury can be detected in a 0.05-ml oil sample; this content is equivalent to 0.2–8 ppm mercury in the oil. Mercury contents of some natural hydrocarbon samples that were analyzed by this method range from <0.2 to 450 ppm.

Many mercury deposits contain hydrocarbon material that is associated with the mercury ore. Yates and Hilpert (1946, p. 248) reported crystalline hydrocarbons, tars, and oils associated with cinnabar in the eastern Mayacmas district of California. In the western part of the Mayacmas district, Bailey (1946, p. 217) observed hydrocarbons and cinnabar that had been deposited contemporaneously. Liquid and solid hydrocarbons occur as gangue in cinnabar ore in the Knoxville district of California (Averitt, 1945, p. 78). Bituminous matter, crystalline and amorphous hydrocarbons, and methane gas are associated with mercury deposits in California, Texas, and New Zealand (White, 1955, 1967).

Some of the oil and gas wells in the Cymric field of Kern County, Calif., produce mercury. Mercury is precipitated in natural-gas pipelines and oil pumps. It has been found in Cymric crude oils and the associated brines and sediments (White, 1967).

The association of mercury with hydrocarbons and oils is evidence that mercury may be trapped and concentrated by hydrocarbon materials, and thus either transported or fixed in place. Any geochemical study of the mercury-crude oil relationship is dependent on the analytical procedure used. Present analytical methods are time consuming and subject to many interferences.

Oxidation of the sample containing mercury is the main problem in analysis. Sample dissolution is most often accomplished by wet oxidation under reflux, using a mixture of hot concentrated nitric, sulfuric, and perchloric acids. The oxidation is a very tedious process, generally requiring 30–40 hours for completion.

Mercury content in the acid-oxidized sample is usually determined by the colorimetric dithizone procedure (Sandell, 1959, p. 621–639; Ward and others, 1963, p. 57–59). However, residual products from the decomposition of the sample oxidize the dithizone solutions used to extract the mercury; even a double-extraction procedure is often unsatisfactory because of these oxidizing agents in the digestate.

The first steps in analysis of the halogen contents of many organic compounds have been the quick oxidation of a sample in a glass oxygen flask and subsequent absorption of the combustion products in an aqueous solution in the flask prior to the halide determination (Schöniger, 1955). This type of oxidation is effective for crude-oil samples also. However, the dithizone colorimetric procedure is not sensitive enough for subsequent mercury determinations to be made on the small samples permitted by the oxygen flask.

Mercury, in 10- to 400-nanogram amounts, is easily determined by the silver-screen procedure developed for natural-water analysis (Hinkle and Learned, 1969). It is collected from an acid solution onto a silver screen. The screen is heated in an induction furnace, and the evolved mercury is measured in a mercury-vapor absorption detector (Vaughn and McCarthy, 1964), an atomic-absorption instrument utilizing the 2537-A line of mercury.

In the procedure described here, the silver-screen method of mercury detection is combined with the Schöniger method of sample oxidation. A small crude-oil sample is oxidized, quickly and cleanly. The fumes from the combustion are absorbed in a chlorine-water solution that contains a silver screen. Any mercury present is collected on the silver screen. The silver screen

U.S. GEOL. SURVEY PROF. PAPER 750-B, PAGES B171–B174

is then heated, and the mercury evolved is measured by the mercury-vapor absorption detector. The simplicity and reduced operating time of this procedure are the advantages over other methods. The smallest mercury concentration that can be measured is 10 nanograms (1×10^{-8} g), or 0.2 parts per million, in a 50-lambda (0.05-ml) oil sample.

EQUIPMENT

In addition to standard laboratory equipment, such as pipets and beakers, the following items are necessary:

Schöniger oxidation equipment, consisting of a 2-liter glass combustion flask, glass and platinum ignition basket, and electrical firing apparatus.
Induction furnace, Leco Model 523, operating at 14.6 MHz.
Mercury-vapor absorption detector (described by Vaughn and McCarthy, 1964).
Silver-gauze screens, 2-inch-diameter, 80-mesh; fold in half to fit through the neck of the Schöniger flask.
Glass screwcap jars for storing the silver screens.
Teflon-coated magnets, 2 inches long.
Magnetic stirrers.
Ashless filter paper.
Syringe, 10-cc capacity.

REAGENTS

All reagents should be prepared with demineralized water.

Hydrochloric acid, 1*N*: Dilute 83 ml of HCl to 1,000 ml with water.
Sodium chlorate solution, 0.1*M*: Dissolve 10.6 g of $NaClO_3$ in 1,000 ml of water.
Sulfuric acid, concentrated.
Acetone.
Oxygen, compressed, tank.
Mercury standard solution: Dissolve 0.1354 g of reagent grade $HgCl_2$ in 100 ml of 1*N* H_2SO_4. This standard contains 1,000 micrograms of Hg per milliliter. By dilution with water, prepare fresh a 1-μg/ml (1,000-ng/ml) standard as needed.
Mercury-saturated air: Place a few grams of mercury in a Dewar flask. Stopper the flask with a 2-hole rubber stopper. Through one hole insert a thermometer; through the other insert a glass tube fitted with a rubber-membrane stopper through which the syringe can be inserted to withdraw mercury-saturated air.

PROCEDURE

All glassware should be rinsed with 1:1 sulfuric acid between runs. The silver screens should also be cleaned between runs by heating in the radiofrequency induction furnace until no measurable mercury is detected by the vapor-absorption detector.

Pipet 50λ (0.05 ml) of crude oil onto a filter paper (about 1¼ inches square, with a ¼- by 1½-inch tail), cut for use in the Schöniger ignition basket. Set the paper aside to dry overnight in a place uncontaminated by mercury vapor. When the oil has dried on the paper, fold the paper and secure it in the ignition basket in the manner specified for proper ignition in the Schöniger flask. Place 25 ml of H_2O, 25 ml of 1*N* HCl, and 5 ml of 0.1*M* $NaClO_3$ in the combustion flask. Also put a Teflon-covered magnet and a folded silver screen in the flask. Flush the flask and contents with oxygen for about 30 seconds and quickly place the ignition basket with sample in the combustion flask. Attach the flask to the ignition apparatus and ignite the sample. After the sample has burned, swirl the chlorine-water solution around the sides of the flask and over the basket, and then place the flask on a magnetic stirrer and stir the contents for 30–45 minutes to absorb the vapors and allow any mercury present to collect on the silver screen. Pour out the sample solution and unfold the silver screen. Rinse the screen three times with demineralized water and once with acetone. Place the screen in a clean jar and allow it to dry. When the screen is dry, cap the jar until ready for analysis in the mercury-vapor absorption detector; screens should be analyzed within 24 hours after sample oxidation because of the possibility of mercury contamination. Place the screen in the induction furnace and vaporize the mercury. Determine the nanograms of mercury measured by the detector from a calibration graph that has been prepared from readings obtained using different volumes of mercury vapor.

Inject different volumes of mercury-saturated air by syringe into the Leco furnace. Heat the furnace to drive the mercury vapor through the detector unit. At any given temperature mercury-saturated air contains a definite concentration of mercury. Plot the curve of quantities of mercury injected versus amperages observed on log-log paper. A calibration graph should be prepared for each set of samples.

Calculate the mercury concentration in the sample on a weight-per-volume basis:

$$\text{Mercury, in parts per million} = \frac{\text{nanograms measured}}{0.05 \text{ ml sample} \times 1{,}000}.$$

DISCUSSION

Most oil samples produce large volumes of gas on combustion. Consequently, sample aliquots larger than 50λ are not used owing to the possibility of explosion in the sealed 2-liter oxygen flask. Samples containing from 0.2- to 8-ppm Hg can be determined on a 50λ sample. Samples containing more than 8 ppm can be analyzed after dilution with a nonchlorinated organic solvent,

such as acetone; aliquots can be taken of the dilution. The combustion products are assumed to be mainly carbon dioxide and water vapor because of the high organic content of the samples.

A waxy residue is often left inside the oxygen flask when only hydrochloric acid is used as a vapor-collecting solution. To prevent the formation of such waxes an oxidizing chlorine-water solution produced by hydrochloric acid and sodium chlorate is used. The chlorine-water solution is made dilute because concentrated chlorine solutions tarnish the silver screens and tarnished silver screens do not collect mercury. Chlorinated hydrocarbon solvents are not used for sample dilution because they too cause tarnish when burned.

As was noted in the silver-screen procedure for natural waters (Hinkle and Learned, 1969), only 80–90 percent of added Hg is recovered from the screens when they are heated in the induction furnace and the evolved mercury is measured by the mercury-vapor absorption detector. This difference in amount of recovery may be due to different methods of calibration of standard mercury solutions and of the mercury detector; standard solutions are prepared from mercury salts, whereas the vapor absorption detector is calibrated with different volumes of mercury vapor. When very accurate analyses are desired, a calibration curve may be prepared to compensate for the loss in recovery by pipeting mercury standards onto filter papers and carrying the standards through the entire combustion, collection, and measurement procedure.

RESULTS

The precision of the described method was checked by placing aliquots of standard mercury solutions on filter papers, drying the papers, and subjecting them to the entire combustion and collection procedure. The relative standard deviation varied from 80 percent at the threshold value to 5.5 percent at the midrange value (table 1), showing acceptable precision for the quantities measured. Repeated analyses of seven samples of crude oils and other hydrocarbons also yielded acceptable data (table 2).

To compare the results obtained by the Schöniger oxidation–silver screen method with the results obtained by other methods, samples were oxidized under reflux with fuming nitric, fuming sulfuric, and 70-percent perchloric acids. Mercury content in the digested samples was determined in two ways: first, by the dithizone colorimetric procedure; and second, by diluting a small aliquot of the digestate with water, making the solution 1*N* in HCl, and collecting the mercury on a silver screen. The silver-screen method is not too satisfactory with acid-digested samples because the strong oxidizing acids tend to tarnish the silver screens. The results of analyses by the Schöniger-oxidation–silver-screen procedure, by the acid-digestion–dithizone procedure, and by a combination of the two procedures compare favorably (table 3).

TABLE 1.—*Mercury recovered from standard solutions*

Mercury added (ng)	Number of runs	Mercury recovered (ng)		Mean and standard deviation (ng)	Relative standard deviation (percent)
		High	Low		
10	4	11	0	5±4	80
20	3	16	10	12±3	25
50	4	46	34	40±4	10
100	4	131	71	97±23	23. 7
200	11	220	185	200±11	5. 5
400	4	407	307	360±35	9. 7

TABLE 2.—*Mercury found, in parts per million, in crude-oil samples*

Sample No.	Number of runs	Mercury found		Mean and standard deviation
		High	Low	
22–256	6	2. 8	1. 3	2. 1±0. 4
57–9G	8	. 6	. 3	. 4±0. 1
W–745–C	8	<. 2	<. 2	<. 2±0
RB–11	10	<. 2	<. 2	<. 2±0
EMF–36	3	. 4	. 3	. 3±0. 1
H–1	4	525	315	450±80
C–3	6	1. 6	. 9	1. 2±0. 2

TABLE 3.—*Comparative results of mercury analyses*

Sample No.	Method of analysis					
	Schöniger oxidation		Acid digestion			
	Silver screen		Dithizone		Silver screen	
	Number of runs	Mean (ppm)	Number of runs	Mean (ppm)	Number of runs	Mean (ppm)
22–256	6	2. 1	5	1. 9	4	2. 2
57–9G	8	0. 4	7	. 5	7	. 4
W–745–C	8	<. 2	3	. 3	2	. 2
RB–11	10	<. 2	2	. 1	2	. 05
EMF–36	3	. 2	3	. 6	3	. 2
H–1	4	450	6	500	2	500

The method of additions was also used to check the reliability of the procedure. Aliquots of standard mercury solutions were placed on filter papers along with oil samples. The filter papers were then subjected to the

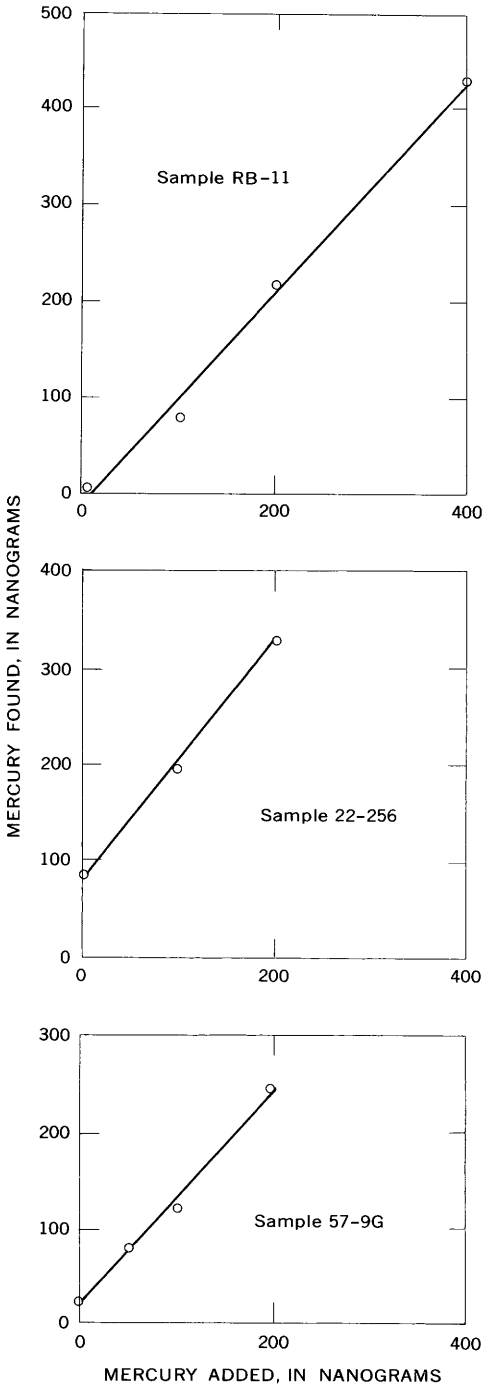

FIGURE 1.—Recovery of mercury from spiked oil samples.

entire combustion and collection procedure. Within the limits of estimation of the procedure, all the added mercury was recovered from the spiked oil samples (fig. 1).

The proposed procedure has been demonstrated to be useful for the determination of mercury in hydrocarbon materials. The time required for sample oxidation has been reduced from the 30–40 hours of older methods to 30–45 minutes; the measurement of dissolved mercury is quick; and the data obtained by the new method are comparable to the data obtained by older methods. This analytical procedure should prove beneficial in studies of the geochemical associations of mercury.

REFERENCES

Averitt, Paul, 1945, Quicksilver deposits of the Knoxville district, Napa, Yolo, and Lake Counties, California: California Jour. Mines and Geology, v. 41, no. 2, p. 65–89.

Bailey, E. H., 1946, Quicksilver deposits of the western Mayacmas district, Sonoma County, California: California Jour. Mines and Geology, v. 42, no. 3, p. 199–230.

Hinkle, M. E., and Learned, R. E., 1969, Determination of mercury in natural waters by collection on silver screens, *in* Geological Survey Research 1969: U.S. Geol. Survey Prof. Paper 650–D, p. D251–D254 [1970].

Sandell, E. B., 1959, Colorimetric determination of traces of metals [3d ed., revised and enlarged]: New York, Interscience Publishers, Inc., 1032 p.

Schöniger, W., 1955, Rapid microanalytical determinations of halogens in organic substances [in German]: Mikrochim. Acta, v. 1955, no. 1, p. 123–129.

Vaughn, W. W., and McCarthy, J. H., Jr., 1964, An instrumental technique for the determination of submicrogram concentrations of mercury in soils, rocks, and gas, *in* Geological Survey Research 1964: U.S. Geol. Survey Prof. Paper 501–D, p. D123–D127 [1965].

Ward, F. N., Lakin, H. W., Canney, F. C., and others, 1963, Analytical methods used in geochemical exploration by the U.S. Geological Survey: U.S. Geol. Survey Bull. 1152, 100 p.

White, D. E., 1955, Thermal springs and epithermal ore deposits, *in* pt. 1 *of* Bateman, A. M., ed., Economic geology: Urbana, Ill., Econ. Geology Pub. Co., p. 99–154.

——— 1967, Mercury and base-metal deposits with associated thermal and mineral waters, p. 575–631 *in* Barnes, H. L., ed., Geochemistry of hydrothermal ore deposits: New York, Holt, Rinehart and Winston, Inc., 670 p.

Yates, R. G., and Hilpert, L. S. 1946, Quicksilver deposits of eastern Mayacmas district, Lake and Napa Counties, California: California Jour. Mines and Geology, v. 42, no. 3, p. 231–286.

APPLICATION OF TRIPLE COINCIDENCE COUNTING AND OF FIRE-ASSAY SEPARATION TO THE NEUTRON-ACTIVATION DETERMINATION OF IRIDIUM

By L. PAUL GREENLAND, J. J. ROWE,
and J. I. DINNIN, Washington, D.C.

Abstract.—Two procedures for the determination of iridium in meteorites, ores, and rocks by neutron activation are described. Both require irradiation of 1-g samples for 12–16 hours in a neutron flux of 7×10^{12}n $cm^{-2}sec^{-1}$. In the first procedure, applicable to the range of iridium concentration of 1–1,000 parts per billion, samples are counted directly (without chemical separations) with three NaI(Tl) detectors which are gated through single-channel analyzers on the 0.308-, 0.296-, and 0.316-MeV Ir^{192} gamma-ray cascade; the associated multichannel analyzer records only those events which simultaneously pass all single-channel analyzers. This counting system is specific to Ir^{192}, but the poor counting efficiency limits its usefulness to samples containing more than 1 ppb of Ir. The second procedure uses a fire-assay separation for iridium concentrations in the 0.001- to 10-ppb range. Samples are fused in the presence of iridium carrier by standard techniques to obtain a Pt-Rh-Ir bead. The final bead is counted in double coincidence to eliminate interference from Ag^{110m} and fission-produced ruthenium which are also present in the bead. Both procedures require long counting times (as much as 24 hours) but are very fast in terms of man-work hours. The simplicity of the procedures makes them well suited to routine analysis.

Studies of the geochemistry of iridium have been limited because of a lack of sensitive analytical methods. The determination of iridium by neutron-activation techniques can be extremely sensitive, and radiochemical separations for the determination of iridium in meteorites have been developed by several laboratories (Baedecker and Ehmann, 1965; Crocket and others, 1967; Kimberlin and others, 1968). Only Baedecker (1967) and Barker and Anders (1968) have analyzed terrestrial materials with such procedures. The difficulties of these techniques, because of the complex chemistry of iridium, have been discussed in detail by Kimberlin and others (1968).

A more promising approach would be the selective counting of iridium without chemical separation. Cobb (1967) and Morgan and Ehmann (1969) used techniques involving a Ge(Li) detector and coincidence counting, respectively, for the direct counting of iridium in meteorites. Neither technique is sufficiently sensitive to be of much geologic interest.

The work of Morgan and Ehmann inspired us to attempt the extension of their double coincidence to a triple coincidence system to attain greater selectivity. The present paper describes this counting system and shows that iridium concentrations in the nanogram/gram region may be determined without chemical separations. However, even this sensitivity is insufficient for the analysis of most rocks, and a rapid technique for the chemical separation of iridium was sought. Grimaldi and Schnepfe (1970) demonstrated the successful concentration of iridium by a simple fire-assay procedure, and we have coupled this separation with double coincidence counting of the final platinum bead to attain a sensitivity of about 10^{-3} ng/g Ir. This paper describes the procedure and reports iridium values for the U.S. Geological Survey standard rocks.

The work reported here is based on the nuclear reaction: $Ir^{191}(n, \gamma)$ Ir^{192}. The 37-percent Ir^{191} has a cross section of 1,000 barns. Ir^{192} decays with a complex γ-ray spectrum; the relevant part is the triple γ cascade of 0.308-, 0.296-, and 0.316-MeV energies.

EXPERIMENTAL METHOD

Fire-assay flux

The flux used was a mixture consisting of 29 percent sodium carbonate, 9 percent silica, 16 percent anhydrous borax, 42 percent lead oxide, and 4 percent flour.

Standards

Grimaldi and Schnepfe (1970) have described the preparation of an ultramafic rock sample containing 10

U.S. GEOL. SURVEY PROF. PAPER 750-B, PAGES B175-B179

ppm of Ir and other noble metals. This sample was diluted with further portions of the rock powder to provide samples containing 1, 0.1, and 0.01 ppm of Ir. The dilutions and the homogeneity of the preparations were checked by neutron-activation analysis. The samples containing 0.1 and 0.01 ppm of Ir were used in later work as standards. Subsequently, the iridium content of the base rock was determined as 0.0005 ppm of Ir, and this correction was applied to the 0.01-ppm Ir standard.

Counting equipment

The system for triple coincidence counting consisted of two 3×3-inch and one 4×4-inch NaI(Tl) detectors which were mounted 120° apart in a horizontal plane and separated from each other by ½-inch lead plates to prevent backscattering. The detectors were connected through preamplifiers and double-delay line amplifiers to timing single-channel analyzers. The output from the analyzers was put into fast coincidence (30 ns resolving time), and the coincidence output was used as a gate for a 1,024-channel analyzer. Signal input to the multichannel analyzer was obtained from a delayed output of the amplifier connected to the 4×4-inch detector. Two of the single-channel analyzers were narrowly gated on the 0.30-MeV peak (composite of the 0.296-, 0.308-, and 0.316-MeV gamma rays) while the third, in the multichannel analyzer branch, passed the 0.20–0.45-MeV range. The double coincidence system was identical, except that only two channels were used and the detectors were mounted 180° apart and face to face. Ehmann (1970) should be consulted for an excellent discussion of coincidence-counting principles and practices.

Treatment of samples and standards for irradiation

Rock samples of 0.5–1 g, meteorite samples of 0.25 g, and 1-g samples of the standard were sealed in ½-dram polyethylene vials and irradiated for 12–16 hours in a neutron flux of $\approx 7\times10^{12}$n cm^{-2}sec^{-1}. The epithermal component of the flux amounted to ≈10 percent, an important contribution to the analytical sensitivity. Samples were irradiated in batches of 20, of which 4 were standards. After irradiation, samples were left to decay for 10–30 days to avoid problems from short-lived isotopes.

Fire-assay procedure

Samples and standards were mixed with about 75 g of flux, 2–5 mg of ammonium chloriridate, and 50 mg of platinum-rhodium wire (13 percent Rh; pure Pt wire is also satisfactory). The fire assay fusion and cupellation are standard techniques (Bugbee, 1940; Beamish, 1966). The final Pt-Rh-Ir bead, containing most of the noble metals, was sealed in a small polyethylene container for counting. The chemical yield of iridium was assumed to be constant.

Counting procedure

Samples expected to be high in iridium content (>0.01 ppm) were counted directly in the triple coincidence system with no chemical processing. Samples were centered in the circle defined by the detectors and counted for periods, depending on the activity, of as long as 24 hours. Before counting each batch of samples, the radial distance of each detector from the center of the circle was adjusted to maintain the counting rate of the most radioactive sample below the level at which pulse pileup became significant. Alternatively, the standard addition technique described by Ehmann (1970) might be considered.

Samples containing less than 0.01 ppm of Ir were subjected to the fire-assay separation, and the final bead was counted in double coincidence for periods of as long as 24 hours. The very low counting rates of the beads precluded difficulties from pulse pileup and backscattering phenomena.

RESULTS AND DISCUSSION

Triple coincidence counting

The system for triple coincidence counting is specific for Ir^{192} as no other element has three coincident gamma rays in the energy range gated by the single-channel analyzers. A very low coincidence-counting rate from Compton scattering of higher energy triply coincident gamma rays, and possibly some double coincident events combined with backscattering, was also observed. This did not interfere with the Ir^{192} peak area determination by the Covell (1959) method from the multichannel-analyzer data, but it makes impossible the determination of iridium by simply counting the total coincidence events.

There appear to be no standard materials of known iridium content that might provide a method of checking triple coincidence counting except for the doped rock prepared and analyzed by Grimaldi and Schenepfe (1970). Dilutions of their 10-ppm Ir standard analyzed by this method and standards prepared from solutions of iridium metal agreed with the nominal value and with their atomic-absorption determination.

Although chondritic meteorites are too variable in composition to serve as standards, they are sufficiently constant to indicate gross (factor of 2) analytical error. Table 1 gives analyses of five meteorites by this method; two of these have been analyzed by Kimberlin and others (1968) by a radiochemical technique, and their results are shown for comparison. The agreement of the two methods is excellent for the Bjurbole and accept-

TABLE 1.—*Iridium content, in parts per million, of chondritic meteorites*

Chondrite	Procedure	
	Triple coincidence (this work)	Radiochemical (Kimberlin and others, 1968)
Pantar	0.46	
Peace River	.37	0.48, 0.57
Ehole	.44	
Mocs	.33	
Bjurbole	.34	0.34, 0.36

able for the Peace River meteorites. Further, all 5 meteorites are well within the range found by Baedecker and Ehmann (1965) for 14 and by Tandon and Wasson (1968) for 21 ordinary chondrites.

Several ore samples were analyzed by triple coincidence, a radiochemical neutron-activation technique,[1] and the fire-assay separation technique described in the next section of this paper. These results (table 2) show good relative agreement.

TABLE 2.—*Iridium content, in parts per billion, of ore materials*

Ore material	Procedure		
	Triple coincidence [1]	Fire assay	Radiochemical
Chromite mill samples:			
Concentrate (ASMV–1)	14±4	16	20
Concentrate (ASBE–2)	16±6		23
Tailing (ASMV–2)	9±4	16	13
Tailing (ASBE–2)	35±5	25	51
Sulfide gossan (1–MVNP–67)	30±8		27

[1] Errors noted are two standard deviations of the counting statistics.

Finally, iridium was determined by triple coincidence in eight Geological Survey standard rocks. All contain <1 ppb of Ir, except the periodotite (PCC–1), in agreement with results obtained by a subsequent fire-assay separation (see table 3). We obtained 3.1 ppb of Ir in the peridotite by direct counting in agreement with 2.6, 2.8, and 3.6 ppb of Ir from the fire-assay separation.

These comparisons demonstrate the specificity and accuracy of the triple-coincidence-counting technique. With the described conditions, 1 ppb of Ir can be detected and 10 ppb of Ir can be readily determined. This method has the advantages of a nondestructive analysis and of simplicity in that very little operator time is required. The method is particularly suited to analysis of ores and meteorites; unfortunately, most geologic materials contain <1 ppb of Ir, and thus other methods are required.

[1] Samples were fused with Na_2O_2 in the presence of Ir carrier, and the cooled melt acidified with HCl. Fe and Cr were removed by extraction with hexone. Ir metal was precipitated with Zn^0 in the presence of Cr and Co holdback carriers. The Ir precipitate was ignited and then fused with NaOH–Na_2O_2 along with added metallic Fe. The fusion cake was dissolved in HCl for the chemical yield determination by the atomic absorption method of Grimaldi and Schnepfe (1970). The acid solution was counted with a 3×3-inch NaI(Tl) detector coupled with a multichannel analyzer.

Double coincidence counting after fire-assay separation

For the determination of iridium after the fire assay described in the section "Fire-assay procedure," to be valid, two assumptions must be made: (1) a constant fraction of the iridium carrier must be recovered from both samples and standards, and (2) isotopic exchange between carrier and radioactive iridium must occur. Both of these assumptions have been validated by experiments described below.

The separation of iridium by fire assay has been discussed by Beamish (1966). Grimaldi and Schnepfe (1970) have shown that as little as 1 μg of Ir can be recovered quantitatively in a gold bead by this technique. Using Ir^{192} tracer, we found that the recovery decreased rapidly below 1 μg of Ir, approaching zero at 0.1 μg of Ir. Substitution of platinum or platinum-rhodium alloy for gold (Ir alloys with Pt but not with Au) and the addition of a few milligrams of ammonium chloriridate as carrier enabled the collection of at least 90 percent Ir^{192} tracer when added at the 0.0005–μg level.

If recovery of iridium in the platinum bead is not quantitative, a reassay of the slag should yield more iridium. Slag from a number of the samples and standards therefore was analyzed: Iridium was not detected in slag from samples having iridium in the 0.00x-ppb range, implying that less than 30 percent of the original iridium was left behind in the first assay; iridium was detected in slag from samples having iridium in the

TABLE 3.—*Iridium content, in parts per billion, in U.S. Geological Survey standard rocks, as determined by different methods*

Standard rock	Source of data	
	This work [1]	Other work [2]
Granite G–1	0.003, .007 .008, .013	[3]<0.07, [4].04
Granite G–2	.005, .009, .028, .039	17.7, 0.2, 0.1
Andesite AGV–1	.003, .004, .006, .029	0.7, 0.5, 0.3
Granodiorite GSP–1	.005, .009, .012	1.1, 0.7, 0.4
Diabase W–1	.22, .23, .24, .26	[3]<.05, [4].26
Basalt BCR–1	.002, .004, .005, .006	1.1, 0.7, 0.2
Peridotite PCC–1	2.6, 2.8, 3.6, [5]3.1	6.6, 0.6, 0.4
Dunite DTS–1	.34, .38, .39, .44, .45, .52, .55, .55, .56, .57, .63, 1.9, 3.9, 4.5	0.5, 0.4, 0.3

[1] Fire-assay separation and double coincidence counting, except as noted.
[2] Neutron activation from Baedecker (1967), except as noted.
[3] From Baedecker and Ehmann (1965).
[4] From Crocket, as cited by Barker and Anders (1968).
[5] Triple coincidence counting, instrumental.

parts-per-billion range, but this amounted to less than 10 percent of the original iridium in all samples.

The iridium standard rocks prepared by Grimaldi and Schnepfe, several ores (table 1), and the Geological Survey peridotite (table 3) have been analyzed both by the triple coincidence and the fire-assay methods with good mutual agreement. This implies that iridium in the parts-per-billion range is being recovered.

The strongly reducing, high-temperature atmosphere of the fire-assay crucible is a nearly ideal environment for isotopic exchange. However, to test specifically for exchange, the lead buttons obtained by fusion of the ore samples (table 1) were cut into four parts and cupelled separately. The specific activity of iridium was the same in each piece of lead, implying that isotopic exchange had occurred.

These results show that isotopic exchange between the carrier and radioactive iridium was achieved and that iridium collection was virtually quantitative by the platinum bead. Further indirect evidence validating this method has been obtained by analysis of rocks from a differentiated dolerite sequence (Greenland, 1970). The observed values vary continuously from 0.006 to 0.25 ppb; when plotted on a differentiation diagram, these yield a clearly defined trend of decreasing iridium content with increasing differentiation rather than the random scatter that would be expected from large analytical errors.

Iridium separated by the fire-assay procedure is not radiochemically pure. Activity from Ag^{110m} and the ruthenium fission products of uranium was observed routinely. The Compton background from these isotopes precluded the direct counting and determination of iridium in the beads. The double-coincidence-counting method greatly reduced the counting rate of extraneous isotopes, leaving a clear Ir^{192} spectrum superimposed on a relatively low Compton background. The residual background, primarily from coincident Compton scatter γ-rays of Ag^{110m}, does not interfere with the peak-area determination of Ir^{192}.

Table 3 compares our results for the U.S. Geological Survey standard rocks with those of Baedecker (1967). Comparison of the two sets of data shows reasonable agreement of the DTS–1 and PCC–1 analyses; however, our analyses of the other rocks (except G–1 and W–1) yield 1–2 orders of magnitude less iridium than Baedecker's results. Different bottles of the standard rocks may differ this much in iridium content, but we regard this as most improbable.

Baedecker (1967) has discussed his problems with isotopic exchange and suggests that his results should be regarded as lower limits; if exchange did not occur, however, it is also possible that more carrier than radioactive iridium was lost in the chemical processing and, thus, that his determinations are upper limits. We believe that a more probable explanation lies in laboratory contamination. The University of Kentucky group, including Baedecker, have been deeply involved in meteorite analysis; Kimberlin and others (1968) note that they are unable to determine iridium in rocks because of previous contamination of laboratory equipment from meteorite analyses. Some support for this view is obtained from the observation that the G–1 and W–1 analyses, published several years before the other standard rocks were issued, are given only as upper limits and imply at least an order of magnitude less iridium than the other standard rocks. Laboratory contamination amounting to a few tenths ppb of Ir would not appreciably affect analyses of DTS–1 and PCC–1 and thus would lead to the pattern of agreements and orders of magnitude discrepancies shown in table 3.

Finally, we note that these new results are in accord with geochemical intuition: the ionic radius of Ir^{+4} is close to that of Cr^{+3}, and thus the two elements might be expected to behave similarly. Our data do show a qualitative correlation with the chromium determinations cited by Flanagan (1969) of the standard rocks, and the analyses of a differentiated dolerite suite (Greenland, 1970) also demonstrate a striking geochemical similarity of iridium with chromium.

REFERENCES

Baedecker, P. A., 1967, The distribution of gold and iridium in meteoritic and terrestrial materials: Kentucky Univ., Ph. D. thesis.

Baedecker, P. A., and Ehmann, W. D., 1965, The distribution of some noble metals in meteorites and natural materials: Geochim. et Cosmochim. Acta, v. 29, no. 4, p. 329–342.

Barker, J. L., Jr., and Anders, Edward, 1968, Accretion rate of cosmic matter from iridium and osmium contents of deep-sea sediments: Geochim. et Cosmochim. Acta, v. 32, no. 6, p. 627–645.

Beamish, F. E., 1966, The analytical chemistry of the noble metals: Oxford, Pergamon Press, 609 p.

Bugbee, E. E., 1940, A textbook of fire assaying, 3d ed.: New York, John Wiley, 314 p.

Cobb, J. C., 1967, A trace-element study of iron meteorites: Jour. Geophys. Research, v. 72, no. 11, p. 1329–1341.

Covell, D. F., 1959, Determination of gamma-ray abundance directly from the total absorption peak: Anal. Chemistry, v. 31, p. 1785–1790.

Crocket, J. H., Keays, R. R., and Hsieh, S., 1967, Precious metal abundances in some carbonaceous and enstatite chondrites: Geochim. et Cosmochim. Acta, v. 31, no. 10, p. 1615–1623.

Ehmann, W. D., 1970, Non-destructive techniques in activation analysis: Fortschr. Chem. Forsch., v. 14, no. 1, p. 49–91.

Flanagan, F. J., 1969, U.S. Geological Survey standards—[pt.] 2, First compilation of data for the new U.S.G.S. rocks: Geochim. et Cosmochim. Acta, v. 33, no. 1, p. 81–120.

Greenland, L. P., 1970, Variation of iridium in a differentiated tholeiitic dolerite: Geochim. et Cosmochim. Acta. [In press].

Grimaldi, F. S., and Schnepfe, M. M., 1970, Determination of iridium in mafic rocks by atomic absorption: Talanta, v. 17, p. 617–621.

Kimberlin, J., Charoonratana, C., and Wasson, J. T., 1968, Neutron activation determination of iridium in meteorites: Radiochim. Acta, v. 10, p. 69–76.

Morgan, J. W., and Ehmann, W. D., 1969, Multiparameter coincidence spectrometry applied to the non-destructive neutron activation analysis of meteorites: Anal. Letters, v. 2, p. 537–545.

Tandon, S. N., and Wasson, J. T., 1968, Gallium, germanium, indium, and iridium variations in a suite of L-group chondrites: Geochim et Cosmochim. Acta, v. 32, no. 10, p. 1087–1109.

DETERMINING FLUORIDE IN ROCKS WITH A SPECIFIC ION ELECTRODE

By BLANCHE L. INGRAM and IRVING MAY,
Washington, D.C.

Abstract.—Fluoride in distillates obtained from rocks can be determined with fluoride specific ion electrodes equally well by linear null-point potentiometry or by electrode calibration. High blanks may result from decomposition products generated during distillation and from organic matter originating from tubing and indicators. Fluoride can be determined with the fluoride electrode in phosphate rocks without separation. Interference by aluminum is controlled by adding sodium citrate.

Most studies of the analytical application of fluoride specific ion electrodes have emphasized methods permitting measurement of fluoride without separations (Edmond, 1969; Ficklin, 1970; Frant and Ross, 1968; Guth and Wey, 1969; Harwood, 1969; Ingram, 1970; Van Loon, 1968; and Weiss, 1969). Direct methods cannot always be used with rocks, however, because of interference from elements such as aluminum which form strong complexes with fluoride. Generally, distillation is used to separate fluoride, and for this reason, use of an electrode to measure fluoride in distillates was studied. Two techniques were studied—an electrode calibration technique using known fluoride solutions, and linear null-point potentiometry (LNPP) (Durst, 1968). Durst, working with microliter quantities of fluoride solutions, concluded that greater precision was obtained for concentrations of fluoride below $10^{-5}M$ when measured by a null-point technique than by an electrode calibration technique. We wished to determine the advantages of each procedure and what problems there were, if any, in measuring fluoride in distillates.

Many phosphate rocks are analyzed for fluoride in this laboratory, and it seemed possible to analyze phosphate rocks without separations. Thus, an investigation of a direct method for phosphate rocks was also included as a part of the study. Since completion of this work, Edmond (1969) has published a direct method for determining fluoride in phosphate rocks that is similar to the method developed here. Both methods use sodium citrate to control aluminum interference, but the details of the methods are somewhat different. A brief summary of the method in use here is given below.

MEASUREMENT OF FLUORIDE IN DISTILLATES

Calibration of Electrode With Known Fluoride Solutions

Apparatus and reagents

An Orion Model 94–09 fluoride-ion electrode and a calomel reference electrode were used in conjunction with a Beckman expanded-scale pH meter for measuring solution potential.

Plastic beakers. Transparent 100-ml beakers and 5-ml disposable beakers.

Potassium nitrate solution, 25 percent (W/V).

Potassium nitrate, $0.1M$.

Potassium hydroxide, $0.1M$.

Standard fluoride solutions. Prepare a stock fluoride solution (1,000 ppm F) by dissolving 1.105 g of primary-standard NaF (Grimaldi and others, 1955) in water and diluting to 500 ml. Dilute the stock solution with $0.1M$ KNO_3 to prepare the following series of standards, 0.02, 0.04, 0.06, 0.10, 0.20, 0.40, 0.60, 1.0, 2.0, 3.0, and 4.0 ppm F. Prepare the 0.02- to 0.6-ppm standards at the time samples are run. Higher standards can be used for several weeks.

Prepare a $1\times10^{-1}M$ F solution in $0.1M$ KNO_3 by dissolving 0.420 g of pure NaF in water, adding 1.0 g of KNO_3, and diluting to 100 ml with water. Prepare solutions that are $1\times10^{-2}M$ F (190 ppm), $1\times10^{-3}M$ F (19 ppm), $1\times10^{-4}M$ F (1.9 ppm), $1\times10^{-5}M$ F (0.19 ppm), and $1\times10^{-6}M$ F (0.019 ppm) in $0.1M$ KNO_3 by serial dilutions using $0.1M$ KNO_3 as diluent.

Procedure

Preparation of distillates.—Select a sample size that will yield a distillate containing 0.02 to 60 ppm F. Decompose the sample and distill the fluorine as directed by Grimaldi and others (1955). If the sample is distilled directly from the perchloric-phosphoric acid medium without preliminary fusion and leaching, add about 15 ml of H_2O to the distillation flask along with the

U.S. GEOL. SURVEY PROF. PAPER 750-B, PAGES B180–B184

acids and sample. Collect the distillate in a 250-ml volumetric flask. Transfer the distillate to a 250-ml beaker and adjust the pH of the solution to between 5.5 and 6, using a pH meter and 0.1*M* KOH added dropwise. Add either 2.5 g of KNO_3 crystals or 10 ml of the 0.25-g/ml KNO_3 solution. Generally, distillates from samples that were fused have such a large volume that solid KNO_3 must be used to keep the distillates from exceeding 250 ml. Transfer the solution back to the flask, allow it to come to room temperature, dilute to volume, and mix well. Measure the potential of this solution.

Measurement of potential.—Potentials of solution are measured as follows: Blot the electrodes with a soft tissue if necessary; pour part of the solution to be measured into a 5-ml plastic beaker and rinse both electrodes with this solution. Pour about 15 to 20 ml of the solution into a 100-ml transparent plastic beaker and immerse the electrodes in this solution. Check the sensing element of the fluoride electrode for air bubbles, shaking the solution gently to dislodge them if present, and read the potential when the electrode has equilibrated.

Prepare a curve for preliminary estimation of fluoride by measuring the potentials of the series of fluoride solutions containing $1\times10^{-6}M$ F to $1\times10^{-2}M$ F, starting with the most dilute solution. Using four-step semilogarithmic paper, plot the fluoride concentrations on the logarithmic axis and millivolts on the linear axis. This curve can be used repeatedly. It can also be used for estimations in the null-point technique. Make a preliminary potential measurement for each distillate. Estimate the fluoride content from the curve, and group the distillates as follows: 4–60 ppm F, 0.2–4 ppm F, and less than 0.2 ppm F. Exact potential readings in the preliminary measurements are not needed. As soon as the indicated potential shows that a distillate is less than 0.2 ppm F, or between 0.2 ppm and 4 ppm F, the reading is interrupted. This is sufficient information for grouping. If the distillate contains more than 4 ppm F, a potential reading is taken, and on the basis of this reading, an aliquot of the distillate is diluted with 0.1*M* KNO_3 so that the diluted solution contains between 1 and 4 ppm F. If a distillate contains more than 60 ppm F, a smaller sample should be decomposed and distilled to insure quantitative distillation of the fluoride. When all necessary dilutions have been made, divide the distillates into two groups, 0.02 to 0.2 ppm F and 0.2 to 4 ppm F. Make the final potential measurements. Measure all the distillates and corresponding standards of one group, and then measure the distillates and standards of the other group. Electrode equilibration takes a minute or two for solutions containing more than 0.2 ppm F, but solutions containing less than 0.2 ppm should be read routinely after a 5-minute immersion period. If two fluoride electrodes are available, it is desirable to reserve one specifically for measurements in the 0.02- to 0.2-ppm range. If only one fluoride electrode is available, immerse the electrode in a 0.02-ppm F solution for 15 minutes before beginning the measurements for the 0.02- to 0.2-ppm F group.

Prepare a calibration curve by plotting the data on semilogarithmic paper.

It is convenient to plot the curve in three sections: 0.02–0.20 ppm, 0.2–1 ppm, and 1–4 ppm, and an accurate interpolation of concentrations is obtained by using 8½- by 11-inch one-cycle paper. Two sheets of paper are combined for the 0.02–0.20 ppm section. This section of the curve is not linear. The concentration of the fluoride in each distillate is read from this calibration curve, and the concentration in the sample is calculated.

Linear Null-point Potentiometry

Apparatus and reagents

A concentration cell connected to a Beckman expanded-scale pH meter was used for the potentiometric titrations. The concentration cell consisted of two half cells contained in transparent plastic beakers connected by a 0.1*M* KNO_3 salt bridge. An Orion Model 94-09 fluoride-ion electrode used in the analate half cell was connected to the glass-electrode input jack of the meter. A second fluoride-ion electrode in the titration half cell was connected to the reference-electrode input of the meter. The titration half cell solution was stirred with a magnetic stirrer. A 10-ml microburet was clamped above the titration half cell so that the tip of the buret dipped into the beaker.

Plastic beakers. Transparent 100- and 250-ml beakers.

Potassium nitrate, 0.1*M*.

Fluoride titrant solutions. The following titrants are needed to cover the entire range of fluoride in the distillates: $1\times10^{-1}M$, $4\times10^{-2}M$, $1\times10^{-2}M$, $4\times10^{-3}M$, $1\times10^{-3}M$, $4\times10^{-4}M$, and $1\times10^{-4}M$. Prepare a $1\times10^{-1}M$ solution as directed above using primary-standard NaF. Prepare a $4\times10^{-2}M$ solution by dissolving 0.168 g of standard NaF in 0.1*M* KNO_3 and diluting to 100 ml with 0.1*M* KNO_3. Other titrants are prepared by diluting with 0.1*M* KNO_3.

Procedure

Distillates are prepared in the same manner as in the procedure above. Measure the potential of the distillates, using the fluoride electrode in conjunction with a calomel electrode. Estimate the molar fluoride concentrations of the solutions, using the curve for estimating prepared in the procedure above. The estimated concentration is used to select a titrant. For solutions that are 1 to $4\times10^{-x}M$ F, select a titrant that is $1\times10^{-(x-2)}M$; for solutions that are 4 to $10\times10^{-x}M$, select a $4\times10^{-(x-2)}M$ titrant. A titrant selected in this way will give an equivalence point with 2 to 8 ml of titrant.

Set up the concentration cell, using 100-ml plastic beakers. Pour 15 to 20 ml of the solution to be titrated into each beaker and immerse the fluoride electrodes

in the solutions. Measure the cell potential which is the null-point potential, the potential at which the concentration of the solution in each half cell is the same. Remove the 100-ml beaker of the titration half cell. Blot the electrode and the part of the bridge that was immersed in the solution. Replace the beaker with a 250-ml plastic beaker containing 200 ml of 0.1*M* KNO_3 and a magnetic stirring bar. Immerse the tip of the buret containing the selected titrant into the solution. Add arbitrary increments of the titrant, stirring until the solution is well mixed after each addition. Stop the stirring and measure the cell potential when the electrode has equilibrated. Before addition of titrant, the cell potential is off scale in the negative direction and becomes more positive during the titration. Measurements of volume and potential are recorded when the potential decreases to about −30 mv. Continue additions past the null-point potential into the positive potential region. Readings of titrant volume and cell potential at the equivalence point itself are unnecessary. About five readings are taken, at least two of which should be past the null-point potential.

Calculate the molar concentration of fluoride in the titration half-cell for each increment of titrant added, using the following formula:

$$C_T = \frac{C_S V_a}{V_0 + V_a},$$

where C_T is the fluoride concentration in the titration half cell, C_S is the concentration of the titrant solution, V_0 is the original volume of inert electrolyte (0.1*M* KNO_3) in the titration half cell, and V_a is the volume of titrant added.

Plot the data semilogarithmically, concentration (C_T) on the logarithmic axis and cell potential on the linear axis. Evaluate the equivalence point by a linear interpolation to the null-point potential. Calculate the percentage of fluoride in the sample.

Results and Discussion

Problems encountered

Blanks.—High and variable blanks can be a major problem in analyzing distillates. The main cause of the problem was traced to the construction of the distillation unit. In the unit used here, circular openings were cut into a Transite board, and during distillation the bottom of the distilling flask rested in this circular opening. The opening was large enough so that a part of the flask protruded below the board, and this part of the flask was heated directly with a bunsen burner. When the volume of solution in the flask was reduced sufficiently to permit distillation at the desired temperature, the liquid level in the flask was below the board also. Although the distillation appeared to be proceeding at the proper temperature, overheating took place at the areas where there was little or no liquid, and products generated from overheating the acids were being carried over into the distillate, causing blank difficulties. This problem was solved by reducing the openings with metal rings so that the liquid level in the flask during distillation was always well above the part of the flask being heated directly.

Organic matter can be the source of blank difficulties also. The organic matter extracted by the steam from the rubber connections used between the steam generator and the distilling flasks caused high blanks. Tygon that had been boiled was substituted for the rubber. Small amounts of Tygon were carried into the distillation flask and into the distillate but caused no difficulty. Methyl red indicator caused an increase in equilibration time for the fluoride electrode in solutions containing very low concentrations of fluoride, and blank solutions in which methyl red was used in the pH adjustment appeared to contain fluoride when a potential reading was made at 5 minutes. For this reason, the indicator was replaced by a pH meter to adjust the acidity of the distillates.

Equilibration time of electrode in electrode calibration technique.—Equilibration time for the electrode in a dilute fluoride solution is much longer if the dilute solution is measured after a concentrated solution. For example, a 0.02-ppm F solution became constant at +172 mv within 5 minutes when read after a 0.15-ppm F solution, but 20 minutes was necessary for a reading of +172 mv when the 0.02-ppm solution was read after a 4-ppm F solution. The change in potential is so slow after 5 to 10 minutes that one may incorrectly judge that equilibrium has been reached. To avoid errors and expedite measurements, the unknown solutions are first sorted into two groups, one containing less than, and one containing more than, 0.2 ppm F, and each group is measured separately. Five minutes is sufficient time for the electrode to equilibrate when solutions are measured that contain 0.2 to 0.02 ppm F.

Stability of solutions.—Fluoride solutions at a pH of 5.5 to 6 in 0.1*M* KNO_3 containing less than 1 ppm F are not stable for long periods. Solutions containing 0.02 to 0.1 ppm F changed on the second day after being made, and solutions containing 0.1 to 0.6 ppm F are stable only 3 or 4 days. Solutions containing 1 to 4 ppm F are stable for at least a month. Distillates containing 0.02 ppm F are stable for several days, if left as collected from the still. Unless it is known that distillates contain more than 0.1 ppm F, they should not be prepared for potential measurement, pH adjustment and addition of KNO_3, if there is insufficient time to measure the potentials on the same day.

Comparison of the two measuring techniques

Fluoride was measured in sodium fluoride standard solutions containing 0.03, 0.12, 0.20, and 60 ppm F, and in distillates of sodium fluoride containing approximately 25 and 60 ppm F, using both electrode techniques. Distillates of eight silicate rocks and U.S. National Bureau of Standards phosphate rocks 120a and 56b were also analyzed by both electrode techniques; the solutions for the electrode analysis of the silicate rocks contained 1 to 4 ppm F. Results of the analysis of the silicate and phosphate rocks are given in table 1. The average difference for the fluoride content obtained by the electrode calibration technique and by LNPP considered as duplicates for each solution was not significant, and the standard deviation (combined analytical error for both methods) calculated for the 0.03- to 0.20-ppm solutions is 0.0009 ppm. This error is 0.15 ppm at the 25- to 60-ppm level, and is 0.0026 percent for the silicate rocks. Distillates of another group of 13 silicate rocks containing from 0.009 to 0.46 percent F were analyzed by the electrode calibration technique and spectrophotometrically with thoron. When the values for each sample obtained by each method of measurement are treated as duplicates, standard deviation is 0.0038 percent.

The average difference between both electrode measuring techniques is not significant by a t test, and both methods gave equally accurate fluoride data. The choice between the two is one of convenience. It is not necessary to dilute distillates when using the null-point technique, and the NaF titrants are stable for weeks. The dilute standards necessary for low concentrations of fluoride (0.02 to 0.6 ppm) in the electrode calibration technique are not stable and are prepared each day that they are needed. If only one or two samples are analyzed at a time, it would probably save time to measure the fluoride by the null-point technique if fluoride in the distillate is less than 0.6 ppm; the time is comparable for other concentrations. When many samples are analyzed at the same time, however, the calibration technique is much faster.

TABLE 1.—*Electrode determination of fluoride in rocks, in percent, by electrode calibration and linear null-point potentiometric (LNPP) techniques*

Sample		Measuring technique		
		Electrode calibration	LNPP	Other [1]
Silicate rock	1	0.328	0.335	0.33
	2	.335	.340	.33
	3	.328	.325	.31
	4	.580	.583	.59
	5	.472	.472	.49
	6	.420	.422	.42
	7	.358	.360	.36
	8	.142	.145	.14
Phosphate rock	NBS–56b	3.39	3.35	[2] 3.4
	NBS–120a	3.96	3.96	[2] 3.92

[1] Samples 1–8, spectrophotometric with thoron; Joseph Budinsky, analyst.
[2] Certificate value.

DIRECT METHOD FOR PHOSPHATE ROCKS

Reagents

0.6M sodium citrate–0.2M potassium nitrate solution. Dissolve 177 g of sodium citrate dihydrate and 20 g KNO_3 in water and dilute to 1 liter.

0.3M sodium citrate–0.1M potassium nitrate solution. Dissolve 88.5 g of sodium citrate dihydrate and 10 g KNO_3 in water, add 2.5 ml of 1+1 HNO_3 and dilute to 1 liter.

Standard fluoride solutions. Prepare standards containing 0.4, 0.6, 1, 2, 3, and 4 ppm F from the stock standard fluoride solution (1,000 ppm F), using the 0.3M sodium citrate–0.1M potassium nitrate solution as diluent.

Procedure

Digest a 100-mg sample with 5 ml of 1+1 HNO_3 for a few minutes on the steam bath to decompose the sample. Filter the solution into a 100-ml volumetric flask, and wash with 1 percent HNO_3. Dilute to volume with water. Transfer a 5-ml aliquot of the sample solution to a 100-ml volumetric flask, add 50 ml of the 0.6M sodium citrate–0.2M KNO_3 solution, and dilute to volume with water. This gives a sample solution in 0.3M sodium citrate—0.1M KNO_3 medium. Measure the fluoride in this solution, using the electrode calibration technique described above.

Results and Discussion

Aluminum interference is controlled by the addition of citrate to the sample solution. Electrode equilibration is slow in a 0.3M citrate–0.1M nitrate medium, and in measuring the potentials of these solutions a 5-minute immersion period for the electrodes is necessary. Generally, phosphate rocks will contain sufficient fluoride so that the sample solution in the citrate-nitrate medium prepared by directions given above will contain 0.4 to 4.0 ppm F (original sample contains 0.8 to 8 percent F). Potential measurements in this range of fluoride in a citrate medium are problem free. If the sample solution in the citrate-nitrate medium is less than 0.4 ppm F, a larger aliquot of the original sample solution can be diluted.

Four samples from the aluminum phosphate (leached) zone of the Florida phosphate deposits, and NBS–120a and NBS–56b were analyzed by this direct procedure. The results are presented in table 2.

413-504 O - 71 - 13

TABLE 2.—*Electrode determination of fluoride, in percent, in phosphate rocks.*

Sample	Aluminum content as Al_2O_3 (percent)	Technique	
		Direct	Distillation
Leached Zone 1	18. 7	0. 90	0. 91
2	16. 6	. 54	. 52
3	10. 2	. 92	. 92
4	17. 6	. 92	. 93
NBS–120a	. 94	3. 90	[1] 3. 92
NBS–56b		3. 44	[1] 3. 4

[1] Certificate value.

REFERENCES

Durst, R. A., 1968, Fluoride microanalysis by linear null-point potentiometry: Anal. Chemistry, v. 40, p. 931–935.

Edmond, C. R., 1969, Direct determination of fluoride in phosphate rock samples using the specific ion electrode: Anal. Chemistry, v. 41, p. 1327–1328.

Ficklin, W. H., 1970, A rapid method for the determination of fluoride in rocks and soils, using an ion-selective electrode, *in* Geological Survey Research 1970: U.S. Geol. Survey Prof. Paper 700–C, p. C186–C188.

Frant, M. S., and Ross, J. W., Jr., 1968, Use of a total ionic strength adjustment buffer for electrode determination of fluoride in water supplies: Anal. Chemistry, v. 7, p. 1169–1171.

Grimaldi, F. S., Ingram, B. L., and Cuttitta, Frank, 1955, Determination of small and large amounts of fluorine in rocks: Anal. Chemistry, v. 27, p. 918–921.

Guth, Jean-Louis, and Wey, Raymond, 1969, Sur un dosage rapide du fluorure dans les mineraux et roches: Soc. Française Minéralogie et Cristallographie Bull., v. 92, p. 105–107.

Harwood, J. E., 1969, The use of an ion-selective electrode for routine fluoride analysis on water samples: Water Research, v. 3, p. 273–280.

Ingram, B. L., 1970, The determination of fluoride in silicate rocks without separation of aluminum using a specific ion electrode: Anal. Chemistry, v. 42, p. 1825–1827.

Van Loon, J. C., 1968, The rapid determination of fluoride in mineral fluorides using a specific ion electrode: Anal. Letters, v. 1, p. 393–398.

Weiss, Dalibor, 1969, Determination of fluoride in mineral raw materials by means of a lanthanum fluoride membrane electrode: Chem. Listy, v. 63, p. 1152–1156.

CHROMIUM CONTENT OF U.S. GEOLOGICAL SURVEY STANDARD ROCKS PCC–1 (PERIDOTITE) AND DTS–1 (DUNITE)

By CLAUDE HUFFMAN, JR., VAN E. SHAW, and J. A. THOMAS, Denver, Colo.

Abstract.—Chromium determinations by colorimetric and atomic absorption spectrophotometric methods were made on PCC–1 (peridotite) and DTS–1 (dunite). The average chromium content of PCC–1 is 2,864 ppm and DTS–1 is 4,275 ppm. The analysis of variance for a three-way cross classification design showed that there was no significant difference between bottles (splits) of either rock; thus the samples may be said to be homogeneous.

The first compilation of data for the six new U.S. Geological Survey standard rocks (Flanagan, 1969) included chromium values for samples PCC–1, a peridotite, and DTS–1, a dunite. The values reported for PCC–1 range from 1,843 to 4,780 ppm with a mean of 3,090 ppm, and for DTS–1 the values range from 2,840 to 5,565 ppm with a mean of 4,230 ppm. This wide range of chromium values indicated the need for additional determinations to better define the chromium content and to study sample homogeneity.

GENERAL PROCEDURE AND DISCUSSION

Five splits of each rock were selected for analysis. These splits were in bottles that had undergone formal randomization after the original loading (Flanagan, 1967). Four weighed portions from each bottle were taken for analysis. Two portions were fused with sodium peroxide in zirconium crucibles by one analyst, and the other two were fused with a mixture of sodium hydroxide and sodium peroxide in nickel crucibles by another analyst. The fused melts were dissolved in water, diluted to 200 ml, and then filtered through a dry filter paper. The four resulting solutions from each bottle were then analyzed for chromium by both colorimetric and atomic absorption methods.

The raw chromium data are given in tables 1 and 2, in which the variables of classification are bottle-split position, method of solution, and method of final determination. The average of 20 colorimetric determina-

TABLE 1.—*Chromium values, in parts per million, obtained for U.S. Geological Survey standard PCC–1 (peridotite)*

Bottle-split position	42–31		3–32		43–11		24–18		48–15	
Method of analysis [1]	C	AA	C	AA	C	AA	C	AA	C	AA
Solution by Na_2O_2										
Run 1	2,800	2,800	2,850	2,800	2,900	2,950	2,850	2,950	2,900	3,000
2	2,800	2,950	2,800	3,000	2,800	2,950	2,850	3,000	2,850	2,950
Solution by $NaOH + Na_2O_2$										
Run 1	2,800	2,750	3,150	2,850	2,900	2,850	2,850	2,800	2,900	2,800
2	2,800	2,800	2,850	2,750	2,800	2,800	2,800	2,800	2,950	2,800
Average per bottle	2,800	2,825	2,913	2,850	2,850	2,888	2,838	2,888	2,900	2,888

[1] C, colorimetric method; AA, atomic absorption method.

NOTE.—The average of 20 colorimetric determinations is 2,860 ppm. The average of 20 atomic absorbtion determinations is 2,868 ppm. The arithmetic mean of all 40 determinations is 2,864 ppm.

U.S. GEOL. SURVEY PROF. PAPER 750–B, PAGES B185–B187

TABLE 2.—*Chromium values, in parts per million, obtained for U.S. Geological Survey standard DTS–1 (dunite)*

Bottle-split position	40–25		16–20		54–18		25–32		25–19	
Method of analysis [1]	C	AA	C	AA	C	AA	C	AA	C	AA
Solution by Na_2O_2										
Run 1	4, 200	4, 300	4, 350	4, 350	4, 350	4, 350	4, 200	4, 150	4, 350	4, 400
2	4, 200	4, 400	4, 200	4, 400	4, 300	4, 400	4, 300	4, 450	4, 150	4, 350
Solution by NaOH + Na_2O_2										
Run 1	4, 300	4, 200	4, 350	4, 200	4, 250	4, 200	4, 250	4, 100	4, 400	4, 200
2	4, 300	4, 100	4, 400	4, 150	4, 400	4, 100	4, 400	4, 200	4, 300	4, 050
Average per bottle	4, 250	4, 250	4, 325	4, 275	4, 325	4, 263	4, 288	4, 225	4, 300	4, 250

[1] C, colorimetric method; AA, atomic absorption method.

NOTE.—The average of 20 colorimetric deteminations is 4,298 ppm. The average of 20 atomic absorption determinations is 4,253 ppm. The arithmetic mean of all 40 determinations is 4,275 ppm.

tions for PCC–1 is 2,860 ppm of chromium and for DTS–1 is 4,298 ppm, whereas 20 atomic absorption determinations yielded averages of 2,868 ppm of chromium in PCC–1 and 4,253 ppm in DTS–1. The arithmetic mean of all 40 determinations is 2,864 ppm of chromium for PCC–1 and 4,275 ppm for DTS–1.

The analyses of variance (table 3) show that there is no significant difference in chromium content between the five bottles of either rock. Further, there is no significant interaction between the bottle-split position and either the analytical method or the method of solution (AB and AC of table 3), or between all three (ABC).

A highly significant interaction variance exists between the colorimetric-atomic absorption (B) and operator-crucible-fusion (C) factors. The variance ratio for this interaction is of the same order of magnitude for each rock: 15.12 for PCC–1 and 26.58 for DTS–1. The mean values (in parts per million) of each of the for combinations that are associated with this interaction are:

Combination	*PCC–1*	*DTS–1*
Analyst 1. Ni–NaOH fusion, with atomic absorption	2, 800	4, 150
Analyst 2. Zr–Na_2O_2 fusion, with colorimetric	2, 840	4, 260
Analyst 1. Ni–NaOH fusion, with colorimetric	2, 880	4, 335
Analyst 2. Zr–Na_2O_2 fusion, with atomic absorption	2, 935	4, 355

Each entry in the preceding tabulation is the mean of 10 values. Although the differences between the means are not large (mostly less than 2 percent of the grand means), they do suggest a slight bias, the basic cause of which cannot be determined from the present design. However, this design does allow study of the variation between bottles, inasmuch as the cause of the significant interaction, whatever it is, is independent of the between-bottle variance.

Chromium values previously obtained by U.S. Geological Survey chemists using conventional rock analysis methods (Flanagan, 1969, table 1) are compared in table 4 with the values of the present report. Although

TABLE 3.—*Analyses of variance of chromium content, in parts per million, in U.S. Geological Survey standard rocks PCC–1 (peridotite) and DTS–1 (dunite)*

Source of variance [1]	Degrees of freedom	Sum of squares	Mean of squares	Variance ratios (F) [2]
PCC–1 (peridotite)				
Main:				
A	4	30, 875. 00	7, 718. 75	1. 5247
B	1	562. 50	562. 50	. 1111
C	1	22, 562. 50	22, 562. 50	4. 4568
Interactions:				
AB	4	16, 625. 00	4, 156. 25	. 8210
AC	4	20, 875. 00	5, 218. 75	1. 0309
BC	1	76, 562. 50	76, 562. 50	15. 1235
ABC	4	10, 625. 00	2, 656. 25	. 5247
Residual	20	101, 250. 00	5, 062. 05	
Total	39	279, 937. 50		
DTS–1 (dunite)				
Main:				
A	4	15, 625. 00	3, 906. 25	0. 5297
B	1	20, 250. 00	20, 250. 00	2. 7458
C	1	42, 250. 00	42, 250. 00	5. 7288
Interactions:				
AB	4	5, 375. 00	1, 343. 75	. 1822
AC	4	7, 125. 00	1, 781. 25	. 2415
BC	1	196, 000. 00	196, 000. 00	26. 5763
ABC	4	5, 875. 00	1, 468. 75	. 1992
Residual	20	147, 500. 00	7, 375. 00	
Total	39	440, 000. 00		

[1] A, between bottles; B, between colorimetric and atomic absorption methods; C, between analyst 1 using Ni crucibles and NaOH fusion and analyst 2 using Zr crucibles and Na_2O_2 fusions.

[2] Critical F values (Davies, 1949):

$F_{0.01}$ (4,20) 4.43	$F_{0.01}$ (1,20) 8.10
$F_{0.05}$ (4,20) 2.87	$F_{0.05}$ (1,20) 4.35
$F_{0.10}$ (4,20) 2.25	$F_{0.10}$ (1,20) 2.97

TABLE 4.—*Comparison of results of analyses for chromium, in parts per million, in U.S. Geological Survey standards PCC–1 (peridotite) and DTS–1 (dunite)*

Sample number	Present report [1]			Previous rock analyses			
	Colorimetric method	Atomic absorption method	Average	(2)	(3)	(4)	Average
PCC–1 (peridotite)	2, 860	2, 868	2, 864	2, 874	2, 874	2, 805	2, 851
DTS–1 (dunite)	4, 298	4, 253	4, 275	4, 448	4, 379	3, 969	4, 265

[1] Average chromium values shown in tables 1 and 2.
[2] Analyst, E. L. Munson, 1964 (U.S. Geological Survey, Denver, Colo.), single conventional analysis.
[3] Analyst, V. C. Smith, 1964 (U.S. Geological Survey, Denver, Colo.), single conventional analysis.
[4] Analyst, L. E. Reichen, 1968 (U.S. Geological Survey, Washington, D.C.), single conventional analysis.

the values agree well, those reported in this paper appear to be high when compared with the average values of chromium for all the analyses of these rocks given by Flanagan (1969, table 4): for PCC–1, 2,682 ppm; for DTS–1, 3,736 ppm.

ANALYTICAL PROCEDURES

Sodium peroxide fusion

Transfer 0.2 g of rock to a zirconium crucible. Add about 1.5 g of Na_2O_2 to the crucible. Heat cautiously over a moderate flame and continue heating for about 1.5 minutes after a quiescent melt is obtained. Allow the melt to cool, then transfer the crucible and its contents to a 250-ml beaker. Add 100 ml of 5-percent solution of alcohol in water to the beaker and heat the solution until the melt is disintegrated. Quantitatively transfer the solution and disintegrated melt to a 200-ml volumetric flask. Allow the solution to cool, dilute to volume with water, and mix. Filter a portion of the solution through an 11-cm dry filter paper into a 150-ml beaker. Reserve the filtrate solution for chromium analyses.

Sodium hydroxide-sodium peroxide fusion

Transfer 0.2 g of rock to a nickel crucible. Add 2.0 g of NaOH and 0.5 g of Na_2O_2 to the crucible. From this point the procedure is the same as that for the sodium peroxide solution method.

Colorimetric determination of chromium

Procedure.—Transfer a portion of the reserved filtrate solution to a 1-cm cell and determine the absorbance of the solution at 370 mμ, using a Beckman D.U. spectrophotometer.

Calibration curve.—Add, separately, 0, 2.0, 4.0, 6.0, and 8.0 ml of a standard 100-ppm chromium solution to 100-ml volumetric flasks. Adjust the alkalinity of each standard to approximate the alkalinity of the reserved filtrate sample solutions. Dilute to a 100-ml volume with water, and mix. Determine the absorbance of the standard solutions (2, 4, 6, and 8 ppm Cr) at 370 mμ against the zero standard as a reference, using 1-cm cells. The same standards were used to obtain a calibration curve for the atomic absorption determinations.

Atomic absorption determination of chromium

Atomize a portion of the reserved filtrate solution into the flame of the atomic absorption spectrophotometer for the chromium determination. Also atomize portions of the colorimetric chromate standard solutions (0, 2, 4, 6, and 8 ppm Cr) in order to obtain a calibration curve.

The chromium values were obtained with a Perkin-Elmer Model 303 atomic absorption spectrophotometer, using an air-acetylene flame and the following instrument parameters recommended by the manufacturer:

Wavelength	3,579 angstroms.
Slit	3.
Acetylene flow setting [1]	9.5.
Airflow setting [1]	8.0.
Burner	Boling 3 slot.
Flame	Reducing.
Acetylene pressure	9 psi.
Air pressure	30 psi.
Scale	X I.

[1] Arbitrary units.

REFERENCES

Davies, O. L., 1949, Statistical methods in research and production, with special reference to the chemical industry [2d ed.]: London, Oliver and Boyd, Ltd., 292 p.

Flanagan, F. J., 1967, U.S. Geological Survey silicate rock standards: Geochim. et Cosmochim. Acta, v. 31, p. 289–308.

———1969, U.S. Geological Survey standards. II. First compilation of data for the new U.S.G.S. rocks: Geochim. et Cosmochim. Acta, v. 33, p. 81–120.

DETERMINATION OF TELLURIUM IN GEOLOGIC MATERIALS IN THE PARTS-PER-BILLION RANGE

By A. E. HUBERT, Denver, Colo.

Abstract.—A sensitive method useful in geochemical exploration has been developed for the determination of tellurium in geologic material. In this method the sample is digested with hydrobromic acid and bromine, and the tellurium is extracted into methyl isobutyl ketone and stripped from the organic phase with water. Tellurium is then measured indirectly by its catalytic action on the reduction of gold by hypophosphorous acid. Results by this method compare favorably with those obtained by atomic absorption. The lower limit of sensitivity by the catalytic method is 5 ppb, whereas existing atomic absorption methods provide a sensitivity of 100 ppb.

The crustal abundance of tellurium is reported by Goldschmidt (1954) at 0.002 ppm (2 ppb). Tellurium in small amounts occurs in halos above deposits of less mobile elements such as gold, and its presence in amounts greater than crustal abundance may indicate targets of mineral potential such as were found in the Cripple Creek district of Colorado (Gott and others, 1967). Small amounts of tellurium also occur as a halo around the copper-rich core in the Ely district of Nevada (Gott and McCarthy, 1966). In the proposed procedure greater sensitivity than available in previous methods offers a better chance to define telluriferous areas related to ore deposits. The method presented here is briefly as follows: The tellurium is brought into solution by a bromine-hydrobromic acid digestion and extracted from the diluted acid (3*N* in HBr) into methyl isobutyl ketone as in the procedure described by Nakagawa and Thompson (1968). Tellurium is extracted into water from the ketone, and the aqueous solution is made 6*N* with hydrochloric acid. Tellurium is finally estimated by its catalytic enhancement of the reduction of gold by hypophosphorous acid (Lakin and Thompson, 1963).

REAGENTS AND APPARATUS

Standard tellurium solution, 0.01 percent: Dissolve 0.0625 g of TeO_2 in 500 ml of 6*N* HCl.

Dilute tellurium solution, 0.0001 percent: Dilute 1 ml of 0.01-percent tellurium solution to 100 ml with concentrated HCl.

Bromine, reagent grade.

Hydrobromic acid, concentrated, reagent grade.

Hydrobromic acid, 1.5*N*: Dilute 172 ml of concentrated HBr to 1 liter with water.

Hydrobromic acid-bromine solution, 1 percent: Dissolve 10 ml of liquid Br in 1 liter of concentrated HBr.

Methyl isobutyl ketone (MIBK), reagent grade.

Hydrochloric acid, concentrated, reagent grade.

Hydrochloric acid, 6*N*: Dilute 1 liter of concentrated HCl with 1 liter of water.

Cupric chloride solution, 3 percent: Dissolve 3 g of cupric chloride ($CuCl_2 \cdot 2H_2O$) in 100 ml of 6*N* of HCl.

Gold solution, 10 mg/ml: Dissolve 2.5 g of Au in aqua regia. Evaporate to near dryness on a hotplate and dissolve the moist residue in 250 ml of 6*N* HCl.

Dilute gold solution, 2 mg/ml: Dilute 20 ml of stock gold solution to 100 ml with 6*N* HCl.

Hypophosphorous acid, 50 percent, reagent grade.

Hotplate, oscillating: A 12×20-inch electric hotplate, with 100°–260°C temperature control, mounted on a constant-speed oscillator base.

Styrofoam cups, insulating, 6 oz.

Test tubes, screwcap, 25×200 mm.

Vacuum filtration equipment, 0.45μ Millipore filter disks.

PROCEDURE

Solution of tellurium sample

Place a 5-g pulverized sample in a 100-ml beaker with 20 ml of 1-percent bromine-hydrobromic acid solution and allow to stand for 1 hour. Put the beaker on an oscillating hotplate and boil the solution gently until the volume is reduced to approximately 10 ml. Remove the beaker from the hotplate and allow to cool.

Extraction of tellurium

Transfer the entire contents (sample and acid) of the beaker to a 25×200-mm test tube fitted with a screwcap. Rinse the beaker with water and add the rinse portion to the tube. Add water to obtain a final volume of about

U.S. GEOL. SURVEY PROF. PAPER 750-B, PAGES B188-B190

300 ml. Add 10 ml of MIBK, screw on the cap, and shake the tube for 5 minutes. Let the contents of the tube settle, or centrifuge until the two layers separate. By pipet transfer the upper MIBK layer to another tube containing 30 ml of 1.5*N* hydrobromic acid. Cap and shake tube for 1 minute and allow the MIBK layer to separate.

Transfer the upper MIBK layer to a tube containing 25 ml of distilled water and shake for 30 minutes. Then remove the MIBK layer and discard. Place the tube containing the water solution on a steam bath to evaporate any remaining MIBK. Cool the tube, add 25 ml of concentrated HCl, and place the tube in the refrigerator to cool to 5°C for the catalytic estimation of tellurium.

Estimation of tellurium

Place 50 ml of 6*N* HCl at 5°C in a styrofoam cup. Add 0.5 ml of gold chloride solution, 0.6 ml of cupric chloride solution, and 0.010γ (obtained by dilution of the dilute, 0.0001 percent, standard solution) of tellurium. Then add 0.3 ml of hypophosphorous acid and allow to stand exactly 5 minutes. At the end of the 5-minute interval, vacuum filter the solution through a 0.45μ Millipore filter paper. If the gold precipitate is pink, the correct concentration of hypophosphorous acid has been used; if no colored precipitate appears, add more hypophosphorous acid, in increments of 0.1 ml to successive trials, until a suitable pink or purple precipitate is obtained. Then make a standard series containing 0, 0.005γ, 0.010γ, and 0.020γ of tellurium and add same amount of hypophosphorous acid as used previously to each standard in the series. The filter disks should appear as a series ranging from colorless on the blank to a deep purple on the highest standard. Once a standard series is obtained, all under the same conditions of time, temperature, and amount of hypophosphorous acid, substitute aliquots of the original sample solution for the tellurium (0.01 percent) standard solution and proceed as in the preparation of the standard series. An aliquot of 0.1 to 10 ml of the same solution can be taken to make a colored spot that matches a color in the standard series.

With a 5-g sample diluted to 50 ml, parts per million in sample $= \frac{\text{micrograms} \times 10 \text{ found}}{\text{milliliters of aliquot}}$.

The tellurium values will range from 0.005 to 1 ppm in a 5-g sample. In practice four samples are run at a time along with a standard as a control. If the control-standard color spot differs in any batch of four samples, change the amount of hypophosphorous acid to obtain the same color in the control as in the previously prepared standard series, and repeat the four samples. Careful control of the temperature of the reactment is essential. If the temperature is above 9°C the spots will be brown and therefore unsatisfactory for any standard series.

DISCUSSION

Hypophosphorous acid is at best marginal in purity inasmuch as it decomposes with time. To obtain consistent results, the bottle of hypophosphorous acid should be opened at least 24 hours before doing the test. Not all bottles of acid are of the same quality, and the rate of reaction will vary from one bottle to another.

Styrofoam cups are used because they help to maintain a constant temperature. Pyrex may be used, but is very difficult to clean for each series of tests.

Interference from iron has been observed to affect the catalytic test. High iron content in the sample will color the MIBK layer reddish brown, and the iron must be removed by successive extractions with 1.5*N* HBr until the MIBK layer is almost colorless. Lakin and Thompson (1963) reported freedom of interference for many elements at expectable concentrations.

PRECISION AND ACCURACY

The precision or repeatability of the catalytic method was investigated by determining the tellurium present in five replicates of six soil sample splits of the same sample, containing various amounts of a standard tellurium solution (table 1). Five replicates of five tellurium

TABLE 1.—*Replicate catalytic determinations of added tellurium in a 5-g soil sample*

Soil sample split No.	Tellurium					Standard deviation (ppm)	Relative standard deviation (percent)
	Added to split (μg)	Calculated in soil (ppm)	Found in soil (ppm)				
			Low	High	Average		
1	None	None	<0.005	<0.005	<0.005	0	0
2	0.025	0.005	.005	.010	.007	.003	43
3	.25	.05	.025	.05	.045	.01	24
4	.5	.1	.05	.1	.09	.02	22
5	1	.2	.2	.2	.2	0	0
6	2.5	.5	.5	1.0	.6	.2	33

composite laboratory-rock standards (contributed by R. L. Erickson, U.S. Geological Survey) compared satisfactorily with atomic absorption values (table 2).

The method is of use below the limit of detection of the atomic absorption method. The method has a sensitivity approaching the value of the crustal abundance of tellurium given by Goldschmidt (1954) and affords an opportunity to study the distribution of tellurium in mineralized areas.

TABLE 2.—*Comparison of the average tellurium values of five catalytic determinations with the average of 20 determinations by atomic absorption on composite laboratory-rock standards*

Sample No.	Determinations	
	Catalytic (ppm)	Atomic absorption (ppm)
1	2.0	2.0
2	.55	1.1
3	.5	.6
4	.39	.46
5	.14	.2

REFERENCES

Goldschmidt, V. M., 1954, Geochemistry: Oxford, Clarendon Press, 730 p.

Gott, G. B., and McCarthy, J. H., Jr., 1966, Distribution of gold, silver, tellurium, and mercury in the Ely mining district, White Pine County, Nevada: U.S. Geol. Survey Circ. 535, 5 p.

Gott, G. B., McCarthy, J. H., Jr., VanSickle, G. H., and McHugh, J. B., 1967, Distribution of gold, tellurium, silver, and mercury in part of the Cripple Creek district, Colorado: U.S. Geol. Survey Circ. 543, 9 p.

Lakin, H. W., and Thompson, C. E., 1963, Tellurium—A new sensitive test: Science, v. 141, no. 3575, p. 42–43.

Nakagawa, H. M., and Thompson, C. E., 1968, Atomic absorption determination of tellurium, *in* Geological Survey Research 1968: U.S. Geol. Survey Prof. Paper 600–B, p. B123–B125.

SUBSTOICHIOMETRIC DETERMINATION OF TANTALUM BY NEUTRON ACTIVATION

By L. PAUL GREENLAND and E. Y. CAMPBELL,
Washington, D.C.

Abstract.—A rapid radiochemical separation of tantalum utilizing substoichiometric extraction of the tantalum tetra-*N*-pentylammonium bromide (TPABr) complex for the chemical yield determination is described. After hydrofluoric-sulfuric acid or sodium peroxide decomposition of silicate rocks, tantalum is radiochemically purified by methyl isobutyl ketone (MIBK) extraction from hydrofluoric-sulfuric acid media, back extraction to ammonium hydroxide, and chloroform extraction of the TPABr complex from hydrofluoric acid. Results from the U.S. Geological Survey rocks are presented.

There has long been a need for a routine analytical method for the determination of tantalum in geological materials. Although neutron activation possesses the requisite sensitivity, published methods are too lengthy for routine use (Greenland, 1968). With the advent of Ge(Li) detectors, rapid nondestructive determinations of tantalum have become possible; however, the sensitivity of these techniques (1 ppm Ta) is inadequate for most purposes (Gordon and others, 1968).

The use of substoichiometric separations to eliminate the chemical yield determination required by activation analysis and thus reduce the analytical time involved is ideally suited to routine analyses (Ruzicka and Stary, 1968; Alimarin and Perezhogin, 1967). We have investigated the use of tetra-*N*-pentylammonium bromide (TAPBr) for the substoichiometric separation of tantalum and have used this separation in a rapid activation determination of tantalum in geologic materials.

The nuclear properties of tantalum relevant to neutron activation analysis have been described previously (Greenland, 1968). The most suitable reaction is: $Ta^{181}(n,\gamma)Ta^{182}$. The Ta^{182} decays with a half life of 115 days, producing many easily measured γ-rays.

REAGENTS

Tantalum carrier solution: Dissolve 7.9 g of $TaCl_5$ in 100 ml of 1+10 HF to give a solution of $\approx$40 mg/ml of Ta. The exact concentration is unimportant.

TPABr solution: Dissolve 1.89 g of tetra-*N*-pentylammonium bromide in 250 ml of $CHCl_3$. The reagent is not stable; prepare fresh daily.

Note.—10 ml of the TPABr solution should correspond stoichiometrically to about 50 percent of the tantalum carrier added to the samples in the procedure. It is advisable to titrate uew batches of TPABr with the tantalum solution and adjust volumes accordingly.

ANALYTICAL PROCEDURE

Irradiation

Approximately 100 mg of each sample was sealed in a polyethylene vial and irradiated for 12–16 hours in a thermal neutron flux of 7×10^{12} n $cm^{-2}sec^{-1}$ at the U.S. Naval Research Laboratory reactor. After irradiation, at least 10 days were permitted for decay of short-lived radioactive products before starting the tantalum radiochemistry.

A natural glass (composite philippinite Po–300), in which tantalum had been determined previously by several neutron activation techniques, was used as a standard. Eighteen samples and 2 standards were irradiated simultaneously and processed through the radiochemistry as a single batch.

Radiochemical purification

Transfer the samples to a platinum dish containing 1.5 ml of Ta carrier, 1–2 ml of H_2SO_4, and 25–30 ml of HF and evaporate overnight on a steam bath. Alternatively, if resistant minerals (such as zircon) are present, fuse the samples with Na_2O_2 in an iron crucible in which 1.5 ml of Ta carrier had been evaporated, leach the fus-

U.S. GEOL. SURVEY PROF. PAPER 750-B, PAGES B191-B193

ion cake with H_2O and centrifuge; discard the supernatant. Dissolve the residue from either decomposition technique in 20–30 ml of 6*M* H_2SO_4–2*M* HF and extract with 15 ml of methyl isobutyl ketone for 10 minutes. Discard the aqueous layer and wash the organic layer for 30 seconds with, successively, 5 ml of 1+20 HNO_3 and 5 ml of H_2O. Discard the wash solutions and back-extract tantalum by shaking the organic layer with 4 ml of 1+10 NH_4OH for 1 minute. $Ta(OH)_5$ appears as a white precipitate at this point; without attempting to separate the phases, add 10 ml of 1+10 HF and swirl to dissolve the precipitate. Drain the aqueous layer to an extraction vessel and add 10.0 ml of TPABr reagent. Extract for 10 minutes, then drain the organic layer quantitatively to a counting vial.

Counting procedure

Count the samples with a 3×3-inch NaI(Tl) well detector coupled to a single-channel analyzer gated to pass the 1.12-, 1.19-, 1.22-, and 1.33-MeV γ-rays. Count the samples twice, obtaining at least 2,000 counts each time. For most samples, counting times less than 10 minutes were required.

DISCUSSION

The chemical procedure was designed to obtain Ta^{182} in a radiochemically pure state with a constant chemical yield. The methyl isobutyl ketone extraction separates tantalum (and Nb) almost completely from other elements, and the two washes remove niobium (Greenland and Campbell, 1970) and surviving traces of other elements. The TPABr extraction is also highly selective for tantalum (Dosch, 1969), and the use of substoichiometric amounts of the reagent increases the selectivity (Ruzicka and Stary, 1968). The selectivity of these separations was confirmed by multichannel analyzer γ-ray spectra of the final fractions which showed only Ta^{182} activity.

The principle of substoichiometric separations and their use to obviate the usual chemical yield determination are described in detail in the excellent monograph by Ruzicka and Stary (1968). Basically, the method relies on the use of a substoichiometric amount of a reagent which reacts quantitatively (or to a constant extent) with the element to be determined to form a complex which can be separated from the excess of unreacted element. In this way a constant amount of the added carrier is obtained in the final solution and, if equal amounts of carrier are added to samples and standards, no correction for chemical losses need be made.

Dosch (1969) described the use of TPABr for the gravimetric separation and determination of tantalum, and we have investigated the application of this reagent to the substoichiometric determination of tantalum. Preliminary experiments showed that both the reagent and its tantalum complex are soluble in chloroform and that this medium provides an easy separation of the complex from unreacted tantalum. With excess TPABr, 90–95 percent of the tantalum is extracted in the range 1–100 mg of Ta.

The reproducibility of the substoichiometric separation of tantalum was studied by extracting increasing amounts of tantalum (at constant specific activity) with a fixed amount of TPABr. The activity of the extracts increased linearly until the stoichiometric amount of tantalum was extracted after which the activity was independent (within ±5 percent) of the tantalum content.

The time required for equilibrium was studied by varying the shaking period (excess Ta) from 2 to 40 minutes. The amount of tantalum extracted was constant in the 5- to 40-minute range and only slightly less for a 2-minute shaking.

The acid concentration was varied over the 2- to 10-percent HF range without effect on the extraction of tantalum.

Table 1 summarizes the chemical losses of tantalum in the procedure up to the TPABr extraction. Most of the loss is due to the incomplete back extraction of tantalum with ammonium hydroxide. However, the total loss of tantalum was less than 40 percent in all analyses and is, therefore, immaterial if the amount of TPABr is limited to that sufficient only to extract 50 percent of the original amount of tantalum carrier.

Analyses of the U.S. Geological Survey standard rocks by this method, using both hydrofluoric–sulfuric acid and sodium peroxide decomposition, are compared with previous values in table 2. Results from the two decomposition methods are in reasonable agreement with each other and with the published results except in the case of G–1. Butler and Thompson (1962) using HF–H_2SO_4 decomposition previously reported values of 0.8–1.0 ppm of Ta in G–1. The low results from the

TABLE 1.—*Losses in chemical separation of tantalum*

Procedural step	*Percentage of original tantalum lost (average of 10 samples)*
Extraction to methyl isobutyl ketone	0.6
HNO_3 wash	2.0
H_2O wash	7.2
Back extraction to NH_4OH	24.1
Total lost prior to tetra-N-pentylammonium bromide extraction	34

TABLE 2.—*Determination of tantalum, in parts per million, in U.S. Geological Survey standard rocks*

Sample	$HF-H_2SO_4$ decomposition		Na_2O_2 decomposition		Previous results [1]
	Individual	Mean	Individual	Mean	
G–1	1.0, .78, .89, .85	0.88	1.4, 1.5, 1.6	1.5	1.6
W–1	.53, .49, .42, .52	.49	.56, .57, .48	.54	.7
G–2	.97, .86, .83, .80	.86	1.0, .99, .88	.96	1.0, .82
GSP–1	1.1, .99, .96, .85	.98	.90, .89, 1.1	.96	1.4, .77
AGV–1	1.1, 1.0, 1.0, .92	1.0	.98, 1.0, 1.0	.99	1.0, .32
BCR–1	.77, .85, .70, .90	.80	.81, .83, .92	.85	.9, .86
PCC–1	<.05, <.05, <.05, <.05	<.05	----------	----------	<.1
DTS–1	<.05, <.05, <.05, <.05	<.05	----------	----------	<.1

[1] G–1 and W–1 results are "recommended values" of Fleischer (1969); others are neutron activation determinations cited by Flanagan (1969).

$HF-H_2SO_4$ decomposition of G–1 suggest that tantalum is concentrated in zircon or other resistant mineral. Although somewhat more tedious, the Na_2O_2 fusion appears to be preferable for the decomposition of silicic (at least) rocks.

The extremes of the replicate determinations shown in table 2 vary by ±10–15 percent from the mean. This variation can be accounted for by the neutron flux variation (±10 percent), the substoichiometric yield (±5 percent), counting statistics (±2 percent), and combined pipeting and transferring errors (±2 percent). Although some of these errors could be reduced if necessary, the precision is adequate for most analyses.

With the system described here, 0.05 ppm of Ta corresponds to a counting rate five times greater than the background rate and is about the lower limit for a reliable determination. This is adequate for most geologic samples but, if necessary, can be decreased by using larger samples and (or) more sophisticated counting equipment.

The major advantages of this method are simplicity and speed. Both the chemical separations and the counting can be done by relatively untrained personnel. Batches of 20 samples can be separated and counted in a single day; if a day is allowed for cleanup and preparation of the next batch, a routine output of 10 samples per man-day can be maintained.

ACKNOWLEDGMENTS

We are indebted to Irving May and J. I. Dinnin for their helpful criticisms of an earlier version of this paper.

REFERENCES

Alimarin, I. P., and Perezhogin, G. A., 1967, Substoichiometric separation in activation analysis—extraction of co-ordinatively-unsolvated salts: Talanta, v. 14, p. 109–119.

Butler, J. R., and Thompson, A. J., 1962, Ta in the granite G–1: Geochim. et Cosmochim. Acta, v. 26, p. 516–517.

Dosch, R. G., 1969, Determination of tantalum and its separation from niobium and other closely associated elements using tetra-N-pentylammonium bromide: Anal. Chemistry, v. 41, p. 193–195.

Flanagan, F. J., 1969, U.S. Geological Survey standards—[pt.] 2, First compilation of data for the new U.S.G.S. rocks: Geochim. et Cosmochim. Acta, v. 33, p. 81–120.

Fleischer, Michael, 1969, U.S. Geological Survey Standards—[pt.] 2, Additional data on rocks G–1 and W–1, 1965–1967: Geochim et Cosmochim. Acta, v. 33, p. 65–79.

Gordon, G. E., Randle, K., Goles, G. G., Corliss, J. B., Beeson, M. H., and Oxley, S. S., 1968, Instrumental activation analysis of standard rocks with high-resolution γ-ray detectors: Geochim. et Cosmochim. Acta, v. 32, p. 369–396.

Greenland, L. P., 1968, Simultaneous determination of tantalum and hafnium in silicates by neutron activation analysis: Anal. Chim. Acta, v. 42, p. 365–370.

Greenland, L. P., and Campbell, E. Y., 1970, Determination of niobium in rocks by an isotope dilution-spectrophotometric method: Anal. Chim. Acta, v. 49, p. 109–114.

Ruzicka, Jaromir, and Stary, Jiri, 1968, Substoichiometry in radiochemical analysis: New York, Pergamon Press, 151 p.

THERMAL METHOD FOR QUANTITATIVE DETERMINATION OF NAHCOLITE IN COLORADO OIL SHALE

By JOHN R. DYNI, WAYNE MOUNTJOY, P. L. HAUFF, and PAUL D. BLACKMON, Denver, Colo.

Abstract.—A simple thermal method for determining the amount of nahcolite ($NaHCO_3$) in Colorado oil shale has been developed. When nahcolite-bearing oil shale is heated at 105°C for 14 hours, the nahcolite decomposes to sodium carbonate by loss of carbon dioxide and water. The amount of nahcolite can be calculated from this weight loss by the following equation: Nahcolite (weight percent) = percent weight loss $\times 2.690 + 0.375$. The statistical accuracy of the method compared to that of chemical analyses is ±2 weight percent at 95-percent confidence limits. The method is reasonably free of interferences and requires a minimum of laboratory equipment. Trona ($Na_2CO_3 \cdot NaHCO_3 \cdot 2H_2O$) can also be determined quantitatively by the thermal method. The technique cannot be used to determine the amount of dawsonite [$NaAl(OH)_2CO_3$] in oil shale because the higher temperatures required to decompose dawsonite also decompose the associated kerogen.

The thick rich-grade oil shales of the Eocene Green River Formation in the Piceance Creek basin, northwestern Colorado, contain large deposits of nahcolite ($NaHCO_3$) that have potential economic value for soda ash (Hite and Dyni, 1967). Because much of the nahcolite is nonbedded and is intimately associated with oil shale, estimating the amount of nahcolite in a core is difficult.

This report describes a new analytical technique for determining the amount of nahcolite in oil shale. The nahcolite-bearing oil shale is heated for 14 hours at 105°C, and the nahcolite decomposes to sodium carbonate by loss of carbon dioxide and water. The amount of nahcolite in the oil shale can be calculated from this weight loss of carbon dioxide and water. The authors' thermal method is simple and reasonably free of interferences, yields relatively accurate and duplicable analyses, and requires a minimum of analytical equipment. The method should be useful in analyzing large numbers of samples for resource and other studies of the nahcolite deposits in the Piceance Creek basin.

The idea for the method was suggested by P. D. Blackmon after he found that nahcolite almost completely decomposes at temperatures as low as 100°C when the mineral was heated for prolonged lengths of time. J. R. Dyni designed the experiments to test the method, and Dyni, P. L. Hauff, and P. C. Beck did the thermal analytical work. Wayne Mountjoy chemically analyzed the samples of oil shale used in these experiments. Fischer assays of samples of oil shale were made by the Laramie Petroleum Research Center, U.S. Bureau of Mines, Laramie, Wyo.

DEVELOPMENT OF METHOD

Sample materials

Sample materials used in this investigation were nahcolite-bearing oil shale, natural and synthetic nahcolite, and trona. The oil shale is from the Joe T. Juhan core hole 4–1 (sec. 4, T. 2 S., R. 98 W., Rio Blanco County, Colo.), a core hole which penetrates the nahcolite-bearing oil-shale deposits in the northern part of the Piceance Creek basin. Composite samples from this core hole were prepared by dry-cutting thin slabs from 2-foot lengths of quartered 1⅛-inch-diameter core. The several slabs from each interval were crushed, ground to pass a 100-mesh screen, and thoroughly mixed.

The natural nahcolite consisted of small clear fragments handpicked from a coarsely crystalline mass of nahcolite obtained from an oil-shale mine in the basin. These fragments unavoidably contained traces of kerogen; however, no mineral impurities were detected by X-ray diffraction. The natural trona, obtained from an operating trona mine in southwest Wyoming, is a satiny white variety which contained no X-ray detectable mineral impurities. The nahcolite and trona were gently hand ground by mortar and pestle to pass a 100-mesh screen. Powdered reagent-grade sodium bicarbonate (synthetic nahcolite) was among the sample materials.

U.S. GEOL. SURVEY PROF. PAPER 750-B, PAGES B194-B198

Thermal decomposition of nahcolite

When heated, sodium bicarbonate decomposes by the following endothermic reaction:

$$2NaHCO_3 \longrightarrow Na_2CO_3 + H_2O + CO_2.$$

The theoretical weight loss in this reaction is 36.91 percent. Published data on the rate of this reaction with respect to time and temperature are incomplete; however, Gautier (1876) reported more than 90 years ago that sodium bicarbonate almost completely decomposes when heated for 18 hours between 100° and 115°C. Other workers found that sodium bicarbonate partly decomposes at even lower temperatures (Mellor, 1952, p. 763).

Differential thermal analysis studies of nahcolite, the natural sodium bicarbonate, show that in an air atmosphere, decomposition begins at 125°, reaches a maximum rate at 205°, and ends at 225°C (Beck, 1950), whereas in a carbon dioxide atmosphere, decomposition reaches a maximum rate at 125°C (Smith and Johnson, 1967). These higher decomposition temperatures found by differential thermal analysis depend partly on the rate of heating. Slowing the rate of heating lowers the temperature at which the reaction occurs.

Recently, Blackmon noted that when nahcolite-bearing Colorado oil shale was heated overnight at 100°C, the nahcolite almost completely decomposed, seemingly without decomposing the kerogen or other constituent minerals of the oil shale that were identified by X-ray diffraction analysis. The resultant weight loss on heating was found to be proportional to the original amount of nahcolite in the oil shale. This finding suggested the quantitative method described.

The feasibility of the thermal method was tested by the following experiments. Most of the samples used in the experiments weighed 1.0–1.5 g, and weights were determined to within 0.1 mg. The samples were heated in open porcelain crucibles in an electric oven. Oven temperatures were determined by a mercury-filled partial immersion glass thermometer, 0°–300°C scale with 1° divisions. The estimated error in the reported temperatures is ±2°C.

To determine the optimum temperature and length of time of heating, weight losses were determined for samples of nahcolite and sodium bicarbonate heated (1) for 14 hours at different temperatures (table 1), and (2) for various lengths of time at 105°C (table 2). The results show that synthetic and natural nahcolite do not completely decompose within the ranges of time and temperature of the experiments. For 14 hours of heating, maximum decomposition is achieved at about 100°C and above (table 1). Samples heated at 105°C show about 95-percent decomposition in the first 4 hours of heating; maximum decomposition is achieved by 12 hours for nahcolite (table 2).

The temperature and length of time of heating were standardized at 105°±2°C and 14 hours. Although somewhat higher temperatures and a longer heating period could be used, these values were selected to minimize the possible interference of thermal decomposition of kerogen. Replicate samples of nahcolite heated under these standard conditions show an average weight loss of 36.61 percent, or about 0.3 percent less than the theoretical value (table 3).

TABLE 1.—*Weight-loss determinations, in percent, for samples of nahcolite and sodium bicarbonate heated for 14 hours at temperatures ranging from 41° to 130°C*

[Analyses by J. R. Dyni]

Temperature (°C)	Nahcolite		Sodium bicarbonate	
	Weight loss	Decomposed	Weight loss	Decomposed
41	0.04	0.11	0.10	0.27
50	.07	.18	.35	.95
60	2.78	7.53	2.82	7.64
71	11.62	31.5	11.18	30.3
80	24.56	66.5	27.48	74.7
89	33.58	91.0	35.63	96.5
100	36.56	99.0	36.70	99.4
110	36.67	99.3	36.65	99.3
119	36.64	99.3	36.69	99.4
130	36.66	99.3	36.68	99.4
Theoretical weight loss	36.91	----------	36.91	----------

TABLE 2.—*Weight-loss determinations, in percent, for samples of nahcolite and sodium bicarbonate heated at 105°C for periods of time ranging from 1 to 24 hours*

[Analyses by J. R. Dyni]

Hours heated	Nahcolite		Sodium bicarbonate	
	Weight loss	Decomposed	Weight loss	Decomposed
1	16.45	44.57	13.04	35.33
2	26.67	72.26	23.91	64.78
3	32.21	87.27	30.08	81.50
4	34.46	93.36	35.46	96.07
5	35.67	96.64	36.40	98.62
6	36.19	98.05	36.59	99.13
7	36.42	98.67	36.66	99.32
8	36.55	99.02	36.68	99.38
10	36.46	98.78	36.67	99.35
12	36.62	99.21	36.70	99.43
14	36.62	99.21	36.67	99.35
16	36.63	99.24	36.69	99.40
18	36.70	99.43	36.69	99.40
20	36.69	99.40	36.67	99.35
22	36.66	99.32	36.73	99.51
24	36.68	99.38	36.66	99.32
Theoretical weight loss	36.91	----------	36.91	----------

During the experimental work, it became evident that trona could also be determined quantitatively by the thermal method. The reaction for the thermal decomposition of trona is

$$2Na_2CO_3 \cdot NaHCO_3 \cdot 2H_2O \longrightarrow 3Na_2CO_3 + 5H_2O + CO_2.$$

In this reaction the weight loss of water and carbon dioxide is 29.66 percent. Replicate samples of trona heated under the standard conditions of the thermal method gave an average weight loss of 29.46 percent, or about 0.2 percent less than the theoretical value (table 3).

TABLE 3.—*Weight-loss determinations, in percent, for replicate samples of nahcolite, sodium bicarbonate, and trona heated for 14 hours at 104° C*

[Analyses by P. L. Hauff]

Nahcolite		Sodium bicarbonate		Trona	
Weight loss	Decomposed	Weight loss	Decomposed	Weight loss	Decomposed
36. 59	99. 12	36. 61	99. 18	29. 46	99. 31
36. 66	99. 31	36. 68	99. 37	29. 46	99. 41
36. 62	99. 20	36. 63	99. 23	29. 45	99. 28
36. 62	99. 20	------	------	29. 45	99. 28
36. 59	99. 12	------	------	29. 50	99. 44
36. 60	99. 15	------	------	29. 45	99. 28
Average:					
36. 61	99. 18	36. 64	99. 26	29. 46	99. 33
Theoretical:					
36. 91	------	36. 91	------	29. 66	------

THERMAL METHOD

Equipment and procedure

Apparatus includes 15-ml porcelain crucibles, desiccators, constant-temperature electric oven, and analytical balance.

The sample of nahcolite-bearing oil shale is crushed, ground to pass a 100-mesh screen, and is thoroughly mixed. To avoid possible thermal decomposition of the nahcolite, the sample should not be allowed to warm up during grinding and mixing. About 1.0 to 1.5 g of sample in a tared oven-dried crucible is dried for 24 hours in a desiccator, weighed accurately to 0.1 mg, then heated for 14 hours at 105°C. The sample and crucible are allowed to cool to room temperature in a desiccator, then reweighed. The weight loss, in percent, is determined and the amount of nahcolite is calculated as follows:

$$\text{Nahcolite (wt percent)} = \text{percent weight loss} \times 2.690 + 0.375.$$

It should be emphasized that this method is quantitative; positive identification of nahcolite by other means, such as X-ray diffraction, is required.

Interferences

Possible interferences in the thermal method include (1) thermal decomposition of kerogen, volatile hydrocarbons, and carbonate minerals other than nahcolite, and (2) presence of adsorbed water.

Table 4 lists weight-loss determinations for oil shales of varying richness from the nahcolite-bearing oil-shale section in the Juhan core hole which were heated for 14 hours at 104°C. The samples, with the exception of two (2427–29 and 2570–72), originally contained nahcolite in amounts ranging from 1.1 to 77.1 weight percent which was removed by water leaching prior to thermal analysis. Semiquantitative X-ray diffraction analysis of the unleached samples found by weight: 0–18 percent dawsonite, 6–25 percent dolomite, and 20–44 percent quartz and feldspar. Samples 2427–29 and 2570–72 (table 4) are from clay-bearing oil shale which underlies the sodium-rich section, and they contained 16 and 31 percent illite, respectively. The weight losses (table 4) are uniformly low and average 0.19 percent. Although these losses show no clear correlation with kerogen or the minerals present, they are probably due to slight decomposition of kerogen, or possibly to small losses of adsorbed water that could not be removed by desiccation prior to analysis.

Possible interference by volatile hydrocarbons was not tested by these samples. Some cores penetrating the nahcolite-bearing oil-shale deposits in Colorado locally contain viscous to solid hydrocarbons in vugs and along fractures. Lighter fractions of these hydrocarbons could

TABLE 4.—*Weight-loss determinations for 13 samples of water-leached moderate- to rich-grade oil shale heated for 14 hours at 104°C*

Sample depth (feet)	Unleached sample		Weight loss for water-leached sample (percent)
	Shale-oil content (gallons per ton)	Nahcolite content (weight percent)	
1861–63	16. 8	36. 0	0. 16
1865–67	21. 2	18. 0	. 12
1961–63	22. 0	37. 6	. 14
1967–69	27. 2	24. 4	. 18
2015–17	29. 7	22. 0	. 17
2145–47	64. 9	1. 1	. 21
2237–39	24. 0	54. 1	. 18
2239–41	27. 9	26. 1	. 16
2321–23	14. 1	77. 1	. 30
2381–83	32. 8	10. 9	. 19
2401–03	37. 1	1. 1	. 19
2427–29	24. 0	0	. 18
2570–72	46. 4	0	. 29

Notes: The samples weighed from 0.5 to 1.2 g and are from the sodium-rich section of oil shale (samples 1861–63 to 2401–03) and underlying clay-bearing oil shale (samples 2427–29 and 2570–72) in the Juhan core hole 4–1. The samples were treated with room-temperature distilled water to remove the nahcolite prior to weight-loss determinations which were run in duplicate by P. L. Hauff. The shale-oil assays (Fischer method) were made on the unleached material by the U.S. Bureau of Mines, Laramie, Wyo., and the nahcolite determinations were run by the thermal method by P. C. Beck, of the U.S. Geological Survey.

be distilled at 100°C. Samples suspected to contain significant amounts of hydrocarbons should be checked by chemical analysis.

Other minerals found elsewhere in the Piceance Creek basin, but not in the Juhan core hole, that are associated with the nahcolite-bearing rocks include wegscheiderite ($Na_2CO_3 \cdot 3NaHCO_3$) and halite. Wegscheiderite probably decomposes at temperatures as low as 100°C. However, this mineral is associated only with halite and has limited distribution in the basin; therefore, it is not considered to be an important interference. Experiments show that halite has no effect on the thermal method.

Accuracy and reproducibility

To test the accuracy and reproducibility of the thermal method, 34 samples of nahcolite-bearing oil shale from the Juhan core hole were analyzed in duplicate by chemical analysis of water-soluble sodium by a similar technique described by Smith and Young (1969), and in duplicate by the thermal method (fig. 1, table 5).

Nahcolite values by chemical analysis plotted against weight-percent losses by the thermal method on figure 1 were evaluated by a least-squares analysis. To reduce operator and instrumental error and sample bias, the duplicate analyses by each method were averaged and the following regression equation at 95-percent confidence limits was obtained:

$$y = 2.690x + 0.375 \pm 2,$$

where

x = thermal weight loss, in percent, and

y = weight-percent nahcolite by chemical analysis.

The regression equation indicates a satisfactory degree of accuracy for the thermal method. If no bias is assumed in analytical techniques, the equation suggests a closer correlation with the theoretical, rather than the actual, thermal weight loss for nahcolite (table 3); however, this is most likely the result of small compensating weight losses, probably from adsorbed water or kerogen (table 4).

Good reproducibility of the thermal analyses is indicated by the data in table 5. The mean and two standard deviations of the differences between duplicate analyses (runs 1 and 2) by the thermal method are 0.2 and 0.3 weight percent, respectively. By comparison, the mean and two standard deviations of like data by chemical analysis are 0.4 and 0.6, respectively.

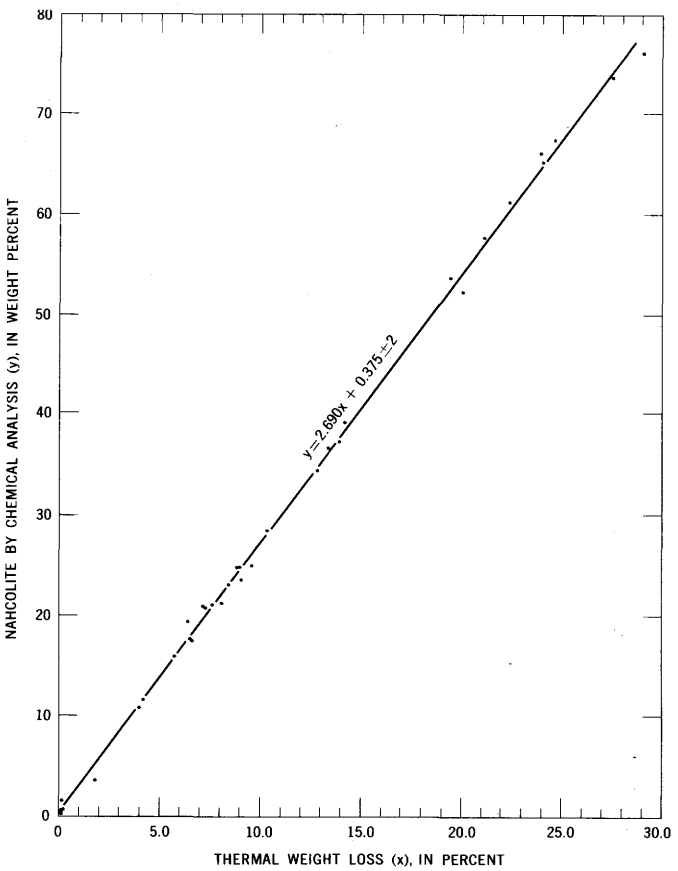

FIGURE 1.—Nahcolite determinations by chemical analysis versus weight-loss determinations by thermal analysis for the samples listed in table 5. Duplicate analyses by each method are averaged.

Applications

Experimental data show that the amount of trona can be determined by the thermal method. Because halite is not an interference, the method could be useful in quantitative determination of trona in the thick widespread beds of mixed trona and halite in the Green River Formation in southwest Wyoming.

The thermal method could possibly be combined with the Fischer assay used to determine shale-oil values

TABLE 5.—*Quantitative determination of nahcolite in 34 samples of nahcolite-bearing oil shale from the Juhan core hole 4–1 by chemical analysis and by thermal analysis*

Sample depth (feet)	Nahcolite determination (weight percent)			
	Chemical analysis		Thermal analysis	
	Run 1	Run 2	Run 1	Run 2
1841–43	11.7	11.8	11.5	11.7
1845–47	36.5	37.3	36.2	36.1
1857–59	61.4	61.0	60.7	60.6
1865–67	17.9	17.2	18.2	18.2
1881–83	24.7	25.2	24.7	24.7
1909–11	34.5	34.8	34.8	34.6
1917–19	66.1	66.1	64.8	64.8
1923–25	24.6	24.9	24.4	24.3
1961–63	36.9	37.6	37.7	37.7
1967–69	24.0	23.4	24.6	25.0
1997–99	.4	.4	1.0	1.1
2015–17	21.3	21.2	22.0	22.1
2031–33	4.2	3.1	5.0	5.3
2053–55	29.0	28.4	27.9	28.4
2079–81	65.4	65.0	65.1	65.0
2085–87	.6	.6	1.0	1.0
2095–97	17.4	17.9	17.9	17.9
2115–17	21.0	21.1	19.5	19.3
2127–29	16.1	15.9	15.6	15.7
2151–53	.3	.3	.9	1.0
2191–97	21.0	21.1	20.8	20.8
2221–23	20.5	21.1	19.9	20.0
2237–39	51.9	52.3	54.3	53.9
2239–41	25.4	24.7	26.1	26.1
2277–79	23.1	23.0	23.1	23.0
2281–83	53.7	54.1	52.5	52.3
2289–91	73.4	74.2	74.3	74.3
2321–23	76.4	76.0	78.0	78.6
2323–25	58.1	57.7	57.3	57.2
2365–67	39.5	39.1	38.7	38.6
3381–83	11.0	10.7	11.0	11.3
2291–93	19.2	19.7	17.3	17.9
2401–03	.8	.8	1.2	1.0
2415–17	1.7	1.7	1.1	1.0

Notes: The chemical determinations of nahcolite were made by Wayne Mountjoy by flame photometric analysis of water-soluble sodium using an internal lithium standard (method of Shapiro and Brannock, 1962). Estimated accuracy is ±1 percent of the amount of sodium found. Leaching with cool water as recommended by Smith and Young (1969, p. 8) is important because hot water increases the basicity of the leachate and dissolves other sodium minerals, such as dawsonite, in the oil shale. The thermal determinations were made by J. R. Dyni and P. L. Hauff.

(Stanfield and Frost, 1949). Although a combined analysis would require more time, the shale-oil and nahcolite determinations could be made on the same sample. Thus, "gas plus" loss and the amount of water, which are commonly determined in a Fischer assay, could be more accurately related to the weight-loss products derived from the thermal decomposition of nahcolite.

The possibility that dawsonite [$NaAl(OH)_2CO_3$], which occurs in large quantities in the Colorado oil-shale deposits, could be analyzed by the thermal method was considered. Preliminary data indicate that dawsonite partly decomposes at temperatures as low as 220°C when heated for 14 hours. Although thermal decomposition of kerogen is negligible at 105°C, appreciable decomposition occurs at 220°C and interferes with the weight-loss products of dawsonite.

REFERENCES

Beck, C. W., 1950, Differential thermal analysis curves of carbonate minerals: Am. Mineralogist, v. 35, nos. 11–12, p. 985–1013.

Gautier, Armand, 1876, Décomposition des bicarbonates alcalins, humides ou secs, sous l'influence de la chaleur et du vide: Acad. Sci. Comptes Rendus, v. 83, p. 275–278.

Hite, R. J., and Dyni, J. R., 1967, Potential resources of dawsonite and nahcolite in the Piceance Creek basin, northwest Colorado *in* Symposium on oil shale, 4th: Colorado School Mines Quart., v. 62, no. 3, p. 25–38.

Mellor, J. W., 1952, A comprehensive treatise on inorganic and theoretical chemistry, v. 2: London, Longmans, Green and Co., Ltd., 894 p.

Shapiro, Leonard, and Brannock, W. W., 1962, Rapid analysis of silicate, carbonate, and phosphate rocks: U.S. Geol. Survey Bull. 1144–A, 56 p.

Smith, J. W., and Johnson, D. R., 1967, Thermal analysis of natural fuels *in* McAdie, H. G., ed., Toronto symposium on thermal analysis, 2d, Toronto, 1967, Proc.: Chem. Inst. Canada, p. 95–116.

Smith, J. W., and Young, N. B., 1969, Determination of dawsonite and nahcolite in Green River Formation oil shales: U.S. Bur. Mines Rept. Inv. 7286, 20 p.

Stanfield, K. E., and Frost, I. C., 1949, Method of assaying oil shale by a modified Fischer retort: U.S. Bur. Mines Rept. Inv. 4477, 13 p. (revision of Rept. Inv. 3977).

IDENTIFICATION OF SERPENTINE VARIETIES BY INFRARED ABSORPTION

By ROBERT W. LUCE, Menlo Park, Calif.

Abstract.—The infrared spectra of 10 chemically and X-ray analyzed serpentines are presented with a tabulation of diagnostic absorption bands. The infrared absorption technique supplements X-ray diffraction for identification purposes. Each serpentine variety has a distinctive spectrum, but a mixture of chrysotile and lizardite cannot be characterized by this method. Serpentine can be distinguished from most common magnesium-rich minerals by spectral differences; however, when mixed with serpentine, minor amounts of brucite cannot be identified by infrared analysis.

In recent years much attention has been given to the petrologic significance of the three serpentine mineral varieties—chrysotile, lizardite, and antigorite (Hostetler and others, 1966; Thayer, 1967; Page, 1967; Černý, 1968). Each of these varieties can be identified by X-ray diffraction (Whittaker and Zussman, 1956), but the differences are subtle. Another method, differential thermal analysis, is too insensitive for most identification purposes. Therefore, an alternative technique was sought in infrared absorption spectrometry. Previous work on a small number of specimens suggested that differences in the infrared spectra might be sufficient to tell the serpentine varieties apart (Brindley and Zussman, 1959; Veniale and van der Marel, 1963). The objectives of this study were to (1) verify the previous findings by using additional good specimens, and (2) determine whether all the mineral constituents in a mixture of several magnesium silicates can be identified by infrared absorption.

The initial part of this work was done as part of the author's doctoral dissertation at Stanford University and was supported by the U.S. Atomic Energy Commission (Contract A (04–3) 326 PA3).

EXPERIMENTAL METHOD

Highly purified serpentine samples were provided by G. T. Faust and R. G. Coleman. X-ray diffraction showed that all but two were single-phase samples. Chrysotile 14N163A contained traces of lizardite, and lizardite 19N163A contained traces of chrysotile.

Specimens with the prefix "F" were described and analyses tabulated by Faust and Fahey (1962); specimens with a numerical prefix were described and analyses given by Page and Coleman (1967). The brucite specimen was collected from New Idria, Calif., by Coleman. The long-fiber chrysotile from Thetford, Quebec, was purchased from Ward's Natural Scientific Establishment, Inc., and has the following composition:

SiO_2	41.3	K_2O	0.07
Al_2O_3	.31	H_2O-	1.0
Fe_2O_3	.78	H_2O+	14.5
FeO	.84	TiO_2	.00
MgO	41.0	P_2O_5	.00
CaO	.09	MnO	.04
Na_2O	.00	Sum	100

Analysis performed in a U.S. Geological Survey laboratory under the supervision of Leonard Shapiro.

Potassium bromide pellets containing 0.25 percent of mineral were prepared by a standard technique (Lyon, 1967; Farmer, 1964) and run in a Perkin-Elmer Model 457 spectrophotometer at 100 cm^{-1} min^{-1} in the range 4,000–2,000 wave numbers and at 50 cm^{-1} min^{-1} in the range 2,000–250 wave numbers. (The wave number is defined as the reciprocal of the wavelength in centimeters.) The error in reproducibility and readability was ± 20 cm^{-1} and ± 10 cm^{-1} in the two ranges, respectively. Supplementary runs on a Beckman IR–9 spectrophotometer showed no differences that were significant for identification purposes. Spectra in the range 10,000–4,000 wave numbers were recorded with a Cary 14RI spectrophotometer. With this instrument, both transparent mineral chips and infrasil plates coated with powdered mineral were used.

U.S. GEOL. SURVEY PROF. PAPER 750-B, PAGES B199-B201

413-504 O - 71 - 14

INFRARED ABSORPTION SPECTRA OF SERPENTINES

The spectra are reproduced in figure 1. They agree substantially with those given by Veniale and van der Marel (1963), Brindley and Zussman (1959), and Moenke (1962). Brindley and Zussman tabulate water bands at about 3,500 cm^{-1} and 1,600 cm^{-1} among those for serpentine. In this work no bands were found that correspond to the weak ones that Brindley and Zussman found at 873 cm^{-1}; moreover, the strong bands that they found between 3,650 and 3,625 cm^{-1} appear at low wave numbers, compared with other published serpentine spectra and with those in this report.

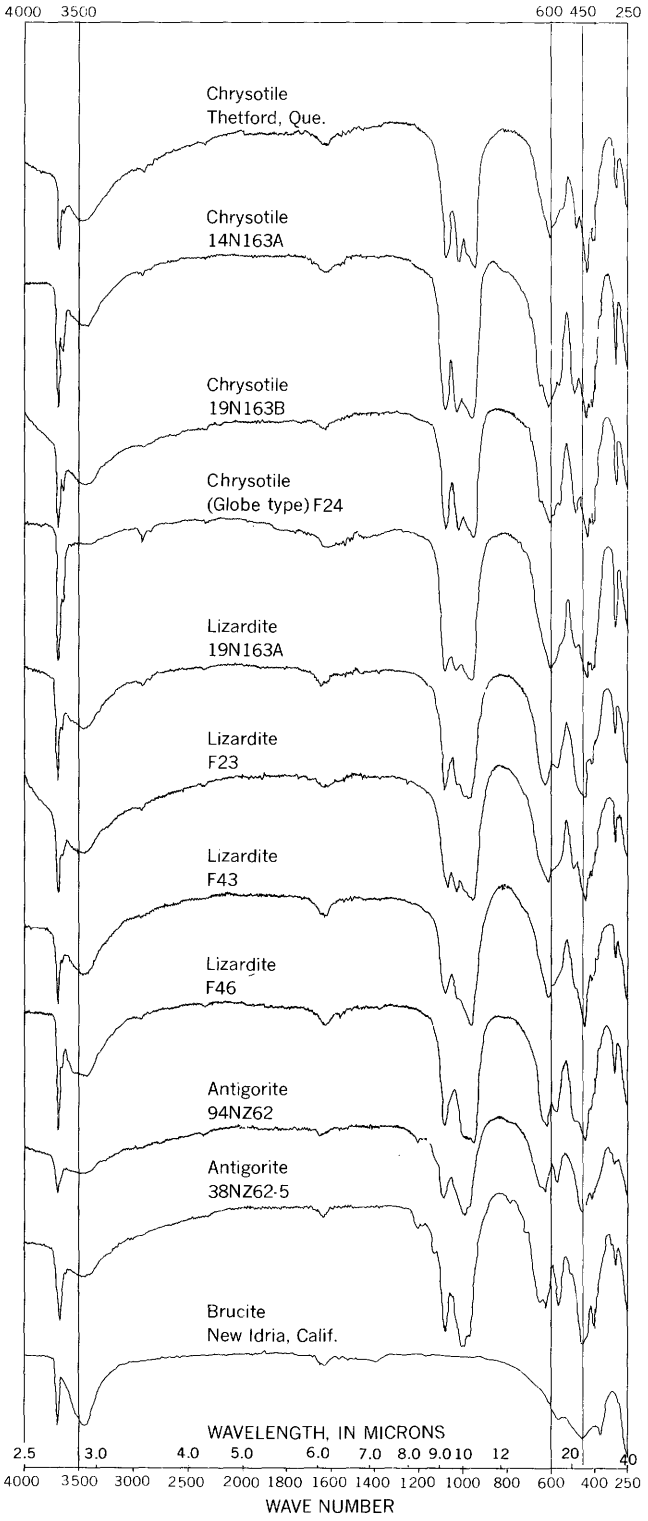

FIGURE 1.—Infrared absorption spectra of the serpentine varieties—chrysotile, lizardite, and antigorite—and brucite.

The infrared absorption bands diagnostic for identification are grouped in table 1 as singlets, doublets, or triplets in three regions. Individual key bands are underlined. Table 2 lists additional nondiagnostic weak to medium bands, including those from the near-infrared region (above 4,000 wave numbers).

The spectrum of antigorite is sufficiently distinct that one can easily identify this serpentine variety. It is also relatively easy to distinguish antigorite from

TABLE 1.—*Diagnostic infrared absorption bands for identifying serpentine mineral varieties*

[S, strong; M, medium; W, weak; parentheses indicate that band is not present in all specimens. Key bands are underlined]

Range in wave numbers	Chrysotile	Lizardite	Antigorite
3, 600–3, 700	Doublet 3, 690 S 3, 640 M	Doublet 3, 690 S 3, 645 M	Singlet 3, 680 S (3, 650 W)
950–1, 100	Triplet 1, 080 S 1, 020 S 955 S	Triplet 1, 080 S 1, 020 M 965 S	Doublet 1, 080 S 990 S (970 W)
400–700	Triplet 605 S 490 M 440 S	Doublet 620 S (485 W) 440 S	Doublet 620 M 455 S

TABLE 2.—*Additional absorption bands for serpentine mineral varieties*

[S, strong; M, medium; W, weak; parentheses indicate band is not present in all specimens]

Chrysotile	Lizardite	Antigorite
		7, 692 W
7, 194 S	7, 194 S	7, 194 S
5, 128 M	5, 128 M	5, 082 M
4, 750 M	4, 785 M	4, 750 M
4, 310 S	4, 310 S	4, 335 M
4, 167 M		4, 210 W
		1, 205 W, 1, 123 W
		780 W, 710 W, 650 W
553 W	575 W	568 M
423 W		
408 M	410 W	404 M
395 W	393 W	
(375 W)	(375 W)	
308 S	308 M	308 M

lizardite and chrysotile by X-ray diffraction and differential thermal analysis.

With the samples used in this study one can make a consistent scheme for the identification of chrysotile and lizardite. However, the spectra are so similar that infrared analysis is not recommended for distinguishing these two serpentine varieties, especially if they occur as mixtures. Infrared absorption should only supplement X-ray diffraction for such purposes.

DETECTION OF OTHER MAGNESIUM MINERALS IN SERPENTINE SAMPLES

Infrared absorption can be successfully used to detect mixtures of common magnesium-rich minerals with serpentine. Examination of Moenke's (1962) reference spectra shows that specifically characteristic medium to strong bands exist for the following minerals: talc, sepiolite, enstatite-hypersthene, forsterite, magnesite, dolomite, chloritoid, clinochlore, ripidolite, and penninite. The spectra for enstatite, bronzite, and forsterite were checked against ones run on well-characterized specimens (Luce, 1969).

Because the coexistence of brucite with serpentine is of petrologic importance, it was decided to investigate the possibility of using infrared absorption to quantitatively identify this mixture of minerals. Selectively dissolving brucite from a serpentinite (Hostetler and others, 1966) is not a wholly satisfactory procedure because serpentine itself is fairly soluble in mild acid solutions (Luce, 1969).

Unfortunately, the spectrum of brucite is, to a first approximation, nearly identical with about half of the serpentine spectrum (see fig. 1). There is a single O–H band at 3,695 cm^{-1} and a broad deep band with three "peaks" between 900 and 350 cm^{-1}. The Mg–O and O–H bands remain in the same positions for serpentine and brucite, whether or not there is a silicate layer lattice joined to the brucite component. A sample containing chrysotile plus 10 percent brucite was made up and an infrared spectrum obtained. No brucite could be positively identified; therefore, the method is not useful for this application.

The less important task of identifying traces of serpentine in brucite, by the Si–O and Mg–O–Si band positions, should be possible with infrared absorption.

REFERENCES

Brindley, G. W., and Zussman, J., 1959, Infrared absorption data for serpentine minerals: Am. Mineralogist, v. 44, p. 185–188.

Černý, P., 1968, Comments on serpentinization and related metasomatism: Am. Mineralogist, v. 53, p. 1377–1385.

Farmer, V. C., 1964, Infra-red spectroscopy of silicates and related compounds, *in* Taylor, H. F. W., ed., The chemistry of cements, v. 2: London, Academic Press, p. 289–309.

Faust, G. T., and Fahey, J. J., 1962, The serpentine group minerals: U.S. Geol. Survey Prof. Paper 384–A, 92 p.

Hostetler, P. B., Coleman, R. G., Mumpton, F. A., and Evans, B. W., 1966, Brucite in alpine serpentinites: Am. Mineralogist, v. 51, p. 75–98.

Luce, R. W., 1969, Dissolution of magnesium silicates: Stanford Univ., Stanford, Calif., Ph. D. thesis, 91 p.

Lyon, R. J. P., 1967, Infrared absorption spectroscopy, *in* Zussman, J., ed., Physical methods in determinative mineralogy: London, Academic Press, p. 371–403.

Moenke, Horst, 1962, Mineralspektren: Berlin, Akademie Verlag, 41 p., plus 355 charts of mineral spectra.

Page, N. J, 1967, Serpentinization considered as a constant volume metasomatic process—A discussion: Am. Mineralogist, v. 52, p. 545–549.

Page, N. J, and Coleman, R. G., 1967, Serpentine-mineral analyses and physical properties, *in* Geological Survey Research 1967: U.S. Geol. Survey Prof. Paper 575–B, p. B103–B107.

Thayer, T. P., 1967, Serpentinization considered as a constant volume metasomatic process—Reply: Am. Mineralogist, v. 52, p. 549–552.

Veniale, Fernando, and van der Marel, H. W., 1963, An interstratified saponite-swelling chlorite mineral as a weathering product of lizardite rock from St. Margherita Staffora (Pavia Province), Italy: Beitr. Mineralogie u. Petrographie, v. 9, p. 198–245.

Whittaker, E. J. W., and Zussman, J., 1956, The characterization of serpentine minerals by X-ray diffraction: Mineralog. Mag., v. 31, p. 107–126.

THERMAL INFRARED DETECTION OF GLACIAL GRAVEL, YELLOWSTONE NATIONAL PARK, WYOMING

By H. A. WALDROP, Denver, Colo.

Work done in cooperation with the National Aeronautics and Space Administration

Abstract.—Well-drained glacial gravel in Yellowstone National Park can be distinguished from bedrock and till by its darker tone on evening thermal infrared imagery. Well-drained gravel supports relatively thin forest, which cools more rapidly at night and which shows a darker infrared tone than thicker forest on different materials. Other conditions that produce dark infrared tone must be considered, but in the report area the dark-tone anomaly is a useful reconnaissance aid in outlining probable deposits of glacial gravel. Hydrothermal activity registers directly on thermal infrared imagery; other geologic features in Yellowstone National Park register indirectly by their topographic expression, which is often more evident on radar imagery and vertical aerial photographs.

Study of thermal infrared imagery of western Yellowstone National Park had two objectives: general inspection of the imagery for geologic features, and detailed examination where areas underlain by well-drained glacial gravel have a characteristically dark infrared tone. Geologic evaluation of the imagery was made by comparison with geologic mapping in progress, radar imagery, vertical aerial photographs, and topographic maps.

Thermal infrared imagery in the 8–14 micrometer band examined in this study was taken on National Aeronautics and Space Administration (NASA) Mission 32, flights 2 through 5; the imagery was obtained at midday, early evening, and shortly after midnight on September 20 and 21, 1966, by means of the Reconofax IV system in a NASA aircraft flying at an altitude of 17,000 feet.

GENERAL RESULTS

General inspection of thermal infrared imagery of western Yellowstone National Park supports results of other remote-sensing studies in the park (Smedes, 1968; Pierce, 1968; Keefer, 1968; Christiansen, 1968) that give detailed examples and analyses. Results of this general inspection are summarized below.

Hydrothermal activity is the only geologic feature registered directly by thermal infrared imagery; other geologic features are shown indirectly, chiefly by their topographic expression. They include: fractures in bedrock (faults and joints), pressure ridges in lava, glacially molded topography, river terraces, alluvial valley fills, talus slopes, and alluvial fans. Chief physiographic and vegetational features that register consistently on imagery are: rivers, lakes, swamps, forests, grasslands, and sun-facing slopes (except on late-evening imagery).

Slopes that face the sun are warmer than shaded slopes and therefore have lighter tones on daytime and early evening imagery. This effect is known as topographic enhancement; it emphasizes geologic features that control topography. Such imagery resembles the prints of standard aerial photographs.

Diurnal changes in relative temperature of natural materials cause important differences in thermal infrared imagery obtained at different hours. Because water has a high specific heat, rivers and deep lakes change temperature much less rapidly than other natural materials. They are relatively cooler than their surroundings during the day and appear black on daytime imagery, but they are relatively warmer than their surroundings at night and appear light gray to white on nighttime imagery. Bedrock, rock rubble, and grasslands are warm and therefore light toned on daytime imagery, but they cool rapidly after sunset and are medium to light gray on nighttime imagery. These reversals in the relative temperature of natural materials

U.S. GEOL. SURVEY PROF. PAPER 750-B, PAGES B202-B206

give nighttime thermal infrared imagery some resemblance to a photographic negative.

On early-evening imagery many valleys and basins appear anomalously dark because dense cold air drains into them from cooling uplands (Geiger, 1950, p. 195–214) and possibly because they are in shadow during late afternoon and have been radiating heat rather than receiving it (Pierce, 1968, p. 7).

Temperature contrasts on nighttime infrared imagery are most pronounced early in the evening. Sun-facing slopes cool and their topographic enhancement fades usually before midnight. And as the forest cools through the night, even the contrast between forest and grassland diminishes before dawn.

The general relations for midday and midnight are summarized in table 1. Relative temperatures of natural materials through the day and night are shown graphically by Pierce (1968, fig. 14).

Few geologic features register directly on thermal infrared imagery of Yellowstone National Park; most that are shown indirectly owe it to their topographic expression, which usually shows more clearly on radar imagery and vertical aerial photographs. The effects of terrain enhancement, forest cover, cold-air drainage, and relative temperature reversals tend to mask rock composition, structure, and distribution, on which most geologic mapping is based. Except for direct registration of thermal features, and for detection of well-drained glacial gravel, which is discussed below, thermal infrared imagery was not as effective as other remote sensors for showing geology in the test area.

TABLE 1.—*Relative temperature and tone of natural materials on thermal infrared imagery of Yellowstone National Park*

Material	Midday		Midnight	
	Relative temperature	Imagery tone	Relative temperature	Imagery tone
Rivers and deep lakes.	Cool	Black	Warm	Light gray.
Bedrock and rubble.	Warm	Light gray.	Cold	Dark gray.
Grasslands	Warm	Light gray to white.	Cold	Dark gray.
Pine forest	Cool	Dark gray.	Warm	Medium to light gray.
Valley bottoms.	Variable	Variable	Cold (from cold air drainage).	Dark gray to black.
Sun-facing slopes.	Warm	Light gray to white.	Cool	Dark gray.
Well-drained glacial gravel.	Variable	Variable	Cool	Medium to dark gray.

DETECTION OF WELL-DRAINED GLACIAL GRAVEL

In an examination for geologic features on thermal infrared imagery of the Yellowstone rhyolite plateau, Christiansen (1968, p. 3) noted a clear local distinction between glacial gravel and bedrock on a small bench near the Gibbon River. Well-drained glacial gravel on the bench had a darker tone than adjacent bedrock on early evening imagery. Because of its potential value in mapping glacial gravel, this tone anomaly was studied in detail where such deposits are widespread.

Much of the Madison Plateau west and north of Lower Geyser Basin is covered by thick gravel and till of the Pinedale Glaciation; west of that area, Quaternary rhyolite of the plateau is unglaciated. Thermal infrared imagery covering the plateau and geyser basin was obtained between 6:30 and 8:00 p.m., less than 2 hours after sunset, when topographic enhancement was still effective and cold-air drainage had begun.

Comparison of the infrared imagery with a generalized geologic map of the same part of the plateau (fig. 1) shows a close correspondence between dark-gray infrared tone and areas covered by thick glacial gravel. The best agreement between infrared imagery and geology on figure 1 is along Sentinel Creek, which separates unglaciated Quaternary rhyolite on the west from well-drained glacial gravel on the east. Northwest of Sentinel Creek this same gravel is also indicated by a dark-gray tone, and several isolated patches of gravel on the plateau are dark gray.

A dark tone on the imagery, however, does not always indicate glacial gravel, and not all glacial gravel on the plateau is indicated by a dark tone. The very dark gray patch at locality *a* on figure 1 is surrounded, as well as underlain, by glacial gravel; the nearly black tone there probably results from ponding of cold air in the outwash channel, as it does in outwash channels to the southwest, and along the north-flowing segment of Sentinel Creek. Such cold-air ponding usually has a darker tone than areas of thin tree cover; it should be anticipated along drainageways. Grassland underlain by both fine alluvium and glacial gravel in Buffalo Meadows has cooled rapidly and appears uniformly black on the imagery. Glacial gravel at points *b* on figure 1 is not dark gray; indeed, it is almost as light as bare or thinly mantled bedrock, an anomaly apparently caused by topographic enhancement and by locally denser tree cover. Hills of hydrothermally cemented gravel at Twin Buttes have a much lighter infrared tone than terrain underlain by uncemented gravel, an effect caused by topographic enhancement, cementation, and continued hydrothermal activity. It

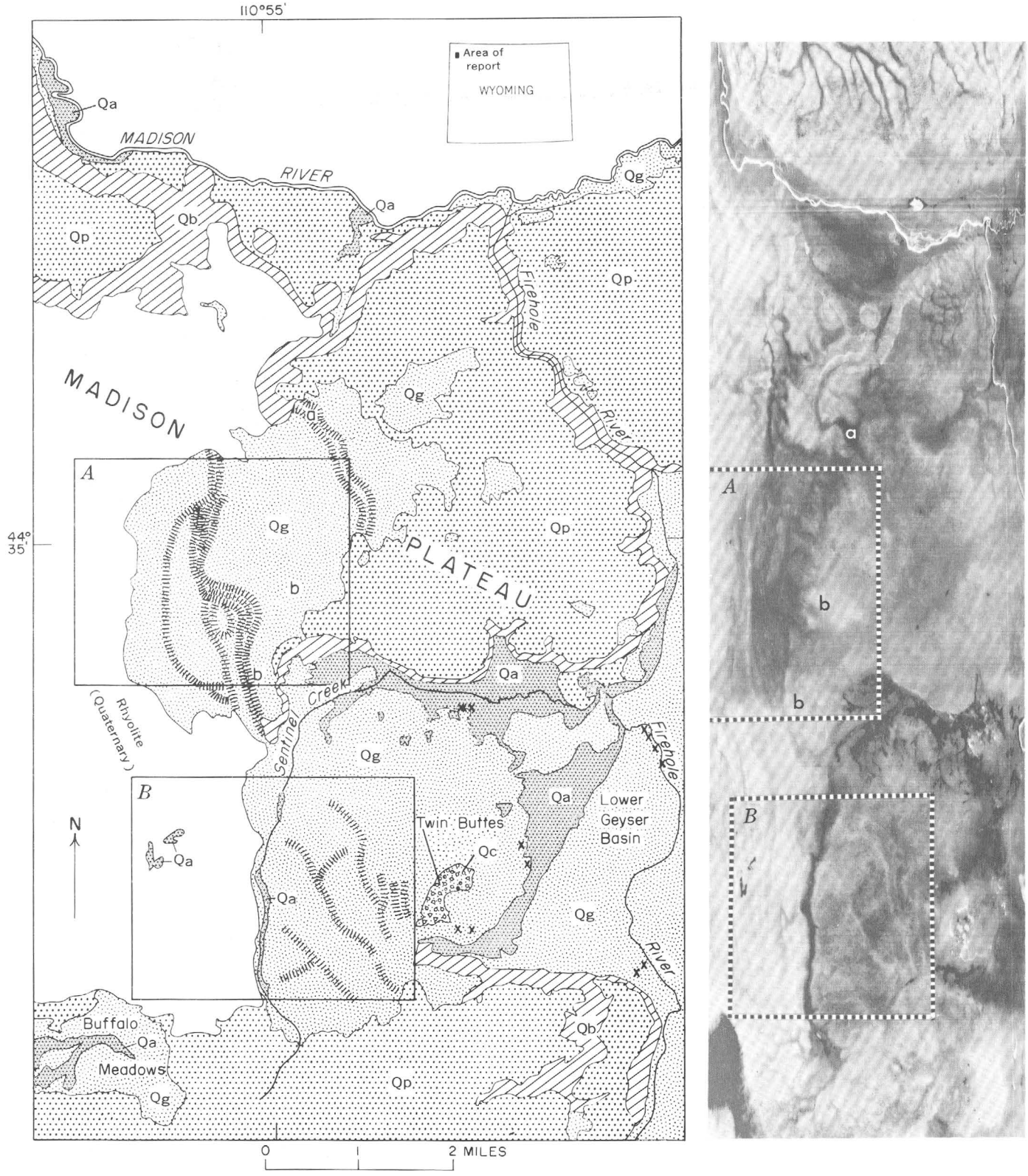
110°55'
Area of report
WYOMING
Qa
MADISON
RIVER
Qb
Qp
Qg
Firehole
River
MADISON
PLATEAU
A
a
b
44°
35'
Rhyolite (Quaternary)
Sentinel Creek
B
N
Twin Buttes
Qc
Lower Geyser Basin
Buffalo Meadows
0
1
2 MILES

FIGURE 1.

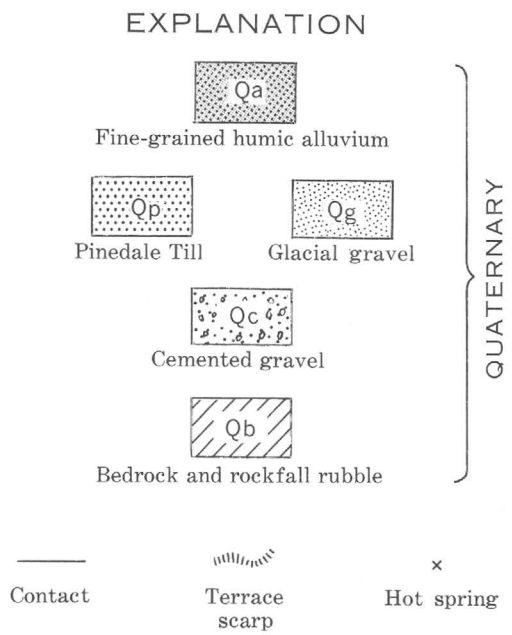

FIGURE 1.—Generalized geologic map and early evening thermal infrared image of part of the Madison Plateau. Unglaciated Quaternary rhyolite on the west side of the image registers light gray to white in contrast to the dark gray of thick glacial gravel to the east. Terrace scarps east of Sentinel Creek show as faint white lines on the image, because they support more trees and have cooled more slowly than adjacent terrace tops. Areas of till are slightly darker on the image than those of rhyolite, but are lighter than those of glacial gravel. Grassland in Buffalo Meadows has cooled rapidly and shows black on the image, masking the contact between fine alluvium and glacial gravel. In the valley of Sentinel Creek a diffuse dark-gray tone caused by cold-air drainage is readily distinguished from the sharply defined black tone of grassland. a, outwash channel; b, anomalously light glacial gravel (explained in text). Rectangles (labeled *A* and *B*) on map and imagery mark areas of aerial photographs on figure 2. Rectangles on the imagery are elongated parallel to direction of flight; they cover the same areas on both the map and photographs.

is necessary to know the cause of the dark-gray tone anomaly and its relation to glacial gravel in order to evaluate these discrepancies between the imagery and the geologic map.

Comparison of the thermal infrared imagery with vertical aerial photographs (fig. 2) shows that darkness of the infrared tone, which indicates relative coolness, is directly related to thinness of forest cover. Thickly forested areas cool slowly at night because ground heat must be transferred to and then reradiated from the tree crowns (Pierce, 1968, p. 13). The thinner the stand of trees the more rapidly will it cool, and the darker will be its infrared tone.

Because density of forest cover depends mainly on soil moisture, it reflects geologic materials. Next to sun exposure, drainage of the substrate is probably the

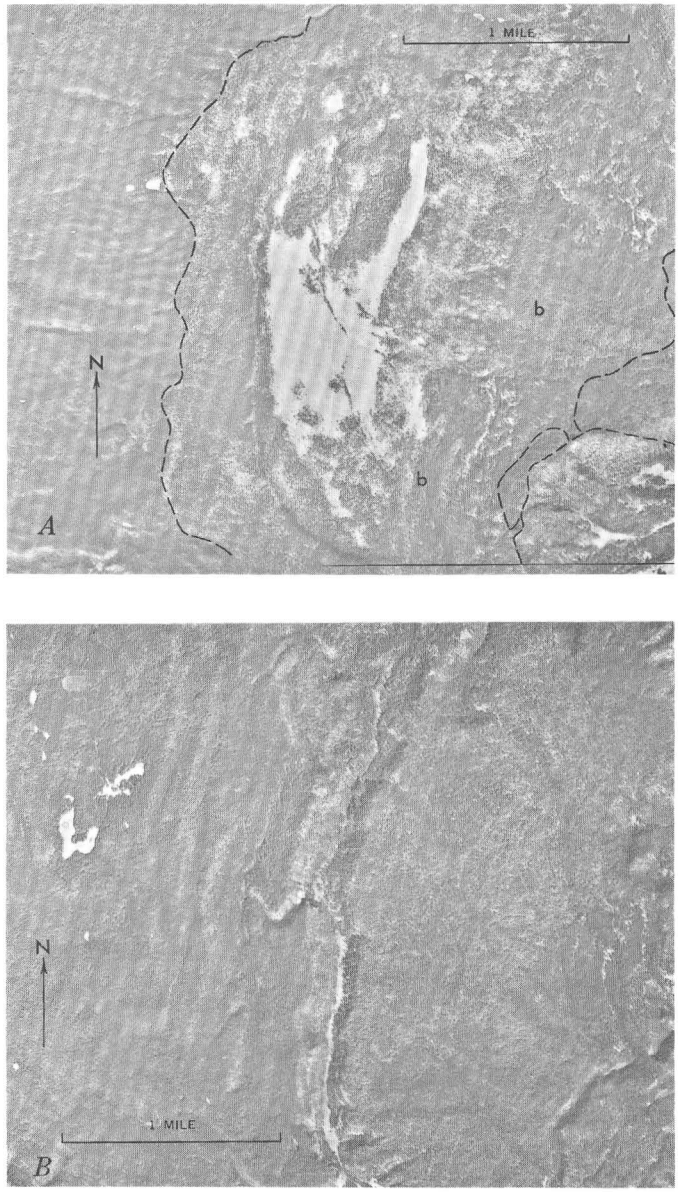

FIGURE 2.—Aerial photographs of parts of the Madison Plateau. Areas covered by these photographs are outlined on the geologic map and infrared imagery of figure 1. *A*, The western quarter of the area is underlain by unglaciated Quaternary rhyolite, the eastern three-quarters by glacial gravel. Thinner forest on the glacial gravel shows faintly on the aerial photograph but is emphasized by dark tone on the infrared imagery of figure 1. The light grassy clearing on the aerial photograph is almost black on the imagery. Areas marked b are underlain by gravel but have a light tone on the imagery because of terrain enhancement and because they support denser stands of trees. Dashed lines mark contact between glacial gravel and unglaciated Quaternary rhyolite to the west, and between glacial gravel and Pinedale Till to the east. *B*, The area west of Sentinel Creek is underlain by unglaciated Quaternary rhyolite, the area to the east by glacial gravel. Thinner forest on glacial gravel shows faintly on the aerial photograph but strongly on the infrared imagery (fig. 1). Pressure ridges in rhyolite west of Sentinel Creek and scarps in the gravel east of it are also emphasized on the infrared imagery.

main control of soil moisture. Unconsolidated glacial gravel drains readily; till, with a larger component of silty material, drains somewhat better than rhyolite bedrock; fine-grained alluvium and lake clays drain so poorly that they commonly support bog and meadow vegetation rather than forest.

On the Madison Plateau the dark-gray-tone anomaly is an indirect expression of a deposit of glacial gravel that drains better, supports fewer trees, and therefore cools more rapidly at night than areas underlain by bedrock and till. However, other factors must be considered in interpreting the infrared imagery. Local conditions, such as sun exposure, topographic position, variation in grain size, and age of the trees, determine forest density in patterns that do not always match distribution of underlying geologic units. Cold-air drainage to low areas can simulate or mask the dark-tone anomaly associated with glacial gravel. For this reason, the anomaly is more diagnostic for deposits on high slopes and the plateau top than for deposits in valleys and basins. The anomaly simply indicates the presence of gravel, regardless of origin; it makes no distinction between outwash gravel, ice-contact gravel, or nonglacial gravelly alluvium. Fine-grained alluvium and lake silts are not shown well by the anomaly. They drain so poorly that they support grass rather than trees; grasslands cool rapidly after sunset and appear black, rather than dark gray, on the imagery (fig. 1).

Despite the problems of interpretation, the relationship between well-drained glacial gravel and dark-gray infrared tone is generally consistent in the test area. And because thermal infrared imagery emphasizes differences in forest density more vividly than aerial photographs do, the dark-gray-tone anomaly is useful as a reconnaissance aid in mapping glacial gravel. It has numerous applications in surficial and engineering geology.

REFERENCES

Christiansen, R. L., 1968, A distinction between bedrock and unconsolidated deposits on 3–5μ infrared imagery of the Yellowstone rhyolite plateau: U.S. Geol. Survey open-file report, 5 p.

Geiger, Rudolf, 1950, The climate near the ground [translated by Milroy N. Stewart and others from 2d German ed. of Das Klima der Bodennahen Luftschicht]: Cambridge, Mass., Harvard Univ. Press, 482 p.

Keefer, W. R. 1968, Evaluation of radar and infrared imagery of sedimentary rock terrane, south-central Yellowstone National Park: U.S. Geol. Survey open-file report, 8 p.

Pierce, K. L., 1968, Evaluation of infrared imagery—applications to studies of surficial geology, Yellowstone Park: U.S. Geol. Survey open-file report, 20 p.

Smedes, H. W., 1968, Geologic evaluation of infrared imagery, eastern part of Yellowstone National Park, Wyoming and Montana: U.S. Geol. Survey open-file report, 27 p.

A CLEAN LABORATORY FOR MINERALOGICAL AND GEOCHEMICAL STUDIES

By MICHAEL B. DUKE and ROBERT F. COMMEAU,
Washington, D.C.

Abstract.—A class–100 (less than 100 particles per cubic foot of air) laminar-flow clean room has been built for mineralogical analyses that must exclude atmospheric particulate contamination. The room is kept clean in two basic ways: (1) air in the room is continuously recycled through high-efficiency particulate air filters, and (2) laminar airflow is maintained so that particles do not settle on material being worked on. The laboratory is used for special problems such as mineralogical studies of lunar soil.

Particulate material suspended in air can contain chemical elements with concentrations high enough to affect the results of sensitive geochemical and mineralogical analyses. It has long been recognized that lead in urban atmospheres, which has been reported in concentrations as high as 3 to 20 micrograms per cubic meter in Los Angeles, Calif. (Working Group on Lead Contamination, 1965), can severely affect the results of lead-isotope determinations on microgram quantities of lead in geochronological studies.

The problem of particulate contamination has been of special interest in the analysis of Apollo 11 lunar soil samples (Duke and others, 1970), which have a median grain size of about 50 micrometers, and in which 20 percent of the material is finer than 15 μm. Many of the geochemical peculiarities of lunar soil, which is different in many isotopic and elemental characteristics from associated crystalline rocks, are apparently most pronounced in the finer fractions. In order to characterize these fractions, it is necessary to exclude terrestrial artifacts or particulate contaminants from the atmosphere.

Owing to the localized nature of many pollution sources and to local atmospheric conditions, air pollution is subject to wide fluctuation in severity; as a result, quantitative information on atmospheric particulate contamination is generally lacking. A sample of settled dust collected outside the clean laboratory described in this report, but inside the building housing it, gave the following analysis (semiquantitative emission spectrography, W. B. Randell, analyst):

Element	Content (percent)	Element	Content (parts per million)
Si	10	Cd	150
Fe	3	V	100
Ca	2	Sr	100
Al	1.5	Ni	100
Zn	1.0	Cr	70
K	.5	Ag	30
Mg	.5	Sn	30
Ti	.34	Y	10
Pb	.2	Co	10
Cu	.1	Mo	5
		Ga	3
		Be	3

The sources of these elements are varied. The common rock-forming elements silicon, iron, calcium, aluminum, potassium, and magnesium are probably derived from soils, natural building materials, and unknown sources; lead is due primarily to automobile exhaust and solder; titanium is due largely to paint flakes; zinc, copper, cadmium, and tin are probably due to construction material, electrical wiring, and plumbing. The sample was collected several months after construction of the clean laboratory, but many of these materials may be related to that construction.

In Washington, D.C. (which lacks heavy industry), electrical generation plants, construction activity, and automobiles are the main sources of contaminants, and the above analysis could be typical. The composition of dust, however, is subject to local variability and probably differs for particulates in different size ranges. An average of 50 tons per square mile per month of particulate material is deposited in downtown urban areas

U.S. GEOL. SURVEY PROF. PAPER 750-B, PAGES B207-B210

in the United States (U.S. Public Health Service, 1966, p. 4), and the average atmospheric particulate contamination is typically 100 $\mu g/m^3$. Scaling the chemical analysis above with these values gives a concentration of 1 $\mu g/m^3$ for each 1 percent of an element in the analysis.

With recent advances in analytical techniques, geochemical analyses are possible at the part-per-million to part-per-billion range on less than a gram of material (neutron activation analysis, isotope dilution mass spectrometry), at a few hundred parts per million in milligram amounts of samples (X-ray fluorescence), and at similar levels in submicrogram samples (electron microprobe). Other techniques offer comparable sensitivities, and new developments will certainly push the sensitivity limits downward. If an element that occurs in the amount of 1 $\mu g/m^3$ of air is being investigated with sensitivity of 100 parts per billion, a 1-g sample cannot be exposed to 0.1 m^3 of unclean air without risking contamination. Air conditioning and filtration remove much of the hazard, but the risks of contaminating a sample by exposing it to the atmosphere must be considered by each analyst. As the detection limits are lowered, the risks become greater, and there is little evidence available as to what contaminants the normal environment contains. It is clear, however, that in order to be able to interpret more and more detailed geochemical data, increasingly cleaner facilities will be required.

It is much easier to design a clean work area than to collect the volumes of information that would be required to support contamination detection in a poorly controlled area. This report describes a laminar-flow clean laboratory designed by and built for the U.S. Geological Survey in Washington, D.C. The laboratory is presently in use for detailed mineralogical analysis of samples when atmospheric particulate contamination must be avoided. "Grain-by-grain" analysis of lunar soil samples collected by the Apollo 11 mission is an example of such studies.

CONVENTIONAL CLEAN ROOMS

Conventional clean rooms have been designed in the past with effective air filtration systems, a pressurization system, and special construction to reduce dust generation and accumulation in the room. Typical levels of contamination attainable in such rooms are in the range of 10,000 particles per cubic foot of air, with all particles 0.5 μm and larger being counted. This is several orders of magnitude better than the normal laboratory environment. Conventional clean rooms, however, suffer from resuspension of the inevitable dust that accumulates in parts of the room with inefficient air circulation and from the irregular flow of air, which may move particles from laboratory personnel or equipment onto samples being processed.

U.S. GEOLOGICAL SURVEY LAMINAR-FLOW CLEAN ROOM

Laminar-flow clean rooms are designed to operate at a level of not more than 100 particles (0.5 μm and larger) per cubic foot (class 100), under conditions of uniform airflow and nearly complete removal of suspended dust (Austin and Timmerman, 1965). Several geometrical layouts are possible; the Geological Survey facility is a class-100 horizontal-crossflow design shown schematically in figure 1 and as it actually looks in figure 2.

Air is pushed by blowers through a plenum and across a bank of HEPA (high-efficiency particulate air) filters which covers one entire wall of the laboratory. These filters are 99.97 percent effective in removing particles 0.3 μm in diameter and larger. The air is blown across the filters at a velocity of 90 feet per minute (a gentle breeze) and is channeled in the filter to emerge in parallel flow (from which the designation "laminar flow" is derived). The air moves across the room, exits through a perforated section of suspended ceiling, and returns to again pass through the filters. Enough new air is added to the system to maintain a 0.015-inch water-pressure differential between the interior and exterior of the room. A portion of the air is recirculated through an air-conditioning system to maintain the desired temperature and humidity.

The laminar flow room is kept clean in two ways. (1) The air in the room is continuously recycled through HEPA filters. Measurements taken with a light-scattering particle detector indicate that the emission rate of dust by the filter wall is less than 5 particles per cubic foot of air. With no operations being carried out

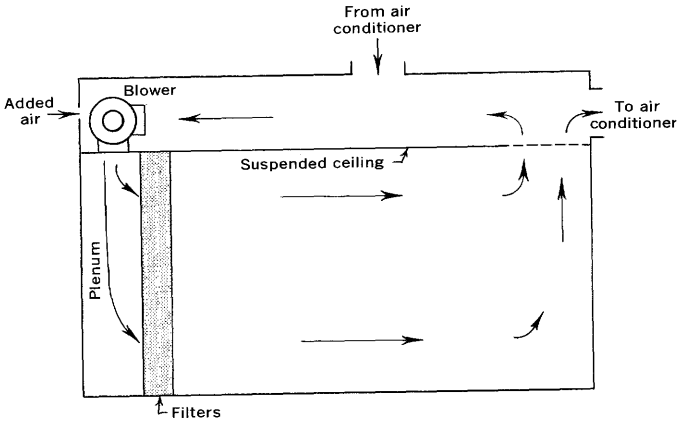

FIGURE 1.—Schematic diagram of horizontal-laminar-flow clean laboratory.

FIGURE 2.—U.S. Geological Survey laminar-flow clean laboratory. Gridded wall at left is a high-efficiency particulate air-filter bank. Airflow is parallel to the end wall. Cleanest work areas are directly in front of the filter wall.

in the laboratory, the dust concentration is generally less than 50 particles per cubic foot. (2) Laminar airflow is maintained so that particles do not settle on material being worked on, thus providing a self-cleaning effect for the room. Laboratory activities (primarily the movement of people) are the main source of particulate contaminants, which locally degrade the cleanliness from class-100 conditions. Walking in front of the particle detector quickly raises the particle count to more than 1,000 particles per cubic foot. However, the speed of air movement is sufficient to carry most fine material out of the room completely and to minimize the settling of larger pieces of dust generated by laboratory operations. Laboratory activities are not generally undertaken downwind from an active work station, although the space can be used for noncritical activities. By restricting work to areas where there is minimum disruption of the laminar airflow, class-100 conditions can be attained at a large number of work stations.

As the personnel working in the laboratory are the main source of contamination, precautions are taken to minimize traffic in the laboratory and to protect work from contamination in handling. All personnel wear complete coveralls, hoods, and shoe covers. Entrance to the laboratory is through an air shower consisting of 20 nozzles that blow air at 60 miles per hour to cleanse outer garments. Access to the laboratory is restricted, and flow of supplies in and out is generally accomplished through air-lock type passthroughs, which are interlocked so that no mixing between outside and inside air occurs. A built-in vacuum system is used for regular cleaning of the laboratory. Despite these rather severe restrictions, the laboratory has proved to be a comfortable work area, and stays of 3 to 4 hours duration are not uncommon.

The design of facilities for chemical laboratory work is a special problem because it is not desirable to recirculate air into which toxic materials have been introduced. The Geological Survey laboratory is provided with special laminar-flow fume hoods, which operate on a separate air supply consisting of 90 percent outside air and 10 percent laboratory air. The hood air is sepa-

rated from the rest of the laboratory by air drawn in across the hood opening and down through the front of the hood counter. HEPA-filtered air flows down from filters, through the rest of the hood, and out through the back of the hood in a laminar flow pattern, to maintain class-100 conditions inside the hood. For use with large amounts of corrosive or highly toxic chemicals, a different design would be required, possibly in which the laboratory as a whole would not use recirculated air.

REFERENCES

Austin, P. R., and Timmerman, S. W., 1965, Design and operation of clean rooms: Detroit, Business News Pub. Co., 427 p.

Duke, M. B., Woo, C. C., Bird, M. L., Sellers, G. A., and Finkelman, R. B., 1970, Lunar soil—Size distribution and mineralogical constituents: Science, v. 167, p. 648–650.

U.S. Public Health Service, 1966, Air pollution—A national sample: U.S. Public Health Service pub. 1562, 27 p.

Working Group on Lead Contamination, 1965, Survey of lead in the atmosphere of three urban communities: U.S. Public Health Service pub. 999–AP–12, 94 p.

DISPERSION COMPUTATION AND TEMPERATURE SIMULATION FOR THE CONNECTICUT RIVER ESTUARY BY MATHEMATICAL MODEL

By L. A. WEISS, Hartford, Conn.

Work done in cooperation with the U.S. Atomic Energy Commission

Abstract.—The dispersive properties of the Connecticut River at Haddam Neck, Conn., have been evaluated and simulated for short time intervals by a one-dimensional mathematical model. The model is based on a thermal survey made on September 9, 1968, at the Connecticut Yankee Atomic Power Co. plant at Haddam Neck. Recorded plant-effluent temperatures, stream temperatures, wind speed, net solar radiation, psychrometer data, air pressure, and river stage are input data for the one-dimensional advection-dispersion model. The longitudinal dispersion coefficients varied from near zero to 3,000 sq ft per sec during a tidal cycle, showing that the dispersion coefficient varies directly with tidal flow. The model was able to predict temperatures at two downstream cross sections within 1° Celsius.

To satisfy the ever-growing demand for electricity, utilities have resorted to atomic-fueled generating plants. In 1968, Northeast Utilities Corp. completed construction of the Connecticut Yankee Atomic Power Co. plant on the Connecticut River at Haddam Neck, Conn. (fig. 1). Public concern over the effects of thermal effluent on the ecology of the river prompted the corporation to contract with the Travelers Research Corp. for a thermal survey of the river in the vicinity of the new powerplant. To make maximum use of the ground-truth data furnished by Northeast Utilities Corp., the U.S. Geological Survey, in cooperation with the Division of Reactor Development and Technology, U.S. Atomic Energy Commission, contracted with H. R. B. Singer Corp. to collect additional thermal data from an aerial survey of the estuary by use of infrared imagery. Ruggles (1970) has described the infrared imagery work, and Merriman (1970) has discussed some of the temperature profiles. This paper presents a mathematical model describing dispersion of heated effluents from a point source into an estuary. Field data collected on September 9, 1968, were used to verify the use of the model in computing dispersion coefficients. The model is believed to be applicable to effluents other than heated effluents and to estuaries other than the Connecticut River.

The purposes of this paper are (1) to propose a new application of a one-dimensional finite-difference model describing thermal dissipation for short time intervals of less than 1 hour in an estuary containing water of homogeneous density, (2) to determine the magnitude of tidal advection in the model using actual flow data for short time intervals, (3) to outline the variation

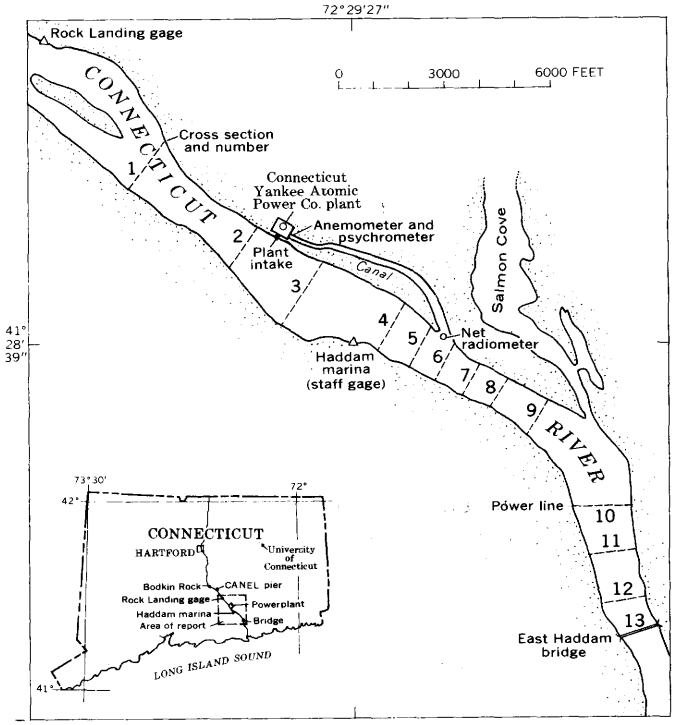

FIGURE 1.—Map of the Connecticut River near Haddam Neck, Conn., showing locations of cross sections, subreaches, and equipment stations.

U.S. GEOL. SURVEY PROF. PAPER 750-B, PAGES B211-B217

of the dispersion coefficient during rapidly changing flow, (4) to simulate river temperature from the model and compare it with field data, and (5) to draw conclusions regarding turbulent dispersion and its future application in modeling the dispersion of pollutants in tidal systems.

MODEL DEVELOPMENT

A one-dimensional mathematical model of an estuary simulating biochemical oxygen demand as well as dissolved oxygen sources and sinks has been developed by Bella and Dobbins (1968). The model described here is a modification applicable to heated inflows. The one-dimensional mass-balance equation describing a thermal effluent discharged into an estuarine environment for time increments of less than 1 day under conditions of unsteady, nonuniform flow is that provided by equation 1:

$$\rho c\frac{\delta(AT)}{\delta t}=-\rho c\frac{\delta(FT)}{\delta L}+\rho c\frac{\delta}{\delta L}\left(AK\frac{\delta T}{\delta L}\right)\pm WQ+\rho c\frac{(FS)(TS)}{\Delta L},$$

where

$\rho c\frac{\delta(AT)}{\delta t}$ represents the change in cross-sectional area and temperature with time,

$\rho c\frac{\delta(FT)}{\delta L}$ is the advective change per unit length of river reach,

$\rho c\frac{\delta}{\delta L}\left(AK\frac{\delta T}{\delta L}\right)$ represents the dispersion change in thermal gradient per unit of reach length,

WQ is the net energy entering or leaving the river reach at the air-water interface, and

$\rho c\frac{(FS)(TS)}{\Delta L}$ represents the thermal load entering the river.

The symbols used in equation 1 are defined as follows:

A=area of stream cross section,
c=specific heat of water,
F=discharge at stream cross section,
FS=plant effluent discharge,
K=longitudinal dispersion at stream cross section,
L=length of subreach,
Q=heat gained or lost in subreach at air-water interface,
ρ=density of water,
t=time interval,
T=temperature at stream cross section,
TS=temperature of plant effluent, and
W=width of subreach.

If river density is homogeneous, river width fairly uniform, and flow positive downstream, the one-dimensional mathematical model for short time intervals can be approximated by expanding equation 1, using a finite-difference scheme as shown in equation 2 for subreach 1. Rearranging terms and solving equation 2 for the dispersion coefficients at cross section j (at time $t=(n+\frac{1}{2})\Delta t$) results in equation 3. If the subreach length is kept short enough, then it can be assumed that $K_{(j,\ n+1/2)}=K_{(j-1,\ n+1/2)}$ and the equation can be solved for $K_{(j,\ n+1/2)}$ as in equation 4. Equation 4 was used to compute dispersion coefficients directly from known temperature, stage, flow, and climatological data.

Equation 2:

$$\begin{aligned}0.25\rho cL_{(i)}&[(A_{(j-1,n+1)}+A_{(j,n+1)})(T_{(j-1,n+1)}+T_{(j,n+1)})\\&-(A_{(j-1,n)}+A_{(j,n)})(T_{(j-1,n)}+T_{(j,n)})]\\&=\rho c\Delta tF_{(j-1,n+\frac{1}{2})}\times 0.5\times(T_{(j-1,n)}\\&+T_{(j-1,n+1)})-0.5\rho c\Delta tF_{(j,n+\frac{1}{2})}(T_{(j,n)}\\&+T_{(j,n+1)})+[0.5\rho c\Delta t(A_{(j-1,n+\frac{1}{2})}/(L_{(i-1)}\\&+L_{(i)}))\times K_{(j-1,n+\frac{1}{2})}(T_{(j-2,n)}+T_{(j-2,n+1)}\\&-T_{(j,n)}-T_{(j,n+1)})]+\rho c\Delta t(FS)_{(i,n+\frac{1}{2})}\\&\times(TS)_{(i,n+\frac{1}{2})}+L_{(i)}W_{(i)}\Delta tQ_{(i,n+\frac{1}{2})}.\end{aligned}$$

Equation 3:

$$\begin{aligned}K_{(j,\ n+\frac{1}{2})}=\{&0.25\rho cL_{(i)}[(A_{(j-1,n+1)}+A_{(j,n+1)})(T_{(j,n+1)}\\&+T_{(j-1,n+1)})-(A_{(j-1,n)}+A_{(j,n)})(T_{(j-1,n)}\\&+T_{(j,n)})]-0.5\rho c\Delta tF_{(j-1,n+\frac{1}{2})}(T_{(j-1,n)}\\&+T_{(j-1,n+1)})+0.5\rho c\Delta tF_{(j,n+\frac{1}{2})}(T_{(j,n)}\\&+T_{(j,n+1)})-0.5\rho c\Delta t\times(A_{(j-1,n+\frac{1}{2})}/(L_{(i-1)}\\&+L_{(i)}))\times K_{(j-1,n+\frac{1}{2})}(T_{(j-2,n+1)}+T_{(j-2,n)}\\&-T_{(j,n+1)}-T_{(j,n)})-\rho c\Delta t(FS)_{(i,n+\frac{1}{2})}\\&\times(TS)_{(i,n+\frac{1}{2})}-L_{(i)}W_{(i)}\Delta tQ_{(i,n+\frac{1}{2})}\}\\&\div[0.5\rho c\Delta t(A_{(j,n+\frac{1}{2})}/(L_{(i)}+L_{(i+1)}))\\&\times(T_{(j+1,n+1)}+T_{(j+1,n)}-T_{(j-1,n+1)}-T_{(j-1,n)}).\end{aligned}$$

Letting $(K_{(j-1,\ n+\frac{1}{2})})\approx(K_{(j,\ n+\frac{1}{2})})$ in equation 2 gives equation 4:

$$\begin{aligned}K_{(j,n+\frac{1}{2})}=\{&0.25\rho cL_{(i)}[(A_{(j-1,n+1)}+A_{(j,n+1)})\\&(T_{(j-1,n+1)}+T_{(j,n+1)})-(A_{(j-1,n)}\\&+A_{(j,n)})(T_{(j-1,n)}+T_{(j,n)})]\\&-0.5\rho c\Delta tF_{(j-1,n+\frac{1}{2})}(T_{(j-1,n)}+T_{(j-1,n+1)})\\&+0.5\rho c\Delta tF_{(j,n+\frac{1}{2})}(T_{(j,n+1)}+T_{(j,n)})\\&-\rho c\Delta t(FS)_{(i,n+\frac{1}{2})}\times(TS)_{(i,n+\frac{1}{2})}\\&-L_{(i)}W_{(i)}\Delta tQ_{(i,n+\frac{1}{2})}\}\\&\div\{0.5\rho c\Delta t[(A_{(j,n+\frac{1}{2})}/(L_{(i)}+L_{(i+1)}))\end{aligned}$$

$$\times(T_{(j+1,n+1)}+T_{(j+1,n)}-T_{(j-1,n+1)}$$
$$-T_{(j-1,n)})+A_{(j-1,n+\frac{1}{2})}/(L_{(i-1)}+L_{(i)}))$$
$$\times(T_{(j-2,n+1)}+T_{(j-2,n)}-T_{(j,n+1)}-T_{(j,n)})\}.$$

The symbols used in equations 2–4 are defined as follows:

$A_{(j-1,\ n+\frac{1}{2})}$=area of stream cross section $j-1$ at time $t_{(n+\frac{1}{2})}$,
c=specific heat of water,
$F_{(j-1,\ n+\frac{1}{2})}$=discharge at stream cross section $j-1$ at time $t_{(n+\frac{1}{2})}$,
$(FS)_{(i,\ n+\frac{1}{2})}$=plant effluent discharge into subreach i at time $t_{(n+\frac{1}{2})}$,
$K_{(j-1,\ n+\frac{1}{2})}$=longitudinal dispersion at cross section $j-1$ at $t_{(n+\frac{1}{2})}$,
Li=Length of subreach i,
$Q_{(i,\ n+\frac{1}{2})}$=heat gained or lost in subreach i as a result of meteorologic conditions between times $t_{(n)}$ and $t_{(n+1)}$,
ρ=density of water,
t=time interval,
$T_{(j-1,\ n+1)}$=temperature at stream cross section $j-1$ at time $t_{(n+1)}$,
$(TS)_{(i,\ n+\frac{1}{2})}$=temperature of plant effluent at mouth of canal, and
W=width of subreach.

Figure 2 is a temporal and spatial scheme of a one-dimensional advection-dispersion model where i=subreach number, j=cross section number, and n=time step.

FLOW COMPUTATION

Discharge at Bodkin Rock and the Haddam marina (table 2) was computed from stage values recorded between these two sections. The flows were computed for 15-minute intervals by unsteady, nonuniform flow equations using the method of characteristics. The method utilized a computer program; previous use of such a program for the Connecticut River was discussed by Lai (1967).

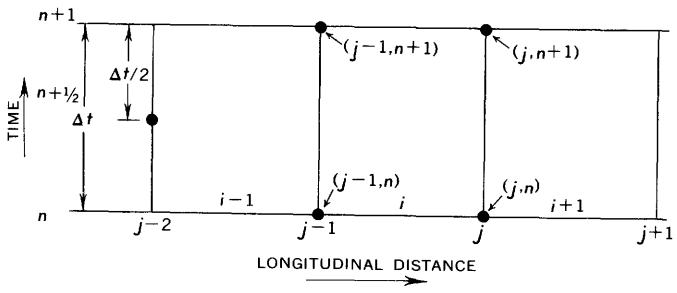

FIGURE 2.—Time and distance scheme.

River stage was not recorded downstream from the Haddam marina at the time of the thermal study. Therefore, flows computed at Bodkin Rock and the Haddam marina were extrapolated to sections 5, 6, and 7. The resulting error is believed to be small because even the farthest station, 7, is less than 4,000 downstream from the marina.

THERMAL SOURCES AND SINKS BETWEEN WATER SURFACE AND ATMOSPHERE

The advection-dispersion model of thermal loading must take into account atmospheric conditions affecting heat flow at the air-water interface. The heat flow from air to water is a source of heat in addition to that from powerplant loading and is positive in sign. Heat flow from water to the air is a heat loss or sink and is negative in sign.

Net incoming radiation Q_R is the sum of incoming solar and atmospheric radiation, minus losses from back radiation of long waves that are emitted at the air-water interface and reflected long-wave and short-wave radiation. Net incoming radiation is the source of heat from the air to the water. Thermal losses or sinks consist chiefly of heat utilized for evaporation Q_E, heat conducted from the water Q_H, and heat advected by evaporation Q_W.

The heat lost by evaporation can be expressed by the equation: $Q_E=EL_c\rho$, where ρ is the density of water, L_c is the heat of vaporization at surface-water temperature, and E is the evaporation, in inches per unit of time. Evaporation was computed by the equation:

$$E=0.001813w(e_o-e_a)+[1-0.03(T_a-T_o)]t,$$

where

t=1 day,
w=wind speed,
e_o=vapor pressure at surface-water temperature (T_o), and
e_a=vapor pressure in air at air temperature (T_a).

Integrating each 15-minute computation of evaporation resulted in a value of 0.15 inch for the day. The University of Connecticut agricultural station (location shown on fig. 1) recorded 0.17 inch of evaporation from a class-A evaporation pan for the same day. Therefore evaporation values used in this study are believed to be well within the desired accuracy.

The heat of conduction is given by the equation $Q_H=R'Q_E$ where R' is the Bowen ratio. The Bowen ratio is given by the equation

$$R'=R\frac{K_{(H)}}{K_{(wv)}}$$

where

$$R=\frac{0.61}{1{,}000}P\frac{T_o-T_a}{e_o-e_a}$$

and $K_{(H)}$ and $K_{(wv)}$ are the thermal and water-vapor diffusivities in air and P is the atmospheric pressure. The ratio

$$\frac{K_{(H)}}{K_{(wv)}}$$

is expressed by the equation

$$\frac{K_{(H)}}{K_{(wv)}}=\sqrt{\frac{(1+3.33R_i)^3}{1+10R_i}}$$

where R_i is the Richardson number. The Richardson number is a value used to express unequal thermal and water-vapor diffusivities due to turbulent wind conditions. The Richardson number is given by the equation

$$R_i=\left(\frac{g}{\theta}\right)\left(\frac{\delta\theta}{\delta z}\right)\Big/\left(\frac{\delta w}{\delta z}\right)^2.$$

This equation relates the thermal gradient to the velocity gradient at 4 meters above ground level. If the velocity of the wind is less than 5 mph, then

$$R_i=0,\ \frac{K_{(H)}}{K_{(wv)}}=1,\text{ and } R'=R.$$

As previously indicated, all wind velocities during the measurement were less than 3.5 mph. In the equation for R_i, the term θ is the potential air temperature at 4 meters, g is the gravitational acceleration, $\frac{\delta\theta}{\delta z}$ is the thermal gradient at 4 meters, and $\frac{\delta w}{\delta z}$ is the velocity gradient at 4 meters.

The heat advected by evaporation is given by the equation $Q_w=c\rho E(T_o-T_b)$ where T_o is the water surface temperature and T_b is the base temperature of the river, which was 0°C in this study. If values of Q_R, Q_E, Q_H, and Q_w for any time are known, the total heat flow to or from the water surface can be calculated from equation 5:

$$Q_{(i,\ n+\frac{1}{2})}=Q_{R(i,\ n+\frac{1}{2})}-(Q_E+Q_H+Q_w)_{(i,\ n+\frac{1}{2})}$$

where

Q_E=energy utilized for evaporation,
Q_H=sensible heat or heat conducted from the water,
$Q_{(i,\ n+\frac{1}{2})}$=total heat flow to or from air-water interface in subreach i at time $n+\frac{1}{2}$,
Q_R=net incoming radiation, and
Q_w=heat advected by evaporation.

FIELD STUDY

To obtain meaningful field results, certain conditions of riverflow and powerplant operation were necessary. The following guidelines determined selection of the specific study date:

1. Minimum fresh-water inflow in the stream.
2. High unaffected river temperature.
3. Uninterrupted powerplant operation for at least 7 days before the study.
4. Little or no wind.

All these conditions were met on September 9, 1968, when the Connecticut Yankee Atomic Power Co. plant at Haddam Neck operated at a power level of 490 megawatts throughout the observation period. During this time, air temperature ranged from 14.7°C to 22.2°C. Hourly dry and wet bulb readings are listed in table 1. Wind direction at the powerplant changed from northeast to southeast but remained below 3.5 mph.

Net radiation measured 4 feet above the water surface at the outlet of the canal ranged from 0 at 0700 e.s.t. to 1.00 g-cal/cm^{2}min^{-1} at 1300 e.s.t. (table 1). River stage values at 15-minute intervals between Bodkin Rock at Middletown and the Haddam marina (see fig. 1) are also shown in the table.

River temperatures were measured with submersible thermometers from four 14-foot outboard-power boats; three patroled different subreaches of the river while the fourth followed the warm water plume to delineate its surface position. Figure 1 shows the locations of the cross sections and of the Haddam marina. Sampling extended over a 4-mile reach using 10 cross sections. Temperature measurements were made at the river surface and at 1-, 3-, and 6-foot depths, and thereafter at 3-foot intervals to and including the river bottom. Temperature observations were scheduled over a 10-hour period centered on low and high tide. Each boat was equipped with a two-way radio, a thermister and bridge with 50-foot lead, range finder, and a plough anchor for maintaining position. Temperatures were measured in degrees Fahrenheit and subsequently converted to degrees Celsius for this report. Point temperatures were integrated in depth and width at five cross sections and shown in table 2. The resulting width-integrated surface temperatures at each of five cross sections are also available in table 2. Point-temperature data are on file with the Environmental Science Section of Northeast Utilities Corp.

Infrared imagery was flown by the H. R. B. Singer Co. under contract with the U.S. Geological Survey in cooperation with the U.S. Atomic Energy Commission.

TABLE 1.—*Stage, climatological, and powerplant effluent data recorded on the Connecticut River, September 9, 1968*

Time (e.s.t.)	Stage (feet)			Air temperature		Air pressure (mbar)[3]	Wind		Net radiation (g-cal/cm² min⁻¹)[4]	Plant effluent		Unaffected river temperature
	Bodkin Rock	CANEL[1] pier	Haddam marina	Dry bulb (°C)[2]	Wet bulb (°C)[2]		Direction	Speed (knots)		Flow (cfs)[5]	Temperature (°C)[2]	(°C)[2]
0700	10.07	9.74	9.21	14.7	14.7	1,023.1	Southeast	2.6	0.00	852	33.5	23.9
0715	9.98	9.66	9.16									
0730	9.88	9.58	9.13									
0745	9.79	9.50	9.13									
0800	9.71	9.44	9.17	15.0	14.5	1,023.7	East	1.7	.15	852	33.4	23.9
0815	9.63	9.41	9.23									
0830	9.55	9.39	9.31									
0845	9.50	9.41	9.44								33.2	
0900	9.47	9.48	9.58	15.0	13.6	1,023.8	Northeast	3.0	.20	852	33.4	23.4
0915	9.47	9.53	9.75									
0930	9.50	9.66	9.95									
0945	9.56	9.85	10.14									
1000	9.67	10.02	10.34	14.7	13.6	1,023.7	Southeast	1.7	.35	852	33.1	23.4
1015	9.81	10.24	10.52								32.0	
1030	9.98	10.40	10.70									
1045	10.15	10.58	10.88									
1100	10.33	10.71	11.05	18.1	15.8	1,023.2	North	1.7	.55	852	32.8	23.4
1115	10.51	10.91	11.19									
1130	10.67	11.06	11.35									
1145	10.83	11.21	11.49									
1200	10.99	11.35	11.65	18.9	15.6	1,022.8	Southeast	1.7	.80	852	32.7	23.4
1215	11.12	11.47	11.74									
1230	11.24	11.59	11.86									
1245	11.36	11.70	11.98									
1300	11.48	11.81	12.05	20.6	17.5	1,022.1	do	1.3	1.00	852	33.2	23.4
1315	11.58	11.90	12.12									
1330	11.69	11.96	12.15								34.4	
1345	11.78	12.04	12.16									
1400	11.87	12.09	12.16	22.2	18.3	1,021.4	do	2.2	.75	852	33.9	24.5
1415	11.95	12.12	12.10									
1430	12.01	12.13	12.02									
1445	12.06	12.12	11.91									
1500	12.10	12.06	11.77	21.0	18.1	1,021.1	do	2.2	.20	852	34.5	25.0
1515	12.09	11.96	11.59									
1530	12.06	11.82	11.41									
1545	12.00	11.67	11.24									
1600	11.90	11.50	11.08	20.6	17.8	1,021.4	do	2.6	.20	852	34.6	25.0
1615	11.77	11.35	10.94									
1630	11.62	11.21	10.80									
1645	11.48	11.10	10.67									
1700	11.34	10.99	10.50	20.6	18.1	1,021.9	do	2.2	.05	852	34.5	25.0
1715	11.21	10.87	10.40									
1730	11.09	10.75	10.26									
1745	10.89	10.65	10.15								34.0	24.6

[1] Connecticut Atomic Nuclear Engine Laboratory.
[2] Degrees Celsius.
[3] Millibars.
[4] Gram-calories per centimeter squared per minute.
[5] Cubic feet per second.

The capability of an infrared-thermal mapping system to delineate the extent of thermal patterns has been discussed by Ruggles (1970). Figure 3 indicates the dispersive characteristics of the surface heat distribution between cross sections 1 and 6 during upstream and downstream flow.

RESULTS OF DISPERSION COMPUTATIONS

Figure 4 shows the results of computations of the dispersion coefficient from the model simulation for the reach between sections 4 and 7 during the period between 0900 and 1700 e.s.t. on September 9, 1968. The figure also shows the flow at the Haddam marina. The dispersion coefficient was 3,060 sq ft per sec when flow was tidal and upstream at 24,300 cfs; it was 3,000 sq ft per sec when flow was downstream at 24,550 cfs, and it dropped to nearly zero just after tide reversal. Equation 4 was used to compute the dispersion coefficients. It is clear that the dispersion coefficient varies directly with tidal flow. The validity of the dispersion coefficients was confirmed by simulating temperature as shown in figure 5. The figure shows sections 7 and 8; the maximum error was 1°C at 1415 e.s.t. The dispersion coefficients and flows at sections 5–7, temperatures at sections 4–6, and air-water heat exchanges in subreaches 5–6 and 6–7 were used as input to simulate temperatures at sections 7 and 8, using equation 2. The temperature simulation was computed by rearranging terms in equa-

413-504 O - 71 - 15

TABLE 2.—*Computed discharge and average river temperatures in the Connecticut River on September 9, 1968*

Time (e.s.t.)	Flow (cfs) [1]		Average temperature in section (° C) [2]					Average surface temperature in section (° C) [2]				
	Bodkin Rock	Haddam marina	4	5	6	7	8	4	5	6	7	8
0700	16,819	16,000										
0715	16,786	15,500										
0730	16,103	15,000										
0745	15,799	14,660										
0800	15,419	13,810	23.8									
0815	14,730	12,450	23.9	----	----	----	24.8	23.9				
0830	13,479	9,524	24.0	23.8	----	----	24.7	23.9	23.8	----	26.9	26.1
0845	12,456	4,082	24.1	23.9	----	----	24.7	23.9	24.0	----	26.7	25.9
0900	10,538	−2,556	24.2	23.9	26.6	24.1	24.7	23.9	24.3	31.1	26.4	25.7
0915	8,009	−10,250	24.4	24.0	26.6	24.2	24.7	24.0	24.6	30.6	26.2	25.6
0930	5,937	−15,210	24.9	24.1	26.4	24.2	24.7	24.2	24.9	30.1	26.0	25.4
0945	1,473	−17,200	24.7	24.2	26.4	24.3	24.7	24.4	25.1	29.7	25.8	25.1
1000	−4,621	−18,970	24.8	24.3	26.3	24.4	24.7	24.8	25.4	29.1	25.4	24.9
1015	−10,177	−19,790	24.9	24.3	26.3	24.6	24.7	25.0	25.8	28.7	25.3	24.9
1030	−15,521	−21,040	24.9	24.4	26.2	24.7	24.8	25.3	26.0	28.2	25.0	24.8
1045	−17,714	−22,590	24.9	24.6	26.4	24.7	24.9	25.6	26.2	27.8	24.8	24.7
1100	−19,574	−23,700	24.9	24.7	26.6	24.8	24.9	25.8	26.2	27.2	24.7	24.7
1115	−19,394	−24,200	25.0	24.8	26.7	24.8	24.9	25.9	26.3	26.9	24.6	24.6
1130	−20,700	−24,530	25.0	24.9	26.7	24.8	25.0	26.0	26.3	27.1	24.7	24.7
1145	−21,200	−24,420	25.0	25.0	26.8	24.9	25.1	26.0	26.4	27.3	24.9	24.9
1200	−21,277	−24,200	25.0	25.1	26.9	24.9	25.1	26.1	26.4	27.6	25.0	25.0
1215	−21,446	−23,800	25.0	25.2	27.0	24.9	25.2	26.1	26.4	27.8	25.1	25.2
1230	−21,475	−23,150	25.1	25.3	27.1	25.0	25.3	26.2	26.6	27.9	25.2	25.3
1245	−21,644	−22,200	25.1	25.4	27.2	25.0	25.4	26.3	26.6	28.1	25.4	25.6
1300	−21,583	−21,290	25.1	25.6	27.2	25.0	25.4	26.3	26.7	28.3	25.6	25.6
1315	−21,500	−20,620	25.2	25.6	27.3	25.0	25.4	26.4	26.7	28.6	25.7	26.1
1330	−21,250	−18,640	25.2	25.6	27.4	25.1	25.5	26.6	26.7	28.8	25.9	26.4
1345	−20,801	−16,500	25.2	25.6	27.6	25.1	25.6	26.6	26.8	28.9	26.0	26.8
1400	−20,086	−14,760	25.2	25.7	27.7	25.1	25.6	26.7	26.8	29.2	26.1	27.1
1415	−19,200	−10,490	25.2	25.7	27.8	25.2	25.7	26.7	26.8	29.3	26.4	27.3
1430	−17,884	−6,129	25.3	25.7	27.9	25.2	25.7	26.6	26.8	29.6	26.7	27.7
1445	−16,104	−425	25.3	25.7	28.0	25.3	25.8	26.6	26.8	29.8	27.0	28.0
1500	−13,760	6,929	25.3	25.8	28.1	25.4	25.8	26.6	26.7	30.0	27.2	28.3
1515	−10,562	13,820	25.4	25.8	28.2	25.4	25.8	26.4	26.7	30.2	27.6	28.6
1530	−5,897	17,270	25.4	25.8	28.3	25.6	25.9	26.4	26.7	30.3	27.8	28.9
1545	106	19,160	25.4	25.8	28.4	25.7	25.9	26.4	26.7	30.6	28.1	29.2
1600	7,110	20,510	25.4	25.9	28.7	25.7	26.0	26.4	26.6	30.8	28.3	29.4
1615	13,519	21,500	25.5	25.9	28.8	25.8	26.0	26.3	26.6	31.0	28.6	29.8
1630	17,250	23,170	25.6	25.9	28.9	25.9	26.0	26.3	26.5	31.1	28.9	30.0
1645	19,409	24,210	25.6	25.9	28.9	26.0	26.1	26.3	26.5	31.3	29.2	
1700	19,480	24,310	25.6	26.0	29.1	26.0	26.1	26.2	26.4	31.6	29.4	
1715	19,373	24,410										
1730	19,079	24,650										
1745	19,168	23,550										

[1] Cubic feet per second.
[2] Degrees Celsius.

tion 2 and solving for $T_{(j+1,\ n+1)}$. Little or no heat dissipated at the air-water interface during the study. Almost all of the heat was dispersed in the estuary.

PRELIMINARY CONCLUSIONS

1. A one-dimensional, continuous time-dependent solution of the mass-balance equation for the longitudinal dispersion of thermal effluents in the Connecticut River is obtainable through numerical methods for short time intervals.

2. The dispersion coefficient in the Connecticut River at any time is highly dependent on the magnitude and direction of instantaneous waterflow.

3. Dispersion coefficients in the Connecticut River vary substantially with time and location.

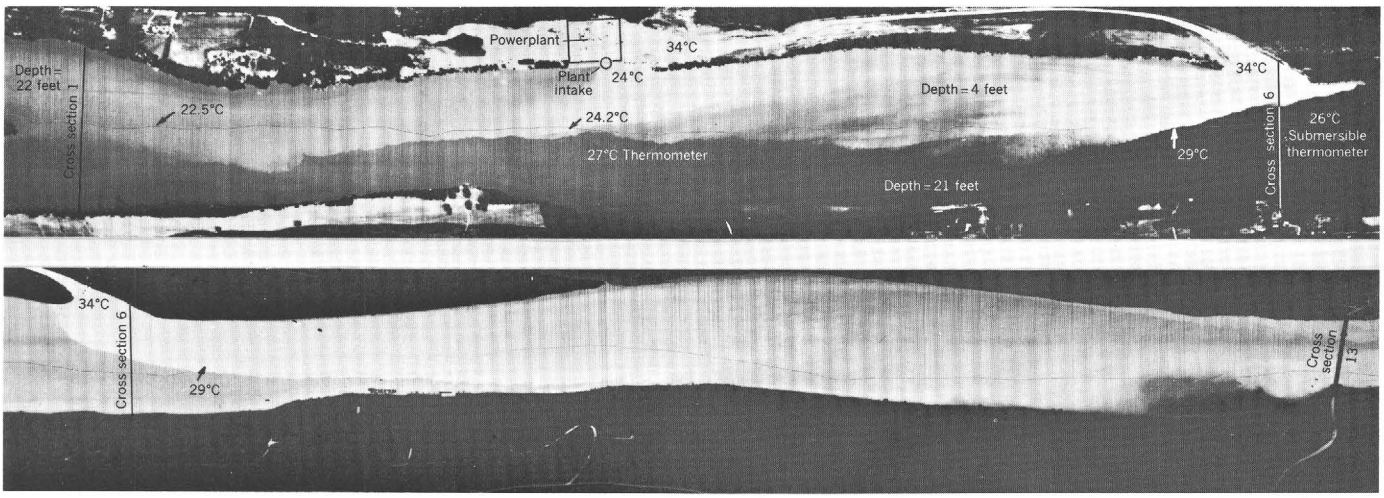

FIGURE 3.—Infrared imagery of thermal dissipation in the Connecticut River near the Connecticut Yankee Atomic Power Co. plant during upstream and downstream flow on September 9, 1968. °C, degree Celsius.

4. Models of this type probably can be applied to other studies, such as those simulating oxygen demand in streams, provided that flow data are available and dispersion coefficients for short time increments can be computed.

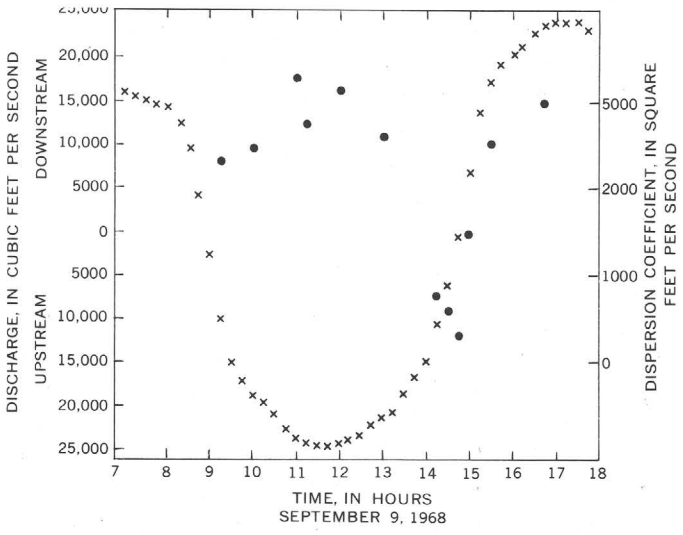

FIGURE 4.—Relation of computed discharge and dispersion coefficient of the Connecticut River at the Haddam marina. x, flow at the Haddam marina; solid circle, dispersion coefficient at cross section 5.

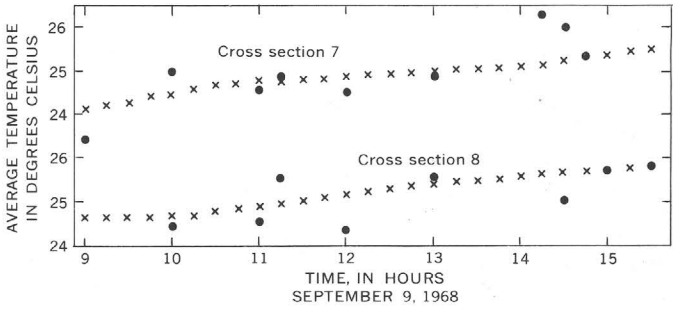

FIGURE 5.—Comparison of field temperature and simulated temperature of the Connecticut River downstream from the Haddam marina. x, field temperature; solid circle, simulated temperature.

REFERENCES

Bella, D. A., and Dobbins, W. E., 1968, Difference modeling of stream pollution: Am. Soc. Civil Engineers Proc., Jour. Sanitary Eng. Div., v. 94, no. SA5, p. 995–1016.

Lai, Chintu, 1967, Computation of transient flows in rivers and estuaries by the multiple-reach method of characteristics, *in* Geological Survey Research 1967: U.S. Geol. Survey Prof. Paper 575–D, p. D273–D280.

Merriman, Daniel, 1970, The calefaction of a river: Sci. American, v. 222, no. 5, p. 42–52.

Ruggles, F. H., Jr., 1970, A thermal survey of the Connecticut River estuary: Proc. 2d Ann. Programs Review, Earth Resources Program, NASA Aircraft Project, v. 111, sec. 41, p. 1–12.

EFFECTS OF URBANIZATION ON SEDIMENT TRANSPORT IN BEL PRE CREEK BASIN, MARYLAND

By THOMAS H. YORKE and WILLIAM J. DAVIS,
College Park, Md.

Work done in cooperation with the District of Columbia Department of Sanitary Engineering, the Maryland–National Capital Park and Planning Commission, and the Washington Suburban Sanitary Commission

Abstract.—The effect of urban expansion on the sediment yield of a 1.7-square-mile drainage basin is described. Streamflow and sediment data were collected at a gaging station on Bel Pre Creek in Montgomery County, Md., between 1963 and 1967. Prior to March 1965, the drainage area was used for pasture and woodland; however, between March 1965 and August 1967, part of the basin was developed for garden apartments and townhouses. A graphical regression analysis indicated that the storm runoff increased 30 percent and the sediment yield was 14 times greater as a result of urban construction on about 15 percent of the drainage basin. The sediment yield from the construction sites was 90 times greater than the yield expected from the area with the original land-use conditions.

The conversion of thousands of acres of land as a result of urban expansion has created serious sediment pollution problems throughout the country. In the Washington, D.C., metropolitan area, increased sediment yields resulting from residential, commercial, and highway construction activities have reduced many of the local streams to unsightly drainage ditches. Once-clean stream channels have become overburdened with sediment, resulting in the destruction of the aquatic life and a general deterioration of the environment of the stream basin.

Numerous investigators have reported on the high sediment yields from urban construction areas. Guy (1965) reported a yield of 189 tons per acre from a small residential construction site in Kensington, Md. In the Scott Run basin, Virginia, a yield of about 100 tons per acre was observed during the construction of an interstate highway (Vice and others, 1969). Each of these studies provides a measure of the extremely high sediment yields associated with construction activities, but neither provides a comparison with the preconstruction conditions. The opportunity for a direct comparison is available with the streamflow and sediment data that was collected on the Bel Pre Creek in Montgomery County, Md., between 1963 and 1967. Measurement of the preurbanization sediment yield was made prior to 1965, and measurement of construction sediment yield was made after 1965 as the land use was altered by the development of a retirement community in the upper half of the basin.

DESCRIPTION OF STUDY AREA

Bel Pre Creek drains a small basin in the headwaters of the Anacostia River. The drainage area above the gaging station is 1.69 square miles (fig. 1). The elevation ranges from 350 feet above mean sea level at the gage to 510 feet near Norbeck. The average slope of the stream channel is 1.3 percent.

The basin is located on the east edge of the Piedmont physiographic province and is characterized by rolling topography, with land slopes ranging from 3 to 15 percent, most of the slopes being less than 8 percent. Igneous and metamorphosed igneous rocks of the Precambrian Era underlie the area. A soft micaceous schist is the predominant rock, and material weathered from this rock is the parent material for the Chester, Manor, and Glenelg soils common to the area (U.S. Dept. of Agriculture,

U.S. GEOL. SURVEY PROF. PAPER 750-B, PAGES B218–B223

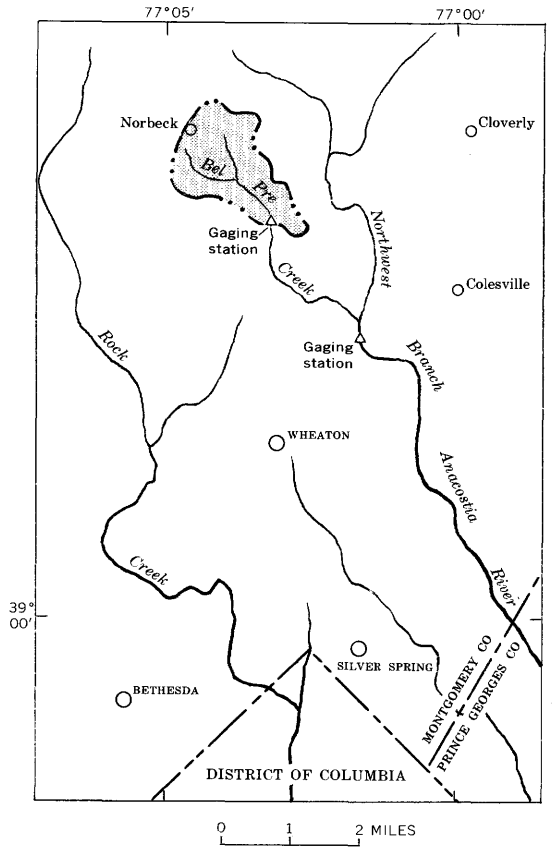

FIGURE 1.—Map showing location of Bel Pre Creek basin, Maryland (stippled).

1961). These soils are predominantly silt loams that are highly susceptible to erosion when exposed to weathering forces. The soils of the Manor series are particularly susceptible in construction areas because of their weakly developed subsoil.

A temperate and rather humid climate, which is typical of the Middle Atlantic States, is characteristic of the area. The average annual precipitation for Washington, D.C., is approximately 41 inches and is fairly evenly distributed throughout the year. The maximum monthly precipitation usually occurs in July or August and the minimum in October or November. Summer precipitation is characterized by short, high-intensity rainfalls from convective storms, and winter precipitation is derived almost exclusively from frontal storms. Average annual runoff from nearby basins is about 14 inches, ranging from about 0.6 inch in September to 1.6 inches in February.

DATA COLLECTION

Streamflow and suspended-sediment data were collected at the Bel Pre Creek gaging station on an intermittent basis from 1963 to 1967. Water-discharge data for storms were obtained by means of a water-stage recorder and current-meter measurements. Suspended-sediment concentrations were determined from samples obtained during storms by using manual and single-stage sampling procedures, as described by the U.S. Inter-Agency Committee on Water Resources, Subcommittee on Sedimentation (1963).

Rainfall was recorded at a site 2 miles northeast of the Bel Pre Creek gaging station. This site was equipped with a standard U.S. Weather Bureau weighing-type recording gage. Additional rainfall data were collected at several sites equipped with wedge-type nonrecording rain gages.

Land-use information was obtained from various aerial photographs taken between 1959 and 1967. The data, as compiled in table 1, represent the land use at the time of the photography. The grass category represents all pastures, abandoned fields, and golf course areas. The construction category accounts for all the area in some phase of active development and includes denuded land and land occupied by partly completed roads and buildings. Once the construction was completed and the areas stabilized with pavements or vegetation, these areas were reclassified in the appropriate category.

LAND-USE CHANGES

The study basin underwent a substantial change in land use during the course of the data collection. In March 1963 the basin was mainly rural. The upper half of the drainage area was woodland, and the lower half was used for a golf club and pasture. Only 1.6 percent of the basin was developed for residential housing or commercial interests, and there were no active construction projects. By 1967, 8.5 percent had been developed for residential housing and another 14 percent was under development. In addition, another 4.9 percent of the basin had been converted from woodland to grassland for a golf course. The development of a retirement community in the upper part of the basin was the primary cause of this rapid change from rural to urban conditions. This residential complex, centered around recreation facilities, is composed of townhouses and garden apartments. It is planned that the community will

TABLE 1.—*Land use, in percent of drainage area, in Bel Pre Creek basin, Maryland, 1959–67*

Date	Cultivated	Grass	Woodland	Urban	Construction
Nov. 1959	12.4	28.5	57.5	1.6	0
Mar. 1963	12.4	28.5	57.5	1.6	0
Dec. 1964	0.6	38.0	56.7	1.6	3.1
July 1965	0	33.6	46.8	1.6	18.0
June 1966	.9	41.4	38.5	5.2	14.0
June 1967	.8	40.4	36.4	8.5	13.9

occupy more than 50 percent of the Bel Pre Creek drainage basin.

EFFECTS OF URBAN DEVELOPMENT

The sediment yield of a drainage basin, as described by Anderson (1957), depends on three sets of variables: natural watershed characteristics, the nature of storms, and land use. Of the three, land use exhibits the greatest effect on sediment yield in that it amplifies or moderates the effect of topographic and geologic factors as well as climatic factors. Steep-sloped watersheds with abundant forest cover generally yield substantially less sediment than much flatter basins under cultivation or in pasture. Also, rainfall has a much greater effect on cultivated fields or open land than it has on woodland (Ursic and Dendy, 1965). The land-use condition that has probably the greatest effect on increased sediment yields is the construction stage in urbanization. Not only is vegetal protection removed from the soil surface, but the stability of the soil structure is destroyed through massive earthmoving for highway rights-of-way and commercial and residential building lots. This leaves the soil unprotected from the forces of rainfall and the accompanying overland runoff. The magnitude of this effect on the Bel Pre Creek basin has been determined in two ways.

Two-storm comparison

One illustration of the effect of urban development on the runoff characteristics and sediment yield of a basin is a comparison of the response of two similar storms, one before and the other during development. The storms of Nov. 6–7, 1963, and Oct. 18–19, 1966, provide this comparison, and they readily exhibit a distinct difference in the response of suspended sediment (fig. 2). The total rainfall of the 1963 storm was 0.9 inch greater than that of the 1966 storm, but the total runoff from the two storms was 40 and 35 cfs-days (cubic feet per second-days), respectively. The peak discharge was 80 cfs in 1963 and 84 cfs in 1966. However, the 1966 storm, which occurred when 14 percent of the basin was under development, yielded nine times more sediment than the storm before development. The yield in suspended sediment was 14.3 tons compared with 124 tons, and the mean concentrations were 70 and 500 mg/l (milligrams per liter), respectively.

It should be noted that the two runoff events used here for comparison were the result of frontal storms, which generally produce less sediment discharge than the convective storms of the summer. For example, the mean concentration of the November 1966 storm was 500 mg/l, as compared with several storms in the summer of 1967 which produced mean concentrations as

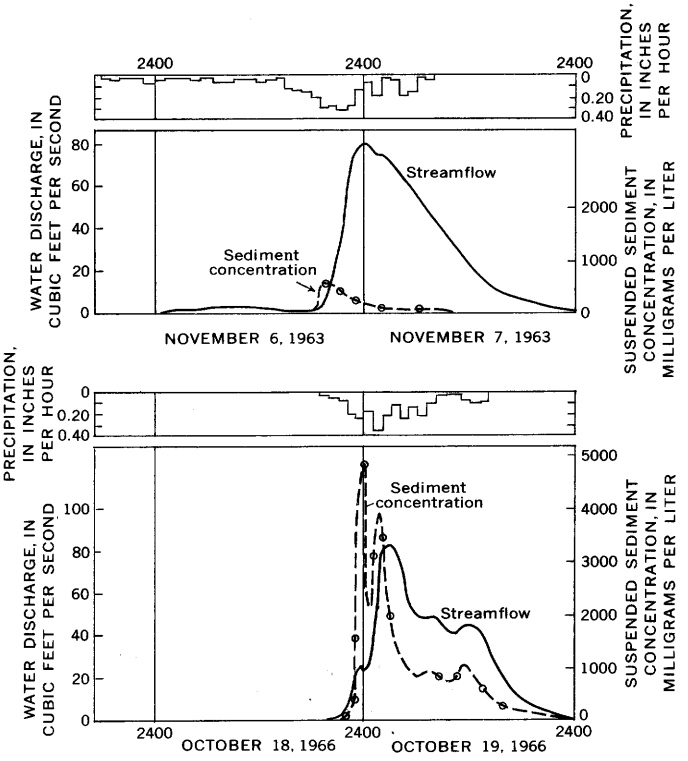

FIGURE 2.—Variation of precipitation, sediment concentration, and water discharge during two storm-runoff periods for Bel Pre Creek, Md.

high as 1,500 mg/l. The estimated peak concentration of suspended sediment for the November 1966 storm was 4,900 mg/l as compared with peak concentrations during summer storms, which reached as high as 32,000 mg/l. This suggests that the effect of construction is substantially greater than the 900-percent increase in sediment yield indicated by the two-storm comparison.

Total suspended-sediment yield

A total of 29 storms were sampled between March 1963 and August 1967. The data for these are listed in table 2. Storm runoff is considered to be total measured runoff minus estimated base flow during a storm. In this study the base flow has been estimated by extending the gage-height graph in a straight line from the point of its initial rise to the point where the recession limb approaches a straight line, then averaging the values at the end points of the line.

The runoff and sediment loads from the sampled storms were plotted as a mass curve to determine the trend of the sediment yield in the Bel Pre Creek basin. As shown in figure 3, the data from the storms between March 1963 and December 1964 approximate a straight line, with a slope that indicates an average concentration of suspended sediment of about 220 mg/l. The plot of data from subsequent storms shows an abrupt upward

break in the slope of the curve. The steeper slope of the second part of the curve, which indicates an average concentration of 2,700 mg/l, shows that the amount of sediment transported by a runoff event between March 1965 and August 1967 was greater than the amount that would have been transported by an equivalent amount of runoff between March 1963 and December 1964. The time of this change in the runoff-sediment relation was approximately coincident with the beginning of a rapid increase in construction area, which changed from 3.1 to 18 percent of the basin between December 1964 and July 1965.

Because the mass curve indicates that the runoff and sediment data from the 29 storms represent two distinct populations, the data have been used for estimating the total sediment yield of Bel Pre Creek both before and during construction. Graphical techniques were employed to develop linear regression relations in order to estimate the runoff and sediment load of unsampled storms during the study period.

Storm runoff from the 21.1-sq-mi drainage basin

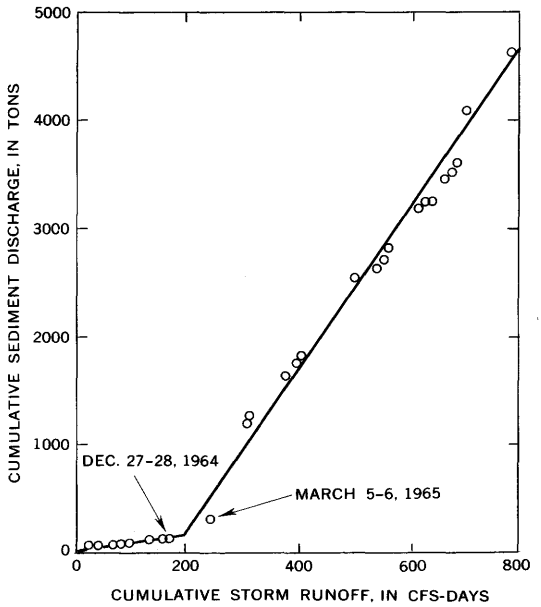

FIGURE 3.—Cumulative sediment and water discharge for sampled storms for Bel Pre Creek, Md., March 1963 to August 1967.

TABLE 2.—*Hydrologic and sediment data for Bel Pre Creek, Md.*

Storm	Precipitation (inches)	Runoff		Peak discharge (cfs)	Suspended sediment	
		Total (cfs-days)	Storm (cfs-days)		Mean concentration (mg/l)	Load (tons)
1963						
Mar. 6–7	.87	26.7	25.3	54	130	28.5
Mar. 12–13	1.46	20.6	19.1	41	64	8.2
Mar. 20–21	.86	7.4	5.4	24	38	2.3
June 2–3	2.95	23.4	22.1	61	110	17.3
Aug. 20–21	2.75	20.4	19.8	102	52	11.3
Sept. 29	2.10	4.5	4.2	18	60	1.3
Nov. 6–7	3.30	39.5	37.8	80	73	14.3
1964						
Jan. 9–10	1.16	27.3	25.7	117	46	11.7
Aug. 3	1.95	1.3	1.2	14	55	.9
Dec. 27–28	.72	11.2	10.4	31	46	3.7
1965						
Mar. 5–6	2.95	75.2	70.7	260	260	181
Aug. 26–27	2.81	71.3	70.3	410	1,730	917
1966						
Jan. 6	.89	6.3	4.5	22	530	20
Feb. 13	1.73	65.0	63.0	180	1,700	394
April 12–13	2.20	22.6	18.6	62	660	121
July 5–6	1.37	5.6	4.1	44	330	25.4
Aug. 11	.91	3.2	2.6	49	710	39
Sept. 14	5.48	107	103	530	1,070	707
Oct. 18–19	2.45	35.0	34.0	84	500	125
Nov. 28–29	1.35	13.4	12.4	63	280	54
1967						
Jan. 27–28	.77	9.5	8.3	56	500	96
Mar. 6–8	2.60	58.9	55.3	192	600	378
Mar. 15–16	.88	17.9	15.3	52	370	57
Apr. 17–18	.66	3.8	2.5	11	270	11.1
May 7–8	2.04	33.9	30.5	96	650	165
June 22–23	1.46	10.1	9.0	130	270	109
July 20–21	.72	7.3	6.6	85	240	57
Aug. 3–5	2.28	25.6	24.1	145	1,110	519
Aug. 24–25	3.45	73	70.5	475	1,500	447

of the Anacostia River near Colesville, Md., was used for estimating runoff from the unsampled events in Bel Pre Creek. The two curves that were developed to define the runoff relation between the two basins are shown in figure 4. Curve 4*A*, based on the 10 sampled runoff periods between March 1963 and December 1964, represents the relation between storm runoff of the two basins before construction was begun in the Bel Pre Creek basin. Curve 4*B* represents this storm runoff relation during construction, from March 1965 to August 1967. The two curves have standard errors of estimate of about 21 and 28 percent, respectively.

Sediment-discharge curves for Bel Pre Creek were developed for the same periods of time that apply to the runoff curves. The curves indicate that the sediment-load and storm-runoff data also represent two distinctly different populations (fig. 5). Curve 5*A* shows the relation between suspended-sediment discharge and storm runoff for the period before residential construction, and curve 5*B* represents the sediment-runoff relation during active construction. The data exhibit considerable scatter, with standard errors of about 38 and 60 percent for curves 5*A* and 5*B*, respectively. This variance probably could be reduced by the introduction of some additional independent variables, such as precipitation intensity, season of the year, duration of runoff, and peakedness of the events. One or more of these variables were used successfully by George (1963), Jones (1966), and Vice, Guy and Ferguson (1969) in their studies of sedimentation and land use. However, in this study,

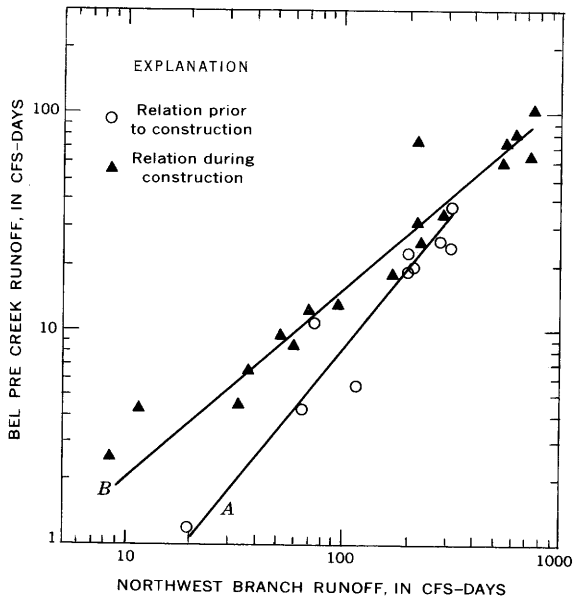

FIGURE 4.—Relation between storm runoff of Bel Pre Creek and Northwest Branch Anacostia River, Md. *A*, prior to construction; *B*, during construction.

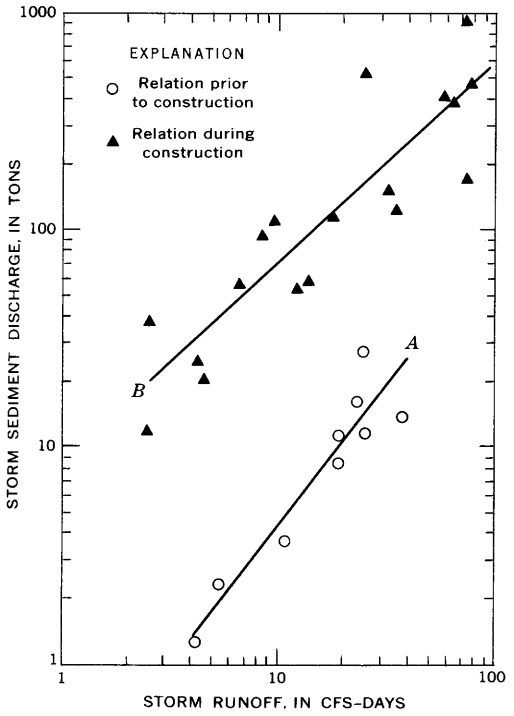

FIGURE 5.—Relation between storm runoff and sediment discharge in Bel Pre Creek basin, Maryland. *A*, prior to construction; *B*, during construction.

the magnitude of the errors from the simple linear regressions of sediment discharge and storm runoff are considered tolerable for the purpose of these regressions.

An inspection of the continuous record of sediment discharge of the Northwest Branch gaging station shows that the suspended-sediment loads from 46 storms during the period March 1965 to August 1967 account for 98.8 percent of the basin yield for the entire 30-month period. Therefore, it is assumed that the loads for the same 46 storms for Bel Pre Creek represent the total suspended-sediment yield from that basin. The loads from 19 of the storms were already known, and the loads of the other 27 storms were estimated on the basis of the runoff of the Northwest Branch and curves 4*B* and 5*B*.

The suspended-sediment loads that would have been transported during the period March 1965 to August 1967 under the original land-use conditions were similarly estimated. Curve *A* of figure 4 was used to estimate what the runoff of Bel Pre Creek would have been for each of the 46 storms between March 1965 and August 1967. The estimated runoff was then applied to sediment-discharge curve *A* of figure 5 to estimate the suspended-sediment load that would have been transported during each storm had no construction taken place.

The suspended-sediment yield for the basin during the period March 1965 to August 1967 for the original land-use conditions was estimated to be 450 tons, transported by about 15 inches of runoff. By comparison, the computed load of 6,200 tons was actually transported by about 19 inches of runoff. Thus, the effect of the construction was to decrease the permeability of a part of the basin, which resulted in a 30-percent increase in storm runoff for the basin, and to provide a greater source of soil particles available for transport, which resulted in a sediment yield for the basin 14 times greater than expected.

Of the total suspended-sediment yield for the 30-month study period, 5,800 tons can be attributed to construction activities. Considering that about 15 percent of the basin, or 160 acres, was always under development, the increased yield of construction sites was approximately 14.5 tons per acre per year. Therefore, the sediment yield from the construction area was approximately 90 times greater than the 0.17 ton per acre per year expected from the original grass and woodland.

SUMMARY AND DISCUSSION

The analysis of the streamflow and sediment data for Bel Pre Creek, although not comprehensive, does establish the magnitude of the sediment yield in a construction area. The unmeasured load moving along the bottom of the streambed and the suspended load during base-flow periods were not accounted for, but the following can be concluded about the storm runoff and suspended-sediment yield of the Bel Pre Creek basin:

1. The storm runoff from the basin during a 30-month period of active construction was about 30 percent higher than that expected with the original grass and forest cover.

2. Construction increased the amount of sediment available for transport and resulted in an average suspended-sediment concentration 12 times greater than that expected with the preurbanization land-use conditions.

3. Urban construction that averaged 15 percent of the basin between March 1965 and August 1967 resulted in a basin sediment yield 14 times more than that expected with the preurbanization land-use conditions.

4. The yield from the construction sites was 90 times more than that expected with the original grass and forest cover.

Measurement of the increase in the yield of suspended sediment as a result of residential construction substantiates the earlier work by Guy (1965), Vice, Guy, and Ferguson (1969), and others who have reported on the effects of urban construction. However, a wide range in the reported effects also points up the need for additional data. For example, what are the reasons for such widely differing yields as 189 tons from each acre converted to residences on a construction site in Kensington, Md., about 100 tons from each acre of highway construction in the Scott Run basin in Virginia, and a yield more on the order of 40 tons per acre of construction in the Bel Pre Creek basin? Differences in climatic factors for different periods and locations account for some of the variation of the sediment yields, but factors of probably greater significance are different topographic features, construction methods, and the proximity of construction sites to stream channels. Further work should be done to analyze the effect of each of these variables and apply the knowledge gained to limit the amount of sediment reaching the streams as a result of urban expansion.

REFERENCES

Anderson, H. W., 1957, Relating sediment yield to watershed variables: American Geophys. Union Trans., v. 38, p. 921–924.

George, J. R., 1963, Sedimentation in the Stony Brook basin, New Jersey, 1956–59: U.S. Geol. Survey open-file rept., 71 p.

Guy, H. P., 1965, Residential construction and sedimentation at Kensington, Maryland, *in* Federal Inter-Agency Sedimentation Conference Proc., 1963: U.S. Dept. Agriculture Misc. Pub. 970, p. 30–37.

Jones, B. L., 1966, Effects of agricultural conservation practices on the hydrology of Corey Creek basin, Pennsylvania, 1954–60: U.S. Geol. Survey Water-Supply Paper 1532–C, 55 p.

Ursic, S. J., and Dendy, F. E., 1965, Sediment yields from small watersheds under various land use and forest covers, *in* Federal Inter-Agency Sedimentation Conference Proc., 1963: U.S. Dept. Agriculture Misc. Pub. 970, p. 47–52.

U.S. Dept. of Agriculture, 1961, Soil Survey of Montgomery County, Maryland: U.S. Dept. Agriculture, Soil Conservation Service, 107 p.

U.S. Inter-Agency Committee on Water Resources, Subcommittee on Sedimentation, 1963, Determination of fluvial sediment discharge: Minneapolis, Minn., Federal Inter-Agency Sedimentation Project, Rept. no. 14, 151 p.

Vice, R. B., Guy, H. P., and Ferguson, G. E., 1969, Sediment movement in an area of suburban highway construction, Scott Run basin, Fairfax County, Virginia, 1961–64: U.S. Geol. Survey Water-Supply Paper 1591–E, 41 p.

WATER-LEVEL SURFACES IN THE AQUIFERS OF WESTERN LONG ISLAND, NEW YORK, IN 1959 AND 1970

By G. E. KIMMEL, Mineola, N.Y.

Work done in cooperation with the Nassau County Department of Public Works and the New York State Department of Environmental Conservation, Division of Water Resources

Abstract.—During the period 1959–70, ground-water levels in northwestern Nassau and east-central Queens Counties declined 20 to 25 feet. The magnitude and extent of the declines in the water table and in the Magothy potentiometric surface were roughly similar. The data suggest a high degree of hydraulic interconnection between the water table and the base of the Magothy aquifer, which includes from 200 to 1,100 feet of saturated unconsolidated deposits. The decline in water levels probably resulted from decreased recharge and increased pumping in an area of relatively low transmissivity.

Ground water in the underlying aquifer system is the sole source of fresh water in Nassau County and is a major source of fresh water in adjacent Queens County, Long Island, N.Y. (fig. 1). Ground-water withdrawals, decreased recharge related to natural phenomena, and decreased recharge related to the activities of man have caused ground-water levels to decline significantly during the past several decades in these counties. The major purpose of this report is to document the water-level declines from 1959 to 1970 in the two most highly developed aquifers. In addition, some hydrologic implications of these declines are considered.

HYDROGEOLOGIC UNITS

The ground-water reservoir of Long Island consists of a wedge-shaped mass of unconsolidated deposits resting on a crystalline bedrock surface which dips gently toward the southeast (fig. 2). The major hydrologic units (after Cohen and others, 1968, p. 18), are described briefly in table 1.

The water table on Long Island mainly is in the upper glacial aquifer but locally is in the Magothy aquifer. In gross aspect, along the ground-water divide near the center of the island, ground water percolates downward from the water table through the ground-water reservoir. Near the shorelines, ground water moves upward and discharges into streams or into the sea.

TABLE 1.—*Hydrogeologic units in Queens and Nassau Counties Long Island, N.Y.*

Hydrogeologic unit	Approximate range in thickness (feet)	Lithology and water-bearing characteristics
Upper glacial aquifer.	50–200	Mainly sand and gravel of moderate to high hydraulic conductivity; also includes clayey deposits of till of low hydraulic conductivity.
Gardiners Clay	0–80	Clay, silty clay, and a little fine sand of low to very low hydraulic conductivity.
Jameco aquifer	0–160	Mainly medium to coarse sand and gravel of moderate to high hydraulic conductivity.
Magothy aquifer	0–900	Coarse to fine sand and silt of moderate hydraulic conductivity, and abundant silt and clay of low to very low hydraulic conductivity. A basal zone of coarse sand and gravel of high hydraulic conductivity is common.
Raritan clay	0–300	Clay of very low hydraulic conductivity; some silt and fine sand of low hydraulic conductivity.
Lloyd aquifer	0–400	Coarse sand and gravel of moderate hydraulic conductivity; some silt and clay of low hydraulic conductivity.
Bedrock		Consolidated crystalline rocks that have little or no interstitial hydraulic conductivity.

U.S. GEOL. SURVEY PROF. PAPER 750-B, PAGES B224–B228

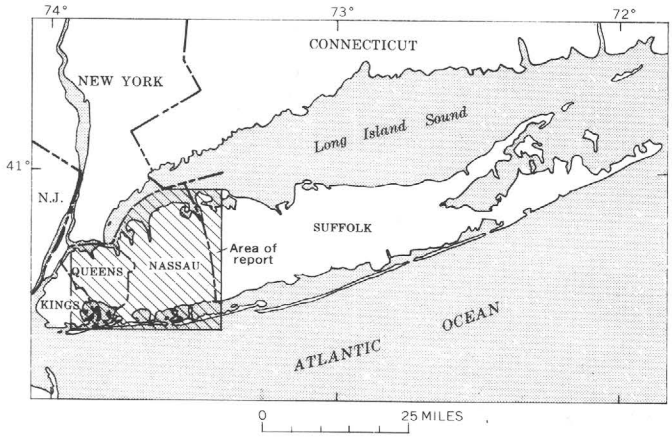

FIGURE 1.—Area of investigation (shaded) on Long Island, N.Y.

WATER-LEVEL SURFACES

Most of the ground-water withdrawals in Queens and Nassau Counties are from the Magothy and upper glacial aquifers, and, accordingly, ground-water levels in these aquifers are emphasized in this report.

Two water-level surfaces are shown on both figures 3 and 4. One surface is the water table (the upper surface of the zone of saturation), and the other is the potentiometric surface defined by the water levels in wells screened at or near the base of the Magothy aquifer. (For convenience, this surface is subsequently referred to in this report as the basal Magothy potentiometric surface.)

Data for the water-table contours were obtained from wetted-tape measurements in 19 wells in Queens County and 166 wells in Nassau County for figure 3, and from 31 wells in Queens County and 199 wells in Nassau County for figure 4. The measurements were made in April and May 1959 for figure 3 and in March 1970 for figure 4. Data for the basal Magothy potentiometric surfaces were obtained mostly from wetted-tape measurements in 55 wells for figure 3 and in 82 wells for figure 4. A few supplementary air-line measurements were used to help define the basal Magothy potentiometric surface in figure 3.

Because of the paucity of simultaneous measurements, the basal Magothy potentiometric surface in figure 3 was developed from data spanning the period 1957 to 1961. During this period, the maximum decline of water levels in Magothy aquifer was about 2 feet, and that decline was in the vicinity of the ground-water divide, where changes in water levels commonly are greatest. Accordingly, the basal Magothy potentiometric surface shown in figure 3 is considered ot be reasonably representative of that surface in 1959.

Throughout most of Nassau County, the heads in both aquifers are nearly the same, and, accordingly, the isopotentials are nearly vertical in most of the county (fig. 2). Directly beneath the ground-water divide, heads decrease with depth, and the isopotentials are virtually horizontal; however, the selected interval in figure 2 precludes showing the horizontal segments of the isopotentials. Near the shorelines, heads increase with depth, and the isopotentials become more nearly horizontal with increasing proximity to the shorelines. In general, these overall head relations reflect the gross directions of ground-water flow that existed under natural conditions; they have been modified only slightly in most of Nassau County.

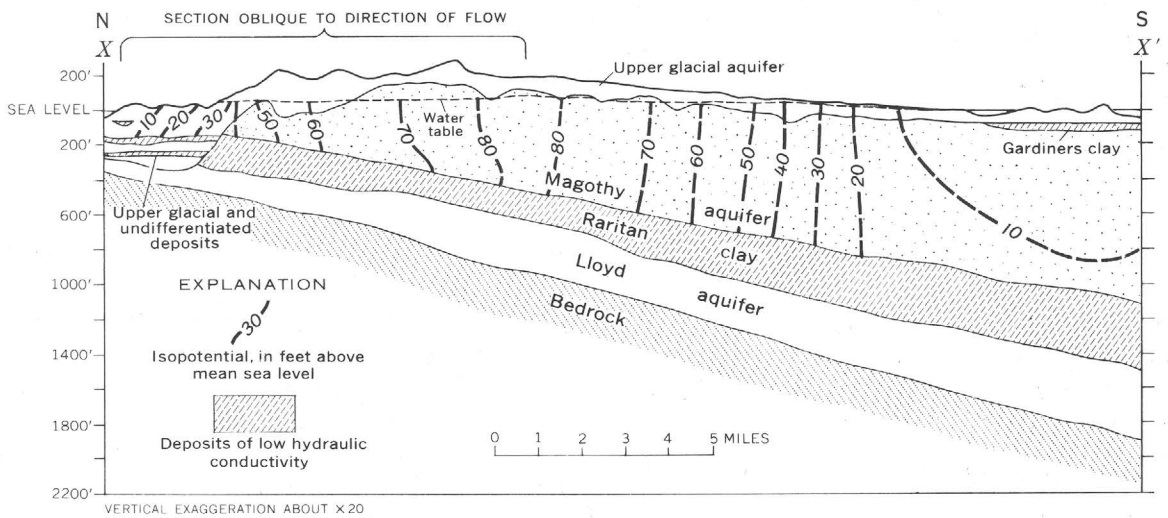

FIGURE 2.—Hydraulic section *X–X'* in eastern Nassau County, Long Island, N.Y., showing isopotentials in the upper glacial and Magothy aquifers in March 1970. Location of the section is shown in figure 4.

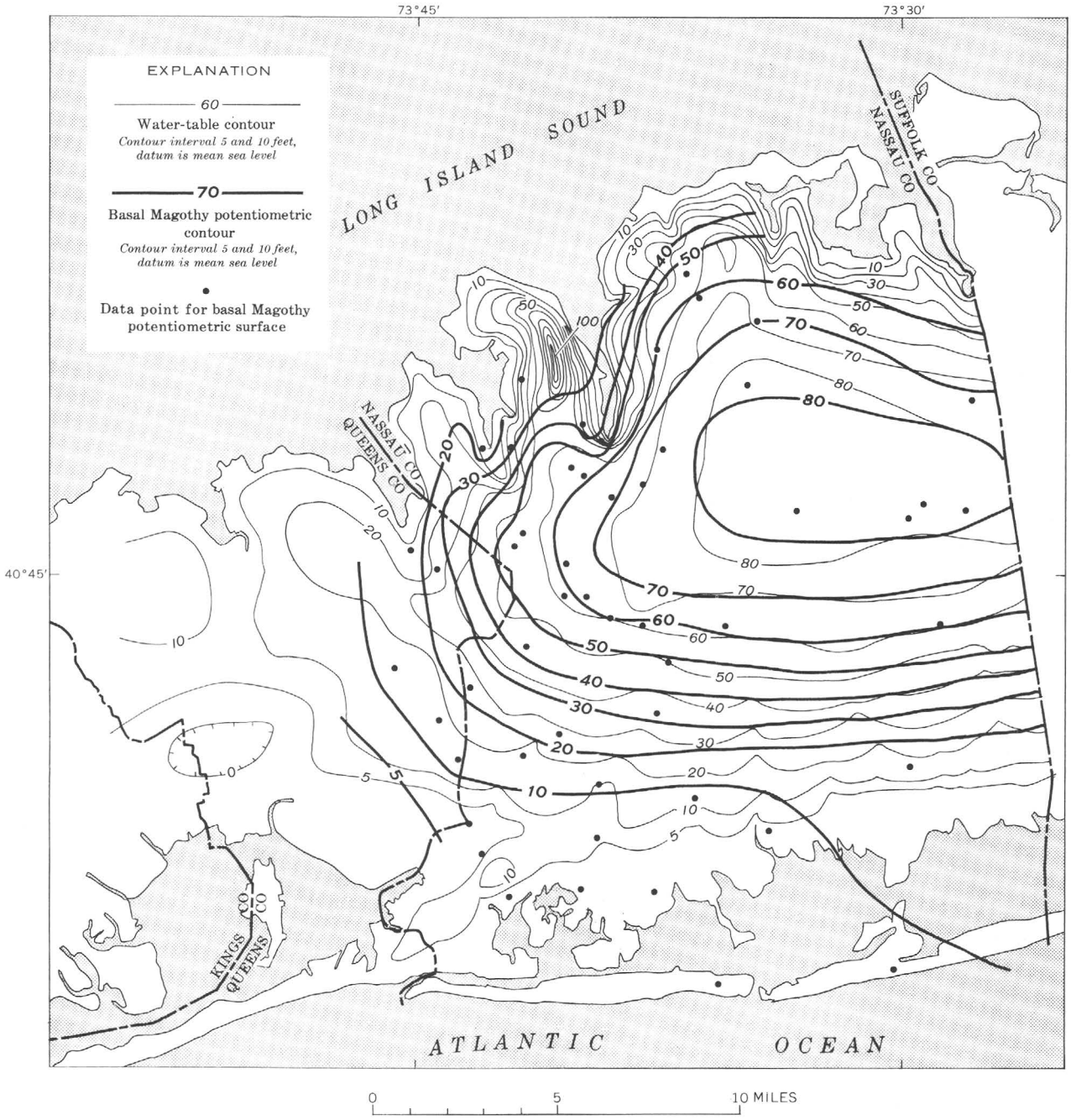

FIGURE 3.—Comparison between the water table and the basal Magothy potentiometric surface in Nassau and Queens Counties, Long Island, N.Y., in spring, 1959.

Both the water table and the basal Magothy potentiometric surface locally are below sea level in central Queens County because of intensive pumping of ground water and several factors related to urbanization.

NET CHANGE IN HEAD

Net declines in the water table and the basal Magothy potentiometric surface from 1959 to 1970 are shown in figures 5 and 6. The water-level declines in the basal part of the Magothy aquifer ranged from about 1 foot near the shorelines to a little more than 20 feet in parts of northeastern Queens and northwestern Nassau Counties. Similar declines occurred in the water table except at the shorelines, where the water table is hydrologically connected to the sea, and, accordingly, the decline was negligible. The general distribution and magnitude of the declines in both net-change maps are roughly similar. The similarity of the water-level declines in both aquifers reflects the high degree of hydraulic interconnection between them. Where the declines do not

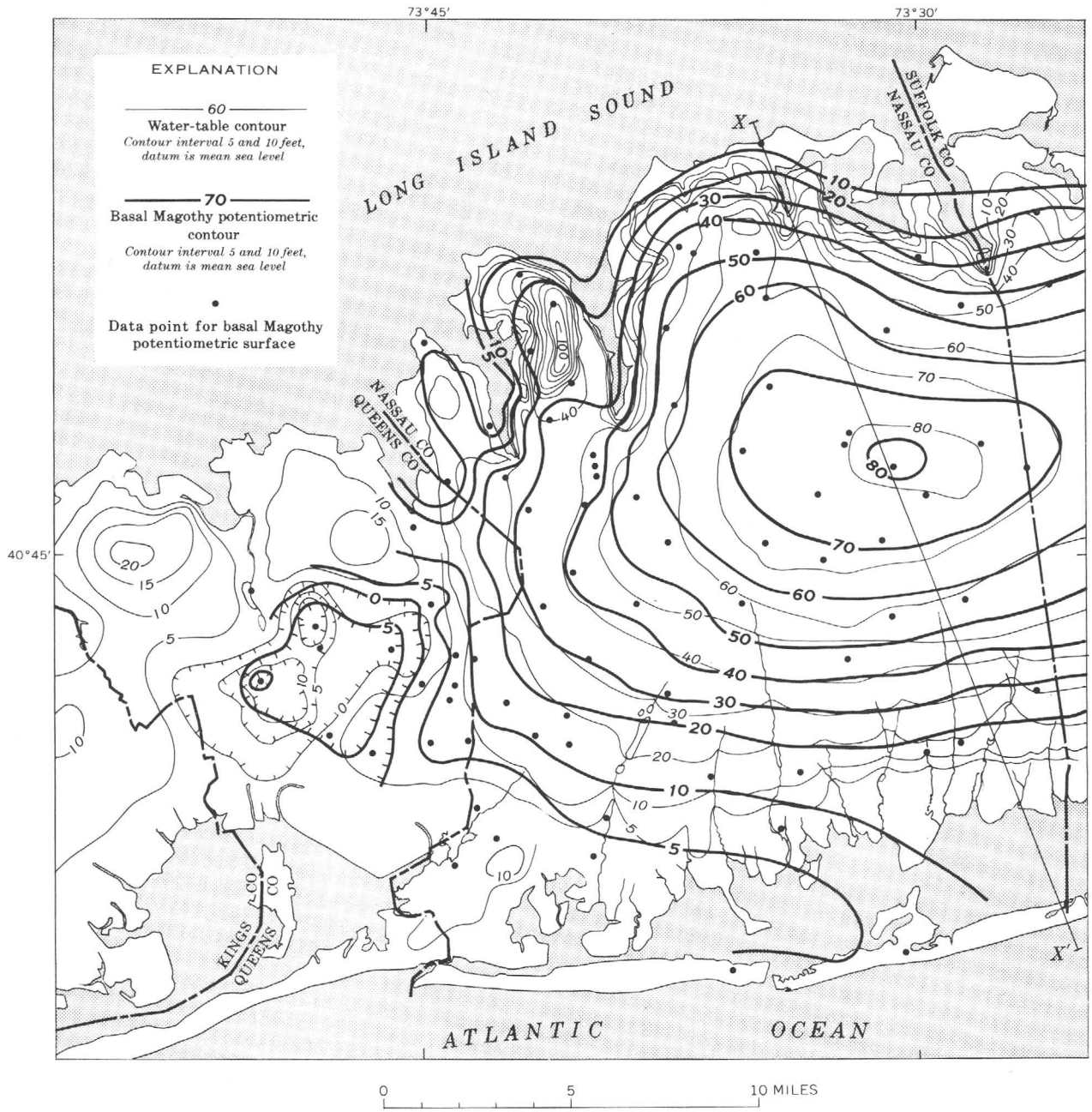

FIGURE 4.—Comparison between the water table and the basal Magothy potentiometric surface in Nassau and Queens Counties, Long Island, N.Y., in March 1970.

roughly coincide, the apparent dissimilarities probably are mainly due to the distortion of head in the aquifer system as a result of local pumping or to inaccuracies in the water-level contours.

Part of the decline in ground-water levels on Long Island from 1962 to 1966 was caused by a severe drought (Cohen and others, 1969). These writers estimated that the maximum net decline in the water table from 1961 to 1966 near the ground-water divide in Nassau County was about 10 feet. Despite 3 years of normal to above-average precipitation from 1967 to 1970, the water table in part of Nassau County has continued to decline, in places by more than the maximum decline of 10 feet shown by Cohen and others (1969, fig. 10), probably partly as a result of continued intensive pumpage.

In Nassau County, public-supply pumpage, which is mainly from the Magothy aquifer, increased from 125 mgd (million gallons per day) in 1959 to 173 mgd in 1968 (New York Water Resources Commission, written commun., 1969). Although the pumpage is fairly

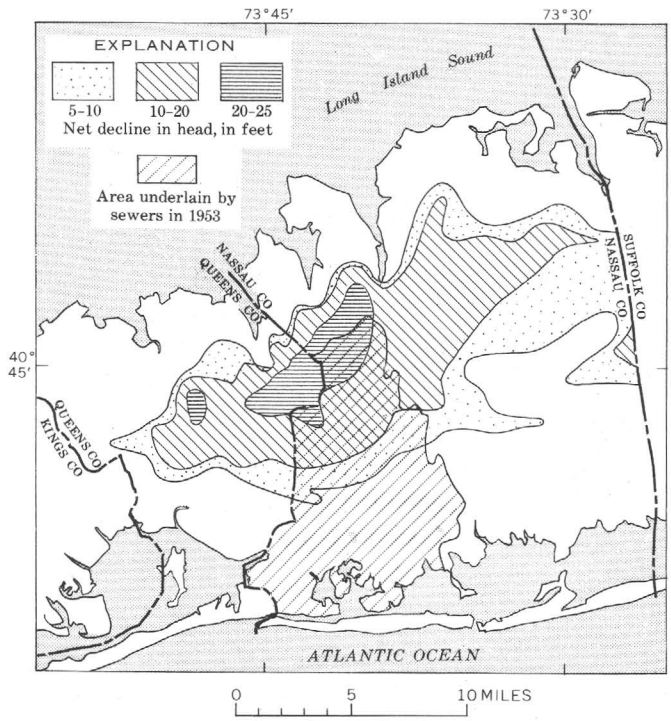

FIGURE 5.—Generalized net decline of the water table in Nassau and Queens Counties, Long Island, N.Y., from 1959 to 1970.

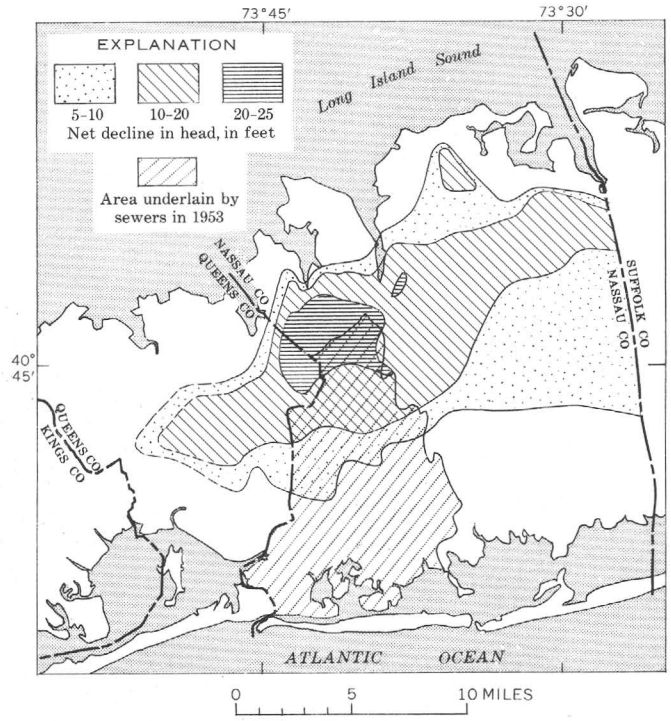

FIGURE 6.—Generalized net decline in the basal Magothy potentiometric surface in Nassau and Queens Counties, Long Island, N.Y., from 1959 to 1970. Dashed lines in left center enclose area of estimated or inferred decline in head.

evenly distributed throughout the county, it is greater in the southern part somewhat south of the area of maximum declines in ground-water levels. The greater net declines in the northern part of the county as compared to the declines in the southern part probably largely reflect the fact that the Magothy aquifer thins markedly northward (fig. 2) and, accordingly, the transmissivity of the aquifer decreases appreciably in that direction.

Ground-water levels in some parts of Nassau County also declined because of the construction of sanitary sewers and the concurrent decrease in recharge resulting from the discontinued use of many thousands of cesspools. Franke (1968, p. 205–209) found that the average decline attributable to sewering in southwestern Nassau County from 1953 to 1966 was about 7 feet. Accordingly, at least part of the net decline in the water table (fig. 5), and perhaps part of the decline in the Magothy potentiometric surface (fig. 6), was related to the construction of sewers.

Pumpage in Queens County, which increased from about 52 mgd in 1959 to 62 mgd in 1968 (New York Water Resources Commission, written commun., 1969), probably is the main cause of the water-level declines in that country since 1959. The net decline is most pronounced in the central and southern part of the county, where the water table and the Magothy potentiometric surface presently are more than 10 feet below sea level.

Since 1903, ground-water levels in Queens County have declined as much as 40 feet, resulting in local but highly significant encroachment of salty water into the fresh ground-water reservoir (Soren, 1970). Periodic chloride determinations (Cohen and Kimmel, 1971) and periodic rounds of water-level measurements and the resulting water-level maps, such as those shown in this report, will help those concerned with the development and management of Long Island's ground water to monitor some of the major effects of present and future ground-water withdrawals.

REFERENCES

Cohen, Philip, Franke, O. L., and Foxworthy, B. L., 1968, An atlas of Long Island's water resources: New York Water Resources Comm. Bull. 62, 117 p.

Cohen, Philip, Franke, O. L., and McClymonds, N. E., 1969, Hydrologic effects of the 1962–66 drought on Long Island, New York: U.S. Geol. Survey Water-Supply Paper 1879–F, 18 p.

Cohen, Philip, and Kimmel, G. E., 1970, Status of salt-water encroachment in 1969 in southern Nassau and southeastern Queens Counties Long Island, New York, *in* Geological Survey Research 1970: U.S. Geol. Survey Prof. Paper 700–D, p. D281–D286.

Franke, O. L., 1968, Double-mass-curve analysis of the effects of sewering on ground-water levels on Long Island, New York, *in* Geological Survey Research 1968: U.S. Geol. Survey Prof. Paper 600–B, p. B205–B209.

Soren, Julian, 1971, Ground-water and geohydrologic conditions in Queens County, Long Island, New York: U.S. Geol. Survey Water-Supply Paper 2001–A, p. A1–A39.

AVAILABILITY OF GROUND WATER FROM LIMESTONE AND DOLOMITE AQUIFERS IN NORTHWEST OHIO AND ITS RELATION TO GEOLOGIC STRUCTURE

By STANLEY E. NORRIS and RICHARD E. FIDLER, Columbus, Ohio

Work done in cooperation with the Ohio Department of Natural Resources, Division of Water

Abstract.—Potentially, the largest ground-water supplies in northwest Ohio are available from limestone and dolomite aquifers in a long, striplike area 7 to 18 miles wide that winds for many miles along the flanks of the north-plunging Cincinnati arch, a structural feature of regional dimensions. The conditions conducive to high water yield are believed to have resulted from ground-water solution of rocks of the periodically emergent Cincinnati arch. Important in defining the regional ground-water system is a highly detailed geologic structure map, based on interpretation of geophysical logs, of the top of the Middle Silurian Lockport Dolomite, showing the location of the arch in the 20-county study area.

An investigation of limestone and dolomite aquifers in northwest Ohio was completed in 1970 by the Division of Water, Ohio Department of Natural Resources, in cooperation with the U.S. Geological Survey. The study area of about 9,000 square miles, or nearly one-fourth of the State, included all or parts of 20 counties (fig. 2). The exploration program consisted mainly of drilling and test pumping approximately 80 wells drilled in the carbonate rock aquifers, to depths ranging from about 200 feet to more than 400 feet. The principal objective was to determine whether or not ground water is available and in what areas it is available for large-scale municipal or industrial use in northwest Ohio.

The U.S. Geological Survey participated in the investigation by making chemical analyses of water samples collected from the test wells, by performing special aquifer tests on selected wells, and by geophysical logging. The logging program, designed to help establish criteria for stratigraphic correlation, consisted of making natural gamma, single-point resistance, self-potential, and caliper logs of the test wells. The logging was done with portable hand-operated equipment of the U.S. Geological Survey. The geophysical logs are presented as part of the appendix to the principal report on the northwest Ohio project, prepared by personnel of the Ohio Division of Water (Walker and others, 1970).

The main purpose of this paper is to describe one of the more important findings of the investigation, stemming largely from the logging program—that geologic structure is the primary control on the yield of wells drilled in the carbonate-rock aquifers of northwest Ohio. Evidence shows that those areas in which well yield is highest are closely associated with the principal structural feature of the area, the Cincinnati arch, a generally north-south-trending anticline of regional dimensions.

As its secondary purpose, this paper describes the interpretation of the geophysical logs. In part, this is an elaboration of an earlier paper (Norris and Fidler, 1969), in which the authors describe the use of natural gamma logs for determining the contact between the principal rock units of Silurian age in northwest Ohio. With the advantage of much additional data, this paper presents a more detailed geologic structure map than did the earlier paper. The revised map was a key element in the interpretation of the regional hydrogeologic system, and it also should prove useful in other geologic applications.

Acknowledgments.—The authors acknowledge the work of Arie E. Janssens, geologist of the Division of Geological Survey, Ohio Department of Natural Resources, whose identification and description of the

U.S. GEOL. SURVEY PROF. PAPER 750-B, PAGES B229-B235

rocks penetrated by the test wells, based on sample studies, was helpful in determining the areal distribution of the principal stratigraphic units. They appreciate also the assistance and cooperation of A. C. Walker, H. B. Eagon, Jr., D. E. Johe, J. J. Schmidt, and R. B. Stein, geologists of the Division of Water, Ohio Department of Natural Resources, all of whom gave freely of the results of their work in the northwest Ohio investigation.

STRATIGRAPHIC UNITS

Carbonate rocks of Middle (Niagara) and Late (Cayuga) Silurian age underlie most of the generally flat, relatively featureless terrain of northwest Ohio. Rocks of both groups are typical dolomites, but those of Niagara age are somewhat more pure, lighter in color, and more crystalline in structure than rocks of Cayuga age. The Lockport Dolomite of Niagara age is exposed at the surface, or crops out beneath a thin covering of glacial till or lake clay, along the crest of the Cincinnati arch in the central and north-central parts of the area, chiefly in Hancock, Seneca, Wood, Ottawa, and Sandusky Counties (see fig. 2). The Lockport Dolomite also constitutes the bedrock in much of Mercer and Van Wert Counties and in parts of Paulding and Auglaize Counties, in the southwestern part of the study area.

The Lockport Dolomite is overlain by rocks of the Bass Islands Group, the aggregate thickness of which increases downdip from zero thickness on much of the crest of the arch where they have been removed by erosion to at least 500 feet in the northwest part of the study area. The Bass Islands Group includes, in ascending order, the Greenfield Dolomite, Tymochtee Formation, Put-in-Bay Dolomite, and the Raisin River Dolomite. These dolomite units, generally distinguishable from one another on the outcrop, are to some extent also separable on natural gamma logs and on self-potential and resistance logs.

The Greenfield Dolomite, typically 50 feet thick, is in part a reef deposit. Contacts of the unit with both the underlying Lockport Dolomite and the overlying Tymochtee Formation range from disconformable, in which the contact is typically characterized by the presence of thin shale or bituminous matter, to conformable and gradational. Contacts of the former type, which predominate in the arch area, usually are identifiable on the geophysical logs. The Tymochtee Formation consists of about 100 feet of generally thin-bedded dolomite, somewhat more shaly in composition than the remainder of the Bass Islands sequence (Carman, 1927, p. 488). The overlying Put-in-Bay Dolomite and the Raisin River Dolomite, both relatively pure dolomites, have a total thickness of at least 350 feet in the study area (A. E. Janssens, 1970, oral communication). In the eastern and northwestern parts of the study area the Bass Islands Group is overlain by progressively younger strata of Devonian and Mississippian ages, chiefly dolomites, interbedded with relatively thin shale units.

INTERPRETATION OF THE GEOPHYSICAL LOGS

Figure 1 shows the complete array of geophysical logs made in test well M–8, drilled near Ottawa in Putnam County. As described previously by the authors (Norris and Fidler, 1969, p. B159) there is a clear distinction on the typical gamma log between rocks of the Niagara Group and those of the overlying Bass Islands Group. The intensity of radiation is markedly less in the Niagara (Lockport Dolomite) section, and that part of the log is relatively featureless compared with the log of the rocks above and below the Niagara section. Al-

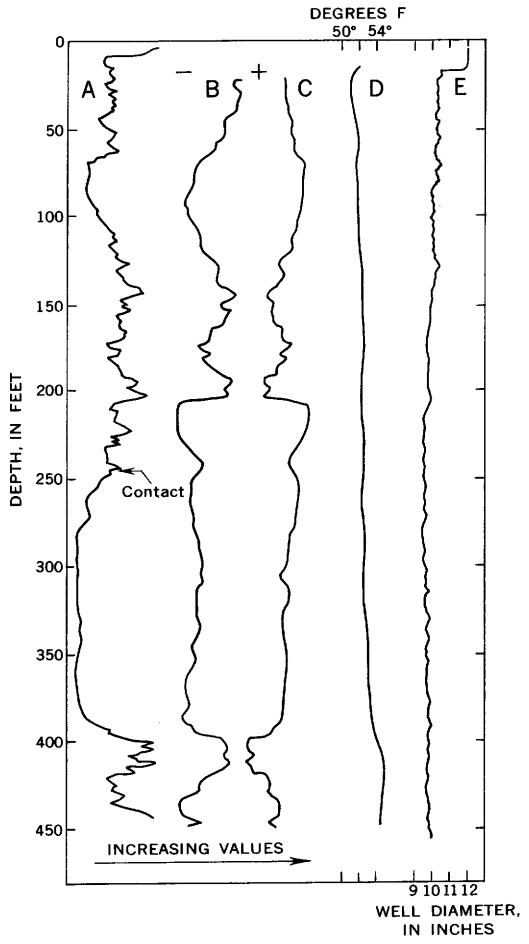

FIGURE 1.—Geophysical logs of well M–8, showing: A, natural gamma; B, self-potential; C, single-point resistance; D, temperature; and E, caliper types. The contact shown is between the Niagara Group, below, and the Bass Islands Group, above.

though gross differences between these rocks usually are clearly evident, precise picking of the contact is largely a matter of practice and judgment.

In their original paper the authors described how a characteristic log section was identified and used as a basis for picking the contact on the logs of the test wells, on the basis of the logging of quarry shotholes which were near enough to the exposed contact to accurately relate its position to the logs. This technique has proved useful in picking the contact with what is believed to be reasonable accuracy on most logs in the study area. Consistency in the results is demonstrated by use of the data in constructing the regional geologic structure map. However, there is considerable variation in and near the top of the Niagara rocks in some wells, with the variable section extending over a range of several feet. Picking the contact in such wells from the gamma log alone becomes a matter of guesswork. In some instances, however, the contact can be picked with confidence, using the self-potential and resistance logs as adjuncts to the gamma log.

The self-potential and resistance logs of well M–8, shown in figure 1, are fairly typical of most wells in the study area. These logs complement one another in that where one curve shows an increase in value the other shows a decrease. When the self-potential and resistance logs are displayed side by side the result is a symmetrical configuration, in this instance somewhat resembling an hourglass. One of the most distinguishing features is a deflection on both logs, generally occurring 40 to 60 feet above the Lockport Dolomite. The authors believe that this point on the logs corresponds to the top of the Greenfield Dolomite. Conspicuous on most of the self-potential and resistance logs, this marker is helpful in estimating the top of the Lockport Dolomite in wells for which the gamma log is difficult to interpret.

The gamma log was useful also in identifying the relatively shaly Tymochtee Formation, which overlies the Greenfield Dolomite. The Tymochtee rocks, about 100 feet thick, produce a characteristic "ragged" appearing section on the gamma log. From this characteristic section it was possible in many instances to estimate the depth to the top of the Lockport Dolomite in relatively shallow wells that did not reach the Lockport.

An attempt to correlate the self-potential and resistance logs with zones of high permeability reported by the drillers yielded inconclusive results. Neither the quality of the logs nor the accuracy with which the driller reported water-yielding zones were considered satisfactory for this purpose. Chief use of the electric logs, other than as an aid in correlating the gamma logs, was in showing accurately the depth of casing in the wells.

Caliper logs, by revealing fractures, solutional cavities, and other openings in the rocks penetrated by the test wells, proved highly useful in this investigation. In support of interpretation advanced later in this paper, caliper-log data indicate that solutional openings in the rocks are more prevalent in some parts of the study area than in others. Caliper logs were not made of all the test wells, as the caliper capability was added late in the program as a substitute for temperature logging. Temperature logs were deemed of too little significance to justify the time required to make them with the equipment available. Most temperature logs of the test wells showed a uniform increase of about 1° or 2° F from the top of the hole to the bottom. This was assumed to reflect the natural heat gradient in the earth. Temperature logs of a few of the test wells, such as that for well M–8, do show small deflections corresponding to differences in the stratigraphic sequence. At least one log shows a deflection which is assumed to indicate a zone of water movement.

GEOLOGIC STRUCTURE AND AREA OF HIGH-YIELD WELLS

The geologic structure map, figure 2, constructed on the Lockport Dolomite, is based on interpretation of geophysical logs of approximately 200 wells, supplemented by 7 control points determined directly from quarry exposures. About 115 of the logs were of State test wells or municipal and industrial wells made in this investigation. The remainder were natural gamma logs of oil and gas wells, made by commercial logging companies, and available from the files of the Division of Geological Survey, Ohio Department of Natural Resources. Although the oil-and-gas-well logs show less detail than do the logs made with the portable equipment used by the U.S. Geological Survey, the logs are basically similar and the same techniques of interpretation were used for both types.

The principal structural feature of northwest Ohio, shown by the contours on figure 2, is the broad, north-plunging Cincinnati arch, or anticline, which extends from south to north across the east-central part of the study area. Known locally as the Findlay arch, the Cincinnati arch is a major structural feature of the mid-continent region. Extending northward from the Nashville dome area in Tennessee to a terminus in southern Ontario, the Cincinnati arch separates the Appalachian basin on the east from the Illinois and Michigan basins on the west and northwest. West of the arch in northwest Ohio the rocks dip northward into the Michigan basin; east of the arch the regional dip is eastward into the Appalachian basin. A small area of uplift centering

413-504 O - 71 - 16

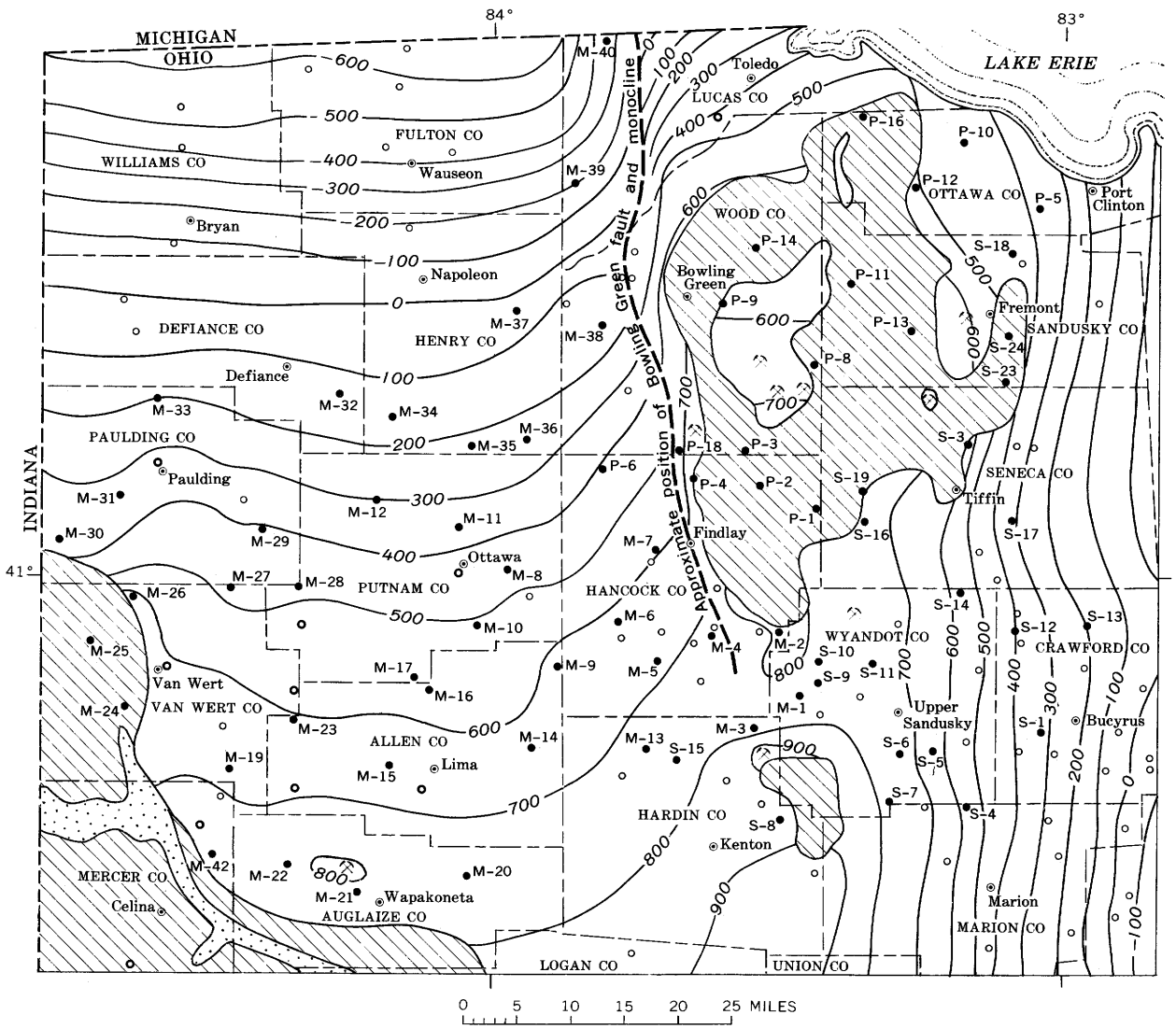

EXPLANATION

300

Approximate altitude of top of Lockport Dolomite
Contour interval 100 feet; datum is mean sea level

Area in which the Lockport Dolomite crops out at the surface or beneath unconsolidated glacial or lake deposits; in part after A. E. Janssens (written commun.) and D. W. Farnsworth (unpublished map in the files of the Division of Geological Survey, Ohio Department of Natural Resources)

Area in which Niagara Group has been removed by erosion in the preglacial Teays River valley

Quarry
Exposed contact of Niagara Group with overlying Bass Islands Group

P-16
State test well

Municipal or industrial well

Oil or gas well

FIGURE 2.—Map of northwest Ohio, showing approximate structure contours on the Lockport Dolomite. Based on data from geophysical logs and quarries.

in Mercer and Van Wert Counties is believed to represent a minor limb of the arch, extending northwest from the main structural axis into the southwestern part of the study area.

Associated with the western flank of the Cincinnati arch in Hancock, Wood, and Lucas Counties is the north-trending Bowling Green fault and monocline, the approximate position of which is shown on the map. Evidence obtained in this investigation is insufficient to define the position and magnitude of the fault accurately. The relatively few control points shown on figure 2 in the immediate vicinity of the fault were useful chiefly in making minor changes in its position, the general location of which is that described by Stout (1941, p. 15–16). Stout traced the location of the fault southward from Michigan to Hardin County, in the southern part of the study area, on the basis of data from oil and gas wells. His data were insufficient to define the fault beyond this latter point. The fault is downthrown on the west side; the maximum displacement, according to Stout (1941, p. 16), is about 200 feet in the vicinity of Bowling Green, in Wood County. The Bowling Green fault is exposed at the surface at only one known place in northwest Ohio, in a quarry near Waterville in southern Lucas County. According to J. E. Carman,[1] north of the Waterville quarry the rocks along the Bowling Green fault are no longer displaced relative to one another, and the fault becomes a monocline with steeply dipping beds.

Structural relief along the crest of the Cincinnati arch, indicated by the contours on figure 2, is in part a depositional feature resulting from an increase in the thickness of the Lockport Dolomite due to reef growth. Typically 180 to 200 feet thick, the Lockport Dolomite thickens markedly near the northern end of the arch where Sparling (1965, p. 236) reports the thickness as more than 400 feet in a quarry test hole in Ottawa County.

Evidence obtained in this investigation shows that wells of highest yield in northwest Ohio are associated with structurally high areas. On figure 3, boundaries have been drawn to set apart the test wells having the highest specific capacities from those of lesser yield. The result is to enclose the high-yield wells within a long, striplike area, 7 to 18 miles wide, that winds for many miles along the flanks of the Cincinnati arch and the structurally uplifted area in the southwest part of the study area. This strip of highly productive rocks extends from Marion County northward along the east flank of the arch for about 80 miles to the vicinity

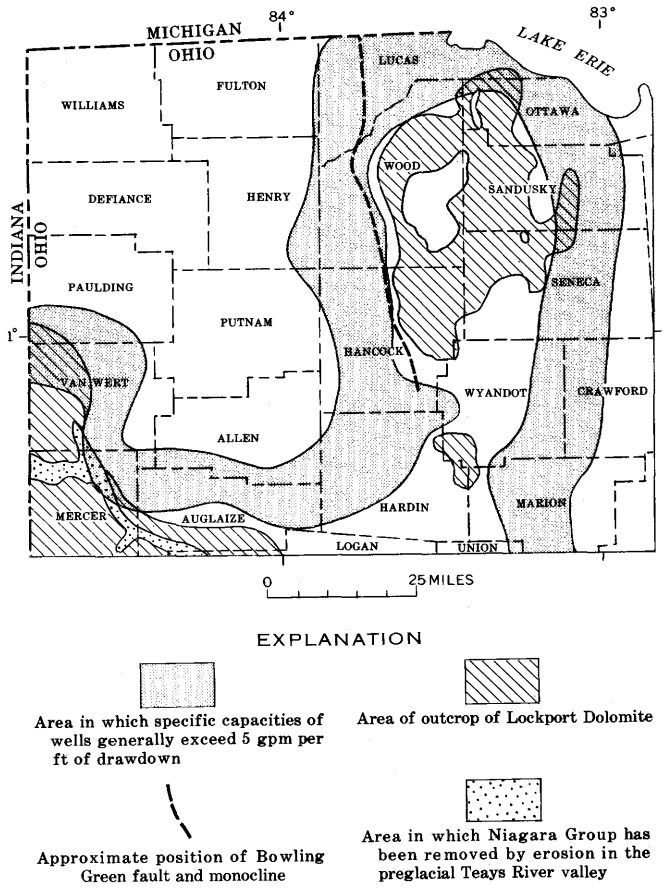

FIGURE 3.—Map of northwest Ohio, showing location of area of high-yield water wells.

of Lake Erie, then swings westward around the nose of the arch and extends southward along the western flank, forming a long narrow loop, the sides of which are separated by 10 to 30 miles along the crest of the arch. As shown here (fig. 3), the inner boundary of the western limb of this loop coincides in part with the location of the Bowling Green fault. From a point near Kenton, in Hardin County, the western limb of the high-yield strip extends west-northwest to the Indiana State line in Van Wert County, paralleling the flank of the minor structural high in Mercer and Van Wert Counties.

The high-yield area of ground water includes approximately 2,500 square miles, or about one-fourth of the study area. Bounded on each side by relatively unproductive strata, the high-yield area partially encloses or borders areas in which the Lockport Dolomite makes up the bedrock beneath a thin covering of glacial till.

Although a few wells in the high-yield area are drilled into the upper part of the Lockport Dolomite, most wells in this area tap the several tens of feet of carbonate strata overlying the Lockport Dolomite,

[1] Carman, J. E., 1948, A study of the geology of Lucas County and the lime-dolomite belt: Ohio Academy of Science, Annual Field Conf. in Geology, p. 6 (mimeo.).

chiefly the Greenfield Dolomite and dolomite of the Tymochtee Formation. A few wells in the high-yield area tap the Put-in-Bay Dolomite and the Raisin River Dolomite.

The high-yield area as drawn on figure 3 is based on the areal distribution of test wells having specific capacities greater than 5 gpm per ft (gallons per minute per foot) of drawdown, as determined from 24-hour pumping tests. Pumping rates during the tests averaged 450 gpm for 26 wells located within the high-yield area, and 160 gpm for 36 wells located outside the high-yield area. The estimated yield of 7 other wells located outside the high-yield area was so low, less than 20 gpm, that specific capacity tests were not made.

The specific capacity of wells in the high-yield area ranged from 5.1 to 93 gpm per ft, and averaged 31 gpm per ft. The specific capacity of wells outside the high-yield area, with one exception, ranged from an estimated 0.1 gpm per ft to 4.9 gpm per ft and averaged 1.8 gpm per ft. The exception, located in northern Allen County, is well M–16, which had a specific capacity of 9 gpm per ft.

Doubtless there are other wells located outside the high-yield areas shown on figure 3 which, like well M–16, also have short-term specific capacities greater than 5 gpm per ft. Similarly, some wells of relatively low yield probably have been drilled in the high-yield area as depicted here. The boundaries on figure 3 are approximate and generalized; they are intended only to show the relation of the high-yield area to the regional geologic structure.

The same rocks that yield water abundantly to wells within the high-yield area yield relatively little water outside this area. An explanation for this geographical distribution of productivity is suggested by a study of caliper logs of the test wells. The logs show that the rocks within the high-yield area contain more cracks and other openings than do the rocks outside this area. The difference is illustrated in figure 4, which compares selected caliper logs of 5 wells located within the high-yield area with logs of 3 wells located outside this area. Although not all the caliper logs show the contrast in the rock openings as well as these examples, the logs are, nevertheless, fairly representative of the respective areas.

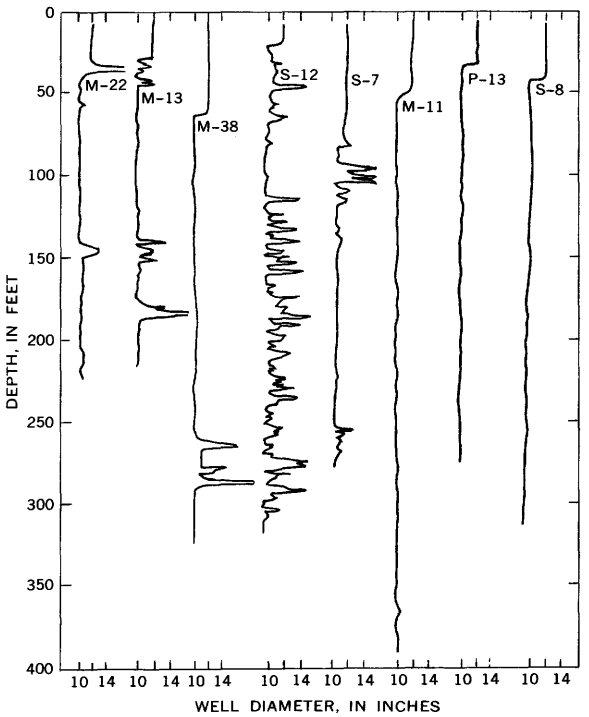

FIGURE 4.—Caliper logs of five wells (M–22, M–13, M–38, S–12, S–7) drilled in the area of high-yield water wells, compared with logs of three wells (M–11, P–13, S–8) drilled outside the high-yield area, showing the difference in solutional openings in the carbonate rocks of the respective areas.

GENESIS OF THE HIGH-YIELD AREA

Temporary emergence above sea level of the Cincinnatic arch area in northwest Ohio is known to have occurred several times in the geologic past, the result in each instance being an elongate peninsula or chain of islands, the sizes of which varied according to the degree of emergence. The large and extensive openings in the rocks within the high-yield area probably resulted from ground-water solution that was restricted for long intervals to the beds comprising these structurally higher, emergent areas. The beds subsequently have been removed from the tops of the structurally higher areas, and the solutional effects now are largely restricted to peripheral areas flanking the crest of the Cincinnati arch and the subsidiary structural high centering in Mercer and Van Wert Counties.

Palegeographic maps presented by Pepper, deWitt, and Demarest (1954, p. 95–107), which illustrate the probable extent of the arch area at selected times in the Mississippian Period, indicate that during much of this time the emergent land mass ranged in width from about 35 to 60 miles. The maximum figure of this range accords well with the distance separating the outside edges of the high-yield area on opposite sides of the arch, shown on figure 3.

Ground-water solution was not confined to the Mississippian Period, however. The Cincinnati arch was a positive palegeographic element throughout most of the Paleozoic Era, and temporary emergence of a narrow, peninsulalike landmass no doubt occurred many times in this long interval. Ground-water solution would have been active whenever the land became

emergent, especially close to the shore where, in an area of ground-water discharge, circulation would have been relatively rapid. Greater solution of the beds in fringing areas along former shorelines would be another factor to account for the present distribution of the high-yield zone around the periphery of the structurally higher area.

Toward the close of the Paleozoic Era the sea retreated from the entire region and the arch area ultimately became a minor part of the Central Lowlands physiographic province. Post-Paleozoic, preglacial erosion, which lasted for a much longer time than did the aggregate of those Paleozoic erosional episodes affecting only the arch area, resulted in the removal of most of the post-Lockport age rocks from the crest of the arch and development of the present bedrock surface.

CONCLUSIONS

The significant result of this investigation is the discovery of the relation between geologic structure and the yield of wells in the carbonate-rock aquifers. Identification of the high-yield area, to which future large-scale ground-water developments inevitably will be drawn, points the way to more effective exploitation of the ground-water resources in northwest Ohio.

Of equal importance is the fact that conditions which here produced the high-yield area are fairly widespread, and not confined to northwest Ohio. Similar belts or zones of high productivity in carbonate-rock aquifers can be expected to occur in other parts of western Ohio and perhaps also in the adjacent States of Indiana and Michigan, in association with structurally higher areas. The geologic structure map thus becomes a useful guide to the availability of large ground-water supplies within a very large area in which limestone and dolomite aquifers are important sources of water supply.

Further investigation will better define the nature and extent of the high-yield area in northwest Ohio, and ultimately will determine whether conditions described here apply also to other areas. Additional quantitative data, in conjunction with studies of recharge and discharge characteristics of the aquifers, will eventually determine the quantity of water available on a long-term basis at specific sites within the high-yield area.

REFERENCES

Carman, J. E., 1927, The Monroe division of rocks in Ohio: Jour. Geology, v. 35, no. 6, p. 481–506.

Norris, S. E. and Fidler, R. E., 1969, Correlation of carbonate rock units in northwest Ohio by natural gamma logging, *in* Geological Survey Research 1969: U.S. Geol. Survey Prof. Paper 650–B, p. B158–B161.

Pepper, J. F., deWitt, Wallace, Jr., and Demarest, D. F., 1954, Geology of the Bedford shale and Berea sandstone in the Appalachian basin: U.S. Geol. Survey Prof. Paper 259, 111 p.

Sparling, D. R., 1965, Geology of Ottawa County, Ohio: Ohio State Univ., unpub. Ph. D. dissert., 265 p.

Stout, Wilber, 1941, Dolomites and limestones of western Ohio: Ohio Geol. Survey Bull. 42, 4th ser., 468 p.

Walker, A. C., Schmidt, J. J., Eagon, H. B., Jr., Johe, D. E., Stein, R. B., with sections by Janssens, A. E., and by Norris, S. E., and Fidler, R. E., 1970, Ground water for planning in northwest Ohio, a study of the carbonate-rock aquifers: Ohio Dept. Nat. Resources, Div. Water, Ohio Water Plan Inventory Rept. 22, 63 p.

PRELIMINARY CONSIDERATION OF MOVEMENT OF GROUND WATER FROM INFILTRATION AREAS ON THE LLANO ESTACADO, TEXAS AND NEW MEXICO

By C. V. THEIS, Albuquerque, N. Mex.

Work done in cooperation with the U.S. Bureau of Reclamation

Abstract.—Consideration of several theoretical models indicates that infiltration canals on the Llano Estacado would probably have to be about 6 or 7 miles apart on the average to provide all parts of their service area with water. Infiltration ponds or lakes, involving radial movement of water, would be somewhat closer—on the average about 3 or 4 miles. The models on which these figures are based are equilibrium models assuming either constant hydraulic conductivity vertically and laterally or constant transmissivity. It is also assumed that the aquifer is isotropic. For the average hydrological condition in this area leading to the values given above, a conductivity of 10,000 feet per year (equivalent to a Meinzer coefficient of permeability of about 200 gpd/ft^2) or a transmissivity equivalent to 30,000 gpd/ft in Meinzer units has been assumed. In areas where these assumed estimates are exceeded, infiltration canals or ponds could be more widely spaced; conversely, in areas where conductivity and transmissivity fall below these assumed averages, infiltration structures would be closer together.

The most obvious way to provide terminal storage for any water imported to the High Plains is to use the tremendous storage capacity of the Ogallala Formation (Pliocene), while at the same time allowing the irrigators to continue to pump their water supply. Two problems are at once apparent: (1) At what rate can water infiltrate (a) from canals and (b) from more or less circular reservoirs, such as the playa lakes? (2) How far can water move underground from such sources; or, in other words, at what distance will such sources be?

The playa lakes are one of the chief sources of recharge of the High Plains under natural conditions, as shown by the reaction of the water table in their vicinity to rainfall. However, the slow disappearance of water in them after they are filled is evidence that the rate of infiltration under natural conditions is very slow. Hence, the problem of inducing significant infiltration will be a serious one, and its solution will require experimentation and sophisticated engineering design and construction.

On the other hand, although some hydraulic features of the Ogallala are now only approximately known, the problem of how far water can flow laterally in the aquifer from an infiltration trench or pond can be approximately solved with the data at hand. In general the lower part of the Ogallala Formation is coarse and permeable, particularly where the formation is unusually thick, as in the neighborhood of Plainview, Tex. This basal material is in part coarse sand and in part gravel with sand and is distinctly fluviatile in origin. Theis, Burleigh, and Waite in 1935 (unpub. report), after obtaining field data on permeability from many localities, estimated a Meinzer coefficient of permeability of 500 gpd/ft^2 (gallons per day per square foot) or a hydraulic conductivity of 67 feet per day for this material. The upper part of the Ogallala Formation is largely windblown sand and silt, which in places where the formation is thin makes up the entire formation. A few channels of more permeable fluviatile material interlace this finer material. The same investigators estimated a Meinzer coefficient of permeability of about 75 gpd/ft^2 or a conductivity of about 10 feet per day for the coarser part of this upper material and considerably less for the average material in this part of the formation.

The sandy gravels probably represent old stream courses and are probably more or less linearly arranged in an east-southeast direction. If so, there is probably a hydraulically anisotropic condition with considerably greater transmissivity in this direction than in the southwesterly direction. If, with further work, values for transmissivity in the two directions can be estimated, the effects of anisotropy can be evaluated.

A preliminary map of variation of transmissivities for the Llano Estacado, based on specific capacities of

U.S. GEOL. SURVEY PROF. PAPER 750-B, PAGES B236-B243

wells, has been prepared in the Austin office of the U.S. Geological Survey. This indicates transmissivities ranging from less than 10,000 gpd/ft (or about 1,300 $ft^2\ day^{-1}$) to about 180,000 gpd/ft (or about 24,000 $ft^2\ day^{-1}$). The zones of equal transmissivity are generally elongated in the east-southeasterly direction.

At the present stage of study of the Llano Estacado, estimates of the rate of ground-water flow from presumed sources of recharge must be approximate and preliminary. However, estimates of flow are necessary at the present time to indicate the nature and magnitude of the recharge problem and to provide data for a conceptual design of the distribution system and terminal storage facilities for water that might be imported to the area.

Ground-water flow from canals or infiltration trenches is mathematically described and analyzed under the following assumptions: (1) the aquifer has a constant hydraulic conductivity, (2) the aquifer has a constant transmissivity, and (3) the aquifer has a varying transmissivity.

A fourth mathematical model considers radial flow from a circular source, simulating recharge from a playa lake or manmade spreading basin. In all cases, isotropic conditions are assumed. It is further assumed that the only source of ground-water flow is induced infiltration from canals or ponds.

MATHEMATICAL MODELS OF GROUND-WATER FLOW FROM CANALS

Movement under conditions of constant hydraulic conductivity

Under the assumptions of uniform areal withdrawal of water, q, from the aquifer, we may write (fig. 1),

$$F=-qx=-Kz\left(\frac{dz}{dx}+s\right),$$

in which z is the thickness of the saturated section (other symbols are defined at end of article)

Let $z=vx$ in which v is a dummy variable.

$$\frac{qx}{K}=vx\left(\frac{v\,dx+x\,dv}{dx}+s\right),\quad q/K=v^2+sv+\frac{xv\,dv}{dx},$$

$$v^2+sv-q/K=-\frac{xv\,dv}{dx},\text{ and}$$

$$-\frac{dx}{x}=\frac{v\,dv}{v^2+sv-q/K}.$$

Integrating, and writing $c=\sqrt{4q/K+s^2}$, $-\ln x=\frac{1}{2}\ln(v^2+sv-q/K)-s/2c\ln\frac{2v+s-c}{2v+s+c}+C/2$, or

$$\ln(x^2(v^2+sv-q/K))=\ln\left(\frac{2v+s-c}{2v+s+c}\right)^{s/c}+C. \qquad (1)$$

In this equation v has the same sign as x. The equation is identically satisfied by considering v as always positive and allowing s to change sign to the negative where the water movement is up the slope of the water body floor. Physically this is equivalent to considering both sides of figure 1 to extend to the right, making x and v positive but changing the direction of slope of the floor. This convention will be used in the following derivation.

Substituting $z=xv$ in the left member of equation 1,

$$\ln(z^2+sxz-qx^2/K)=\ln\left(\frac{2v+s-c}{2v+s+c}\right)^{s/c}+C.$$

As $x\to 0$, $z\to a$ and $\frac{2v+s-c}{2v+s+c}\to 1$,

$$C=\ln a^2,\text{ and}$$

$$\ln(x^2/a^2(v^2+sv-q/K))=\ln\left(\frac{2v+s-c}{2v+s+c}\right)^{s/c}.$$

Eliminating the log form and substituting $z/v=x$,

$$\frac{z^2}{a^2v^2}(v^2+sv-q/K)=\left(\frac{2v+s-c}{2v+s+c}\right)^{s/c}. \qquad (2)$$

As $a\to 0$, $v^2+sv\to q/K$. Writing v_0 for v at $a=0$,

$$\left.\begin{aligned}&v_0^2+sv_0=q/K,\text{ and}\\&c=\sqrt{4q/K+s^2}=\sqrt{4v_0^2+4sv_0+s^2}=2v_0+s\end{aligned}\right\} \qquad (3)$$

Now let $v=v_0+w$, in which w is a new variable and v_0 is a constant for a given q, K, and s, and let $z_0=v_0x$.

$$\left.\begin{aligned}&z-z_0=x(v-v_0)=wx,\text{ and}\\&z=(z-z_0)z/(z-z_0)=(z-z_0)v/w=(z-z_0)(1+v_0/w)\end{aligned}\right\} \qquad (4)$$

Making these substitutions in the members of equation 2,

$$\frac{z^2(v^2+sv-q/K)}{a^2v^2}=\frac{(z-z_0)^2}{a^2}$$

$$\left(\frac{v_0^2+2v_0w+w^2+s(v_0+w)-(v_0^2+sv_0)}{w^2}\right)$$

$$=\left(\frac{z-z_0}{a}\right)^2\left(\frac{2v_0+s+w}{w}\right)$$

$$=\left(\frac{z-z_0}{a}\right)^2\left(\frac{c+w}{w}\right).$$

$$\left(\frac{2v+s-c}{2v+s+c}\right)^{s/c}=\left(\frac{2v_0+s+2w-c}{2v_0+s+2w+c}\right)^{s/c}$$

$$=\left(\frac{w}{w+c}\right)^{s/c}.$$

Equation 2 is therefore equivalent to:

$$\left(\frac{z-z_0}{a}\right)^2=\left(\frac{w}{w+c}\right)^{1+s/c}, \text{ or}$$

$$\left(\frac{z-z_0}{a}\right)=\left(\frac{w}{w+c}\right)^{1/2(1+s/c)}. \quad (5)$$

It will be found convenient for computation to write $M=s/c$, and to let $w=\alpha c/2$. Then,

$$\frac{z-z_0}{a}=\left(\frac{\alpha}{\alpha+2}\right)^{1/2(1+M)}. \quad (6)$$

The sign of $M=s/c$ is by our convention positive where the water moves down the slope of the water-body floor and negative where the water moves up the slope of the floor.

$$M=s(4q/K+s^2)^{-1/2}=(s/2)/\sqrt{q/K+(s/2)^2}.$$

From equation 4,

$$x/a=(z-z_0)/aw=2[(z-z_0)/a]/\alpha c,$$
$$x/a=2[z-z_0)/a]M/\alpha s, \text{ and}$$
$$x(s/2)/a=[(z-z_0)/a]M/\alpha. \quad (7)$$

Also from equations 4 and 3,

$$z/a=[(z-z_0)/a][1+v_0/w]$$
$$=[(z-z_0)/a][1+2(c-s)/2\alpha c]$$
$$=[(z-z_0)/a][1+1/\alpha-M/\alpha]$$
$$=[(z-z_0)/a][1+1/\alpha]-x(s/2)/a. \quad (8)$$

If we divide both sides of equation 7 by $s/2$, we obtain at s=zero:

$$\left.\begin{aligned} x/a&=\sqrt{K/q}(z-z_0)/a\alpha, \text{ and}\\ z/a&=[(z-z_0)/a][1+1/\alpha]. \end{aligned}\right\} \quad (9)$$

By substituting the value of $(z-z_0)$ from the second equation into the first, we obtain:

$$x=\sqrt{K/q}\, z/(1+\alpha). \quad (9a)$$

These equations express x and z for $s=0$ in parameters desirable for the general solution. A more direct expression can be obtained by rewriting equation 2 for $s=0$:

$$(z^2/a^2)(1-q/Kv^2)=1,$$
$$z^2-qz^2/Kv^2=a^2,$$
$$z^2-qx^2/K=a^2,$$
$$x^2=K(z^2-a^2)/q, \text{ and}$$
$$x=a\sqrt{K/q}\sqrt{(z/a)^2-1}, \quad (9b)$$

for $s=0$, $L=2x$.

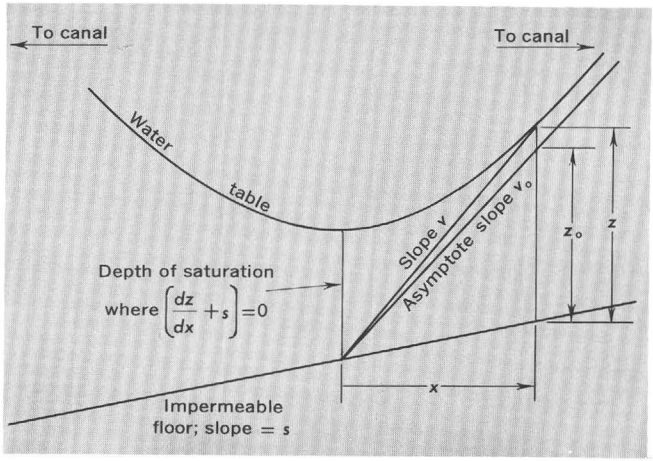

FIGURE 1.—Nomenclature for water movement from canals through the aquifer under assumption of uniform hydraulic conductivity, K.

A chart can be prepared giving values of the parameters z/a and $\frac{xs/2}{a}$ in terms of

$$(z-z_0)/a=\left[\frac{\alpha}{\alpha+2}\right]^{1/2(1+M)}.$$

In practice, a value of α is assumed and a desk-top computer can be programed to compute all needed data for all relevant values of M for this α. Figure 2 is such a chart. A series of values of α defines all the profiles given.

On this chart the series of lines converging to the lower left represents profiles of the water table, in terms of the parameters mentioned above, for the region down the slope of the floor of the water body (positive M) from the infiltration canal; those converging to the right represent profiles up the slope (negative M). The negative values are given on the upper scale and the positive values on the lower scale. In using the chart the same absolute value must be used for both positive M and negative M.

Inasmuch as the thickness of the water body must be the same under both canals, the values of z/a must be the same for both upslope and downslope sections. In using the chart, allowable minimum and maximum thicknesses for the water body are chosen. The ratio of maximum to minimum gives the control for entering the chart. If, for instance, the minimum depth is regarded as 50 feet and the depth under the canal is to be 250 feet, the value of z/a for entering the chart is 5.

The value of M is taken from the relation $M=(s/2)/\sqrt{(q/K)+(s/2)^2}$. If K is taken as 10,000 feet per year (equivalent to a Meinzer coefficient of permeability

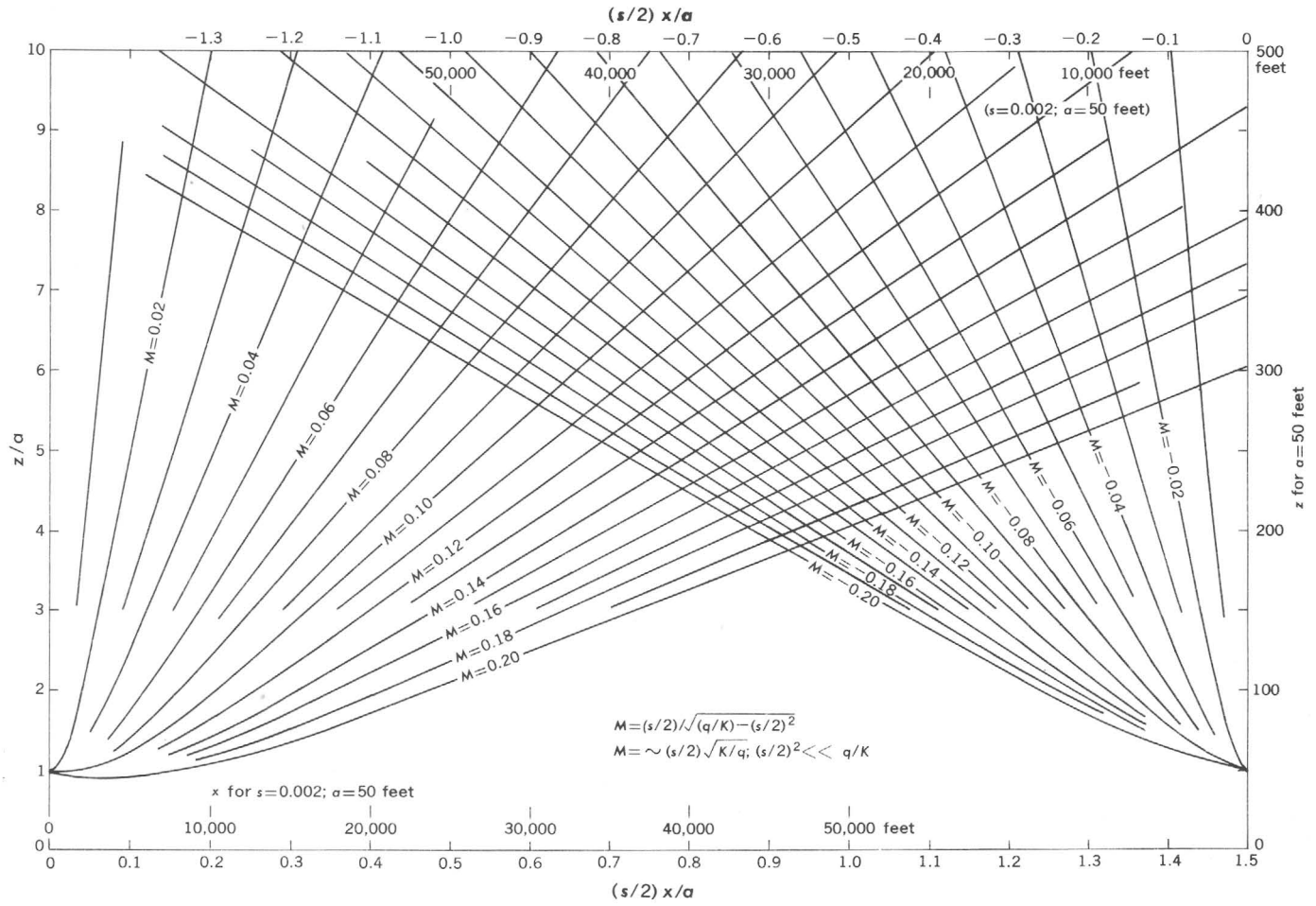

FIGURE 2.--Graph for determining the spacing of canals under conditions of uniform hydraulic conductivity, K.

of about 200 gpd/ft^2), q as 2 feet per year so that $K/q=5{,}000$, and s as 0.002, $M\approx 0.07$. The $z/a=5$ line intersects the $M=-0.07$ line at $(s/2)\ x/a=-0.315$ and the $M=+0.07$ at 0.375. The distance L between canals in terms of the $(s/2)\ x/a$ values is the sum of the absolute values, or $(s/2)\ L/a=0.690$, and the distance under these assumptions is $L=0.69\times(50/10^{-3})=34{,}500$ feet.

Some properties of M are of interest. For low values of $s/2$, such as the average slope of the sub-Ogallala floor, $M\approx(s/2)\sqrt{K/q}$. Further, it can be shown for the range of values pertinent to the Llano Estacado that the distance between recharging canals is $L\approx 2M\ (z/a)\ a/(s/2)$, or for a z/a value of 5, $L\approx 10Ma/(s/2)$. For the values assumed above, $L=0.7\times 50\times 1{,}000=35{,}000$ feet.

Equation 9b, derived for $s=0$, yields a value of $L=2x$ for the same assumed values of K/q, z, and a as follows:

$$L=2\times 50\ \sqrt{5{,}000}\ \sqrt{25-1},\ \text{or}$$
$$L=34{,}641\ \text{feet}.$$

It is apparent that for hydraulic factors pertinent to the Llano Estacado and for preliminary conceptual design, the slopes of the water table and of the sub-Ogallala floor may be disregarded. The only effect of the slope of the floor will be to shift the trough of the water table under these conditions of recharge somewhat downslope from the midpoint between canals.

The quantity of water which must infilter through such a canal is qL. For $L=35{,}000$ feet and $q=2$ feet per year, the quantity is 70,000 ft^2/yr or 192 ft^2/day or 192 ft^3/day per lineal foot of trench.

Movement under conditions of constant transmissivity

It may be considered that the permeability of the Ogallala Formation of the southern High Plains may be largely in gravels and sands in the basal part of the formation. In such a case the formation may be considered to have a constant transmissivity, any additional permeability in the upper section being considered negligible. In general, the problem is mathematically identical with the situation of defining flow in an

artesian aquifer that is recharged along some line and pumped at a uniform areal rate. From figure 3 we may write the equation for this condition as follows:

$$F=-qx=-T\,(dz/dx+s), \text{ or}$$
$$qx-Ts=T\,dz/dx.$$

Integrating,

$$qx^2/2-Tsx=Tz+C.$$

At $x=0$, $z=a$; $C=-Ta$,

$$qx^2/2-Tsx=T(z-a), \text{ or}$$
$$qx^2/2T-sx=z-a. \tag{10}$$

By completing the square we obtain:

$$\left.\begin{aligned} x&=\pm\sqrt{(T/q)\ [2(z-a)+Ts^2/q]}+Ts/q, \text{ and}\\ sx&=\pm\sqrt{(Ts^2/q)\ [2(z-a)+Ts^2/q]}+Ts^2/q. \end{aligned}\right\} \tag{11}$$

If we write x_1 for the absolute value of the distance through which the water moves down the slope of the impervious floor and x_2 for the absolute value of the distance through which water moves upslope, we have:

$$sx_1=\sqrt{(Ts^2/q)\ [2(z-a)+Ts^2/q]}+Ts^2/q, \text{ and}$$
$$sx_2=\sqrt{(Ts^2/q)\ [2(z-a)+Ts^2/q]}-Ts^2/q.$$

It is evident that:

$$\left.\begin{aligned} x_1&=x_2+2Ts^2/q, \text{ and}\\ L&=x_1+x_2=2x_2+2Ts^2/q. \end{aligned}\right\} \tag{12}$$

Hence all relevant information can be gathered from one set of curves. Figure 4 is a set of curves of $(z-a)$ plotted against sx for various values of $2Ts^2/q$.

It is to be noted that, in general, a, which is the depth of saturation at the point of lowest head, is not the least depth of saturation. Letting the derivative of equation 10 equal zero to find the position of the minimum value of z,

$$d(z-a)/dx=dz/dx=qx/T-s=0,$$
$$x=Ts/q, \text{ and}$$
$$sx=Ts^2/q. \tag{13a}$$

Substituting these values in equation 10,

$$(z-a)_{min}=qT^2s^2/2Tq^2-Ts^2/q, \text{ or}$$
$$(z-a)_{min}=-Ts^2/2q \tag{13b}$$

If the slope of the flow is zero, the s-terms drop out in equations 10 and 11, and

$$\left.\begin{aligned} z-a&=qx^2/2T, \text{ and}\\ x&=\sqrt{2T(z-a)/q}. \end{aligned}\right\} \tag{14}$$

In using figure 4, the quantity of $2Ts^2/q$ is computed, and values of a and of maximum z chosen. The value of sx is found for the intersection of the proper curve with the value of $z-a$. This is the value of sx for which water is moving against the slope of the floor. The value of sx in the other direction is obtained according to equation 12 by adding $2Ts^2/q$ to the value of sx read from the chart.

For instance, if a is taken as 50 feet and the maximum depth as 250 feet, and a value of 6 for $2Ts^2/q$ is assumed, the chart is entered at $z-a=200$ and the curve $\delta=2Ts^2/q=6$ intersected. The value of sx is found to be 32. The corresponding sx for the downslope part of the water body is $32+6=38$, and the total distance between canals is $sL=70$. If $s=2\times10^{-3}$ the total distance between canals is 35,000 feet.

The value of T/q used in this example is 750,000 feet. If this is substituted in equation 14, which disregards the slope of the floor, the distance between canals is computed as 34,640 feet.

This example is somewhat comparable to that used in the previous section, where the distance between canals of 34,500 feet was determined. If average thickness of saturated section is taken as 150 feet and multiplied by a K/q of 5,000 used in the previous section, the value of $2Ts^2/q$ represented is 6.0. If the rate of withdrawal is 2 feet per year the Meinzer transmissivity represented is about 30,000 gpd/ft. For values of hydraulic conductivity and transmissivity common to the High Plains, and for preliminary purposes, the type of model chosen is apparently not of critical importance.

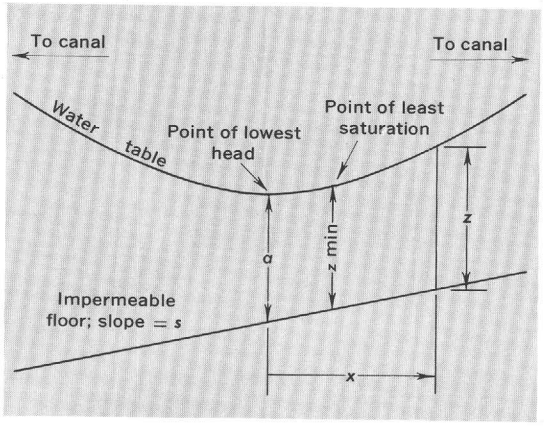

FIGURE 3.—Nomenclature for water movement from canals through the aquifer, assuming uniform transmissivity, T.

Movement under conditions of varying transmissivity

Any prescribed conditions of hydraulic conductivity and recharge can be treated numerically by assuming that all the conditions of flow are constant through a

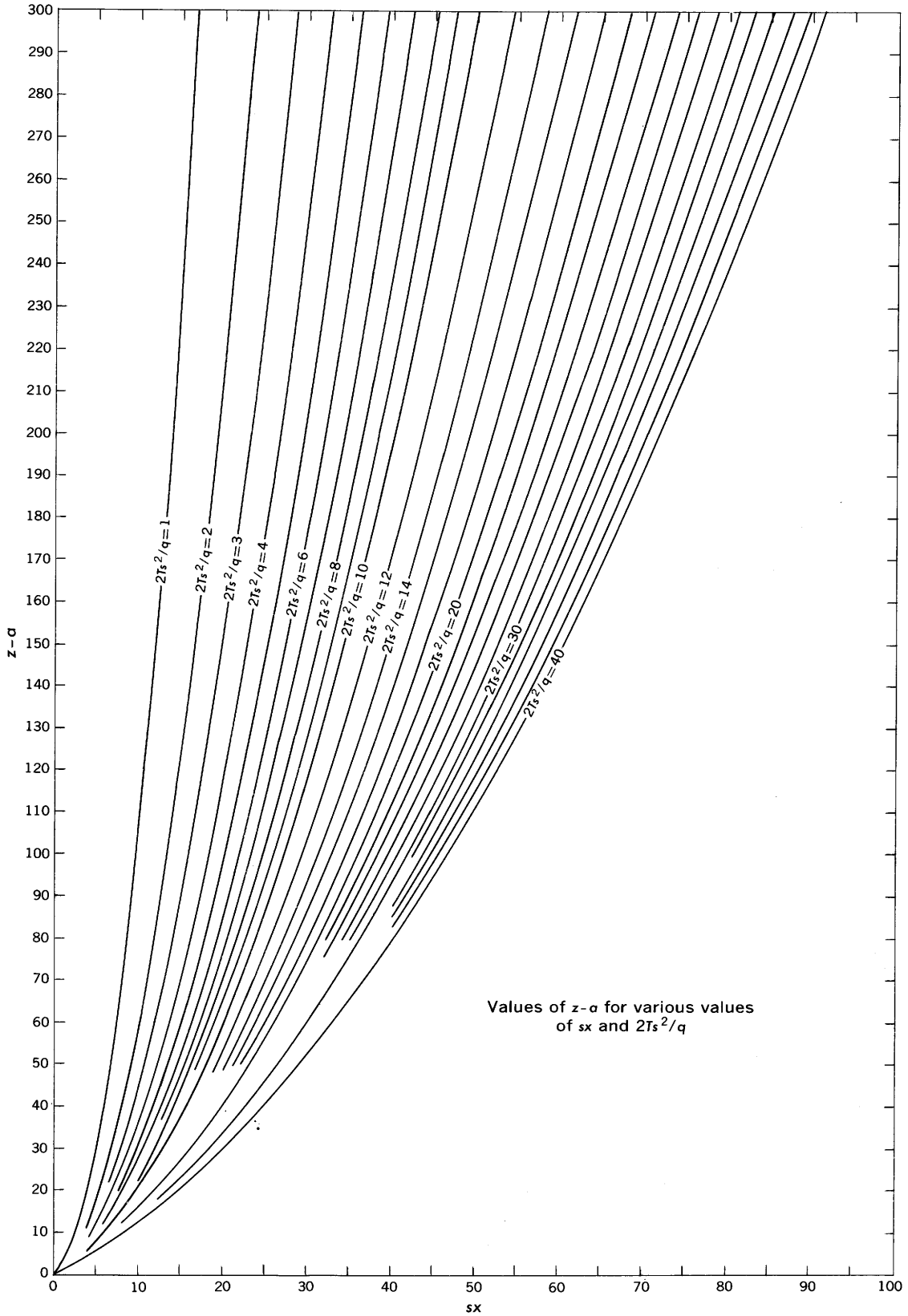

FIGURE 4.—Graph for determining the spacing of canals, assuming uniform transmissivity, T.

small increment of distance, but that these conditions may change from one group of increments to another.

The differential equation for flow is:

$$F=-qx=-Kz\left(\frac{dz}{dx}+s\right),$$

$$\frac{qx}{Kz}=\frac{dz}{dx}+s, \text{ or}$$

$$\frac{qx}{Kz}-s=\frac{dz}{dx}.$$

Expressed in terms of finite differences this is:

$$\Delta z=\Delta x\left(\frac{\Sigma\Delta x}{(K/q)\Sigma\Delta z}-s\right).$$

If a is the minimum thickness of saturation, then

$$\Delta z=\Delta x\left(\frac{\Sigma\Delta x}{(K/q)(a+\Sigma\Delta z)}-s\right).$$

The depth of saturation is given by $a+\Sigma\Delta z$ and the distance by $\Sigma\Delta x$. Hydraulic conductivities can be changed at appropriate depths of saturation or at appropriate distances. Negative values may be inserted for Δx, to describe conditions for flow up the slope of the floor.

With the aid of even the smallest of computers, the position of the water table for any assumed distribution of conductivity can be rapidly computed as accurately as by any of the previous methods.

MATHEMATICAL MODEL OF GROUND-WATER FLOW FROM A CIRCULAR AREA SIMULATING A PLAYA LAKE OR MANMADE SPREADING BASIN

It appears from the treatment of data for canals that for small slopes of the sub-Ogallala floor and for transmissivities characteristic of the Ogallala, the slope of the floor can be disregarded. In the following treatment of movement from a circular area such as one of the lakes or sinks of the Llano Estacado, it is considered that the floor is horizontal.

Consider a circular lake of radius ρ from which water seeps at a rate p to feed a circular area of radius R, from which water is withdrawn at a uniform rate, q, throughout the area. Let K be the hydraulic conductivity of the aquifer. The total quantity used must equal the quantity infiltered.

$$\pi q(R^2-\rho^2)=\pi p\rho^2,$$
$$qR^2=(p+q)\rho^2,$$
$$\rho^2=qR^2/(p+q), \text{ and}$$
$$\rho=R\sqrt{q/(p+q)}. \quad (15)$$

This gives the ratio between infiltering area and area served.

Assuming an areally uniform rate of withdrawal and a level floor,

$$\pi q(R^2-r^2)=-2\pi rKz\,dz/dr, \text{ or}$$
$$(q/K)(R^2-r^2)dr/r=-2z\,dz.$$

Integrating,

$$(q/K)(R^2\ln r-r^2/2)=-z^2+C.$$

At $r=R$, $z=a$, a minimum depth, $C=a^2+(q/K)(R^2\ln R-R^2/2)$, and $(q/K)(R^2\ln r-r^2/2)=a^2-z^2+(q/K)(R^2\ln R-R^2/2)$, and $z^2-a^2=(q/K)[R^2\ln R/r-(R^2-r^2)/2]$.

Let $z=z_1$ at $r=\rho$. Then

$$z_1^2-a^2=(q/K)[R^2\ln R/\rho-(R^2-\rho^2)/2]. \quad (16)$$

For flow conditions below the infiltration pond, assuming a uniform rate of leakage, p:

$$\pi pr^2=-2\pi rKz\,dz/dr,$$
$$(p/K)r\,dr=-2z\,dz, \text{ and}$$
$$(p/2K)r^2=-z^2+C.$$

The maximum thickness of saturation, Z, is at the center of the pond at $r=0$. Therefore, $C=Z^2$, and $(p/2K)r^2=Z^2-z^2$.

At the perimeter of the pond, $z=z_1$, and

$$(p/2K)\rho^2=Z^2-z_1^2. \quad (17)$$

Adding equations 16 and 17,

$$Z^2-z_1^2+z_1^2-a^2=(q/2K)[2R^2\ln R/\rho - R^2+\rho^2]+(p/2K)\rho^2.$$

Substituting the value of ρ from equation 15,

$$Z^2-a^2=(1/2K)[qR^2\ln(p+q)/q - qR^2+q(p+q)R^2/(p+q)],$$
$$Z^2-a^2=q\,R^2\ln(1+p/q)/2K,$$
$$\left.\begin{aligned} R^2&=2K(Z^2-a^2)/q\ln(1+p/q), \text{ and}\\ R^2&=K(Z^2-a^2)/1.15\,q\log_{10}(1+p/q).\end{aligned}\right\} \quad (18)$$

If we make the previous assumptions that $K/g=5{,}000$, equivalent to the use of 2 feet of water per year, and that the Meinzer permeability is 200, and we further assume that $p=1$ foot per day$=365$ feet per year, and assume maximum and minimum depths of 300 feet and 50 feet, then

$$R^2=5{,}000\ (8.75\times10^4)/1.15 \log 183.5$$
$$=4.375\times10^8/2.603$$
$$=1.68075\times10^8\ \text{ft}^2.$$

Area served$=\pi R^2=5.2802\times10^8$ ft$^2=18.94$ mile^2.
Radius of area served$=R=12{,}964$ feet.
Area of lake$=\pi R^2/183.5=2.88\times10^6$ ft$^2=0.1$ mile^2.

NOMENCLATURE

a=thickness of water body chosen, where water velocity equals zero [L],
F=total flux through a unit width of section [L^2T^{-1}],
K=hydraulic conductivity [$L\ T^{-1}$],
L=horizontal distance between parallel canals that lose water to the aquifer [L],
P_m=Meinzer coefficient of (field) permeability [gpd/ft^2],
p=rate of infiltration [$L\ T^{-1}$],
q=average depth of water used in area (total water used divided by total area) [$L\ T^{-1}$],
R=maximum radius of area served from circular pond [L],
r=radius to point of interest [L],
s=slope of floor of water body [dimensionless],
T=transmissivity [$L^2\ T^{-1}$],
x=horizontal distance [L],
z=depth of saturation [L],
Z=maximum depth of saturation [L], and
ρ=radius of infiltering pond [L].

ORIGIN OF MINERALIZED GROUND WATER IN PRECAMBRIAN ROCKS, NORTHEAST BRAZIL

By STUART L. SCHOFF, Washington, D.C.

Work done in cooperation with the U.S. Agency for International Development and the Brazilian Superintendência do Desenvolvimento do Nordeste

Abstract.—The upper Rio Paraíbo basin, northeast Brazil, an area of about 12,000 square kilometers, has ground water ranging in dissolved solids from about 350 to 25,000 milligrams per liter. It is underlain by crystalline bedrock of Precambrian age, and saprolite and alluvium derived from it. The crystalline rocks are types that yield water of excellent chemical quality in the United States. The common concept that fresh water enters the rocks and is becoming progressively more mineralized through contact with the rocks and concentration through evaporation seems hardly to be tenable in the area studied. It is suggested that the water originated as sea water and is being slowly and unevenly diluted and drained out of the rocks.

Ground water in the Precambrian rocks of northeastern Brazil contradicts the usual American experience that water in crystalline rocks, although meager in quantity, is excellent in chemical quality, as indicated by reported dissolved solids in the low hundreds, if not the tens, of milligrams per liter (Todd, 1959, p. 178; White and others, 1963, p. 5–6, 14, 16–17, 25–26; Feth and others, 1964, p. 16; Johnston, 1962, p. 45). Brazilians in the northeast are content with drinking water having as much as 1,000 mg/l of dissolved solids, and accept as commonplace for use by cattle water having 2,000 to 5,000 mg/l.

The high mineral content of the ground water creates problems in the use of the water. Speculating about the cause of the mineralization, recent writers [1] (Costa, 1963, 1965; Siqueira, 1963) have sought to relate regional and local geologic structure, ground-water circulation, and lithology to the observed chemical composition of the water. They have, for example, debated the relative importance of biotite and sodic feldspar as contributors to the mineralization. Fundamental to this thinking is the concept that infiltrating water—presumably rainwater—having picked up carbon dioxide and other substances, dissolves the rocks and with the help of evaporation becomes progressively mineralized. This would have to continue, in the Brazilian situation discussed here, until some of the water has dissolved-solids concentrations of 10,000 to 25,000 mg/l. Water quality, therefore, would be deteriorating.

Skepticism of the solution-and-evaporation hypothesis arose during the examination of 212 chemical analyses representing water from 106 wells in the upper part of the Rio Paraíba basin, an area of about 12,000 square kilometers in northeastern Brazil (fig. 1). All the wells had been drilled for the Brazilian Superintendency for Development of the Northeast, and into rocks described as gneiss, schist, migmatite, and granite. The water samples were collected by, or at the direction of, the geologists who had supervised the drilling operations, and were analyzed chemically in two Brazilian government laboratories. The dissolved solids in the water ranged from 334 to 25,500 mg/l and averaged 4,300 mg/l. The chloride concentration ranged from 14 to 13,700 mg/l and averaged nearly 2,000 mg/l.

WATER COMPOSITION AND LITHOLOGY

The composition of the water has no identifiable relationship to the rock in which it occurs. In analyses representing water from 40 wells drilled into gneiss, the dissolved solids ranged from the second lowest to the highest in the area. Most of these wells had chloride

[1] Texeira, J. A., and Oliveira, S. P. B., 1962, Perfuração de poços tubularares e levantamento geológico, Petrolina, Pe [Pernambuco]: Superintendência de Desenvolvimento do Nordeste, (ms. rept.) 22 p.

U.S. GEOL. SURVEY PROF. PAPER 750–B, PAGES B244–B247

FIGURE 1.—Map showing distribution of rocks of Cretaceous age (K, stippled) in northeast Brazil.

water, but about 25 percent had bicarbonate water. The concentrations of the other ions ranged widely. No doubt the rocks contributed something to the chemical composition of the water, but their influence was not predominant.

SIMILARITY TO SEA WATER

Although lacking clear-cut relationships to host rocks, the water has characteristics resembling those of sea water. The concentrations of dissolved solids and of chloride in the most mineralized water sample from the upper Rio Paraíba basin are somewhat more than 70 percent of the concentrations in sea water. Sodium chloride increases as total solids increase.

Magnesium predominated over calcium in a majority of the water samples, as it does in sea water, whereas, in ground water from continental sources calcium generally predominates (Hem, 1959, p. 82). Expressed as the ratio of magnesium to calcium (Mg/Ca), this relationship is shown in figure 2. The ratios for Paraíba water are mostly greater than 1.0, and as a group they fall closer in figure 2 to the sea-water reference line (ratio 5.24) than do the ratios for a group of continental waters, which are based on published analyses (White and others, 1963, tables). The published analyses represent water from several types of rock, including crystalline rock, in places which are as scattered as Washington State, South Africa, and India, and where climates range from humid to arid. In these analyses, with one exception, the dissolved-solids content is well below 1,000 mg/l, and it presumably is due to solution of rock material by infiltrating water.

The ratios of calcium plus magnesium to sodium (Ca+Mg/Na), calcium plus magnesium to chloride (Ca+Mg/Cl), and calcium plus magnesium to sodium plus chloride (Ca+Mg/Na+Cl) likewise show the Paraíba water to be closer in composition to sea water than are the same continental waters. These ratios also show the more mineralized Paraíba water to be closer to sea water than is the less mineralized Paraíba water.

POSSIBLE SOURCE OF CONSTITUENTS

Some of the principal constitutents of the water are more readily available within the area than others. The cations—calcium, magnesium, sodium, and potassium—could have been dissolved from the feldspars, pyroxenes, amphiboles, and micas in the igneous and metamorphic rock of the area. Calcium and magnesium could also be obtained from marble, limestone, and magnesite, which occur sparingly in the Precambrian rocks.

The anions, on the other hand, are not as available in the country rock. The concentrations of bicarbonate in the ground water, for example, seem to be out of proportion to the amount of carbonate rock. They are, in fact, greater than the concentrations of bicarbonate in sea water, and constitute a special problem not considered in this paper. The sulfate, least important of the anions in the water of the Paraíba basin, might come from the weathering of the sulfides of the metals, which, however, are not especially abundant components of the country rock. Chloride, chief among the anions in the water, probably is exceedingly scarce in the rocks, Chloride ordinarily amounts to only 0.05 percent or less in igneous rocks (Parker, 1967, table 20). A frequently

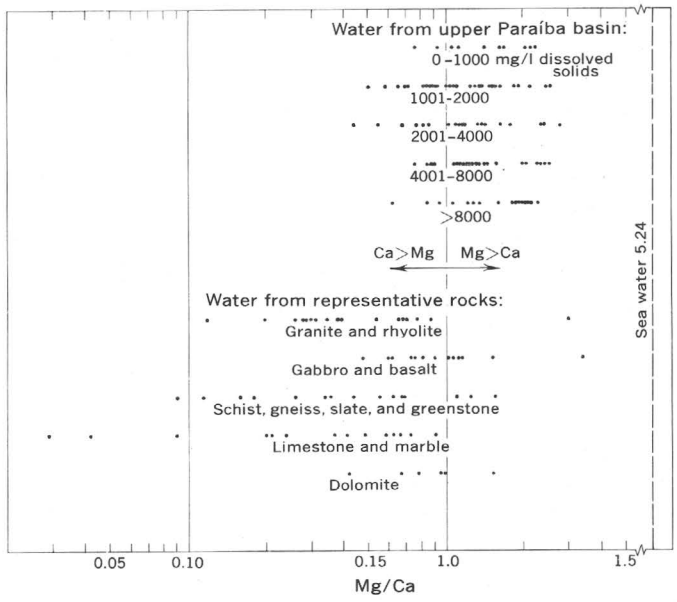

FIGURE 2.—The ratio of magnesium to calcium in ground water in the upper Rio Paraíba basin compared with the same ratio in sea water and in water from several groups of rock. Published representative analyses of water from the several groups of rock are from White, Hem, and Waring (1963).

quoted figure is 314 parts per million of chloride, and on this basis 6.4 kilograms of average rock would have to be decomposed in releasing the chloride in an average liter of Paraíba ground water. It could require the destruction of more than a billion kilograms of rock to furnish the chloride in the water that might be pumped out of the ground in a year by 100 windmill wells. The fate of other constituents taken in solution more abundantly by the water and the disposition of the insoluble remainder are problems that need only be mentioned here.

CONCENTRATION BY EVAPORATION

The solution of mineral matter from the rock is supposed to be accompanied by concentration of the water through evaporation, and in some respects the semiarid climate of the Paraíba basin seems to be favorable to the process. The average annual precipitation at one weather station is about 280 millimeters per year, and at the other, 640 millimeters, most of it coming in the 3 months, March–May. This is not abundance, but is enough to provide occasional recharge to the groundwater reservoirs, maintaining a modest supply of water. Temperatures are high the year around, making annual evaporative capacity great.

On the other hand, evaporation under present conditions would affect mainly the water en route to the water table and the ground water about to be discharged to the land surface. In 40 of 50 wells reported by Costa (1965, p. 21–22), the depth to static water level is more than 3 meters, placing a severe limitation on evaporation from the zone of saturation. Although not to be ignored, evaporation may be less potent than it is generally credited with being.

The process of concentration would, it seems, have to be selective. The chloride in average igneous rocks is only one sixty-fifth the amount of magnesium, yet the highest chloride in the Paraíba water is 13 times the amount of magnesium. A process of concentration that would boost the ratio of chloride to magnesium from 1 : 65 to 13 : 1 is hard to visualize.

MARINE INVASION AND DECREASING MINERALIZATION

In view of the difficulties with the solution-and-evaporation hypothesis as applied to the upper-Rio Paraíba basin, it is suggested that the mineralized water originated as sea water introduced during the latest marine invasion of northeast Brazil. Remnants of sedimentary rock remaining in the region show that the ocean last advanced into some parts of northeast Brazil during late Cretaceous time (fig. 1), but no evidence of that invasion remains within the upper Rio-Paraíba basin, unless it is the water itself.

The case therefore rests on the possibility of a marine invason of the basin, the resemblance of the ground water to sea water, with considerable allowance necessary for subsequent changes in the relative proportions of some constituents, together with the fact that so much chloride could more easily be obtained from sea water than from the rocks.

Sea water must certainly have been drained out of some rocks and replaced by fresh water. The Chapada do Araripe (fig. 1), for example, is an outlier containing a 600-meter section of Cretaceous rock made up, from the base upward, of fluviatile conglomerate and sandstone, a sequence of brackish or marine strata, and an upper fluviatile sandstone (Prof. Karl Beurlen, 1964, p. 337, and oral communication, Aug. 31, 1967). The lower sandstone must have been submerged and full of sea water while the brackish-to-marine strata were being deposited on top of it, but today the average dissolved-solids concentration of the water in this sandstone is 500 mg/l, and the maximum is only 1,000 mg/l (dos Anjos, 1963, p. 14). The Cretaceous strata bordering the north coast would have been last to emerge from the sea, and the water in them, though dilute compared with sea water, is more mineralized than the ground water in the Chapada do Araripe, ranging from 219 to 4,800 mg/l, and averaging about 1,600 mg/l.

The fracture systems in the Precambrian rocks would have been full of sea water after the sea had advanced over them, and this water ultimately would have begun to drain out. The process would have been deferred, however, so long as sediments covered them, and it would have gone more slowly than in the sediments because the permeability of the Precambrian rock is less. The process would also go unevenly—faster or slower, according to differences in permeability from one fracture system to another. These differences are great, and account for sharp contrasts in water quality between adjacent wells in the basin. Dilution by infiltrating rain water would have accompanied the draining process, and would have been similarly uneven, and for the same reason. And, at the same time, the solution of some materials from the rock and the precipitation of some from solution would have modified the proportions of the various constituents in the water.

Under this hypothesis, the chemical quality of the ground water in the upper Rio Paraíba basin is improving, although imperceptibly. Acts of man, such as artifically recharging the underground reservoir with fresh water or pumping mineralized water from it, tend

in the same direction as the natural process. Systematic pumping of a well, suitably coordinated with the season of recharge, might ultimately lead to worthwhile improvement in the quality of the water coming into the well. Regional improvement sought by pumping many wells, however, probably is too uncertain to be practical.

REFERENCES

dos Anjos, Nelson da F. R., 1963, Novos elementos sôbre a hidrogeologia do alto Jaguaribe, Ceará: Superintendência do Desenvolvimento do Nordeste, (mimeo), 19 p.

Beurlen, Karl, 1964, Introdução à estratigrafia geral e comparada: Expansão Gráfica, Recife, 1st ed., 440 p.

Costa, W. D., 1963, Roteiro de excursão, hidrogeologia no cristalino, região Monteiro-Sumé, Pb [Paraíba]: 17 Congresso Nac. Geol., Rio de Janeiro 1963, 22 p.

——— 1965, Resumo hidrogeológico da região centro-sul da Paraíba: Água subterrânea, Mar.-May, p. 18–24.

Feth, J. H., Roberson, C. E., and Polzer, W. L., 1964, Sources of mineral constituents in water from granite rocks, Sierra Nevada, California and Nevada: U.S. Geol. Survey Water-Supply Paper 1535–I, 170 p.

Hem, J. D., 1959, Study and interpretation of the chemical characteristics of natural water: U.S. Geol. Survey Water-Supply Paper 1473, 269 p., 2 pl. 40 figs.

Johnston, P. M., 1962, Geology and ground-water resources of the Fairfax quadrangle, Virginia: U.S. Geol. Survey Water-Supply Paper 1539–L, 61 p.

Lamego, A. R., ed., 1960, Mapa geológico do Brasil: Div. Geologia e Mineralogia, scale 1:5,000,000.

Parker, R. L., 1967, Composition of the earth's crust, *in* Fleischer, Michael, technical editor, Data of geochemistry, sixth edition: U.S. Geol. Survey Prof. Paper 440–D, 19 p.

Siqueira, Luis, 1963, Contribuicão da geologia à pesquisa de água subterrânea no cristalino: Clube de Eng. de Pe [Pernambuco], Revista, ano X, Sept.–Oct., 17 unnumb. p.; *also*, 1967, Água subterrânea, Jan.-Mar., p. 1–29.

Todd, D. K., 1959, Ground water hydrology: New York, John Wiley & Sons, 336 p.

White, D. E., Hem, J. D., and Waring, G. A., 1963, Chemical composition of subsurface waters, *in* Fleischer, Michael, technical editor, Data of geochemistry, sixth edition: U.S. Geol. Survey Prof. Paper 440–F, 67 p.

413-504 O - 71 - 17

REGIONAL SPECIFIC YIELD OF COAMO FAN, PUERTO RICO, COMPUTED BY WATER-BUDGET METHOD

By ENNIO V. GIUSTI, San Juan, P.R.

Work done in cooperation with the Commonwealth of Puerto Rico

Abstract.—A regional value of 0.16 for specific yield was computed by the water-budget method for the Coamo alluvial fan in southern Puerto Rico for calendar year 1967. This method may be used where dewatering of the aquifer is a major component of the water budget and where infiltration from rainfall and surface water is negligible or its effect can be calculated. For the Coamo fan, which is irrigated for agriculture, an average of one-third of the irrigation water was recirculated through the aquifer during the study year 1967.

One of the two most important hydraulic properties of a water-table aquifer is the specific yield. It usually is computed from data obtained in pumping tests along with another important hydraulic property, the transmissivity. The water-budget method was used to compute the specific yield of the Coamo alluvial fan, in southern Puerto Rico, using data for the study year 1967. The study is part of an investigation of the water resources of the Coamo area.

ELEMENTS OF THE WATER BUDGET

The items of the water budget are the inflow, the outflow, and the change in storage. In a coastal alluvial fan subject to pumping, the outflow is the water pumped out plus ground-water outflow to the sea, plus evapotranspiration. The inflow is the ground-water inflow at the head of the fan plus infiltration at the land surface of the fan (rainfall, streamflow, irrigation). For any time period, the algebraic difference between the inflow and the outflow equals the change in storage during that time.

Written explicitly, the water-budget equation for the Coamo alluvial fan can be stated as:

$$(I_s+I_{gw})-(O_p+O_{gw}+O_{ET}+O_s)=\pm\Delta S) \qquad (1)$$

where

I_s = inflow of surface water (recharge from rainfall, streamflow, and irrigation),
I_{gw} = inflow of ground water,
O_p = pumpage from the fan,
O_{gw} = outflow of ground water to sea,
O_{ET} = outflow as evapotranspiration,
O_s = outflow as runoff, and
ΔS = change in storage.

DATA AVAILABLE

The data for the water budget were collected in 1967, a drought year with an average frequency of occurrence of roughly once in 50 years. The data consist of continuous streamflow records from 5 stations at the head and the mouth of the fan (fig. 1) monthly and bimonthly water-level measurements from about 40 wells scattered throughout the fan, daily inflow from diversion canals, daily pumpage from all wells (about 70), and daily rainfall from 6 stations.

Monthly and continuous water-level measurements (fig. 2) allowed us to prepare maps of monthly change in water level. The change in water level in part of the Coamo fan is shown in figure 3.

COMPUTATION OF SPECIFIC YIELD

The change in storage, term ΔS of equation 1, is by definition the bulk volume of dewatered alluvium multiplied by the specific yield of the aquifer. In order to compute the specific yield, one must evaluate the other

U.S. GEOL. SURVEY PROF. PAPER 750-B, PAGES B248-B251

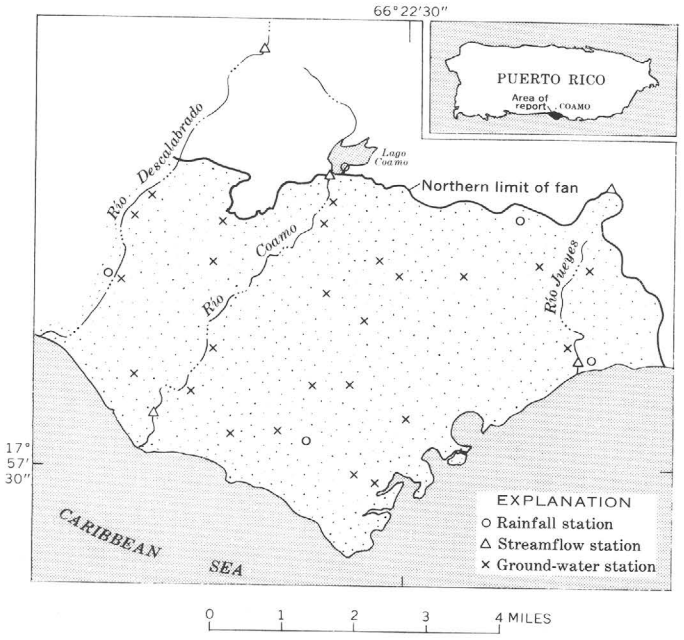

FIGURE 1.—Location of Coamo fan and the hydrologic stations used in the study.

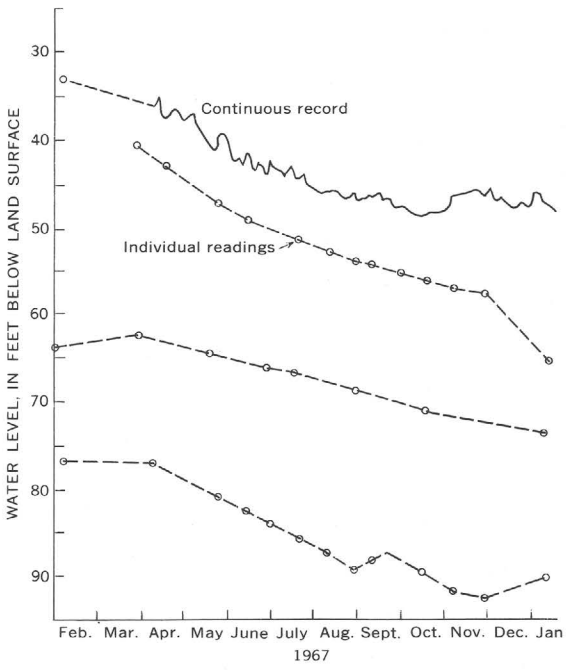

FIGURE 2.—Water-level fluctuations of some wells in the Coamo fan, 1967.

items of the water budget. Consider equation 1 and the data of table 1. For the months of April and May 1967 with practically no rainfall, one can write equation 1 as:

$$O_p = aI + S_y \Delta V, \quad (2)$$

where

O_q = outflow, pumpage from the fan,
I = irrigation water applied on the fan,
ΔV = volume of dewatered alluvium,
S_y = specific yield, and
a = a coefficient representing the fraction of irrigation water infiltrating into the aquifer.

TABLE 1.—*Data for water budget of Coamo fan, 1967*

Month	Pumpage Q (acre-ft)	Volume of dewatered alluvium ΔV (acre-ft)	Ratio $Q/\Delta V$	Total applied water—irrigation, streamflow, and rainfall (acre-ft)	Rainfall (inches)
Jan	3, 700	12, 700	0. 29	8, 000	1. 8
Feb	3, 600	11, 000	. 32	6, 000	. 8
Mar	3, 400	12, 000	. 26	5, 300	. 5
Apr	3, 600	16, 900	. 21	5, 300	. 2
May	4, 000	20, 000	. 20	4, 700	. 1
June	5, 000	22, 000	. 23	6, 800	1. 0
July	5, 400	24, 000	. 23	6, 800	. 8
Aug	5, 100	15, 000	. 35	7, 400	1. 4
Sept	4, 500	10, 100	. 44	8, 900	3. 3
Oct	4, 800	8, 000	. 60	12, 000	4. 3
Nov	3, 900	1, 900	2. 00	8, 800	2. 0
Dec	4, 430	5, 500	. 80	6, 400	. 3
Total for year	51, 430	159, 100		86, 400	16. 5

In writing equation 2, the following assumptions were made:

1. The inflow and outflow of ground water, represented by the terms I_{gw} and O_{gw} of equation 1, were considered to be negligible and their difference $I_{gw} - O_{gw}$ to be close to zero. This is justified by trial computations of inflow and outflow around the boundaries of the fan, using water-table gradients observed in the field.

2. The term O_{ET} was considered to be equal to the fraction of applied water that did not infiltrate; or $O_{ET} = (1-a)\ I_s$. This assumption is justified by the fact that no river outflow occurred ($O_s = 0$), that rainfall was nearly zero, and that no surface outflow of irrigation water took place.

3. Although coefficient a of equation 2 is properly a function of I, it was assumed that a was the same for the months of April and May.

The volume of dewatered alluvium was computed by integration within the lines of decline of water level, as shown in maps like figure 3, with the aid of a plastic grid superimposed on the map. The data for I_s and O_p were inventoried in the field.

The coefficients a and S_y of equation 2, obtained by simultaneous solution of the equation with the data for April and May of table 1 came to be

$$a = 0.17 \text{ and } S_y = 0.16.$$

The computed value of the specific yield is comparable to that computed from pumping tests in alluvium.

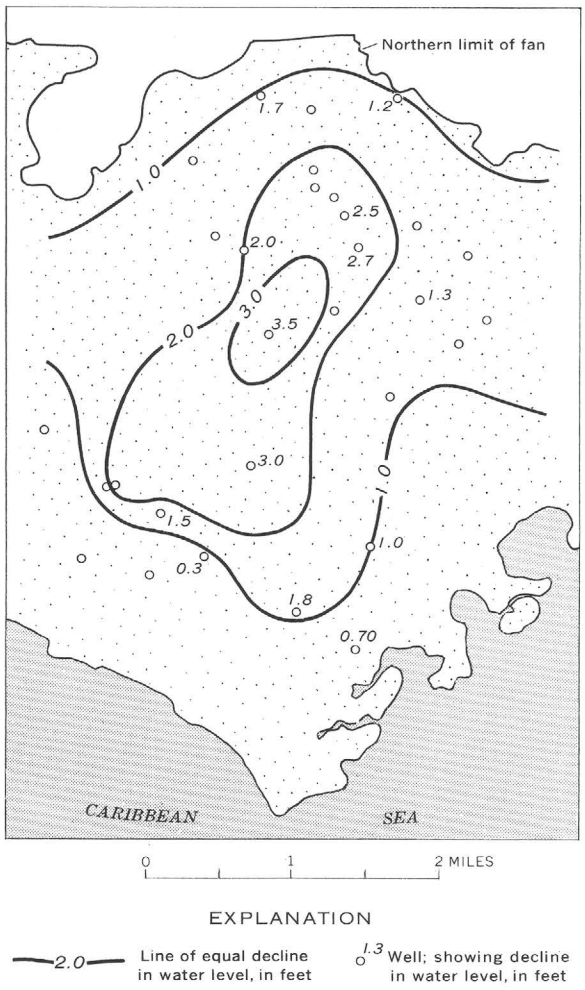

FIGURE 3.—Decline in water level during May 1967 in the central part of the Coamo fan.

The coefficient a represents the fraction of the applied water that reached the water table as recharge. The value of 0.17 for this coefficient probably is nearly a minimum, as it was computed from data for two practically rainless months, when evapotranspiration was at a maximum because potential evaporation was high. The variation in the fraction of applied water reaching the water table with increase in the quantity of water applied is illustrated by figure 4. In this figure the recharge, or withdrawal minus change in storage (computed using the storage coefficient as 0.16), is plotted versus the quantity of applied water (irrigation, streamflow, and rainfall). The points represent data taken for the months during the study year. The values for coefficient a ranged from about 0.17 to about 0.55 during the year.

The ratio of recharge to applied water, as shown by any point on the graph, gives the fraction of applied

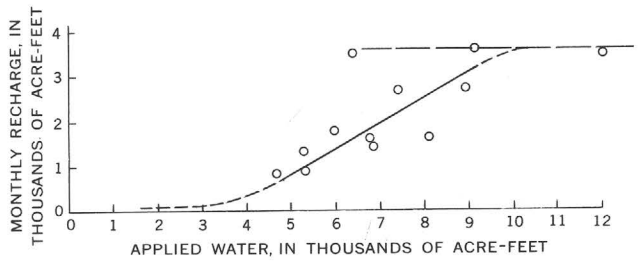

FIGURE 4.—Relation between recharge and applied water. Monthly recharge determined as pumpage minus dewatering (O_p—0.16$\triangle V$).

water reaching the water table as recharge at that level of water application. The lower (dashed) part of the graph is inferred to approach the abscissa asymptotically; at very low levels of water application all pumpage is thought to be derived from storage. The upper horizontal line, or "ceiling", suggested that there is a limit to the quantity of water that can infiltrate during a month; the excess would evaporate or run off as streamflow.

WATER BUDGET OF COAMO FAN, 1967

We prepared the water budget (fig. 5) from the data in table 1 and from other collected data on streamflow. The results are derived by inserting the annual values into equation 1 and assuming the term $I_{gw}-O_{gw}$ to be zero for the year (steady-state condition for regional ground-water flow). The term I_s for the year is separated into its three components as follows:

1. Recharge from the rivers is obtained simply by subtracting streamflow at the head of the fan from streamflow at the mouth.

2. Recharge from rainfall is calculated by using an average infiltration rate of 0.15, which in turn is estimated from rainfall-runoff ratios applicable in this area of Puerto Rico for low rainfall (Giusti and López, 1967).

3. The recharge from irrigation is arrived at through the "back door," the water budget having accounted for the other items. Indeed, to make up the difference between O_p (the pumpage, 52,000 acre-ft) and the loss of storage (0.16$\triangle V$=25,000 acre-ft), one needs 27,000 acre-ft. Substracting the 5,000 acre-ft from river and rainfall infiltration still leaves 22,000 acre-ft, which can come only from return flow of irrigation. Since irrigation was 66,000 acre-ft (52,000 from pumping plus 14,000 from canal diversions), the ratio of return flow to total was 0.33. In simple terms, one-third of the applied irrigation returned to the body of ground water.

The evapotranspiration was computed as a residual of all other factors of equation 1.

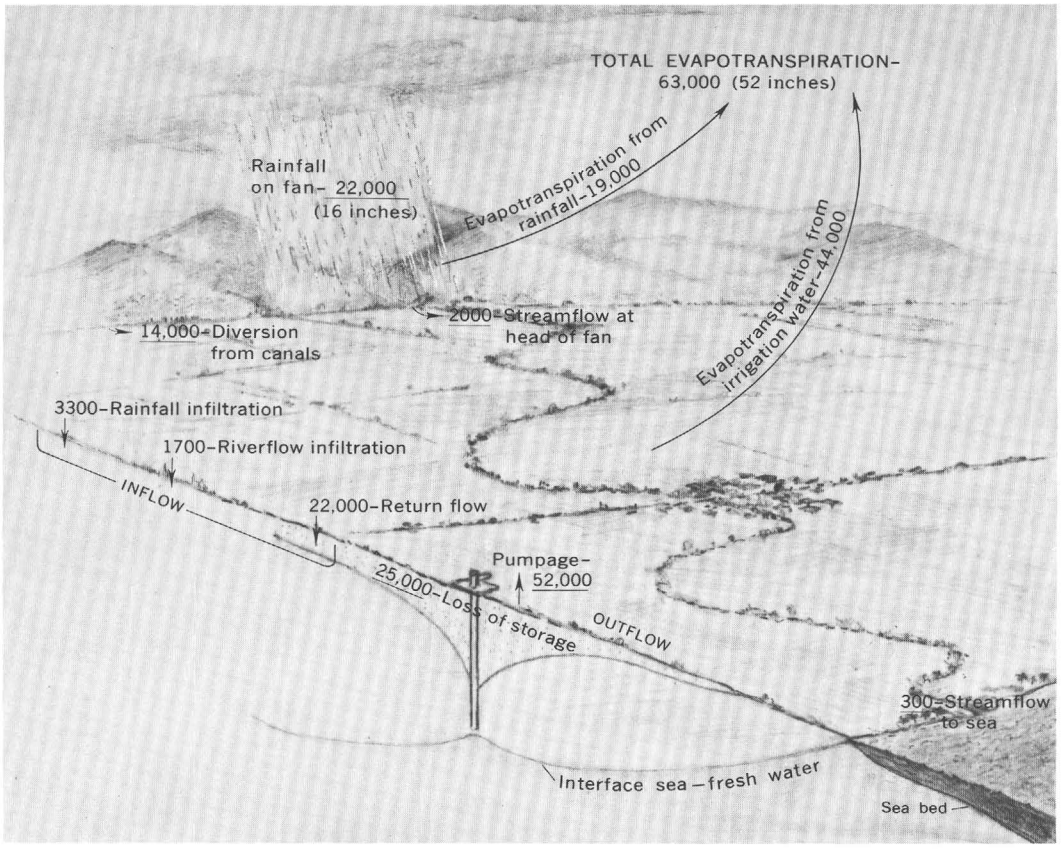

FIGURE 5.—Water budget of the Coamo fan, 1967. Budget values are in acre-feet; underlined numbers are measured values.

The accuracy and utility of this method to compute the specific yield of an aquifer hinge, of course, on the accuracy of the figures used to make the water budget. More than that, dewatering due to pumpage must be clearly separable from any regional decrease of water levels due to seasonal effects or to infiltration of surface water. It is suggested that techniques used by geophysicists to remove "the regional" in gravity and magnetic surveys may be helpful.

REFERENCE

Giusti, E. V., and López, M. A., 1967, Climate and streamflow of Puerto Rico: Caribbean Jour. Sci., vol. 7, no. 3–4, p. 87–93.

EARTHQUAKE-ACCELERATED DECLINE OF WATER LEVEL IN AN OBSERVATION WELL IN ST. THOMAS, VIRGIN ISLANDS

By TULLY M. ROBISON, San Juan, P.R.

Work done in cooperation with the Government of the Virgin Islands of the United States

Abstract.—A minor local earthquake caused a precipitate decline in the water level of an observation well in St. Thomas, Virgin Islands. The decline continued for over 3 months. The cause of the decline is assumed to be fracturing of the aquifer.

At about 4:32 p.m. on March 29, 1968, a mild earthquake was felt in the Virgin Islands and Puerto Rico. The shocks were felt most strongly on St. Thomas, V.I. The shocks reportedly lasted about 3 seconds and were heard as a rumbling noise. The preliminary determination of the epicenter by the U.S. Coast and Geodetic Survey was given as lat 18.8° N and long 64.8° W. This placed the epicenter at about 30 miles north of St. Thomas and just south of the Puerto Rico trench. The depth and magnitude (Richter scale) were given as 60 km and 4.7, respectively.

It is not unusual for severe earthquakes to be recorded in instrumented observation wells at great distances from the epicenters. The Alaskan earthquake was recorded in many observation wells throughout the United States. The shocks normally are recorded as a series of rapid oscillations of the water level, with the amplitude diminishing with time. There typically is no lasting effect on the water level.

This was not the effect on a U.S. Geological Survey observation well on St. Thomas, V.I. The well was equipped with a continuous water-level recorder. The recorder graph, which was traced for figure 1, registered the tremor as a single asymmetrical blip having a double amplitude of a little less than 0.03 foot. The sensitivity of the well is indicated by the twice-daily earth-tide fluctuations having an average amplitude of about 0.01 foot. Despite the modest response to the tremor, the water level showed a relatively steep decline afterward. In the first 24 hours, the water level declined 0.11 foot, more than 10 times the pre-earthquake rate of 0.01 foot per day. As shown by figure 2, the decline continued for more than 3 months, although at a decreasing rate.

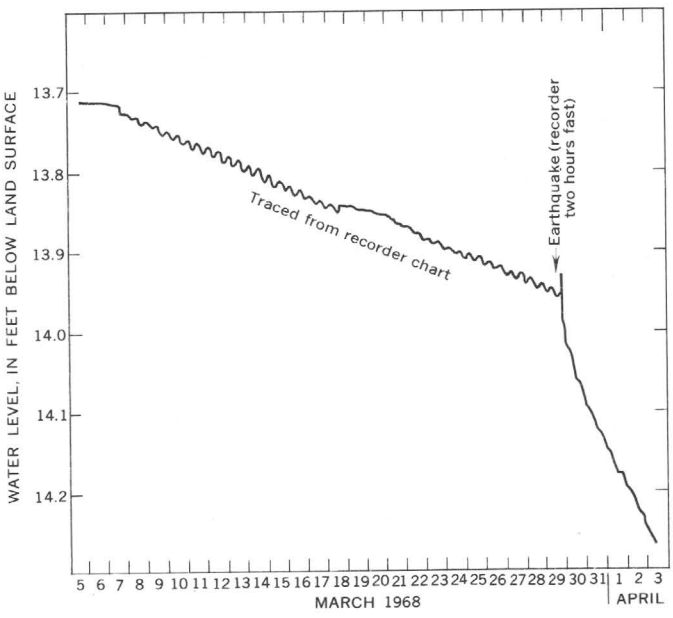

FIGURE 1.—Hydrograph of well USGS–11, showing immediate effect of earthquake.

To give some geohydrologic background, the well (USGS–11) is located at Estate Brookman in a narrow valley in southeastern St. Thomas. The well is close to a stream which was dry for several months before and after the earthquake. There was no nearby pumpage at the time. The valley floor is alluviated to a depth of 20 to 30 feet, and the alluvium is underlain by volcanic flows, tuffs, and breccias of Tertiary age.

U.S. GEOL. SURVEY PROF. PAPER 750-B, PAGES B252–B253

The well is at an elevation of 30 feet above mean sea level, is 60 feet deep, is cased with 6-inch casing to 38 feet (slotted 20–38 feet), and has an open bore from 38 feet to the bottom. The principal water-bearing zone is between 28 and 38 feet. The log of the well is as follows:

Lithology	Thickness (feet)	Cumulative depth (feet)
Quaternary:		
Alluvium, brown	28	28
Water Island Formation of Donnelly (1960):		
Volcanic tuff, brownish gray, highly weathered.	12	40
Volcanic breccia, varicolored, brown, gray, green; weathered.	20	60

It is the author's belief that the decline in water level was caused by fracturing of the volcanic aquifer that underlies the alluvium, increasing its ability to transmit water, and thereby enabling the ground water in the vicinity to seek a lower level more readily. On July 3, 1968, about 3 months after the earthquake, the water level reached 16.58 feet below land surface, an all-time low for the well. The total decline since the earthquake had been 2.63 feet. Recovery began on July 4. The recovery is attributable to heavy rains which ended a prolonged period of low rainfall. On July 15, 1968, the well was converted to a production well.

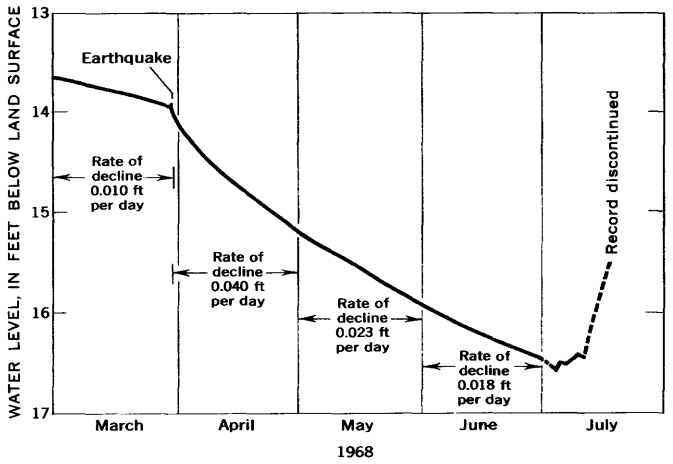

FIGURE 2.—Hydrograph of well USGS–11, showing long-term effect of earthquake.

REFERENCE

Donnelly, T. W., 1960, The geology of St. Thomas and St. John, Virgin Islands: Caribbean Geol. Conf., 2d, Mayagüez, Puerto Rico, Jan. 4–9, 1959, trans., p. 153–155.

RESISTANCE TO FLOW IN FLAT-BED SAND CHANNELS

By C. H. SCOTT and J. K. CULBERTSON,
Albuquerque, N. Mex., Washington, D.C.

Abstract.—The flat bed that is characteristic of upper regime flow commonly occurs at high discharge in sand channels. Data from many channels with sand beds show that for a flat bed or for a dune bed the velocity varies with hydraulic radius to the one-half power, indicating a constant value of Chezy C or of C_*. Values of C_* for upper regime flow for 24 channels were used in a regression analysis to determine the effect of median particle diameter of bed material and of slope on values of C_*. The analysis showed that C_* could be expressed as a function of median particle diameter alone. The relation developed from the analysis,

$$C_* = \frac{10.2}{(d_{50})^{1/2}},$$

with d_{50} expressed in millimeters, predicts the actual value of C_* within plus or minus 25 percent about 70 percent of the time. The relationship of Manning's n to median diameter of bed material and hydraulic radius, based on the relationship expressed above, is given in graphical form.

The bed forms most commonly observed in natural channels are (1) dune and transition forms of lower regime flow and (2) flat bed, standing wave, and antidune forms of upper regime flow. This progression of bed forms may be observed in an open channel as shear is increased. In many natural streams, the increase in shear with increase in discharge is sufficient to cause a change from lower to upper regime flow.

In this paper, parameters used to express resistance to flow for upper regime flow of sand-channel streams are examined in terms of relationships among the basic variables of velocity, depth, slope, and particle size of bed material. The study was limited to upper regime flow because this flow condition commonly occurs with high discharge, the magnitude of which may have to be determined by indirect methods. The purpose of the study was to develop a better definition of parameters used to express resistance to flow for the upper regime in sand channels.

FORMS OF RESISTANCE COEFFICIENTS

One of the earliest formulas for resistance to flow was proposed by Chezy. An important assumption made by Chezy was that the resisting force per unit area is proportional to the square of the velocity. The total resisting force for a length of channel at a cross section then is

$$F_r = K_C U^2 P L, \quad (1)$$

where

F_r = the total resisting force,
K_C = a constant of proportionality,
U = the mean velocity of flow,
P = the wetted perimeter, and
L = the length of channel.

In order to develop the Chezy equation, use is made of the most basic principle of uniform steady flow in an open channel. This principle states that the total force resisting flow is equal to the component of force acting in the direction of flow if the flow is uniform and steady. The component of force acting in the direction of flow is the component of weight of a volume of water parallel to the energy gradient, or

$$F_d = \gamma D W L S, \quad (2)$$

where

F_d = the component of force acting in the direction of flow,
γ = the unit weight of water,
D = the mean depth of flow,
W = the width of flow,
L = the length of channel, and
S = the energy slope.

U.S. GEOL. SURVEY PROF. PAPER 750-B, PAGES B254-B258

If we equate the forces expressed by equations 1 and 2,

$$K_c U^2 PL = \gamma\, DWLS, \tag{3}$$

and with DW equal to the area, A,

$$U^2 = \frac{\gamma}{K_c}\frac{A}{P} S. \tag{4}$$

The area divided by the wetted perimeter is the hydraulic radius, R, and

$$U^2 = \frac{\gamma}{K_c} RS, \tag{5}$$

from which

$$U = C\,(RS)^{1/2}. \tag{6}$$

This is the expression for Chezy C commonly given in which C has the dimensions of $ft^{1/2}/sec$. If gamma in equation 5 is expressed as the product of the mass density and the acceleration of gravity, then

$$U = \left(\frac{\rho}{K_c} gRS\right)^{1/2} \tag{7}$$

and

$$U = C_* (gRS)^{1/2}. \tag{8}$$

The coefficient C_*, which is more properly termed a parameter of flow conductance than a parameter of flow resistance, is dimensionless in this expression, which is derived for steady uniform flow in a channel of finite width. The coefficient C_* is numerically equal to Chezy C divided by the square root of the acceleration of gravity.

The Manning equation can be written in the same form as equation 8, with

$$C_* = \frac{0.263 R^{1/6}}{n}. \tag{9}$$

Although the Manning relation is more commonly used, the Chezy relation expressed as equation 8 is used in relationships developed in this paper. The relationships developed for predicting C_* are then converted to relationships for predicting Manning's n on the basis of equation 9.

DESCRIPTION OF DATA

Basic data used in this report were obtained from several sources which are briefly described below.

Data from the Rio Grande conveyance channel near Bernardo, N. Mex., were obtained by the U.S. Geological Survey as part of a field research study. Bed forms in the conveyance channel range from well-developed dunes in lower regime flow to a flat bed in the upper regime. Hydraulic data for the flat-bed condition were obtained over a range of discharge from about 600 to 1,200 cubic feet per second. The depths ranged from about 2.2 to 4.5 feet. Samples of bed material were obtained at each cross section for analysis of particle size by the visual-accumulation-tube method (Colby and Christensen, 1956). A complete description of the study reaches, data-collection procedures, and a listing of the basic data for the conveyance channel are given by Culbertson and Scott (written commun., 1970).

Data on velocity and depth for the Rio Grande at Cochiti, near Bernalillo, and for Galisteo Creek at Domingo, N. Mex., were taken from Culbertson and Dawdy (1964). Velocity, depth, and bed-material particle-size data for these stations were supplemented with data from routine water-discharge and sediment measurements.

Data on velocity, depth, slope, and bed-material particle size for Balloki Sulemanke and Marala Ravi link canals were taken from the West Pakistan Water and Power Development Authority publication of canal data (1963). The slopes and median diameters of bed material were averaged to determine means for these values.

Data on mean velocity, mean depth, slope, and bed-material particle size for the Elkhorn River near Waterloo, Nebr., were taken from Beckman and Furness (1962). Mean velocities and mean depths from the upper cable section were used in the analysis in this paper. The bed-material particle size used was that reported from analysis of the composite of 39 samples from 40 tons of bed material taken from the reach in June 1959.

Data on mean velocity, mean depth, slope, and particle size distributions for the Middle Loup River at Dunning, Nebr., and near Arcadia, Nebr., were obtained from summaries of special measurements made by personnel of the Nebraska District of the Geological Survey.

Average values of Chezy C, from which C_*'s were computed, and median diameter of particle size of bed material were taken from Dawdy (1961, table 1) for the following stations:

Browns Wash near Green River, Utah
Canadian River at Logan, N. Mex.
Cherry Creek near Franktown, Colo.
Cherry Creek near Melvin, Colo.
Cheyenne River near Spencer, Wyo.
Cuffawa Creek at Chulahoma, Miss.
Lance Creek at Spencer, Wyo.
Middle Loup River at St. Paul, Nebr.
Pigeon Roost Creek near Byhalia, Miss.
Republican River at Stratton, Nebr.
Rio Grande at San Antonio, N. Mex.

Rio Grande at San Marcial, N. Mex.
White River, South Fork, below White River, S. Dak.
Willie Wilkins Creek near Holly Springs, Miss.

ANALYSIS OF DATA

For many channels with sand beds, mean velocity varies with the one-half power of the hydraulic radius for flows over a flat bed. As shown previously by Dawdy (1961), an average Chezy C, which is constant as hydraulic radius varies, can be computed on the basis of the average relationship between velocity and hydraulic radius, if a constant slope for the channel is used. In this analysis, the use of an average relation between mean velocity and hydraulic radius is assumed to approximate an average steady uniform flow, and the average channel slope is assumed to approximate the average energy slope.

The value of C_*, based on the average relation of velocity to hydraulic radius for upper regime flow and on average slope, was determined for those channels for which the value of Chezy C had not been previously determined. The values of Chezy C reported by Dawdy, and used in this analysis, were converted to C_* by dividing by the square root of the acceleration of gravity. The values of C_* were then plotted as a function of the median diameter of bed material (fig. 1, curve 1). The effect of slope on the functional relation was checked by plotting the residuals of C_* from curve 1 as a function of the average slope of each channel (fig. 1, curve 2). The analysis shows that C_* can be expressed as a function of the median diameter of bed material alone, and that slope has no apparent effect on the relationship of C_* to median diameter. The relationship between C_* and median diameter can be expressed empirically as

$$C_*=\frac{10.2}{(d_{50}{}^{1/2})}, \tag{10}$$

with d_{50} expressed in millimeters.

Because the Manning coefficient, n, is more commonly used than either Chezy C or C_*, the values of C_* given in equation 10 are converted to values of n by the relation expressed in equation 9. Because hydraulic radius enters the relation in equation 9, n is expressed in terms of the median diameter of bed material and of hydraulic radius (fig. 2).

An exact mathematical analysis of the error involved in estimating C_* from equation 10 is not possible because instantaneous values of slope were not available for computation of instantaneous values of C_*. However, an approximation of this error can be obtained by considering the error involved in estimating the average C_* for a channel on the basis of curve 1 of figure 1, and adding to that error an approximation of the possible variation of instantaneous values of C_* from the average C_* for any given channel.

On curve 1 of figure 1, about 90 percent of the points defining the relationship are within plus or minus 15 percent of the curve. The values of C_* shown on figure 1 are averages for each channel; therefore, it is necessary to consider the possible deviation of C_* from the average C_* for a given channel. The variation of C_* from the average C_* is directly proportional to the variation of velocity from the average relationship of velocity to hydraulic radius, assuming an average slope for the

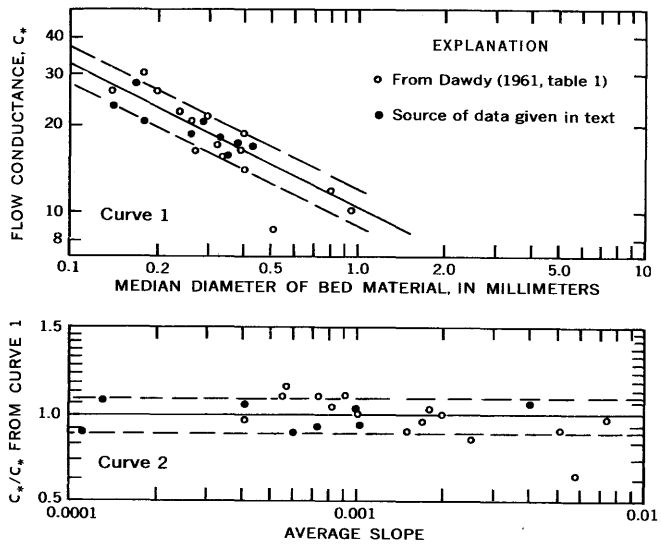

FIGURE 1.—C_* for upper regime flow as a function of median diameter of bed material and of slope. Dashed lines define area within 15 percent of the curves.

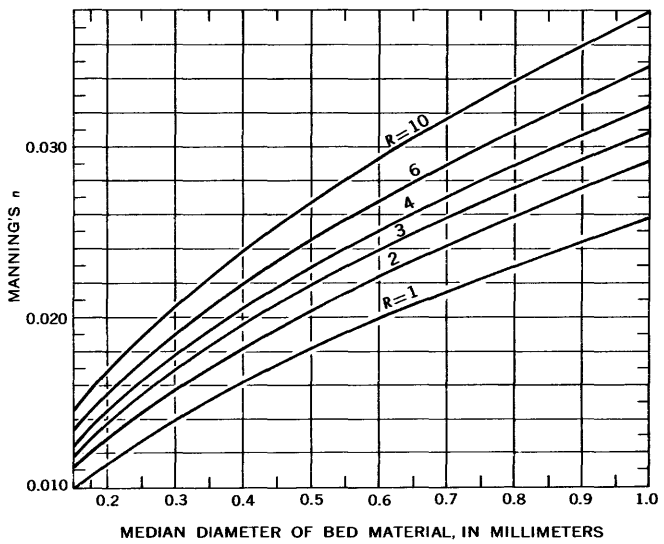

FIGURE 2.—Manning's n for upper regime flow as a function of median diameter of bed material and hydraulic radius.

channel. The relation of velocity to hydraulic radius for the Rio Grande conveyance channel near Bernardo, N. Mex., (fig. 3) is used as an example to illustrate the variation of velocity from the average curve. For those values of velocity and hydraulic radius for which bed form was known to be flat, about 80 percent of the points are within plus or minus 10 percent of the average curve. This estimate is not inconsistent with estimates for other channels for which the relationships of velocity to hydraulic radius were plotted and is not inconsistent for relationships for several channels shown by Dawdy (1961). Combining the two errors indicates that a value of C_* computed from equation 10 on the basis of a median diameter of bed material would be within plus or minus 25 percent of the actual value about 70 percent of the time. The same error applies to a value of n selected on the basis of figure 2.

APPLICATION

Equation 10 provides an independent means of estimating conductance of flow for flat beds in sand channels, from which the mean velocity in the cross section can be estimated by application of equation 8, if the hydraulic radius and slope are known. A representative sample of bed material should be obtained for analysis to determine size distribution. One possible source of error in application occurs because a representative sample of bed material at one point in time may not be representative of bed material at some other time. In some channels, such as the Rio Grande conveyance channel near Bernardo, N. Mex., somewhat finer bed material may be associated with a flat bed form than with a dune bed form (fig. 4). Such condition can be detected only by analysis of samples obtained when the different bed forms exist.

Furthermore, in a channel such as the conveyance channel near Bernardo, where bed form may range from dune bed to flat bed over a wide range of hydraulic radius (fig. 3), the only certain method of determining the bed form at any given point in time is by direct observation. However, for channels with discontinuous rating curves of the type described by Dawdy (1961), an estimate of the bed form that existed in the past is possible by a method suggested by Simons and Richardson (1966, fig. 28).

Average channel slope was used in the computation of the values of C_*, and average channel slope was assumed in the analysis of error for the relationship of figure 1 because instantaneous slope was not available. However, the use of instantaneous slope in the analysis

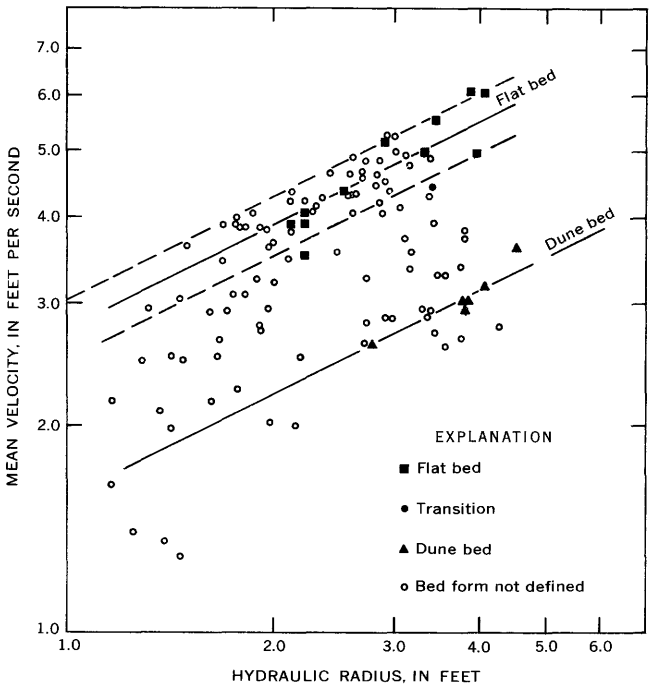

FIGURE 3.—Mean velocity as a function of hydraulic radius, Rio Grande conveyance channel near Bernardo, N. Mex. Dashed lines define area within 10 percent of the curve.

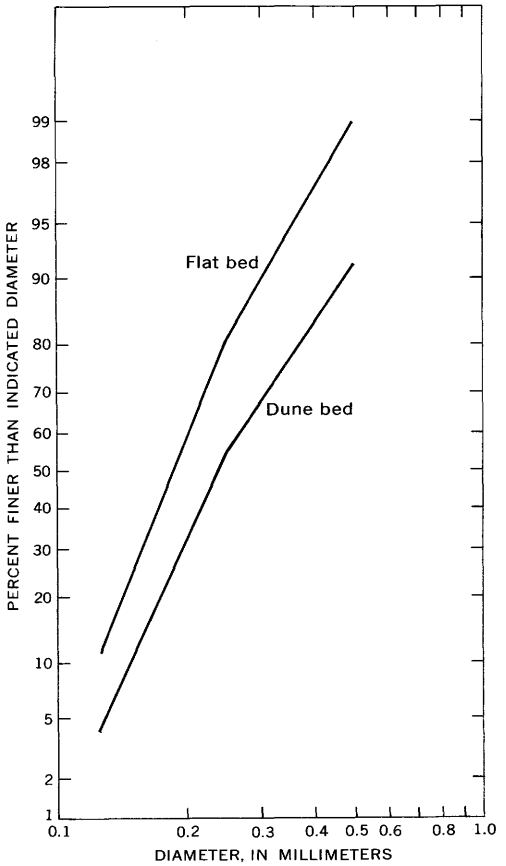

FIGURE 4.—Particle-size distribution for a flat bed and a dune bed, Rio Grande conveyance channel near Bernardo, N. Mex.

of error probably would have had little effect on the indicated error developed by the method used in this paper. Although either instantaneous slope or average slope can be used in the computation of mean velocity, use of instantaneous slope is recommended. The instantaneous slope used in the computation should be determined for a reach of channel that is reasonably straight and of fairly uniform width. The reach for which the slope is determined should be not less than 10 channels widths in length.

Equation 10 is valid for flat beds, but some of the channels used in the analysis, such as Pigeon Roost Creek near Byhalia, Miss., and Galisteo Creek near Domingo, N. Mex., are known to have standing waves at high flow. The relationship is probably valid for mild standing waves but would tend to overestimate conductance of flow for antidune flow.

REFERENCES

Beckman, E. W., and Furness, L. W., 1962, Flow characteristics of Elkhorn River near Waterloo, Nebraska: U.S. Geol. Survey Water-Supply Paper 1498–B, 34 p.

Colby, B. C., and Christensen, R. P., 1956, Visual accumulation tube for size analysis of sands: Am. Soc. Civil Engineers Proc., Jour. Hydraulics Div., v. 82, no. HY3, p. 1–17.

Culbertson, J. K., and Dawdy, D. R, 1964, A study of fluvial characteristics and hydraulic variables, middle Rio Grande, New Mexico: U.S. Geol. Survey Water-Supply Paper 1498–F, 72 p.

Dawdy, D. R., 1961, Depth-discharge relations of alluvial streams—discontinuous rating curves: U.S. Geol. Survey Water-Supply Paper 1498–C, 16 p.

Simons, D. B., and Richardson, E. V., 1966, Resistance to flow in alluvial channels: U.S. Geol. Survey Prof. Paper 422–J, 61 p.

West Pakistan Water and Power Development Authority, 1963, Canal and headworks data observation programme 1962–63 data tabulation: Harza Engineering Co. Internatioanl, Chicago, Ill., pt. 1, 342 p.

THE UNIT HYDROGRAPH—A TECHNIQUE FOR ROUTING RESERVOIR RELEASES

By V. B. SAUER, Washington, D.C.

Work done in cooperation with the Sabine River Authorities of Texas and Louisiana

Abstract.—The unit-hydrograph technique was successfully used to route power-demand reservoir releases from Toledo Bend Reservoir to 3 locations as far as 50 miles downstream on the Sabine River. The method is empirical and requires that the storage-discharge relation of the channel be basically linear, and that flood-wave traveltime be relatively constant through the range of discharge being routed. The basic equation is

$$Q_t = q_1 Q_{R\,(t-T)} + q_2 Q_{R\,(t-T-D)} + q_3 Q_{R\,(t-T-2D)} + \ldots q_n Q_{R\,(t-T-nD+D)},$$

where Q_t is the flow at the desired site at time t, $q_1, q_2 \ldots q_n$ are the unit hydrograph ordinates, and Q_R is the average reservoir release during a selected duration period, D. The parenthetical subscript denotes the midtime of reservoir release, and T is the flood-wave traveltime to the desired site.

Toledo Bend Reservoir, located on the Sabine River between Texas and Lousiana, is used for power generation on a peak-load demand basis. Normal operation of the powerplant results in a rather irregular pattern of flow releases, with sudden changes of flow. So that discharge of paper mill effluent into the Sabine River at a point 37 miles downstream from the reservoir can be keyed to the flow, a forecast of the flow in the Sabine is required. Standard routing techniques, such as the Muskingum method, do not provide flow estimates of suitable accuracy.

The routing of flow releases from reservoirs to downstream locations is not usually successful with standard routing techniques based solely on the continuity concept (outflow equals inflow plus change in storage). The reason for this lack of success is that the change in storage in the channel downstream from the reservoir cannot be easily determined during times of rapidly changing flow conditions imposed by reservoir releases. This paper describes a routing method based on the commonly used unit-hydrograph technique of flow lagging and flow summation. This method of routing was used for the Sabine River study, and comparisons of computed flow with actual flow at three locations downstream from the reservoir indicate satisfactory results. The procedure requires (1) a unit hydrograph for the site at which a flow hydrograph is desired, (2) a record of releases from the reservoir, and (3) a time, T, representative of flood-wave traveltime. The large volume of computations requires the use of a digital computer.

THEORY

The unit-hydrograph technique is basically a routing technique, whether it is used to develop the hydrograph for a basin based on rainfall excess, or, as in this case, to route water from a reservoir to some downstream location. Its success depends largely on the storage characteristics of the basin or channel that it is designed to represent. If storage is linearly related to discharge, the concept of proportionality will be valid, and outflow hydographs will be in direct proportion to the associated inflow. The amount of error which can be tolerated will determine the degree to which prototype nonlinearity can be tolerated.

A given quantity of water released from a reservoir at a rate, Q_R (in cubic feet per second), for a duration of D hours will result in a specific hydrograph at a downstream location, A. If we assume no losses or gains in the channel reach between the reservoir and point A, the volume of flow at point A will equal the release volume, but the shape of the hydrograph at point A will be determined by the storage characteristics

U.S. GEOL. SURVEY PROF. PAPER 750-B, PAGES B259-B264

of the channel. The time of arrival of the release water at point A will be determined by the speed at which the flood wave travels in the channel. Flood-wave traveltime is generally defined by factors such as leading edge, peak, and inflection points. For use in this study, flood-wave traveltime, T, has been defined as the time from the beginning of the reservoir release to the first impulse of the resultant flood wave at site A. See figure 1 for a definition sketch. If we assume a reservoir-release rate of 1 cfs for D hours, the resulting hydrograph at point A can be considered a unit hydrograph for that site. In this sense, the meaning of the term "unit hydrograph" is somewhat different from the usual meaning, as it refers here to a unit rate rather than a unit volume.

The hydrograph at point A for any release rate, Q_{R1}, for D hours can be computed by multiplying the ordinates of the unit hydrograph by Q_{R1} and displacing it in time by T hours. If releases Q_{R2} are made during the next duration period, the resulting hydrograph is computed by multiplying the unit-hydrograph ordinates times Q_{R2} and displacing that hydrograph T hours from the beginning of the second duration period. A summation of ordinates at simultaneous times will yield the hydrograph for the combined releases of Q_{R1} and Q_{R2}.

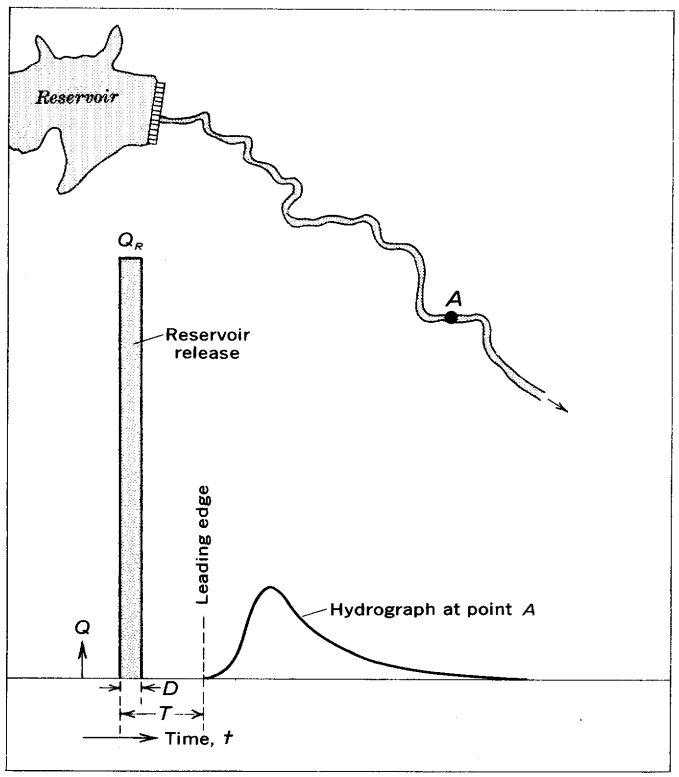

FIGURE 1.—Definition sketch showing relation of downstream hydrograph to reservoir release. See text for explanation of symbols.

Figure 2 is a graphical illustration of this process. Any number of release periods can be combined in this way to form the actual hydrograph at point A.

The flow at site A can be computed for a specific time, t, by computing the hydrographs resulting from the known releases, lagging them by time T, and summing the individual ordinates at time t. The equation for this process can be expressed in terms of the flow releases and the unit-hydrograph ordinates, and can also account for the time lag, T. Let the unit-hydrograph ordinates be designated as $q_1, q_2, q_3, \ldots, q_n$, and the time interval equal D. The discharge at site A at time t is designated Q_t and the equation is

$$Q_t = q_1 Q_{R(t-T)} + q_2 Q_{R(t-T-D)} + q_3 Q_{R(t-T-2D)} + \ldots q_n Q_{R(t-T-nD+D)}. \quad (1)$$

The parenthetical subscripts denote the midtime of the release, Q_R. Positive values indicate future time, and negative values indicate past time; therefore, to work on the basis of known releases, t must not exceed T. A given site on the channel downstream from a reservoir will have specific values for $q_1, q_2, q_3, \ldots q_n, T, n$, and D. Then the only variable necessary for computing the downstream flow, Q_t, becomes the reservoir release, Q_R. This relation assumes that T does not vary appreciably with discharge and that the storage-discharge relation is basically linear, as stated previously.

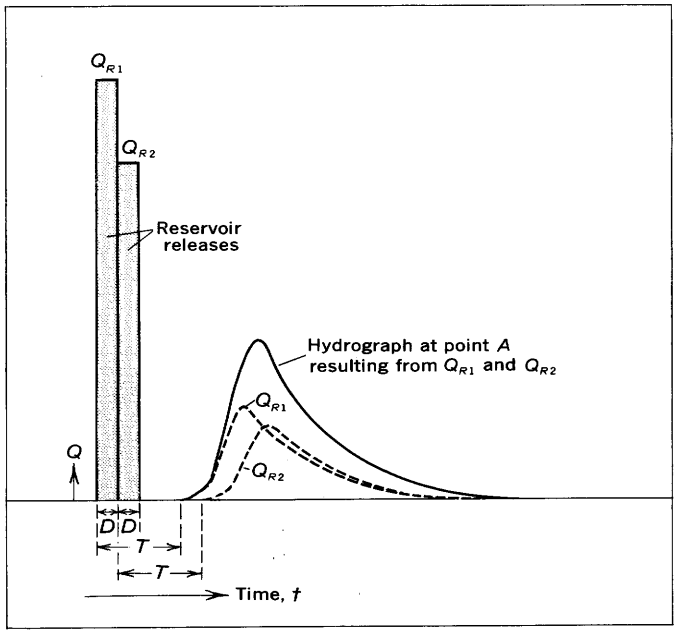

FIGURE 2.—Definition sketch showing relation of downstream hydrograph to multiple release pattern. See text for explanation of symbols.

THE UNIT HYDROGRAPH

The unit hydrograph for a site is a critical item necessary for the practical application of equation 1. It is beyond the scope of this paper to describe a method of determining the unit hydrograph; any of the accepted procedures can be used. Actual streamflow data at the desired site are preferable for the unit-hydrograph derivation, but data for a site upstream or downstream can sometimes be transferred to the desired site. Synthetic methods can also be used.

The unit hydrographs for the Sabine River study were derived from a family of dimensionless model hydrographs obtained from W. D. Mitchell through personal communication. Although this family of dimensionless model hydrographs is not published, the method of deriving them is explained by Mitchell (1962; 1967).

TEST RESULTS

The Sabine River project furnished rather extensive data for developing and testing the unit-hydrograph routing technique. Three gage sites—Burkeville, Tex., Merryville, La., and Bon Wier, Tex.—are located, respectively, at points 11, 37, and 50 miles downstream from the powerhouse at Toledo Bend Dam. Continuous records of stage and discharge are available at Burkeville and Bon Wier. Continuous records of stage only are available at the Merryville gage; however, a provisional stage-discharge relation was used to estimate a continuous record of discharge at this site for one of the test periods. Hourly values of reservoir releases are available from the powerplant records. Figure 3 is a sketch showing the relative location of the dam and gages.

The actual records at the three gage sites were used to develop the factors necessary in the routing equations. A tabulation of these factors is given in table 1. The duration, D, was selected so that sufficient points would be computed to define the outflow hydrograph. The last ordinate of the unit hydrograph is the nth term for that site.

Substituting values of table 1 into equation 1 provides specific routing equations for each site. These equations are:

for Burkeville,

$$Q_t = q_1 Q_{R(t-3)} + q_2 Q_{R(t-5)} + q_3 Q_{R(t-7)} + \ldots q_{23} Q_{R(t-47)}; \quad (2)$$

for Merryville,

$$Q_t = q_1 Q_{R(t-12)} + q_2 Q_{R(t-16)} + q_3 Q_{R(t-20)} + \ldots q_{17} Q_{R(t-76)}; \quad (3)$$

and for Bon Wier,

$$Q_t = q_1 Q_{R(t-17)} + q_2 Q_{R(t-21)} + q_3 Q_{R(t-25)} + \ldots q_{18} Q_{R(t-85)}. \quad (4)$$

The parenthetical subscript for the first Q_R term in each equation indicates the limit for which Q_t can be computed from known releases. For instance, the discharge at Merryville cannot be predicted more than 12 hours into the future on the basis of known releases.

The computations were performed by computer. The results of two test periods each for Burkeville and Bon Wier and one test period for Merryville are shown graphically in figures 4 and 5. Comparative data for the June test period were not available for the Merryville site. Intervening inflow into the channel reach during both test periods, which was the result of base flow and leakage from the dam, was considered constant during each period. The quantity of intervening flow was estimated for each period on the basis of actual records at each site. Comparisons are good except for timing in the low discharge range, where errors of up to 8 hours occurred.

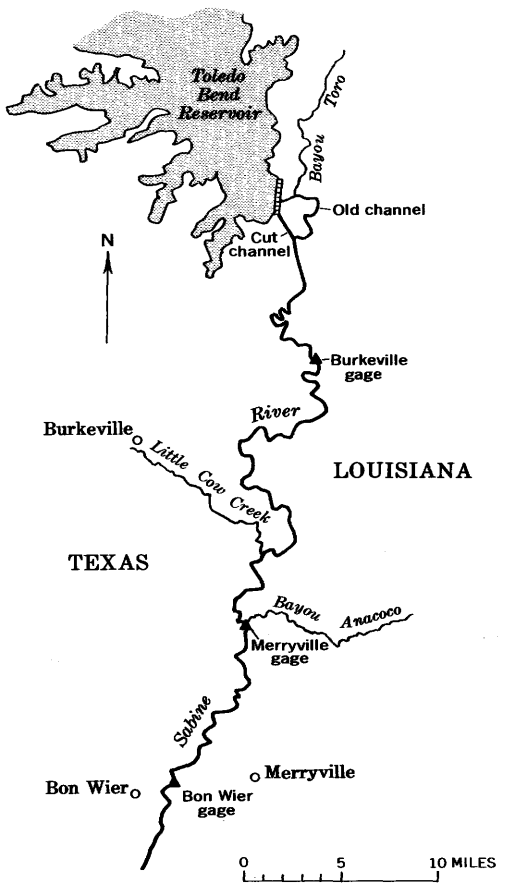

FIGURE 3.—Map of study area.

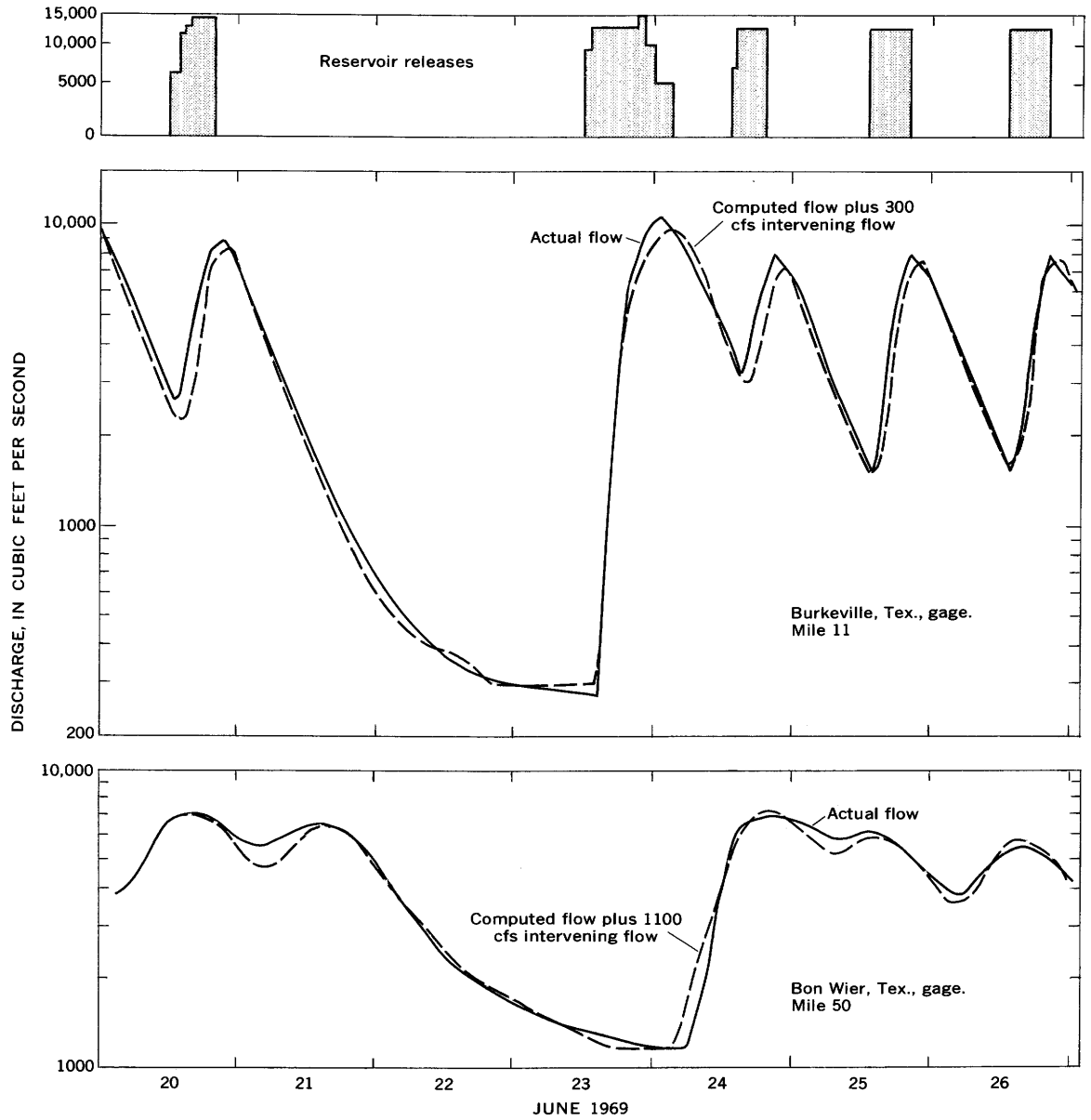

FIGURE 4.—Comparison of routed flow to actual flow for period June 20–26, 1969, Sabine River, Texas-Louisiana.

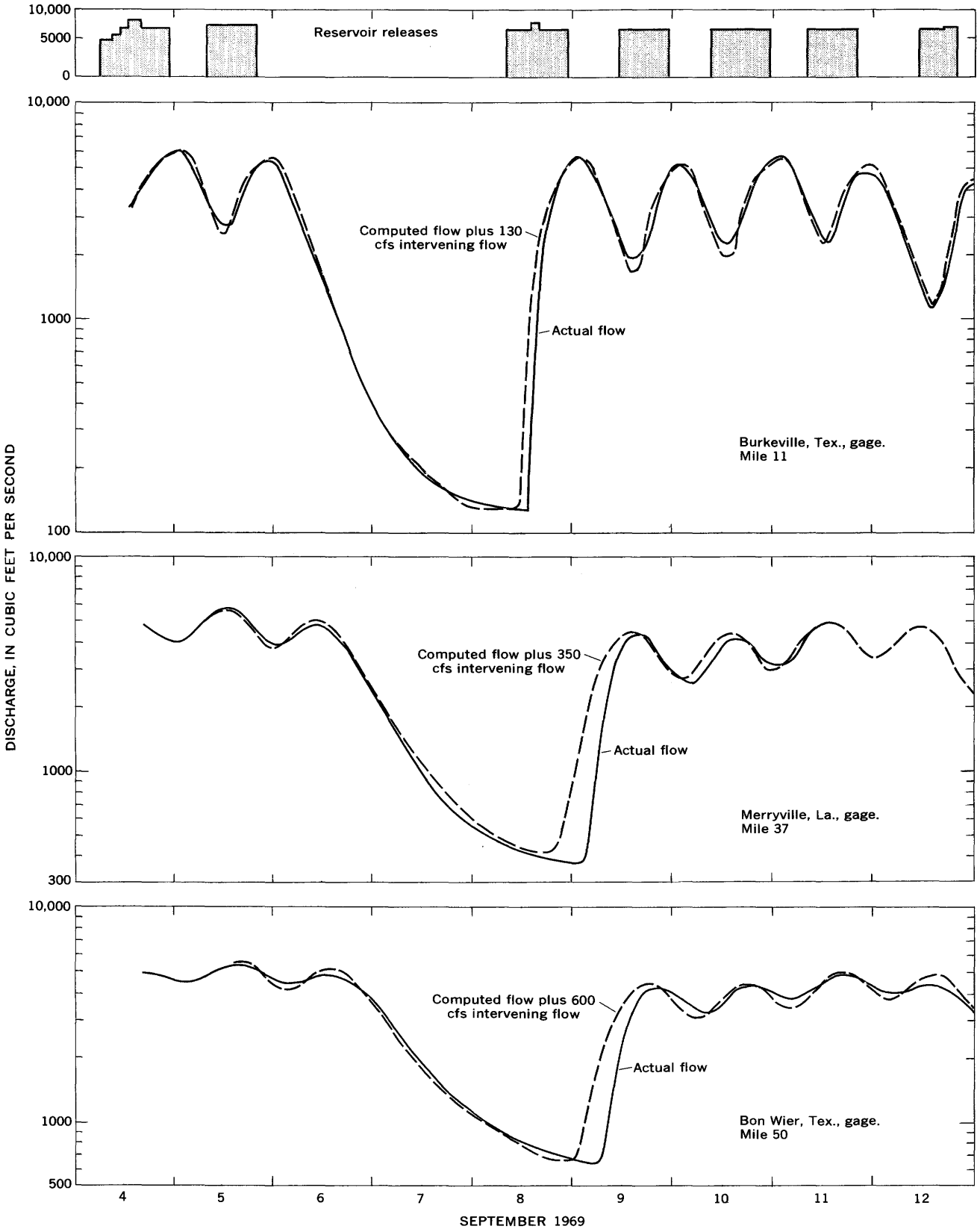

FIGURE 5.—Comparison of routed flow to actual flow for period September 4–12, 1969, Sabine River, Texas-Louisiana.

413-504 O - 71 - 18

TABLE 1.—*Sabine River routing data*

	Gage site		
	Burkeville, Tex.	Merryville, La.	Bon Wier, Tex.
	***D* and *T* (hours)**		
D	2	4	4
T	3	12	17
	Unit hydrograph ordinates (cfs)		
q_1	0. 066	0. 027	0. 072
q_2	. 201	. 147	. 162
q_3	. 166	. 219	. 180
q_4	. 128	. 173	. 155
q_5	. 099	. 124	. 111
q_6	. 077	. 089	. 082
q_7	. 060	. 064	. 062
q_8	. 046	. 046	. 046
q_9	. 036	. 032	. 034
q_{10}	. 028	. 023	. 025
q_{11}	. 021	. 017	. 019
q_{12}	. 017	. 013	. 015
q_{13}	. 013	. 009	. 012
q_{14}	. 010	. 007	. 009
q_{15}	. 008	. 005	. 007
q_{16}	. 006	. 003	. 005
q_{17}	. 005	. 002	. 003
q_{18}	. 004	----------	. 001
q_{19}	. 003	----------	----------
q_{20}	. 002	----------	----------
q_{21}	. 002	----------	----------
q_{22}	. 001	----------	----------
q_{23}	. 001	----------	----------

SUMMARY

The unit-hydrograph technique is a workable method of routing flow from a reservoir even though rapid changes of large magnitude may occur in the flow releases. It requires that the storage-discharge relation in the channel reach be basically a linear relation, and that flood-wave traveltime be relatively constant through the range of discharges to be routed. The Sabine River test results indicated good comparisons of actual flow to computed flow. There was, however, an indication that traveltime in the low discharge range is somewhat slower than in the high range, causing timing errors of up to 8 hours for one of the test periods. This magnitude of error was not considered objectional for the purposes of this study. Additional studies are being made to introduce a variable time factor to reduce the timing error.

Use of the unit-hydrograph method requires a digital computer to handle large quantities of data. Once the routing equation is established, the only input to the computer is the record of flow releases from the reservoir. The program is written in FORTRAN IV for a Univac 494 computer and has been adapted for use on an IBM 360 computer.

REFERENCES

Mitchell, W. D., 1962, Effect of reservoir storage on peak flow: U.S. Geol. Survey Water-Supply Paper 1580–C, 25 p.

——— 1967, Linear analysis of hydrographs: Water Resources Research, v. 3, no. 3, p. 891–895.

A METHOD OF CALCULATING PERMEABILITY FROM ELECTRIC LOGS

By M. G. CROFT, Bismarck, N. Dak.

Work done in cooperation with the North Dakota State Water Commission and North Dakota Geological Survey

Abstract.—A method is described for calculating permeability and transmissivity from resistivity curves of electric logs of water wells. The transmissivity calculated from electric logs was reasonably accurate when compared with aquifer tests at two sites. The method should prove useful for the construction of transmissivity maps in areas where electric logs of water wells are abundant.

Much has been written on the interpretation of electric logs for use in the search for oil and gas, but in contrast, little has been written on the interpretation of electric logs in the water-well industry. This investigation was made to evaluate a method developed by earlier workers for determining the permeability of fresh-water deposits with electric logging devices. The method gives reasonably accurate results if used in conjunction with core samples, aquifer tests, or other well data.

In some areas a large percentage of drilled water wells are logged by commercial geophysical logging companies. Multiple-electrode resistivity logs are a valuable tool for estimating water quality, and many types of logs are used for correlating lithologic units. In addition to these uses, graphs (fig. 1) modified from data reported by Turneaure and Russell (1940), Jones and Buford (1951), and Alger (1966, p. 19) make possible the estimation of permeability and transmissivity from the resistivity curves of electric logs. An investigation of the method suggested by these authors indicates that use of the graphs for these purposes is feasible. The method should prove useful in the construction of transmissivity maps of clastic sediments in areas where multiple-electrode resistivity logs of water wells are abundant. The transmissivity maps, in turn, can be used for the construction of ground-water models.

METHOD

The most widely used empirical relationship among theoretical water resistivity, porosity, and water saturation is reported by Archie (1942). He showed that for core samples, the formation resistivity factor, water resistivity, and rock or sediment resistivity are related over wide ranges of porosity and water salinity by the expression $F=\frac{R_0}{R_w}$ where F is the formation factor, R_0 is the resistivity of a water-saturated rock, and R_w is the resistivity of the water with which the rock is saturated.

Jones and Buford (1951) described a method using electric logs for estimating the quality of ground water in granular aquifers penetrated by rotary-drilled holes. Of particular interest in their report is the relationship of grade-sized samples to formation factor and permeability (1951, p. 121). Jones and Buford's data are presented in this report in graph form (fig. 1). These same data are also presented in graph form by Alger (1966, figs. 12 and 13). The data in figure 1 indicate that the smaller the grain size, the smaller the value of the formation factor. This is the opposite of the relationship normally found with brine-filled sandstone in oil-field work. Alger (1966, p. 13–19) believed that this reverse relation among permeability, formation factor, and grain size in fresh-water aquifers was due to the increased importance of surface conductance and the decreased importance of electrolytic conductance.

Figure 1 illustrates the data presented by Jones and Buford (1951, p. 121), upon which the method is based. The figure can be used to estimate the transmissivity of an aquifer with the resistivity multiple-electrode curves. Jones and Buford used sieved samples of sand

U.S. GEOL. SURVEY PROF. PAPER 750-B, PAGES B265–B269

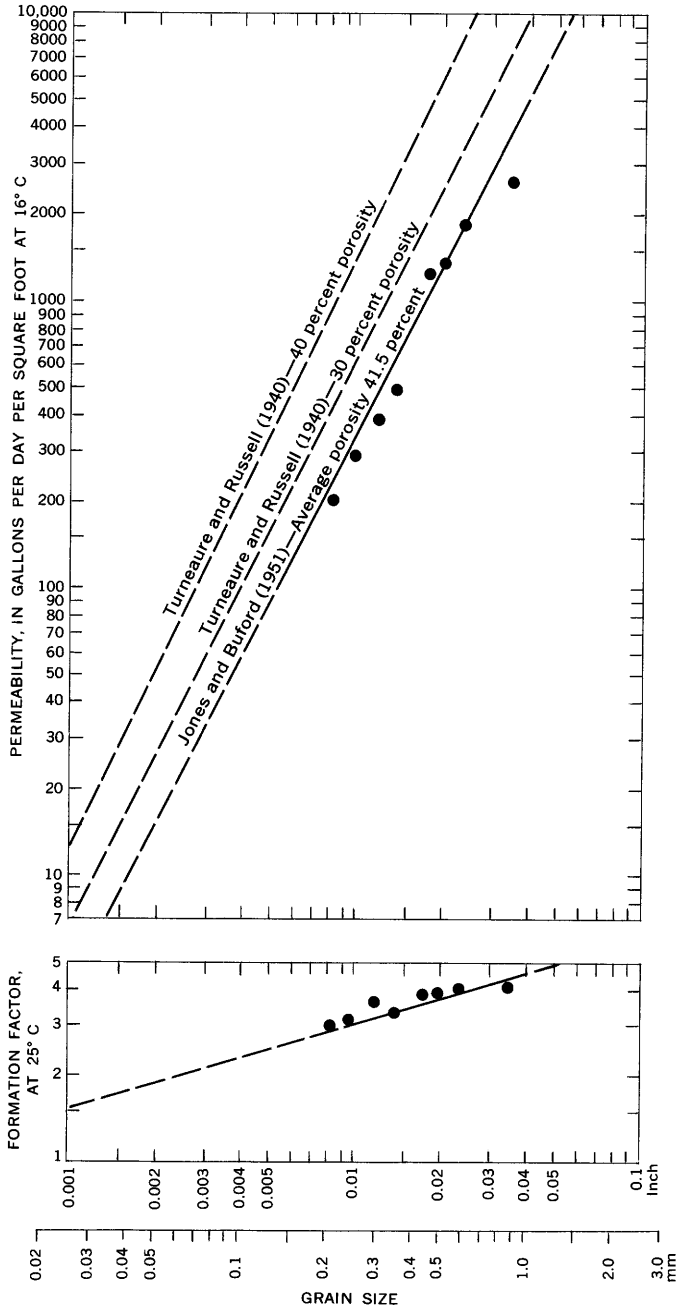

FIGURE 1.—Graphs relating grain size to permeability and formation factor (modified from Alger, 1966).

of one size grade of nearly equal porosity that had a lower permeability than the samples (fig. 1) reported by Turneaure and Russell (1940, p. 97). The graphs (fig. 1) were extended so that they are usable with a minimum F of about 1.7, in order to estimate the permeability of the least transmissive beds shown on numerous logs. While it is possible that the results from using the extended part of the graph are fortuitous, the following examples strongly suggest that reasonable estimates of permeability and transmissivity can be obtained with the graph in its present form despite the scanty data upon which the graph is based and the fact that the samples were grade sized. Figure 2, constructed from the data in figure 1, is much easier to use to convert formation factor to permeability.

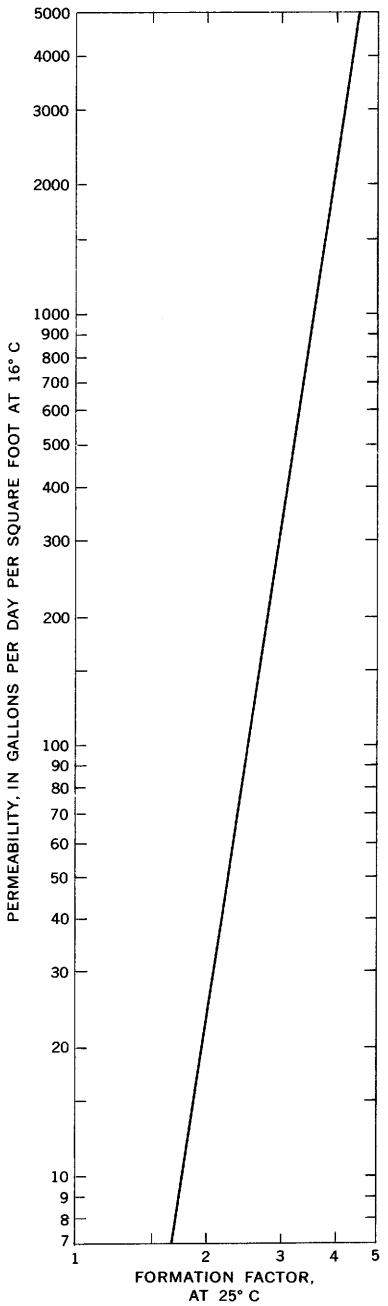

FIGURE 2.—Permeability versus formation factor.

EXAMPLES

Croft and Wesolowski (1970, table 1) made 11 flow tests and 38 recovery tests of wells penetrating the Fox Hills Sandstone and Hell Creek Formation in Mercer and Oliver Counties, N. Dak. The values obtained for transmissivity ranged from 13 to 3,100 gpd (gallons per day) per foot and averaged 510 gpd per foot. Permeabilities were obtained by dividing the thickness of the aquifer, obtained from a driller's log or electric log of the well, into the value for transmissivity. The average permeability obtained by this method was 16 gpd per square foot. The transmissivity of the aquifer in the southwestern part of Mercer County, determined by ground-water flow analysis of a large pumping depression, was 1,400 gpd per foot (Croft and Wesolowski, 1970, p. B194).

A selected section from the upper part of an electric log of an oil and gas test well a few miles west of the pumping depression is shown in figure 3. Formation factors and values for permeability calculated for beds of sandstone forming the aquifer (1,190–1,505 feet) with the long-normal resistivity curve are shown in table 1. The formation factor $\frac{R_0}{R_w}$ for the interval from 1,250 to 1,280 feet was determined as follows:

1. The long-normal R_0 reading of 8.5 ohms m²/m (ohms square meter per meter) was corrected to a standard temperature of 25°C (77°F) with a Schlumberger chart (Schlumberger Technology Corp., 1968, p. 9). The average temperature of water from flowing wells which tap the aquifer was 13.3°C (56°F). The corrected resistivity is 6.4 ohms m²/m.
2. R_w, the resistivity of the water, was determined from conductivity readings of water from nearby wells to be about 3.5.
3. Hence,

$$F=\frac{R_0}{R_w}=\frac{6.4}{3.5}=1.8.$$

The formation factor, is converted to permeability by use of figure 2. The total transmissivity of the beds of sandstone forming the upper Fox Hills and lower Hell Creek aquifer was calculated by this method to be 1,485 gpd per foot. This value, converted to transmissivity at field temperature, becomes 1,400 gpd per foot, the same value obtained from the ground-water flow analysis.

Alger (1966, p. 13) believed that the resistivity value obtained from a 16-inch normal curve is very close to the true formation resistivity (R_0) in many shallow water wells, provided that (1) the well was drilled with fresh mud that had a resistivity close to that of the formation water, (2) mud invasion was shallow, and (3) the sand beds were relatively thick. The long-normal curve was used in the above example because these conditions were not completely met. Generally the long-normal curve was found to give the better results in most tests.

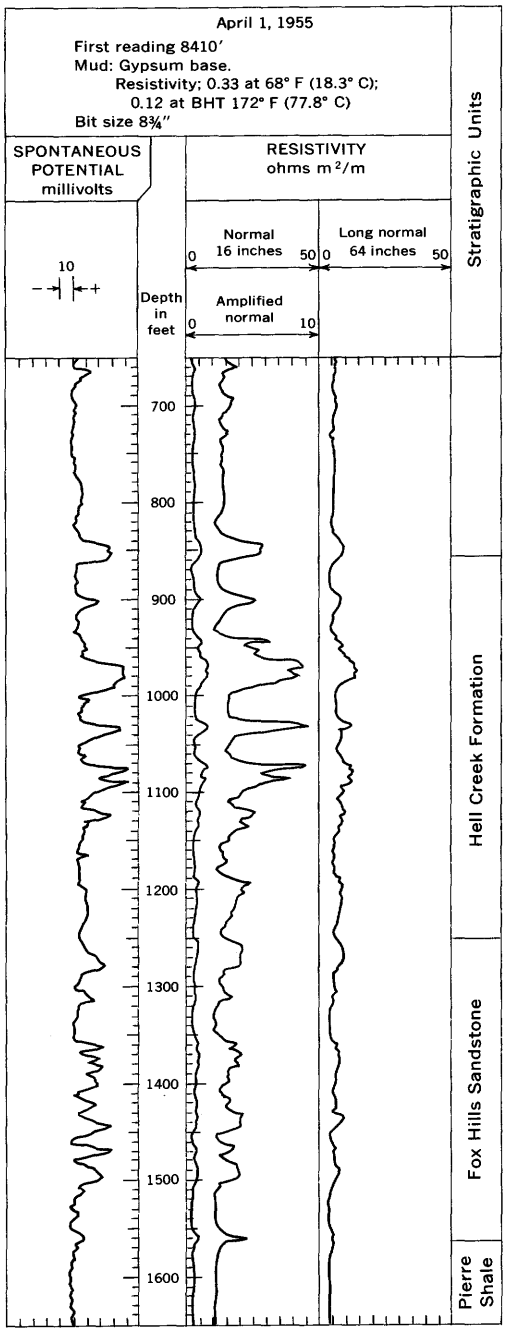

FIGURE 3.—Electric log of well in T. 141 N., R. 41 W., sec. 8, Dunn County, N. Dak.

TABLE 1.—*Formation factors and values for permeability calculated from an electric log (fig. 3) of well in T. 141 N., R. 91 W., sec. 8, Dunn County, N. Dak.*

Depth (feet)	$\frac{R_0}{R_w}$	Formation factor, F	Permeability, P (gpd per sq ft)	Aquifer thickness (feet)	Transmissivity, T (gpd per ft)
1,190–1,210	$\frac{6.2}{3.5}$	1.8	12	20	240
1,250–1,280	$\frac{6.4}{3.5}$	1.8	12	30	360
1,350–1,390	$\frac{5.8}{3.5}$	1.7	9	40	360
1,430–1,455	$\frac{6.4}{3.5}$	1.8	12	25	300
1,480–1,505	$\frac{5.8}{3.5}$	1.7	9	25	225
Total					1,485

An aquifer test in well 20S–19E–25A1, about 2 miles southwest of Stratford, in the San Joaquin Valley, Calif., is reported by Croft and Gordon (1968, p. 28). The well-numbering system is described by Croft and Gordon (1968, p. 9). The casing of the pumped well was perforated in the zone from 1,018 to 2,023 feet below land surface. The coefficient of transmissivity was calculated to be about 70,000 gpd per foot at the site.

The electric log of well 20S–19E–25C1, an observation well with the casing perforated in the zone from 702 to 1,666 feet, is shown in figure 4. The E clay, a widespread lacustrine deposit that occurs from 695 to 750 feet in the log, forms the top of the aquifer (Croft and Gordon, 1968, pl. 5). A lacustrine deposit at a depth of about 1,900 feet probably forms the base of the aquifer. Water from the observation well had a temperature of 26.7°C (80°F) and a resistivity of 7.2 ohms m²/m. Calculations from the log of this well were made by use of the short-normal resistivity curve, with the aid of a chart published by Schlumberger Technology Corp. (1968, p. 44). The sand at a depth of 1,590 to 1,620 feet had a resistivity on the short-normal curve of about 18 ohms m²/m. The corrected resistivity is about 20 ohms. m²/m. The formation factor is 2.8, and the permeability is about 230 gpd per square foot. Therefore, the bed of sand has a transmissivity of about 6,900 gpd per foot. The sum of all calculations for each bed of sand shown by the log for the interval from 750 to 1,620 feet indicates a transmissivity of about 45,000 gpd per foot. The transmissivity of 45,000 gpd per foot converted to transmissivity at field temperature is 60,000 gpd per foot, which compares favorably with the value obtained from the aquifer test, considering the fact that the lower 280 feet of the aquifer was not logged.

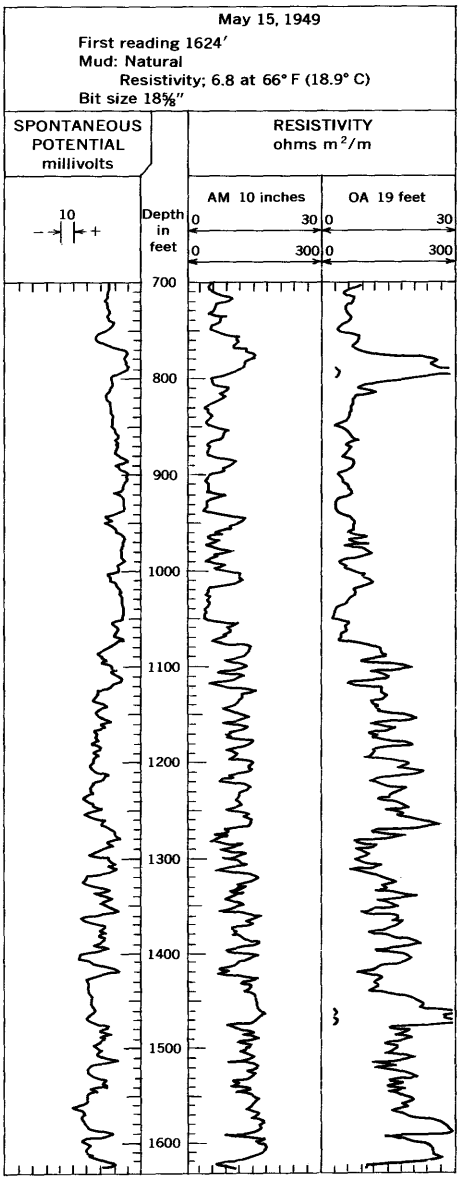

FIGURE 4.—Electric log of well in T. 20 S., R. 19 E., sec. 25C1, San Joaquin Valley, Calif.

REFERENCES

Alger, R. P., 1966, Interpretation of electric logs in fresh water wells in unconsolidated formations: Society of Professional Well Log Analysts Trans., Seventh Annual Logging Symposium, sec. CC, p. 1–25.

Archie, G. E., 1942, The electrical resistivity log as an aid in determining some reservoir characteristics: Am. Inst. Mining Metall. Engineers Trans., v. 146, p. 54–62.

Croft M. G., and Gordon, G. V., 1968, Geology, hydrology, and quality of water in the Hanford-Visalia area, San Joaquin Valley, California: U.S. Geol. Survey open-file report, 63 p.

Croft, M. G., and Wesolowski, E. A., 1970, Transmissivity and storage coefficient of aquifers in the Fox Hills Sandstone and Hell Creek Formation, Mercer and Oliver Counties, North Dakota, *in* Geological Survey Research 1970: U.S. Geol. Survey Prof. Paper 700–B, p. B190–B195.

Jones, P. H., and Buford, T. B., 1951, Electric logging applied to ground-water exploration: Geophysics, v. 16, no. 1, p. 115–139.

Schlumberger Technology Corp., 1968, Log interpretation charts: Houston, Texas, Schlumberger Technology Corp., 68 p.

Turneaure, F. E., and Russell, H. L., 1940, Public water supplies, 4th ed.: New York, John Wiley and Sons, 704 p.

THE USE OF WELL LOGGING IN RECHARGE STUDIES OF THE OGALLALA FORMATION IN WEST TEXAS

By W. S. KEYS and R. F. BROWN,
Denver, Colo., Lubbock, Tex.

Abstract.—As a part of a study of artificial-recharge processes by the U.S. Geological Survey, a series of test holes were drilled in the Ogallala Formation in the southern High Plains of west Texas. Drive cores taken in each lithologic unit were analyzed for moisture content, specific retention, total porosity, specific yield, permeability, and grain-size distribution. Some of these parameters are correlated with neutron, natural gamma, and gamma-gamma geophysical logs. These correlations permit a better delineation of the hydrologic characteristics of the Ogallala Formation than had previously been possible. An apparent relationship between the ratios of naturally occurring radioisotopes and calcium carbonate may prove useful for detecting caliche in boreholes.

The U.S. Geological Survey initiated a major study of artificial recharge, centered at Lubbock, Tex., in fiscal year 1969. The study resulted from the obvious need to replenish ground water in the Ogallala Formation to minimize or halt the decline of the water table and to provide a continuing supply of water from the Ogallala aquifer system. Several areas of research relative to artificial recharge are being investigated at the present time. This paper deals with the use of geophysical well logging in investigations of artificial recharge through water spreading on the land surface. All the illustrations depict conditions at a recharge site near the Lubbock airport (fig. 1). Logging techniques are also used to study recharge through wells. Some preliminary results of this work were described by Schneider, Jones, and Signor (1971). Most of the logging described in this report was done by the staff of a U.S. Geological Survey research project on borehole geophysics as applied to geohydrology, which is headquartered in Denver, Colo. This paper, in slightly modified form, is to be published in the proceedings of the Ogallala Aquifer Symposium, Texas Tech University, May 1970.

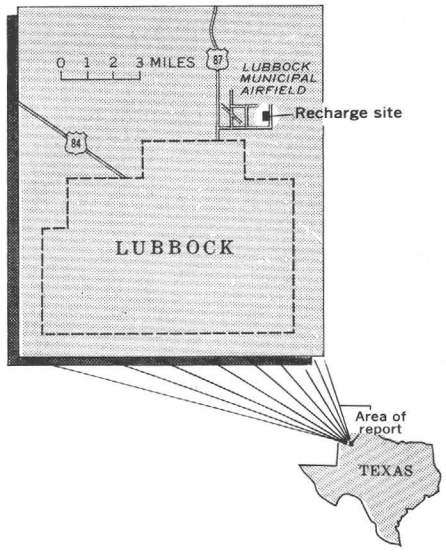

FIGURE 1.—Map showing location of the recharge site at the Lubbock, Tex., municipal airfield.

The most critical factor affecting artificial recharge through a spreading basin is the vertical permeability of the beds between the bottom of the spreading basin and the water table. If the vertical permeability of these intervening beds is low, the time required for water to percolate from the basin to the water table will be so great that artificial recharge might be impractical in many situations. Accordingly, one of the major research efforts is to develop methods for measuring or estimating the vertical permeability of the unsaturated zone so that favorable sites for surface spreading can be selected on the basis of drilling, logging, and testing.

To do this, the vertical permeability of the beds to air was determined in place, using a method described by Stallman and Weeks (1969). Present plans are to test

U.S. GEOL. SURVEY PROF. PAPER 750-B, PAGES B270-B277

a method for relating air to water permeability proposed by E. P. Weeks (written commun., 1970). Logging is used to guide construction of air-permeability holes and to describe the unsaturated part of the Ogallala Formation with sufficient accuracy to permit development of a correlation between air and water permeabilities and other lithologic parameters. It is hoped that the relationships between sample analyses and geophysical logs will be sufficiently consistent that logging alone can be used to predict permeability.

All this work is in a preliminary phase and, rather than applying proven methods, new techniques are being developed. A brief description of the drilling, sampling, hole-completion methods, and the analytical techniques employed in the laboratory are necessary to establish a basis for a discussion of the logging results.

DRILLING AND SAMPLING TECHNIQUES

Most drilling to date has been done with a 4- to 5½-inch flight auger. Where possible, the drilling is done without the addition of water so as to minimize the disturbance of moisture content in core samples and in the material penetrated by the hole.

Drive-core samples were taken through the unsaturated section of the Ogallala at several locations. The cores were obtained by driving a split-tube sampler containing three aluminum liners, each 6 inches long by 1½ inches in diameter, through a hollow-stem auger. After each 18-inch drive, the core barrel was retrieved and the sample removed. As soon as the samples were obtained, the aluminum core liners were sealed with plastic caps, wrapped with electrical tape, and sealed in plastic and wax. This procedure is essential to ensure that there is no moisture change in the sample after it is obtained and before it is analyzed in the laboratory.

After each sample was obtained, a solid plug was placed in the auger bit and the auger rotated down the 18-inch section that had been sampled. When the auger reached the bottom of the cored section, the plug was removed and the split-tube sampler was inserted and driven through an 18-inch section. By this method, practically undisturbed core samples were obtained. However, it was not possible to obtain continuous drive samples from the entire unsaturated thickness.

Geophysical logs were run in many of the holes as soon as the drilling was completed and the auger flights were removed. In some holes logging was done first in the open hole; second, in 2-inch inside-diameter steel pipe; and third, in this same casing after various kinds of backfill had been placed in the annular space between the pipe and the 4- to 5½-inch-diameter auger hole. The following types of backfill were used: dry top soil, sand, dry cement, neat expanding-cement grout, and AM–9 chemical grout. All these backfill materials had some effect on the nuclear logs made in the 2-inch pipe.

Several holes have been drilled with wire-line coring equipment. The wire-line core holes are smaller in diameter and, therefore, superior for quantitative geophysical logging. In addition, core can be obtained in caliche-cemented units where recovery is not possible with drive coring. Compacting of clay samples is minimized by the use of wire-line coring techniques.

LABORATORY ANALYSES

Drive-core samples have been analyzed for permeability, total porosity, moisture content by weight and volume, particle-size distribution, specific retention, and specific yield. The coefficient of permeability was determined by saturating the sample in a 6-inch liner and measuring the flow rate through it under either constant-head or variable-head conditions (Wenzel, 1942).

The total porosity was determined by ovendrying the saturated samples to determine the total volume of water that was lost through complete drying. Moisture content by weight was determined as the weight loss due to ovendrying divided by the total weight measured at the time of sampling. Moisture content by volume was determined by assuming a density of 1.00 g/cc for water, computing a water volume, and dividing by the total sample volume. The particle-size distribution was determined by sieve and hydrometer analysis of the sample after it had been prepared by crushing by mortar and pestle. The specific retention and specific yield were determined by saturating and then centrifuging a sample which was reconstituted from all the material which passed a U.S. Standard No. 10 sieve.

Initial determinations of permeability were affected by clay compaction and by the chemical characteristics of the water used to make the tests; moisture contents were affected by carbonate content. Analyses by more adequate techniques are not yet complete, so the preliminary comparisons of log and sample data shown in this report may be erroneous.

Cores taken by wire-line method have been analyzed radiometrically for radium-equivalent uranium, thorium, and potassium.[1] Fractions of these same cores were analyzed for calcium carbonate content by chemical means.

Core samples are the chief basis for the qualitative and quantitative interpretation of geophysical logs in a newly investigated geohydrologic environment. Geophysical logs indicate lithology and grain-size distri-

[1] Radiometric analyses were made by Carl Bunker, U.S. Geological Survey, Denver, Colo.

bution, and may be calibrated in percentage moisture, porosity, or bulk density by logging core holes and correlating the results with those of laboratory analyses of the core samples. The logs are then used to extrapolate the core data laterally and vertically, resulting in a significant reduction in cost compared to that for obtaining cores and performing laboratory analyses for each hole. The relationship of logs and sample analyses should be consistent within a given lithology where the hole construction is the same.

PRINCIPLES OF LOGGING TECHNIQUES EMPLOYED

Investigations described in this report were carried out above the water table, and most of the logging was done in cased holes; therefore, only a limited number of logging techniques were employed. These included making caliper (in uncased holes), natural gamma, gamma-gamma, and neutron logs.

The caliper log is a record of changes in the average diameter of a drill hole with depth. Its major uses are to evaluate the borehole environment in which other logs are made in order to correct for hole-diameter effects and to provide information on lithology. The probe contains three motor-actuated arms or feelers which open at the bottom of the hole. As the probe is withdrawn from the hole, the spread of the feelers is constricted by the diameter of the borehole.

The natural gamma log is a continuous record of the intensity of gamma radiation produced by all naturally occurring radioisotopes in all rocks. The log, which is made with a sodium iodide detector, is routinely used for the identification of lithology and for stratigraphic correlation. However, it does not show the relative abundance of potassium-40, and uranium and thorium series. This may be done in boreholes by a special technique called gamma spectrometry (Keys and Boulogne, 1969).

The gamma-gamma probe contains a source of gamma photons, cobalt-60, separated from a sodium iodide detector by tungsten-alloy spacers. The gamma-gamma log is a record of the intensity of gamma radiation from the source after it is attenuated and backscattered by the borehole and surrounding rocks. The main uses of gamma-gamma logs are for the identification of lithology, hole-construction parameters, and the measurement of the bulk density and porosity of rocks. Gamma transmittance logging, a variation of this technique, utilizes a source in one drill hole and a detector in a nearby hole. The source and detector are synchronously moved to provide a log of a very large volume of material. The log can provide absolute values only if the distance between holes is constant. However, it does provide a sensitive means of logging changes in the environment, and it is relatively free from borehole effects.

The neutron log is made with a neutron source and a scintillation detector arranged in a probe so that the output is primarily a function of the hydrogen content of the borehole environment. Neutron logs are chiefly used for the measurement of moisture content above the water table and total porosity below the water table.

In this investigation two different types of neutron probes have been employed, one commonly used in soils investigations, and the other in oil-well logging. The neutron moisture probe commonly used in soils investigations utilizes a 100-millicurie americium-beryllium source positioned several inches from the detector. This tool can be used only in relatively small diameter holes, and the count rate increases with higher moisture content. For most logging, a neutron tool was used with a 3-curie americium-beryllium source positioned at least 17 inches from the detector. This probe, commonly used in oil-well logging, may be used under a wide variety of hole conditions. The count rate decreases as the moisture content or saturated porosity increases; thus, in this report, the neutron trace shows moisture increasing to the left. Neutron transmittance logging is done in the same way as gamma transmittance and provides a log that is remarkably free of borehole effects and thus is more effective for monitoring changes in the environment.

Most of the preliminary investigations on the use of geophysical logs in the Ogallala Formation consist of comparing laboratory data on cores with data from logs. An important factor in this process is the great difference in the volume of material sampled by the two techniques. The radiation detector for each of the nuclear logs utilized should be visualized as the center of a roughly sphere shaped volume of the formation which contributes to the signal recorded as a log. Within the radius of investigation, the material closest to the detector contributes the greatest part of the signal, and the material farthest away the least. For the natural gamma log, the volume investigated is about 250 times the volume of a drive-core sample of the same depth interval. For the neutron log the volume may be more than 600 times as great, depending on the moisture content.

A further difference in sample size is introduced by laboratory procedures which involve splitting of the core. For these reasons, exact correspondence of sample analyses and log values is not to be expected in a nonhomogeneous lithologic unit like the Ogallala. Depth errors, owing to core loss, add an additional difficulty to the collation of logs and core.

APPLICATION OF LOGS

Lithology and correlation

Composite interpretation of several different types of logs based on one cored hole is the best way to identify and correlate units within the Ogallala Formation. Lithology seems to be best identified by the natural gamma log. Project work in other sedimentary environments indicates that the response of the natural gamma log can be semiquantitatively related to the percentage clay fraction. To date, sufficient mechanical analyses of samples from the Ogallala are not available to make such a comparison, but the natural gamma log is the best available for use both above and below the water table in identification of sand and clay sections.

The neutron log is outstanding for lithologic identification above the water table. Clay beds have a higher specific retention than sand and silt beds and, therefore, a higher moisture content. Below the water table, the lithologic separation based on water content is less pronounced but is still useful. Some correlation of units is evident from gamma-gamma logs, and caliche zones are indicated by solution cavities or extremely uniform diameter holes shown by caliper logs in some wire-line core holes.

Stratigraphic correlation of lithologic units in the Ogallala is easily accomplished at the Lubbock airport recharge site by use of natural gamma and neutron logs. The clay beds are the most readily identified and are the most continuous lithologic units at the site. Clay beds only a few inches thick extend for hundreds of feet, and a thick clay such as that shown on the logs between depths of 90 and 100 feet (fig. 2) may have a very great lateral extent.

Permeability

The ultimate objective of most geophysical logging in hydrology is the measurement of some parameter related to permeability. No geophysical log measures permeability directly. In a well-recharge project northwest of Lubbock, it was found that the zone having the lowest gamma intensity also exhibited the highest permeability. Above and below this zone, a high gamma intensity indicated interstitial clay which decreased the permeability of the sand. In contrast, at the surface spreading site near the Lubbock airport, the natural gamma log does not appear to be a measure of permeability in the upper part of the Ogallala. The clay beds shown on figure 2 are much less permeable than the clean sands. However, the presence of the caliche or calcium carbonate also seems to decrease the permeability of the sands. Caliche is here defined as gravel or sand cemented by calcium carbonate, or the calcium carbonate itself.

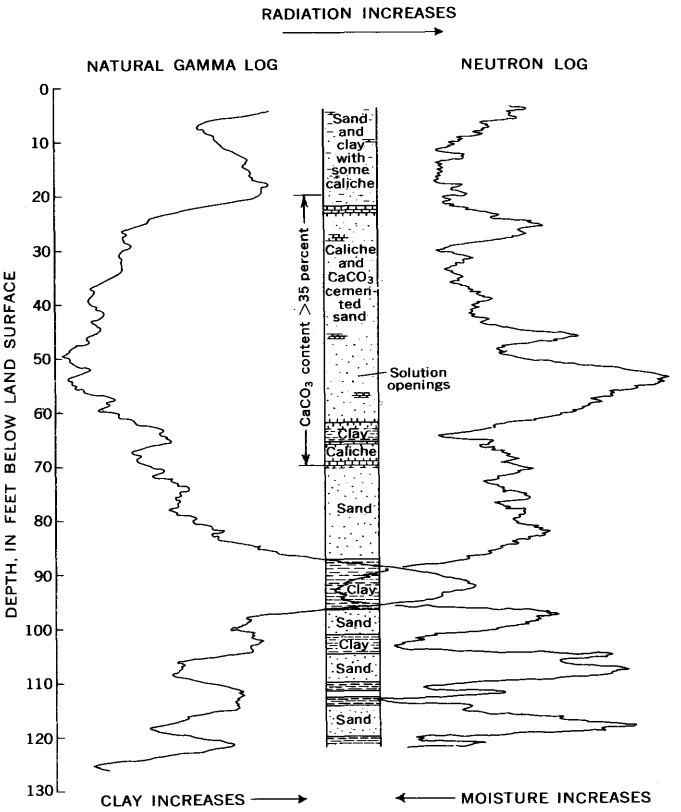

FIGURE 2.—Neutron, natural gamma, and lithologic logs made at the Lubbock airport recharge site.

On the basis of preliminary laboratory analyses of data from cores, the highest vertical permeabilities in the Ogallala at the Lubbock airport recharge site are in the zones that are relatively low in both clay and calcium carbonate content. Laboratory data on a series of samples from a test hole at this site showed only one sample with a coefficient of permeability greater than 7 gallons per day per square foot (gpd per sq ft) within the zone where $CaCO_3$ is more than 35 percent (fig. 3) or within the clay beds shown on figure 3. The high permeability measured in the caliche zone was not substantiated by an adjacent sample.

In contrast, the zones having lower carbonate and clay contents have permeabilities as high as 180 gpd per sq ft; most of the higher values were found between depths of 108 and 128 feet. Below the caliche zone, all the samples having coefficients of permeability greater than 10 gpd per sq ft contained less than 30 percent clay and silt-size grains. In contrast, the permeabilities measured on core samples from the clay bed between 90 and 100 feet deep, averaged 0.004 gpd per sq ft, and the silt and clay fraction averaged 64 percent. In this area, logs that provide data on clay and $CaCO_3$ content are likely to be the most useful for predicting the vertical permeability of the unsaturated zone.

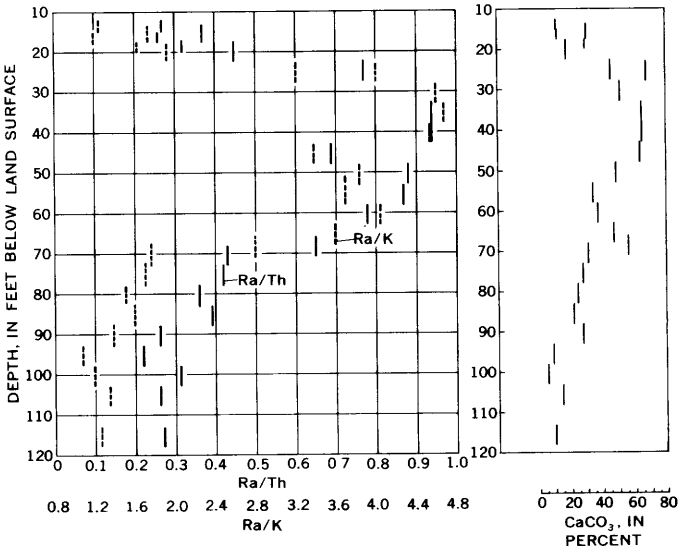

FIGURE 3.—Relationship of radiometric content, expressed as the ratios of radium to thorium (Ra/Th) and of radium to potassium (Ra/K), to the calcium carbonate content, in dry-weight percent, for 25 core samples from the Lubbock airport recharge site.

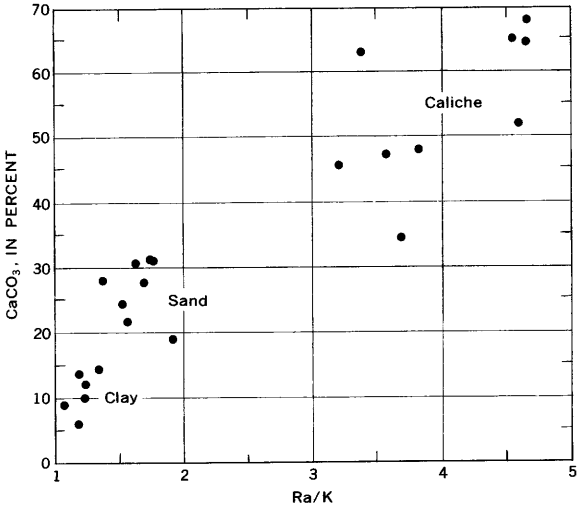

FIGURE 4.—Graph of calcium carbonate versus ratio of radium to potassium content, by dry weight.

Caliche content

A unique problem that is related to recharge of the Ogallala by surface spreading concerns the identification and quantitative determination of caliche or calcium carbonate content. Neither natural gamma, neutron, nor gamma-gamma logs have provided useful information on the caliche content to date.

To date, the most effective method for identifying the caliche-rich zones is gamma spectrometry. Radiometric ratios for 25 wire-line core samples are shown in figure 3. Note the general correspondence of the radium-potassium ratios and the calcium carbonate content. Figure 4 is a graph of $CaCO_3$ and Ra/K. There is a sharp break between those samples with less than 31 percent $CaCO_3$ and those with more than 34 percent $CaCO_3$.

On the basis of these few samples, clay and sand also appear to be distinguished by Ra-K ratios. The reason for these relationships are not clear at this time. However, potassium and thorium are consistently low in the caliche, and radium is quite variable, probably owing to leaching. The content of all three elements is low in the sand below the caliche and high in the clay.

It has been demonstrated that the identification of radioisotopes in boreholes can be accomplished with the equipment used on this project (Keys and Boulogne, 1969). In boreholes, the determination of ratios between natural radioisotopes should be easier than the quantitative determination of the individual isotopes because of the difficulty of maintaining a constant relationship between the detector and sample investigated. Research on the relation of natural radiosotopes to the lithology and water-bearing characteristics of the Ogallala will continue, and in-hole radiometric analyses will be carried out in the near future. Caliper or hole-diameter logs also have some potential for locating caliche in open holes because the walls of the hole through caliche-cemented sections are commonly smooth and the hole is of smaller diameter than in sand or clay sections.

Moisture content

Neutron logs are widely used for the measurement of moisture content above the water table. In the Ogallala, we have used the long-spaced, oil-well type, neutron probe for most of our logging because of the reduced effect of borehole parameters.

Figure 5 shows the correlation between moisture content (by volume) as measured on cores in the laboratory and by a neutron log of the core hole. In view of the limitations described under "Principles of Logging Techniques Employed" in this report, the correlation is good. No major differences in character are seen between the open-hole log of the core hole and a log made in a hole 2 feet away after a 2-inch pipe was inserted and the hole was backfilled. The clay beds have the highest moisture content because of their high specific retention, and the caliche and sand have the lowest moisture content. Neutron logs have been made over a period of a year at this site, and the only significant changes above the water table have been due to hole-construction techniques. The logs, however, show that there was a 2.5- to 3-foot rise in the water table during this period (fig. 6).

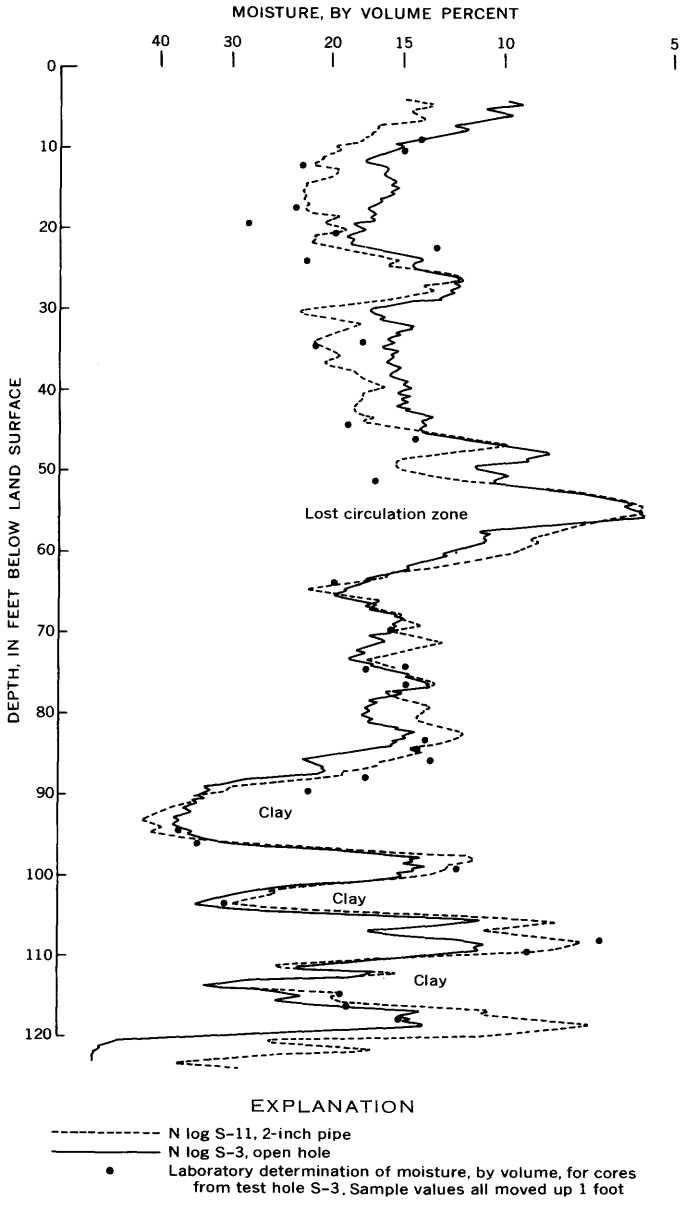

FIGURE 5.—Moisture content as determined from cores in the laboratory and from neutron logs of the holes from which the cores were taken.

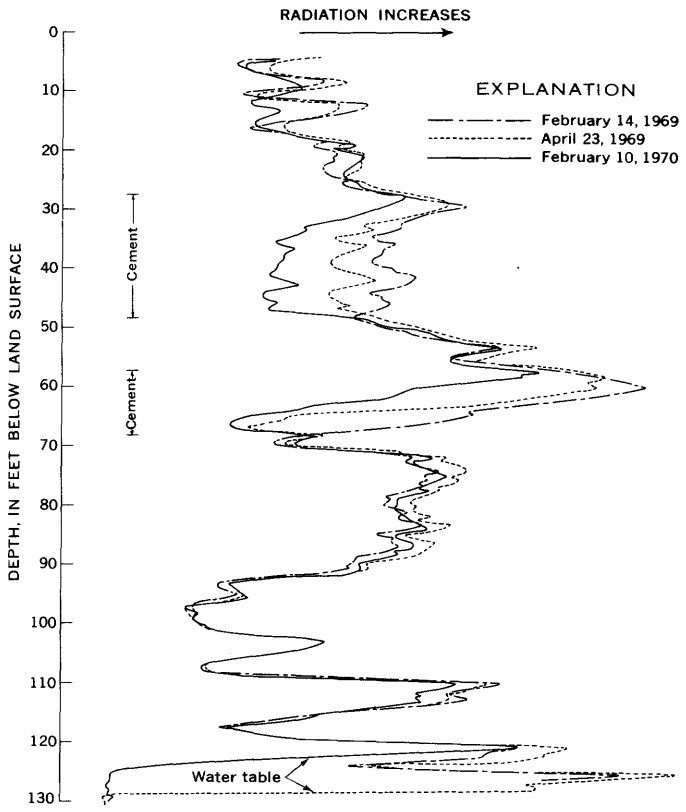

FIGURE 6.—Periodic neutron logs of the Ogallala Formation.

Porosity and bulk density

The neutron log may be interpreted in terms of porosity below, but not above, the water table.

The output of a gamma-gamma probe is inversely proportional to the bulk density of the material penetrated by a drill hole. Unfortunately, such a measurement of bulk density also includes the varying density of the liquid-gas mixture in the pore spaces. Total porosity is related to bulk density by the following equation:

$$\text{Porosity} = \frac{\text{Grain density} - \text{bulk density}}{\text{Grain density} - \text{fluid density}}.$$

Average grain density may be assumed to be 2.65 g/cc (quartz), or it may be determined by laboratory analysis. Fluid density may be assumed to be 1.00 g/cc below the water table. Bulk density may be related to caliche content below the water table because calcite ($CaCO_3$) has a density of 2.71 g/cc. The high content of $CaCO_3$ in the caliche zones should, therefore, be indicated by a higher bulk density. In practice the log trace has not been definitive—perhaps in part because of the susceptibility of the gamma-gamma log to borehole effects.

Neutron and gamma-gamma logs can be used to calculate total porosity below the water table. The measurement of effective porosity is important to calculations of the amount of water that may be stored in the Ogallala. However, at this stage in the investigations, it is not certain whether there is a significant difference between total and effective porosity in the Ogallala. Effective porosity may be calculated from quantitative resistivity logs of the saturated portion of the Ogallala. Guyod (1966) presents a chart which enables the determination of effective porosity for granular aquifers from resistivity and water-quality data.

Effects of recharge

A potential use for well logging in the Ogallala is to study the effects of artificial recharge. Gamma-transmittance logs have been used to study plugging of the aquifer by sediment near a recharge well, and temperature logs used to trace the flow of recharge water (Schneider and others, 1971). Transmittance logs may also be used to measure plugging caused by sediment in surface-spreading operations. The much greater volume of material investigated by this technique increases the sensitivity to changes in the formation and decreases sensitivity to changes in the annulus of the well. Another potential use of logging is for the in situ detection of tracers added to recharge water. Neutron activation in boreholes may be used to detect nonradioactive tracers through the casing. Resistivity logging may be used to monitor changes in water quality caused by recharge. Logs that measure vertical flow within a well may be used to locate zones taking water injection recharge as well as zones which have become plugged as a result of recharge operation. Logs may enable the selection of the most permeable zones where screens should be set or casing perforated for maximum recharge. As part of this study, multielectrode resistivity logs have been made through plastic well screen. These logs measure effective porosity and therefore offer another potential means of locating plugged zones in the aquifer caused by sediment in recharge water.

PROBLEMS IN USE OF LOGS

This report describes actual and potential uses of geophysical well logs in the Ogallala without discussing the several problems inherent in their use. When adequate logging equipment is available, problems in the quantitative use of logs can be separated into three general categories: Drilling and hole construction, sampling, and sample analysis. The latter two categories are included because of the importance of samples as a guide to log interpretation in a new area and for the calibration of logs. Research in drilling, sampling, and analytical techniques should proceed hand in hand with logging investigations in a new area.

Drilling and hole construction

It is impossible to drill a hole without disturbing, in some way, the environment that is to be measured. If moisture determination is the objective, drilling with water will increase the moisture content near the hole. However, frictional heat and the circulation of air caused by augering will also dry out the wall of the hole. Any deviation from standard hole size will have some effect on the output of logging probes that are not decentralized and side collimated. If drilling is done with water or mud, differential pressure will cause some mud filtrate to enter the formation and a mud cake to form.

In the Ogallala any holes that are to be used for periodic logging must be cased so that they will stay open. Unless the casing fits the hole very tightly, backfill material should be added to maintain the hole and prevent water circulation in the annulus. Any variation in the casing, backfill, or hole diameter will have some effect on nuclear logs. Figure 6 compares three neutron logs of a hole at the spreading site that were made over a period of 1 year. After 2-inch pipe was inserted, the hole was backfilled with fine dry topsoil, and dry cement was added in the two intervals shown in order to prevent the movement of water in the annulus. The major difference between these logs was caused by the gradual increase in the moisture content of the dry cement. (A rising water table is also shown.) Obviously, dry cement is not a satisfactory material for backfilling. Both chemical grout and expanding cement have also been found unsatisfactory from the standpoint of moisture logging because they have a high equivalent moisture content and penetrate the formation to varying degrees. Research will continue on improved techniques and materials for backfilling test holes.

Figure 7 shows the effect of nonuniform backfill on a neutron log made with a 3-curie source in a core hole. The shift on the right-hand log, which was made after

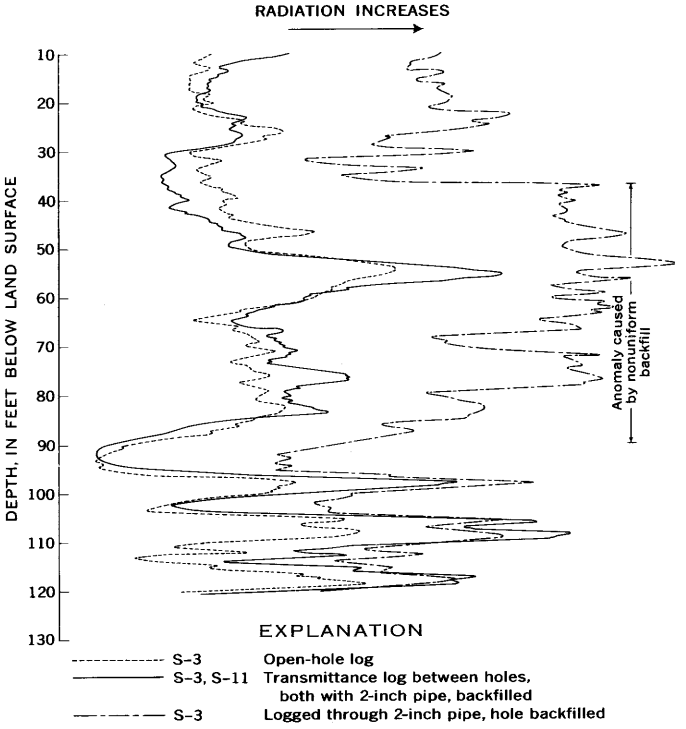

FIGURE 7.—Comparison of three neutron logs made under different borehole conditions.

installing 2-inch pipe and backfilling, was even greater on logs made with a neutron moisture probe. The neutron log shown by a solid line was made by the transmittance technique between holes S–3 and S–11 which are about 2 feet apart. Note that the effect of backfill is completely eliminated. Although the sensitivity of the transmittance log is somewhat greater, it conforms very closely to the open-hole log of S–3.

Sampling

Most of the samples taken in the Ogallala, to date, have been drive cores. The chief difficulties with drive coring have been the compaction of clay samples and the inability to penetrate caliche-cemented sections. Furthermore, it is difficult to determine the degree to which samples of various lithologies are disturbed. Presently, experiments with wire-line coring techniques are being conducted in order to improve recovery and reduce disturbance of the cores. The technique appears to have considerable promise. Penetration of the hole wall by drilling fluid is apparently insignificant when one considers the radius of investigation of the neutron device. A normal-moisture log is obtained within several days after termination of drilling. Holes drilled by the wire-line technique have the advantage of being at least 2 inches smaller in diameter than holes drilled using the hollow-stem auger. For logging these holes, tight-fitting pipe will be installed which will eliminate the necessity for backfill.

Sample analysis

Only a brief mention of some of the problems in sample analysis will be made here. However, the importance of recognizing these difficulties cannot be overemphasized. Use of erroneous laboratory data will obviously lead to incorrect interpretation of geophysical logs. Compaction or channeling of the sample will affect moisture, porosity, and permeability data. Determination of grain-size distribution is meaningless unless (1) it is preceded by quantitative analyses for carbonate or other nondetrital cement and (2) a thin-section study is made to determine its mode of occurrence. Furthermore, significant differences in permeameter readings are noted when there are differences in the quality of water used and that with which the formation would be in equilibrium. This factor will, of course, have a major bearing on recharge of the Ogallala.

CONCLUSIONS

Geophysical well logging is most useful in investigations of the feasibility of artificial recharge of the Ogallala aquifer. Logs can be used to extrapolate sample and test data laterally and vertically. They can provide information that is not otherwise obtainable from some cased irrigation wells. Logs may enable the prediction of the yield or recharge potential of specific sections of the Ogallala. They can provide data of use for proper well construction. If enough logs are made they will provide the basis for the construction of more accurate lithofacies maps of the aquifer. Finally, borehole geophysics provides methods for the in situ measurement of changes in the aquifer caused by artificial recharge.

REFERENCES

Guyod, Hubert, 1966, Interpretation of electric and gamma ray logs in water wells: The Log Analyst, v. 6, no. 5, p. 29–44.

Keys, W. S., and Boulogne, A. R., 1969, Well logging with californium-252: The Log Analyst, v. 10, no. 6, Nov.–Dec., p. 11–24.

Schneider, A. D., Jones, O. R., and Signor, D. C., 1971, Recharge of turbid water to the Ogallala aquifer through a dual purpose well: Texas A and M University Experiment Station Misc. Pub. [In press.]

Stallman, R. W., and Weeks, E. P., 1969, The use of atmospherically induced gas-pressure fluctuations for computing hydraulic conductivity of the unsaturated zone: Geol. Soc. America Program and Abs., 1969, pt. 7.

Wenzel, L. K., 1942, Methods for determining permeability of water-bearing materials, with special reference to discharging-well methods: U.S. Geol. Survey Water-Supply Paper 887, 192 p.

SUBJECT INDEX

[For major headings such as "Economic geology," "Geochemistry," "Ground water," see under State names or refer to table of contents]

413-504 O - 71 - 19

AUTHOR INDEX

U.S. GOVERNMENT PRINTING OFFICE:1970 O—413-504